A SOLID STATE AND MECHANISTIC STUDY OF MULTIDENTATE LIGAND ZIRCONIUM(IV) HALIDO COMPLEXES

By

MARYKE STEYN

A thesis submitted to meet the requirements for the degree of

PHILOSOPHIAE DOCTOR

In the

DEPARTMENT OF CHEMISTRY

FACULTY OF NATURAL- AND AGRICULTURAL SCIENCES

At the

UNIVERSITY OF THE FREE STATE

SUPERVISOR: PROF. HENDRIK G.VISSER

CO-SUPERVISOR: PROF. ANDREAS ROODT

FEBRUARY 2014

Acknowledgements

First and foremost, I thank the Lord Almighty for the countless opportunities He has granted me. Only by His blessing, by His guidance this has been possible.

To Prof. Roodt, a simple "thank you" isn't sufficient. For all the opportunities, the patience, the inspiration through your passion for chemistry, I have grown into a passable scientist. Thank you, for always asking more questions than I am able to answer, for always pushing me to give a 110 %.

To Prof. Visser, Blits-Vis, thank you for your guidance throughout this project. All the advice, new ideas and supportive humour is greatly appreciated. Thank you for allowing me to express myself in long-winded scientific deliberations, more times than should ever be necessary.

To my mother, Annemarie Zaayman, thank you for putting up with my eccentricities. Thank you for the support and for always checking up on me, making sure I give it my all. I would not have come this far without your endless support. To my 'new dad' Ockie Zaayman, thank you for your support as well, it is greatly appreciated.

To Annél, Linda and Eben Oosthuysen, thank you for the support you have given me. Thank you for the confidence you have put in me and know that I truly appreciate all your support.

To my close friends, you know who you are, thank you for never-ending support and camaraderie, the time you have spent listening to all my troubles, my depressions and aggressions, and especially for being there to celebrate all the good things that have come my way. Without you all to lean on, to keep me sane and to keep me grounded, I wouldn't have made it this far.

More, for sure, the future waits,

and ever more, my courage fails.

but on the greener side awaits.

Destiny, a mystery,

Success, an uncertainty.

And as I brace, for the fight,

my eyes are blinded by the Light,

my solace found in His Holy Might.

My doubt, drowned for ever more,

the righteous, wisest, highest ever soar.

~~ Wishful Thinker

Table of Contents

Chapter 3

Synthesis of Zirconium(IV) Complexes – Experimental Techniques & Preliminary Characterisation

Chapter 4

X-Ray Diffraction Studies of Zirconium(IV) Complexes Containing 5,7-Halogen Substituted 8-Hydroxyquinoline Ligands

Chapter 5

X-Ray Diffraction Studies of Zirconium(IV) Complexes Containing Non-Halogen Substituted 8-Hydroxyquinoline Ligands

Chapter 6

X-Ray Diffraction Studies of Zirconium(IV) Complexes Containing O,O'-Donating Ligands

Chapter 7

Solution Formation Kinetics Study of Tetrakis(oxine-type)zirconium(IV) Complexes

Chapter 8

Theoretical Study of Zirconium(IV) O,O- and N,O-Bidentate Ligand Complexes

List of Abbreviations

Abbreviation	Meaning
acac	Acetylacetone - organic ligand
Acac	Acetylacetone - ligand family reference
ox	8-Hydroxyquinoline - organic ligand
Ox	8-Hydroxyquinoline - ligand family reference
Lig	Ligand
Lig#	Specific numbered ligand, with # = ligand number as coordinated
IR	infra-red
UV/Vis	ultra violet/visible
NMR	nuclear magnetic resonance
XRD	x-ray diffraction
mg	milligram
mmol	millimol
M	$mol.dm^{-3}$
°C	degrees Celsius
v	IR stretching frequency
λ	UV/Vis wavelength
δ	chemical shift
ppm	(unit of chemical shift) parts per million
C_3D_6O	Deuterated Acetone
MeOD	Deuterated Methanol
DMF	N,N'-Dimethylformamide
Z	number of molecules in a unit cell
Å	angstrom
°	degrees
π	pi
A	absorbance (theoretical)
A_{obs}	observed absorbance
k_x	rate constant for a forward equilibrium reaction
k_{-x}	rate constant for a backward equilibrium reaction
K_x	equilibrium constant for an equilibrium reaction
k_{obs}	observed rate constant
DFT	Density Functional Theory
RMS	Quadratic mean (root-mean-square)

Chapter 1

Zirconium and the Nuclear Industry –

A Brief History and Insight

Zirconium, as *element*, was discovered in 1789 by Martin Heinrich Klaproth, a German chemist, while analysing the composition of the mineral jargon ($ZrSiO_4$).[1] It has been known as a gem mineral since biblical times, known more commonly as *hyacinth*, *jacinth* or *ligure*. Furthermore, the *metal* zirconium was first produced in its impure form by Jöns Jacob Berzelius, a Swedish chemist, in 1824, by heating a mixture of potassium and potassium hexafluorozirconate by activating a decomposition process. It was a century later, in 1925 that the first industrial process for the production of pure metallic zirconium was developed by Anton Eduard van Arkel and Jan Hendrik de Boer.[2] This process is known today as the "Crystal Bar Process" or "Iodide Process". In 1938 William J. Kroll further advanced the production of this metal with the application of his "Kroll Process", by which zirconium tetrachloride is reduced by molten magnesium. This technology was widely used since the 1950's as an economically viable method.[3]

---

[1] David R. Lide, ed.; *CRC Handbook of Chemistry and Physics* (**2005**), *Section 4: Properties of the Elements and Inorganic Compounds*, Int.Vers. (http://www.hbcpnetbase.com), CRC Press, Boca Raton, FL, 36.
[2] R. Nielsen & T.W. Chang; *"Zirconium and Zirconium Compounds"*,*Ullmann's Encyclopaedia of Industrial Chemistry* (**2005**), Wiley-VCH, Weinheim, 1-2.
[3] G. Roza; *"Zirconium"* (**2009**), 1st Ed., Rosen Publishing Group, 24-25.

It was later discovered that zirconium had excellent application value in the nuclear industry, and in particular as cladding material for fuel rods. This is due to the fact that it has a very low thermal neutron absorption cross section, but also exhibits outstanding anti-corrosion properties and high thermal stability.[4] Unfortunately, zirconium is always found together with its chemical twin hafnium, from natural/mining sources. Hafnium, with its very high affinity for thermal neutrons is most often employed as control rods, used for controlling the rate of fission in nuclear reactors.[5] For this application alone, it is apparent why the separation of these metals to their chemically pure state, is so important. Even the smallest impurity of one metal in the other would seriously degrade the ability if the metal to function in its role in a nuclear reactor. Separation of these metals can be accomplished *via* several means, but separation is a difficult and labour intensive process, due to their very similar chemical characteristics (See Chapter 2 for elaboration).

1.1. Zirconium in Industry

Zirconium as metal has a wide range of applications, in many diverse industrial technologies. It is extensively employed as catalyst for synthesis of organic compounds,[6,7,8] but also in ceramics,[9] the manufacturing of surgical equipment[1] and applied in semi-conductors.[10] Furthermore, its anti-corrosive properties and high thermal stability makes it ideal for use in refractory material in furnaces and crucibles.[11]

However, as indicated above, the most noteworthy application of this metal is found in die nuclear industry, as cladding material for fuel rods.[12] Nuclear grade zirconium is required to be essentially hafnium free (<100 ppm),[13] due to hafnium's high low thermal neutron

---

[4] R.H. Nielsen, J.H. Schlewitz & H. Nielsen; *"Zirconium and Zirconium Compounds"*, *26* (**2000**), Kirk-Othmer Encyclopaedia of Chemical Technology, John Wiley & Sons, Inc., 637.

[5] David R. Lide, ed.; *CRC Handbook of Chemistry and Physics* (**2005**), *Section 4: Properties of the Elements and Inorganic Compounds*, Int.Vers. (http://www.hbcpnetbase.com), CRC Press, Boca Raton, FL, 4-36.

[6] M. Ozawa; *J. Alloy. Compd. 275/277* (**1998**), 886–890.

[7] H. Ishitani, M. Ueno & S. Kobayashi; *J. Am. Chem. Soc. 122* (**2000**), 8180-8186.

[8] D.W. Stephan; *Angew. Chem. Int. Ed. 39* (**2000**), 314 – 329.

[9] G. Roza; *"Zirconium"* (**2009**), 1st Ed., Rosen Publishing Group, 34-35.

[10] R. Nielsen & T.W. Chang; *"Zirconium and Zirconium Compounds"*,*Ullmann's Encyclopaedia of Industrial Chemistry* (**2005**), Wiley-VCH, Weinheim, 1-13.

[11] R.E. Smallman & R.J. Bishop; *"Modern Physical Metallurgy and Materials Engineering"* (**1999**), 6th Ed., Elsevier Ltd., 330-331.

[12] R.H. Nielsen, J.H. Schlewitz & H. Nielsen; *"Zirconium and Zirconium Compounds"*, *26* (**2000**), Kirk-Othmer Encyclopaedia of Chemical Technology, John Wiley & Sons, Inc., 630.

[13] M. Benedict, T.H. Pigford & H.W. Levi; *Nuclear Chemical Engineering* (**1981**), McGraw-Hill, USA, 318–347.

absorption cross section (Hf = 104 barns *vs.* Zr = 0.184 barns).[14] It is in this case that the separation of these two metals becomes such a significant endeavour, since impurities can cause serious degradation of the metal's application in this field. Zirconium metal is applied as a variation of alloys in cladding material, commonly referred to as Zircaloy.[4] These alloys contain other metals with similarly low thermal neutron absorption cross sections, but in very low quantities. The composition of some of these alloys is as follows:

- Zircaloy-2[15] (Zry-2): Zirconium (98.5 %), tin (1.4%), oxygen (0.12 %), chromium (0.10 %), iron (0.10 %), and nickel (0.05 %).

- Zircaloy-4[16] (Zry-4): Zirconium (98.5 %), tin (1.4%), iron (0.20 %), oxygen (0.12 %) and chromium (0.10%).

- Zr-2.5Nb:[17] Zirconium (97.5 %), niobium (2.6 %) and oxygen (0.14%).

- Zirconium Low Oxidation[18] (ZIRLO): Zirconium (97 %), niobium (1 %), tin (1 %) and iron (0.1 %).

The predominant commercial source of zirconium has long been its silicate mineral zircon ($ZrSiO_4$), obtained as a by-product from mining and processing of the titanium minerals such as ilmenite and rutile.[19] This mineral is rarely found in economically viable minable rocks, due to natural weather erosion that strips away the zircon grains, which is why the greater deposits available are found in river delta and beach sands.[20] Of this mineral sand, South Africa is one of the world's largest suppliers of zircon sand, producing 30 % of the global demand in 2006.[21] At this stage, a clearer picture can be drawn as to the economic impact the purification of zirconium has on South Africa and world-wide.

---

[14] N.N. Greenwood & A. Earnshaw; *"Chemistry of the Elements", 2nd Ed.* (**1997**), Reed Educational and Professional Publishing Ltd, Butterworth-Heinemann, Woburn, MA, 954-975.
[15] MatWeb Material Property Data; *Zircaloy-2 Zirconium Alloy* (**2014**); http://www.matweb.com/search/datasheet.aspx?matguid=eb1dad5ce1ad4a1f9e92f86d5b44740d, Last Accessed 03/02/2014.
[16] MatWeb Material Property Data*; Zircaloy-4 Zirconium Alloy* (**2014**);http://www.matweb.com/search/datasheet.aspx?MatGUID=e36a9590eb5945de94d89a35097b7faa, Last Accessed 03/02/2014.
[17] MatWeb Material Property Data; *Zr-2.5Nb Zirconium Alloy, Nuclear Grade* (**2014**); http://www.matweb.com/search/datasheet.aspx?MatGUID=9c996807673f4208bc99c655c388072d, Last Accessed 03/02/2014.
[18] H.K. Yueh, R.L. Kesterson, R.J. Comstock, H.H. Shah, D.J. Colburn, M. Dahlback & L. Hallstadius; *J. ASTM Int. 2* (**2005**), 6, 330-315.
[19] R.H. Nielsen, J.H. Schlewitz & H. Nielsen; *"Zirconium and Zirconium Compounds"*, *26* (**2000**), Kirk-Othmer Encyclopaedia of Chemical Technology, John Wiley & Sons, Inc., 622-623.
[20] R. Nielsen & T.W. Chang; *"Zirconium and Zirconium Compounds"*,*Ullmann's Encyclopaedia of Industrial Chemistry* (**2005**), Wiley-VCH, Weinheim, 4-5.
[21] Roskill; *"The Economics of Zirconium" (***2007**). 12thEd., London, Roskill Information Services Ltd., 1-4.

1.2. Economic Indicators and Considerations

The global zirconium consumption market per annum has grown in the last decade to an expected capacity of 115 000 tons per year. This includes all industries such as ceramics, chemical, refractory and metal/metal alloys.[22] The principle market for zirconium as metal is for the Zircaloy material utilized in the aforementioned nuclear reactors as cladding material. The global consumption of this product is estimated 5500 tons in 2010 with a global increase in demand expected of around 4 % per annum.

Iluka Resources, an Australian sand mining company and a major producer of zircon in the global market, mentioned in their December 2013 report[23] that the average price for zircon in 2013 is estimated to be US$1150/t. Furthermore, according to the 2011 Roskill[24] report on zirconium market indicators, the forecast is expected to reach US$1800/t by 2015. This is a clear indicator of a global demand that is growing every year.

Therefore, since zirconium finds such a significant application as metal alloy in the nuclear industry as cladding material, a noteworthy influence into the economy weighs heavily on the cheaper production of nuclear grade zirconium. Additionally, since South Africa is a leading producer of the zircon sand, the predominant mineral source supplying this metal, the effect on the national economy also comes into play.

By investigation and design of cheaper/easier and more sustainable separation/purification methods, enhancing the metallurgic knowledge base already available, the impact on a wide range of aspects becomes worth considering here. First and foremost, the financial implications involved lead to a stronger local economy. Secondly, the intellectual property of method and patent design and implementation leads to employment propagation. Finally, by being able to affect all the downstream processes involved from basic mining, directly to refinement and metal production, South Africa will benefit in all aspects concerned.

---

[22] Roskill; *"Zirconium: Global industry markets and outlook" (***2011**). 13th Ed., London, Roskill Information Services Ltd., 4-6.

[23] Iluka; Quarterly Production Report - 31 December 2013, http://www.iluka.com/docs/default-source/asx-releases/december-2013-quarterly-production-report.pdf?sfvrsn=6, Last Accessed: 03/02/2014.

[24] Roskill; *"Zirconium: Global industry markets and outlook" (***2011**). 13th Ed., London, Roskill Information Services Ltd., 5.

1.3. The aim of this study

The information presented here clearly show that there is scope for improvements in the metallurgical methods of purification of zirconium and separation from hafnium. A field of study that can yield vital information regarding chemical behaviour of these metals revolves around metallic chelation experimentation. By studying the solid state and solution behaviour of zirconium with selected coordination agents, as well as the rates at which these interactions take place, may provide a clearer image of how improvements on known methods can be made can be identified.

<u>The explicit aims of this study, therefore, are as follows:</u>

I.   Synthesis of novel zirconium(IV) coordination compounds with a wide range of N- and O-donating multidentate ligands and subsequent characterisation thereof by means of analytical techniques, such as IR-, UV/Vis- and NMR spectroscopies. The ligands intended for this study are discussed and described in detail in Chapter 2.

II. Solid state structural characterisation of crystalline products of the above, intended at elucidating the nuances of chelation that can be observed by means of single crystal X-Ray Diffraction (XRD). With this type of investigation, a comparison with similar hafnium(IV) compounds could yield valuable insight into physical and/or chemical state differences to be exploited for purification/separation endeavours.

III. Solution behavioural evaluation of the intrinsic formation mechanism of the synthesised and characterised compounds of zirconium(IV). This is achieved by means of UV/Vis kinetics studies and reaction rate modelling with the intention of shedding light into the equilibrium influences in this process that could be exploited for solution extraction methodology.

IV. Theoretical optimization of complexes, by means of computational chemistry techniques, of solid state structures obtained and sourced from literature, with the intention of determining whether or not these three-dimensional entities as obtained from XRD studies, can be predicted by simulation. If it is possible, then this technique can also be further employed to quantify previously unknown/unobtainable structures, for comparative purposes. These structural comparisons, just as with XRD analysed compounds, can in principle yield information as to certain smaller but significant differences that would allow for solid state or solution manipulation studies for purification of zirconium and separation from hafnium.

In the following chapter, a brief insight into the theoretical considerations regarding the known techniques of zirconium-hafnium separation is presented. Furthermore, a discussion regarding the chosen organic chelation agents identified for this study is also included, emphasising the reasoning as to why they would lead to valuable and novel insights into zirconium(IV) coordination behaviour.

1.4. Technical Considerations of This Study

Throughout this thesis, in discussion on the coordination study considerations, theoretical and applied, there will often be related to a correlation of zirconium and hafnium aspects for separation purposes. This particular document, however, reports only the results of the zirconium counterpart of the overarching research endeavour.

This is due to the fact that it is but one half of a tandem study on the separation of these metals, from the inorganic chemistry point of view. The corresponding hafnium co-project is in progress by Mr. J.A. Viljoen (UFS), focusing on the same aims of investigation.

Both these PhD research projects are parented by their related M.Sc. precursors, also individually focussing on zirconium[25] and hafnium[26] coordination behaviour in the solid and solution states. Referral will often be made throughout this thesis of the original M.Sc. dissertation that was completed in 2009, as basis for several correlations regarding crystallographic structural characterisation as well as solution kinetic mechanistic considerations.

---

[25] M. Steyn; *Speciation And Interconversion Mechanism Of Mixed Halo And O,O- And O,N Bidentate Ligand Complexes Of Zirconium*, M.Sc. Dissertation (**2009**), University of the Free State, South Africa.
[26] J.A. Viljoen; *Speciation And Interconversion Mechanism Of Mixed Halo And N,O- Bidentate Ligand Complexes Of Hafnium*, M.Sc. Dissertation (**2009**), University of the Free State, South Africa.

Chapter 2

Theoretical Considerations – Purification and Coordination Studies of Zirconium(IV)

Zirconium and hafnium, the chemical twins of the titanium triad on the periodic table, have found considerable interest the world over in research.[1,2,3,4,5] As transitions metals they function over a wide range of applications, from catalysis[6,7,8] to alloyed metal components.[9,10,11] However, they find their most predominant use in the nuclear industry for their very different characteristics in this field. It is in their nuclear properties they show themselves to be complete opposites.

Zirconium,[12] with its very low affinity for thermal neutrons, high thermal stability and exceptional anti-corrosive properties, is widely used as cladding material for nuclear reactor

[1] T. J. Pinnavaia & R. C. Fay; *Inorg. Chem. 7* (**1968**), 502-508.

[2] H.K. Chun, W.L. Steffen & R.C. Fay; *Inorg.Chem. 18* (**1979**), 2458-2465.

[3] A. Clearfield & D.S. Thakur; *Appl. Catal. 26* (**1986**), 1–26.

[4] F. Calderazzo, U. Englert, C. Maichle-Mössmer, F. Marchetti, G. Pampaloni, D. Petroni, C. Pinzino, J. Strähle & G. Tripepi; *Inorg. Chim.Acta 270* (**1998**), 177-188.

[5] M.B. Pomfret C. Stoltz, B. Varughese, & R.A. Walker; *Anal. Chem. 77* (**2005**), 1791-1795.

[6] M. Ozawa; *J. Alloy. Compd. 275/277* (**1998**), 886–890.

[7] H. Ishitani, M. Ueno & S. Kobayashi; *J. Am. Chem. Soc. 122* (**2000**), 8180-8186.

[8] D.W. Stephan; *Angew. Chem. Int. Ed. 39* (**2000**), 314 – 329.

[9] M. Griffiths; *J. Nucl. Mater. 159* (**1988**) 190–218.

[10] B. Cox; *J. Nucl. Mater. 170* (**1990**), 1, 1–23.

[11] M.P. Pulls; *J. Nucl. Mater. 393* (**2009**) 2, 350–367.

[12] David R. Lide, ed.; *CRC Handbook of Chemistry and Physics* (**2005**), *Section 4: Properties of the Elements and Inorganic Compounds*, Int.Vers. (http://www.hbcpnetbase.com), CRC Press, Boca Raton, FL, 4-36.

fuel rods. Hafnium,[13] on the other hand, with its very high affinity for thermal neutrons is most often employed as control rods, used for controlling the rate of fission in reactors. For this application alone, it is apparent why the separation of these metals to their chemically pure state, is so important. Even the smallest impurity of one metal in the other would seriously degrade the ability if the metal to function in its role in a nuclear reactor.

Separation of these metals can be accomplished *via* several means, but is a difficult and labour intensive process. This is due to their overwhelming chemical similarities (as shown in Table 2.1).

Table 2.1 Comparison of characteristic properties of zirconium and hafnium.[14]

Property	Zr	Hf
Group	4	4
Period	5	6
Block	d	d
Atomic number	40	72
Boiling point (°C, K)	1854 , 2127.15	2233 , 2506.15
Boiling point (°C, K)	4406 , 4679.15	4600 , 4873.15
Density (kg.m^{-3})	6507	13276
Relative atomic mass	91.224	178.49
Common oxidation states	4	4
Atomic radius, non-bonded (Å)	2.23	2.23
Covalent radius (Å)	1.64	1.64
Electronegativity (Pauling scale)	1.330	1.300
Heat of fusion (kJ.mol^{-1})	14	27.2
Heat of vaporization (kJ.mol^{-1})	573	571
Molar heat capacity (J.mol^{-1}.K^{-1})	25.36	25.73
Thermal conductivity (W.m^{-1}.K^{-1})	22.6	23
Thermal expansion (@25 °C, µm.m^{-1}.K^{-1})	5.7	5.9
Thermal Neutron Capture Cross Section (barns, 10^{-28} m^2)	0.184	104

---

[13] David R. Lide, ed.; *CRC Handbook of Chemistry and Physics* (**2005**), *Section 4: Properties of the Elements and Inorganic Compounds*, Int.Vers. (http://www.hbcpnetbase.com), CRC Press, Boca Raton, FL, 4-14.
[14] N.N. Greenwood & A. Earnshaw; *"Chemistry of the Elements", 2nd Ed.* (**1997**), Reed Educational and Professional Publishing Ltd, Butterworth-Heinemann, Woburn, MA, 954-975.

2.1. Production of Zirconium Metal – The Kroll Process

This pyrometallurgical production method, also known as the magnesium reduction process, has been employed widely since the 1950's to produce pure zirconium.[15] This method was initially developed for the production of metallic titanium[16] but was later adapted for zirconium production. The process involves the reduction of zirconium tetrachloride in an inert atmosphere with molten magnesium.[17] Initial difficulties encountered with this method revolved around the physical characteristics of the metal chloride. $ZrCl_4$ is a solid at room temperature, which only sublimes at 331 °C and can only be liquefied under pressure at 335 atm. Furthermore, this compound is readily hydrolysed by atmospheric moisture to the metal oxychloride and produces hydrochloric acid in the process. Kroll and co-workers solved the hydrolysis problem by designing novel reduction furnaces that allowed for only gaseous zirconium chloride to come into contact with the magnesium reducing agent. This prevented the contamination of the chlorinated zirconium with oxygen.

The specific method[18] involves the fluidisation of hafnium-free zirconium dioxide in an induction-heated chlorinator. The reaction process at 900 °C yields $ZrCl_4$ and CO_2, which passes through a nickel lined condenser, to form the metal powder after cooling to below 200 °C. This powder product is then purified by sublimation in an inert atmosphere along with the reducing agent - magnesium - to yield the metallic zirconium as metal beads in a slurry with the magnesium chloride. This slurry is then distilled at 980 °C, to drain off the liquidised magnesium chloride, yielding a porous zirconium sponge after cooling.

This metallurgic method in itself is steadily being replaced by other methods that focus on other types of technologies. One such method is the FFC Cambridge Process, which is an electrochemical method that reduces metal oxide to metal powder by means of electrolysis of solids.[19]

[15] G. Roza; *"Zirconium"* (**2009**), 1st Ed., Rosen Publishing Group, 24-25.
[16] W. Kroll; *"Method for Manufacturing Titanium"* (**1940**), US Patent 2205854.
[17] A.L. Lowe & G.W. Parry; *"Zirconium in the Nuclear Industry: Proceedings of the Third International Conference"*, *633* (**1976**), 7.
[18] R.H. Nielsen, J.H. Schlewitz & H. Nielsen; *"Zirconium and Zirconium Compounds"*, *26* (**2000**), Kirk-Othmer Encyclopedia of Chemical Technology, John Wiley & Sons, Inc., 630.
[19] A.J. Fenn, G. Cooley, D. Fray & L. Smith; *Advanced Materials & Processes 162* (**2004**), 51-53.

2.2. Separation of Zirconium and Hafnium

2.2.1. Liquid-Liquid Extraction

Liquid-Liquid Extraction, or Solvent Extraction, is a separation method that utilises the differences in relative solubilities of compounds in solution in different, immiscible solvents. This is usually performed *via* water and different organic solvents, but other variations also exist. For the separation of zirconium and hafnium this method exploits the difference in solubility of the respective chelated compounds of these metals in different solvents.
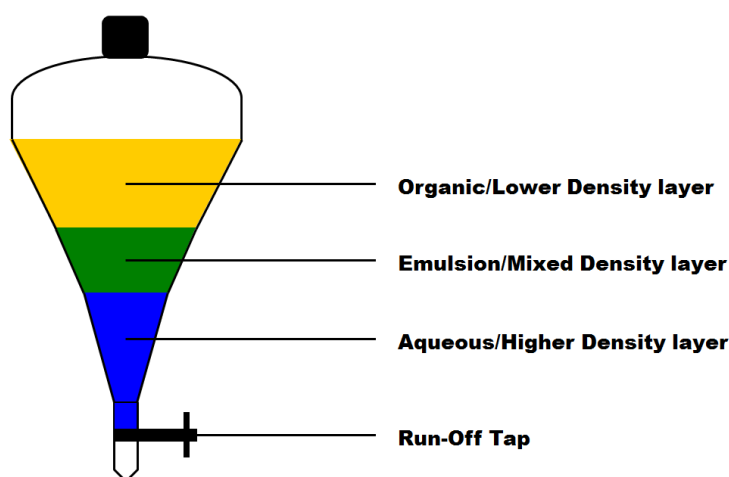
Figure 2.1 Schematic illustration of the rudimentary laboratory setup of the liquid-liquid/solvent extraction technique. From initial agitation of the mixed solution, the emulsion or mixed density layer separates over time into a single density layer that can be run off individually.

One such a process involves the thiocyanate compounds of these metals extracted from water by methyl isobutyl ketone (MIBK).[20] The hafnium moiety has a slightly greater solubility in the organic phase, which allows for extraction of the zirconium counterpart from the acidified (by dilute sulphuric acid) aqueous phase. The metals are then recovered by means of precipitation as zirconium sulphate and hafnium oxide. This method is widely used in the USA.[21]

---

[20] R.H. Nielsen, J.H. Schlewitz & H. Nielsen; *"Zirconium and Zirconium Compounds"*, *26* (**2000**), Kirk-Othmer Encyclopedia of Chemical Technology, John Wiley & Sons, Inc., 630.
[21] R.H. Nielsen; *"Hafnium and Hafnium Compounds"*, *13* (**2000**), Kirk-OthmerEncyclopedia of Chemical Technology, John Wiley & Sons, Inc., 82.

In another method, zirconium is preferentially extracted from an acidified (hydrochloric-nitric acid mix or nitric acid) heptane solution by reaction with tributyl phosphate (TBP). Hafnium and other impurities are retained in the aqueous layer, while the zirconium is recovered from the organic phase *via* precipitation after neutralization. With this precipitation method, no further purification of the zirconium powder is required.
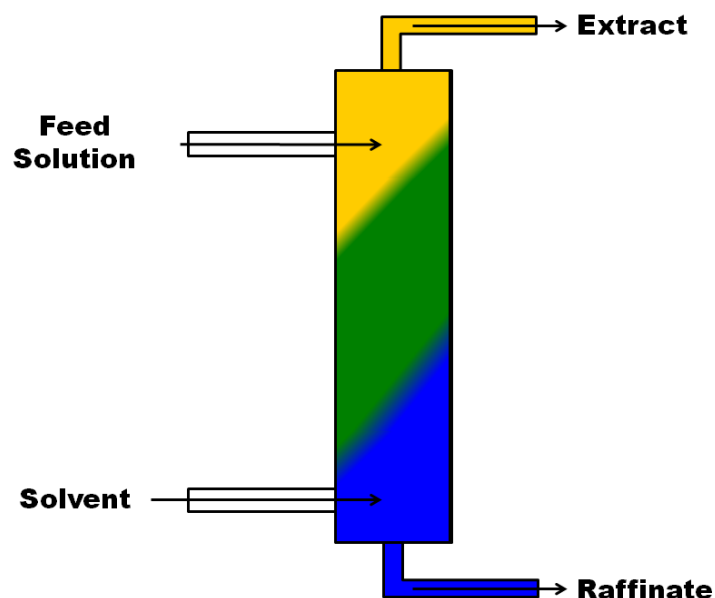
Figure 2.2 Schematic illustration of a rudimentary industrial extraction column[22] of the liquid-liquid/solvent extraction technique. Mixing occurs along the length of the column from the "Feed" and "Solvent" solutions, after which the "Extract"-solution flows out at the top. The "Raffinate"-solution is considered to contain insoluble or un-extractable components, and may be resourced for further extraction.

In yet other methods, high molecular weight amines are employed to separate these metals in hydrochloric acid solutions. It has been shown that higher selectivities for zirconium can be found from tertiary amines in sulphuric acid, but secondary and primary amines are also utilized.[20] With the addition of nitric acid, the separation can be greatly influenced, but unfortunately decreases the yield of zirconium recovered. In Japan, this method was implemented employing trioctylamine in kerosene.

---

[22] E. Muller; *"Liquid-Liquid Extraction", Ullmann's Encyclopedia of Industrial Chemistry* (**2005**), Wiley-VCH, Weinheim, 1-4.

2.2.2. Extractive Distillation

Extractive (or Fractional) Distillation is a method of separation distillation in the presence of a miscible, high boiling, relatively non-volatile component (the solvent), that forms no azeotropes with any of the dissolved compounds or other volatiles present.[23] This method is mostly used in cases where separation of compounds in a mixture cannot be accomplished *via* simple distillation, due to the fact that the compounds present in the mixture are equally (or near equally) volatile in solution. Therefore, the compounds in solution would evaporate at the same temperature, making normal distillation techniques unfeasible.
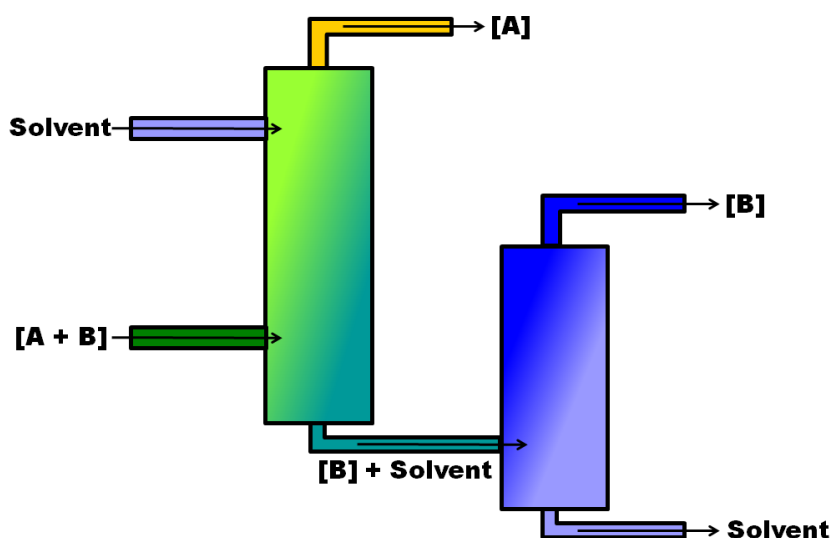
Figure 2.3 Schematic illustration of a rudimentary Two-Column Extractive Distillation Setup.[24] Separation occurs in two separate phases; initially only one compound (A) is distilled off, followed by further distillation in another column to obtain compound B as well as recovering the solvent.

This method of distillation takes advantage of the fact that the solvent employed is of high boiling temperature, allowing for all desired products to be volatilised (boiled/ distilled off) before the solvent would. The solvent interacts differently with each component in the mixture, and thus alter their relative volatility, allowing for previously similar compounds to be fractionally distilled, where it is not possible in the general sense. Furthermore, the fact that the solvent does not form azeotropic mixtures with the compound, the distilled fractions can be considered pure, and would not require any further purification/ separation steps.

---

[23] J.G. Speight; *"The Refinery of the Future"*, (**2010**), London: William Andrew, 134-136.
[24] Z. Lei, C. Li & B. Chen; *Separation and Purification Reviews 32* (**2003**), 2, 121-213.

In the case of the separation of zirconium and hafnium employing this method, the anhydrous metal tetrachlorides ($ZrCl_4$ and $HfCl_4$) have different volatilities at higher pressures.[25] These metal tetrachlorides are dissolved in a molten solvent salt mix of potassium chloride and aluminium chloride, in which both metals are soluble without complex formation. The entire system is pressurised (30-45 atm) and heated above 4000 °C. At this point, all of the $HfCl_4$ and a small amount of $ZrCl_4$ are distilled off, and pure $ZrCl_4$ remains behind. [26]

2.2.3. Fractional Crystallization

Fractional Crystallization, or even Fractional Precipitation, is a purification method most often used in chemistry for the refining of substances based on solubilities and tendencies for one compound to form a solid state product under different conditions from other impurities in solution.[27]

In the case of separation of zirconium and hafnium, these metals can be separated by means of selective (fractional) crystallization of their potassium hexafluoro metal (K_2MF_6) compounds. The hafnium compound is more soluble in the hydrofluoric acid solution utilised, and allows for pure potassium hexafluorzirconate crystal to be collected.[28]

This was, in fact, the very first laboratory method for separation of zirconium and hafnium.[29] Von Hevesy *et al.* reported as early as 1925 that this method had been the easiest way to separate these metals. Initial methods used either potassium or ammonium fluorides to zirconium/hafnium fluorides solutions. The process involves a series of batch crystallizations, wherein each cycle the products become increasingly more pure.

[25] R.H. Nielsen, J.H. Schlewitz & H. Nielsen; *"Zirconium and Zirconium Compounds", 26* (**2000**), Kirk-Othmer Encyclopedia of Chemical Technology, John Wiley & Sons, Inc., 630-631.
[26] R.H. Nielsen; *"Hafnium and Hafnium Compounds", 13* (**2000**), Kirk-OthmerEncyclopedia of Chemical Technology, John Wiley & Sons, Inc., 84.
[27] L.A. Cisternas, C.M. Vásquez & R.E. Swaney; *AIChE J. 52* (**2006**), 5, 1754-1769.
[28] R.H. Nielsen; *"Hafnium and Hafnium Compounds", 13* (**2000**), Kirk-OthmerEncyclopedia of Chemical Technology, John Wiley & Sons, Inc., 84.
[29] G. von Hevesy; *Chem. Rev.2* (**1925**), 1-41.

2.2.4.   Ion Exchange Separation

Ion Exchange separation is a form of separation or purification that utilises chromatographic principles of solid and liquid state interactions of different ions on a stationary phase. In principle, the process involves the retention and release of different ions in solution on this stationary phase as it moves along the span of the experimental setup (usually a column uniformly packed with this substrate). The speed, at which certain compounds/analytes are passed along this setup, is dependent on both the type of stationary phase as well as the composition of the analytes to be separated.[30]
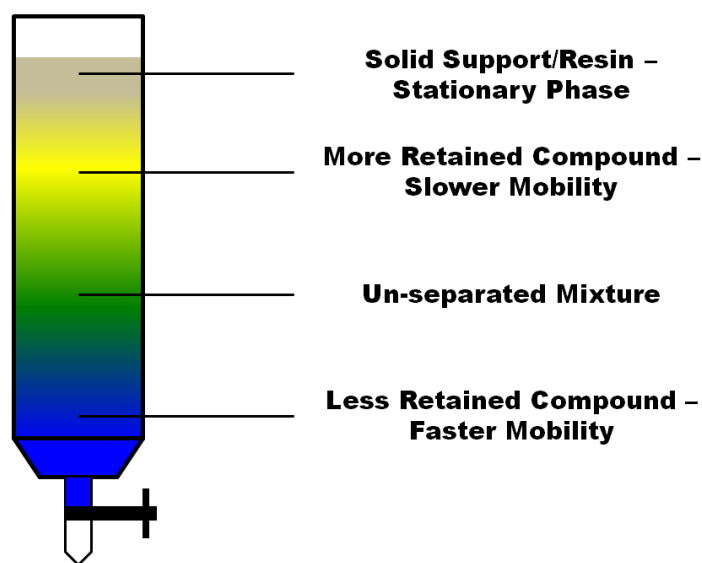
Figure 2.4 Schematic illustration of a rudimentary Liquid Chromatography separation setup, indicating different elution stages of compounds/analytes being separated over time.

In the case of Ion Exchange separation of zirconium and hafnium, standard ion exchange resins are utilised with a wide variety of possible acidifiers. These resins fall into four general categories of functionality:[31]

- *Cation-Exchange Resins:* (**a**) Strong acidity (sulfonic groups) & (**b**) Weakly acidity (carboxylic groups)
- *Anion-Exchange Resins:* (**c**) Strong basicity (quaternary amino groups) & (**d**) Weak basicity (primary, secondary or tertiary amino groups)

---

[30] D.A. Skoog, D.M. West, F.J. Holler & S.R. Crouch, *Fundamentals of Analytical Chemistry*, Brooks Cole, **2004**, 8th Ed, 916-918.
[31] F. de Dardel & T.V. Arden; *"Ion Exchangers"*, *Ullmann's Encyclopaedia of Industrial Chemistry* (**2005**), Wiley-VCH, Weinheim, 4-5.

Metal oxides are separated during the process of acidification as the dissolved components are passed along such an ion-exchange separation column. Earlier examples, such as Machlan & Hague[32] showed that sulphuric-hydrofluoric acid solutions could effectively separate these metals to a pure reactor grade composition. Benedict *et al.*[33] found that Nitric Acid-Citric Acid mixtures are also feasible as solvent phase and Qureshi and Husain[34] later found formic acid to be just as favourable an acidifier as all the rest.

The large amount of research findings currently available in this field suggests that ion-exchange separation has its place as highly favoured method.[35,36,37] The main reason for this is due to the fact that on industrial scale, it is a point of concern to minimize the amount of organic wastes from other methods such as solvent extraction processes.[38] In this case it is a better technique since the process in most cases involves a reusable stationary phase or cylindrical column resin bed through which the purification mixture is passed. This minimizes the fallout wastes, in that it takes less solvent to purify the metals through this approach.

2.2.5. Concluding Remarks – Separation Methods

When one considers the above mentioned overview of known separation techniques for metallic zirconium and hafnium, the industrially applied methods as well as others that are only feasible in a small scale/ laboratory setup, definite points of interest arise. In all cases, the differences of physical properties of these metals are exploited but only *via* small differences in chemical behaviour in certain physical states.

- *Liquid-Liquid Extraction* – takes advantage of solubility differences of chelated organometallic compounds of the metals.

- *Extractive Distillation* – takes advantage of a difference in volatility of metal compounds in the presence of a solvent that does not react directly with the metal itself, but which alters their solution behaviour (affecting boiling point for metal compounds).

---

[32] L.A. Machlan & J.L. Hague; *J. Res. Nat. Bur. Stand. 66A* (**1962**), 6, 517-520.
[33] J.T. Benedict, W.C. Schumb & C.D. Coryell; *J. Am. Chem. Soc.*, **1954**, 76 (8), 2036–2040.
[34] M. Qureshi & K. Husain; *Anal. Chem. 43* (**1971**), 3, 447–449.
[35] M. Taghizadeh, M. Ghanadi & E. Zolfonoun; *J. Nuclear Materials 412* (**2011**), 334–337.
[36] M. Taghizadeh, R. Ghasemzadeh, S.N. Ashrafizadeh & M. Ghannadi; *Hydrometallurgy 96* (**2009**), 77–80.
[37] M. Smolik, A. Jakobik-Kolon&M. Poranski, *Hydrometallurgy 95* (**2009**), 350-353.
[38] F.Shohreh, F.Z.Hamid, K. Masoud& S. Zeynab; *Iran. J. Chem. Eng. 26* (**2007**), 3, 61-71.

- ***Fractional Crystallization*** – takes advantage of a difference of tendency of one metal complex to change physical state, from solute to precipitate or crystalline solid, at a different rate or at different environmental conditions than the other.

- ***Ion Exchange Separation*** – takes advantage of a difference in the rate of elution of different metal complex ions on a chromatographic separation setup. This rate of elution is directly linked to the tendency for one metal ion to be retained or released along such an ion-exchange column, which is in turn dependant on the chemical effect of the mobile phase on the specific metal or metal complex.

Taking these principles into consideration, it becomes potentially plausible to predict the way forward for easier and better separation techniques for zirconium and hafnium. When embarking on new and revisiting some previous research approaches for this process, one would need to focus specifically on key points, as highlighted previously:

a. Developing methods that exploit chemical behaviour, reactions or states that in some way alter physical attributes or characteristics of these metals.

b. Investigating the aspects which govern chemical behaviour, etc. in an attempt to allow for the theoretical prediction of idealised conditions for separation.

c. Focus specifically on studying the trends, and especially solution behaviour for these metals as well as their respective coordination compounds, as far as the general field of structural focus allows.

This then forms an ideal basis for an applied coordination chemistry study of metal-ligand interactions and effects.

These points of interest themselves are extremely important and are the key focus areas in any study motivated by improving on metal-complex models in the fields they find high applicability, for example:

- Catalytic studies focus on (*i*) organic ligand effects, as well as (*ii*) comparisons of metal centres on the efficiency of the catalyst's performance for the process it is designed.

- Radiopharmaceutical, chemotherapeutic and metal based drug development studies in general focus greatly on improving on known compounds that are (*i*) more effective in therapy or diagnosis, and (*ii*) less harmful to the patient's health than their precursors, as well as (*iii*) developing new methods or substrates that can replace out-dated technologies

- Agrochemical studies focus on developing or improving substances used for a wide range of applications in the agricultural industries. Great emphasis is placed on designing novel substrates that are more environmentally friendly than their predecessors, depending on the field of application.

As a fundamental point, the proposal to study novel zirconium and hafnium coordination compounds as well as their solution behavioural characteristics, for the separation of these metals from their base ores, it is important to take into account the successes in this field with regard to known chelators, solvents and other contributors that have already been successfully applied on an industrial scale.

It is worth considering building on the published knowledge of long standing research initiatives, not only for the separation of these metals, but also when considering the specific area of focus for research in structural and behavioural characterisation endeavours. Some organic chelators are already well known for being effective for industrial scale separation, such as phosphates and phosphonates in the case of solvent extraction methods.

Nevertheless it is also worth considering the study of structural and behavioural characteristics of zirconium and hafnium in coordination with a range of similar organic chelators that are well characterised and researched in their own regard. It is a known fact that the steric and electronic effects of organic ligands can have a great impact on the behaviour of their respective metal complexes in different solution media. These aspects become of paramount importance when considering improving on known conditions for a method such as Solvent Extraction Separation, for example.

2.3. Zirconium and Organic Chelators

The key to effective and easy separation of zirconium and hafnium could in principle be found in the larger differences between chemical properties of complexes of these metals, containing similar ligands. In the search for a unique chemical state difference, it is

necessary to investigate metal compounds with ligands, which allow for characterization and evaluation of said metal complexes. The postulation of the reaction mechanism and step-wise analysis thereof can also assist in the development of a process to clarify the intrinsic chemical behaviour which the metal itself undergoes during substitution with organic chelates.

Zirconium metal complexes have received moderate amounts of interest from research group's worldwide.[39,40,41] The general focus of research concerning zirconium as coordinating metal revolves around structural defining studies with particular reference to coordination geometries. Other research reports focus heavily on the development of new complexes for industrial applications in catalysis, with particular interest in polymerisation catalytic processes.[42,43,44,45,46]

Very little is however known about the mechanism of ligand coordination and the interchange for zirconium and hafnium complexes, since most synthetic projects focus on merely characterizing certain aspects of a specific complex and evaluating the *thermodynamic* aspects of systems. A number of research projects on the coordination geometries and prediction of coordination from characterization by methods not using three-dimensional structural analysis (X-ray diffraction) have been done.[47,48,49] However the aspects involved for control of the extent of coordination is generally unresolved.

2.3.1. *β*-Diketones

The *β*-diketone family (Figure 2.5) of bidentate ligands are a widely used type of conjugated ligand system in coordination chemistry. In particular, the acetylacetone branch of this family is distinct. It is a well know ligand system employed for its ease of coordination to all known non-radioactive elements. Zirconium and hafnium are unique in this case as they are the only elements which have been reported to form

[39] R.C. Fay; *Coord. Chem. Rev. 71* (**1986**); 113-138.

[40] E.M. Page & S.A. Wass; *Coord. Chem. Rev. 152* (**1996**), 411-466.

[41] R.L. Davidovicha, D.V. Marinina, V. Stavilab & K.H. Whitmire; *Coord. Chem. Rev. 257* (**2013**), 3074-3088.

[42] R. Vollmerhaus, M. Rahim, R. Tomaszewski, S. Xin, N.J. Taylor & S. Collins; *Organometallics 19* (**2000**), 2161-2169.

[43] J. Kim, J.W. Hwang, Y. Kim, M.H. Lee, Y. Han & Y. Do; *J. Organomet. Chem. 620* (**2001**), 1-7.

[44] M.J. Scott & S.J. Lippard; *Inorg. Chim. Acta 263* (**1997**), 287-299.

[45] M. Rahim, N.J. Taylor, S. Xin & S. Collins; *Organometallics 17* (**1998**), 1315-1323.

[46] H. V. Rasika Dias, W. Jin & Z. Wang; *Inorg.Chem. 35* (**1996**), 6074-6079

[47] J.V. Silverton & J.L. Hoard; *Inorg. Chem. 2* (**1963**), 243-249.

[48] H.K. Chun, W.L. Steffen & R.C. Fay; *Inorg.Chem. 18* (**1979**), 2458-2465.

[49] F. Calderazzo, U. Englert, C. Maichle-Mössmer, F. Marchetti, G. Pampaloni, D. Petroni, C. Pinzino, J. Strähle & G. Tripepi; *Inorg. Chim. Acta 270* (**1998**), 177-188.

β-diketonates in which the metal may exhibit coordination numbers of six, seven and eight.[50] Another interesting aspect of the *tetrakis*(acetylacetonato) zirconium(IV)-type complexes are classic examples of square-antiprismatic coordination geometries.[51]

Research with regard to zirconium complexes of acetylacetone and functionalised derivatives thereof has found a fair amount of interest in literature.[47,48,49,50,51] Several zirconium(IV) complexes were investigated and discussed in the previous M.Sc. dissertation parenting this project.[52] Functionalization of the methyl groups on the β-diketone backbone are most commonly found with a replacement of methyl (acetylacetone or 2,4-pentanedione) with favoured organic groups such as phenyl (1,3-diphenyl-1,3-propanedione), tertiary-butyl (2,2,7,7-tetramethyl-3,5-heptanedione) and trifluoromethyl (hexafluoroacetylacetone/1,1,1,5,5,5-hexafluoro-2,4-pentanedione) moieties. Unsymmetrical moieties are also produced such as the substitution of a single methyl group with trifluoro methyl (trifluoroacetylacetone/ 1,1,1-Trifluoro-2,4-pentanedione). Most notably these complexes are published in abundance as the *tris*- or *tetrakis*-chelated moiety, but very few examples of lesser coordinated complexes are available.
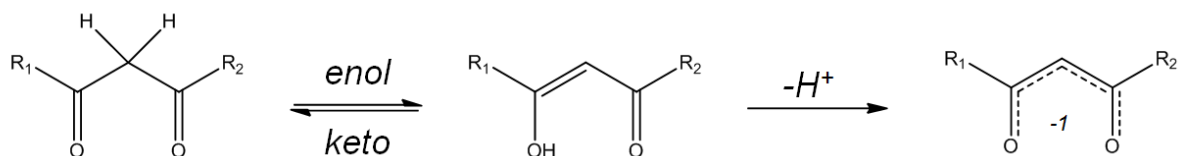
Figure 2.5 Graphic representation of basic Acac type ligand structure. For acac, $R_1=R_2=CH_3$; phacac, $R_1=R_2=$ph; ^{t}Buacac, $R_1=R_2=^t$Bu; hfacac, $R_1=R_2=CF_3$; tfacac, $R_1=CF_3$ & $R_2=CH_3$.

2.3.2. Amines

As discussed earlier with regard to Liquid-Liquid Separation methods of zirconium and hafnium, there are several known approaches in which high molecular weight amines are employed to separate these metals in acidic solutions.[53,54,55] Bearing this in mind, it

---

[50] T. J. Pinnavaia & R. C. Fay; *Inorg. Chem. 7* (**1968**), 502-508.

[51] W. Clegg; *Acta Cryst. C43* (**1987**), 789-791.

[52] M. Steyn; *Speciation And Interconversion Mechanism Of Mixed Halo And O,O- And O,N Bidentate Ligand Complexes Of Zirconium*, M.Sc. Dissertation, *Chapter 2* (**2009**), University of the Free State, South Africa.

[53] A.L. Lowe & G.W. Parry, *"Zirconium in the Nuclear Industry: Proceedings of the Third International Conference", 633* (**1976**), 46-56.

[54] F.L. Moore; *Anal. Chem. 29* (**1957**), 11, 1660–1662.

[55] N. M. Sundaramurthi & V. M. Shinde; *Analyst 114* (**1989**), 201-205.

is highly favourable to consider certain amines for chelators when aiming to study and compare zirconium and hafnium complexes for separation method development.

If one were to design novel amine ligands for a comparative study, one would have to consider not only a range of ligands with different electronic properties, but also a wide range of steric characteristics. Amines in the general sense can be commercially obtained or prepared in a wide range of variances to fit these points of interest.
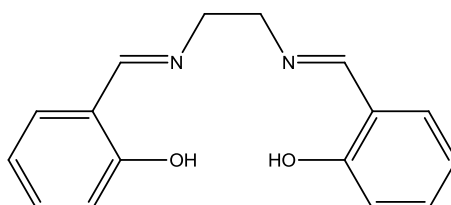
Figure 2.6 Salen - [N,N'-Ethylenebis(salicylimine)]

A specific group of amines that falls squarely in this category are those of the Salen [N,N'-Ethylenebis(salicylimine)] family of chelators (See Figure 2.6).These ligands are highly adjustable when modifying the diamine portion at the centre of the tetradentate chelator.[56,57,58] These types of chelators can be prepared by merely altering the initial diamine that is condensed with salicylaldehyde and some of these derivatives are commercially available (See Figure 2.7).
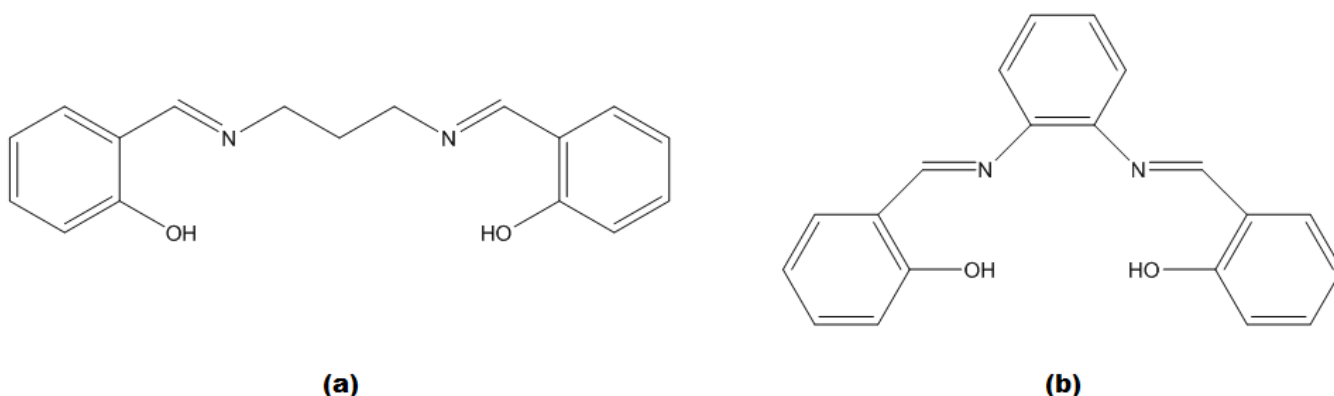
Figure 2.7 Illustration of commercially available Salen-type tetradentate ligands;
(**a**) N,N'-Bis-(salicylidene)-1,3-propanediamine, (**b**) N,N′-Bis(salicylidene)-1,2-phenylenediamine.

This, in itself, allows for greatly affecting the electronic and steric contributors to organometallic complexes of zirconium and hafnium. This aspect could yield valuable information as to the chelation preferences of these metals as well as the differences

[56] E.N. Jacobsen, W. Zhang, M.L. Guler; *J. Am. Chem. Soc. 113* (**1991**), 17, 6703–6704.
[57] E.J. Campbell & S.T. Nguyen; *Tetrahedron Lett. 42* (**2001**), 1221-1225.
[58] H. Zhu, M. Wang, C. Ma, B. Li, C. Chen & L. Sun; *J. Organomet. Chem. 690* (**2005**), 3929-3936.

between solution behaviour and solid state product characteristics. Furthermore, these types of complexes of zirconium has, in fact, been studied in the past for catalytic applications.[59,60,61] However, as with the *β*-diketone-complexes, these compounds are rarely compared critically with hafnium counterparts.

2.3.3. Pyridines and Pyridine-based Ligands

Pyridine compounds are defined by the presence of a six-membered heterocyclic ring consisting of five carbon atoms and one nitrogen atom. The arrangement of atoms is similar to benzene except that one of the carbon–hydrogen ring sets has been replaced by a nitrogen atom. Furthermore, it has been the most studied of all the known heterocycles.[62] In organic reactions, pyridine behaves both as a tertiary amine (undergoing protonation, alkylation, acylation, and N-oxidation at the nitrogen atom) and as an aromatic compound (undergoing nucleophilic substitutions). Bearing this in mind, it becomes worth considering the derivative pyridine ligand types for similar structural characterisation studies of metal complex behaviour.

As a chelating ligand, it is most often used in a derivative form with a wide range of substituents around the heterocycles. The most commonly known moieties are undoubtedly 2,2'-bipyridine, terpyridine (2,2';6',2"-terpyridine) and 1,10-phenanthroline (See Figure 2.8) but other varieties of carboxylate- and alkyl-pyridines are also widely used in industry.
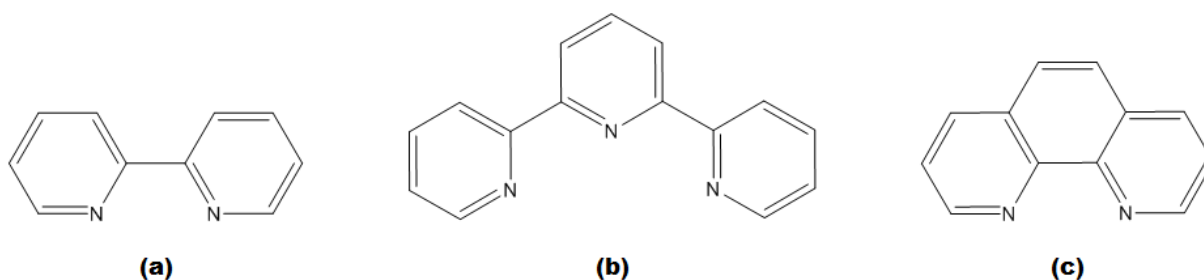
Figure 2.8 Graphical representation of common pyridines; **(a)** 2,2'-Bipyridine, **(b)** Terpyridine (2,2';6',2"-terpyridine) and **(c)** 1,10-Phenanthroline

[59] T. Repo, M. Klinga, P. Pietikainen, M. Leskela , A. Uusitalo, T. Pakkanen, K. Hakala, P. Aaltonen & B. Lofgren; *Macromolecules 30* (**1997**), 171-175.
[60] B. Schweder, D. Walther, T. Dohler, O. Klobes & H. Gorls; *J. Prakt. Chem. 341* (**1999**) 736-747.
[61] J. Huang, B. Lian, L. Yong & Y. Qian; *Inorg. Chem. Commun. 4* (**2001**) 392-394.
[62] E. F. V. Scriven & R. Murugan, *"Pyridine and Pyridine Derivatives"*, *20* (**2000**), Kirk-Othmer Encyclopedia of Chemical Technology, John Wiley & Sons, Inc., 28.

Just as with the standard amine ligands discussed before, derivative pyridine ligands can also be designed to fit the criteria of electronic and steric property influencers desired for such a comparative evaluation of metal complex characteristics. Interesting examples of commercially available pyridines of this sort (See Figure 2.9) include the dipyridyl sub-set of ligands. These ligands are known to more commonly yield catena-type (chained) crystalline structures.[63,64,65]
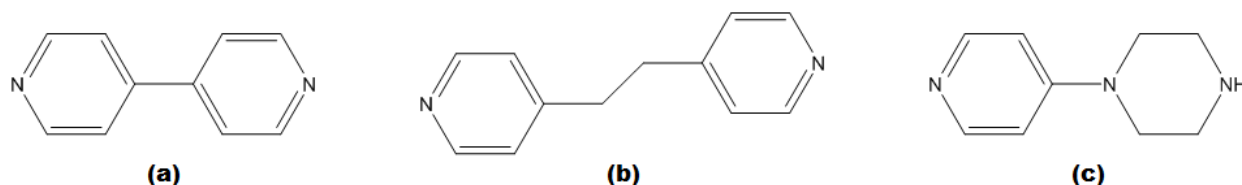
Figure 2.9 Graphical representation of common dipyridyls; (**a**) 4,4'-Dipyridyl, (**b**) 1,2-Bis(4-pyridyl)ethane, (**c**) 1-(4-Pyridyl)piperazine.

This characteristic of ligand coordination behaviour opens up another aspect of chelation manipulation possibilities, especially when considering that zirconium and hafnium are known to favour mainly the square-antiprismatic coordination geometry about the metal centre. By taking advantage of ligand structure rigidity, one could in theory force different chelation geometries on these metal centres.

Another subset of pyridine ligands also showing great potential for this type of separation study are the pyridine-carboxylic acids (Figure 2.10). These ligands are widely used as organic chelators as well, for a wide range of applications.[66,67,68,69]
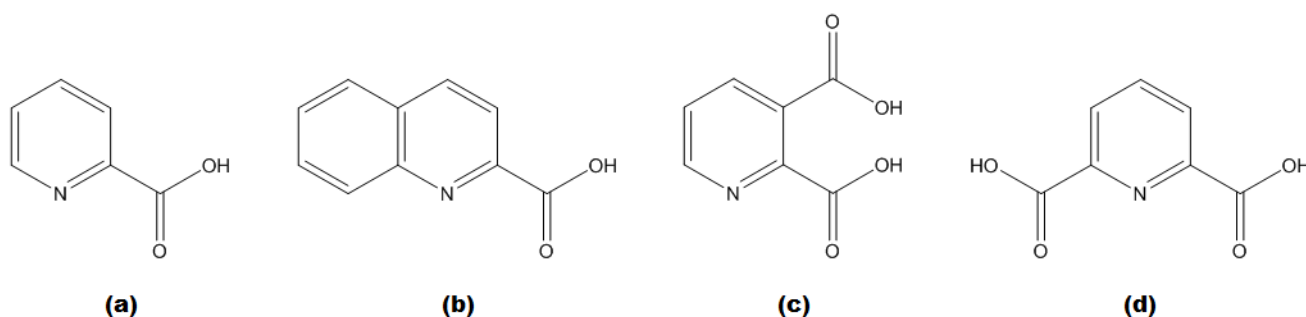
Figure 2.10 Graphical representation of common pyridine-carboxylic acids; (**a**) *Picolinic Acid* (Pyridine-2-carboxylic acid), (**b**) *Quinaldic acid* (2-Quinolinecarboxylic acid), (**c**) *Quinolinic acid* (2,3-Pyridinedicarboxylic acid), (**c**) *Dipicolinic acid* (2,6-Pyridinedicarboxylic acid).

[63] S.W.Lee, H.J. Kim, Y.K. Lee, K. Park, J.H. Son & Y.U. Kwon; *Inorg. Chim. Acta 353* (**2003**) 151-158.
[64] J. Wu & S. Huang; *Cryst. Eng. Comm. 13* (**2011**), 2062-2070.
[65] P. Phuengphai, S. Youngme, I. Mutikainen, P. Gamez & J. Reedijk; *Polyhedron 42* (**2012**), 10-17.
[66] M.A.S. Goher, A.A. Youssef, Z.Y. Zhou, T.C.W. Mak; *Polyhedron 12* (**1993**), 1871-1878.
[67] K. Hashimoto, S. Nagatomo, S. Fujinami, H. Furutachi, S. Ogo, M. Suzuki, A. Uehara, Y. Maeda, Y. Watanabe, T. Kitagawa; *Angew. Chem., Int. Ed. 41* (**2002**), 1202-1205.
[68] T. Hirano, M. Kuroda, N. Takeda, M. Hayashi, M. Mukaida, T. Oi & H. Nagao; *J. Chem. Soc. Dalton Trans.* (**2002**), 2158-2162.
[69] H.J. van der Westhuizen, R. Meijboom, M. Schutte & A. Roodt; *Inorg. Chem. 49* (**2010**), 9599-9608.

These ligands have the added structural benefit of allowing for comparisons of coordinative preferences of metals to N's or O's. Furthermore, the relative placement of carboxylic groups dictates the denticity of the chelator. In the case of Picolinic acid or Quinaldic acid, simple bidentate binding is obvious, only influenced by the sterics of the aromatic ring/rings of the main structure. However, in the case of the di-carboxylic examples Quinolinic acid and Dipicolinic acid, variations of bi- or tri-denticity could in theory be achieved. For the former, bidentate chelation across either the N,O[66,70] or O,O[71,72] sites could occur, allowing for detection of preference for either these possibilities. For the latter, bi-[73] or tridentate[74] coordination can in theory take place.

2.3.4. Quinolines

Quinolines are heterocyclic organic compounds that like naphthalene and pyridine are aromatic, but less intensely so than benzene. In the particular interest of this study, 8-hydroxyquinolines/quinolinols/oxines (oxH) are specifically focused upon. Oxine can be considered a combination of catechol and 2,2'-bipyridine chelators (See Figure 2.11).

(a)   **(b)**   **(c)**
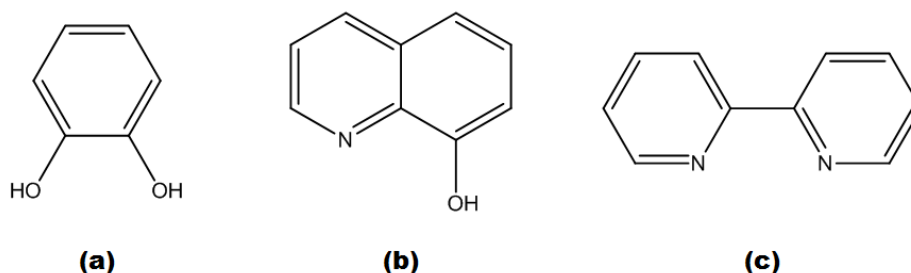
Figure 2.11 Comparison of coordinative aspects of (**a**) catechol, (**b**) 8-hydroxyquinoline and (**c**) 2,2'-bipyridine.

8-Hydroxyquinoline in its deprotonated form contains a phenolic portion as found in a catechol, but also the pyridine coordinative element of the bipyridine, yielding a monoanionic coordinative intermediate of the dianionic catechol and the neutral

[70] B. Barszcz, M. Hodorowicz, A. Jablonska-Wawrzycka, J. Masternak, W. Nitek & K. Stadnicka; *Polyhedron 29* (**2010**), 1191-1200.
[71] L.J. Li & Y. Li; *J. Mol. Struct. 694* (**2004**), 199-203.
[72] S. Shit, J. Chakraborty, J.A.K. Howard, E.C. Spencer, C. Desplanches & S. Mitra; *Struct. Chem. 19* (**2008**), 553-558.
[73] A. Moghimi, H.R. Khavassi, F. Dashtestani, D. Kordestani, A.E. Jafari, B. Maddah & S.M. Moosavi; *J. Mol. Struct. 996* (**2011**), 38-41.
[74] H. Aghabozorg, M. Ghadermazi, F. Zabihi, B. Nakhjavan, J. Soleimannejad, E. Sadr-khanlou & A. Moghimi; *J. Chem. Cryst. 38* (**2008**), 645-654.

bipyridine. Furthermore, the presence of both a carbocyclic and a heterocyclic ring enables a wide variety of chemical reactions.[75]

Quaternary alkylation on the nitrogen takes place readily, but unlike pyridine, quinolines show addition by subsequent reaction with nucleophiles. Nucleophilic substitution is promoted by the heterocyclic nitrogen portion. Electrophilic substitution takes place much more easily than in pyridine, and the substituents are generally located in the carbocyclic ring.The oxine ligand family forms a significant portion of the interest in this case, partially due to the fact that they are known as potential extracting agents of metal ions in dilute solutions.[76] This chelator has in the past actually been studied as a possible extractant of zirconium and niobium from uranium sources.[77]

Oxines can be commercially purchased in many structural substituent derivative forms. Substituents in this ligand family range from halides, carboxylic acids, nitryl and alkyl groups (See Figure 2.12).
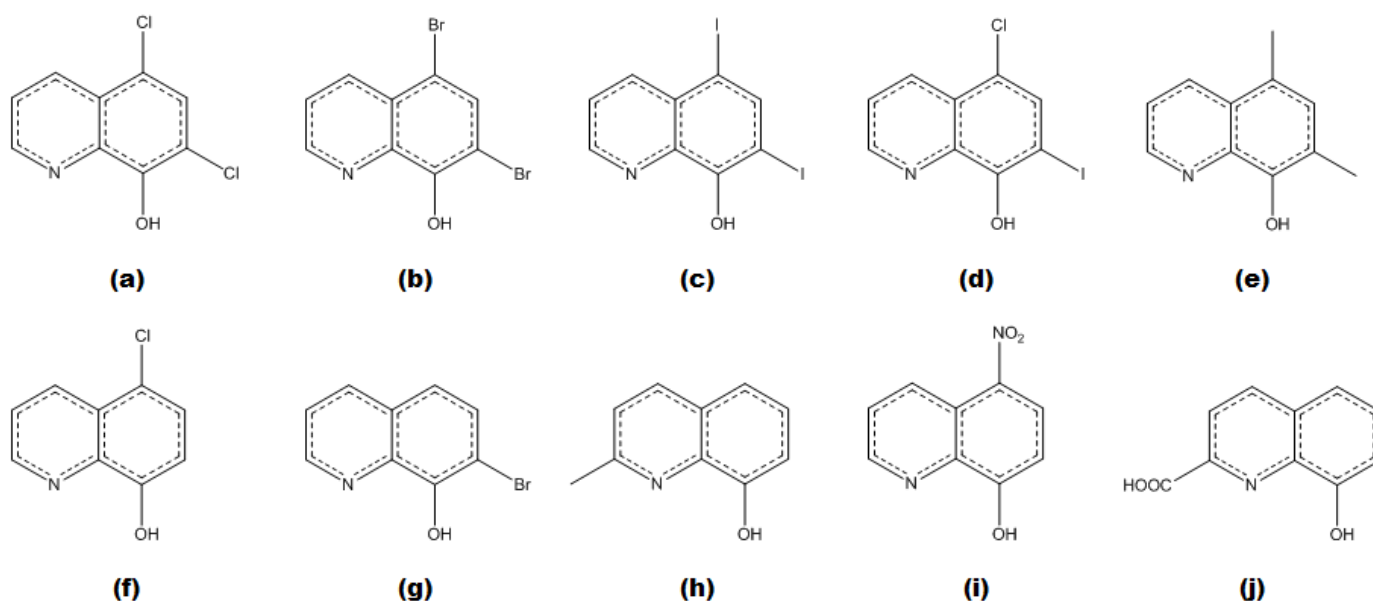
Figure 2.12 Graphical representation of the quinoline/oxine ligand family with different substituents present. (**a**) *5,7-Dichloro-8-hydroxyquinoline* (diClOxH), (**b**) *5,7-Dibromo-8-hydroxyquinoline* (diBrOxH), (**c**) *5,7-Diiodo-8-hydroxyquinoline* (diIOxH), (**d**) *5-Chloro-7-iodo-8-hydroxyquinoline* (CliOxH), (**e**) *5,7-Dimethyl-8-hydroxyquinoline* (diMeOxH), (**f**) *5-Chloro-8-hydroxyquinoline* (5-ClOxH), (**g**) *7-Bromo-8-hydroxyquinoline* (7-BrOxH), (**h**) *2-Methyl-8-hydroxyquinoline* (2-MeOxH), (**i**) *5-Nitro-8-hydroxyquinoline* (5-NO$_2$OxH), (**j**) *Hydroxy-2-quinolinecarboxylic acid* (2-COOHOxH).

[75] K.T. Finley, *"Quinolines and Isoquinolines"*, *9* (**2000**), Kirk-OthmerEncyclopedia of Chemical Technology, John Wiley & Sons, Inc., 2.

[76] D.L. Huges & M.R. Truter; *J. Chem. Soc. Dalton Trans.* (**1979**), 520.

[77] K. Motojima, H. Hashitani, S. Bando & H. Yoshida; *J. Nucl. Sci. Technol. 3* (**1966**), 8, 326-332.

2.4. Kinetic/Mechanistic Studies – Zirconium & Hafnium

There is limited data available in literature concerning the kinetic and associated mechanistic studies on zirconium and hafnium complexes, regarding *specifically* the formation processes of coordination compounds.[78,79] Solution behaviour studies involving such compounds generally tend towards catalytic investigations focusing on catalyst activity[80,81,82] or catalytic conversion mechanism processes.[83,84,85]

During the related M.Sc. project previously concluded,[86] a preliminary investigation into the solution behaviour of the formation of the *tetrakis*(8-hydroxyquinoline)zirconium(IV) complex was performed. During the course of this endeavour, a step-wise mechanism for the coordination of the four oxine ligands to the Zr(IV) metal centre was postulated from experimental results. The overall mechanism proposed from this, as illustrated in Scheme 2.1, describes an intricate and very complex process of bidentate ligand coordination with a fast initial reaction, followed by three multi-phase reaction steps wherein it is assumed that the chloride ligand is liberated as HCl (H$^+$ from oxH) in the ring-closing step in each of the four processes.

Furthermore, an assessment of equilibrium manipulation was also included, effectively evaluating the effect of a suppressant on the reaction rate of the formation of the Zr(IV) complex as well as intermediate species involved. It was concluded from these experiments that the coordination of the 3rd and 4th oxine ligand could be substantially restrained/slowed, however not reversed or completely inhibited. The information gathered in this preliminary study, in principle, could yield vital insights into the possibilities of solution extraction purification of zirconium by means of coordination chemistry manipulation.

[78] A.C. Adams & E.M. Larsen; *Inorg. Chem. 5* (**1966**), 814-819.

[79] J. Woo-Sik, T. Nakagawa & H. Tomiyasu; *Inorg. Chim. Acta 209* (**1993**), 79-83.

[80] G.D. Yadav & T.S. ThoratInd; *Ind. Eng. Chem. Res. 35* (**1996**), 721-731.

[81] K.J. Blackmore, N. Lal, J.W. Ziller & A.F. Heyduk; *J. Am. Chem. Soc. 130* (**2008**), 2728-2729.

[82] F. Coleman & A. Erxleben; *Polyhedron 48* (**2012**), 104–109.

[83] S. Yamada, I. Yamauchi & A. Murata; *Anal. Sci. 11* (**1995**), 903-908.

[84] J. Rose, G. Chauveteau, R. Tabary, S. Moustier & J.-L. Hazemann; *Colloid Surface A 217* (**2003**), 159-164.

[85] P.D. Knight, G. Clarkson, M.L. Hammond, B.S. Kimberley, P. Scott; *J. Organomet. Chem. 690* (**2005**), 5125–5144.

[86] M. Steyn; *Speciation And Interconversion Mechanism Of Mixed Halo And O,O- And O,N Bidentate Ligand Complexes Of Zirconium*, M.Sc. Dissertation, *Chapter 7* (**2009**), University of the Free State, South Africa.

Step 1: $ZrCl_4$ + oxH $\underset{k_{-1}}{\overset{K_1,\,k_1}{\rightleftharpoons}}$ $[ZrCl_3(ox)]$ + HCl $\quad\big\}$ **Fast Stopped Flow Kinetic Study**

Step 2: $[ZrCl_3(ox)]$ + oxH $\underset{k_{-2a}}{\overset{K_{2a},\,k_{2a}}{\rightleftharpoons}}$ $[ZrCl_3(ox)(ox^*)]$

$[ZrCl_3(ox)(ox^*)]$ $\xrightarrow{k_{2b}}$ $[ZrCl_2(ox)_2]$ + HCl

Fast Stopped Flow – Slow UV/Vis Correlation

Step 3: $[ZrCl_2(ox)_2]$ + oxH $\underset{k_{-3a}}{\overset{K_{3a},\,k_{3a}}{\rightleftharpoons}}$ $[ZrCl_2(ox)_2(ox^*)]$

$[ZrCl_2(ox)_2(ox^*)]$ $\xrightarrow{k_{3b}}$ $[ZrCl(ox)_3]$ + HCl

Step 4: $[ZrCl(ox)_3]$ + oxH $\underset{k_{-4a}}{\overset{K_{4a},\,k_{4a}}{\rightleftharpoons}}$ $[ZrCl(ox)_3(ox^*)]$

$[ZrCl(ox)_3(ox^*)]$ $\xrightarrow{k_{4b}}$ $[Zr(ox)_4]$ + HCl

Slow UV/Vis Kinetic Study
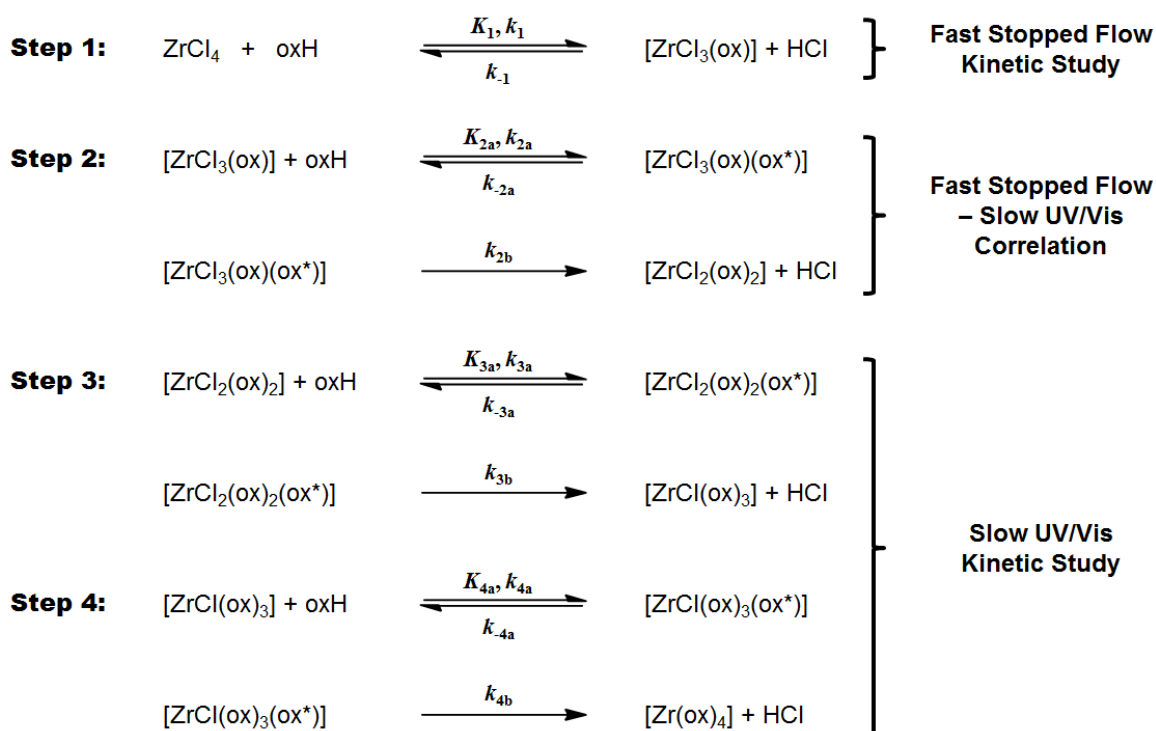
Scheme 2.1 Proposed overall scheme for the observed coordination of four oxine ligands to tetrachloridozirconium(IV) [intermediate products denoted by presence of (ox*)].

It is thus imperative that this evaluation is expanded on in a systematic study, utilizing more modern and advanced equipment and backed by computing strategies, to broaden the knowledgebase on time-resolved behaviour of zirconium and hafnium.

2.5. Some Aspects of the Geometry of Eight-Coordindate Complexes Related to Isomer Descriptions

It has been stated here (§ 2.4.1) and in the previous M.Sc. dissertation parenting this project,[52] that zirconium and hafnium compounds tend to prefer a certain "maximum extent" of coordination when reacted with bidentate ligands. In fact, it is a point of interest as to *why* most known, published structures of these metals containing bidentate ligands necessarily hold four ligands (*tetrakis*-coordinated complexes). It has previously been postulated that the solid state products of this sort appear to prefer this maximum state of coordination, most likely as lowest crystallization state. This is in accordance of what is expected in these symbiotic systems.[87]

---

[87]J. E. Huheey, E. A. Keiter & R. L. Keiter; *Inorganic Chemistry - Principles of Structure and Reactivity, 4ᵗʰ Ed.* (**1993**) HarperCollins College Publishers, New York.

Furthermore, it has also been widely accepted that, not only do these metals most often exhibit an eight coordinated solid state structure, but are also classic examples of what is known as a square antiprismatic coordination polyhedra or geometry.[47,88] A classic square antiprism (or *anti-cube*) is defined as an eight cornered structure, with sets of four corners on two parallel sides, where one set of corners is displaced away from the right-angled cube shape, so as to give triangle side planes connecting all corners (Figure 2.13).
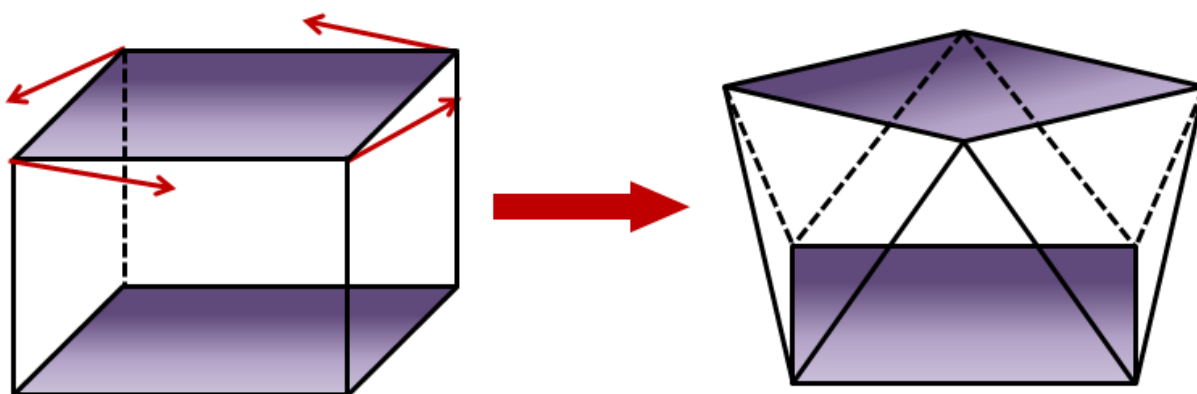
Figure 2.13 Illustration of the transformation of a (**left**) standard cube to yield a (**right**) square antiprism by displacement of only the bottom four corners.

The way that this description relates to an organometallic compound's coordination geometry can best be illustrated as in Figure 2.14, where the square antiprism is drawn in, using the eight coordination atoms as the corners of the polyhedra.
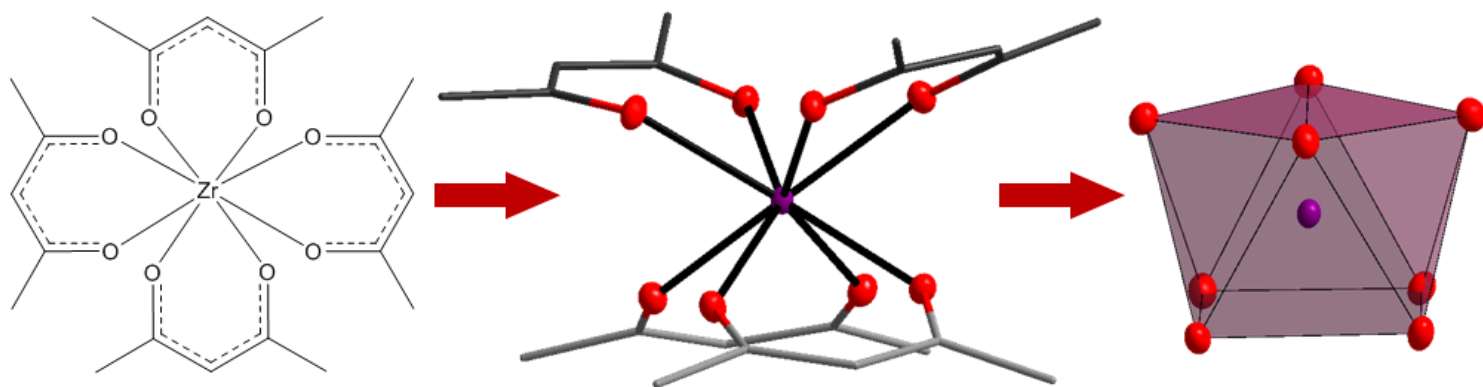
Figure 2.14 Illustration of coordination geometry identification for *Tetrakis*(acetylacetonato) zirconium(IV); (**left**) Schematic drawing of the four acac-ligands chelated to zirconium, (**middle**) obtained solid state 3D structure by means of crystallography,[47] (**right**) simplified polyhedra showing only the metal center and the eight coordinating oxygen atoms as square antiprism corners.

---

[88] J.L. Hoard & J.V. Silverton; *Inorg.Chem. 2* (**1963**), 235-242.

From the previous image, one can also deduce that there is not simply one isomer obtainable for this square antiprismatic coordination geometry. As a point of particular interest for this project, the coordinative possibilities for metal complexes containing four identical bidentate ligands will be described and elaborated on here.
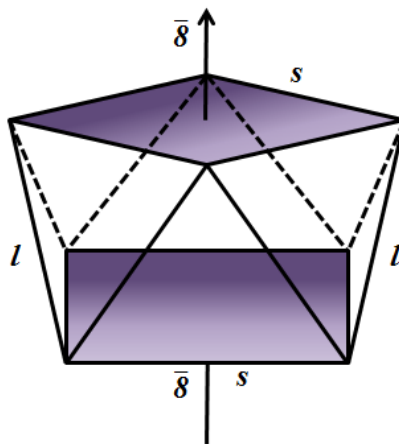
Figure 2.15 Illustration and notation for the D_{4d}- $\bar{8}$2m antiprism

From literature,[88,89] three possible isomers are possible, specifically for metal complexes containing four identical bidentate ligands with *O,O'*-coordination atoms. Hoard *et al.*[76] defined this geometry as the D_{4d}-$\bar{8}$2m antiprism (Figure 2.15), with all vertices (ligand coordination sites) equivalent. Furthermore, the 16 structural edges divide equally between two symmetry types, *s* and *l* and the polyhedron centre (central metal atom) is the intersection point of the unique $\bar{8}$ axis and 4 two-fold axes. Each of these two-fold axes passes through the mid-points of two opposed *l* edges. Subsequently, the three possible isomers for metal complexes, containing four *O,O'*-donating bidentate ligands, with a square antiprismatic coordination polyhedron, are as follows:

I. *D$_2$ – Corner-Bonded Ligands*

The 1st possible isomer, defined as D_2-222 or *ssss* isomer is a commonly found example. Published structures of this species include *Tetrakis*(acetylacetonato) zirconium(iv),[47,51] *Tetrakis*(trifluoro acetylacetonato)zirconium(iv)[90,91] and *Tetrakis*(1,3-diphenyl-1,3-propanedionato)zirconium(iv).[92]

[89] M.A. Porai-Koshits & L.A. Aslanov; *J. Struct. Chem. (Engl. Transl.) 13* (**1972**), 244-253.
[90] K.V.Zherikova, N.B.Morozova, N.V.Kurat'eva, I.A.Baidina, P.A.Stabnikov & I.K.Igumenov; *J.Struct.Chem. 48* (**2007**), 513-522.
[91] M.Steyn, A.Roodt & G.Steyl; *Acta Cryst. E64* (**2008**), m827
[92] H.K. Chun, W.L. Steffen & R.C. Fay; *Inorg.Chem. 18* (**1979**), 2458-2465.
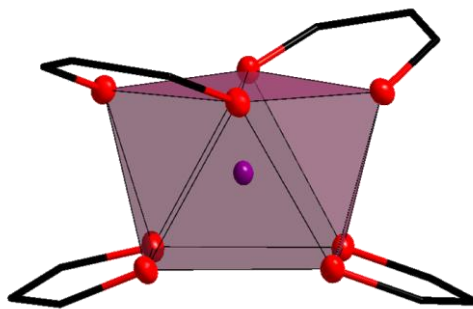
Figure 2.16 Illustration of the typical D_2 corner-bonded square antiprismatic isomer.

Interestingly, this is also the isomer that is easiest to visualize from the three-dimensional structure, due to the fact that the ligands appear to be "pinched" inward at the top and bottom of the antiprism.
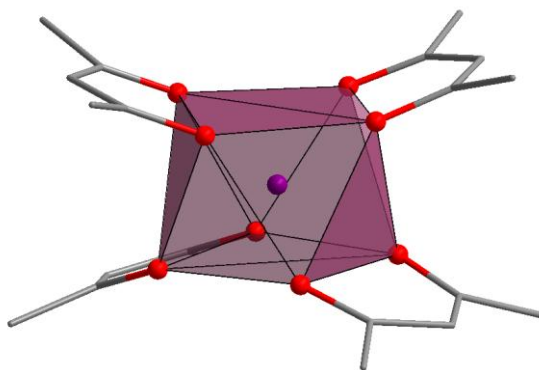
Figure 2.17 Graphical illustration of the structure of *Tetrakis*(acetylacetonato)zirconium(IV), showing the square antiprismatic coordination polyhedra around the metal center.

II.   *D₄ – Side-Bonded Ligands*
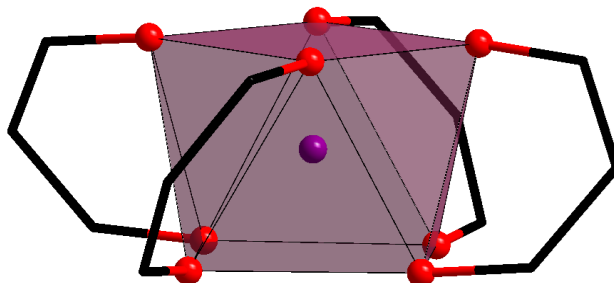
Figure 2.18 Illustration of the typical D_4 side-bonded square antiprismatic isomer.

The 2nd isomer, defined as D$_4$-422 or *llll* isomer is also theoretically possible for zirconium complexes. Unfortunately no examples currently exist in literature. This could most likely be due to excessive straining of ligand structure to accommodate the larger bite-angles required to achieve this geometry.

One such example exists of a *Tetrakis*(2,2,6,6-tetramethyl-3,5-heptanedionato) niobium(IV)[93] complex and the average bite angle reported for the ligands across the Nb(IV)-metal centre was *ca.* 80 °, much larger than the known average bite angle of 75 ° for these type of zirconium compounds.
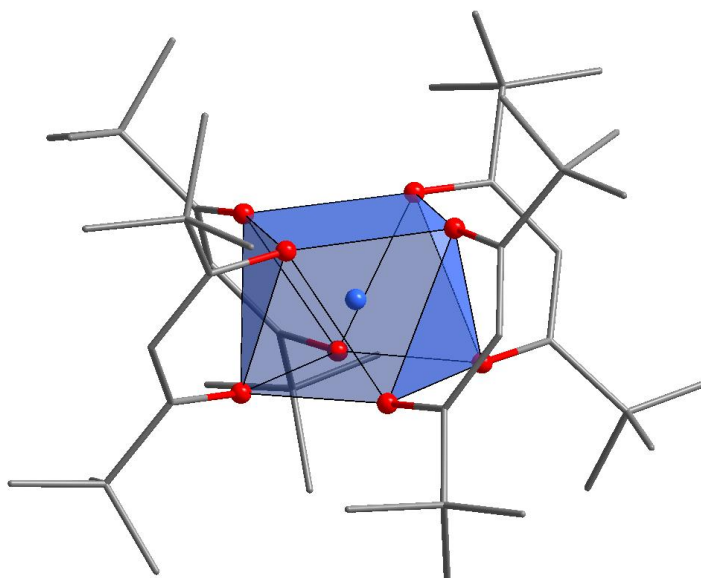
Figure 2.19 Graphical illustration of the structure of *Tetrakis*(2,2,6,6-tetramethyl-3,5-heptanedionato)niobium(IV), showing the square antiprismatic coordination polyhedra around the metal center.

III.   C$_2$ – Combined D$_2$/D$_4$, Corner- and Side-Bonded Ligands
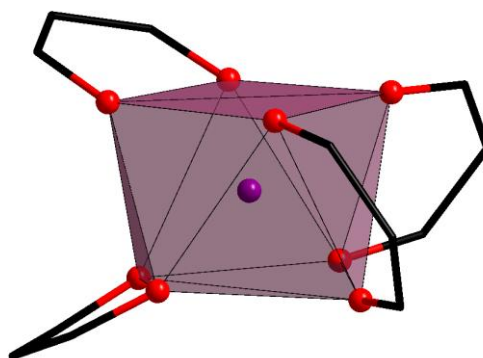
Figure 2.20 Illustration of the typical C$_2$ mixed bonding square antiprismatic isomer.

[93] T.J. Pinnavaia, B.L. Barnett, G. Podolsky & A. Tulinsky; *J.Am.Chem.Soc. 97* (**1975**), 2712-2717.

The final isomer, defined as C_2-2 or *llss* isomer is also commonly found for zirconium complexes. Published structures of this species include *Tetrakis*(hexafluoro acetylacetonato)zirconium(IV)[45] and *Tetrakis*(t-Butyl-3-oxobutanoato)zirconium(iv).[94] For these examples the ligand bite angles still average *ca.* 75 °, as expected for zirconium-acac complexes.
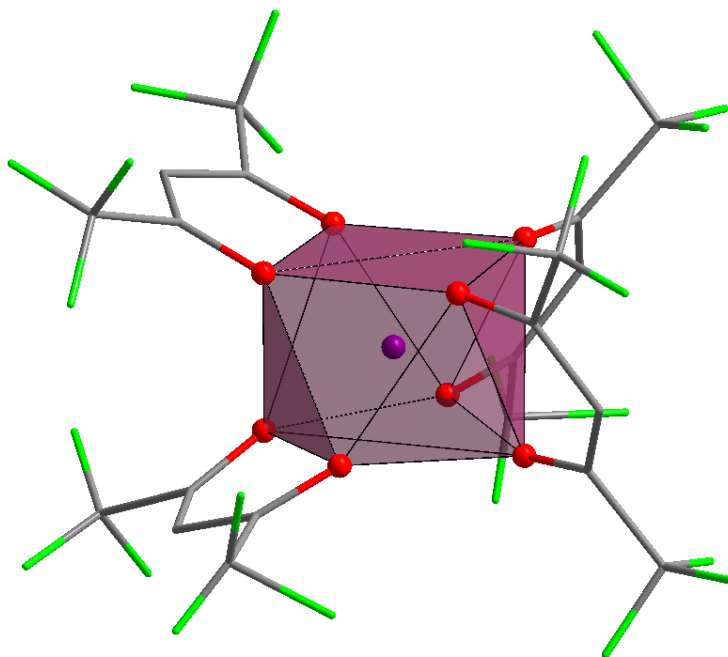
Figure 2. 21 Graphical illustration of the structure of *Tetrakis*(hexafluoro acetylacetonato) zirconium(IV), showing the square antiprismatic coordination polyhedra around the metal center.

The point of interest related to such coordination geometry isomers, lies in the fact that it still needs to be determined if the same theory holds for other types of ligands, specifically the N,O-donating oxine family described earlier. Since very few examples of tetrakis(oxine)zirconium(IV) complexes are known, speculating on trends is not possible.

During the course of this project, particularly the crystallographic solid state structural characterisation, emphasis is placed on the discoveries made in this regard. The reason for this depends heavily on the matter of identifying ligand characteristics, that influence organometallic chelation more than that of the metals studied. The overarching aim here is to identify certain ligands or families that can manipulate solid state structural properties to induce different physical or chemical behaviours for zirconium and hafnium. If this can be achieved then separation of these metals would be possible by means of organometallic chelation.

---

[94] U.K. Urs, M.S. Dharmaprakash, S.A. Shivashankar & T.N.G. Row; *Acta Cryst. E59* (**2003**), m83-m84.

2.6. Conclusion

In order for the advancement in research on the separation techniques for zirconium and hafnium, it is very important to emphasize investigative aims based on known methods already viable for industrial processes. The focus of any study which is targeted at applying ligand chelation aspects for separation procedures would necessarily have to start at developing novel compounds of the metals that are to be studied. It is however imperative for the development of such compounds, that sufficient knowledge exists regarding the basic principles of all contributing factors in coordination reactions.

In all chemical processes involving metal complexes, the coordinated ligands govern the reactions to a large extent. It is therefore very important that all properties (electronic, steric, reactivity, etc.) of various ligands are clearly understood in order to enable intelligent adjustment to be made, inducing the effects of choice. Moreover, the time-resolved aspects (kinetics) and general intimate and stoichiometric mechanistic principles should constantly be incorporated into argument. When taking these rules into consideration, it becomes apparent that a study facing the immense challenge of investigating the effects of ligand coordination on solution behaviours of zirconium and hafnium complexes, especially for the separation of these metals by known methods, it becomes of paramount importance to focus on a very select field of chelators.

Furthermore, it is also vital that such a research project focus on discerning exactly which nuances in adaptation of ligand design affect which reaction process during coordination/ product formation. In order to successfully execute this research endeavour, it necessitates the full characterisation of all novel zirconium compounds proposed. This implicates the structural characterisation of complexes by means of crystallographic methods, as well as solution behavioural quantification of product formation and formation influencing (inhibitors, quenchers, extractants) by means of kinetic rate evaluations via UV/Vis absorbance and NMR spectroscopies.

The following chapters discuss the process, progress and results obtained from these synthetic and characterisation endeavours. Chapter 3 includes the detailed description of zirconium complex synthesis as well as broad characterisation of said compounds. Chapters 4-6 contain solid state structural characterisation by means of single crystal X-ray diffractometry while Chapter 7 describes the solution behavioural studies of certain compounds by means of UV/Vis absorbance spectroscopic kinetics. Finally, Chapter 8 involves theoretical optimization of solid state structures of zirconium, aimed at correlation of calculated complexes with published counterparts.

Chapter 3

Synthesis of Zirconium(IV) Complexes –

Experimental Techniques & Preliminary Characterisation

The synthesis of zirconium(IV) complexes forms a fundamental part of a project focusing on the study of solid state characterisation of these types of compounds. Furthermore, without specific synthetic aims as far as the intended Zr(IV) products are concerned, a detailed solution behavioural kinetic study would be futile.

During the course of this study, a wide range of organic, bi- and multidentate ligands were subjected to chelation with zirconium, with the explicit purpose of producing novel complexes for expanding the knowledge base and publication, as well as comparative identification of behavioural trends for this metal. The latter here relating directly to finding specific nuances of zirconium crystallization tendencies that could be exploited in separation investigations. In other words, if zirconium compounds show certain characteristics, in comparison to other, similar moieties or more specifically to their hafnium counterparts, solution extraction experiments could make direct use of certain reaction tendencies to separate these metals.

In this chapter, a number successful syntheses are reported and the complexes characterised by IR-, UV/Vis- and NMR spectroscopy. In this case, only complexes that yielded crystalline products are described, as they held the highest value for structural investigations by means of single crystal XRD. The characterisation of solids, which yielded usable structural data, are described in detail in Chapters 4, 5 and 6.

3.1. Chemical and Apparatus detail

3.1.1. Reagents and Solvents

All reagents used for the synthesis and characterization were of analytical grade and were purchased from Sigma-Aldrich, South Africa. Reagents and solvents were used as received, without further purification or drying, respectively.

3.1.2. Nuclear Magnetic Resonance Spectroscopy

The ^{13}C and ^{1}H FT-NMR solution-state spectra were recorded on a Bruker Advance II 600 (^{1}H: 600.28 MHz; ^{13}C: 150.96 MHz). ^{1}H NMR spectra were referenced internally using residual protons in the deuterated solvents, Acetone-d_6 [C_3D_6O = 2.05(5) ppm] and Methanol-d_4 [MeOD = 4.78(1) ppm & 3.31(5) ppm]. ^{13}C NMR spectra were similarly referenced internally to the solvent resonance [C_3D_6O = 29.92(7) ppm & 206.68(13) ppm; MeOD = 49.15(7) ppm] with values reported relative to tetramethylsilane (δ 0.0 ppm).

3.1.3. Infrared Spectroscopy

Solid state FT-IR spectra were recorded as neat samples on a Digilab FTS 2000 Fourier transform spectrometer (ATR) utilizing a He-Ne laser at 632.6 nm, in the range of 3000 to 600 cm^{-1}.

3.1.4. UV/Vis Spectroscopy

UV/Vis absorbance spectra were collected in a 1.000(1) cm tandem quartz cuvette on a Varian Cary 50 Conc. spectrophotometer, which was equipped with a Julabo F12-mV temperature cell regulator accurate within 0.1 °C. All λ_{max} values reported in this chapter were collected at 25.0 °C.

3.2. Metal Complex Synthesis

The general method for synthesis of zirconium metal complexes was carried over from the previously determined idealised procedure, for producing collectable crystals of lesser sensitivity, as described in the related M.Sc. projected concluded in 2009.[1] This method involves a simple bench-top, atmospheric condition, addition method of combining both the $ZrCl_4$ and ligand, previously dissolved in N,N'-dimethylformamide (DMF), at slightly elevated temperatures (40 - 60 °C). The reaction solution is stirred vigorously for 30 minutes. The heating of the reaction solution is then stopped, the solution covered and allowed to slowly cool, which induces crystallization. Specific quantities of reagents, other reaction conditions and rate of crystallization are described below.

3.2.1. Oxine Complexes of Zirconium
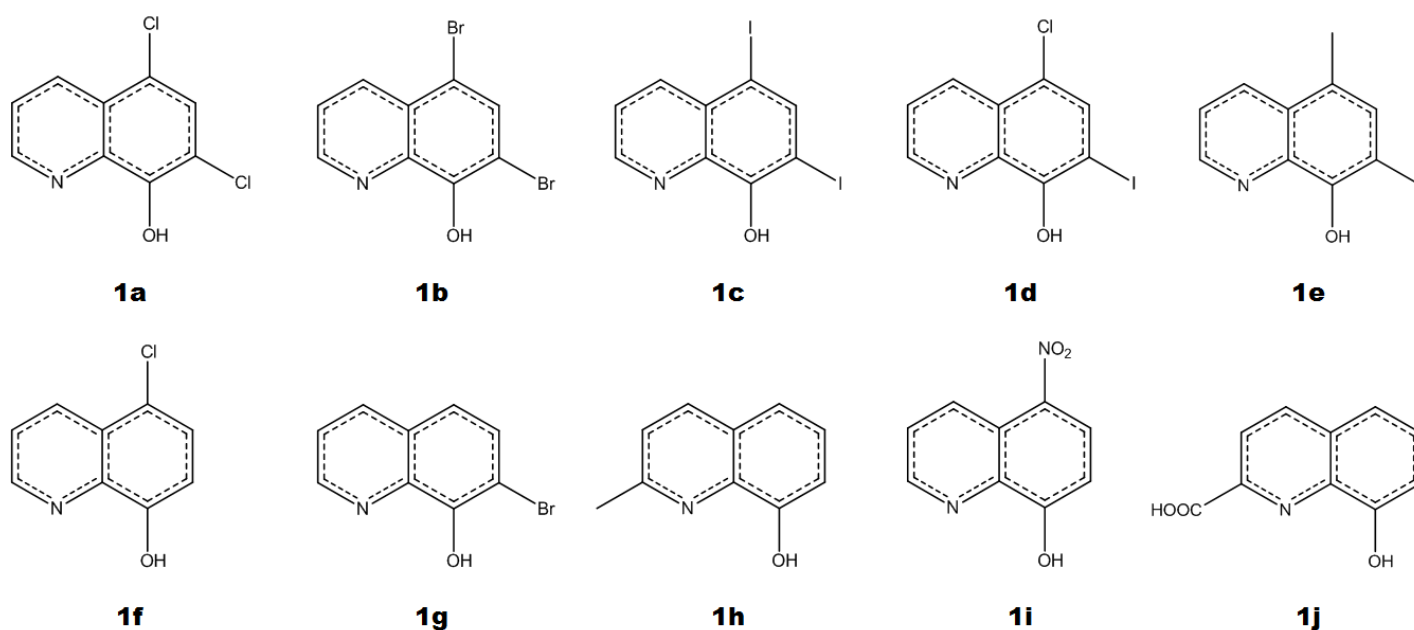
Figure 3.1 Graphical representation of the quinoline/oxine ligands employed in synthesis of zirconium(IV) complexes. (**1a**) *5,7-Dichloro-8-hydroxyquinoline* (diClOxH), (**1b**) *5,7-Dibromo-8-hydroxyquinoline* (diBrOxH), (**1c**) *5,7-Diiodo-8-hydroxyquinoline* (diIOxH), (**1d**) *5-Chloro-7-iodo-8-hydroxyquinoline* (CliOxH), (**1e**) *5,7-Dimethyl-8-hydroxyquinoline* (diMeOxH), (**1f**) *5-Chloro-8-hydroxyquinoline* (5-ClOxH), (**1g**) *7-Bromo-8-hydroxyquinoline* (7-BrOxH), (**1h**) *2-Methyl-8-hydroxyquinoline* (2-MeOxH), (**1i**) *5-Nitro-8-hydroxyquinoline* (5-NO₂OxH), (**1j**) *Hydroxy-2-quinolinecarboxylic acid* (2-AOxH).

---

[1] M. Steyn; *Speciation And Interconversion Mechanism Of Mixed Halo And O,O- And O,N Bidentate Ligand Complexes Of Zirconium*, M.Sc. Dissertation, *Chapter 4* (**2009**), University of the Free State, South Africa.

3.2.1.1. Tetrakis(5,7-dichloroquinolin-8-olato-$\kappa^2 N,O$)zirconium(IV) dimethylformamide disolvate – [Zr(diClOx)$_4$]·2DMF

ZrCl$_4$ (104.2 mg, 0.447 mmol) combined with **1a** - 5,7-Dichloro-8-quinoline (diClOxH) (279.7 mg, 1.307 mmol) in a total DMF volume of 11 ml. Dark yellow plate-like crystals, suitable for single X-Ray diffraction, formed after *ca.* 10 days. (Yield: 253 mg, 82 %). Crystallographic structural characterisation of **Zr_1a** is discussed in § 4.2, solution formation kinetic investigations in § 7.4 and theoretical optimization in § 8.3.3.

IR (ATR): $v_{C=O}$ = 1567 cm^{-1}; UV/Vis: λ^{DMF}_{max} = 400 nm, ε = 226.8 cm^{-1}.M^{-1}; ^{1}H NMR (600.28 MHz, Acetone-d_6): δ = 9.04 (d, 1H), 8.71 (d, 1H), 8.03 (s, 1H), 7.81 (q, 1H); ^{13}C NMR (150.96 MHz, Acetone-d_6): δ = 154.4 (CH), 148.8 (C), 139.1 (C), 127.9 (CH), 124.6 (C), 123.0 (CH), 120.6 (C), 118.9 (C), 115.9 (C).

3.2.1.2. Tetrakis(5,7-dibromoquinolin-8-olato-$\kappa^2 N,O$)zirconium(IV) dimethylformamide solvate – [Zr(diBrOx)$_4$]·nDMF

ZrCl$_4$ (103.9 mg, 0.446 mmol) and **1b** - 5,7-dibromoquinoline (diBrOxH) (391.8 mg, 1.293 mmol) in a total DMF volume of 12 ml. Dark yellow cuboid crystals, suitable for single X-Ray diffraction, formed after *ca.* 10 days. (Yield: 312 mg, 74 %). Although crystals were obtained, no adequate reflection data could be recorded for this product, due to poor crystal quality.

IR (ATR): $v_{C=O}$ = 1560 cm^{-1}; UV/Vis: λ^{DMF}_{max} = 402 nm, ε = 278.6 cm^{-1}.M^{-1}; ^{1}H NMR (600.28 MHz, Acetone-d_6): δ = 9.18 (d, 1H), 8.70 (d, 1H), 7.98 (s, 1H), 7.71 (q, 1H); ^{13}C NMR (150.96 MHz, Acetone-d_6): δ = 152.4 (CH), 151.2 (C), 136.4 (C), 131.9 (CH), 128.2 (C), 123.2 (CH), 121.8 (C), 119.9 (C).

3.2.1.3. Tetrakis(5,7-diiodoquinolin-8-olato-$\kappa^2 N,O$)zirconium(IV) dimethylformamide solvate – [Zr(diIOx)$_4$]·nDMF

ZrCl$_4$ (103.7 mg, 0.445 mmol) and **1c** - 5,7-diiodoquinoline (diIOxH) (518.9 mg, 1.307 mmol) in a total DMF volume of 13 ml. Dark yellow needle crystals, suitable for single X-Ray diffraction, formed after *ca.* 10 days. (Yield: 434 mg, 79 %). Although crystals were obtained and reflection data was collected, the data was not of good enough quality to refine into a usable crystallographic description of this product.

IR (ATR): $v_{C=O}$ = 1549 cm^{-1}; UV/Vis: λ^{DMF}_{max} = 406 nm, ε = 401.2 cm^{-1}.M^{-1}; ^{1}H NMR (600.28 MHz, Acetone-d_6): δ = 9.24 (d, 1H), 8.80 (d, 1H), 8.40 (q, 1H), 7.61 (s, 1H); ^{13}C NMR (150.96 MHz, Acetone-d_6): δ = 155.6 (C), 153.3 (CH), 147.4 (C), 139.8 (CH), 129.4 (C), 127.1 (C), 125.9 (CH), 85.8 (C), 80.1 (C).

3.2.1.4. μ-oxo-bis[di(5-Chloro-7-iodoquinolin-8-olato-κ^{2}N,O)-dichloro-(dimethylformamido-κO)zirconium(IV)] dimethylformamide solvate – [ZrCl(CliOx)$_2$(DMF)$_2$O]$_2$·DMF

ZrCl$_4$ (100.2 mg, 0.430 mmol) and **1d** - 5-Chloro-7-iodo-8-hydroxyquinoline (CliOxH) (400.6 mg, 1.002 mmol) in a total DMF volume of 12 ml. Dark yellow cuboid crystals, suitable for single X-Ray diffraction, formed after *ca.* 10 days. (Yield: 208 mg, 59 %). Crystallographic structural characterisation of **Zr_1d** is discussed in § 4.4.

IR (ATR): $v_{C=O}$ = 1531 cm^{-1}; UV/Vis: λ^{DMF}_{max} = 398 nm, ε = 1.067 x 10^3 cm^{-1}.M^{-1}; ^{1}H NMR (600.28 MHz, Methanol-d_4): δ = 9.28 (d, 1H), 8.58 (d, 1H), 8.03 (s, 1H), 7.11 (q, 1H); ^{13}C NMR (150.96 MHz, Methanol-d_4): δ = 155.3 (CH), 152.2 (C), 140.4 (C), 135.9 (CH), 125.7 (C), 124.2 (CH), 118.6 (C), 110.2 (C), 78.2 (C).

3.2.1.5. Tetrakis(5,7-dimethylquinolin-8-olato-κ^{2}N,O)zirconium(IV) dimethylformamide disolvate – [Zr(diMeOx)$_4$]·2DMF

ZrCl$_4$ (100.3 mg, 0.430 mmol) and **1e** - 5,7-Dimethyl-8-hydroxyquinoline (diMeOxH) (228.2 mg, 1.317 mmol) in a total DMF volume of 10 ml. Dark yellow cuboid crystals, suitable for single X-Ray diffraction, formed after *ca.* 10 days. (Yield: 203 mg, 79 %). Crystallographic structural characterisation of **Zr_1e** is discussed in § 5.2, solution formation kinetic investigations in § 7.6 and theoretical optimization in § 8.3.2.

IR (ATR): $v_{C=O}$ = 1544 cm^{-1}; UV/Vis: λ^{DMF}_{max} = 405 nm, ε = 462.3 cm^{-1}.M^{-1}; ^{1}H NMR (600.28 MHz, Methanol-d_4): δ = 9.17 (d, 1H), 8.99 (d, 1H), 8.01 (q, 1H), 7.55 (s, 1H), 2.69 (s, 3H), 2.53 (s, 3H); ^{13}C NMR (150.96 MHz, Methanol-d_4): δ = 143.7(CH), 142.7 (C), 141.9 (C), 133.6 (CH), 130.4 (CH), 128.6 (C), 127.8 (C), 126.9 (C), 120.2 (CH), 15.6 (CH$_3$), 16.2 (CH$_3$).

3.2.1.6. Tetrakis(5-chloroquinolin-8-olato-$\kappa^2 N,O$)zirconium(IV) dimethylformamide disolvate – [Zr(5-ClOx)$_4$]·nDMF

ZrCl$_4$ (100.4 mg, 0.431 mmol) and **1f** - 5-Chloro-8-hydroxyquinoline (5-ClOxH) (232.2 mg, 1.293 mmol) in a total DMF volume of 10 ml. Dark yellow cuboid crystals, suitable for single X-Ray diffraction, formed after *ca.* 14 days. (Yield: 217 mg, 83 %). Crystallographic structural characterisation of **Zr_1f** is discussed in § 4.3 and solution formation kinetic investigations in § 7.5.

IR (ATR): $v_{C=O}$ = 1550 cm^{-1}; UV/Vis: λ^{DMF}_{max} = 400 nm, ε = 426.4 cm^{-1}.M^{-1}; ^{1}H NMR (600.28 MHz, Methanol-d_4): δ = 9.17 (d, 1H), 8.55 (d, 1H), 7.92 (q, 1H), 7.46 (d, 1H), 6.88 (d, 1H); ^{13}C NMR (150.96 MHz, Methanol-d_4): δ = 147.7 (CH), 144.0 (C), 143.5 (C), 130.6 (CH), 129.1 (C), 123.2 (C), 122.5 (CH), 115.9 (C), 112.3 (CH).

3.2.1.7. Tetrakis(7-bromoquinolin-8-olato-$\kappa^2 N,O$)zirconium(IV) dimethylformamide solvate – [Zr(7-BrOx)$_4$]·nDMF

ZrCl$_4$ (103.3 mg, 0.443 mmol) and **1g** - 7-Bromo-8-hydroxyquinoline (7-BrOxH) (288.1 mg, 1.286 mmol) in a total DMF volume of 10 ml. Yellow cuboid crystals, suitable for single X-Ray diffraction, formed after *ca.* 14 days. (Yield: 248 mg, 78 %). Although crystals were obtained and reflection data was collected, the data was not of good enough quality to refine into a usable crystallographic description of this product.

IR (ATR): $v_{C=O}$ = 1554 cm^{-1}; UV/Vis: λ^{DMF}_{max} = 378 nm, ε = 313.7 cm^{-1}.M^{-1}; ^{1}H NMR (600.28 MHz, Methanol-d_4): δ = 9.12 (d, 1H), 8.14 (d, 1H), 7.79 (q, 1H), 7.46 (d, 1H), 7.22 (d, 1H); ^{13}C NMR (150.96 MHz, Methanol-d_4): δ = 146.3 (CH), 144.1 (C), 134.2 (C), 132.3 (CH), 130.0 (C), 129.5 (C), 122.3 (CH), 121.7 (C), 120.3 (CH).

3.2.1.8. Tetrakis(2-methylquinolin-8-olato-$\kappa^2 N,O$)zirconium(IV) dimethylformamide solvate – [Zr(2-MeOx)$_4$]·nDMF

ZrCl$_4$ (105.0 mg, 0.451 mmol) and **1h** - 2-Methyl-8-hydroxyquinoline (2-MeOxH) (202.7 mg, 1.273 mmol) in a total DMF volume of 10 ml. Light yellow cuboid crystals, suitable for single X-Ray diffraction, formed after *ca.* 14 days. (Yield: 189 mg, 82 %). Although crystals were obtained and reflection data was collected, the data was

not of good enough quality to refine into a usable crystallographic description of this product.

IR (ATR): $v_{C=O}$ = 1538 cm^{-1}; UV/Vis: λ^{DMF}_{max} = 313 nm, ε = 303.6 cm^{-1}.M^{-1}; ^{1}H NMR (600.28 MHz, Methanol-d_4): δ = 8.96 (d, 1H), 7.91 (d, 1H), 7.74 (q, 1H), 7.56 (q, 1H), 7.47 (d, 1H), 3.32 (m, 3H). ^{13}C NMR (150.96 MHz, Methanol-d_4): δ = 157.3 (CH), 147.6 (C), 146.1 (C), 129.8 (CH), 128.7 (C), 128.5 (CH), 123.8 (CH), 118.6 (CH), 116.1 (CH), 19.3 (CH$_3$).

3.2.1.9. *Tetrakis(5-nitroquinolin-8-olato-κ^{2}N,O)zirconium(IV) – [Zr(5-NO$_2$Ox)$_4$]*

ZrCl$_4$ (105.7 mg, 0.454 mmol) and **1i** - 5-Nitro-8-hydroxyquinoline (5-NO$_2$OxH) (254.5 mg, 1.338 mmol) in a total DMF volume of 10 ml. Dark yellow cuboid crystals, suitable for single X-Ray diffraction, formed after *ca.* 21 days. (Yield: 205 mg, 72 %). Crystallographic structural characterisation of **Zr_1i** is discussed in § 5.3.

IR (ATR): $v_{C=O}$ = 1540 cm^{-1}; UV/Vis: λ^{DMF}_{max} = 394 nm, ε = 228.7 cm^{-1}.M^{-1}; ^{1}H NMR (600.28 MHz, Acetone-d_6): δ = 9.62 (d, 1H), 9.25 (d, 1H), 8.83 (q, 1H), 8.38 (d, 1H), 7.55 (d, 1H); ^{13}C NMR (150.96 MHz, Acetone-d_6): δ = 159.6 (C), 151.2 (CH), 143.2 (C), 138.6 (C), 132.1 (CH), 126.7 (CH), 126.4 (CH), 123.7 (C), 113.4 (CH).

3.2.1.10. *Tetrakis(2-carboxyquinolin-8-olato-κ^{2}N,O)zirconium(IV) dimethylformamide solvate – [Zr(2-AOx)$_4$]·nDMF*

ZrCl$_4$ (109.1 mg, 0.468 mmol) and **1j** - 8-Hydroxy-2-quinolinecarboxylic acid (2-AOxH) (245.3 mg, 1.297 mmol) in a total DMF volume of 11 ml. Orange cuboid crystals, suitable for single X-Ray diffraction, formed after *ca.* 10 days. (Yield: 216 mg, 79 %). Although crystals were obtained, no adequate reflection data could be recorded for this product, due to crystal instability.

IR (ATR): $v_{C=O}$ = 1595 cm^{-1}; UV/Vis: λ^{DMF}_{max} = 416 nm, ε = 779.0 cm^{-1}.M^{-1}; ^{1}H NMR (600.28 MHz, Methanol-d_4): δ = 8.48 (d, 1H), 8.20 (d, 1H), 7.62 (q, 1H), 7.50 (q, 1H), 7.22 (d, 1H); ^{13}C NMR (150.96 MHz, Methanol-d_4): δ = 163.5 (C), 145.1 (C), 138.0 (CH), 137.7 (C), 130.5 (C), 130.2 (CH), 120.8 (CH), 120.4 (CH), 117.6 (C), 111.9 (CH).

3.2.2. O,O'-Donating Bidentate Ligand Complexes of Zirconium
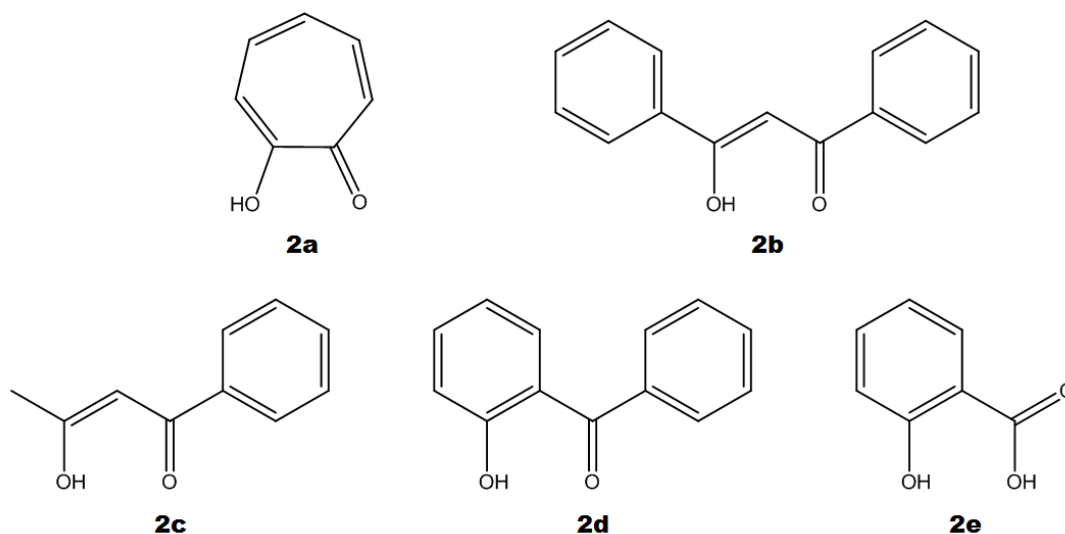
Figure 3.2 Graphical representation of the O,O'-donating bidentate ligands employed in synthesis of zirconium(IV) complexes. (**2a**) *Tropolone* (TropH), (**2b**) *Dibenzoylmethane* (DBMH), (**2c**) *Benzoylacetone* (bzAcacH), (**2d**) *2-Hydroxybenzophenone* (BzAcH), (**2e**) *Salicylic acid* (SalAH),

3.2.2.1. Tetrakis(tropolonato-κ^2O,O')zirconium(IV) dimethylformamide solvate – [Zr(Trop)$_4$]· DMF

ZrCl$_4$ (101.5 mg, 0.436 mmol) and **2a** - Tropolone (TropH) (163.1 mg, 1.336 mmol) in a total DMF volume of 8 ml. Light yellow cuboid crystals, suitable for single X-Ray diffraction, formed after *ca.* 14 days. (Yield: 162 mg, 84 %). Crystallographic structural characterisation of **Zr_2a** is discussed in § 6.2.

IR (ATR): $v_{C=O}$ = 1588 & 1514 cm^{-1}; UV/Vis: λ^{DMF}_{max} = 336 nm, ε = 3.973 x 10^3 cm^{-1}.M^{-1}; ^{1}H NMR (600.28 MHz, Methanol-d_4): δ = 7.95 (d, 1H), 7.81 (d, 1H), 7.60 (q, 1H), 7.46 (q, 1H), 7.39(q, 1H); ^{13}C NMR (150.96 MHz, Methanol-d_4): δ = 181.1 (C), 180.9 (C), 141.1 (CH), 140.4 (CH), 129.8 (CH), 126.6 (CH), 125.8 (CH).

3.2.2.2. Tetrakis(1,3-diphenyl-1,3-propanedionato-κ^2O,O')zirconium(IV) – [Zr(DBM)$_4$]

ZrCl$_4$ (101.2 mg, 0.434 mmol) and **2b** - Dibenzoylmethane (DBMH) (396.6 mg, 1.769 mmol) in a total DMF volume of 20 ml. Yellow trapezoid crystals, suitable for single X-Ray diffraction, formed after *ca.* 21 days. (Yield: 382 mg, 89 %). Crystallographic structural characterisation of **Zr_2b** is discussed in § 6.3.

IR (ATR): $v_{C=O}$ = 1591 & 1519 cm^{-1}; UV/Vis: λ^{DMF}_{max} = 352 nm, ε = 2.751 x 10^3 cm^{-1}.M^{-1}; ^{1}H NMR (600.28 MHz, Acetone-d_6): δ = 8.21 (d, 4H), 7.97 (s, 1H), 7.51 (q, 2H), 7.38 (q, 4H); ^{13}C NMR (150.96 MHz, Acetone-d_6): δ = 184.5 (2C), 134.9 (2C), 128.7 (4C), 126.4 (6C), 92.1 (1C).

3.2.2.3. Tetrakis(1-Phenyl-1,3-butanedionato-κ^2O,O')zirconium(IV) dimethylformamide solvate – [Zr(bzAcac)₄]·nDMF

ZrCl₄ (50.3 mg, 0.216 mmol) and **2c** - Benzoylacetone (bzAcacH) (102.3 mg, 0.631 mmol) in a total DMF volume of 10 ml. Light yellow cuboid crystals, suitable for single X-Ray diffraction, formed after *ca.* 4 days. (Yield: 101 mg, 87 %). Although crystals were obtained, no adequate reflection data could be recorded for this product, due to poor crystal quality.

IR (ATR): $v_{C=O}$ = 1591 & 1516 cm^{-1}; UV/Vis: λ^{DMF}_{max} = 332 nm, ε = 4.663 x 10^3 cm^{-1}.M^{-1}; ^{1}H NMR (600.28 MHz, Acetone-d_6): δ = 8.48 (d, 2H), 8.15 (q, 2H), 8.03 (d, 1H), 7.04 (s, 1H), 3.32 (s, 3H); ^{13}C NMR (150.96 MHz, Acetone-d_6): δ = 184.3 (C), 180.2 (C), 136.1 (CH), 134.7 (C), 129.4 (2CH), 128.4 (2CH), 97.2 (CH), 24.3 (CH₃).

3.2.2.4. Tetrakis(2-(benzoyl)phenolato-κ^2O,O')zirconium(IV) dimethylformamide solvate – [Zr(bzAc)₄]·nDMF

ZrCl₄ (50.3 mg, 0.216 mmol) and **2d** - 2-Hydroxybenzophenone (bzAcH) (132.1 mg, 0.666 mmol) in a total DMF volume of 10 ml. Light yellow plate-like crystals, suitable for single X-Ray diffraction, formed after *ca.* 4 days. (Yield: 95 mg, 65 %). Although crystals were obtained, no adequate reflection data could be recorded for this product, due to crystal instability.

IR (ATR): $v_{C=O}$ = 1648 & 1624 cm^{-1}; UV/Vis: λ^{DMF}_{max} = 333 nm, ε = 1.593 x 10^3 cm^{-1}.M^{-1}; ^{1}H NMR (600 MHz, Methanol-d_4): δ = 8.10 (d, 2H), 7.81 (d, 1H), 7.74 (d, 1H), 7.65 (q, 2H), 7.61 (q, 1H), 7.51 (q, 1H), 7.00 (d, 1H); ^{13}C NMR (150.96 MHz, Methanol-d_4): δ = 201.2 (C), 164.3 (C), 137.8 (C), 135.7 (2CH), 132.8 (CH), 131.9 (2CH), 130.7 (2CH), 128.9 (CH), 120.1 (C), 118.67 (CH).

3.2.2.5. Tetrakis(salicylato-*κ²O,O'*)zirconium(IV) dimethylformamide solvate – [Zr(Sal)₄]·nDMF

ZrCl₄ (50.3 mg, 0.216 mmol) and **2e** - Salicylic acid (SalH₂) (98.2 mg, 0.711 mmol) in a total DMF volume of 10 ml. Colourless plate-like crystals, suitable for single X-Ray diffraction, formed after *ca.* 4 days. (Yield: 117 mg, 86 %). Although crystals were obtained, no adequate reflection data could be recorded for this product, due to poor crystal quality.

IR (ATR): $v_{C=O}$ = 1655 & 1610 cm⁻¹; UV/Vis: λ^{DMF}_{max} = 305 nm, ε = 3.058 x 10³ cm⁻¹.M⁻¹; ¹H NMR (600.28 MHz, Methanol-d_4): δ = 7.87 (d, 1H), 7.47 (d, 1H), 6.92 (q, 1H), 6.85 (q, 1H); ¹³C NMR (150.96 MHz, Methanol-d_4): δ = 172.5 (C), 162.1 (C), 135.3 (CH), 130.2 (CH), 116.8 (CH), 112.47 (CH).

3.2.3. Pyridine Complexes of Zirconium
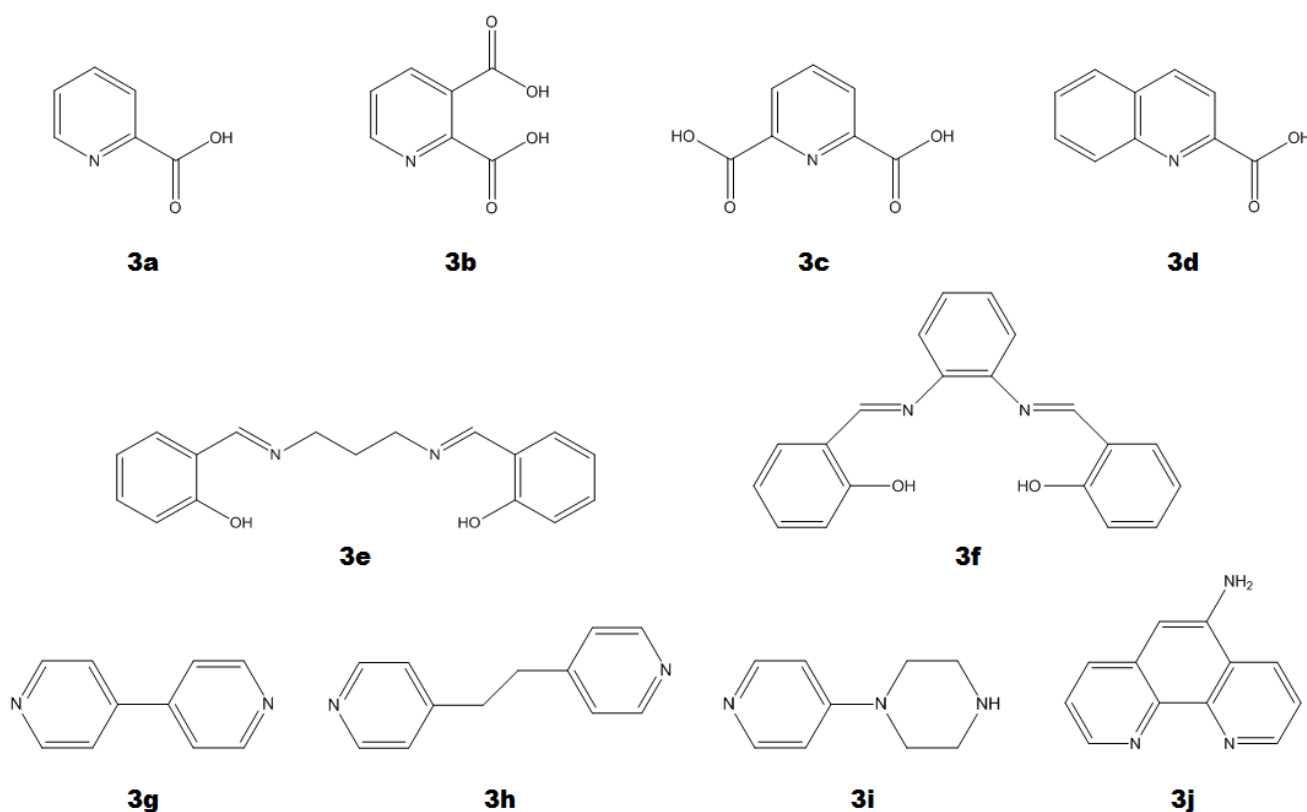
Figure 3.3 Graphical representation of the quinoline/oxine ligands employed in synthesis of zirconium(IV) complexes. (**3a**) *Picolinic Acid* (PicH), (**3b**) *Quinolinic acid* (QnH), (**3c**) *Dipicolinic acid* (DipicH), (**3d**) *Quinaldic acid* (QdH), (**3e**) *N,N'-Bis-(Salicylidene)-1,3-propanediamine* (SalpnH), (**3f**) *N,N'-Bis(salicylidene)-1,2-phenylenediamine* (SalophenH), (**3g**) *4,4'-Dipyridyl* (DiPyrH), (**3h**) *1,2-Bis(4-pyridyl)ethane* (DPyrH), (**3i**) *1-(4-Pyridyl)piperazine* (PiPyrH), (**3j**) *1,10-Phenanthroline-5-amine* (APhenH),

3.2.3.1. Tetrakis(picolinato-$\kappa^2 N,O$)zirconium(IV) dihydrate – [Zr(Pic)$_4$].2H$_2$O

ZrCl$_4$ (103.3 mg, 0.443 mmol) and **3a** - Picolinic acid (PicH) (175.2 mg, 1.423 mmol) in a total DMF volume of 10 ml. Colourless cuboid crystals, suitable for single X-Ray diffraction, formed after *ca.* 30 days. (Yield: 178 mg, 86%). Crystallographic structural characterisation of **Zr_3a** is discussed in § 5.4.

IR (ATR): $v_{C=O}$ = 1653 cm^{-1}; UV/Vis: λ^{DMF}_{max} = 301 nm, ε = 4.589 x 10^3 cm^{-1}.M^{-1}; ^{1}H NMR (600.28 MHz, Acetone-d_6): δ = 8.39 (d, 1H), 8.31 (d, 1H), 8.11 (q, 1H), 8.01 (q, 1H); ^{13}C NMR (150.96 MHz, Acetone-d_6): δ = 171.1 (C), 145.1 (CH), 144.4 (C), 132.8 (CH), 127.6 (CH), 125.8 (CH).

3.2.3.2. Tetrakis(pyridine-2,3-dicarboxylate-$\kappa^2 N,O$)zirconium(IV) dimethylformamide solvate – [Zr(Qn)$_4$]·nDMF

ZrCl$_4$ (50.2 mg, 0.215 mmol) and **3b** - Quinolinic acid (QnH$_2$) (74.8 mg, 0.448 mmol) in a total DMF volume of 10 ml. Colourless needle-like crystals, suitable for single X-Ray diffraction, formed after *ca.* 4 days. (Yield: 77 mg, 91%). Although crystals were obtained, no adequate reflection data could be recorded for this product, due to poor crystal quality.

IR (ATR): $v_{C=O}$ = 1732 cm^{-1}; UV/Vis: λ^{DMF}_{max} = 316 nm, ε = 9.180 x 10^3 cm^{-1}.M^{-1}; ^{1}H NMR (600 MHz, Methanol-d_4): δ = 8.85 (d, 2H), 8.61 (d, 1H), 7.95 (q, 1H); ^{13}C NMR (150.96 MHz, Methanol-d_4): δ = 168.5 (C), 164.2 (C), 163.5 (CH), 162.9 (C), 150.26 (CH), 138.8 (CH), 126.48 (C).

3.2.3.3. Tetrakis(pyridine-2,6-dicarboxylate-$\kappa^2 N,O$)zirconium(IV) dimethylformamide solvate – [Zr(Dipic)$_4$]·nDMF

ZrCl$_4$ (50.2 mg, 0.215 mmol) and **3c** - Dipicolinic acid (DipicH$_2$) (74.4 mg, 0.447 mmol) in a total DMF volume of 10 ml. Colourless cuboid crystals, suitable for single X-Ray diffraction, formed after *ca.* 4 days. (Yield: 49 mg, 89%). Although crystals were obtained, no adequate reflection data could be recorded for this product, due to poor crystal quality.

IR (ATR): $v_{C=O}$ = 1736 cm^{-1}; UV/Vis: λ^{DMF}_{max} = 314 nm, ε = 4.736 x 10^3 cm^{-1}.M^{-1}; ^{1}H NMR (600 MHz, Acetone-d_6): δ = 8.26 (d, 2H), 8.12 (q, 1H); ^{13}C NMR (150.96 MHz, Acetone-d_6): δ = 171.3 (2C), 144.2 (2C), 138.8 (CH), 127.2 (2CH).

3.2.3.4. Tetrakis(quinoline-2-carboxylato-$\kappa^2 N,O$)zirconium(IV) dimethylformamide solvate – [Zr(Qd)$_4$]·nDMF

ZrCl$_4$ (50.2 mg, 0.215 mmol) and **3d** - Quinaldic acid (QdH) (77.4 mg, 0.447 mmol) in a total DMF volume of 10 ml. Colourless cuboid crystals, suitable for single X-Ray diffraction, formed after *ca.* 21 days. (Yield: 76 mg, 87%). Although crystals were obtained, no adequate reflection data could be recorded for this product, due to crystal instability.

IR (ATR): $v_{C=O}$ = 1650 cm^{-1}; UV/Vis: λ^{DMF}_{max} = 315 nm, ε = 7.607 x 10^3 cm^{-1}.M^{-1}; ^{1}H NMR (600 MHz, Methanol-d_4): δ = 9.18 (d, 1H), 8.52 (d, 1H), 8.48 d, 1H), 8.35 (d, 1H), 8.20 (q, 1H), 8.02 (q, 1H); ^{13}C NMR (150.96 MHz, Methanol-d_4): δ = 148.9 (C), 145.8 (C), 143.6 (C), 140.9 (CH), 139.3 (CH), 134.8 (CH), 130.6 (C), 128.8 (CH), 123.3 (CH), 121.0 (CH).

3.2.3.5. Bis(N,N'-o-phenylene-bis(salicylideneiminato)-$\kappa^4 N,N',O,O'$)zirconium(IV) dimethylformamide solvate – [Zr(Salpn)$_2$]·nDMF

ZrCl$_4$ (50.2 mg, 0.215 mmol) and **3e** - N,N'-Bis-(Salicylidene)-1,3-propanediamine (SalpnH$_2$) (136.4 mg, 0.483 mmol) in a total DMF volume of 10 ml. Orange plate-like crystals, suitable for single X-Ray diffraction, formed after *ca.* 10 days. (Yield: 119 mg, 84%). Although crystals were obtained, no adequate reflection data could be recorded for this product, due to crystal instability.

IR (ATR): $v_{C=O}$ = 1652 cm^{-1}; UV/Vis: λ^{DMF}_{max} = 373 nm, ε = 3.923 x 10^3 cm^{-1}.M^{-1}; ^{1}H NMR (600 MHz, Methanol-d_4): δ = 7.97 (s, 2H), 7.85 (d, 1H), 7.69 (d, 1H), 7.54 (t, 1H), 7.49 (t, 1H), 7.34 (d, 1H), 7.26 (d, 1H), 7.17 (t, 1H), 7.10 (t, 1H), 3.08 (d, 4H), 2.08 (t, 2H); ^{13}C NMR (150.96 MHz, Methanol-d_4): δ = 155.2 (C), 154.9(C), 136.5 (CH), 135.5(CH), 128.0(CH), 127.9(CH), 127.3(CH), 127.1(CH), 119.0 (C), 118.8 (C), 117.0 (CH), 116.8 (CH), 115.2 (CH), 114.5 (CH), 59.7 (CH$_2$), 34.0 (CH$_2$).

3.2.3.6. Bis(N,N'-bis(salicylidene)-1,3-propanediaminato-$\kappa^4 N,N',O,O'$) zirconium(IV) dimethylformamide solvate – [Zr(Salophen)$_2$]·nDMF

ZrCl$_4$ (50.2 mg, 0.215 mmol) and **3f** - N,N′-Bis(salicylidene)-1,2-phenylenediamine (SalophenH$_2$) (135.2 mg, 0.427 mmol) in a total DMF volume of 10 ml. Red plate-like crystals, suitable for single X-Ray diffraction, formed after *ca.* 4 days. (Yield: 132 mg, 85%). Although crystals were obtained, no adequate reflection data could be recorded for this product, due to crystal instability.

IR (ATR): $v_{C=O}$ = 1661 cm^{-1}; UV/Vis: λ^{DMF}_{max} = 376 nm, ε = 7.682 x 10^3 cm^{-1}.M^{-1}; ^{1}H NMR (600 MHz, Methanol-d_4): δ = 9.04 (s, 2H), 8.28 (d, 1H), 7.90(d, 1H), 7.71 (d, 2H), 7.62 (t, 2H), 7.47 (t, 1H), 7.37 (t, 1H), 7.33(t, 1H), 7.15 (d, 1H), 7.09 (t, 1H), 6.98(d, 1H); ^{13}C NMR (150.96 MHz, Methanol-d_4): δ = 159.1 (2CH), 148.9 (2C), 134.4 (CH), 133.5 (CH), 132.4 (CH), 131.6 (CH), 130.8 (CH), 130.1 (CH), 128.0 (2CH), 125.4 (2C), 121.9 (CH), 121.2 (CH), 120.9 (C), 119.9 (C), 116.6 (CH), 116.2 (CH).

3.2.3.7. Poly[dichlorobis(μ_2-4,4'-Bipyridyl)zirconium(IV)] dimethylformamide solvate – [ZrCl$_2$(DiPyr)$_2$]·nDMF

ZrCl$_4$ (50.2 mg, 0.215 mmol) and **3g** - 4,4'-Dipyridyl (DiPyrH) (70.0 mg, 0.448 mmol) in a total DMF volume of 10 ml. Colourless plate-like crystals, suitable for single X-Ray diffraction, formed after *ca.* 21 days. (Yield: 213 mg, 78%). Although crystals were obtained, no adequate reflection data could be recorded for this product, due to poor crystal quality.

UV/Vis: λ^{DMF}_{max} = 302 nm, ε = 7.391 x 10^3 cm^{-1}.M^{-1}; ^{1}H NMR (600 MHz, Methanol-d_4): δ = 8.89 (d, 4H), 8.18 (d, 4H); ^{13}C NMR (150.96 MHz, Methanol-d_4): δ = 148.1 (2C), 147.3 (4CH), 123.3 (4CH).

3.2.3.8. Poly[dichlorobis(μ_2-1,2-bis(4-pyridyl)ethane)zirconium(IV)] dimethylformamide solvate – [ZrCl$_2$(DPyr)$_2$]·nDMF

ZrCl$_4$ (50.2 mg, 0.215 mmol) and **3h** - 1,2-Bis(4-pyridyl)ethane (DPyrH) (79.7 mg, 0.433 mmol) in a total DMF volume of 10 ml. Colourless cuboid crystals, suitable for single X-Ray diffraction, formed after *ca.* 21 days. (Yield: 247 mg, 83%). Although crystals were obtained, no adequate reflection data could be recorded for this product, due to poor crystal quality.

UV/Vis: λ^{DMF}_{max} = 307 nm, ε = 9.972 x 10^3 cm^{-1}.M^{-1}; ^{1}H NMR (600 MHz, Methanol-d_4): δ = 8.63 (d, 4H), 7.73 (d, 4H), 3.29 (s, 2H); ^{13}C NMR (150.96 MHz, Methanol-d_4): δ = 156.9 (2C), 144.8 (4CH), 125.9 (4CH), 34.9 (2CH$_2$)

3.2.3.9. Poly[dichlorobis(µ$_2$-1-(4-pyridyl)piperazine)zirconium(IV)] dimethylformamide solvate – [ZrCl$_2$(PiPyr)$_2$]·nDMF

ZrCl$_4$ (50.2 mg, 0.215 mmol) and **3i** - 1-(4-Pyridyl)piperazine (PiPyrH) (71.9 mg, 0.441 mmol) in a total DMF volume of 10 ml. Colourless cuboid crystals, suitable for single X-Ray diffraction, formed after *ca.* 21 days. (Yield: 215 mg, 77%). Although crystals were obtained, no adequate reflection data could be recorded for this product, due to poor crystal quality.

UV/Vis: λ^{DMF}_{max} = 309 nm, ε = 5.314 x 10^3 cm^{-1}.M^{-1}; ^{1}H NMR (600 MHz, Methanol-d_4): δ = 8.23 (d, 2H), 7.20 (d, 2H), 3.89 (t, 4H), 3.32 (t, 4H); ^{13}C NMR (150.96 MHz, Methanol-d_4): δ = 156.8 (C), 141.9 (2CH), 108.1 (2CH), 43.7 (2CH$_2$), 43.1 (2CH$_2$).

3.2.3.10. Tetrakis(1,10-phenanthroline-5-amine-κ^2N,O)zirconium(IV) dimethylformamide solvate – [Zr(APhen)$_4$]·nDMF

ZrCl$_4$ (50.2 mg, 0.215 mmol) and **3j** - 1,10-Phenanthroline-5-amine (APhenH) (87.1 mg, 0.446 mmol) in a total DMF volume of 10 ml. Orange cuboid crystals, suitable for single X-Ray diffraction, formed after *ca.* 4 days. (Yield: 83 mg, 85%). Although crystals were obtained, no adequate reflection data could be recorded for this product, due to crystal instability.

UV/Vis: λ^{DMF}_{max} = 361 nm, ε = 5.458 x 10^3 cm^{-1}.M^{-1}; ^{1}H NMR (600 MHz, Methanol-d_4): δ = 9.14 (d, 2H), 8.77 (d, 2H), 8.72 (d, 2H), 8.68 (d, 2H), 8.01 (dd, 2H), 7.95 (dd, 2H); ^{13}C NMR (150.96 MHz, Methanol-d_4): δ = 150.1 (C), 145.5 (2C), 141.3(C), 138.7 (CH), 137.3 (CH), 132.4 (C), 132.3 (C), 130.7 (CH), 124.9 (C), 124.3 (CH), 122.7 (CH).

3.3. Conclusion

During the course of the synthesis part of this project, many novel and re-synthesised complexes of zirconium were prepared and characterised. The more significant focus area revolved around the oxine-type ligand family, of which very few examples of zirconium-compounds were available in literature.[2] It can now however be confirmed that these ligands can easily be chelated to zirconium.

Leading out from previously investigated ligands,[1] other *O,O'*-donating ligands were also studied. A range of new *β*-diketone ligands was employed in synthesis as well as tropolone, as an aromatic steric-bulk example. Furthermore, a range of pyridine type ligands was also chelated to zirconium. In all cases, by simply utilizing DMF as reaction solvent and without enforcing any special precautions on reaction environment (i.e. standard bench-top, aerobic conditions), several zirconium products could easily be obtained. In this chapter, 25 examples have been described that yielded crystalline material, within 4-30 days, in the DMF reaction solvent, without any special/elaborate crystallization technique.

It may further be concluded, from these rudimentary findings, that zirconium as metal centre, with the starting form of $ZrCl_4$, reacts in DMF very readily with most ligands. Furthermore, this metal shows to favour crystalline products in most cases observed and described here. From the absorbance maxima data reported in Table 3.1, there appears to be no specific trend for product colouration, as far as electronic or steric properties of ligands species are concerned. However, it does appear as though the O,O-Ligand complexes all tend toward shorter wavelength colouration than the N- and/or O-donating Oxines and Pyridines, with the Oxine complexes, on average, displaying absorbance maxima at longer wavelengths.

It is also interesting to note that, even though complex solutions yielded certain colouration (and subsequently a specific wavelength related to this colouration), the crystalline products in some cases had a completely different colouration. As for the examples of [Zr(APhen)$_4$]·nDMF (Zr_3j – orange crystals), [Zr(Salpn)$_2$]·nDMF (Zr_3e – orange crystals) and [Zr(Salophen)$_2$]·nDMF (Zr_3f – red crystals), of which all complexes dissolved in DMF gave yellow solutions, although their crystalline products had a much darker colouration (i.e., a bathochromic shift). This could be indicative of solution state behaviour that differs substantially from crystalline lattice packing. In other words, for these examples, the specific molecular structure of the zirconium(IV) complexes are different for these two states and is

---

[2] The Cambridge Structural Database, Licence Update Feb 2013; F. H. Allen; *Acta Cryst. B58* (**2002**), 380-388.

worth investigating in future to determine how these moieties behave in different environments.

Table 3.1 λ^{DMF}_{max} and ε values as determined during Zr(IV)-complex characterization. Data sorted in ascending order of λ^{DMF}_{max} for each ligand type.

Zr(IV) Compound	Formula	Donating Atoms	λ^{DMF}_{max} (nm)	ε (cm^{-1}.M^{-1})
Oxines				
Zr_1h	[Zr(2-MeOx)$_4$]·nDMF	**N,O**	**313**	303.6
Zr_1g	[Zr(7-BrOx)$_4$]·nDMF	**N,O**	**378**	313.7
Zr_1i	[Zr(5-NO$_2$Ox)$_4$]	**N,O**	**394**	228.7
Zr_1d	[ZrCl(CliOx)$_2$(DMF)$_2$O]$_2$·DMF	**N,O**	**398**	1.067 x 10^3
Zr_1a	[Zr(diClOx)$_4$]·2DMF	**N,O**	**400**	226.8
Zr_1f	[Zr(5-ClOx)$_4$]·nDMF	**N,O**	**400**	426.4
Zr_1b	[Zr(diBrOx)$_4$]·nDMF	**N,O**	**402**	278.6
Zr_1e	[Zr(diMeOx)$_4$]·2DMF	**N,O**	**405**	462.3
Zr_1c	[Zr(diIOx)$_4$]·nDMF	**N,O**	**406**	401.2
Zr_1j	[Zr(2-AOx)$_4$]·nDMF	**N,O**	**416**	779
O,O-Ligands				
Zr_2e	[Zr(Sal)$_4$]·nDMF	**O,O**	**305**	3.058 x 10^3
Zr_2c	[Zr(bzAcac)$_4$]·nDMF	**O,O**	**332**	4.663 x 10^3
Zr_2d	[Zr(bzAc)$_4$]·nDMF	**O,O**	**333**	1.593 x 10^3
Zr_2a	[Zr(Trop)$_4$]·DMF	**O,O**	**336**	3.973 x 10^3
Zr_2b	[Zr(DBM)$_4$]	**O,O**	**352**	2.751 x 10^3
Pyridines				
Zr_3a	[Zr(Pic)$_4$]·2H$_2$O	**N,O**	**301**	4.589 x 10^3
Zr_3g	[ZrCl$_2$(DiPyr)$_2$]·nDMF	**N,N**	**302**	7.391 x 10^3
Zr_3h	[ZrCl$_2$(DPyr)$_2$]·nDMF	**N,N**	**307**	9.972 x 10^3
Zr_3i	[ZrCl$_2$(PiPyr)$_2$]·nDMF	**N,N**	**309**	5.314 x 10^3
Zr_3c	[Zr(Dipic)$_4$]·nDMF	**N,O**	**314**	4.736 x 10^3
Zr_3d	[Zr(Qd)$_4$]·nDMF	**N,O**	**315**	7.607 x 10^3
Zr_3b	[Zr(Qn)$_4$]·nDMF	**N,O**	**316**	9.180 x 10^3
Zr_3j	[Zr(APhen)$_4$]·nDMF	**N,N**	**361**	5.458 x 10^3
Zr_3e	[Zr(Salpn)$_2$]·nDMF	**N,N,O,O**	**373**	3.923 x 10^3
Zr_3f	[Zr(Salophen)$_2$]·nDMF	**N,N,O,O**	**376**	7.682 x 10^3

In the following Chapters (4-6), the crystallographic characterisation of some of these compounds is described in detail. Furthermore, in Chapter 7, a solution behavioural kinetic study of three oxine ligands in complex formation reactions with zirconium(IV) are also evaluated and Chapter 8 includes the theoretical optimization of selected zirconium(IV) compound structures.

Chapter 4

X-Ray Diffraction Studies of Zirconium(IV) Complexes Containing 5,7-Halogen Substituted 8-Hydroxyquinoline Ligands

This chapter contains a detailed discussion of Zr(IV) complexes containing halogen-substituted-8-hydroxyquinoline (oxine; 5,7-XOx) ligands. The importance of structural characterisation of zirconium and hafnium complexes, as discussed in detail in Chapter 2, lies also in the value of finding anomalies in the chemical behaviours of these two metals, with an overarching aim of exploiting these differences for separation purposes from base ore sources. In this case a study of solid state characteristics is evaluated with similar ligands chelated to zirconium, specifically.

The oxine ligand family forms a significant part of the interest in this case, partially due to the fact that they are known as potential extracting agents of metal ions in dilute solutions.[1] An integral part of this project has been focused on employing different commercially available oxine ligands, with various substituents on the 5 and 7 positions of the quinoline back-bone (Figure 4.1). These substituents alter the electronic characteristics of the ligand as a whole, influencing the chelation aspects of the final organometallic complex. Furthermore, when considering that very little of these zirconium and hafnium complexes have been structurally characterised,[2] it becomes apparent that a crystallographic study of metal complexes containing this ligand family could have a considerable influence on experimental design regarding separation studies utilizing such ligands.

---

[1] D.L. Huges & M.R. Truter; *J. Chem. Soc. Dalton Trans.* (**1979**), 520-527.
[2] The Cambridge Structural Database, Licence Update Feb 2013; F. H. Allen; *Acta Cryst. B58* (**2002**), 380-388.

In the following paragraphs, the crystallographic structure determination of three zirconium-oxine complexes is presented in detail as well as the correlation of each structure with other similar structures of zirconium and hafnium. An in depth discussion of the literary and theoretical interest in these types of ligands can be found in § 2.3.4.
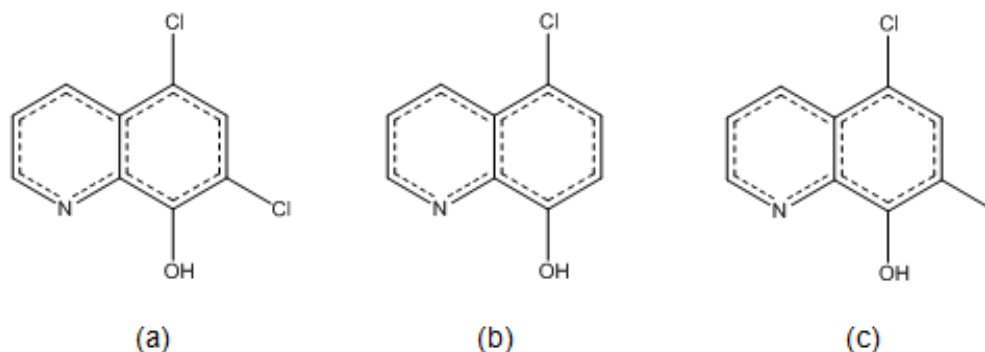
Figure 4.1 Oxine ligands chelated to zirconium and discussed in this chapter.
(**a**) 5,7-Dichloro-8-hydroxyquinoline (diClOxH); (**b**) 5-Chloro-8-hydroxyquinoline (5-ClOxH);
(**c**) 5-Chloro-7-iodo-8-hydroxyquinoline (CliOxH).

4.1. Experimental

The X-ray intensity data was collected on a Bruker X8 ApexII 4K Kappa CCD area detector diffractometer, equipped with a graphite monochromator and MoKα fine-focus sealed tube (λ = 0.71069 Å, T = 100(2) K) operated at 2.0 kW (50 kV, 40 mA). The initial unit cell determinations and data collections were done by the SMART[3] software package. The collected frames were integrated using a narrow-frame integration algorithm and reduced with the Bruker SAINT-Plus and XPREP software packages[4] respectively. Analysis of the data showed no significant decay during the data collection. Data was corrected for absorption effects using the multi-scan technique SADABS,[5] and the structure was solved by the direct methods package SIR97[6] and refined using the WinGX[7] software incorporating SHELXL.[8] The final anisotropic full-matrix least-squares refinement was done on F^2.

---

[3] Bruker SMART-NT Version 5.050.Bruker AXS Inc. Area-Detector Software Package; Madison, WI, USA, **1998.**
[4] Bruker SAINT-Plus Version 6.02 (including XPREP), Bruker AXS Inc. Area-Detector Integration Software, Madison, WI, USA, **1999.**
[5] Bruker SADABS Version 2004/1.Bruker AXS Inc. Area Detector Absorption Correction Software, Madison, WI, USA, **1998.**
[6] A. Altomare, M.C. Burla, M. Camalli, G.L. Cascarano, C. Giacovazzo, A. Guagliardi, A.G.G. Moliterni, G. Polidori & R. Spagna; *J. Appl. Cryst. 32* (**1999**), 115-119.
[7] L.J. Farrugia; *J. Appl. Cryst. 32* (**1999**), 837-838.
[8] G.M. Sheldrick; SHELXL97. *Program for crystal structure refinement*, University of Göttingen, Germany, **1997.**

The methyl and aromatic protons were placed in geometrically idealized positions (C–H = 0.93 – 0.98 Å) and constrained to ride on their parent atoms with $U_{iso}(H) = 1.2U_{eq}(C)$. Non-hydrogen atoms were refined with anisotropic displacement parameters. The graphics were obtained with the DIAMOND[9] program with 50% probability ellipsoids for all non-hydrogen atoms.

Note: General Considerations throughout the following text

1. Oxine ligands are numbered from the N-atom, following sequentially around both rings (Figure 4.2).
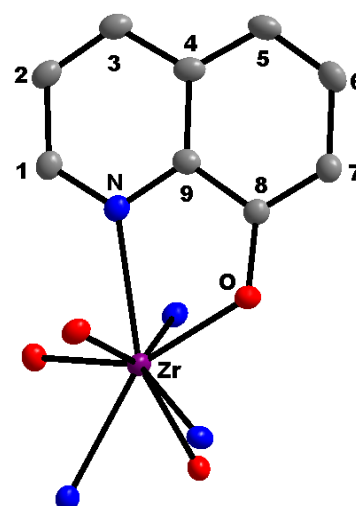
Figure 4.2 Oxine atom numbering

2. Each individually characterised ligand (i.e. independent ligands not symmetrically generated) around the metal centre is numbered consecutively, and referred to in short "Lig#" with # = 1 - 4. Ligands are identified by the numbering of the nitrogen and oxygen atoms of the ligand coordinated to the metal centre. Furthermore, independent ligand planes are coloured systematically throughout the text (Figure 4.3)
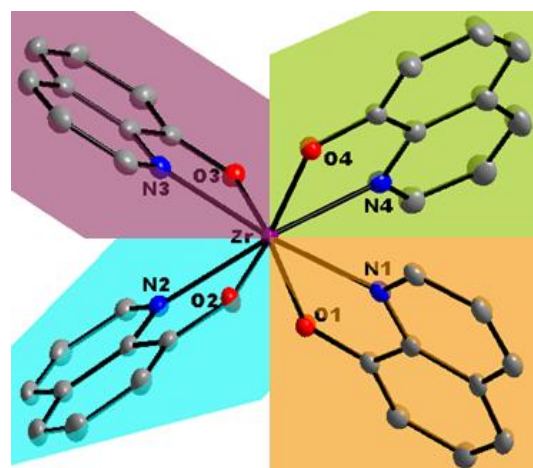
Figure 4.3 Ligand numbering and plane colours.

3. Ligands in *tetrakis*-coordinated zirconium(iv) structures are generally arranged in a space filling fan-like arrangement, with no specific geometric planes as a point of reference, due to the square-antiprismatic coordination polyhedron. The higher coordination isomeric description of these structures is illustrated in two ways.

---

[9] K. Brandenburg & H. Putz; DIAMOND, *Release 3.0e, Crystal Impact GbR*, Bonn, Germany, **2006.**

a. Firstly, the placement of the N- and O- coordination atoms of the oxine ligands are observed as either *mirrored* or *alternating* in the positioning of these atoms across the metal centre (Figure 4.4).
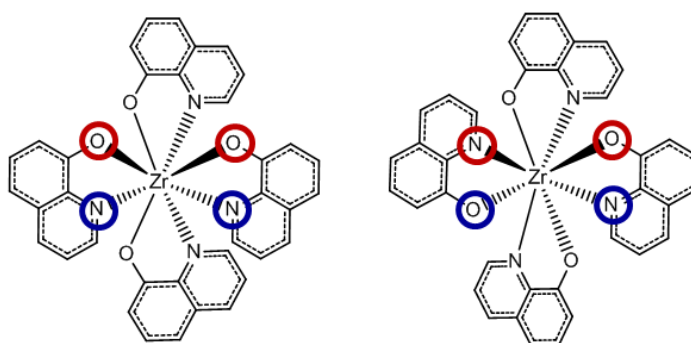
Figure 4.4 Coordinate ox-ligand arrangement around the metal centre when considering the N- and O- coordination sites; (**left**) Mirrored; (**right**) Alternating.

b. Secondly, from the discussion on eight-coordinated and square antiprismatic geometry found in metal complexes included in § 2.5, three possible isomers are observed and classified. As described earlier, for complexes with four O,O-donating bidentate ligands chelated (specifically the β-diketone type ligands) and exhibiting a square antiprismatic arrangement of these ligands around the metal centre, the specific position of the bidentate ligands on the square antiprism dictates the named isomer.[10] As illustrated in Figure 4.5, the three possible isomers that can be visualised are a corner-clipped ligand placement (Fig 4.5a - D_2), side-clipped coordination (Fig 4.5b - D_4) or a combination of these two (Fig 4.5c - C_2).

(a) (b) (c)
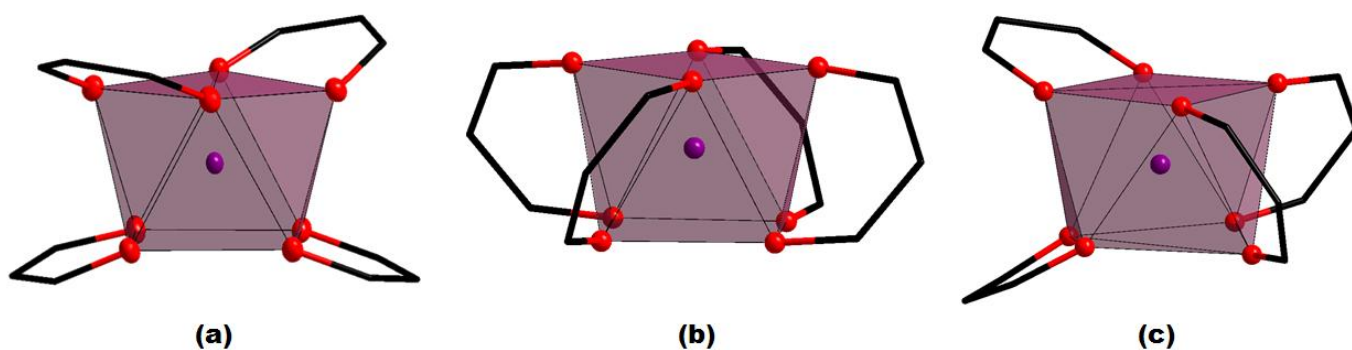
Figure 4.5 Coordination isomers as defined for *tetrakis*(β-diketone)metal complexes exhibiting a square antiprismatic coordination polyhedron. (**a**) D_2 - Corner-clipped ligands; (**b**) D_4 - Side-clipped ligands; (**c**) C_2 - Combination corner- and side-clipped ligands.

---

[10] C.W. Haigh; *Polyhedron 15* (**1995**), 605-643.

In the case of these N,O-donating oxine ligands, the same isomers are possible but with a further addition of two subcategories of the D_2 corner-clipped isomer. These two isomers are directly dependant on the placement of the oxine ligands with respect to each other across the metal centre, as illustrated in Figure 4.4 earlier. As depicted in Figure 4.6, the corner-clipped ligands display two distinct directionalities in which they are coordinated with respect to each other on the square antiprism frame. Depending on the *mirrored* or *alternating* placement of N- and O-coordination sites, either a D_2^x (ligands placed across the *x*-axis) or a D_2^z (ligands placed across the *z*-axis) is possible. This specific sub-category of isomer is only observed in this case of N,O-donating oxine ligands, as described here. Furthermore, they are distinctly defined by the reference location of the coordinating atoms on the eight corners of the square antiprism, for these unsymmetrical ligands.
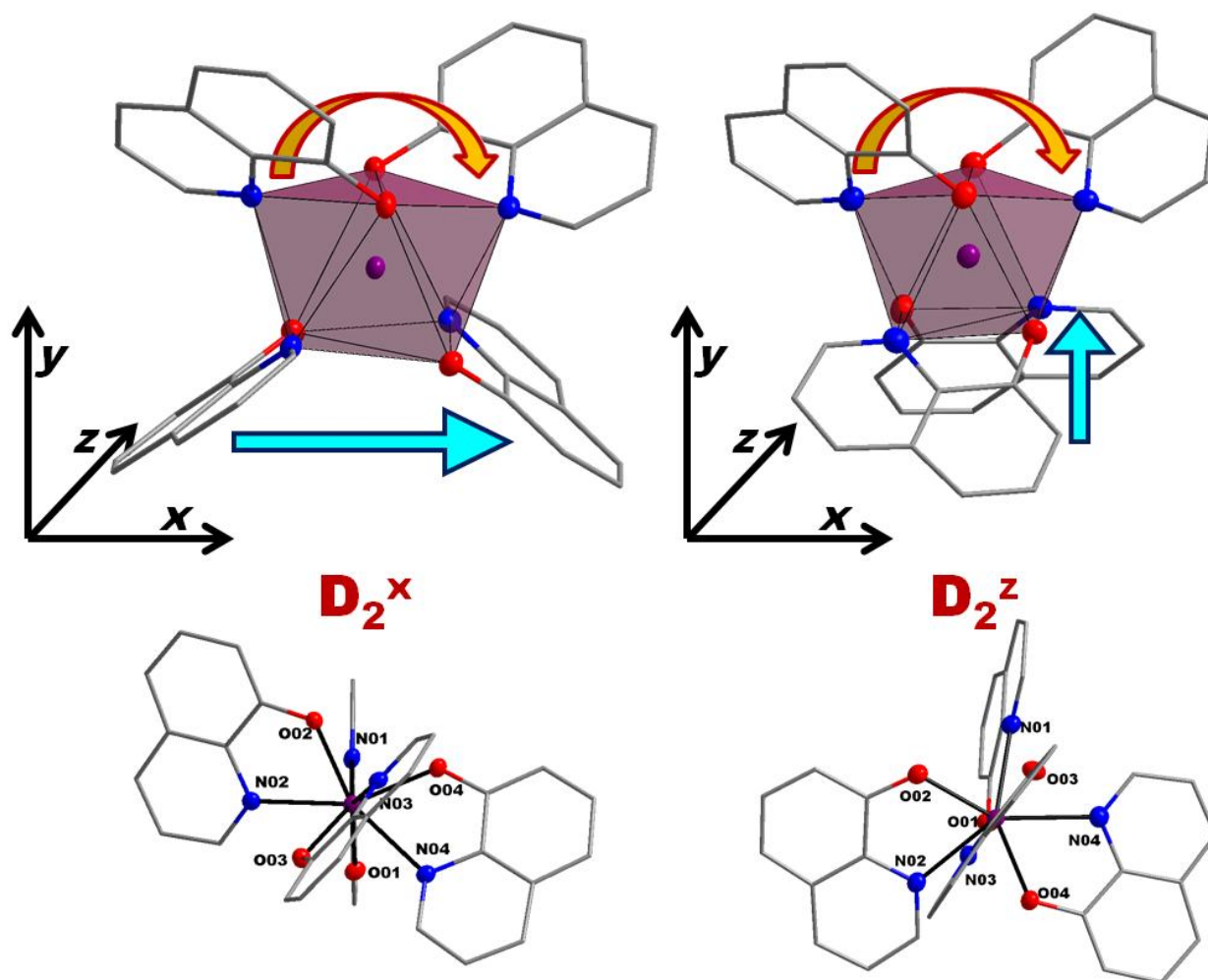
Figure 4.6 Coordination isomer sub-category illustration of the corner-clipped D_2 species observed, when considering the arrangement of the ligands at the bottom square of the antiprism (**left**) D_2^x - ligands arranged across the *x*-axis; (**right**) D_2^z - ligands arranged across the *z*-axis.

Table 4.1 Crystallographic and Refinement Details for structures discussed in this chapter.

Crystal Formula	[Zr(diClOx)$_4$]·2DMF (Zr_1a)	[Zr(5-ClOx)$_4$]·2DMF (Zr_1f)	[ZrCl(CliOx)$_2$(DMF)$_2$O]$_2$·DMF (Zr_1d)
Empirical formula	C$_{42}$ H$_{30}$ Cl$_8$ N$_6$ O$_6$Zr	C$_{78}$ H$_{54}$ Cl$_8$ N$_{10}$ O$_{10}$ Zr$_2$	C$_{45}$ H$_{37}$ Cl$_6$ I$_4$ N$_7$ O$_8$ Zr$_2$
Formula weight (g.mol^{-1})	2175.57	1757.35	853.28
Crystal system, Space Group	Monoclinic, C2/c	Monoclinic, P2$_1$/c	Monoclinic, P2$_1$/c
Unit cell dimensions:			
a, b, c (Å)	30.357(4), 13.037(5), 26.386(4)	18.678(3), 21.176(5), 20.148(2)	14.634(5), 13.712(4), 14.710(4)
α, β, γ (°)	90.0, 118,343(5), 90.0	90.0, 90.894(4), 90.0	90.00, 114.073(5), 90.0
Volume (Å^3), Z	9191(4), 4	7968(2), 4	2695.0(16), 4
Density (calculated, mg.cm^{-3})	1.572	1.465	2.103
Crystal morphology	plate	cuboid	cuboid
Crystal Colour	yellow	yellow	yellow
Crystal size (mm^3)	0.086 x 0.179 x 0.274	0.074 x 0.101 x 0.219	0.072 x 0.163 x 0.170
Absorption coefficient μ (mm^{-1})	0.758	0.593	3.033
F(000)	4376	3552	1628
Theta range	2.10 to 28.00	2.28 to 26.00	2.78 to 28.00
Index ranges	-40 ≤ h ≤ 40	-23 ≤ h ≤ 22	-19 ≤ h ≤ 19
	-16 ≤ k ≤ 17	-26 ≤ k ≤ 26	-18 ≤ k ≤ 16
	-34 ≤ l ≤ 33	-24 ≤ l ≤ 24	-19 ≤ l ≤ 19
Reflections collected, Independent Reflections, R$_{int}$	59147, 11076, 0.0343	63079, 15607, 0.0487	37888, 6485, 0.0299
Completeness to 2θ (°, %)	28.0, 99.8	26.00, 99.7	28.00, 99.7
Max. and min. transmission	-	-	0.8158 and 0.6266
Data, restraints, parameters	11076, 25, 607	15607, 150, 1044	6485, 4, 342
Goodness-of-fit on F^2	1.047	1.024	1.047
Final R indices [I>2σ(I)]	R$_1$ = 0.0409	R$_1$ = 0.0677	R$_1$ = 0.0314
	wR$_2$ = 0.0962	wR$_2$ = 0.1842	wR$_2$ = 0.0737
R indices (all data)	R$_1$ = 0.0573	R$_1$ = 0.1010	R$_1$ = 0.0393
	wR$_2$ = 0.1087	wR$_2$ = 0.2212	wR$_2$ = 0.0791
Largest diff. peak and hole (e.Å^{-3})	0.925 and -1.045	1.501 and -0.757	2.346 and -1.787

4.2. Crystal Structure of [Zr(diClOx)₄].2DMF – Zr_1a

The structure of this *tetrakis*-coordinated zirconium - 5,7-dichloro-8-hydroxyquinoline complex[11] (**Zr_1a**) is one of few examples of zirconium-oxine crystallographically characterised structures available in published literature to date. Synthesis of **Zr_1a** and the resulting yellow crystals obtained for this was discussed in § 3.2.1.1.

A summary of the general crystal data is given in Table 4.1, while the numbering scheme of the solvated complex is shown in the perspective drawing in Figure 4.7. Table 4.2 presents selected bond lengths and angles of the title compound. Atomic coordinates, anisotropic displacement parameters, bond distances and angles and hydrogen coordinates, are given in the supplementary data (Appendix A.1). Hydrogen atoms and/or solvent molecules are omitted in some figures for clarity.
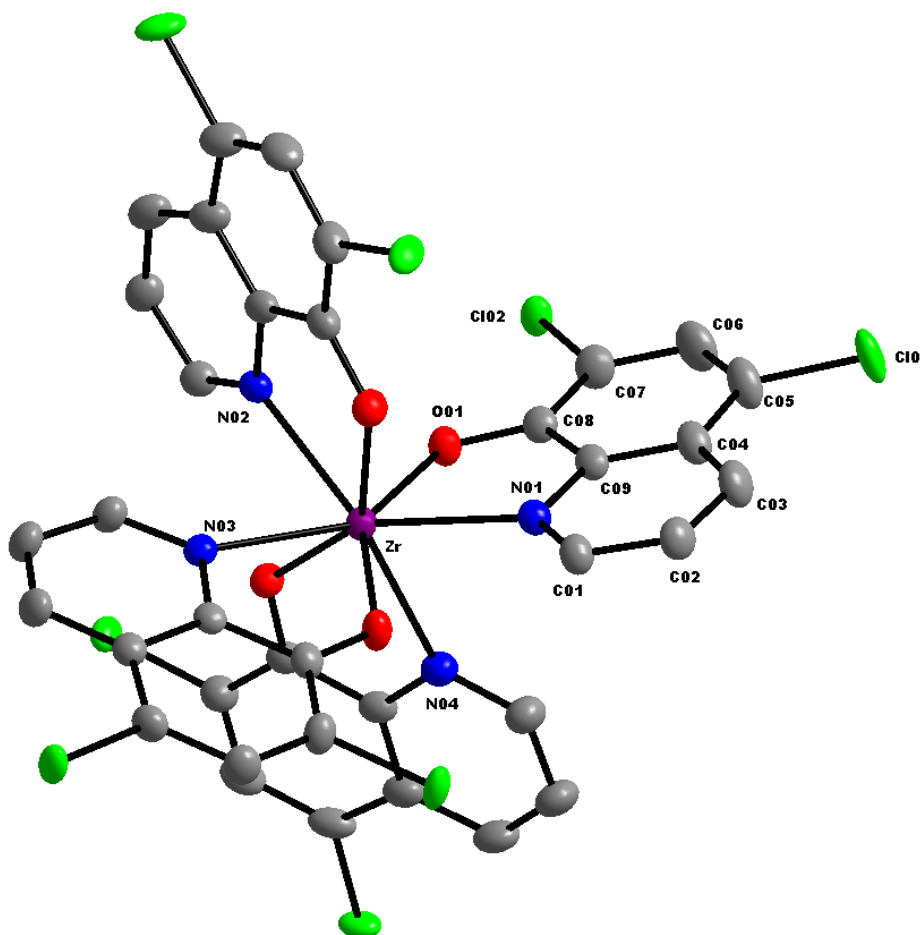
Figure 4.7 Graphic illustration of [Zr(diClOx)₄].2DMF showing general numbering of atoms. Displacement ellipsoids drawn at 50% probability. Hydrogen atoms and solvent molecules omitted for clarity.

[11] M. Steyn, H.G. Visser & A. Roodt; *Z. Kristallogr. - New Cryst. Struct. 228* **(2013)**, 3, 413-415.

The compound *tetrakis*(5,7-dichloroquinolin-8-olato-κ^2N,O)zirconium(IV) dimethylformamide disolvate, crystallizes in the monoclinic space group, *C*2/*c*. The asymmetric unit consists of a Zr(IV) metal centre coordinated to four bidentate ligands (5,7-dichloroquinolin-8-olate = diClOx⁻). Two crystallographically independent N,N'-dimethylformamide (DMF) solvent molecules fill the rest of the asymmetric unit. Both these solvent molecules are separately disordered, each in a different manner. One DMF molecule is disordered in a 68.7(1) %:31.3(1) % ratio over the carbonyl N—C—O section of the molecule. The other DMF solvent is placed in a disordered arrangement of 52.3(5) % : 47.7(5) % with a translation of the entire molecule.

Table 4.2 Selected Geometric Parameters for [Zr(diClOx)$_4$].2DMF (**Zr_1a**).

Selected Bond Lengths (Å)			
Zr—N$_{01}$	2.417(2)	Cl$_{01}$—C$_{05}$	1.739(3)
Zr—N$_{02}$	2.415(2)	Cl$_{02}$—C$_{07}$	1.735(3)
Zr—N$_{03}$	2.485(2)	Cl$_{03}$—C$_{14}$	1.740(3)
Zr—N$_{04}$	2.491(2)	Cl$_{04}$—C$_{16}$	1.729(3)
Zr—O$_{01}$	2.113(2)	Cl$_{05}$—C$_{23}$	1.741(3)
Zr—O$_{02}$	2.110(2)	Cl$_{06}$—C$_{25}$	1.732(3)
Zr—O$_{03}$	2.075(2)	Cl$_{07}$—C$_{32}$	1.739(3)
Zr—O$_{04}$	2.081(2)	Cl$_{08}$—C$_{34}$	1.728(3)
Selected Bite Angles (°)			
N$_{01}$—Zr—O$_{01}$	70.21(7)	N$_{03}$—Zr—O$_{03}$	69.28(7)
N$_{02}$—Zr—O$_{02}$	70.43(7)	N$_{04}$—Zr—O$_{04}$	69.17(7)
Selected Geometric Coordination Angles (°)			
N$_{01}$—Zr—N$_{02}$	127.85(7)	O$_{01}$—Zr—O$_{02}$	94.51(8)
N$_{01}$—Zr—N$_{03}$	135.11(7)	O$_{01}$—Zr—O$_{03}$	141.28(7)
N$_{01}$—Zr—N$_{04}$	75.36(7)	O$_{01}$—Zr—O$_{04}$	90.82(7)
N$_{02}$—Zr—N$_{03}$	74.76(7)	O$_{02}$—Zr—O$_{03}$	90.78(8)
N$_{02}$—Zr—N$_{04}$	135.33(7)	O$_{02}$—Zr—O$_{04}$	141.24(7)
N$_{03}$—Zr—N$_{04}$	118.11(7)	O$_{03}$—Zr—O$_{04}$	108.41(8)
Selected Torsion Angles (°)			
N$_{01}$—C$_{09}$—C$_{08}$—O$_{01}$	0.14(40)	N$_{03}$—C$_{27}$—C$_{26}$—O$_{03}$	1.19(37)
N$_{02}$—C$_{18}$—C$_{17}$—O$_{02}$	1.17(39)	N$_{04}$—C$_{36}$—C$_{35}$—O$_{04}$	0.79(39)
Ligand Plane Angles (°)			
Lig1/Lig2	80.45(4)	Lig3/Lig4	84.69(4)
Lig2/Lig3	84.75(5)	Lig4/Lig1	86.84(4)
Lig1/Lig3	151.21(4)	Lig2/Lig4	152.34(4)

The N,O-donating ligands surrounding the metal centre, are placed in a space filling, fan-like arrangement to give an approximate square-antiprismatic coordination polyhedron (Figure 4.8), with a slight outward distortion towards dodecahedral geometry. This distortion from the ideal square antiprism is associated with an outward bend of 19.46(7) °, as illustrated in Figure 4.9.

In this structure the average Zr—N and Zr—O bond distances are 2.452(2) Å and 2.095(2) Å, respectively, and the average N—Zr—O bite angle is found to be 69.77(7) ° (Table 4.2). The measured N—C—C—O torsion angles of the ligand frame facing the N—Zr—O bite angles are found to range from 0.14(40) ° to 1.19(37) °, indicating very little deviation from the planarity of the ligands themselves.
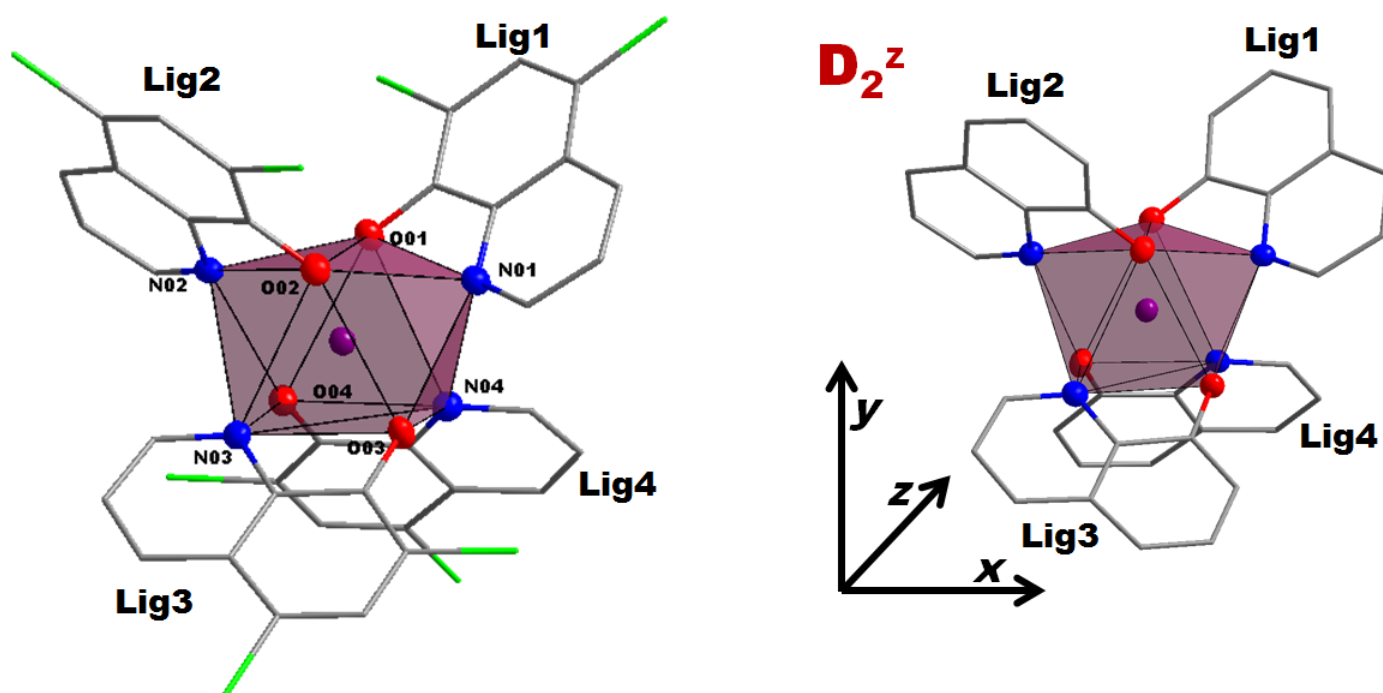
Figure 4.8 Graphic illustration of the square-antiprismatic coordination polyhedron of [Zr(diClOx)$_4$]. (**left**) Side view showing upper and lower four corners represented by the N- and O-coordinating atoms of the ligands; (**right**) Isomer description as determined from the placement of the ox-ligands on the square antiprism - in this case the corner-clipped D$_2^z$.
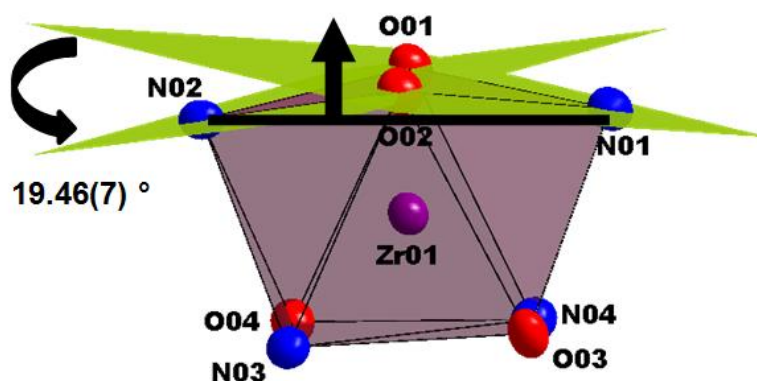
Figure 4.9 Illustration of the distortion of the square-antiprismatic coordination polyhedron found in [Zr(diClOx)$_4$], showing the outward bend of the top-most atoms at an angle of 19.46(7) °.

From Figure 4.10 it can be seen that each coordinated ligand is duplicated by an opposite facing one *via* an approximate two-fold rotation axis, when looking diagonally (from top to bottom) of the square antiprism. In other words Lig4 is duplicated by Lig2, and so on. Although these duplicated ligands do not lie in a flat plane opposite each other, it is clear that the ligands are chelated to the metal centre with an *alternating* placement of the N- and O-coordinating sited. With regard to the overall coordination description of the ligands as viewed in the square antiprism (Figure 4.8), the title compound crystallises as a D_2^z corner-clipped isomer.
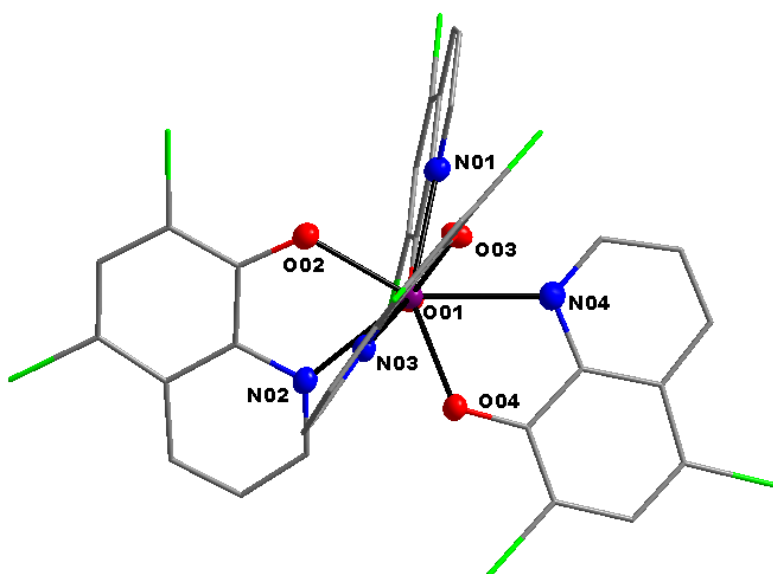
Figure 4.10 Graphical illustration of the *alternating* placement of the diClOx ligands across the metal centre in the title molecule, with the arrangement of N_{01} & O_{03} and O_{02} & N_{04} opposite each other, respectively. Hydrogens and solvent molecules omitted for clarity.

The coordinating ligands are thus characterised by "opposite" ligand pairs and "adjacent" ligand pairs, and are described further as such, respectively. The planes defined by each individual ligand appear flat, with no deviation of any one atom out of the plane. This is also illustrated by the torsion angles for these ligands as reported in Table 4.2. These "ligand-planes" (Figure 4.11) lie across the metal centre at angles of 151.21(4) ° (Lig1/Lig3) and 152.34(4) ° (Lig2/Lig4) for each opposite facing pair. The dihedral angles between adjacent ligand planes range from 80.45(4) ° at the smallest (Lig1/ Lig2) to 86.84(4) ° at the largest (Lig1/Lig4) as reported in Table 4.2.
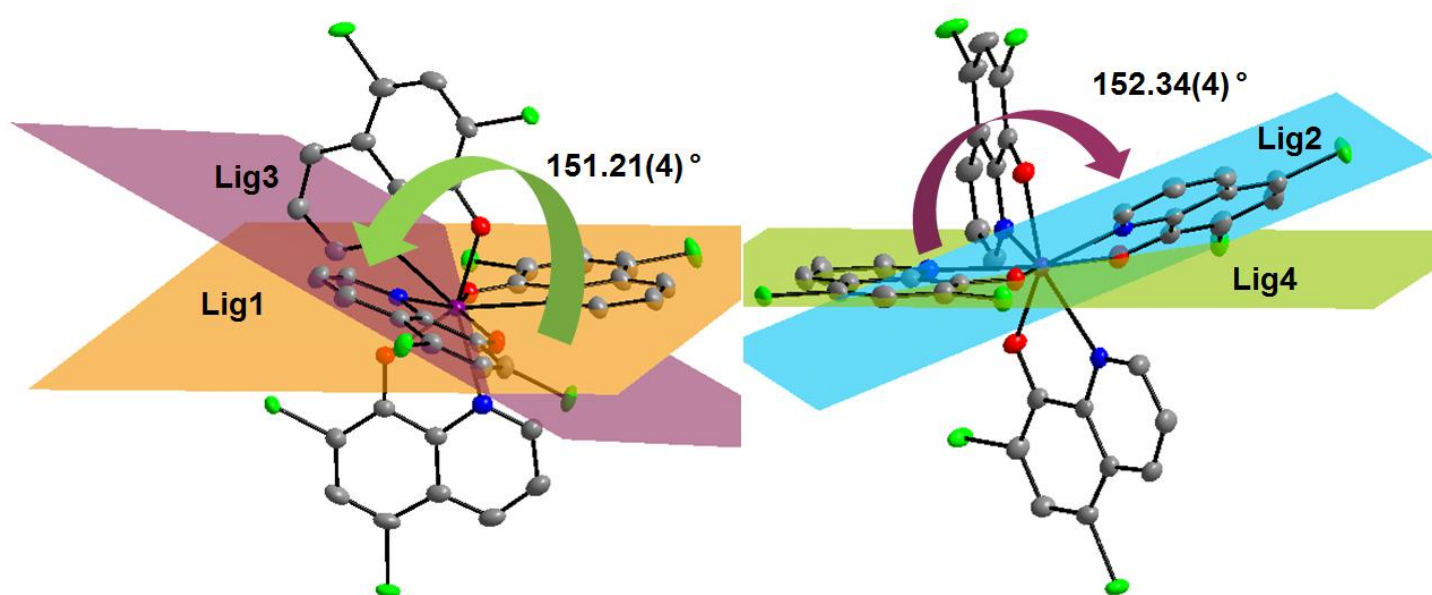
Figure 4.11 Illustration of the different ligand planes measured across the Zr metal centre. (**left**) Lig1/Lig3 at an angle of 151.21(4) °; (**right**) Lig2/Lig4 at an angle of 152.34(4) °.

Only one intra-molecular C—H•••O hydrogen bonding interaction is observed between two diClOx-ligands, Lig1 & Lig3 (Figure 4.12, Table 4.3).
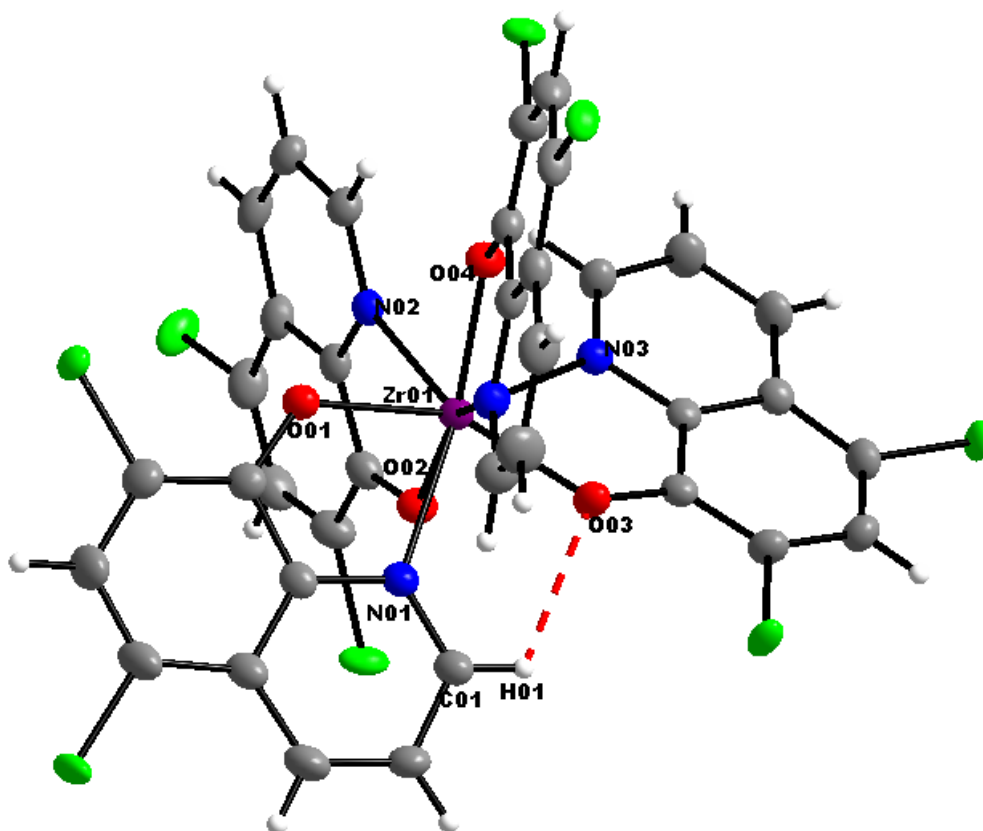
Figure 4.12 Illustration of the intra-molecular hydrogen bonding interaction found in the title molecule.
C_{01}—H_{01}•••O_{03} (Table 4.3).

Table 4.3 Hydrogen-bond geometry in the title compound (Å, °).

D—H···A	*D—H*	*H···A*	*D···A*	*D—H···A*
C_{01}—H_{01}···O_{03}	0.93	2.37	2.878(4)	113.9(2)

Crystal lattice stabilization is further influenced by π–π interactions between the benzene rings of the diClOx-ligands and symmetry generated counterparts (-x,-y,-z) of neighbouring molecules, with interplanar and centroid-to-centroid distances of 3.410(4) Å and 3.682(1) Å, respectively (Figure 4.19). Furthermore, a Cl•••C interaction is observed between Cl_{07} and C_{27}(-x,-y,-z), of neighbouring molecules. The effects of the π–π stacking and Cl•••C interactions form a network of molecule pairs packing diagonally across the *ab*-plane (Figure 4.13).
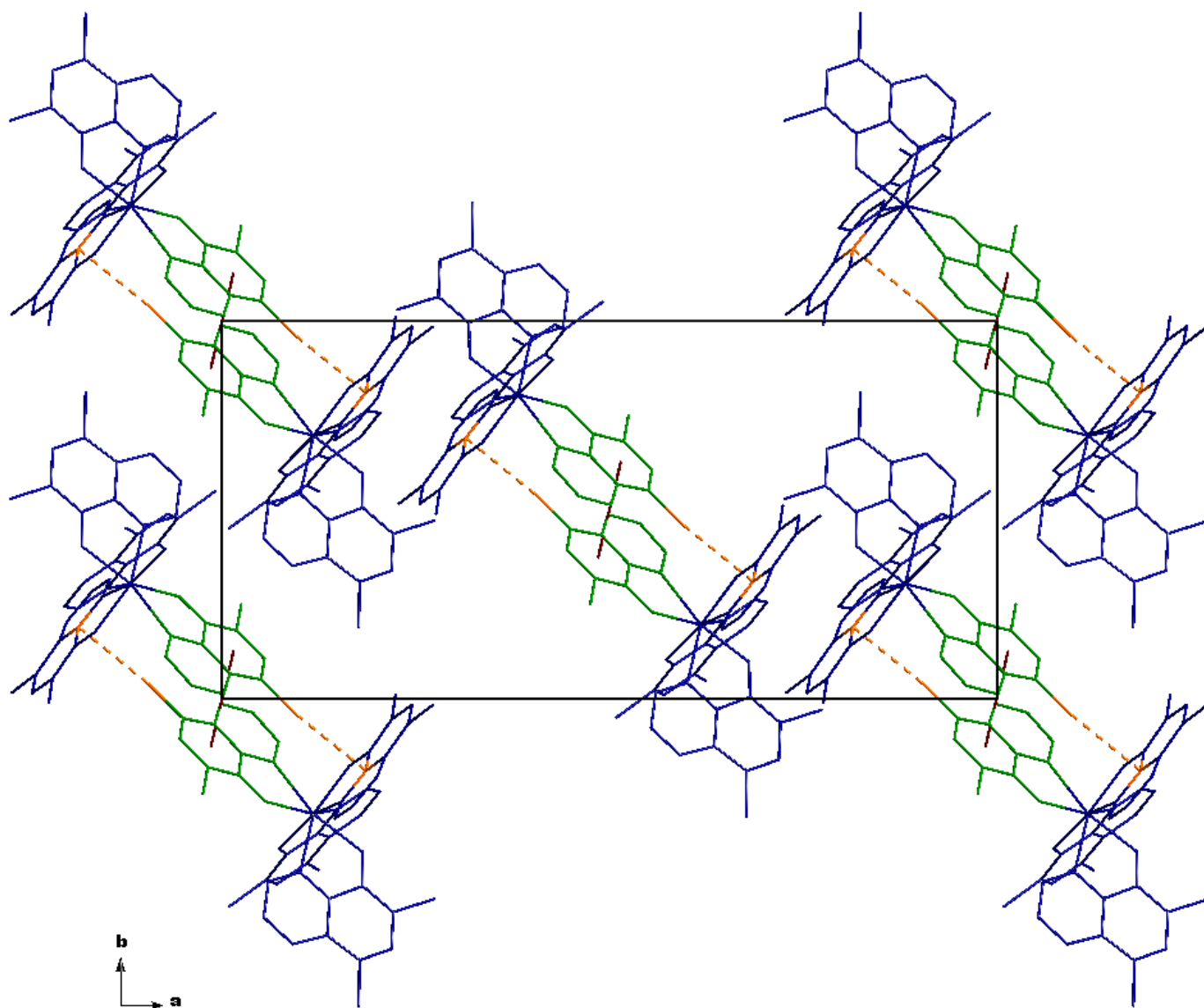
Figure 4.13 Graphical illustration of the head-to-head packing found in the title compound, depicting the paired π–π interactions between the benzene rings of the diClOx Lig4 and symmetry generated counterpart (-x,-y,-z) (— — —), as well as Cl•••C interaction between neighboring molecules; Cl_{07}•••C_{27} (-x,-y,-z), 3.152 Å, (— — — — —).

4.3. Crystal Structure of [Zr(5-ClOx)$_4$].2DMF – Zr_1f

The structure of this *tetrakis*-coordinated zirconium - 5-chloro-8-hydroxyquinoline complex (**Zr_1f**) is one of few examples of zirconium-oxine structures exhibiting two unique molecules in the asymmetric unit. Synthesis of **Zr_1f** and the resulting yellow crystals obtained for this was discussed in § 3.2.1.6.

A summary of the general crystal data is given in Table 4.1, while the numbering scheme of the solvated complex is shown in the perspective drawing in Figure 4.14. Table 4.4 presents selected bond lengths and angles of the title compound. Atomic coordinates, anisotropic displacement parameters, bond distances and angles and hydrogen coordinates, are given in the supplementary data (Appendix A.2). Hydrogen atoms and/or solvent molecules are omitted in some molecular presentations for clarity.
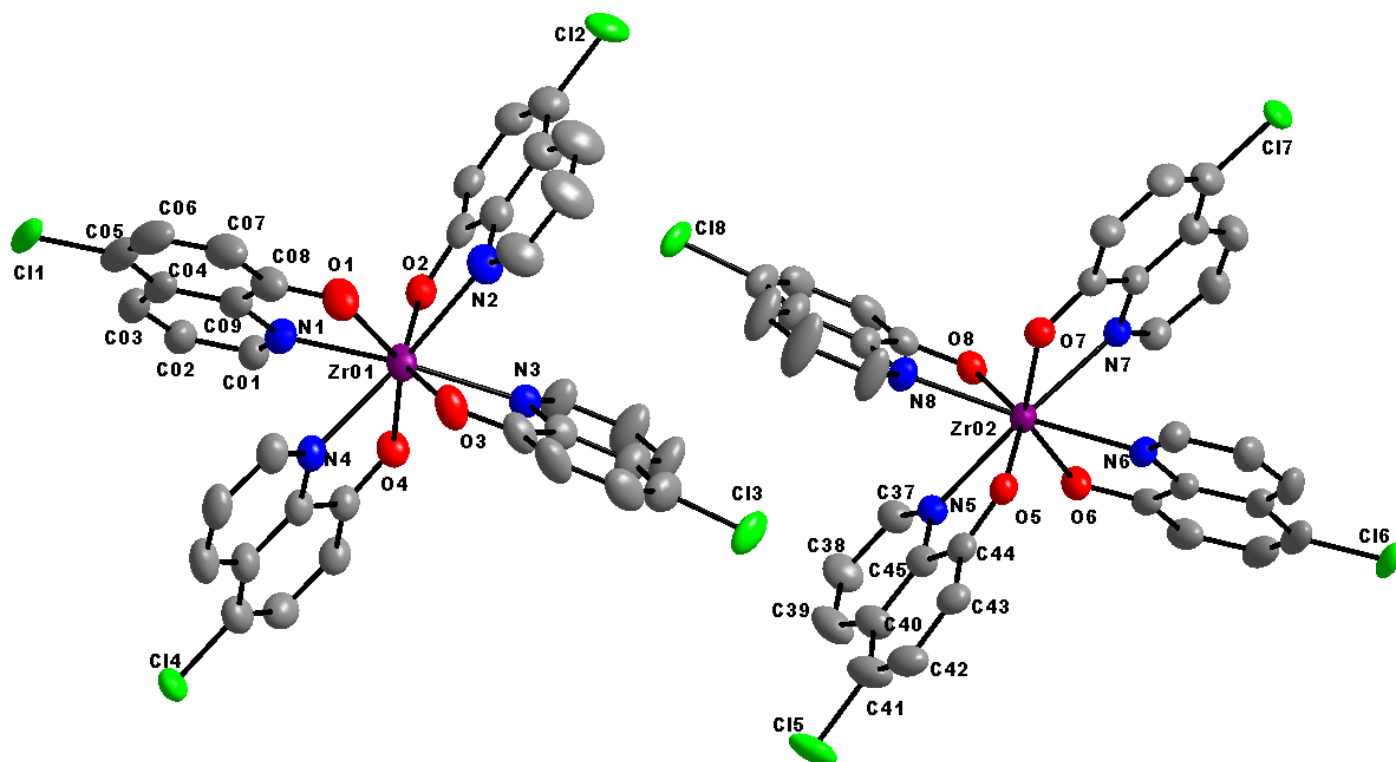
Figure 4.14 Graphic illustration of [Zr(5-ClOx)$_4$].2DMF showing general numbering of atoms. Displacement ellipsoids drawn at 50% probability. Hydrogen atoms and solvent molecules omitted for clarity.

The compound *tetrakis*(5-chloroquinolin-8-olato-$\kappa^2 N,O$)zirconium(IV)dimethylformamide disolvate, crystallizes in the monoclinic space group, *P2$_1$/c*. The asymmetric unit consists of two Zr(IV) metal centres, each coordinated to four bidentate ligands (5-chloroquinolin-8-olate = 5-ClOx$^-$). Two crystallographically independent N,N'-dimethylformamide (DMF) solvent molecules fill the rest of the asymmetric unit. One of the DMF solvent molecules is disordered over 3 positions in a 38.1(5) %: 37.9(5) %: 24.2(7) % ratio.

Table 4.4 Selected Geometric Parameters for [Zr(5-ClOx)$_4$].2DMF (**Zr_1f**). For Zr$_n$—X$_m$, molecule Zr$_1$: n = 01, m = 01-04; molecule Zr$_2$: n = 02, m = 05-08; X = N, O, Cl.

Selected Bond Lengths (Å)					
Zr$_{01}$—N$_{01}$	2.423(5)	**Zr$_{01}$—O$_{01}$**	2.103(4)	**Cl$_{01}$—C$_{05}$**	1.746(7)
Zr$_{01}$—N$_{02}$	2.429(5)	**Zr$_{01}$—O$_{02}$**	2.103(4)	**Cl$_{02}$—C$_{14}$**	1.757(6)
Zr$_{01}$—N$_{03}$	2.410(4)	**Zr$_{01}$—O$_{03}$**	2.091(4)	**Cl$_{03}$—C$_{23}$**	1.739(6)
Zr$_{01}$—N$_{04}$	2.448(4)	**Zr$_{01}$—O$_{04}$**	2.100(4)	**Cl$_{04}$—C$_{32}$**	1.734(6)
Zr$_{02}$—N$_{05}$	2.431(4)	**Zr$_{02}$—O$_{05}$**	2.110(3)	**Cl$_{05}$—C$_{41}$**	1.755(6)
Zr$_{02}$—N$_{06}$	2.411(4)	**Zr$_{02}$—O$_{06}$**	2.097(3)	**Cl$_{06}$—C$_{50}$**	1.741(6)
Zr$_{02}$—N$_{07}$	2.449(4)	**Zr$_{02}$—O$_{07}$**	2.098(3)	**Cl$_{07}$—C$_{59}$**	1.739(6)
Zr$_{02}$—N$_{08}$	2.416(4)	**Zr$_{02}$—O$_{08}$**	2.096(3)	**Cl$_{08}$—C$_{68}$**	1.741(5)

Selected Bite Angles (°)			
N$_{01}$—Zr—O$_{01}$	70.05(15)	**N$_{05}$—Zr—O$_{05}$**	69.84(13)
N$_{02}$—Zr—O$_{02}$	69.55(15)	**N$_{06}$—Zr—O$_{06}$**	70.30(14)
N$_{03}$—Zr—O$_{03}$	70.31(14)	**N$_{07}$—Zr—O$_{07}$**	69.65(13)
N$_{04}$—Zr—O$_{04}$	69.76(14)	**N$_{08}$—Zr—O$_{08}$**	70.29(13)

Selected Geometric Coordination Angles (°)			
N$_{01}$—Zr—N$_{02}$	121.25(16)	**O$_{01}$—Zr—O$_{02}$**	105.06(16)
N$_{01}$—Zr—N$_{03}$	144.79(15)	**O$_{01}$—Zr—O$_{03}$**	84.95(16)
N$_{01}$—Zr—N$_{04}$	69.30(15)	**O$_{01}$—Zr—O$_{04}$**	142.91(15)
N$_{02}$—Zr—N$_{03}$	72.10(15)	**O$_{02}$—Zr—O$_{03}$**	142.54(14)
N$_{02}$—Zr—N$_{04}$	145.99(14)	**O$_{02}$—Zr—O$_{04}$**	87.65(14)
N$_{03}$—Zr—N$_{04}$	119.69(14)	**O$_{03}$—Zr—O$_{04}$**	106.08(16)
N$_{05}$—Zr—N$_{06}$	121.18(14)	**O$_{05}$—Zr—O$_{06}$**	104.73(14)
N$_{05}$—Zr—N$_{07}$	145.79(13)	**O$_{05}$—Zr—O$_{07}$**	88.07(13)
N$_{05}$—Zr—N$_{08}$	71.42(14)	**O$_{05}$—Zr—O$_{08}$**	142.41(13)
N$_{06}$—Zr—N$_{07}$	69.09(14)	**O$_{06}$—Zr—O$_{07}$**	143.58(13)
N$_{06}$—Zr—N$_{08}$	144.79(14)	**O$_{06}$—Zr—O$_{08}$**	85.32(14)
N$_{07}$—Zr—N$_{08}$	120.90(14)	**O$_{07}$—Zr—O$_{08}$**	105.26(13)

Selected Torsion Angles (°)			
N$_{01}$—C$_{09}$—C$_{08}$—O$_{01}$	-1.59(80)	**N$_{05}$—C$_{45}$—C$_{44}$—O$_{05}$**	-0.67(63)
N$_{02}$—C$_{18}$—C$_{17}$—O$_{02}$	0.11(75)	**N$_{06}$—C$_{54}$—C$_{53}$—O$_{06}$**	1.19(71)
N$_{03}$—C$_{27}$—C$_{26}$—O$_{03}$	-2.13(76)	**N$_{07}$—C$_{63}$—C$_{62}$—O$_{07}$**	0.08(62)
N$_{04}$—C$_{36}$—C$_{35}$—O$_{04}$	-0.05(71)	**N$_{08}$—C$_{72}$—C$_{71}$—O$_{08}$**	2.94(63)

Selected Torsion Angles (°)			
Lig1/Lig2	80.55(23)	**Lig5/Lig6**	80.63(21)
Lig2/Lig3	75.91(24)	**Lig6/Lig7**	56.10(22)
Lig3/Lig4	80.22(19)	**Lig7/Lig8**	76.82(20)
Lig4/Lig1	59.10(20)	**Lig8/Lig5**	74.70(21)
Lig1/Lig3	146.09(11)	**Lig5/Lig7**	132.27(16)
Lig2/Lig4	134.22(17)	**Lig6/Lig8**	146.49(11)

For both molecules in the asymmetric unit, the four 5-ClOx-ligands lie around the metal centre in a space filling, fan-like arrangement to give an approximate square-antiprismatic coordination polyhedron (Figure 4.15), with an almost negligible outward distortion towards dodecahedral geometry. This distortion from the ideal square antiprism is associated with an outward bend of 4.86(13) ° and 4.04(14) °, for the Zr_{01} and Zr_{02} molecules respectively, as illustrated in Figure 4.16.

In this structure the average Zr—N and Zr—O bond distances are 2.427(4) Å and 2.100(3) Å, respectively, and the average N—Zr—O bite angle is found to be 69.97(14) ° (Table 4.4). The measured N—C—C—O torsion angles of the ligand frame facing the N—Zr—O bite angles are found to range from -2.13(76) ° to 2.94(63) °, indicating very little deviation from the planarity of the ligands themselves.
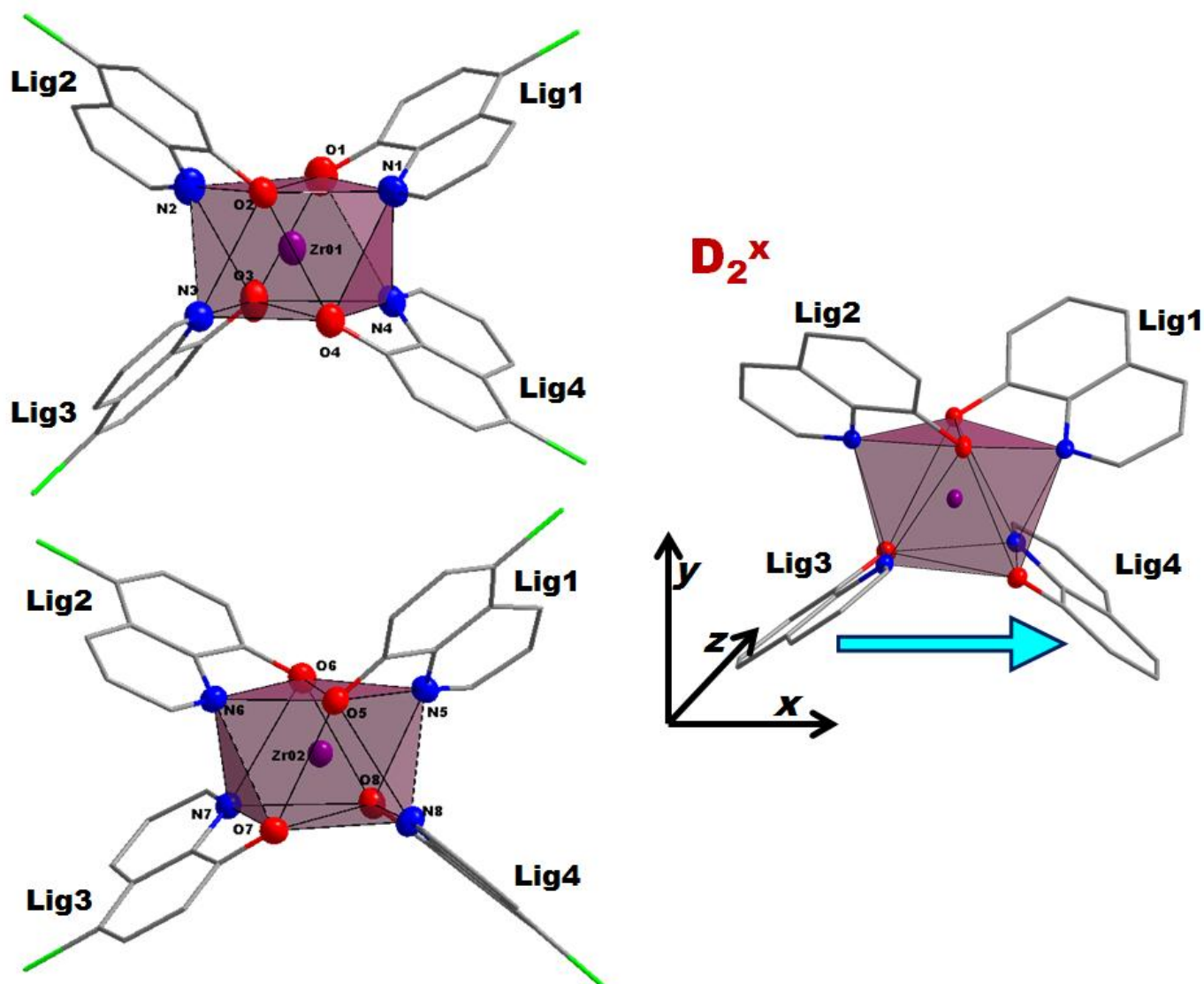
Figure 4.15 Graphic illustration of the square-antiprismatic coordination polyhedron of both [Zr(5-ClOx)$_4$] molecules in the asymmetric unit of the title compound, (**left**) Side views showing upper and lower four corners represented by the N- and O-coordinating atoms; (**right**) Isomer description as determined from the placement of the ox-ligands on the square antiprism.
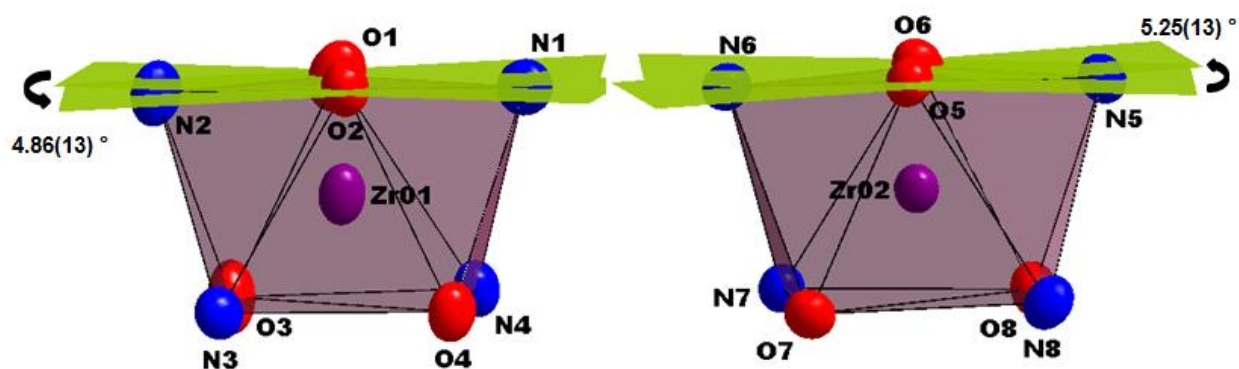
Figure 4.16 Illustration of the distortion of the square-antiprismatic coordination polyhedron found in [Zr(5-ClOx)$_4$], showing the outward bend of the top-most atoms; (**left**) Zr$_{01}$-molecule - 4.86(13) °, (**right**) Zr$_{02}$-molecule - 5.25(13) °.
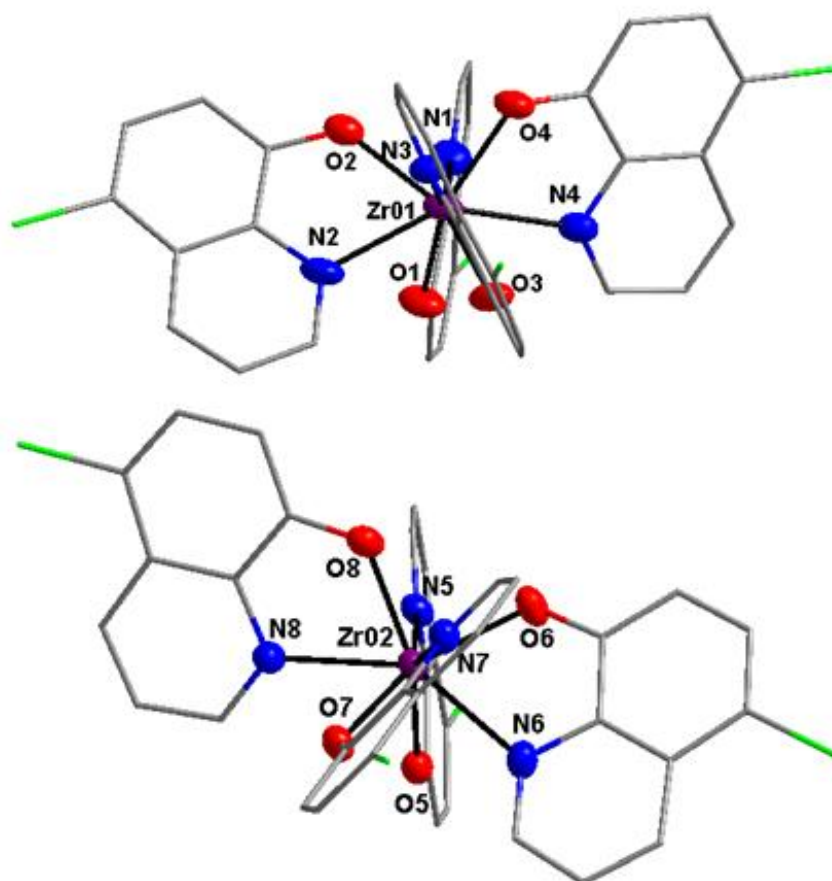
Figure 4.17 Graphical illustration of the *mirrored* placement of the 5-ClOx ligands across the two metal centers in the title molecule. Hydrogens and solvent molecules omitted for clarity. Graphical illustration of the *mirrored* placement of the 5-ClOx ligands across the metal centers in the title molecule, with the arrangement of O- and N-atoms.

From Figure 4.17 it can be seen that each coordinated ligand is duplicated by an opposite facing one *via* an approximate two-fold rotation axis, when looking diagonally (from top to bottom) of the square antiprism. In other words Lig4 is duplicated by Lig2, and so on. Although these duplicated ligands do not lie in a flat plane opposite each other, it is clear that the ligands are chelated to the metal centre with a *mirrored* placement of the N- and O- coordinating sited. With regard to the overall coordination description of the ligands as viewed in the square antiprism (Figure 4.15), the title compound crystallises as a D_2^x corner-clipped isomer for both Zr(IV)-molecules in the asymmetric unit.
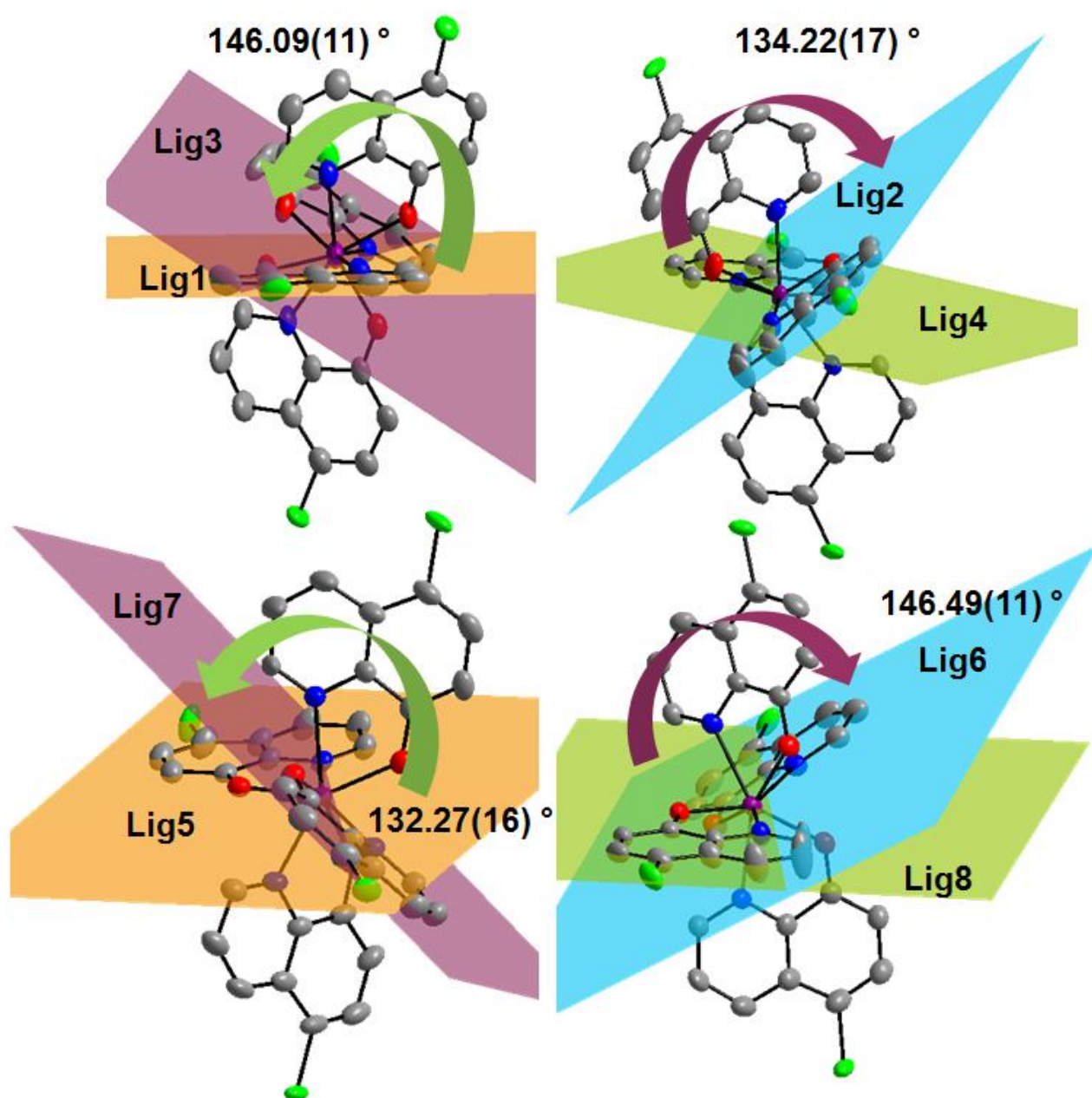
Figure 4.18 Illustration of the different ligand planes measured across the Zr metal centers in the title compound. (**top-left**) Lig1/Lig3 of the Zr_{01}-Molecule; (**top-right**) Lig2/Lig4 of the Zr_{01}-Molecule; (**bottom-left**) Lig5/Lig7 of the Zr_{02}-Molecule; (**bottom-right**) Lig6/Lig8 of the Zr_{02}-Molecule.

The coordinating ligands are thus characterised by "opposite" ligand pairs and "adjacent" ligand pairs, and are described further as such, respectively. The planes defined by each individual ligand appear flat, with no deviation of any one atom out of the plane. This is also illustrated by the torsion angles for these ligands as reported in Table 4.4. These "ligand-planes" (Figure 4.18) lie across the metal centre at angles of 146.09(11) ° (Lig1/Lig3), 134.22(17) ° (Lig2/Lig4), 132.27(16) ° (Lig5/Lig7) and 146.49(11) ° (Lig6/Lig8) for each opposite facing pair. The dihedral angles between adjacent ligand planes range from 56.10(22) ° at the smallest (Lig6/Lig7) to 80.63(21) ° at the largest (Lig5/Lig6) as reported in Table 4.4.

Many noteworthy C—H$\cdots$O hydrogen bonding interactions are observed in this structure (Table 4.5). Three *intermolecular* interactions are found in C_{48}—$H_{48}\cdots O_9^i$ (*i = x, −y+1/2, z+1/2*) - Lig6 to the non-disordered DMF solvent; C_{61}—$H_{61}\cdots O_4^i$ and C_{34}—$H_{34}\cdots O_7^{ii}$ (*ii = x, −y+1/2, z−1/2*) - double interaction between Lig4 and Lig7 of neighbouring, as illustrated in Figure 4.19.
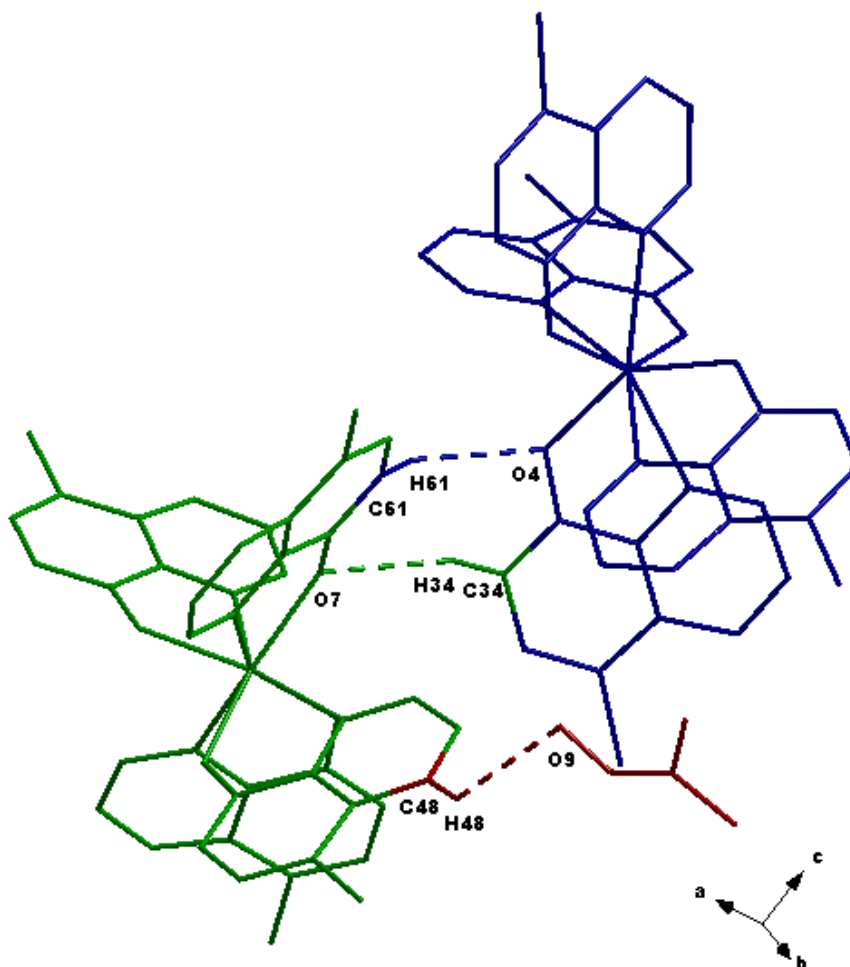
Figure 4.19 Illustration of the i*ntermolecular* hydrogen bonding interaction found in the title molecule. (**blue**) C_{61}—$H_{61}\cdots O_4$; (**green**) C_{34}—$H_{34}\cdots O_7$ and (**red**) C_{48}—$H_4 8\cdots O_9$.

Table 4.5 Hydrogen-bond geometry in the title compound (Å, °).

$D-H \cdots A$	$D-H$	$H \cdots A$	$D \cdots A$	$D-H \cdots A$ (°)
$C_{10}-H_{10} \cdots O_3$	0.93	2.56	3.044(8)	113
$C_{37}-H_{37} \cdots O_8$	0.93	2.57	3.049(6)	113
$C_{48}-H_{48} \cdots O_9^{i}$	0.93	2.56	3.197(9)	126
$C_{61}-H_{61} \cdots O_4^{i}$	0.93	2.56	3.387(7)	148
$C_{34}-H_{34} \cdots O_7^{ii}$	0.93	2.56	3.403(7)	151
Symmetry codes: (i) x, −y+1/2, z+1/2; (ii) x, −y+1/2, z−1/2.				

Moreover, two *intramolecular* C—H⋯O hydrogen bonding interactions are found between $C_{10}-H_{10} \cdots O_3$ (Lig2 to Lig3) and $C_{37}-H_{37} \cdots O_8$ (Lig5 to Lig8) in this bimolecular asymmetric unit, as shown in Figure 4.20. In other words, each of the crystallographically independent Zr-molecules interacts with each other in such a way as to form tandem pairs of metallic molecule units. Crystal lattice packing is further stabilized by Cl•••π interactions between Cl_3 (Lig3) to the benzene ring of Lig5 (Cl_3•••Bz5 = 3.339(3) Å, 177.1(3) °) and Cl_8 to the benzene ring of Lig2 (Cl_8•••Bz2 = 3.366(3) Å, 175.2(2) °). This tightly knit two-dimensional interaction network rigidly ties the crystal lattice together, influencing the overall packing in pairs of these two zirconium molecules dispersed in a head-to-head packing fashion throughout the system.
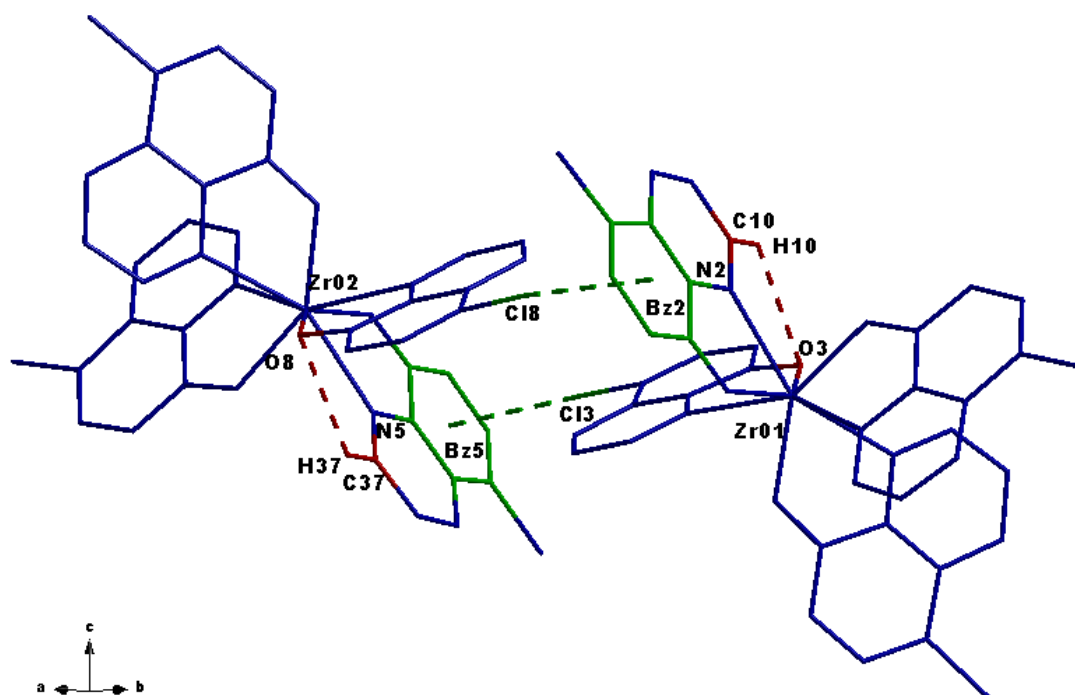
Figure 4.20 Graphical illustration of the intermolecular Cl•••π interactions (***green***) and intramolecular C—H⋯O interactions (***red***) observable between the two zirconium molecules in the asymmetric unit of the title compound. Hydrogen atoms and solvent molecules omitted for clarity.

4.4. Crystal Structure of [ZrCl(CliOx)$_2$(DMF)$_2$O]$_2$.DMF – Zr_1d

The structure of this mono-oxo bridged zirconium - Clioquinoline complex[12] (**Zr_1d**) is a unique example of zirconium-oxine (and more significantly of zirconium-bidentate ligand complexes) structures available in literature to date. Synthesis of **Zr_1d** and the resulting yellow crystals obtained for this was discussed in § 3.2.1.4.

A summary of the general crystal data is given in Table 4.1, while the numbering scheme of the solvated complex is shown in the perspective drawing in Figure 4.21. Table 4.6 presents selected bond lengths and angles of the title compound. Atomic coordinates, anisotropic displacement parameters, all bond distances and angles and hydrogen coordinates, are given in the supplementary data (Appendix A.3). Hydrogen atoms and/or solvent molecules are omitted in some portions of the molecular representations for clarity.
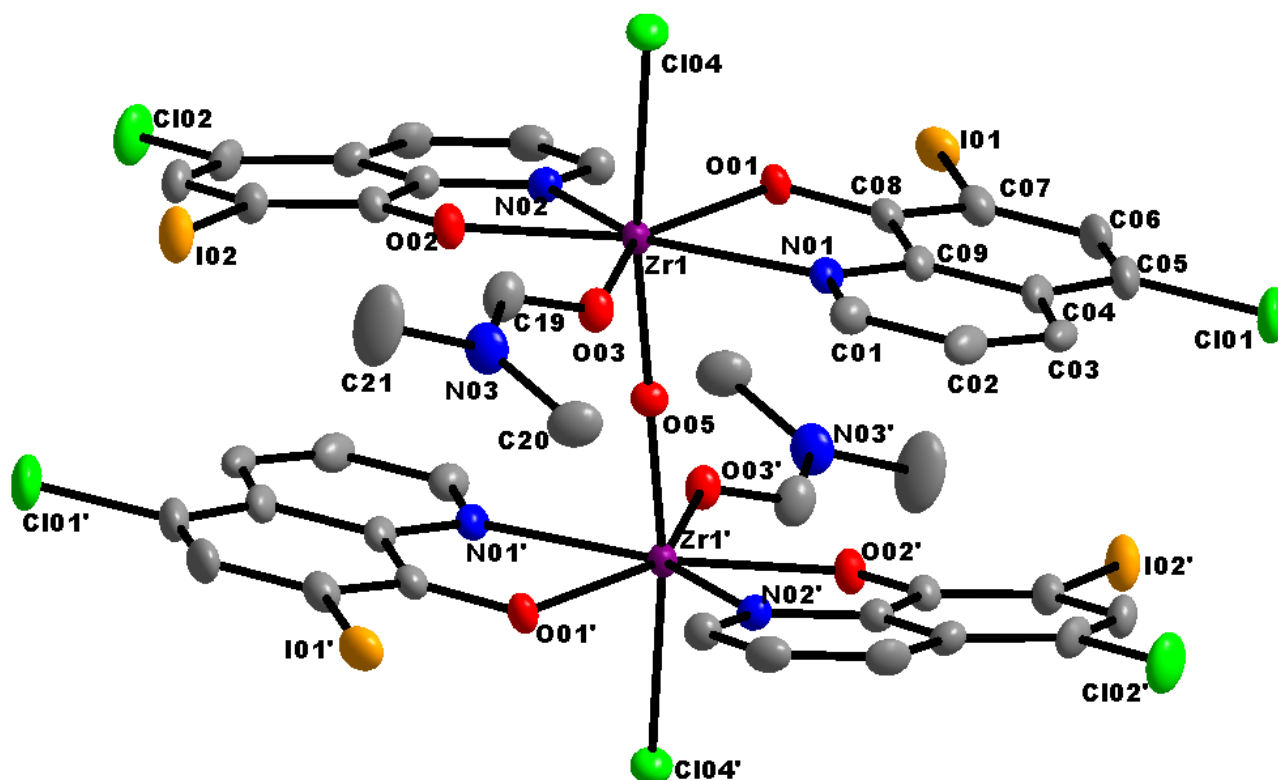
Figure 4.21 Graphic illustration of [ZrCl(CliOx)$_2$(DMF)$_2$O]$_2$.DMF showing general numbering of atoms. Displacement ellipsoids drawn at 50% probability. Hydrogen atoms and solvent molecules omitted for clarity. Symm. Code: (') 2 - *x*, 2 - *y*, 2 - *z*.

[12] M. Steyn, H.G. Visser & A. Roodt; *Z. Kristallogr. - New Cryst. Struct. 229* **(2014)**, 1, 67-69.

The compound, *µ*-oxo-bis[di(5-Chloro-7-iodoquinolin-8-olato-*$\kappa^2 N,O$*)-dichloro-(dimethylformamido-*κO*)zirconium(IV)] dimethylformamide solvate, crystallizes in the monoclinic space group, *P*2$_1$/*c*. The asymmetric unit consists of a Zr(IV) metal centre coordinated to two unique bidentate CliOx (5-Chloro-7-iodo-8-hydroxyquinoline) ligands, a monodentate N,N'-dimethylformamide (DMF) ligand, an axial chloride atom and an oxygen atom situated on an inversion centre. In the molecule, the coordinated O atom forms a bridge to another Zr(IV) metal centre which is generated by symmetry. Furthermore, a disordered (50:50) DMF solvent molecule is also found in the asymmetric unit.

Table 4.6 Selected Geometric Parameters for [ZrCl(CliOx)$_2$(DMF)$_2$O]$_2$.DMF (**Zr_1d**).

Selected Bond Lengths (Å)			
Zr—N$_{01}$	2.426(3)	Zr—Cl$_{04}$	2.559(13)
Zr—N$_{02}$	2.414(3)	Cl$_{01}$—C$_{05}$	1.744(4)
Zr—O$_{01}$	2.115(2)	Cl$_{02}$—C$_{14}$	1.741(4)
Zr—O$_{02}$	2.116(3)	I$_{01}$—C$_{07}$	2.088(4)
Zr—O$_{03}$	2.227(3)	I$_{02}$—C$_{16}$	2.082(4)
Zr—O$_{05}$	1.932(7)		
Selected Bite Angles (°)			
N$_{01}$—Zr—O$_{01}$	70.13(10)	N$_{02}$—Zr—O$_{02}$	69.22(10)
Selected Geometric Coordination Angles (°)			
N$_{01}$—Zr—N$_{02}$	143.03(10)	O$_{01}$—Zr—O$_{02}$	141.19(10)
N$_{01}$—Zr—O$_{02}$	147.75(10)	O$_{01}$—Zr—N$_{02}$	73.60(10)
N$_{01}$—Zr—O$_{03}$	73.56(10)	O$_{01}$—Zr—O$_{03}$	143.64(9)
N$_{01}$—Zr—O$_{05}$	85.07(7)	O$_{01}$—Zr—O$_{05}$	89.97(7)
N$_{01}$—Zr—Cl$_{04}$	85.75(7)	O$_{01}$—Zr—Cl$_{04}$	88.54(8)
N$_{02}$—Zr—O$_{03}$	142.62(10)	O$_{02}$—Zr—O$_{03}$	74.61(9)
N$_{02}$—Zr—O$_{05}$	88.05(7)	O$_{02}$—Zr—O$_{05}$	99.36(8)
N$_{02}$—Zr—Cl$_{04}$	100.37(8)	O$_{02}$—Zr—Cl$_{04}$	87.53(8)
O$_{03}$—Zr—Cl$_{04}$	86.95(7)	O$_{03}$—Zr—O$_{05}$	88.79(7)
O$_{05}$—Zr—Cl$_{04}$	170.65(3)		
Selected Torsion Angles (°)			
N$_{01}$—C$_{09}$—C$_{08}$—O$_{01}$	-2.03(57)	N$_{02}$—C$_{18}$—C$_{17}$—O$_{02}$	0.89(56)

The coordination polyhedron around the central metal atom can best be described as a pentagonal bipyramid, with an approximate pentagonal plane formed by the two CliOx ligands and the coordinated DMF ligand (Figure 4.22). This in itself is a unique case for a Zr-Ox type complex, since it is generally assumed that a tetrakis, 8-coordinate species with a square-antiprismatic (or dodecahedral) geometry would be obtained for this type of complexes of zirconium.[13,14]

---

[13] J.V. Silverton & J.L. Hoard; *Inorg. Chem. 2* (**1963**), 243-249.
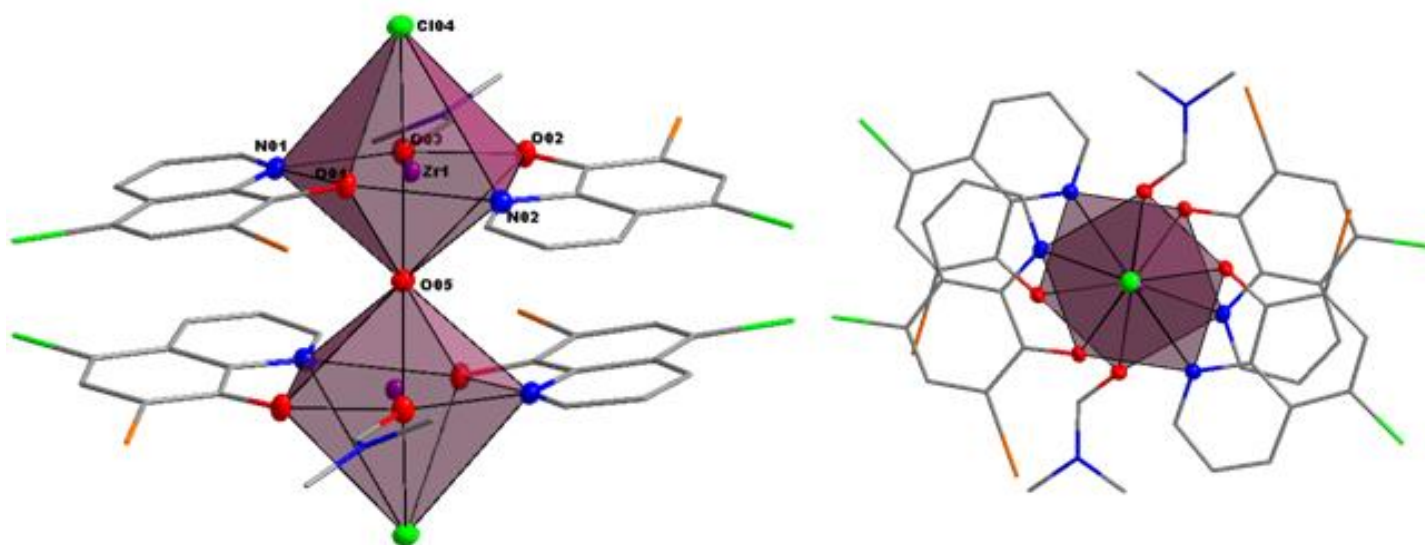
Figure 4.22 Graphic illustration of the pentagonal bipyramid coordination polyhedron of [ZrCl(CliOx)$_2$DMF)$_2$O]$_2$. (**left**) Side view showing the pentagonal planes of upper and lower pyramids with CliOx and DMF ligands placed over the metal inversion centre; (**right**) Top view showing the alternating spacing of the coordinative atoms. Hydrogens and solvent molecules omitted for clarity.

This compound displays average Zr—N and Zr—O bond distances of 2.420(3) Å and 2.115(3) Å, respectively and an average N—Zr—O bite angle of 69.68(10) ° (Table 4.6). The bridged Zr—O and DMF Zr—O bond distances are found to be 1.9322(7) Å and 2.227(3) Å, respectively. The axial Zr—Cl distance is 2.5597(13) Å. The measured N—C—C—O torsion angles of the ligand frame facing the N—Zr—O bite angles are found to range from -2.03(57) ° to 0.89(56) °, indicating very little deviation from the planarity of the ligands themselves.

The dihedral planes defined by the two CliOx ligands (Figure 4.23) lie at an angle of 169.27(9) ° to each other. The plane defined by the coordinated DMF molecule lie at an angle of 161.56(3) ° and 150.95(3) ° to the planes of Lig1 and Lig2, respectively.

---

[14] W. Clegg; *Acta Cryst.C43* (**1987**), 789 -791.
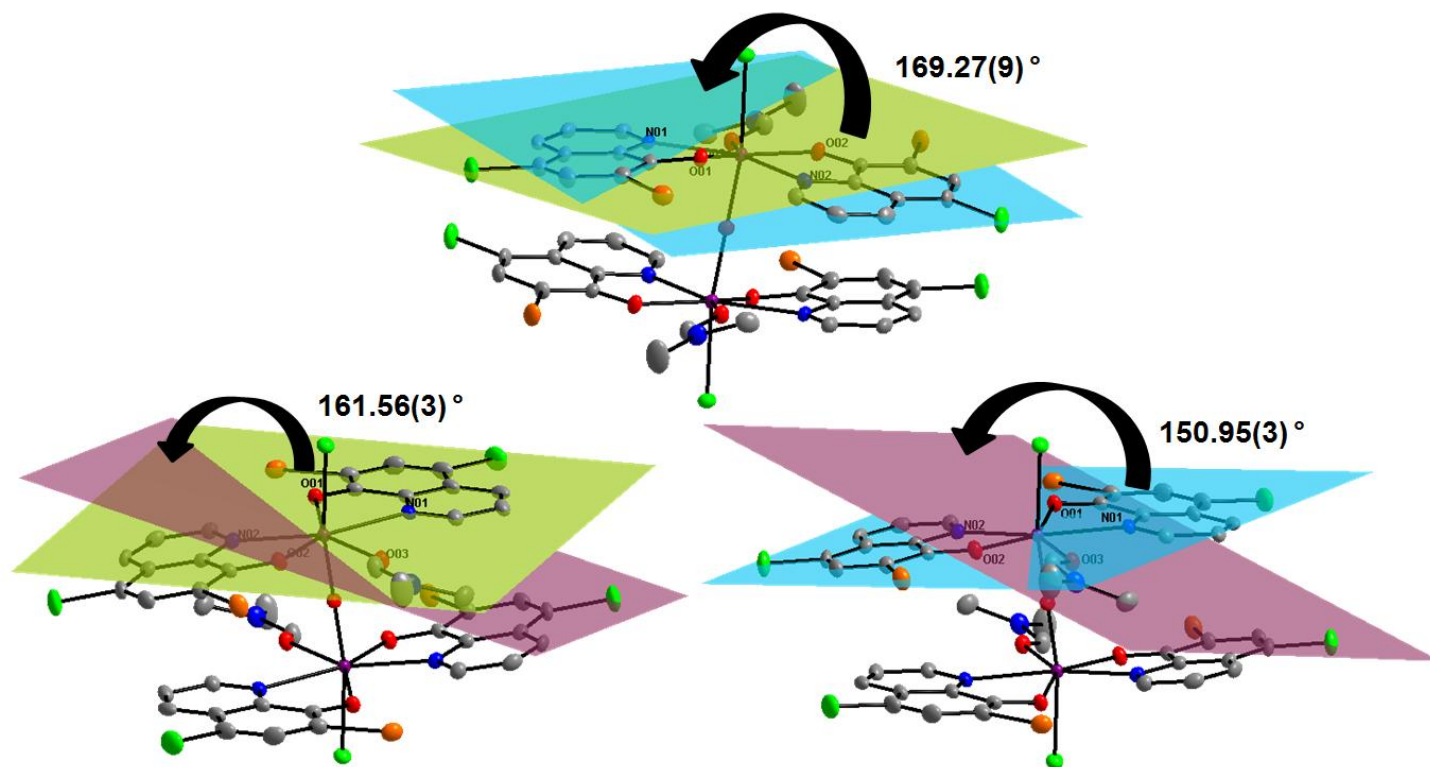
Figure 4.23 Illustration of the different ligand planes measured across the Zr metal centre. (**top**) Lig1/Lig2 at an angle of 169.27(9) °; (**bottom left**) Lig1/DMF at an angle of 161.56(3) °; (**bottom right**) Lig2/DMF at an angle of 150.95(3) °.
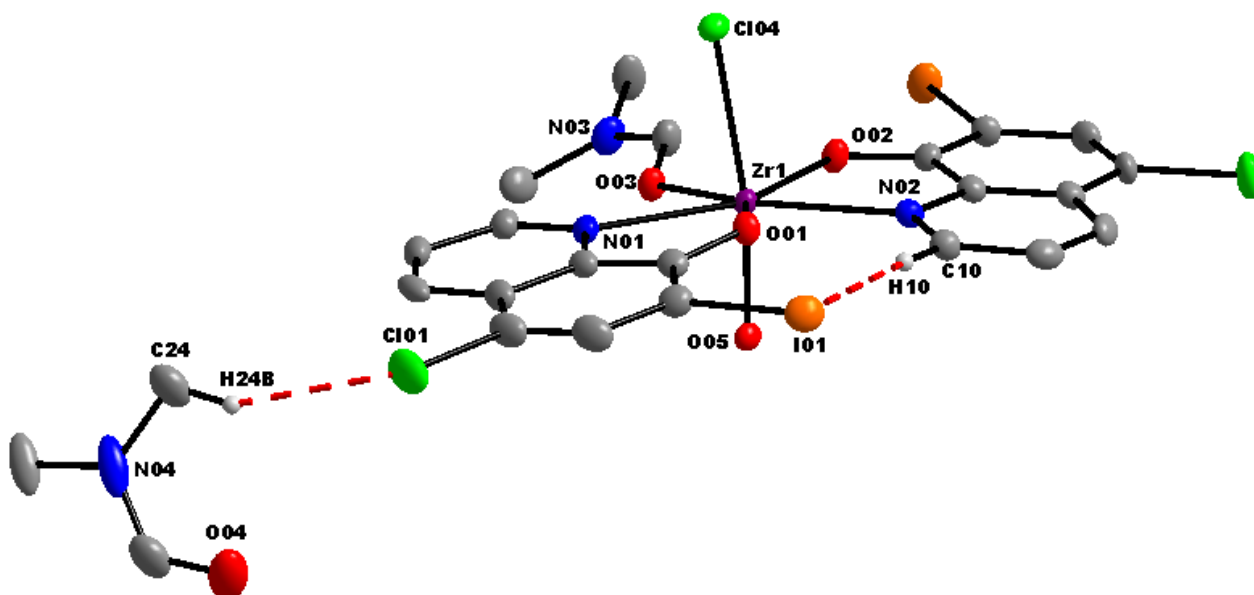
Figure 4.24 Illustration of the intra-molecular hydrogen bonding interactions found in the title molecule. C_{10}—H_{10}···I_{01} & C_{24}—H_{24B}···Cl_{01} (x−1, y−1, z−1), (Table 4.7).

Halide-hydrogen bonding interactions, C—H⋯X, are observed *intermolecularly* between a CliOx ligand (Lig1) and the DMF solvent molecule, as well as *intramolecularly* between the hydrogen atom of C_{10}—H_{10} of a CliOx-ligand (Lig2) to I_{01} of the other (Lig1), (Table 4.7, Figure 4.24).

Table 4.7 Hydrogen-bond geometry in the title compound (Å, °).

D—H⋯A	*D—H*	*H⋯A*	*D⋯A*	*D—H⋯A*
C_{10}—H_{10}⋯I_{01}	0.93	2.99	3.905 (4)	169
C_{24}—H_{24B}⋯Cl_{01} ii	0.96	2.7	3.585 (15)	154
Symmetry code: (ii) x−1, y−1, z−1.				

(a)

(b)
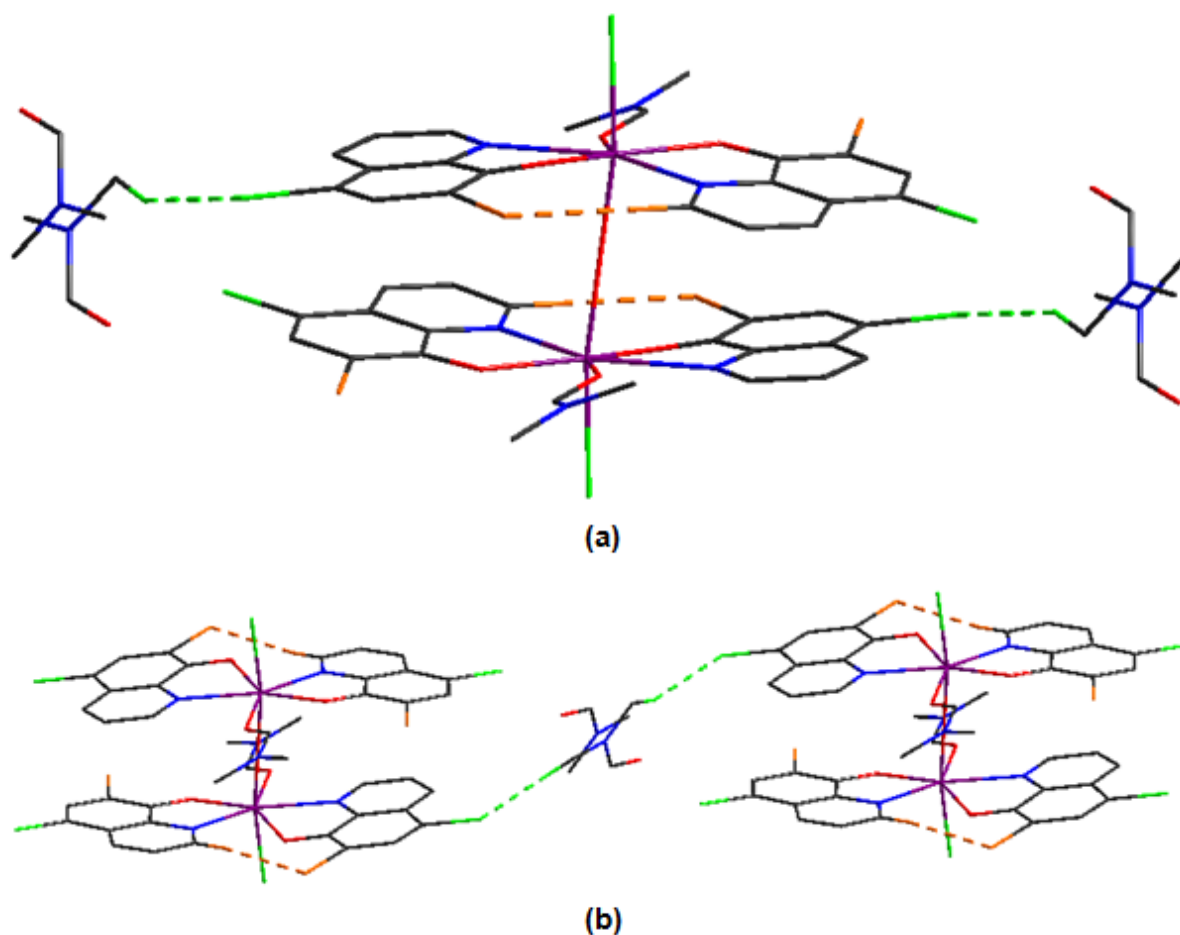
Figure 4.25 Graphical illustration of the crystal lattice stabilization by means of hydrogen bonding, as found in the title compound. ***Green Dotted Line*** - C_{24}—H_{24B}⋯Cl_{01} (x−1, y−1, z−1); ***Orange Dotted Line*** - C_{10}—H_{10}⋯I_{01}. **(a)** Depicting solvent-to-solvent linking through the bridged Zr_2-molecule; **(b)** Depicting cross-solvent linking over the disordered DMF solvent molecule to two different Zr_2-molecules.

The crystal lattice stabilization effect created by these hydrogen bonding interactions is illustrated in Figure 4.26. The solvent-to-solvent linking (Fig 4.25a) through the bridged Zr_2-molecule as well as the cross-solvent linking (Fig 4.25b) utilizes the disordered placement of the DMF solvent molecule to stabilize the entire network of *oxo*-bridged molecules. Furthermore, the two-dimensional supra-molecular network is further stabilized by *intramolecular* π-π interactions between the pyridine and benzene rings of overlapping CliOx ligands within the dimeric structure as well as *intermolecular* π-π interactions between the pyridine rings of neighbouring CliOx ligands as illustrated in Figure 4.26. The centroid-to-centroid distances for the *intra-* and *intermolecular* π-π interactions are 3.541(3) Å and 3.642(3) Å, respectively.
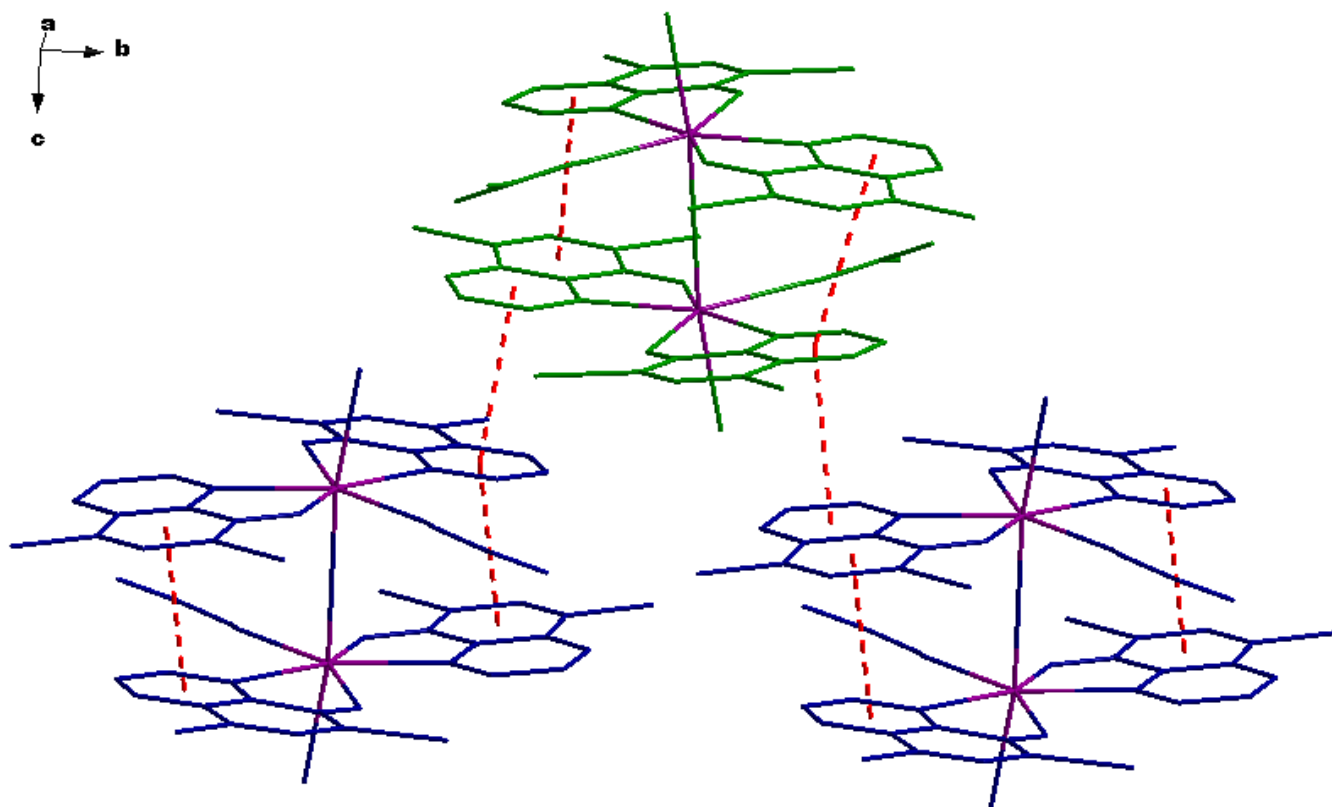
Figure 4.26 Illustration of the two-dimensional packing enabled by π-π interactions (***Red Dotted Lines***) along the *c*-axis in the crystal lattice.

4.5. Evaluation of Structural Characteristic Comparisons

In order to effectively evaluate the structural data presented above and before, a comparison of certain structural aspects of the zirconium-oxine complexes, as determined crystallographically, need to be taken into consideration. Specific aspects worth considering consist of the following general focus areas when discussing zirconium(IV) complexes containing bidentate ligands like oxine:

- Extent of coordination - limitation of the amount of ligands coordinated.

- Coordination mode/geometry around the metal centre specifically (Directly caused by the above) - two possibilities appear to be prevalent throughout literature for these specific complexes containing singular nature ligands, i.e. dodecahedral or square-antiprismatic.

- Nature of specific bond lengths - in bidentate complexes, the characteristics observed in bond length comparisons.

- Effective packing, as influenced by presence/absence of solvate molecules.

- Packing/stabilization - specific influencers to be investigated/predicted in model compounds.

With these factors in mind, a comparative evaluation of the presented zirconium and hafnium solid state structures can be summarised as in Table 4.8.

In general, it is observed that zirconium(IV) and hafnium(IV) complexes of oxine-type ligands appear to not specifically favour solid state crystal packing in any specific space group, but do tend towards monoclinic systems over all. The coordination environment around the metal centre for these oxine complexes tends to favour the square-antiprismatic polyhedron with minimal distortion towards the dodecahedral geometry. This then goes a long way into allowing for the prediction of solid state behaviour of zirconium(IV) N,O-bidentate ligand complexes. It has been established many decades ago that zirconium(IV) O,O'-bidentate ligand complexes, in particular the *tetrakis*(β-diketone)zirconium(IV) complexes,[11,12] prefer the square-antiprismatic coordination mode. Now the same conclusion can be drawn for N,O-bidentate ligand complexes, or at the very least for oxine-complexes in general. This is of course excluding the case of the $[ZrCl(CliOx)_2(DMF)_2O]_2$.(DMF) complex, which in itself is a structural anomaly that cannot be clearly explained at this stage.

Furthermore, it is concluded that in an overarching comparison of the data currently available, the average Zr — N and Zr — O bond lengths are 2.430(3) Å and 2.104(2) Å, respectively, with an average N — Zr — O bite angle of 70.23(8) °. A comparison of the zirconium and hafnium bond lengths shows that the Zr — N bonds tend to be *ca.* 0.1 Å longer than the Hf — N bonds of the same ligand-complex. With respect to other structural properties, the zirconium and hafnium oxine complexes are in general very similar.

Table 4.8 Selected crystallographic characteristics, bond lengths and angles of zirconium(IV) and hafnium(IV) - oxine complexes.

	$[Zr(ox)_4]$[a]	$[Zr(diClOx)_4]$[b]	$[Hf(diClOx)_4]$[c]	$[Zr(5\text{-}ClOx)_4]$[d]	$[ZrCl(CliOx)_2(DMF)_2O]_2$[e]	$[Hf(CliOx)_4]$[f]
Crystal system	Triclinic	Monoclinic	Monoclinic	Monoclinic	Monoclinic	Monoclinic
Space group	$P\bar{1}$	$C2/c$	$P2_1/n$	$P2_1/c$	$P2_1/c$	$P2_1/a$
***a, b, c* (Å)**	11.342(2), 12.209(5), 12.538(4)	30.357(5), 13.037(4), 26.386(4)	22.428(2), 15.789(1), 28.335(2)	18.678(3), 21.176(5), 20.148(2)	14.634(3), 13.712(2), 14.710(5)	19.901 (3), 15.247(5), 32.947(1)
***α , β, γ* (°)**	91.728(2), 103.419(3), 99.250(3)	90.0, 118.343(4), 90.0	90.0, 112.527(2), 90.0	90.0, 90.894(4), 90.0	90.0, 114.073(4), 90.0	90.0, 105.97(3) , 90.0
Cell Volume ($Å^3$)	1662.7(12)	9191(4)	9268.9(12)	7968(2)	2695.0(16)	9611(4)
Z	2	4	8	4	4	4
Coordination Polyhedra	Sq-Anti prismatic	Sq-Anti prismatic	Sq-Anti prismatic	Sq-Anti prismatic	Pentagonal-Bipyramidal	Sq-Anti prismatic
Bidentate Ligands Coordinated	4	4	4	4	2	4
Avg. M — N (Å)	2.420(2)	2.452(2)	2.386(5)	2.427(4)	2.420(3)	2.393(3)
Avg. M — O (Å)	2.106(2)	2.095(2)	2.098(4)	2.100(3)	2.116(2)	2.192(2)
Avg. N — M — O (°)	70.43(7)	69.77(7)	70.85(2)	69.97(14)	69.68(10)	69.81(8)

a) Ref. 15, **b**) § 4.2, **c**) Ref. 16, **d**) § 4.3, **e**) §4.4, **f**) Ref. 17.

[15] M. Steyn, H.G. Visser & A. Roodt; *J. S. Afr. Inst. Min. Metall 113* (**2013**), 105-108.

[16] J.A. Viljoen, H.G. Visser & A. Roodt; *Z. Kristallogr. - New Cryst. Struct.* (**2014**), In Press.

[17] J.A. Viljoen; *Unpublished.*

With regard to the influence of solvent molecules in effective packing of these organometallic molecules, it can be concluded that hydrogen bonding between coordinated ox-ligands and these solvents influence the stability of the lattice as a whole. However, the most noteworthy packing stabilizer is undoubtedly the π-stacking interactions observed in all cases characterised thus far. In some cases direct π-π stacking between coordinated ligands ([Zr(ox)$_4$][15] & [ZrCl(CliOx)$_2$(DMF)$_2$O]$_2$[§4.4]) and in others halogen-π stacking ([Zr(5-ClOx)$_4$][§4.3] & [Zr(diClOx)$_4$][§4.2]) are observed. In all these cases we find that the aromatic nature of the ox-ligands (both the pyridine and benzene portions) significantly influences this π stacking tendency of the greater molecular structure as a whole. This stacking dictates the overall stability and arrangement in the crystal lattice as a whole, as is evident from the structural descriptions above.

In the following chapter, Chapter 5, three additional zirconium oxine-type complexes are structurally evaluated and described. With all of this data, a clearer description of the solid state behaviour of these complexes will be attempted. The results presented here will be further discussed with regard to the geometric characteristics observed in each case (ligand plane angles, square anti-prism deviations, etc.) in § 6.4.

Chapter 5

X-Ray Diffraction Studies of Zirconium(IV) Complexes Containing Non-Halogen Substituted 8-Hydroxyquinoline Ligands

This chapter contains a detailed discussion of Zr(IV) compounds with other, non-halogen substituted, variations of 8-hydroxyquinoline (oxine; ox) ligands. The importance of structural characterisation of zirconium and hafnium complexes, as discussed in detail in Chapter 2, lies also in the value of finding anomalies in the chemical behaviours of these two metals, with an overarching aim of exploiting these differences for separation purposes from base ore sources. In this case, as in Chapter 4, a study of the solid state characteristics is evaluated with similar ligands chelated to zirconium, specifically.

An integral part of this project has been focused on employing different commercially available oxine or oxine-type ligands, with variation in the electronic bulk of the quinoline back-bone (Figure 5.1). These variations of the oxine structure as a whole could in principal alter the intimate coordination around the metal centre, but also the solid state arrangement of the crystal lattice as a whole.

In the following paragraphs, the crystallographic structure determination of three zirconium-oxine-type complexes is presented in detail as well as the correlation of each structure with similar structures of zirconium and hafnium. An in depth discussion of the literary and theoretical interest in these types of ligands can be found in § 2.3.4.
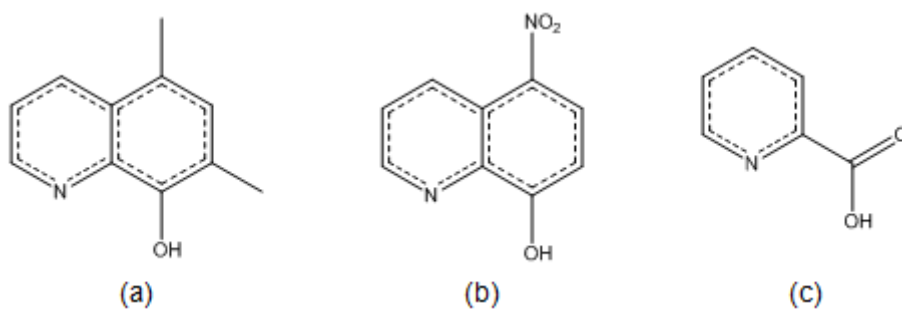
Figure 5.1 Oxine ligands chelated to zirconium and discussed in this chapter.
(**a**) 5,7-Dimethyl-8-hydroxyquinoline (diMeOxH); (**b**) 5-Nitro-8-hydroxyquinoline (5-NO$_2$OxH);
(**c**) Picolinic Acid (Pic).

5.1. Experimental

The X-ray intensity data was collected on a Bruker X8 ApexII 4K Kappa CCD area detector diffractometer, equipped with a graphite monochromator and MoKα fine-focus sealed tube (λ = 0.71069 Å, T = 100(2) K) operated at 2.0 kW (50 kV, 40 mA). The initial unit cell determinations and data collections were done by the SMART[1] software package. The collected frames were integrated using a narrow-frame integration algorithm and reduced with the Bruker SAINT-Plus and XPREP software packages[2] respectively. Analysis of the data showed no significant decay during the data collection. Data was corrected for absorption effects using the multi-scan technique SADABS,[3] and the structure was solved by the direct methods package SIR97[4] and refined using the WinGX[5] software incorporating SHELXL.[6] The final anisotropic full-matrix least-squares refinement was done on F^2. The methyl and aromatic protons were placed in geometrically idealized positions (C–H = 0.93 – 0.98 Å) and constrained to ride on their parent atoms with U$_{iso}$(H) = 1.2U$_{eq}$(C). Non-hydrogen atoms were refined with anisotropic displacement parameters. The graphics were obtained with the DIAMOND[7] program with 50% probability ellipsoids for all non-hydrogen atoms.

---

[1] Bruker SMART-NT Version 5.050.Bruker AXS Inc. Area-Detector Software Package; Madison, WI, USA, **1998.**
[2] Bruker SAINT-Plus Version 6.02 (including XPREP), Bruker AXS Inc. Area-Detector Integration Software, Madison, WI, USA, **1999.**
[3] Bruker SADABS Version 2004/1.Bruker AXS Inc. Area Detector Absorption Correction Software, Madison, WI, USA, **1998.**
[4] A. Altomare, M.C. Burla, M. Camalli, G.L. Cascarano, C. Giacovazzo, A. Guagliardi, A.G.G. Moliterni, G. Polidori & R. Spagna; *J. Appl. Cryst. 32* (**1999**), 115-119.
[5] L.J. Farrugia; *J. Appl. Cryst. 32* (**1999**), 837-838.
[6] G.M. Sheldrick; SHELXL97. *Program for crystal structure refinement*, University of Göttingen, Germany, **1997.**
[7] K. Brandenburg & H. Putz; DIAMOND, Release 3.0e, Crystal Impact GbR, Bonn, Germany, **2006.**

Note: General Considerations throughout the following text

1. Oxine Ligands are numbered from the N-atom, following sequentially around both rings (Figure 5.2).
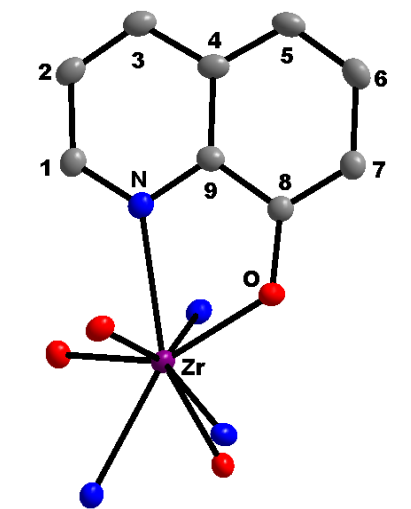
Figure 5.2 Oxine atom numbering

2. Each individually characterised ligand (i.e. independent ligands not symmetrically generated) around the metal centre is numbered consecutively, and referred to in short "Lig#" with # = 1 - 4. Ligands are identified by the numbering of the nitrogen and oxygen atoms of the ligand coordinated to the metal centre. Furthermore, independent ligand planes are coloured systematically throughout the text (Figure 5.3).
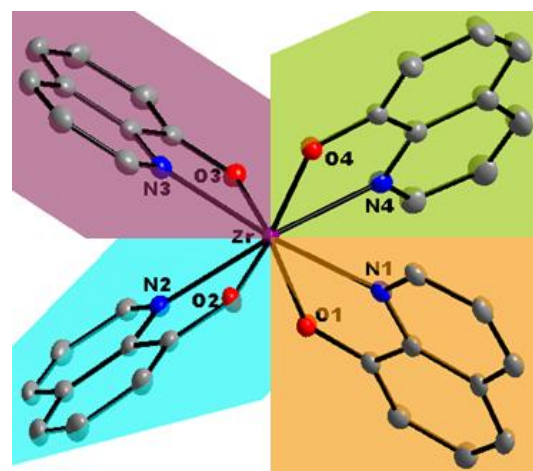
Figure 5.3 Ligand numbering and plane colours.

3. Ligands in *tetrakis*-coordinated zirconium(iv) structures are generally arranged in a space filling fan-like arrangement, with no specific geometric planes as a point of reference, due to the square-antiprismatic coordination polyhedron. The higher coordination isomeric description of these structures is illustrated in two ways.

a. Firstly, the placement of the N- and O- coordination atoms of the oxine ligands are observed as either mirrored or alternating in the positioning of these atoms across the metal centre (*Figure 5.4*).
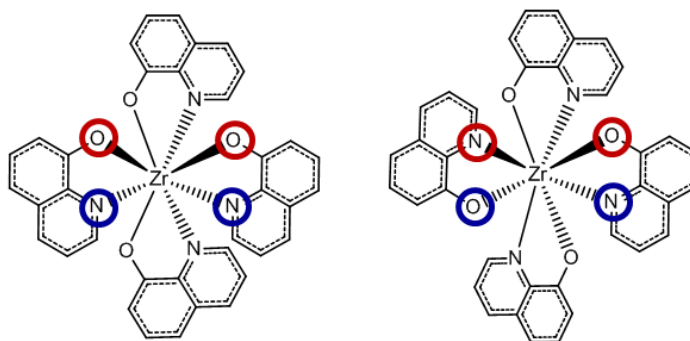
Figure 5.4 Coordinate ox-ligand arrangement around the metal centre when considering the N- and O-coordination sites; (**left**) Mirrored; (**right**) Alternating.

b. Secondly, from the discussion on eight-coordinated and square antiprismatic geometry found in metal complexes included in § 2.5, three possible isomers are observed and classified. As described earlier, for complexes with four O,O-donating bidentate ligands chelated (specifically the *β*-diketone type ligands) and exhibiting a square antiprismatic arrangement of these ligands around the metal centre, the specific position of the bidentate ligands on the square antiprism dictates the named isomer.[8] As illustrated in Figure 5.5, the three possible isomers that can be visualised are a corner-clipped ligand placement (Fig 5.5a - D_2), side-clipped coordination (Fig 5.5b - D_4) or a combination of these two (Fig 5.5c - C_2).

(a) (b) (c)
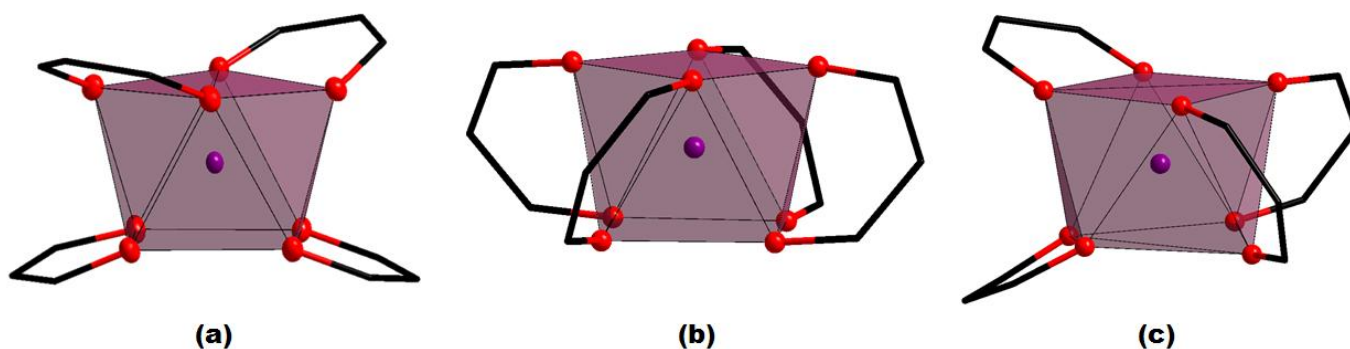
Figure 5.5 Coordination isomers as defined for *tetrakis*(*β*-diketone)metal complexes exhibiting a square antiprismatic coordination polyhedron. (**a**) D_2 - Corner-clipped ligands; (**b**) D_4 - Side-clipped ligands; (**c**) C_2 - Combination corner- and side-clipped ligands.

---

[8] C.W. Haigh; *Polyhedron 15* (**1995**), 605-643.

In the case of these N,O-donating oxine ligands, the same isomers are possible but with a further addition of two subcategories of the D_2 corner-clipped isomer. These two isomers are directly dependant on the placement of the oxine ligands with respect to each other across the metal centre, as illustrated in Figure 5.4 earlier. As depicted in Figure 5.6, the corner-clipped ligands display two distinct directionalities in which they are coordinated with respect to each other on the square antiprism frame. Depending on the *mirrored* or *alternating* placement of N- and O-coordination sites, either a D_2^x (ligands placed across the *x*-axis) or a D_2^z (ligands placed across the *z*-axis) is possible. This specific sub-category of isomer is only observed in this case of N,O-donating oxine ligands, as described here. Furthermore, they are distinctly defined by the reference location of the coordinating atoms on the eight corners of the square antiprism, for these unsymmetrical ligands.
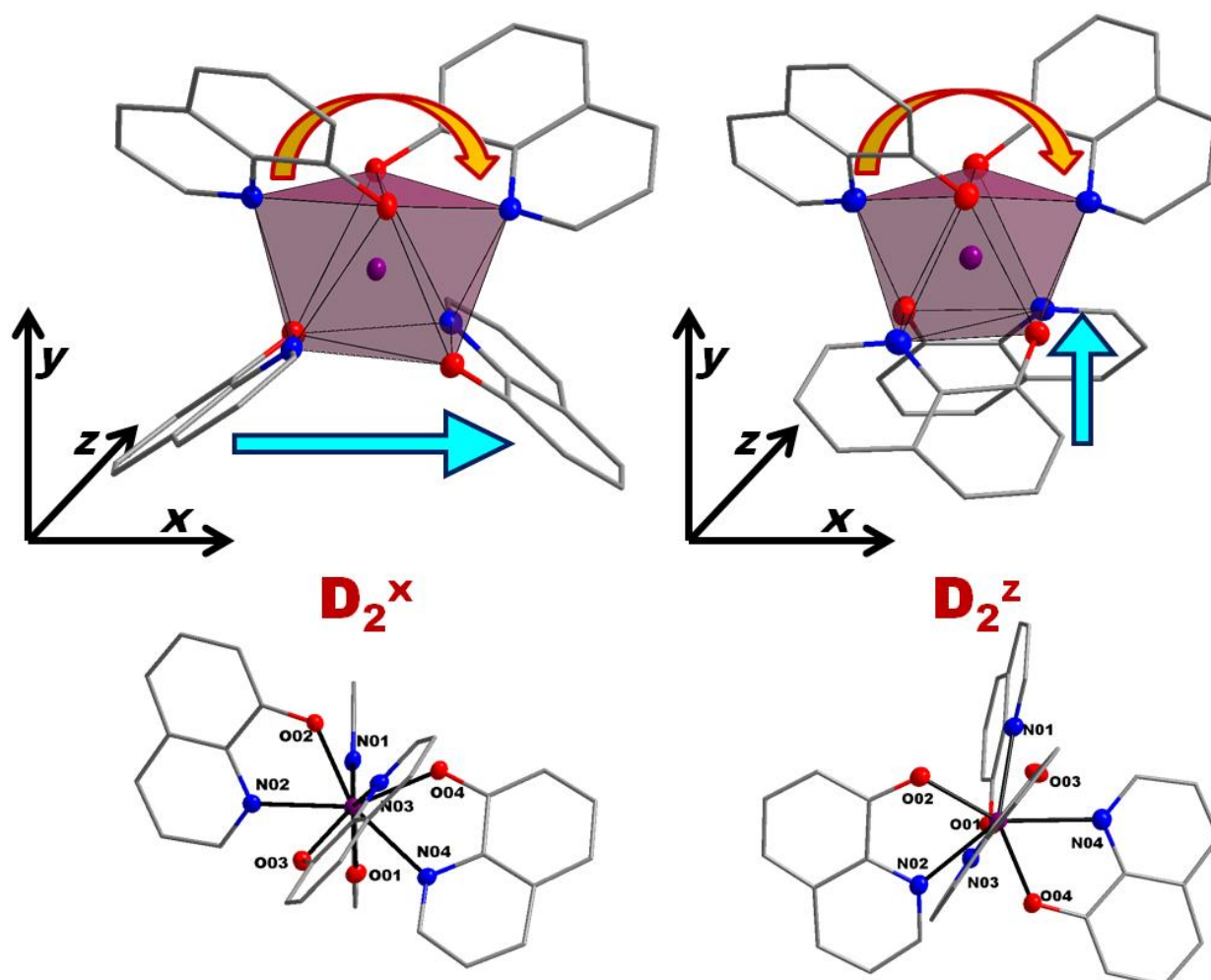
Figure 5.6 Coordination isomer sub-category illustration of the corner-clipped D_2 species observed, when considering the arrangement of the ligands at the bottom square of the antiprism (**left**) D_2^x - ligands arranged across the *x*-axis; (**right**) D_2^z - ligands arranged across the *z*-axis.

Table 5.1 Crystallographic and Refinement Details for structures discussed in this chapter.

Crystal Formula	[Zr(diMeOx)$_4$].2DMF (Zr_1e)	[Zr(5-NO$_2$Ox)$_4$] (Zr_1i)	[Zr(Pic)$_4$].2H$_2$O (Zr_3a)
Empirical formula	C$_{50}$ H$_{48}$ N$_6$ O$_6$Zr	C$_{36}$ H$_{20}$ N$_8$ O$_{12}$Zr	C$_{24}$ H$_{20}$ N$_4$ O$_{10}$Zr
Formula weight (g.mol^{-1})	920.16	423.91	153.92
Crystal system, Space Group	Orthorhombic *Pna*2$_1$	Tetragonal, *I*$\bar{4}$2*d*	Tetragonal, *P*4$_2$/*n*
Unit cell dimensions:			
a, b, c (Å)	15.572(5), 18.706(4), 15.853(4)	14.795(4), 14.795(5), 22.082(5)	11.083(3), 11.083(5), 9.548(3)
α, β, γ (°)	90.0, 90.0, 90.0	90.0, 90.0, 90.0	90.0, 90.0, 90.0
Volume (Å^3), Z	4618(2), 4	4834(3), 8	1172.8(10), 8
Density (calculated, mg.cm^{-3})	1.324	1.16	1.743
Crystal morphology	cuboid	cuboid	cuboid
Crystal Colour	red	yellow	colourless
Crystal size (mm^3)	0.136 x 0.257 x 1.332	0.197x 0.261 x 0.312	0.043 x 0.091 x 0.123
Absorption coefficient *μ* (mm^{-1})	0.293	0.285	0.539
F(000)	1912	1712	624
Theta range	2.13 to 28.00	2.68 to 25.99	2.60 to 28.47
Index ranges	-20 ≤ h ≤ 20	-18 ≤ h ≤ 16	-14 ≤ h ≤ 13
	-22 ≤ k ≤ 24	-18 ≤ k ≤ 18	-14 ≤ k ≤ 14
	-20 ≤ l ≤ 20	-27 ≤ l ≤ 27	-12 ≤ l ≤ 12
Reflections collected, Independent Reflections, R$_{int}$	61276, 11142, 0.0641	37002, 2374, 0.0302	27234, 1477, 0.0736
Completeness to 2*θ* (°, %)	28.00, 99.8	25.99, 99.6	28.47, 99.3
Max. and min. transmission	0.9629 and 0.9276	0.9452 and 0.9169	0.9381 and 0.9788
Data, restraints, parameters	11142, 305, 672	2374, 10, 215	1477, 1, 87
Goodness-of-fit on F^2	1.026	1.187	1.098
Final R indices [I>2σ (I)]	R$_1$ = 0.0415	R$_1$ = 0.0540	R$_1$ = 0.0374
	wR$_2$ = 0.0895	wR$_2$ = 0.1478	wR$_2$ = 0.0943
R indices (all data)	R$_1$ = 0.0664	R$_1$ = 0.0582	R$_1$ = 0.0447
	wR$_2$ = 0.1009	wR$_2$ = 0.1567	wR$_2$ = 0.1002
Largest diff. peak and hole (e.Å^{-3})	0.436 and -0.406	0.706 and -0.507	0.638 and -0.917

5.2. Crystal Structure of [Zr(diMeOx)₄].2DMF– Zr_1e

The published structure of this *tetrakis*-coordinated zirconium - 5,7-dimethyl-8-hydroxyquinoline complex[9] (**Zr_1e**) is one of few examples of zirconium-oxine structures available in literature to date. Synthesis of **Zr_1e** and the resulting red crystals obtained for this was discussed in § 3.2.1.5.

A summary of the general crystal data is given in Table 5.1, while the numbering scheme of the solvated complex is shown in the perspective drawing in Figure 5.7. Table 5.2 presents selected bond lengths and angles of the title compound. Atomic coordinates, anisotropic displacement parameters, all bond distances and angles and hydrogen coordinates, are given in the supplementary data (Appendix A.4). Hydrogen atoms and/or solvent molecules are omitted in some molecular presentations for clarity.

Figure 5.7 Graphic illustration of [Zr(diMeOx)₄].2DMF showing general numbering of atoms. Displacement ellipsoids drawn at 50% probability. Hydrogen atoms and solvent molecules omitted for clarity.

---

[9] M. Steyn, H.G. Visser & A. Roodt; *ActaCryst. E68* (**2012**), m1344–m1345.

The compound *tetrakis*(5,7-dimethylquinolin-8-olato-$\kappa^2 N,O$)zirconium(IV) dimethylformamide disolvate, crystallizes in the orthorhombic space group, *Pna*2_1. The asymmetric unit consists of a Zr(IV) metal centre coordinated to four bidentate ligands (5,7-dimethylquinolin-8-olate = diMeOx⁻). Two crystallographically independent N,N'-dimethylformamide (DMF) solvent molecules fill the rest of the asymmetric unit. Of these solvent molecules, one is disordered over 3 positions in a 36.2(8) % : 35.8(1) % : 28.0(7)% ratio.

Table 5.2 Selected Geometric Parameters for [Zr(diMeOx)$_4$].2DMF.

Selected Bond Lengths (Å)			
Zr—N$_{1A}$	2.493(17)	Zr—N$_{1B}$	2.340(20)
Zr—O$_{1A}$	2.078(15)	Zr—O$_{1B}$	2.134(11)
N$_{2A}$—O$_{2A}$	1.198(15)	N$_{2B}$—O$_{2B}$	1.195(17)
N$_{2A}$—O$_{3A}$	1.170(20)	N$_{2B}$—O$_{3B}$	1.177(19)
N$_{2A}$—C$_{5A}$	1.459(13)	N$_{2B}$—C$_{5B}$	1.484(18)
Selected Bite Angles (°)			
N$_{1A}$—Zr—O$_{1A}$	67.1(5)	N$_{1B}$—Zr—O$_{1B}$	68.6(4)
Selected Geometric Coordination Angles (°)			
N$_{1A}$—Zr—N$_{1A}$^{i}	69.1(7)	N$_{1B}$—Zr—N$_{1B}$^{i}	70.0(8)
N$_{1A}$—Zr—N$_{1A}$^{ii}	132.7(7)	N$_{1B}$—Zr—N$_{1B}$^{ii}	132.2(5)
O$_{1A}$—Zr—O$_{1A}$^{i}	133.0(6)	O$_{1B}$—Zr—O$_{1B}$^{i}	150.4(5)
O$_{1A}$—Zr—O$_{1A}$^{ii}	99.1(2)	O$_{1B}$—Zr—O$_{1B}$^{ii}	93.7(1)
Symmetry codes: (i) −x+1, −y, z; (ii) y+1/2, −x+1/2, −z+3/2.			
Selected Torsion Angles (°)			
N$_{1A}$—C$_{9A}$—C$_{8A}$—O$_{1A}$	9.8(19)	N$_{1B}$—C$_{9B}$—C$_{8B}$—O$_{1B}$	−6.6(18)
Ligand Plane Angles (°)			
Lig1/Lig2	78.29(45)	Lig3/Lig4	78.29(49)
Lig2/Lig3	55.130(35)	Lig4/Lig1	53.69(28)
Lig1/Lig3	102.42(47)	Lig2/Lig4	102.42(48)

The four diMeOx-ligands lie around the metal centre in a space filling, fan-like arrangement to give an approximate square-antiprismatic coordination polyhedron (Figure 5.8), with an almost negligible outward distortion towards dodecahedral geometry. This distortion from the ideal square antiprism is associated with an outward bend of 5.02(12) °, as illustrated in Figure 5.9.

In this structure the average Zr—N and Zr—O bond distances are 2.418(3) Å and 2.104(2) Å, respectively, and the average N—Zr—O bite angle is found to be 70.16(8) ° (Table 5.2). The measured N—C—C—O torsion angles of the ligand frame facing the N—Zr—O bite angles are found to range from 0.49(41) ° to 2.85(41) °, indicating very little deviation from the planarity of the ligands themselves.
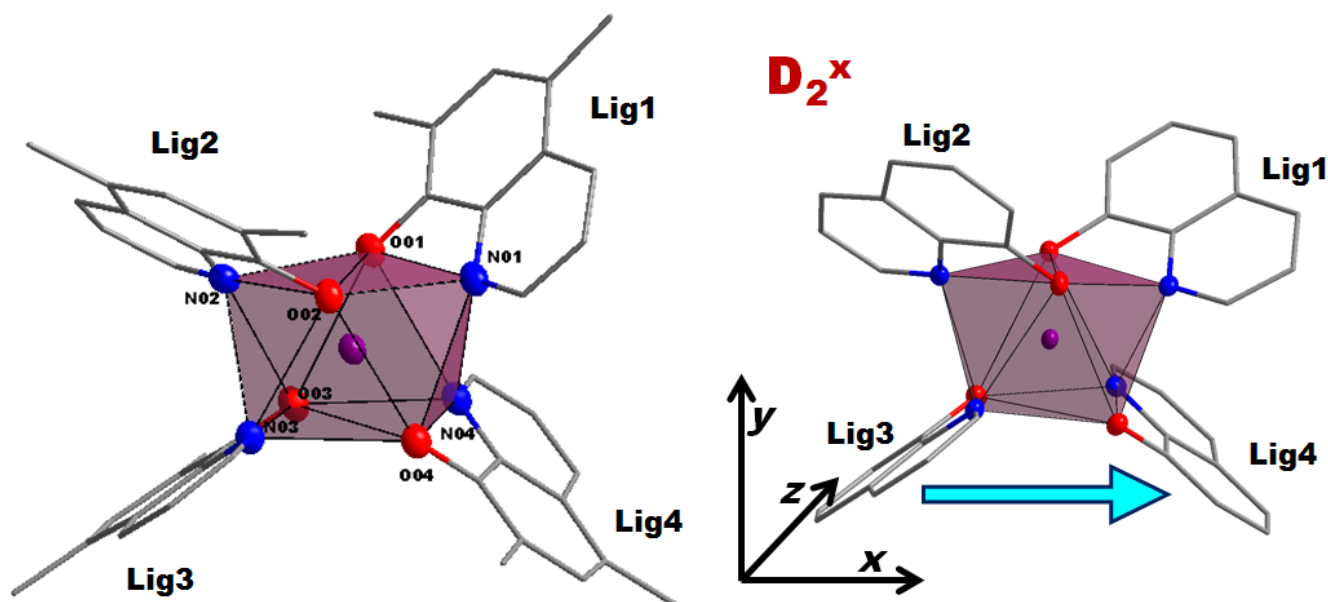
Figure 5.8 Graphic illustration of the square-antiprismatic coordination polyhedron of [Zr(diMeOx)$_4$]. **(left)** Side view showing upper and lower four corners represented by the N- and O-coordinating atoms of the ligands; **(right)** Isomer description as determined from the placement of the ox-ligands on the square antiprism - in this case the corner-clipped D_2^x.

Figure 5.9 Illustration of the distortion of the square-antiprismatic coordination polyhedron found in [Zr(diMeOx)$_4$], showing the outward bend of the top-most atoms at an angle of 5.02(12) °.

From Figure 5.10 it can be seen that each coordinated ligand is duplicated by an opposite facing one *via* an approximate two-fold rotation axis, when looking diagonally (from top to bottom) of the square antiprism. In other words Lig4 is duplicated by Lig2, and so on. Although these duplicated ligands do not lie in a flat plane opposite each other, it is clear

that the ligands are chelated to the metal centre with a *mirrored* placement of the N- and O-coordinating sited. With regard to the overall coordination description of the ligands as viewed in the square antiprism (Figure 5.8), the title compound crystallises as a D_2^x corner-clipped isomer.
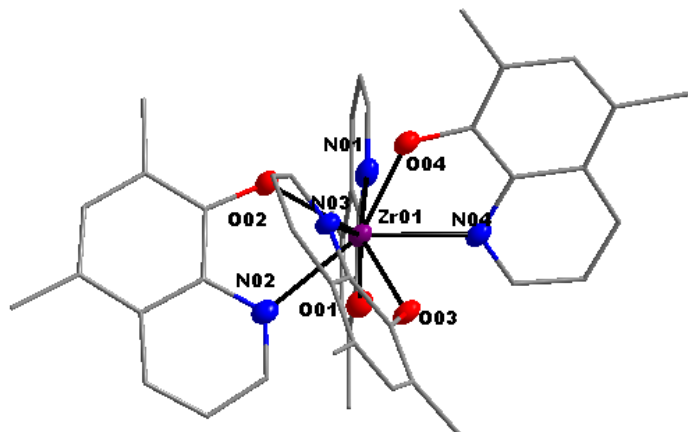
Figure 5.10 Graphical illustration of the *mirrored* placement of the diMeOx ligands across the metal centre in the title molecule, with the arrangement of O_{02} & O_{04} and N_{01} & N_{03} opposite each other, respectively. Hydrogens and solvent molecules omitted for clarity.

Figure 5.11 Illustration of the different ligand planes measured across the Zr metal centre. (**left**) Lig1/Lig3 at an angle of 140.73(6) °; (**right**) Lig2/Lig4 at an angle of 142.21(6) °.

The coordinating ligands are thus characterised by "opposite" ligand pairs and "adjacent" ligand pairs, and are described further as such, respectively. The planes defined by each individual ligand appear flat, with no deviation of any one atom out of the plane. This is also illustrated by the torsion angles for these ligands as reported in Table 5.2. These "ligand-planes" (Figure 5.11) lie across the metal centre at angles of 140.73(6) ° (Lig1/Lig3) and 142.21(6) ° (Lig2/Lig4) for each opposite facing pair. The dihedral angles between adjacent ligand planes range from 61.26(7) ° at the smallest (Lig2/Lig3) to 88.92(7) ° at the largest (Lig1/Lig2) as reported in Table 5.2.

Only one significant C—H⋯O hydrogen bonding interaction is observed between the methyl group of a diMeOx-ligand (Lig4) and the non-disordered DMF molecule (Figure 5.12, Table 5.3).
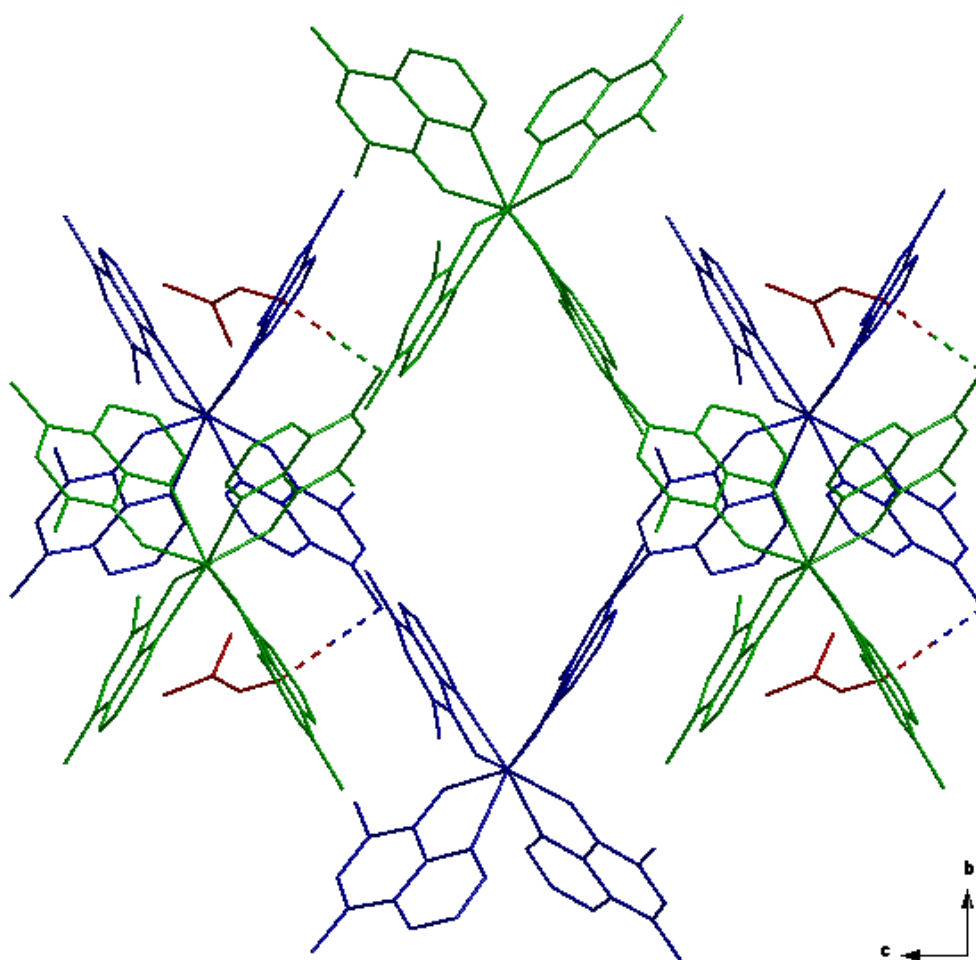
Figure 5.12 Illustration of the hydrogen bonding interaction found in the title molecule. As viewed along the *a*-axis, depicting the alternating placement of ligand-to-solvent interaction, with front facing molecules (***blue***) and rear-facing molecules (***green***) of the DMF solvent (***red***).

Table 5.3 Hydrogen-bond geometry in the title compound (Å, °).

D—H···A	D—H	H···A	D···A	D—H···A
C_{4A}—H_{4A2}···O_{05}ⁱ	0.96	2.44	3.363(7)	161.3
Symmetry code: (i) −x+3/2, y+1/2, z−1/2.				

Crystal lattice packing is further stabilized by π–π interactions between the benzene rings of the diMeOx ligand groups 2 and 3 with symmetry generated counterparts (1-x,1-y,1/2+z; 1-x,1-y,-1/2+z) of neighbouring molecules, with interplanar and centroid-to-centroid distances of 3.433(4) Å and 3.671(3) Å, respectively (Figure 5.13).

Figure 5.13 Graphical illustration of the head-to-tail packing found in the title compound, depicting the 'threaded' π–π interactions between the benzene rings of the diMeOx ligand 2 and 3 (***red dotted line***) as viewed along the *a*-axis.

5.3. Crystal Structure of [Zr(5-NO$_2$Ox)$_4$] – Zr_1i

The structure of this *tetrakis*-coordinated zirconium - 5-nitro-8-hydroxyquinoline complex (**Zr_1i**) is an interesting example of the more symmetrical coordination possibilities of zirconium-oxine structures. Synthesis of **Zr_1i** and the resulting yellow crystals obtained for this was discussed in § 3.2.1.9.

A summary of the general crystal data is given in Table 5.1, while the numbering scheme of the complex is shown in the perspective drawing in Figure 5.14 and in Figure 5.15 the comparison of the two disordered halves are overlayed. Table 5.4 presents selected bond lengths and angles of the title compound. Atomic coordinates, anisotropic displacement parameters, all bond distances and angles and hydrogen coordinates, are given in the supplementary data (Appendix A.5). Hydrogen atoms and/or solvent molecules are omitted in some molecular presentations for clarity.
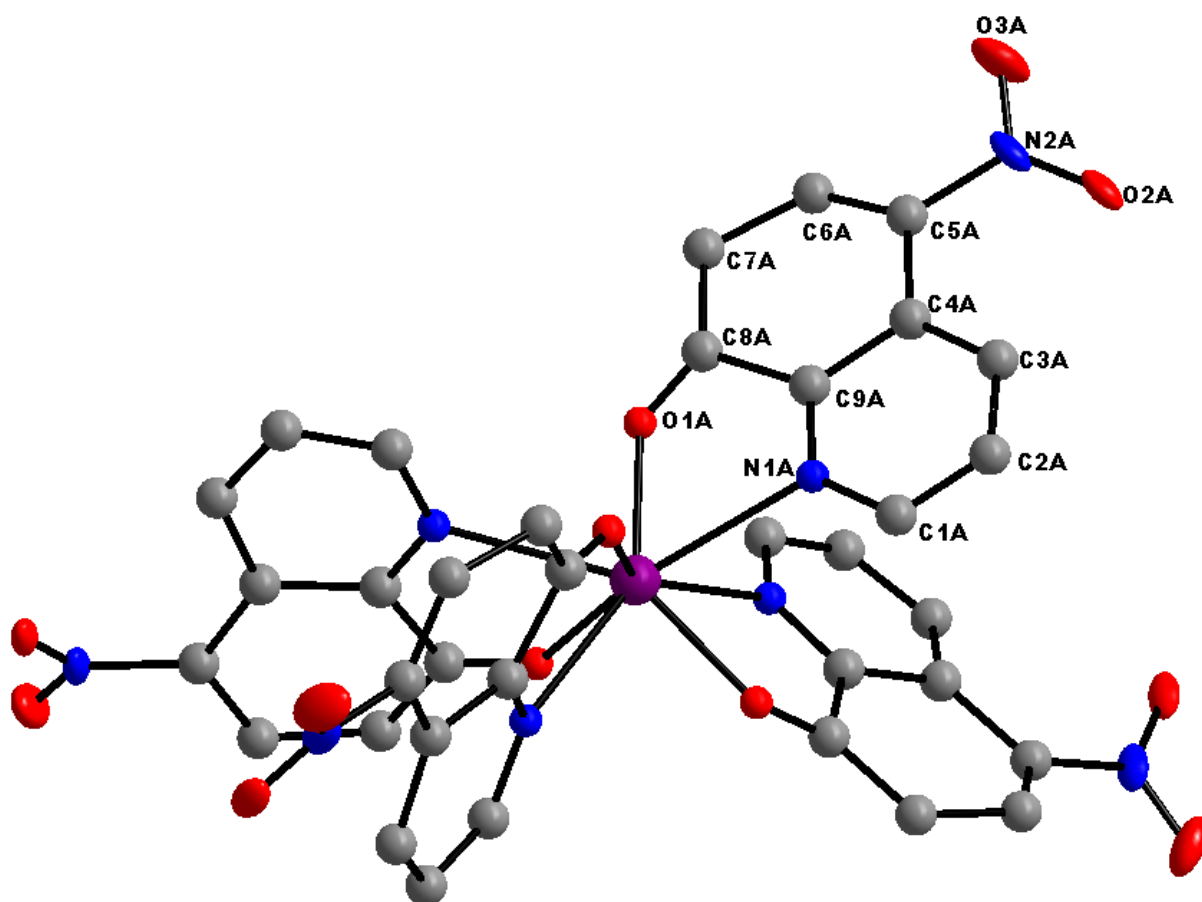
Figure 5.14 Graphic illustration of [Zr(5-NO$_2$Ox)$_4$] showing general numbering of atoms.
Numbering of the disordered ligand atoms denoted by A = 51%, B = 49%.
Displacement ellipsoids drawn at 50% probability. Hydrogen atoms omitted for clarity

The compound *tetrakis*(5-nitroquinolin-8-olato-$\kappa^2 N,O$)zirconium(IV) crystallizes in the tetragonal space group, $\bar{4}2d$. The asymmetric unit consists of a Zr(IV) metal centre located on crystallographic fourfold roto-inversion axis and is coordinated to one crystallographically independent, disordered bidentate ligand (5-nitroquinolin-8-olate = 5-NO$_2$Ox$^-$) without any solvent molecules present. The other three ligands of this eight-coordinate metal molecule are generated *via* symmetry. The disordered chelation of the 5-NO$_2$Ox ligand exists in a 51.2(8) % (Zr$_A$) : 48.8(8) % (Zr$_B$) ratio.
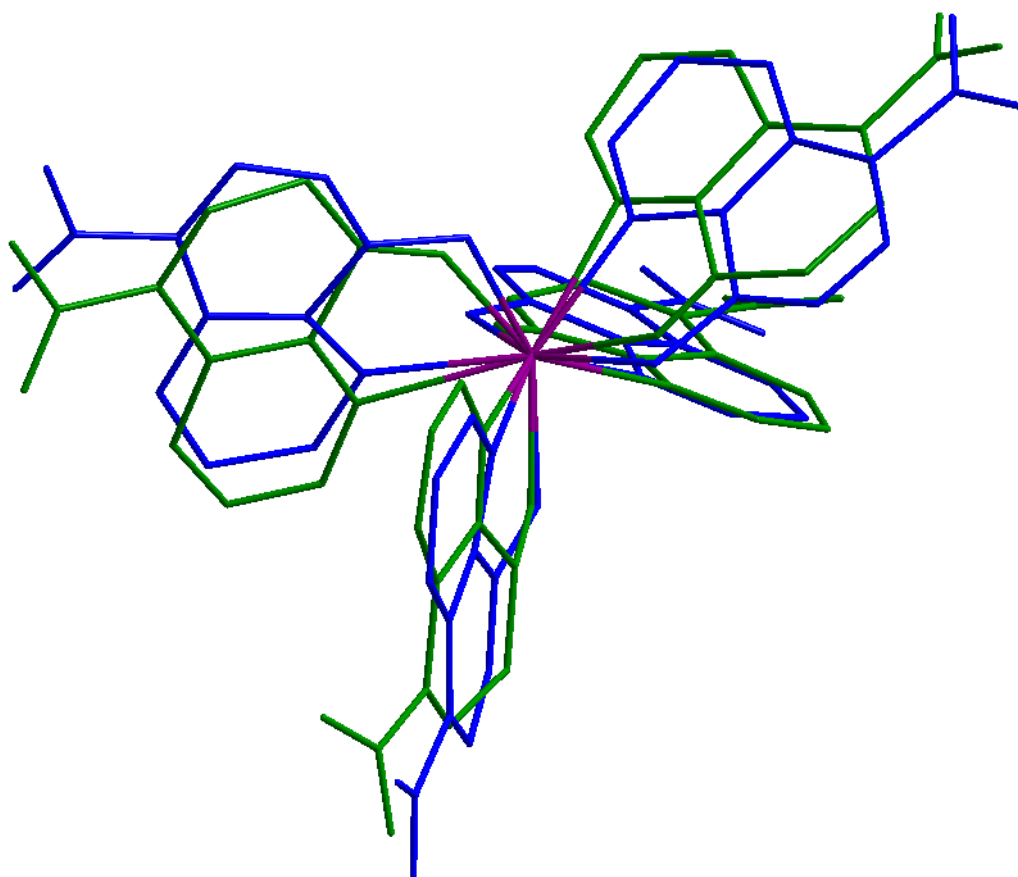
Figure 5.15 Graphic illustration of [Zr(5-NO$_2$Ox)$_4$] showing overlay of this disordered compound. (**green**) A = 51%; (**blue**) B = 49%. Hydrogen atoms omitted for clarity

In this compound two different coordination geometries are observed. The N,O-donating ligands for each of the disordered Zr-molecules surrounding the metal centres, are placed in a space filling, fan-like arrangement. At first it appears that both Zr$_A$ and Zr$_B$ exhibits the expected approximate, slightly distorted, square-antiprismatic coordination polyhedron (Figure 5.16). However, when the distortion from the ideal square antiprism is measured, it becomes evident that two different geometries are present. The Zr$_A$-molecule (with an outward bend of 17.53(55) °) characteristically illustrates the slightly distorted, square-antiprismatic coordination polyhedron, but the Zr$_B$-molecule (with an outward bend of 28.33(63) °) exhibits a distorted dodecahedral geometry, as illustrated in Figure 5.17.

Table 5.4 Selected Geometric Parameters for [Zr(5-NO$_2$Ox)$_4$].

Selected Bond Lengths (Å)			
Zr—N$_{1A}$	2.493(17)	Zr—N$_{1B}$	2.340(20)
Zr—O$_{1A}$	2.078(15)	Zr—O$_{1B}$	2.134(11)
N$_{2A}$—O$_{2A}$	1.198(15)	N$_{2B}$—O$_{2B}$	1.195(17)
N$_{2A}$—O$_{3A}$	1.170(20)	N$_{2B}$—O$_{3B}$	1.177(19)
N$_{2A}$—C$_{5A}$	1.459(13)	N$_{2B}$—C$_{5B}$	1.484(18)
Selected Bite Angles (°)			
N$_{1A}$—Zr—O$_{1A}$	67.1(5)	N$_{1B}$—Zr—O$_{1B}$	68.6(4)
Selected Geometric Coordination Angles (°)			
N$_{1A}$—Zr—N$_{1A}$^{i}	69.1(7)	N$_{1B}$—Zr—N$_{1B}$^{i}	70.0(8)
N$_{1A}$—Zr—N$_{1A}$^{ii}	132.7(7)	N$_{1B}$—Zr—N$_{1B}$^{ii}	132.2(5)
O$_{1A}$—Zr—O$_{1A}$^{i}	133.0(6)	O$_{1B}$—Zr—O$_{1B}$^{i}	150.4(5)
O$_{1A}$—Zr—O$_{1A}$^{ii}	99.1(2)	O$_{1B}$—Zr—O$_{1B}$^{ii}	93.7(1)
Symmetry codes: (i) −x+1, −y, z; (ii) y+1/2, −x+1/2, −z+3/2.			
Selected Torsion Angles (°)			
N$_{1A}$—C$_{9A}$—C$_{8A}$—O$_{1A}$	9.8(19)	N$_{1B}$—C$_{9B}$—C$_{8B}$—O$_{1B}$	−6.6(18)
Ligand Plane Angles (°)			
Lig1/Lig2	78.29(45)	Lig3/Lig4	78.29(49)
Lig2/Lig3	55.130(35)	Lig4/Lig1	53.69(28)

Figure 5.16 Graphic illustration of the square-antiprismatic coordination polyhedron of [Zr(5-NO$_2$Ox)$_4$]. Side view showing upper and lower four corners represented by the N- and O-coordinating atoms of the ligands. Hydrogen atoms omitted for clarity.
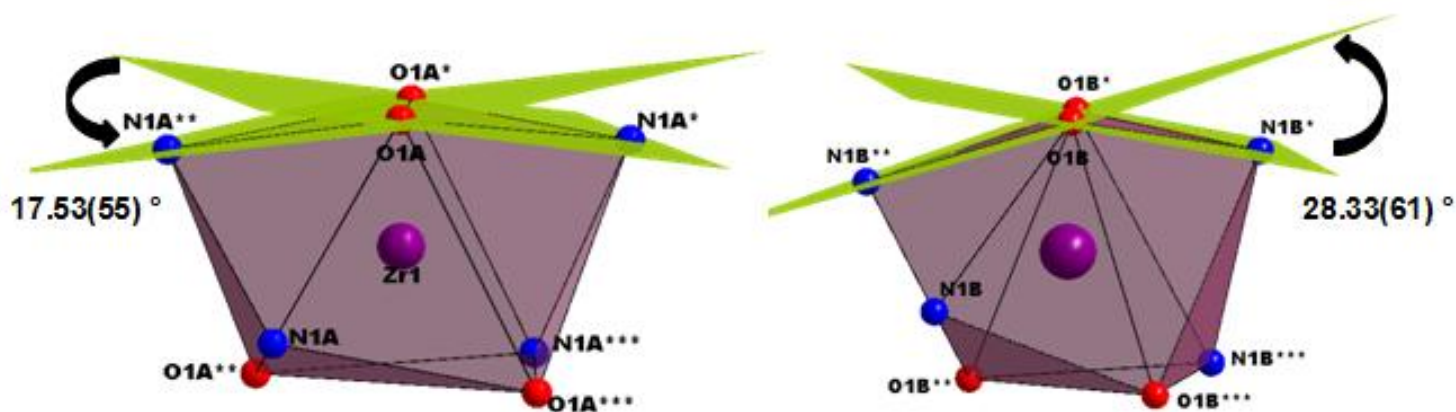
Figure 5.17 Illustration of the distortion of the square-antiprismatic coordination polyhedron found in [Zr(5-NO$_2$Ox)$_4$], showing the outward bend of the top-most atoms; (**left**) Zr$_A$-molecule - 17.53(55) °, (**right**) Zr$_B$-molecule - 28.33(63) °.

In this structure the Zr—N and Zr—O bond distances are 2.417(18) Å and 2.106(13) Å, respectively, and the N—Zr—O bite angle is found to be 69.9(4) ° (Table 5.4). The measured N—C—C—O torsion angles of the ligand frame facing the N—Zr—O bite angles are found to range from −6.6(18) ° to 9.8(19) °, indicating negligible deviation from the planarity of the ligands themselves.
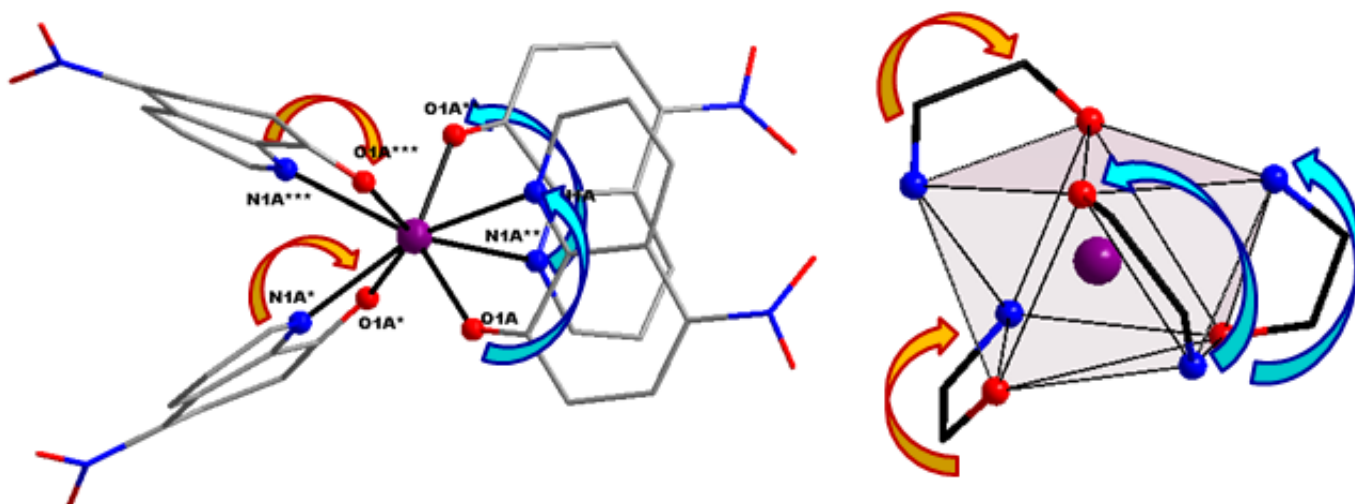
Figure 5.18 Graphic illustration of the coordination manner and isomer as found for [Zr(5-NO$_2$Ox)$_4$]. **Yellow arrows** indicating corner-coordinated ligands, **blue arrows** for side-coordinated ligands on the antiprismatic polyhedra. **(left)** Side view showing the arrangement of the ligands around the metal centre; **(right)** Isomer description as determined from the placement of the ox-ligands on the square antiprism - in this case the mixed C$_2$ isomer.

The ligands in this compound are arranged around the metal centre in a manner that does not conform to the previously described species. The ligands themselves do not lie across the metal centre in the manner that allows a discernable description of *alternating* or *mirrored* chelation of components. The reason for this becomes apparent when the coordination isomer for this compound is defined, as illustrated in Figure 5.18. When one considers the arrangement of the four oxine ligands along the edges of the square antiprismatic chelation geometry, it becomes clear that this compound exhibits the C_2 isomer, with a combination of corner- and side-clipped ligands. As such, when only visualising the ligands as they are spaced around the metal centre, there appears to be an alternating swivelling of ligands in the fan-like arrangement, with a 102.42(47) ° angle between the planes of opposite facing ligands (Figure 5.18a & 5.19). In other words, ligands opposite each other are not perpendicularly swivelled either.

Furthermore, the planes defined by each individual ligand are not perfectly flat. There is an outward bend of the C_6 and C_7 atoms out of the average plane defined by most of the ligand atoms, at an average distance of 0.121(17) Å and 0.113(19) Å, respectively. These "average ligand-planes" lie adjacent to each other at dihedral angles ranging from 55.13(35) ° at the smallest (Lig2/Lig3) to 78.29(49) ° at the largest (Lig3/Lig4) as reported in Table 5.4.
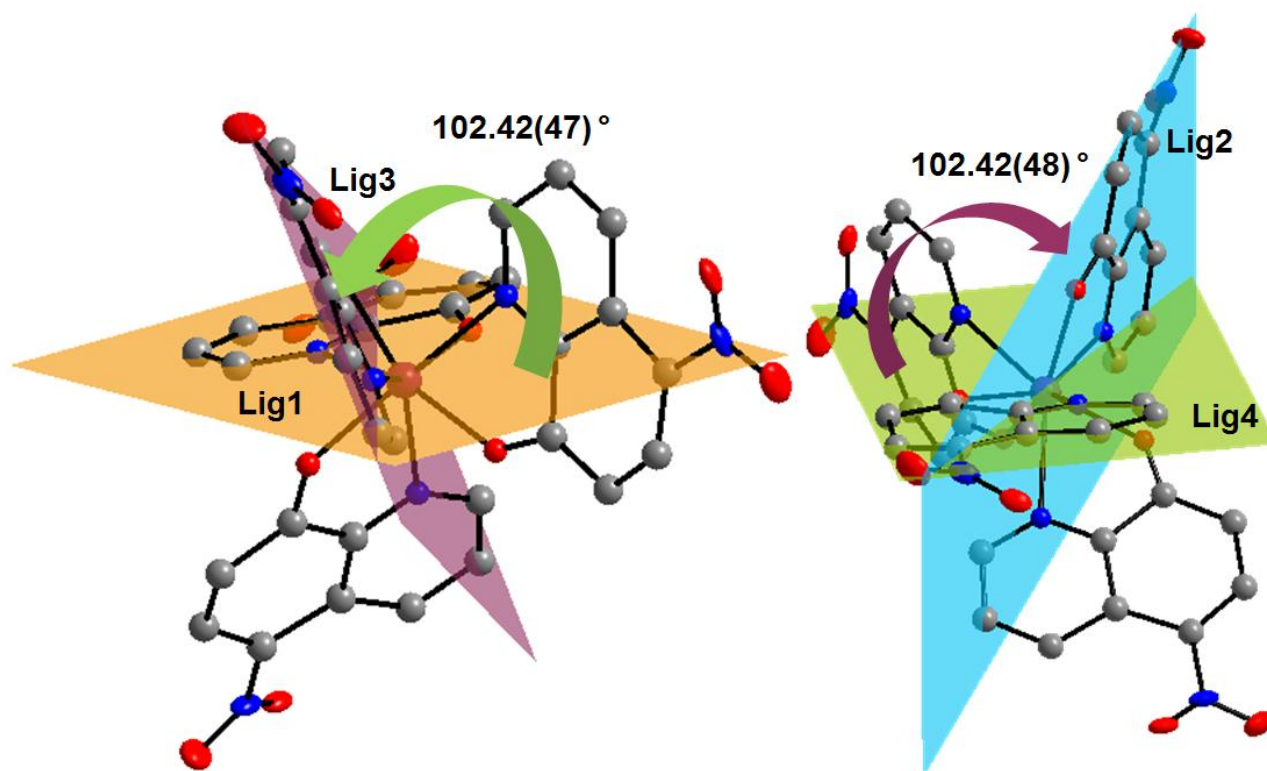
Figure 5.19 Illustration of the different ligand planes measured across the Zr metal centre. (**left**) Lig1/Lig3 at an angle of 102.42(47) °; (**right**) Lig2/Lig4 at an angle of 102.42(48) °.

Only two *intramolecular* C—H•••O (Table 5.5) hydrogen bonding interactions are observed in this structure. As illustrated in Figure 5.20, both interactions are linked to the NO_2-section of the ox-ligand, with C_{1A}—H_{1A}•••O_{2A}^{iii} (*iii* = *y, x−1/2, z+1/4*) and C_{2A}—H_{2A}•••O_{3A}^{iv} (*iv = y, −x+1, −z+1*) from symmetry generated molecule linking the crystal lattice as a whole.

Table 5.5 Hydrogen-bond geometry in the title compound (Å, °).

D—*H*⋯*A*	*D*—*H*	*H*⋯*A*	*D*⋯*A*	*D*—*H*⋯*A*
C_{1A}—H_{1A}⋯O_{2A}^{iii}	0.95	2.38	3.29(2)	162
C_{2A}—H_{2A}⋯O_{3A}^{iv}	0.95	2.21	3.11(3)	156
Symmetry codes: (iii) y, x−1/2, z+1/4; (iv) y, −x+1, −z+1.				
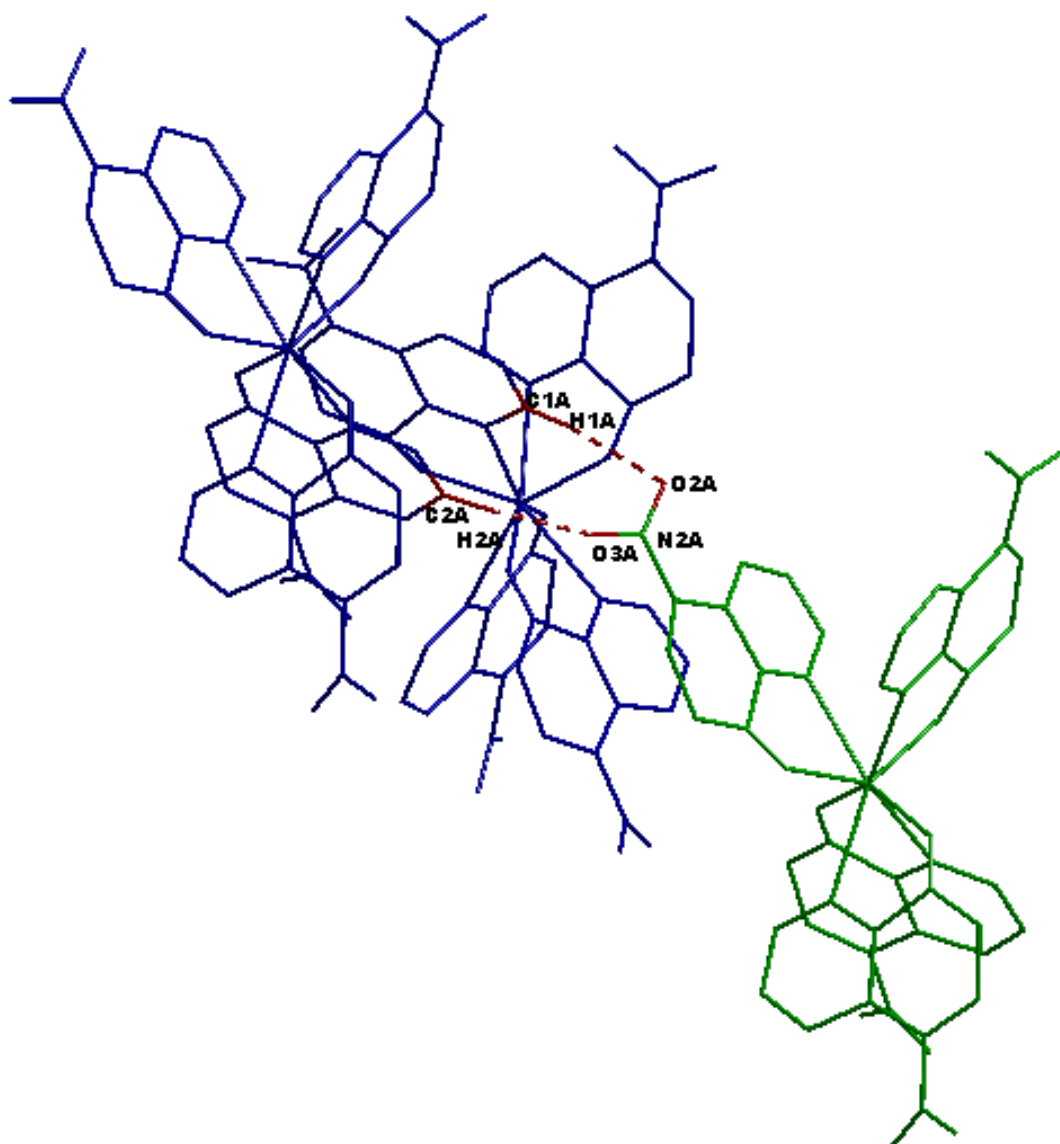
Figure 5.20 Illustration of the intra-molecular hydrogen bonding interaction found in the title molecule. C_{01}—H_{01}⋯O_{03} (Table 5.5).

Crystal lattice stabilization is further influenced by π–π interactions between the benzene and pyridine rings of both the Zr_A and Zr_B disordered molecules (Figure 5.21). Benzene rings are found to pack with a centroid-to-centroid and interplanar distances of 3.624(11) Å and 3.541(8) Å, respectively. Pyridine rings pack with centroid-to-centroid and interplanar distances of 3.522(10) Å and 3.406(7) Å.
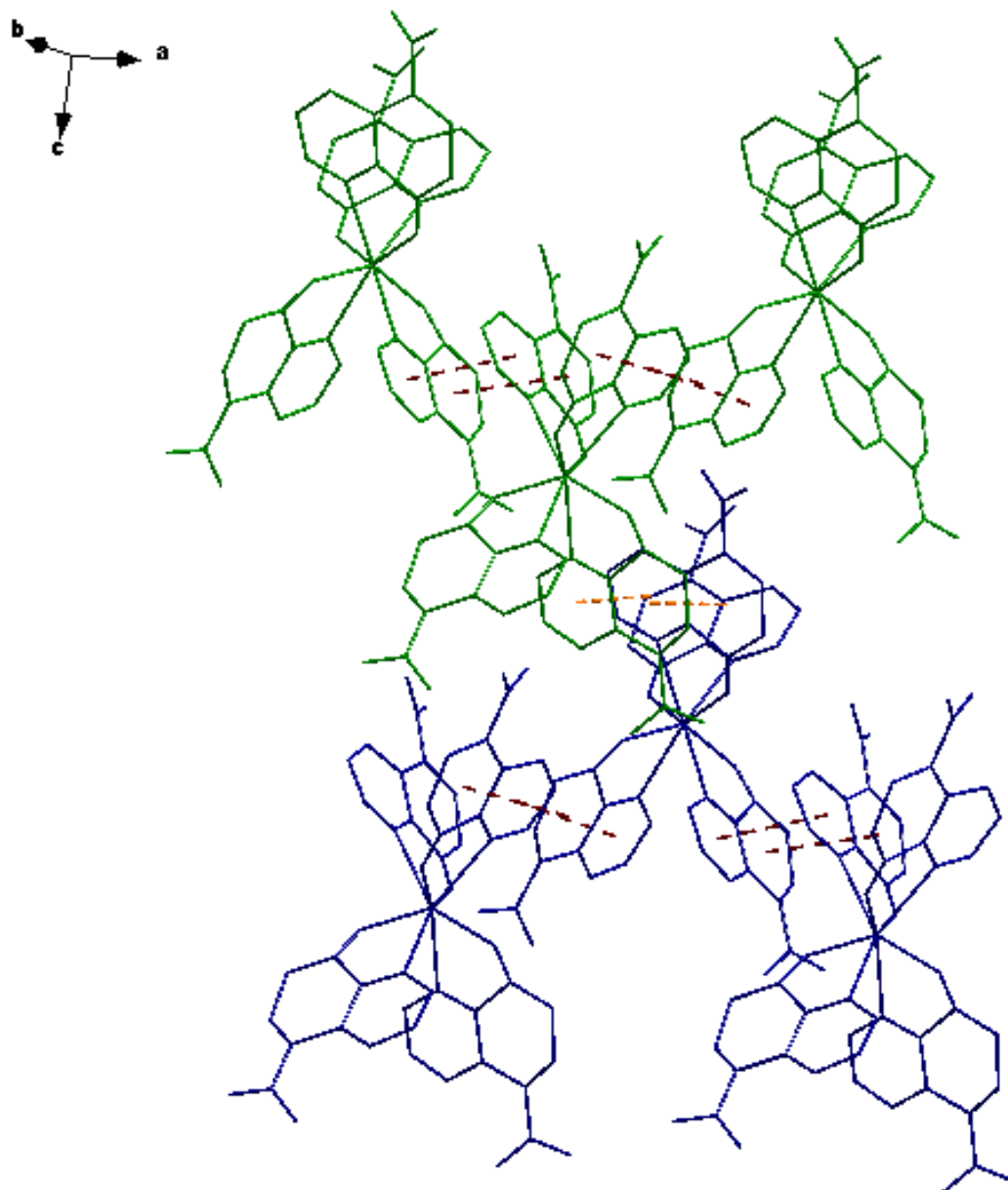
Figure 5.21 Graphical illustration of the head-to-head packing found in the title compound, depicting the paired π–π interactions between the benzene and pyridine rings of the 5-NO_2Ox Ligands along the *ac*-plane (***red dotted line***), as well along the *bc*-plane (***orange dotted line***) linking the entire crystal lattice into a tightly packed network.

5.4. Crystal Structure of [Zr(Pic)$_4$].2H$_2$O – Zr_3a

The structure of this *tetrakis*-coordinated zirconium - picolinic acid complex[10] (**Zr_3a**) is another significant example of the more symmetrical coordination specimens of zirconium-oxine-type crystallographically characterised structures. Synthesis of **Zr_3a** and the resulting colourless crystals obtained for this was discussed in § 3.2.3.1.

A summary of the general crystal data is given in Table 5.1, while the numbering scheme of the solvated complex is shown in the perspective drawing in Figure 5.22. Table 5.6 presents selected bond lengths and angles of the title compound. Atomic coordinates, anisotropic displacement parameters, all bond distances and angles and hydrogen coordinates, are given in the supplementary data (Appendix A.6). Hydrogen atoms and/or solvent molecules are omitted in some molecular presentations for clarity.
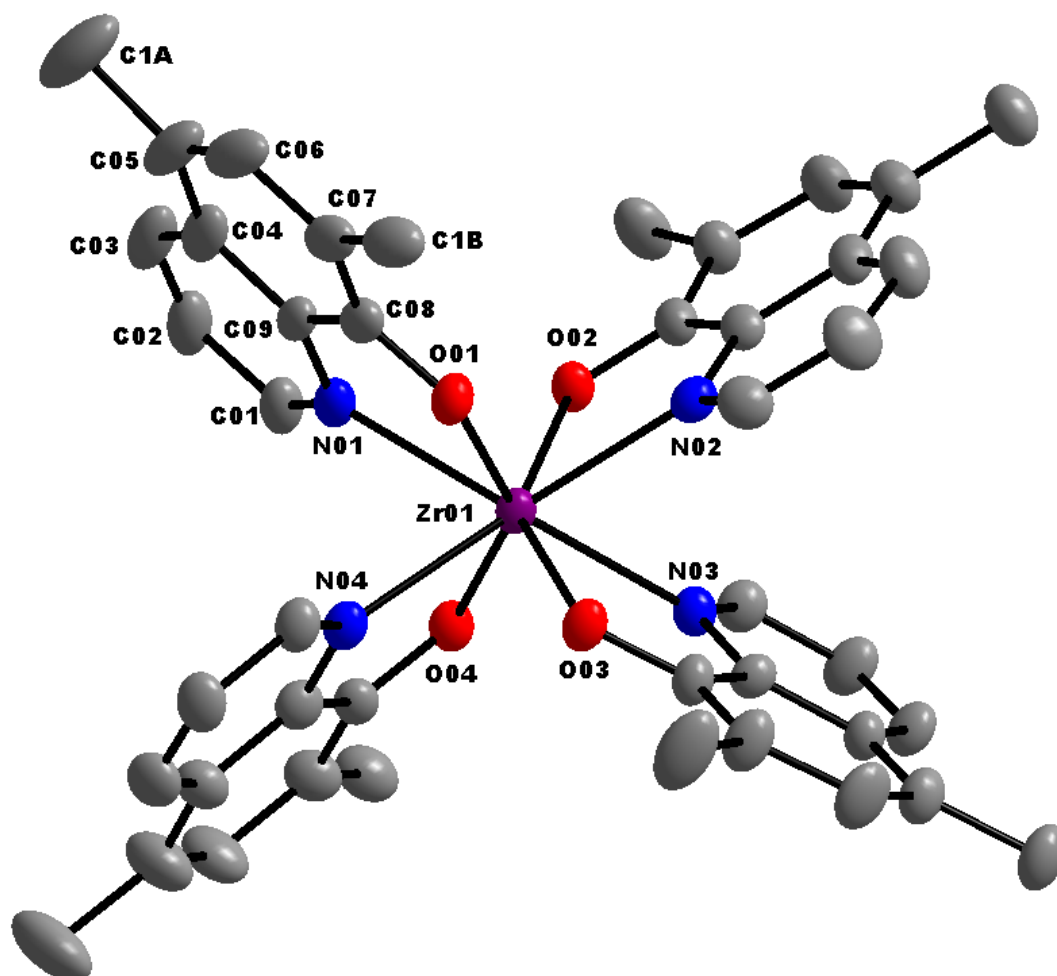
The compound *tetrakis*(picolinato-$\kappa^2 N,O$)zirconium(IV) dihydrate crystallizes in the tetragonal space group, *P*4$_2$/*n*. The asymmetric unit consists of a Zr(IV) metal centre located on a crystallographic fourfold rotoinversion axis and is coordinated to one crystallographically independent bidentate ligand (Picolinic Acid = Pic) with half of a water solvent molecule present. The other three ligands, as well as water solvent molecules sections, of this eight-coordinate metal molecule are generated *via* symmetry.
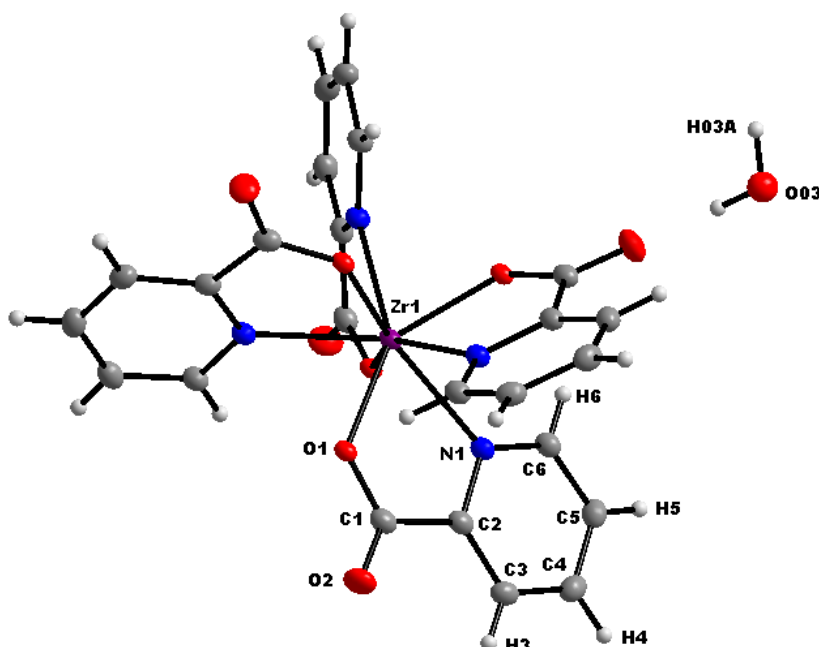
Figure 5.22 Graphic illustration of [Zr(Pic)$_4$].2H$_2$O showing general numbering of atoms. Displacement ellipsoids drawn at 50% probability.

---

[10] M. Steyn, H.G. Visser, A. Roodt & T.J. Muller; *Acta Cryst. E67* (**2011**), m1240-m1241 .

Table 5.6 Selected Geometric Parameters for [Zr(Pic)$_4$].2H$_2$O.

Selected Bond Lengths (Å)			
Zr1—N$_1$	2.393(2)	O$_1$—C$_1$	1.294(3)
Zr1—O$_1$	2.120(2)	O$_2$—C$_1$	1.218(3)

Selected Geometric Coordination Angles (°)			
N$_1$—Zr—O$_1$	69.79(7)		
N$_1$—Zr—O$_1$[i]	73.05(7)	O$_1$—Zr—N$_1$[i]	145.95(7)
N$_1$—Zr—O$_1$[ii]	78.95(7)	O$_1$—Zr—N$_1$[ii]	78.95(7)
N$_1$—Zr—O$_1$[iii]	145.95(7)	O$_1$—Zr—N$_1$[iii]	73.05(7)
N$_1$—Zr—N$_1$[i]	129.78(7)	O$_1$—Zr—O$_1$[i]	96.47(3)
N$_1$—Zr—N$_1$[ii]	73.76(11)	O$_1$—Zr—O$_1$[ii]	140.77(10)

Symmetry codes: (i) y, −x+1/2, −z+3/2; (ii) −x+1/2, −y+1/2, z; (iii) −y+1/2, x, −z+3/2.

Selected Torsion Angles (°)			
N$_1$—C$_2$—C$_1$—O$_1$	6.42(31)	O$_2$—C$_1$—C$_2$—C$_3$	7.96(39)

| Ligand Plane Angles (°)			
Lig1/Lig2	74.28(5)	Lig3/Lig4	74.29(5)
Lig2/Lig3	68.62(5)	Lig4/Lig1	68.62(5)
Lig1/Lig3	111.38(5)	Lig2/Lig4	111.38(5)
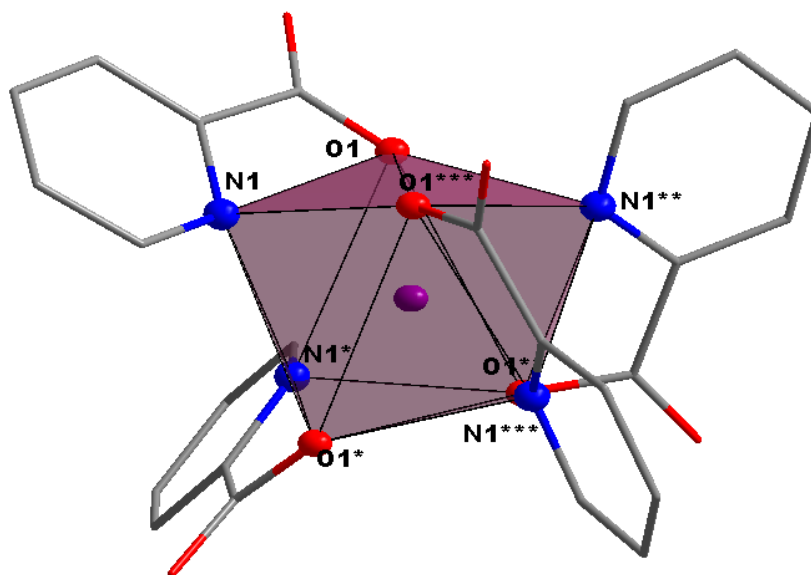
Figure 5.23 Graphic illustration of the square-antiprismatic coordination polyhedron of [Zr(Pic)$_4$]. **(left)** Side view showing upper and lower four corners represented by the N- and O-coordinating atoms of the ligands; **(right)** Top view showing the alternating spacing of the coordinative atoms. Hydrogens and solvent molecules omitted for clarity.

The N,O-donating ligands surrounding the metal centre, are placed in a space filling, fan-like arrangement to give an approximate square-antiprismatic coordination polyhedron (Figure 5.23), with a slight outward distortion towards dodecahedral geometry. This distortion from the ideal square antiprism is associated with an outward bend of 21.02(7) °as illustrated in Figure 5.24.
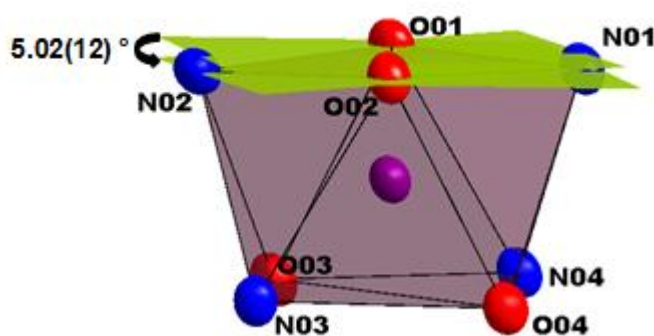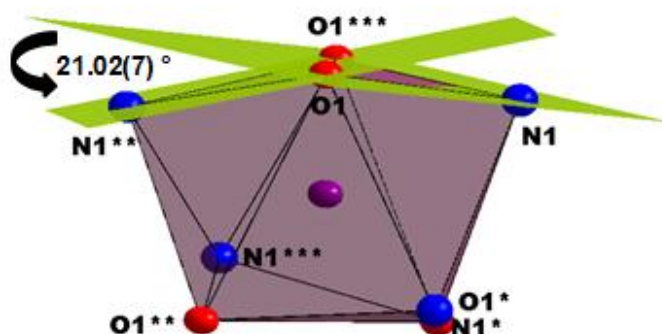

Figure 5.24 Illustration of the distortion of the square-antiprismatic coordination polyhedron found in [Zr(Pic)$_4$], showing the outward bend of the top-most atoms at an angle of 21.02(7) °.

In this structure the Zr—N and Zr—O bond distances are 2.393(2) Å and 2.120(2) Å, respectively, and the average N—Zr—O bite angle is found to be 69.79(7) ° (Table 5.6). The measured N—C—C—O torsion angle of the ligand frame facing the N—Zr—O bite angle is found to be 6.42(31) °, indicating very little deviation from the planarity of the ligands themselves.

The ligands in this compound are arranged around the metal centre in a manner that does not conform to the previously described species. The ligands themselves do not lie across the metal centre in the manner that allows a discernable description of *alternating* or *mirrored* chelation of components. The reason for this becomes apparent when the coordination isomer for this compound is defined, as illustrated in Figure 5.25 and 5.26. When one considers the arrangement of the four oxine ligands along the edges of the square antiprismatic chelation geometry, it becomes clear that this compound exhibits the C$_2$ isomer, with a combination of corner- and side-clipped ligands. As such, when only visualising the ligands as they are spaced around the metal centre, there appears to be an alternating swivelling of ligands in the fan-like arrangement, with a 111.38(5) ° angle between the planes of opposite facing ligands (Figure 5.26). In other words, ligands opposite each other are not perpendicularly swivelled either.
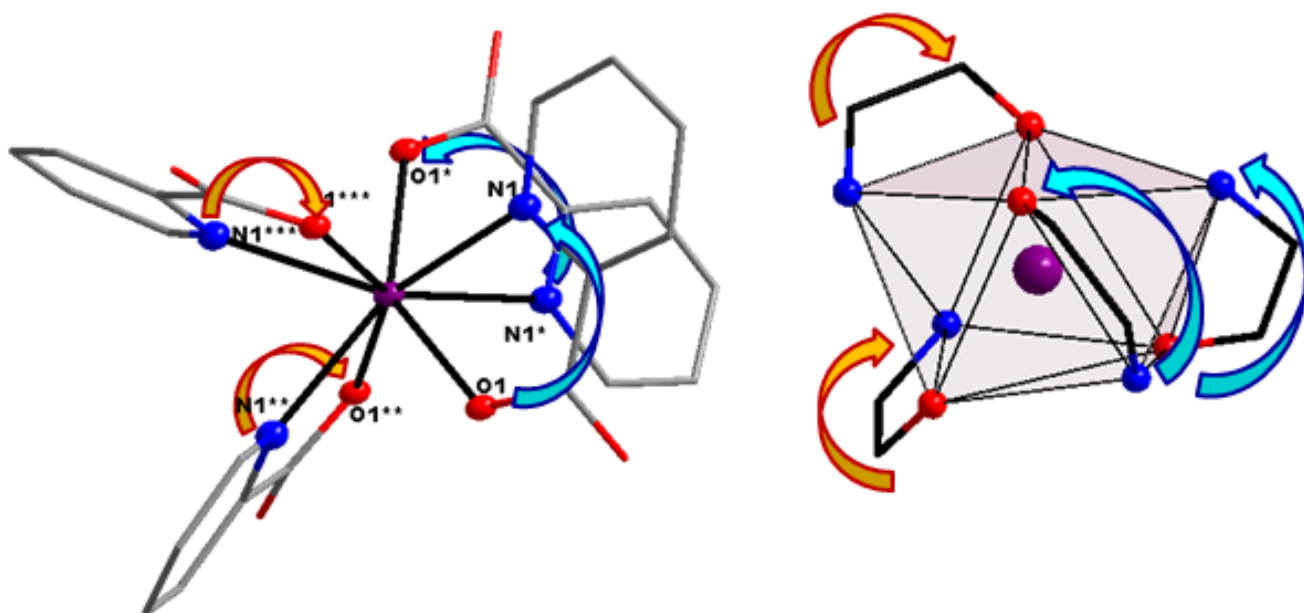
Figure 5.25 Graphic illustration of the coordination manner and isomer as found for [Zr(Pic)$_4$]. *Yellow arrows* indicating corner-coordinated ligands, *blue arrows* for side-coordinated ligands on the antiprismatic polyhedra. **(left)** Side view showing the arrangement of the ligands around the metal centre; **(right)** Isomer description as determined from the placement of the ligands on the square antiprism - in this case the mixed C$_2$ isomer.

Furthermore, the planes defined by each individual ligand appear flat, with no deviation of any one atom out of the plane. These "average ligand-planes" lie adjacent to each other at dihedral angles ranging from 68.62(5)° at the smallest (Lig2/Lig3; Lig4/Lig1) to 74.29(5) ° at the largest (Lig1/Lig2; Lig3/Lig4) as reported in Table 5.6.
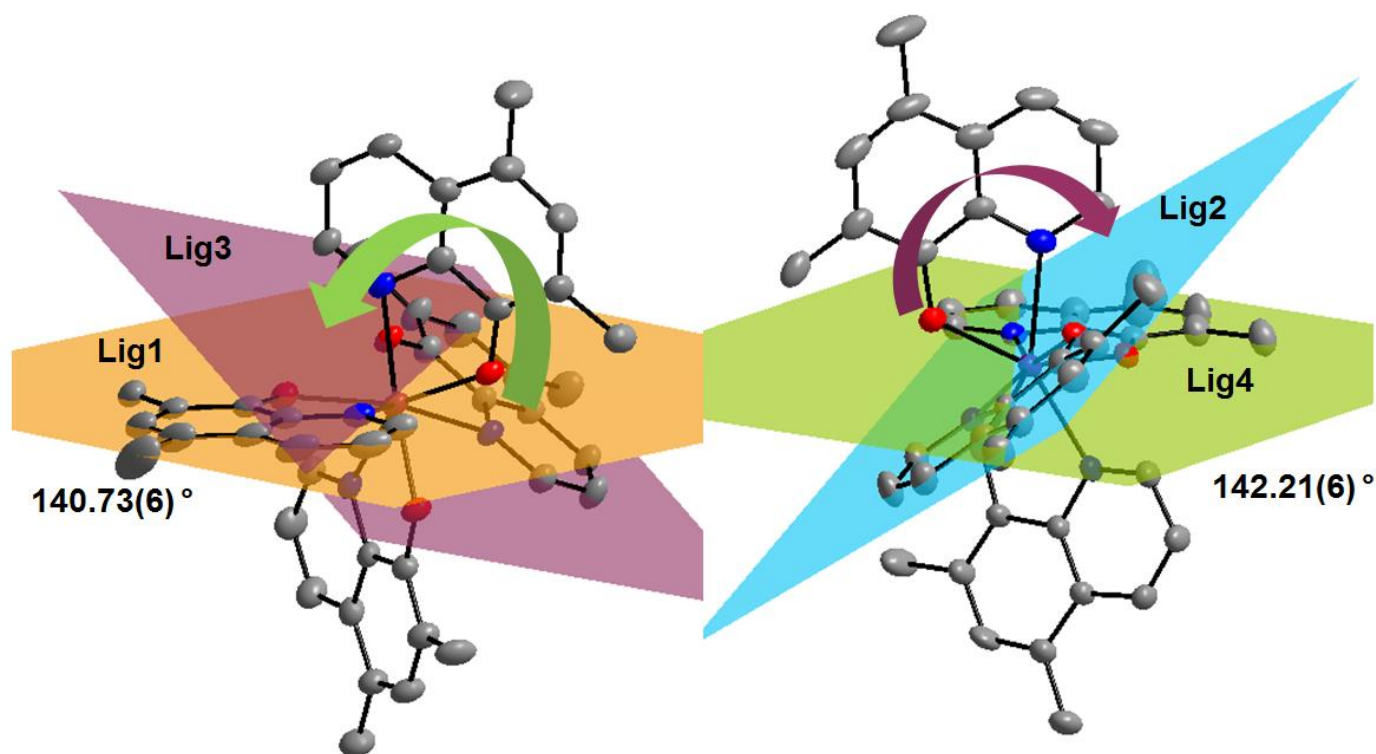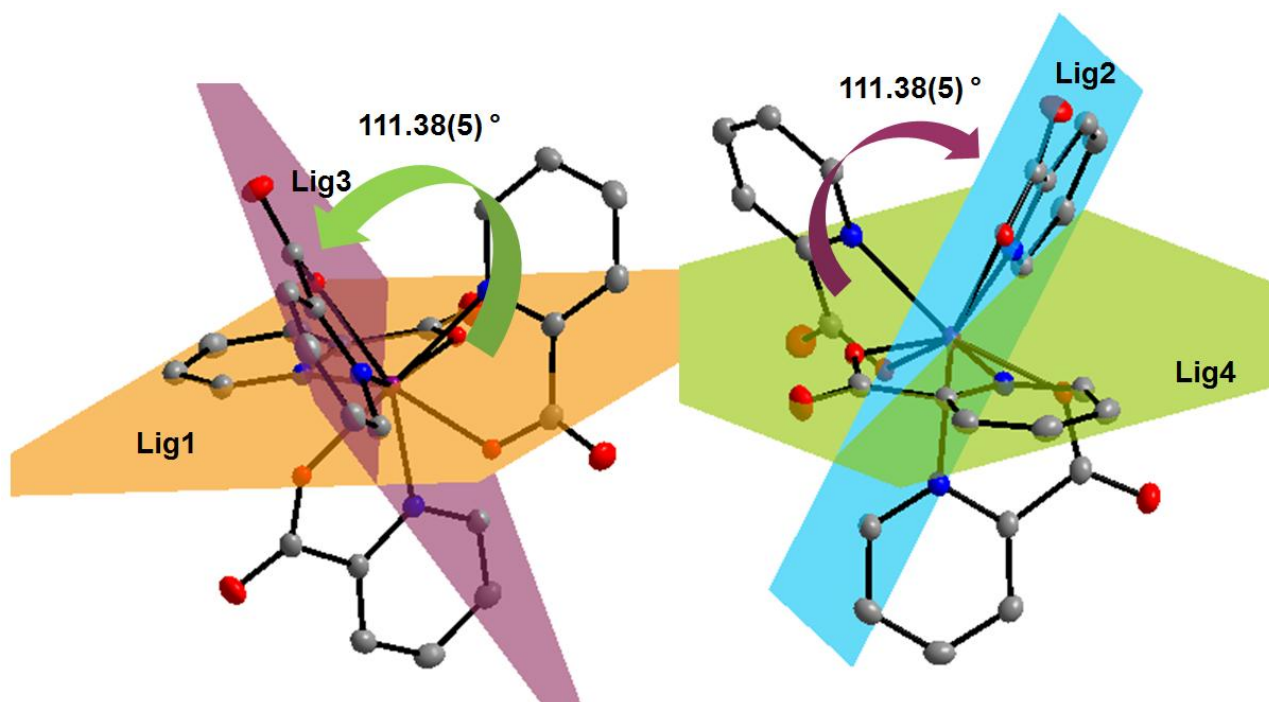

Figure 5.26 Illustration of the different Ligand Group Planes measured across the Zr metal center. **(left)** Lig1/Lig3 at an angle of 111.38(5) °; **(right)** Lig2/Lig4 at an angle of 111.38(5) °.

Intra-molecular C—H•••O hydrogen bonding interactions are observed between the solvent water and the C=O substituent on the Pic-ligand. The effect of this hydrogen bonding interaction network appears to clip the entire lattice in place at the corners where each water molecule is placed (Figure 5.27, Table 5.7).

Table 5.7 Hydrogen-bond geometry in the title compound (Å, °).

D—H$\cdots A$	D—H	H$\cdots A$	$D\cdots A$	D—H$\cdots A$
O_{03}—$H_{03A}\cdots O_2^{iv}$	0.94 (2)	1.89 (2)	2.829 (3)	175 (5)
Symmetry code: (iv) y, $-x+3/2$, $-z+3/2$.				
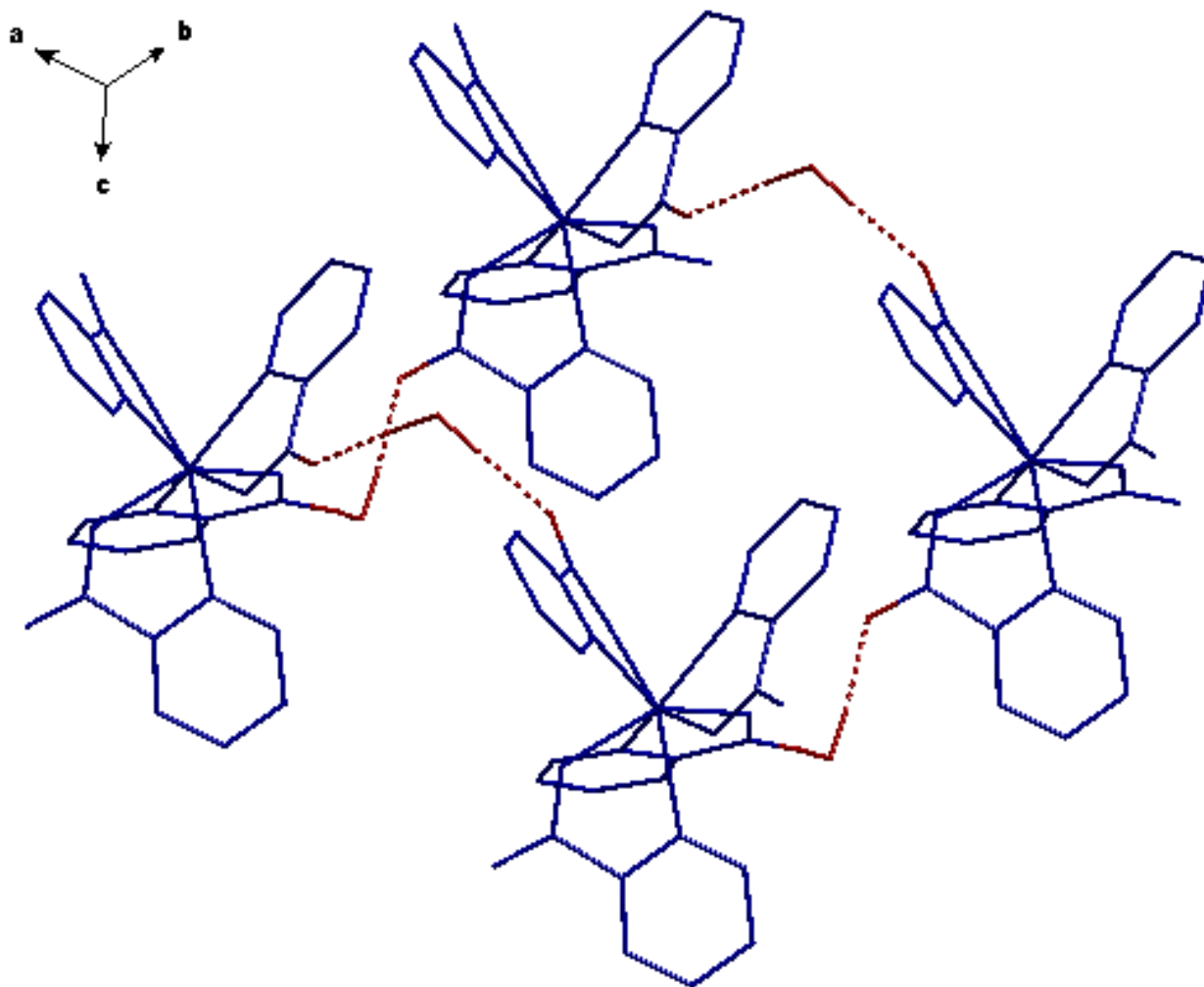
Figure 5.27 Illustration of the intra-molecular hydrogen bonding interaction found in the title molecule. O_{03}—$H_{03A}\cdots O_2$ (Table 5.7).

Crystal lattice stabilization is further influenced by π–π interactions through each Pic pyridine ring with its neighbour in a criss-cross pattern (Figure 5.28). These π-π stacking interactions are arranged with interplanar and centroid-to-centroid distances of 3.271(35) Å and 3.6391(15) Å, respectively. The greater effect of this criss-cross π–π stacking has the entire lattice arranged in a head-to-tail packing of the crystal network, with alternate direction of packing for each neighbouring column, as illustrated in Figure 5.28.
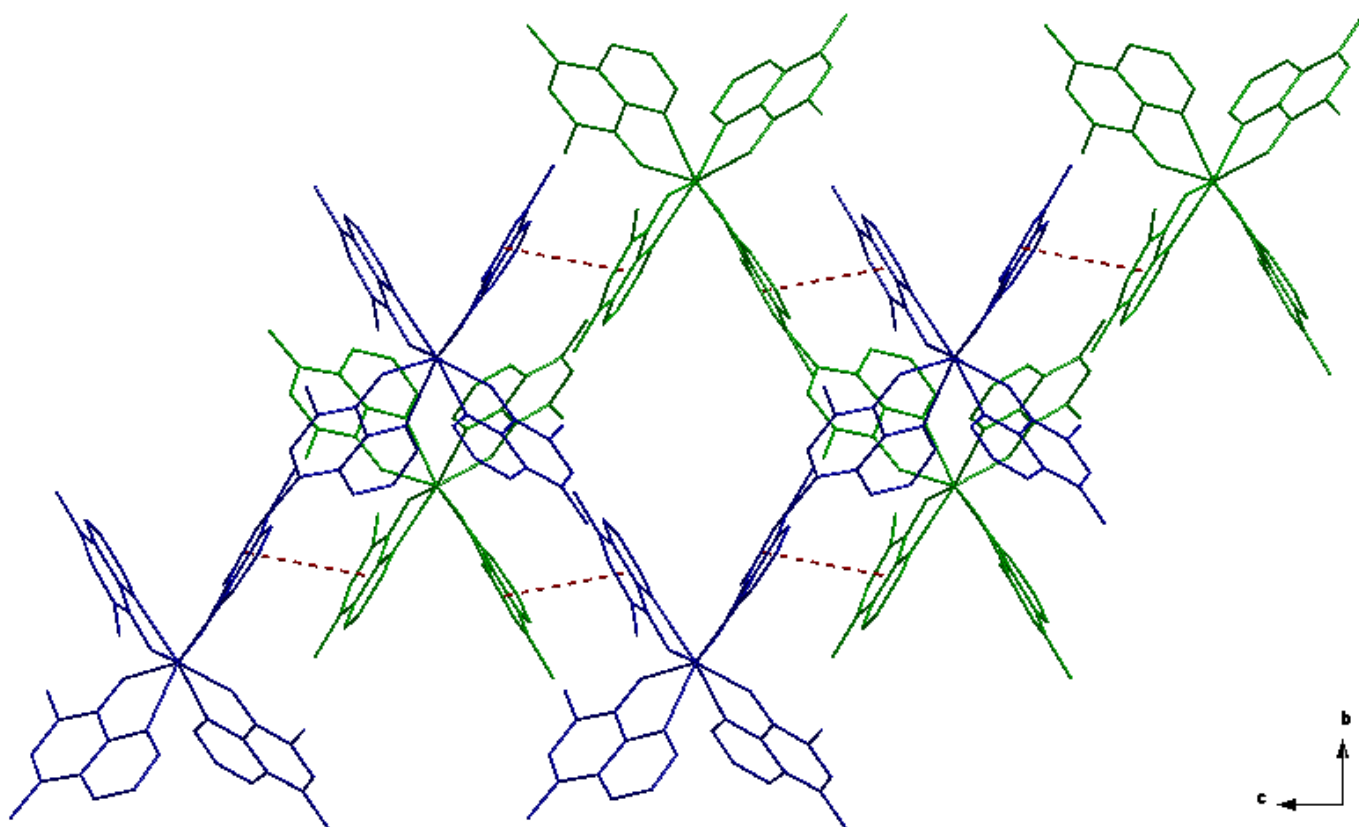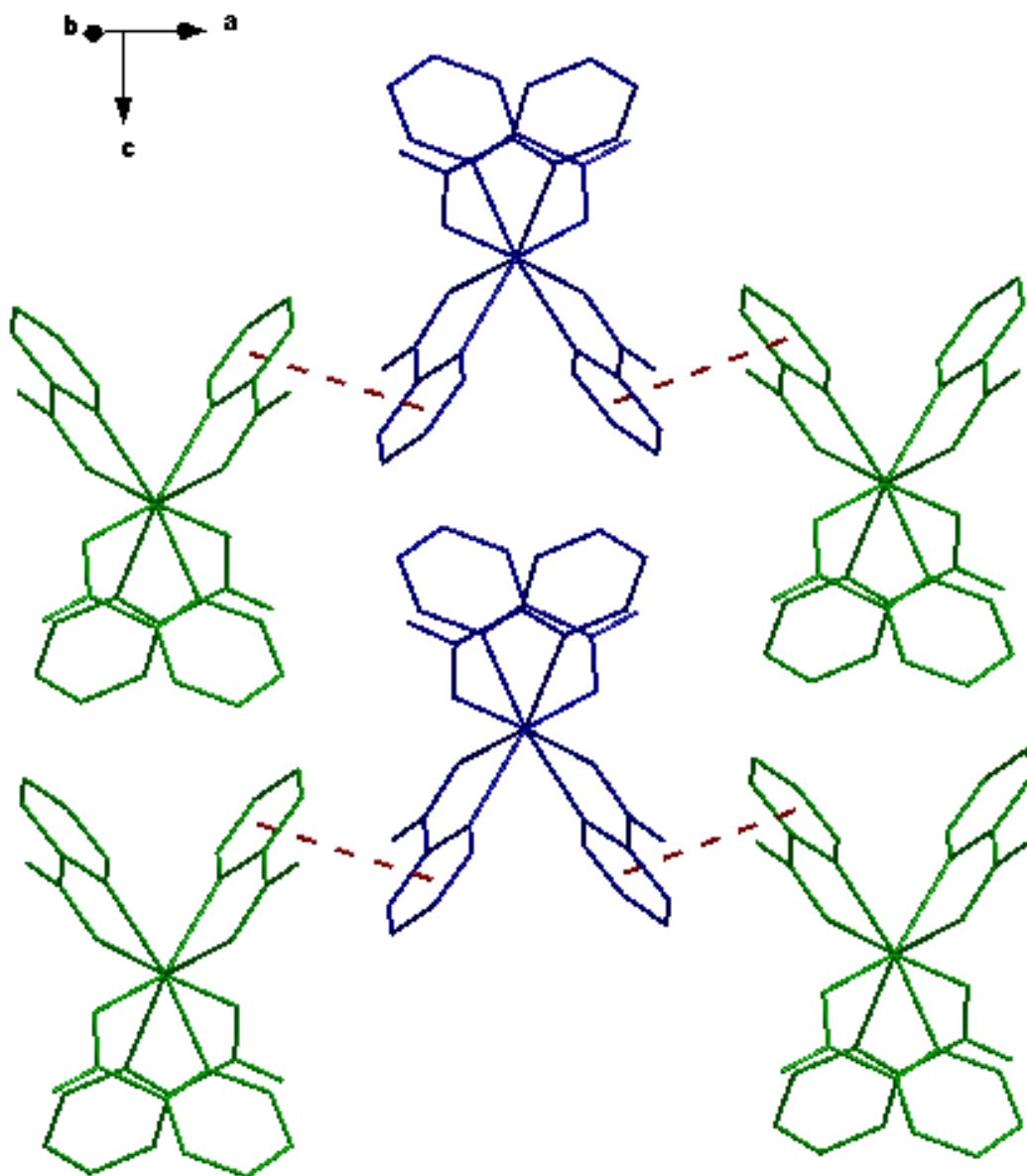

Figure 5.28 Graphical illustration of the head-to-tail packing found in the title compound, depicting the paired *π–π* interactions between the pyridine rings of the Pic ligands (***red dotted line***). Hydrogen atoms and solvent molecules omitted for clarity.

5.5. Evaluation of Structural Characteristic Comparisons

In order to effectively evaluate the structural data presented here and in the previous chapter, a comparison of certain structural aspects of the zirconium-oxine complexes, as determined crystallographically, need to be taken into consideration. Specific aspects, as mentioned in the previous chapter, worth considering consist of the following general focus areas when discussing these complexes:

- Extent of coordination - limitation of the amount of ligands coordinated.

- Coordination mode/geometry around the metal centre specifically- two possibilities appear to be prevalent throughout literature for these specific complexes containing singular nature ligands, i.e. dodecahedral or square-antiprismatic.

- Nature of specific bond lengths - in bidentate complexes, the characteristics observed in bond length comparisons.

- Effective packing, as influenced by presence/absence of solvate molecules.

- Packing/stabilization - specific influencers to be investigated/predicted in model compounds.

With these factors in mind, a comparative evaluation of the presented zirconium solid state structures as well as structures hafnium counterparts in literature can be summarised as in Tables 5.8 and 5.9 below. In general, with the greater group of structurally characterised complexes available at this stage, there can be a more certain set of assumptions made with regard to the solid state behaviours of zirconium(IV) and hafnium(IV) complexes of oxine-type ligands.

When considering the summarized data from Tables 5.8 and 5.9, it becomes clear that there is no definite trend for the favoured solid state crystal packing in any one particular space group. Furthermore, no specific crystal systems is favoured either, when considering the wide range of monoclinic, triclinic, orthorhombic and tetragonal examples presented.

Table 5.8 Selected crystallographic characteristics, bond lengths and angles of zirconium(IV) and hafnium(IV) - oxine complexes

	[Zr(ox)$_4$].DMF.H$_2$O[a]	[Hf(ox)$_4$].DMF.H$_2$O[b]	[Hf(ox)$_4$].Tol[c]	[Zr(diClOx)$_4$].2DMF[d]	[Hf(diClOx)$_4$].2DMF[e]	[Zr(5ClOx)$_4$].2DMF[f]
Crystal system	Triclinic	Triclinic	Triclinic	Monoclinic	Monoclinic	Monoclinic
Space group	$P\bar{1}$	$P\bar{1}$	$P\bar{1}$	$C2/c$	$P2_1/n$	$P2_1/c$
***a, b, c* (Å)**	11.342(2), 12.209(5), 12.538(4)	11.360 (5), 12.245 (4), 12.504 (5)	11.3323(5), 12.5539(5), 15.7126(7)	30.357(5), 13.037(4), 26.386(4)	22.428(2), 15.789(1), 28.335(2)	18.678(3), 21.176(5), 20.148(2)
***α , β, γ* (°)**	91.728(2), 103.419(3), 99.250(3)	91.817 (4), 103.333 (5), 99.190 (5)	69.746(2), 69.700(2), 75.787(2)	90.0, 118.343(4), 90.0	90.0, 112.527(2), 90.0	90.0, 90.894(4), 90.0
Cell Volume (Å^3)	1662.7(12)	1666.5(11)	1946.79(14)	9191(4)	9268.9(12)	7968(2)
Z	2	2	2	4	8	4
Coordination Polyhedra	Sq-Anti prismatic	Sq-Anti prismatic	Sq-Anti prismatic	Sq-Anti prismatic	Sq-Anti prismatic	Sq-Anti prismatic
Bidentate Ligands Coordinated	4	4	4	4	4	4
Avg. M — N (Å)	2.420(2)	2.399(2)	2.398(3)	2.452(2)	2.386(5)	2.427(4)
Avg. M — O (Å)	2.106(2)	2.096(2)	2.096(3)	2.095(2)	2.098(4)	2.100(3)
Avg. N — M — O (°)	70.43(7)	70.92(8)	70.94(11)	69.77(7)	70.85(2)	69.97(14)

a) Ref. 11, **b**) Ref. 12, **c**) Ref. 13, **d**) § 4.2, **e**) Ref. 14, **f**) § 4.3.

The coordination environment around the metal centre for most oxine complexes tends to definitively favour the square-antiprismatic polyhedron with minimal distortion towards the dodecahedral geometry. With this in mind, and from the discussion on the matter in § 4.5, it can now be more accurately theorized that zirconium(IV) [and even hafnium(IV)] N,O-bidentate ligand complexes should in most cases certainly yield a square-antiprismatic geometry around the metal centre.

[11] M. Steyn, H.G. Visser & A. Roodt; *J. S. Afr. Inst. Min. Metall. 113* (**2013**), 105-108.

[12] J.A. Viljoen, H.G. Visser, A. Roodt & M. Steyn; *Acta Cryst. E65* (**2009**), m1514–m1515.

[13] J.A. Viljoen, H.G. Visser, A. Roodt & M. Steyn; *Acta Cryst. E65* (**2009**), m1367–m1368.

[14] J.A. Viljoen, H.G. Visser & A. Roodt; *Z. Kristallogr. - New Cryst. Struct. 228* (**2013**), 3, 413-415.

Table 5.9 Selected crystallographic characteristics, bond lengths and angles of zirconium(IV) and hafnium(IV) - oxine complexes

	[ZrCl(CliOx)$_2$ (DMF)$_2$O]$_2$ .DMF[a]	[Hf(CliOx)$_4$] .2DMF[b]	[Zr(diMeOx)$_4$]. 2DMF[c]	[Hf(diMeOx)$_4$] .2DMF[d]	[Zr(5NO$_2$Ox)$_4$][e]	[Zr(Pic)$_4$] .2H$_2$O[f]
Crystal system	Monoclinic	Monoclinic	Orthorhombic	Monoclinic	Tetragonal	Tetragonal
Space group	$P2_1/c$	$P2_1/a$	$Pna2_1$	$P2_1/c$	$I\bar{4}2d$	P4(2)/n
a, b, c (Å)	14.634(3), 13.712(2), 14.710(5)	19.901 (3), 15.247(5), 32.947(1)	15.572(5), 18.706(4), 15.853(4)	9.978(5), 16.0584(3), 28.2474(5)	14.795(5), 14.795(5), 22.082(5)	11.083(5), 11.083(5), 9.548(5)
α , β, γ (°)	90.0, 114.073(4), 90.0	90.0, 105.97(3) , 90.0	90.0, 90.0, 90.0	90.0, 101.582(1), 90.0	90.0, 90.0, 90.0	90.0, 90.0, 90.0
Cell Volume (Å^3)	2695.0(16)	9611(4)	4618(2)	4475.2(15)	4834(3)	1172.8(10)
Z	4	4	4	4	8	8
Coordination Polyhedra	Pentagonal-Bipyramidal	Sq-Anti prismatic	Sq-Anti prismatic	Sq-Anti prismatic	Sq-Anti prismatic	Sq-Anti prismatic
Bidentate Ligands Coordinated	2	4	4	4	4	4
Avg. M — N (Å)	2.420(3)	2.393(3)	2.418(3)	2.398(2)	2.417(18)	2.393(2)
Avg. M — O (Å)	2.116(2)	2.192(2)	2.104(2)	2.098(2)	2.106(13)	2.120(2)
Avg. N — M — O (°)	69.68(10)	69.81(8)	70.16(8)	70.18(8)	67.9(4)	69.79(7)

a) § 4.4, **b**) Ref. 15, **c**) § 5.2, **d**) Ref. 16, **e**) § 5.3, **f**) § 5.4.

As mentioned previously, it has been established in literature that zirconium O,O'-bidentate ligand complexes, in particular the *tetrakis(β*-diketone)zirconium(IV) complexes,[17,18] prefer the square-antiprismatic coordination mode. Now the same conclusion can be drawn for N,O-bidentate ligand complexes, or at the very least for oxine-complexes in general. This is of course excluding the case of the [ZrCl(CliOx)$_2$(DMF)$_2$O]$_2$.DMF complex (see § 4.4), which in itself is a structural anomaly that cannot be clearly explained at this stage. The implication of this measured characteristic of zirconium chelation behaviour tends to suggest that the extent of coordination and even the intimate geometry around the metal centre is governed directly by the zirconium(IV) [and hafnium(IV)] tending towards a maximum state of

[15] J.A. Viljoen; *Unpublished.*
[16] J.A. Viljoen, H.G. Visser & A. Roodt*; Acta Cryst. E67* (**2011**), m1428-m1429**.**
[17] J.V. Silverton & J.L. Hoard; *Inorg. Chem. 2* (**1963**), 243-249.
[18] W. Clegg; *Acta Cryst.C43* (**1987**), 789 -791.

coordination, as preference, or as lowest energy crystallization state. This is in accordance of what is expected in these symbiotic systems.[19] It is worth noting at this stage that the Zr-CliOx and Hf-CliOx complexes exhibit completely different solid state structures, regardless of the fact that synthesis of said complexes occurred via identical techniques. This in itself is a potentially significant step forward in the basic coordination chemistry of these metals, and for advancing knowledge for separation/purification experiments of these metals.

Furthermore, we can conclude with even more certainty than before, that in an overarching comparison of the data currently available, the average Zr — N and Zr — O bond lengths are 2.421(3) Å and 2.107(2) Å, respectively, with an average N — Zr — O bite angle of 70.14(8) °. A comparison of the zirconium and hafnium bond lengths show that, across the board, the Zr — N bonds tend to be *ca.* 0.1 Å longer than the Hf — N bonds of the same ligand-complex. However, with regard to most other structural properties, the zirconium and hafnium oxine complexes are in general similar.

With regard to the effective packing of organometallic molecules on the matter of influences of the solvent molecules present, we can conclude that hydrogen bonding between coordinated ox-ligands and these solvents influence the stability of the lattice as a whole. However, the most noteworthy packing stabilizer is undoubtedly the π-stacking interactions observed in all cases characterised thus far. In some cases we observe direct π-π stacking between coordinated ligands {$[Zr(ox)_4]$,[10] $[ZrCl(CliOx)_2(DMF)_2O]_2$,[§4.4] $[Zr(diMeOx)_4]$,[§5.2] $[Zr(5NO_2Ox)_4]$[§5.3] & $[Zr(Pic)_4]$[§5.4]} and in others halogen-π stacking ($[Zr(5-ClOx)_4]$[§4.3] & $[Zr(diClOx)_4]$[§4.2]). In all these cases we find that the aromatic nature of the ox-ligands (both the pyridine and benzene portions) significantly influences this π stacking tendency of the greater molecular structure as a whole. This stacking dictates the overall stability and arrangement in the crystal lattice as a whole, as is evident from the structural descriptions above.

In the following chapter, Chapter 6, two additional zirconium O,O'-bidentate ligand complexes are structurally evaluated and described. Furthermore, comparisons with literary sources are made with regard to the nature of these zirconium complexes. With even more comparable structures, a clearer picture of the solid state behaviours of these organometallic complexes can be drawn.

The results presented here will be further discussed with regard to the geometric characteristics observed in each case (ligand plane angles, square anti-prism deviations, etc.) in § 6.4.

---

[19] J.E. Huheey, E.A. Keiter & R.L. Keiter; *Inorganic Chemistry - Principles of Structure and Reactivity, 4th Ed.* (**1993**) HarperCollins College Publishers, New York.

Chapter 6

X-Ray Diffraction Studies of Zirconium(IV) Complexes

Containing *O,O'*-Donating Ligands

This chapter contains a detailed discussion of two *O,O'*-bidentate ligand complexes of zirconium(IV) prepared as part of this project. In this case a study of solid state characteristics is evaluated with similar ligands chelated to zirconium in a comparative manner to similar structures found in literature of each ligand type. For each ligand, the intended aim has been to re-synthesize and re-determine the structural characteristics for a new complex obtained from N,N-Dimethylformamide (DMF) as reaction and crystallization solvent.

Firstly, tropolone (2-Hydroxy-2,4,6-cycloheptatrien-1-one = TropH) was employed in synthesis of a zirconium complex, by means of the standard DMF bench-top technique thus far broadly utilized in this project. Trop with its 7-membered aromatic ring could shed light on the effect of steric influencing of the coordination environment around the metal centre studied. Furthermore, the known tendency of this ligand to form extensive π-π stacked crystal lattice network stabilization[1] can prove useful for the studying of ligand-dictated solid state behaviours of zirconium bidentate-ligand complexes.

Secondly, dibenzoylmethane (1,3-Diphenylpropane-1,3-dione = DBMH) was also employed in the synthesis of a zirconium complex, by means of the standard DMF bench-top technique. DBM is an excellent example of a *β*-diketone ligand suitably adjusted for a study

---

[1] G. Steyl & A. Roodt; *Models, Mysteries and Magic of Molecule, Chapter 15* (**2008**), Springer Netherlands, 325-340.

on steric hindrance as influencing factor in solid state behaviours of zirconium and hafnium organometallic complexes.
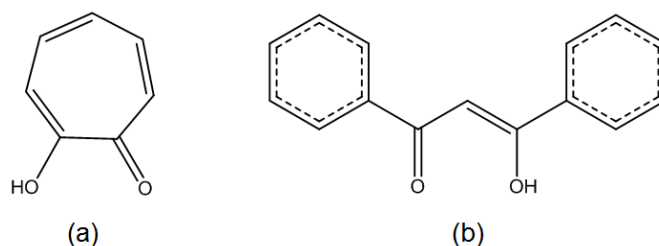
Figure 6.1 *O,O'*-bidentate ligands chelated to zirconium and discussed in this chapter. (**a**) Tropolone (TropH); (**b**) Dibenzoylmethane (DBMH).

6.1. Experimental

The X-ray intensity data was collected on a Bruker X8 ApexII 4K Kappa CCD area detector diffractometer, equipped with a graphite monochromator and MoKα fine-focus sealed tube (λ = 0.71069 Å, T = 100(2) K) operated at 2.0 kW (50 kV, 40 mA). The initial unit cell determinations and data collections were done by the SMART[2] software package. The collected frames were integrated using a narrow-frame integration algorithm and reduced with the Bruker SAINT-Plus and XPREP software packages[3] respectively. Analysis of the data showed no significant decay during the data collection. Data was corrected for absorption effects using the multi-scan technique SADABS,[4] and the structure was solved by the direct methods package SIR97[5] and refined using the WinGX[6] software incorporating SHELXL.[7] The final anisotropic full-matrix least-squares refinement was done on F^2. The methyl and aromatic protons were placed in geometrically idealized positions (C–H = 0.93 – 0.98 Å) and constrained to ride on their parent atoms with U$_{iso}$(H) = 1.2U$_{eq}$(C). Non-hydrogen atoms were refined with anisotropic displacement parameters. The graphics were obtained with the DIAMOND[8] program with 50% probability ellipsoids for all non-hydrogen atoms.

---

[2] Bruker SMART-NT Version 5.050.Bruker AXS Inc. Area-Detector Software Package; Madison, WI, USA, **1998.**
[3] Bruker SAINT-Plus Version 6.02 (including XPREP), Bruker AXS Inc. Area-Detector Integration Software, Madison, WI, USA, **1999.**
[4] Bruker SADABS Version 2004/1.Bruker AXS Inc. Area Detector Absorption Correction Software, Madison, WI, USA, **1998.**
[5] A. Altomare, M.C. Burla, M. Camalli, G.L. Cascarano, C. Giacovazzo, A. Guagliardi, A.G.G. Moliterni, G. Polidori & R. Spagna; *J. Appl. Cryst. 32* (**1999**), 115-119.
[6] L.J. Farrugia; *J. Appl. Cryst. 32* (**1999**), 837-838.
[7] G.M. Sheldrick; SHELXL97. Program for crystal structure refinement, University of Göttingen, Germany, **1997.**
[8] K. Brandenburg & H. Putz; DIAMOND, Release 3.0e, Crystal Impact GbR, Bonn, Germany, **2006.**

Table 6.1 Crystallographic and Refinement Details for structures discussed in this chapter.

Crystal Formula	[Zr(Trop)$_4$].DMF **(Zr_2a)**	[Zr(DBM)$_4$] **(Zr_2b)**
Empirical formula	C$_{31}$ H$_{27}$ N O$_9$Zr	C$_{60}$ H$_{44}$O$_8$Zr
Formula weight (g.mol^{-1})	648.76	984.17
Crystal system, Space Group	Triclinic, $P\bar{1}$	Monoclinic, $P2_1/c$
Unit cell dimensions:		
a, b, c (Å)	10.454(5), 11.734(5), 12.827(5)	24.769(5), 10.216(5), 19.314(5)
α, β, γ (°)	100.050(5), 97.575(5), 113.999(5)	90.0, 101.541(5), 90.0
Volume (Å^3), Z	1378.9(10), 2	4788(3), 4
Density (calculated, mg.cm^{-3})	1.562	1.365
Crystal morphology	cuboid	trapezoid
Crystal Colour	colourless	colourless
Crystal size (mm^3)	0.202 x 0.290 x 0.364	0.331 x 0.630 x 0.792
Absorption coefficient μ (mm^{-1})	0.458	0.288
F(000)	664	2032
Theta range	4.11 to 27.00	1.68 to 28.00
Index ranges	$-13 \le h \le 13$	$-32 \le h \le 32$
	$-14 \le k \le 14$	$-13 \le k \le 13$
	$-16 \le l \le 16$	$-25 \le l \le 25$
Reflections collected, Independent Reflections, R$_{int}$	11655, 5144, 0.0877	88438, 11558, 0.0303
Completeness to 2θ (°, %)	27.00 94.9	28.00 100.0
Max. and min. transmission	0.9140 and 0.8526	0.9110 and 0.8044
Data, restraints, parameters	5144, 0, 382	11558, 0, 622
Goodness-of-fit on F^2	1.057	1.023
Final R indices [I>2σ(I)]	R$_1$ = 0.0767	R$_1$ = 0.0279
	wR$_2$ = 0.2170	wR$_2$ = 0.0665
R indices (all data)	R$_1$ = 0.1031	R$_1$ = 0.0333
	wR$_2$ = 0.2504	wR$_2$ = 0.0700
Largest diff. peak and hole (e.Å^{-3})	3.546 and -2.195	0.407 and -0.529

6.2. Crystal Structure of [Zr(Trop)$_4$].DMF – Zr_2a

The structure of this *tetrakis*-coordinated zirconium - tropolone complex **Zr_2a** is an attempt at the re-synthesis of a published structure[9] reported with a chloroform solvent in the asymmetric unit. Due to the recent successes with the synthetic methodology employing N,N'-dimethylformamide (DMF) as solvent, and subsequently often observing this solvent crystallize along with the studied zirconium bidentate-ligand complexes, the recollection of a new zirconium - tropolone structure was deemed essential. The broader interest in a new structure with a different solvent in the crystal lattice could potentially give insight into solvent effects on the solid state characteristics of zirconium complexes as a whole.

 Synthesis of **Zr_2a** and the resulting colourless crystals obtained for this was discussed in § 3.2.2.1. A summary of the general crystal data is given in Table 6.1, while the numbering scheme of the solvated complex is shown in the perspective drawing in Figure 6.2. Table 6.2 presents selected bond lengths and angles of the title compound. Atomic coordinates, anisotropic displacement parameters, all bond distances and angles and hydrogen coordinates, are given in the supplementary data (Appendix A.7). Hydrogen atoms and/or solvent molecules are omitted in some molecular presentations for clarity.
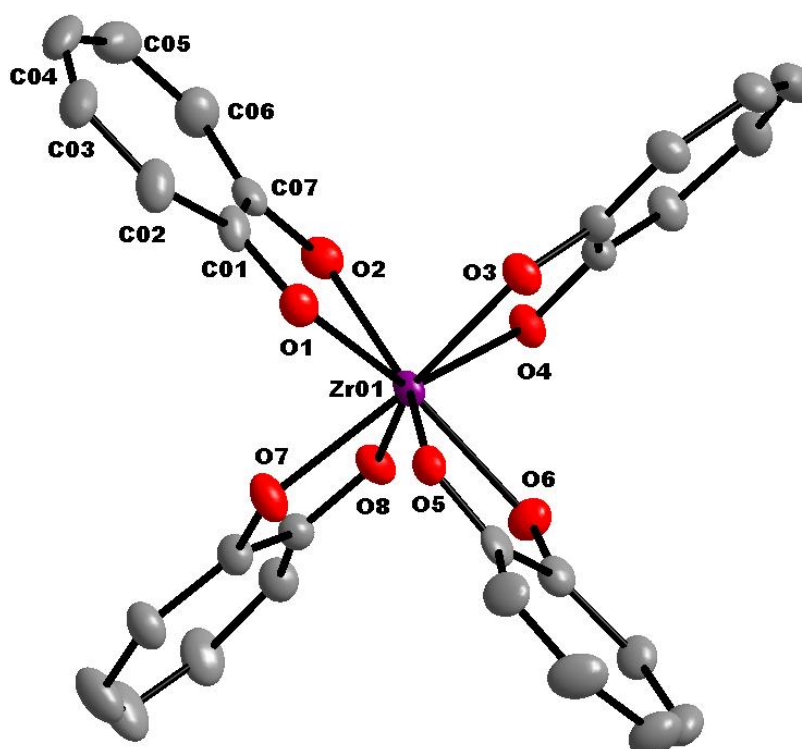
Figure 6.2 Graphic illustration of [Zr(Trop)$_4$].DMF showing general numbering of atoms. Displacement ellipsoids drawn at 50% probability. Hydrogen atoms and solvent molecules omitted for clarity.

---

[9] A.R. Davis & F.W.B. Einstein; *Acta Cryst. B34* (**1978**), 2110-2115.

Table 6.2 Selected Geometric Parameters for [Zr(Trop)$_4$].DMF.

Selected Bond Lengths (Å)			
Zr—O$_1$	2.190 (4)	Zr—O$_2$	2.177 (4)
Zr—O$_3$	2.193 (3)	Zr—O$_4$	2.184 (3)
Zr—O$_5$	2.207 (3)	Zr—O$_6$	2.179 (4)
Zr—O$_7$	2.176 (3)	Zr—O$_8$	2.203 (3)
C$_{01}$—C$_{07}$	1.453 (7)	C$_{15}$—C$_{21}$	1.448 (7)
C$_{08}$—C$_{14}$	1.462 (6)	C$_{22}$—C$_{28}$	1.450 (7)

Selected Bite Angles (°)			
O$_1$—Zr—O$_2$	69.88 (13)	O$_5$—Zr—O$_6$	69.56 (13)
O$_3$—Zr—O$_4$	69.56 (12)	O$_7$—Zr—O$_8$	69.11 (12)

Selected Geometric Coordination Angles (°)			
O$_1$—Zr—O$_3$	78.85 (13)	O$_3$—Zr—O$_5$	78.63 (12)
O$_1$—Zr—O$_4$	131.65 (12)	O$_3$—Zr—O$_6$	93.50 (13)
O$_1$—Zr—O$_5$	72.19 (13)	O$_3$—Zr—O$_7$	149.78 (12)
O$_1$—Zr—O$_6$	141.75 (13)	O$_3$—Zr—O$_8$	141.11 (12)
O$_1$—Zr—O$_7$	76.54 (13)	O$_4$—Zr—O$_5$	131.95 (12)
O$_1$—Zr—O$_8$	130.41 (13)	O$_4$—Zr—O$_6$	77.29 (13)
O$_2$—Zr—O$_3$	92.56 (12)	O$_4$—Zr—O$_7$	140.65 (12)
O$_2$—Zr—O$_4$	75.84 (13)	O$_4$—Zr—O$_8$	71.56 (12)
O$_2$—Zr—O$_5$	142.04 (13)	O$_5$—Zr—O$_7$	77.34 (12)
O$_2$—Zr—O$_6$	148.34 (13)	O$_5$—Zr—O$_8$	129.80 (12)
O$_2$—Zr—O$_7$	95.19 (14)	O$_6$—Zr—O$_7$	95.03 (13)
O$_2$—Zr—O$_8$	78.63 (13)	O$_6$—Zr—O$_8$	77.23 (13)

Selected Torsion Angles (°)			
O$_1$—C$_{01}$—C$_{07}$—O$_2$	-4.59(68)	O$_5$—C$_{15}$—C$_{21}$—O$_6$	1.35(67)
O$_3$—C$_{08}$—C$_{14}$—O$_4$	2.27(65)	O$_7$—C$_{22}$—C$_{28}$—O$_8$	-3.53(67)

Ligand Plane Angles (°)			
Trop1/Trop2	89.85(9)	Trop3/Trop4	89.58(10)
Trop2/Trop3	89.65(9)	Trop4/Trop1	89.17(11)
Trop1/Trop3	176.01(9)	Trop2/Trop4	176.79(12)

The compound *tetrakis*(tropolonato-κ^2O,O')zirconium(IV) dimethylformamide solvate, crystallizes in the monoclinic space group, $P2_1/c$. The asymmetric unit consists of a Zr(IV) metal centre coordinated to four bidentate ligands (tropolonate; Trop) and a crystallographically independent N,N'-dimethylformamide (DMF) solvent molecule.

The four Trop-ligands lie around the metal centre in a space filling, fan-like arrangement to give a distorted dodecahedral geometry (Figure 6.3). The distortion from the flat topped expected square antiprismatic coordination polyhedron in this case is calculated to be 30.82(17) °, as illustrated in Figure 6.4. With a distortion of this extent, the geometry around the metal centre is considered "distorted dodecahedral".

As suggested previously by Davis *et.al.*[9] smaller bite angles of *O,O'*-donor ligands will result in dodecahedron geometries. In the case of *β*-diketone ligands (acac-type ligands specifically) with average bite angles of 75 °, the square antiprismatic geometries are more commonplace.

In this structure two different sets of Zr—O bond distances are notable. For each Trop-ligand, one of the Zr—O coordinative bonds are slightly shorter than the other. These Zr—O_{longer} and Zr—$O_{shorter}$ average 2.198(3) Å and 2.179(4) Å, respectively, with an overall average of 2.189(3) Å (Table 6.2). The average O—Zr—O bite angle is found to be 69.53(12) °. The measured O—C—C—O torsion angles of the ligand frame facing the O—Zr—O bite angles are found to range from -4.59(68) ° to 2.27(65) °, indicating very little deviation from the planarity of the ligands themselves.
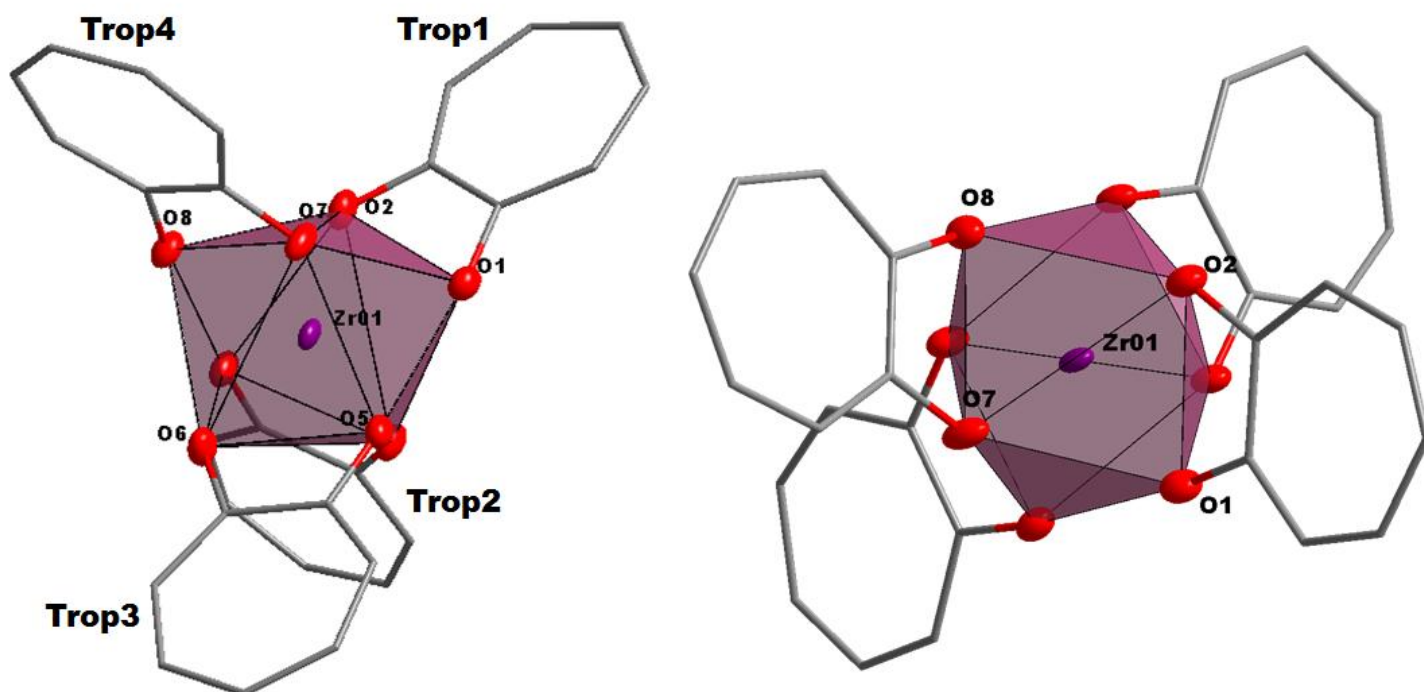
Figure 6.3 Graphic illustration of the distorted square-antiprismatic coordination polyhedron of [Zr(Trop)$_4$]. (**left**) Side view showing upper and lower four corners represented by the O-coordinating atoms of the ligands; (**right**) Top view showing the alternating spacing of the coordinative atoms. Hydrogen atoms and solvent molecules omitted for clarity.
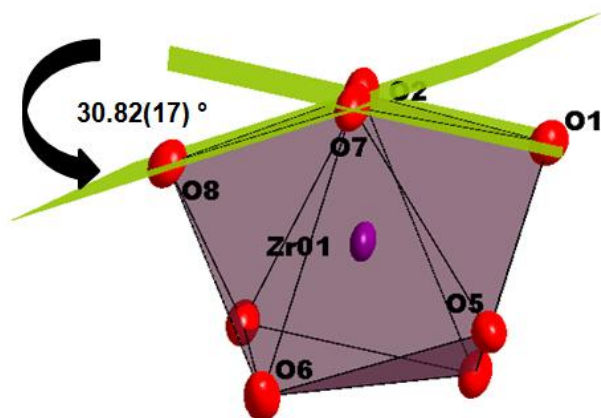
Figure 6.4 Illustration of the distortion out of the ideal square-antiprismatic coordination polyhedron, yielding a distorted dodecahedral geometry, as found in [Zr(Trop)$_4$].

The ligands lie across the metal centre in pairs of near planar ligand sets (Figure 6.5a), as also evident from the torsion angles reported in Table 6.2. Furthermore a notable tilt of each Trop ligand is observable in respect to the perpendicular ligand-pair-plane it lays on (Figure 6.5b). These tilted angles are measure by means of a line drawn through the centre of the entire ligand and the angle it forms with the ligand-pair-plane it is situated on is calculated. These tilting angles range from 16.23(7) ° at the smallest (Trop4) to 23.11(7) ° at the largest (Trop2).
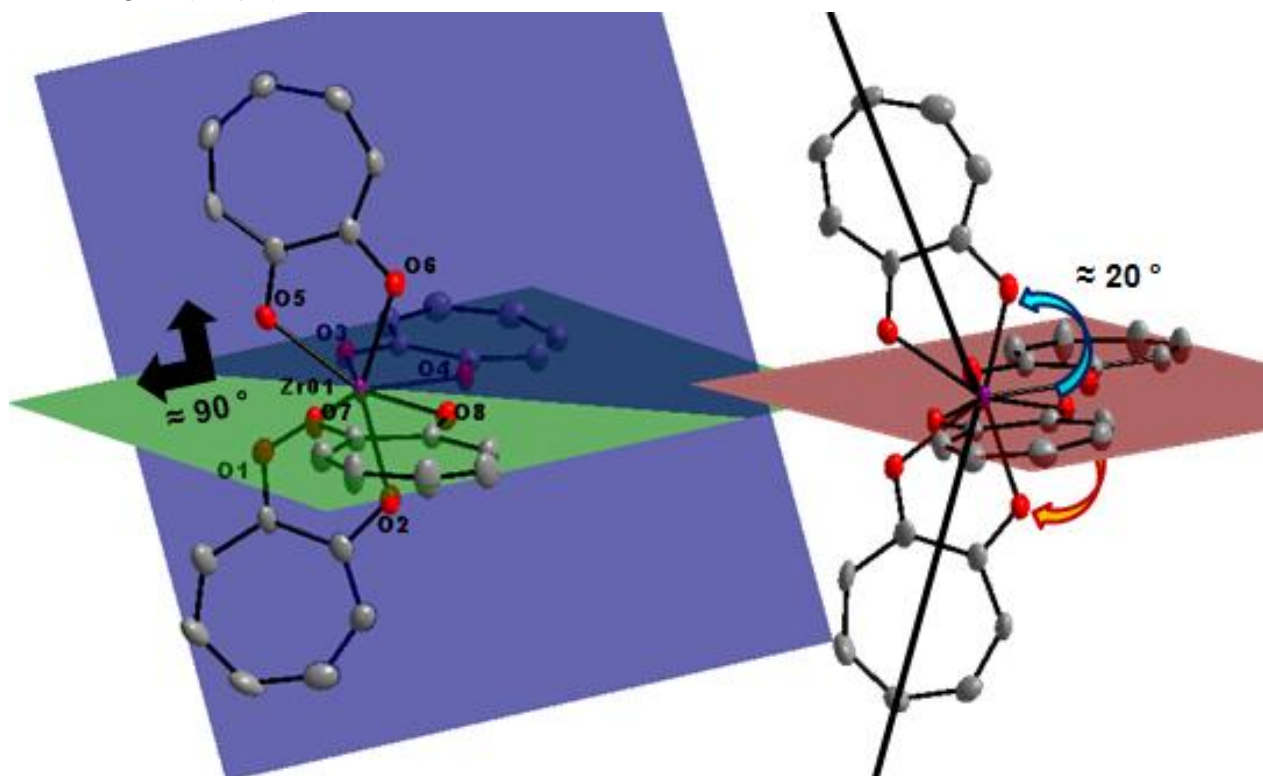
Figure 6.5 Graphical illustration of the different ligand-pair-planes observed in the title structure. (**left**) Ligand-pair-planes of Trop1/Trop3 (*blue*) and Trop2/Trop4 (*green*) intersecting at an angle of 89.45(8) °; (**right**) Tilting of individual Trop-ligands on the ligand-pair-planes they lie on.

Furthermore, the planes defined by each individual ligand appear flat, with no deviation of any one atom out of the plane. These "ligand-planes" (Figure 6.6) lie across the metal centre at angles of 176.01(9) ° (Trop1/Trop3) and 176.79(12) ° (Trop2/Trop4) for each opposite facing pair. The angles between adjacent ligand planes range from 89.17(11) ° at the smallest (Trop4/Trop1) and 89.85(9) ° at the largest (Trop1/Trop2) as reported in Table 6.2.
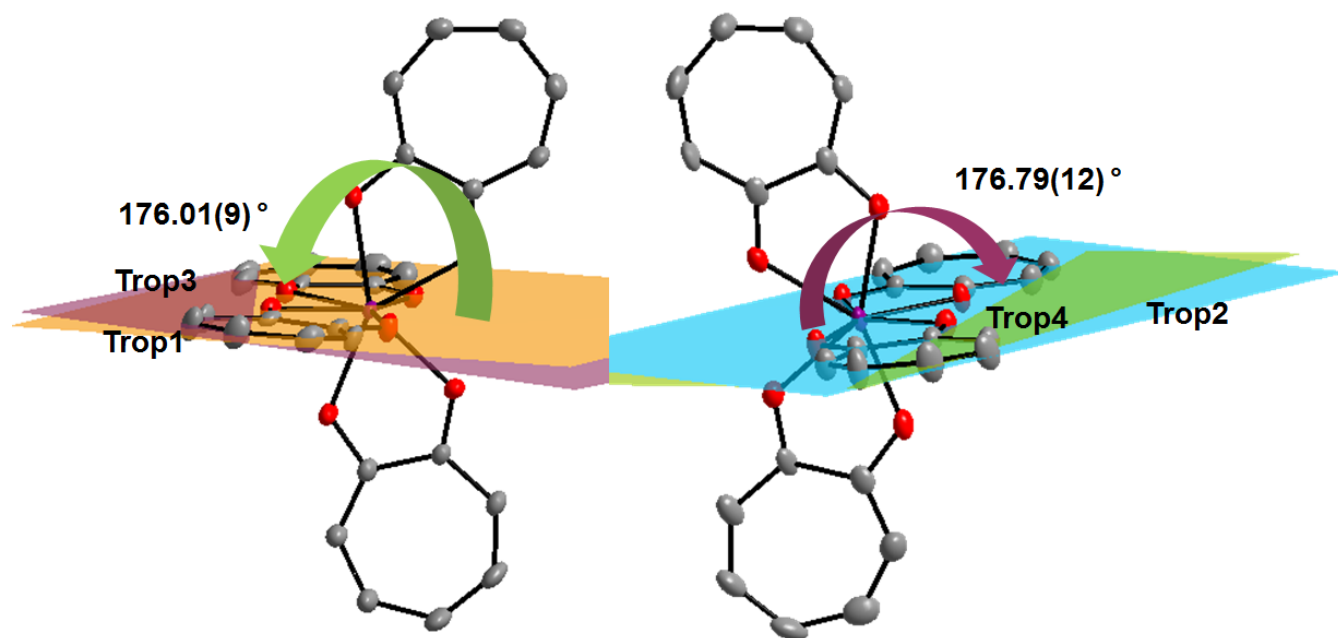
Figure 6.6 Illustration of the different ligand planes measured across the Zr metal center. (**left**) Trop1/Trop3 at an angle of 176.01(9) °; (**right**) Trop2/Trop4 at an angle of 176.79(12) °.

Crystal lattice packing is stabilized by π–π interactions between Trop1 and neighbouring molecules. This stacking of the Trop-ligands is observed with interplanar and centroid-to-centroid distances of 3.950(10) Å and 3.991(11) Å, respectively (Figure 6.7).

Table 6.3 Hydrogen-bond geometry in the title compound (Å, °).

D—H⋯A	D—H	H⋯A	D⋯A	D—H⋯A
C_{02}—H_{02}⋯O_9^i	0.95	2.49	3.184 (10)	130
C_{03}—H_{03}⋯O_9^i	0.95	2.57	3.228 (10)	127
C_{12}—H_{12}⋯O_2^{ii}	0.95	2.56	3.278 (6)	132
Symmetry codes: (i) −x+2, −y, −z+1; (ii) −x+1, −y+1, −z.				

Intermolecular C—H⋯O hydrogen bonding interactions are observed in this structure. Two of these are found between C_{02}—H_{02} as well as C_{03}—H_{03} of Trop1 to O_9 of the DMF solvent molecule present (Table 6.3) as illustrated in Figure 6.7. The third interaction is found between C_{12}—H_{12} of Trop2 to O_2 of Trop1 (Figure 6.8).
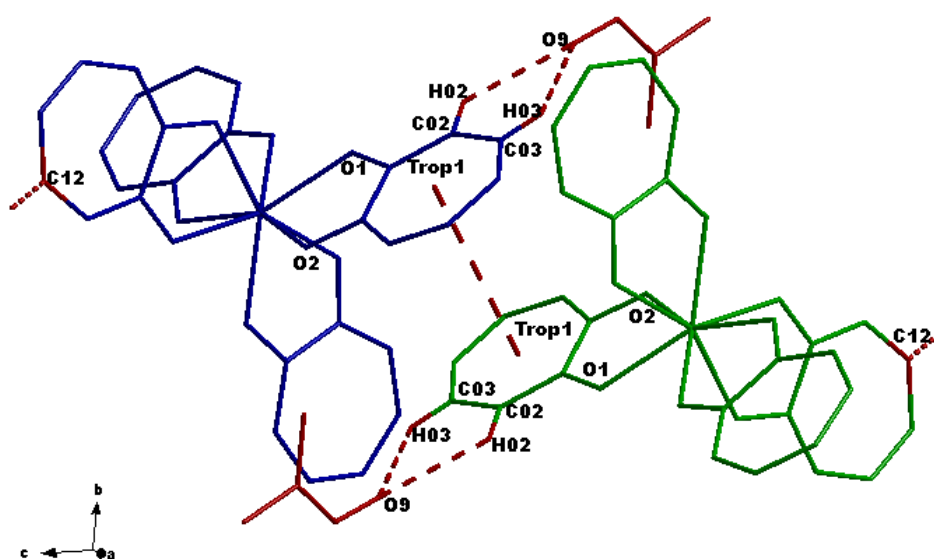
Figure 6.7 Illustration of the hydrogen bonding and the π–π interactions found in the title molecule. Interactions of C_{02}—H_{02}···O_9 and C_{02}—H_{02}···O_9 on the edges of the π–π interaction of Trop1 on neighboring molecule.
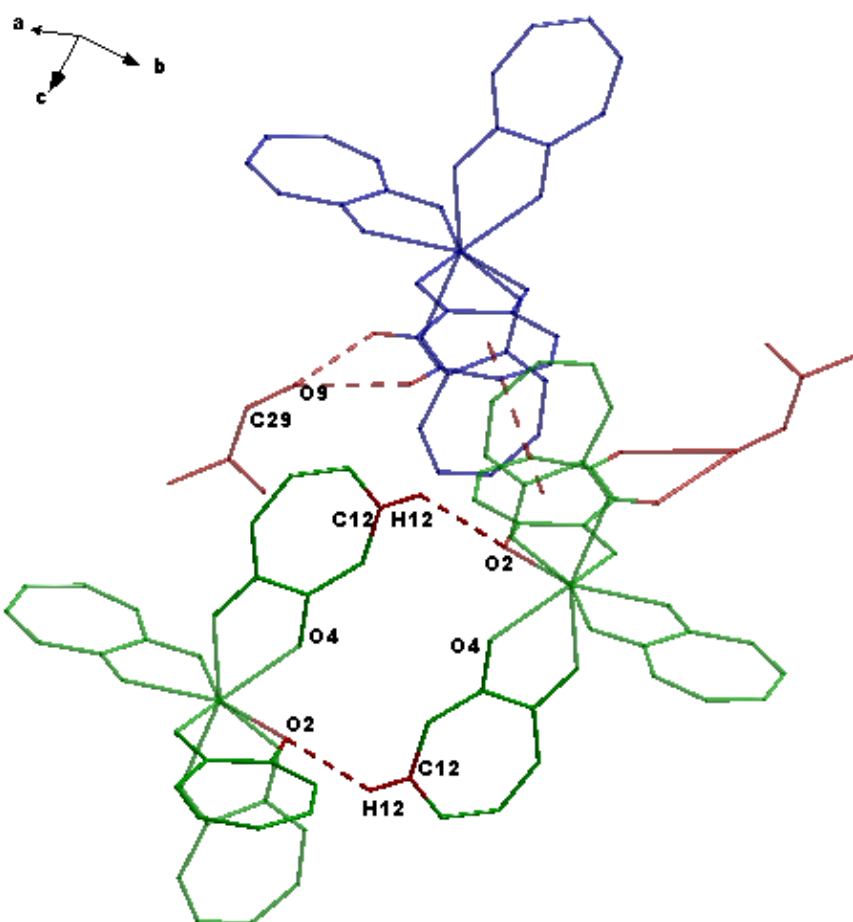
Figure 6.8 Graphical illustration of the C—H···O interactions observed in the title molecule. Other C—H···O and π–π interactions faded in the background (see also Figure 6.7), showing the overall stabilization found in the crystal lattice.

A comparative summary of the known [Zr(Trop)$_4$] and [Hf(Trop)$_4$] structural information is summarized below in Table 6.4. The structure of the [Hf(Trop)$_4$].DMF[10] was also published in the 1970's, a year prior to the [Zr(Trop)$_4$].(CHCl$_3$) structural paper. Both of these literature examples go into extensive detail with regard to intricate structural characteristics of both complexes, specifically in describing the coordination geometry around the metal centre.

In both cases, the final conclusions drawn with regard to the matter of defining the polyhedron as dodecahedral or square-antiprismatic, both concluded the same, a near dodecahedral geometry. As described by Davis *et.al.*[9] smaller bite angles of *O,O'*-donor ligands will result in dodecahedron geometries. In the case of *β*-diketone ligands (acac-type ligands specifically) with average bite angles of 75 °, the square antiprismatic geometries are more commonplace.

Table 6.4 Selected crystallographic characteristics, bond lengths and angles
of zirconium and hafnium tropolone complexes.

	[Zr(Trop)$_4$].DMF[a]	[Zr(Trop)$_4$].CHCl$_3$[b]	[Hf(Trop)$_4$].DMF[c]
Crystal system	Triclinic	Triclinic	Triclinic
Space Group	$P\bar{1}$	$P\bar{1}$	$P\bar{1}$
Coordination Polyhedra	Distorted Dodecahedron	Distorted Dodecahedron	Distorted Dodecahedron
Unit cell dimensions:			
a, b, c (Å)	10.454(5), 11.734(5), 12.827(5)	11.714(3), 15.163(4), 10.317(3)	12.839(3), 10.706(4), 11.708(2)
α, β, γ (°)	100.050(5), 97.575(5), 113.999(5)	91.74(2), 73.91(3), 100.94(2)	67.32(1), 101.10(1), 83.60(1)
Volume (Å^3)	1378.9(10)	1728.24	1426.12
Z	2	2	2
R-Factor %	7.7	7.5	6.0
Average Zr—O (Å)	2.189(3)	2.188(6)	2.182(5)
Shortest Zr—O (Å)	2.176 (3)	2.158(6)	2.168(6)
Longest Zr—O (Å)	2.207 (3)	2.209(6)	2.199(4)
Average O—Zr—O (°)	69.53(12)	68.53(2)	69.66(1)

a) This work, **b**) Ref 9, **c**) Ref 10.

---

[10] D. Tranqui, A. Tissier, J. Laugier & P. Boyer; *Acta Cryst. B33* (**1977**), 392-397.

What is interesting to note from these three examples, is that regardless of solvent molecules present in each respective case, the structural characteristics across the board are very similar. Although Davis *et.al.*[9] concluded that the chloroform solvent molecule in their case influences the lattice packing to a great extent, both the Zr- and Hf-DMF examples show similar packing influencers dictated more by the Trop ligand, as a whole. In other words, ligand stabilization tendencies are as predictable, if not more so, than hydrogen bonding interactions of solvent molecules in these organometallic compounds.

6.3. Crystal Structure of [Zr(DBM)₄] – Zr_2b

As part of this on-going study investigating coordination behaviour of O,O'- and N,O-bidentate ligands with zirconium and hafnium for possible influencing factors in the purification/separation of these metals, we have been able to refine methods of synthesis and crystallization of zirconium complexes. This is in particular as a reference/comparison with much older literary reported/published methods and results. Herein is described and elaborated on the synthesis and crystallographic characterisation of the structure [*tetrakis*(1,3-diphenyl-1,3-propanedionato)-zirconium(IV)][11] - [Zr(DBM)₄] (**Zr_2b**) as a redetermination and comparison to a previously published structure[12] and as a comparison to the hafnium(IV)-counterpart.[13]

Synthesis of **Zr_2b** and the resulting colourless crystals obtained for this was discussed in § 3.2.2.2. A summary of the general crystal data is given in Table 6.1, while the numbering scheme of the solvated complex is shown in the perspective drawing in Figure 6.9. Table 6.5 presents selected bond lengths and angles of the title compound. Atomic coordinates, anisotropic displacement parameters, all bond distances and angles and hydrogen coordinates, are given in the supplementary data (Appendix A.8). Hydrogen atoms and/or solvent molecules are omitted in some molecular presentations for clarity.

This zirconium *β*-diketone complex crystallizes in the monoclinic space group, *P2₁/c*. The asymmetric unit consists of a Zr(IV) metal centre coordinated to four unique bidentate, oxygen donating ligands, Dibenzoylmethane (DBM) ligands. No solvent molecule is present in the crystal lattice, even though the compound was synthesised and crystallized in N,N'-dimethylformamide (DMF).

[11] M. Steyn, H.G.Visser & A. Roodt; *J. S. Afr. Inst. Min. Metall. 114* (**2014**), 183-188.
[12] H.K. Chun, W.L. Steffen & R.C. Fay; *Inorg. Chem. 18* (**1979**), 2458-2465.
[13] J. A. Viljoen, H. G. Visser & A. Roodt; *Acta Cryst. E66* (**2010**), m1053–m1054.

Table 6.5 Selected Geometric Parameters for [Zr(DBM)$_4$].

Selected Bond Lengths (Å)			
Zr—O$_1$	2.141(1)	C$_{01}$—C$_{101}$	1.494(2)
Zr—O$_2$	2.207(1)	C$_{03}$—C$_{201}$	1.488(2)
Zr—O$_3$	2.190(1)	C$_{04}$—C$_{301}$	1.489(2)
Zr—O$_4$	2.162(1)	C$_{06}$—C$_{401}$	1.498(2)
Zr—O$_5$	2.158(1)	C$_{07}$—C$_{501}$	1.490(2)
Zr—O$_6$	2.201(1)	C$_{09}$—C$_{601}$	1.491(2)
Zr—O$_7$	2.213(1)	C$_{10}$—C$_{701}$	1.496(2)
Zr—O$_8$	2.152(1)	C$_{12}$—C$_{801}$	1.492(2)

Selected Bite Angles (°)			
O$_1$—Zr—O$_2$	74.91(4)	O$_5$—Zr—O$_6$	74.59(4)
O$_3$—Zr—O$_4$	74.53(4)	O$_7$—Zr—O$_8$	74.10(4)

Selected Geometric Coordination Angles (°)			
O$_1$—Zr—O$_3$	78.78(4)	O$_3$—Zr—O$_5$	72.88(4)
O$_1$—Zr—O$_4$	143.62(3)	O$_3$—Zr—O$_6$	115.37(4)
O$_1$—Zr—O$_5$	79.29 (5)	O$_3$—Zr—O$_7$	141.02(4)
O$_1$—Zr—O$_6$	144.15(4)	O$_3$—Zr—O$_8$	142.86(3)
O$_1$—Zr—O$_7$	72.65(3)	O$_4$—Zr—O$_5$	114.90(4)
O$_1$—Zr—O$_8$	112.35(4)	O$_4$—Zr—O$_6$	71.14(4)
O$_2$—Zr—O$_3$	77.65(3)	O$_4$—Zr—O$_7$	141.54(3)
O$_2$—Zr—O$_4$	75.58(4)	O$_4$—Zr—O$_8$	77.58(4)
O$_2$—Zr—O$_5$	143.92(3)	O$_5$—Zr—O$_7$	76.16(3)
O$_2$—Zr—O$_6$	138.44(4)	O$_5$—Zr—O$_8$	142.50(4)
O$_2$—Zr—O$_7$	118.29(4)	O$_6$—Zr—O$_7$	77.10(4)
O$_2$—Zr—O$_8$	71.98(4)	O$_6$—Zr—O$_8$	77.52(3)

Selected Torsion Angles (°)			
O$_1$—C$_{01}$—C$_{03}$—O$_2$	6.02(11)	O$_5$—C$_{07}$—C$_{09}$—O$_6$	10.98(11)
O$_3$—C$_{04}$—C$_{06}$—O$_4$	-1.39(11)	O$_7$—C$_{10}$—C$_{12}$—O$_8$	-1.54(11)

Ligand Plane Angles (°)			
Lig1/Lig2	39.52(4)	Lig3/Lig4	33.69(4)
Lig2/Lig3	35.07(5)	Lig4/Lig1	44.38(4)
Lig1/Lig3	163.88(4)	Lig2/Lig4	164.23(4)
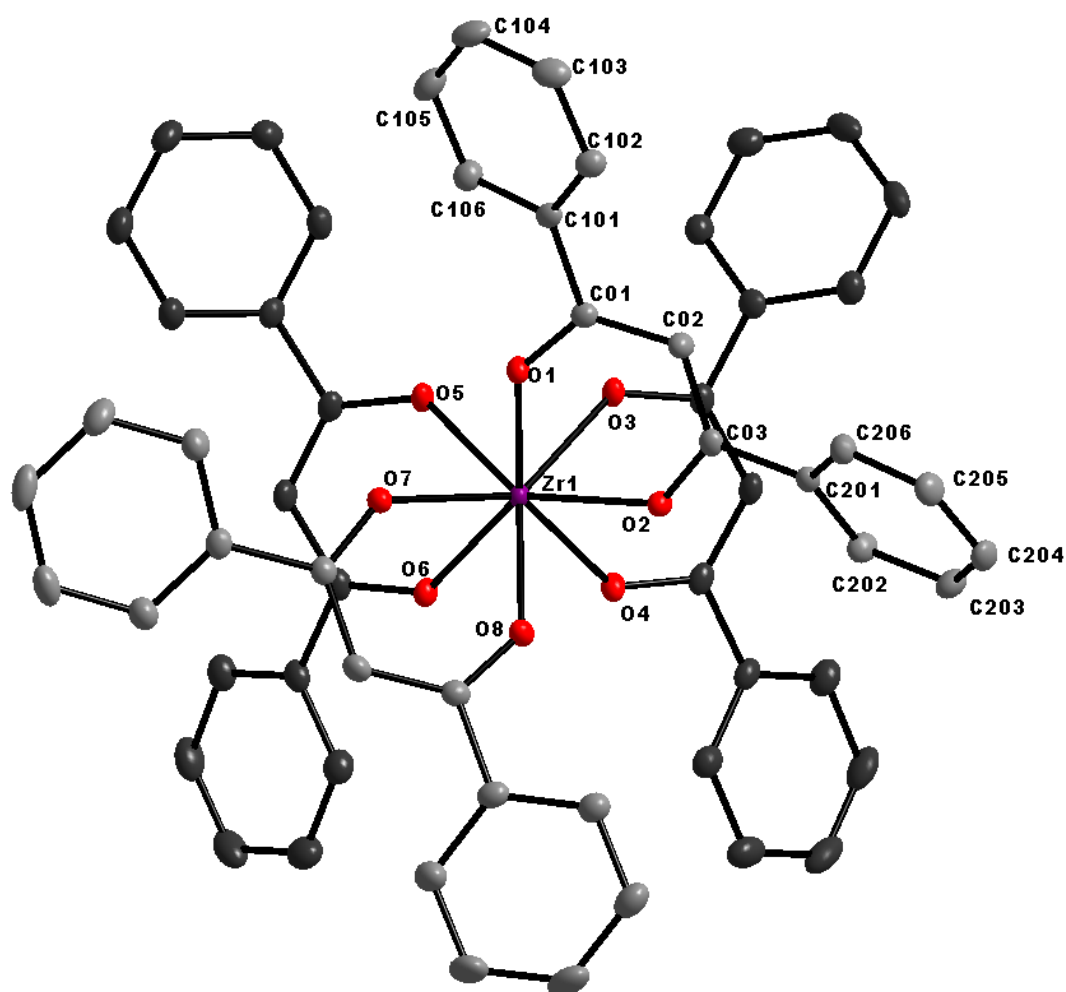
Figure 6.9 Graphic illustration of [Zr(DBM)$_4$] showing general numbering of atoms. Displacement ellipsoids drawn at 50% probability. Hydrogen atoms omitted for clarity.

The four DBM-ligands are arranged around the metal centre in a space filling, fan-like arrangement to give a square-antiprismatic coordination polyhedron (Figure 6.10), with an almost negligible outward distortion towards dodecahedral geometry. This distortion of the ideal square antiprism is associated with an outward bend of 3.71(4) °, as illustrated in Figure 6.11. With regard to the overall coordination description of the ligands as viewed in the square antiprism (Figure 6.10a), the title compound displays a D$_2$ corner-clipped isomer species.

In this structure the Zr—O bond distances range from 2.141(1) Å to 2.2125(1) Å (Table 6.5). The average O—Zr—O bite is found to be 74.53(4) °. The measured O—C—C—O torsion angles of the ligand frame facing the O—Zr—O bite angles are found to range from -1.54(11) ° to 10.98(11) °, indicating negligible deviation from the planarity of the ligands themselves.
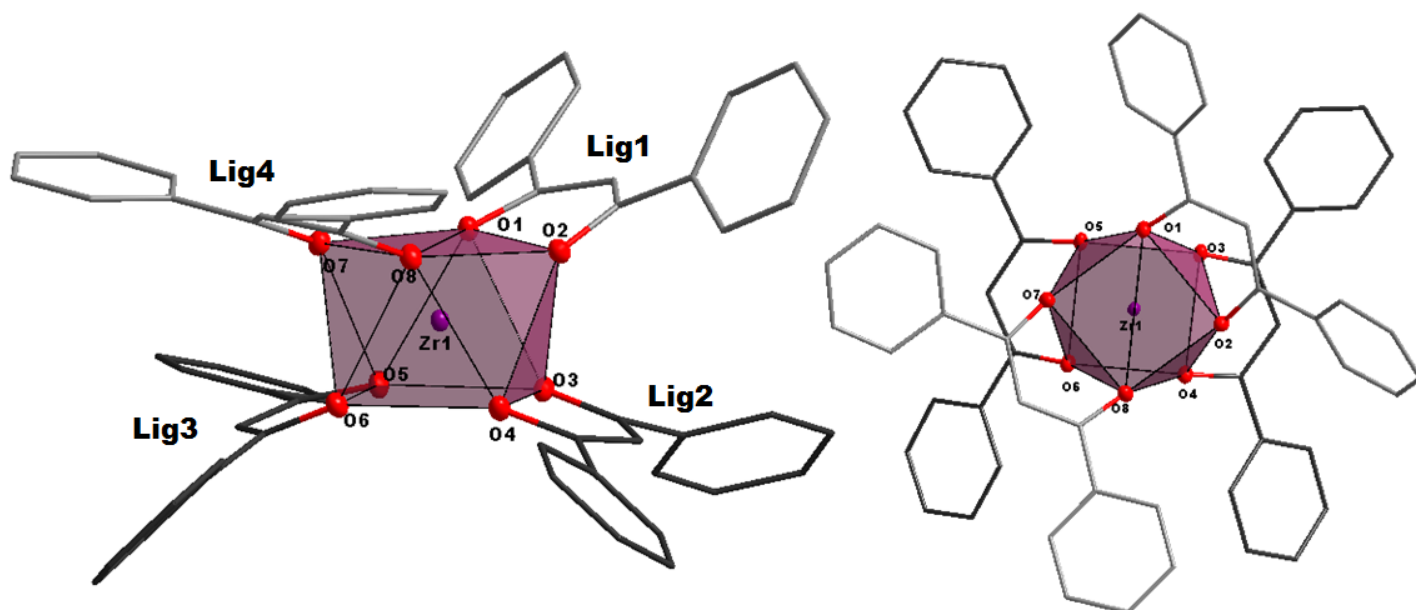
Figure 6.10 Graphic illustration of the square-antiprismatic coordination polyhedron of [Zr(DBM)$_4$], also displaying the D$_2$ isomer character (corner clipped ligands). (**left**) Side view showing upper and lower four corners represented by the N- and O-coordinating atoms of the ligands; (**right**) Top view showing the alternating spacing of the coordinative atoms.
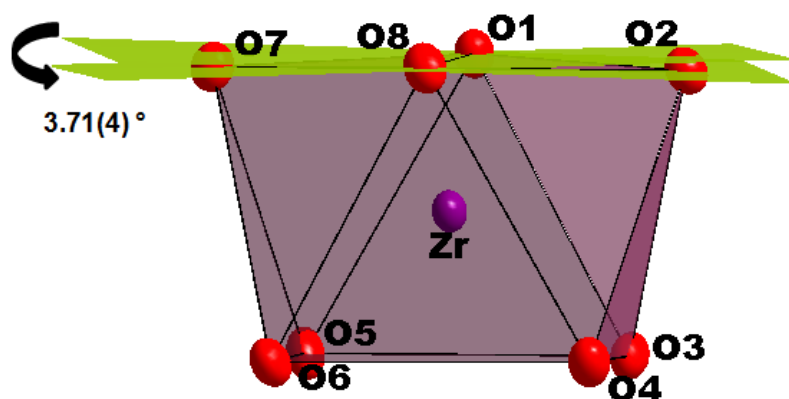
Figure 6.11 Illustration of the distortion of the square-antiprismatic coordination polyhedron found in [Zr(DBM)$_4$], showing the outward bend of the top-most atoms at an angle of 3.71(4) °.

A noteworthy characteristic of the zirconium metal centre is observed in this structure, in that it distorts the backbone of the bidentate (acac-type) ligands from its preferred coordination geometry of ca. 180 ° towards a highly distorted bent-like geometry to accommodate the overall polyhedron geometry around the metal centre. These ligands are chelated around the metal centre with a bend in the ligand at the intersection of the two planes formed by the ligand-backbone (O—C—C—C—O) and the O—Zr—O bite angle (Figure 6.12). The extent of this ligand-distortion ranges from 16.64(5) to 25.76(4) °.
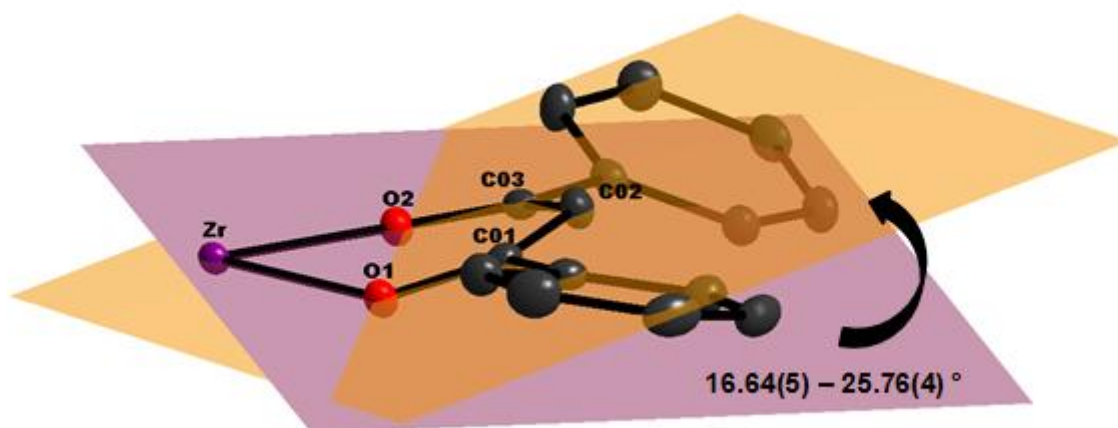
Figure 6.12 Illustration of ligand bending as found in the title compound.
The two planes intersect at the O,O'-coordination site.

The ligand backbone itself also displays a swivelling in the arrangement of each individual phenyl-ring at the edges of the C—C—C-backbone. Each Ph-ring is swivelled at distinct angles (See Table 6.6) with respect to their parent β-diketone structural plane (Figure 6.13a), ranging from 136.24(4) to 159.64(5) °. Furthermore the angle at which each phenyl pair are swivelled away from each other over the β-diketone backbone plane ranges from 119.80(5) to 158.41(4) ° (Figure 6.13b). This planar swivelling found for each individual phenyl ring is directly related to the manner in which the crystal lattice packing is arranged, as described below.
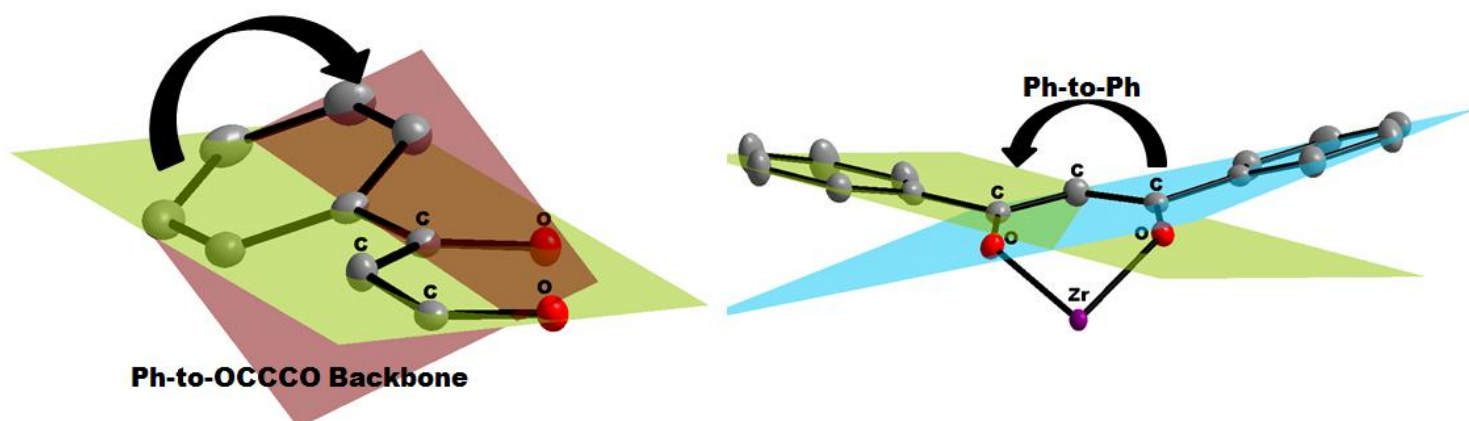
Figure 6.13 Illustration of ligand phenyl swiveling as found in the title compound;
(**Left**) Swivel of the phenyl with regard to the parent backbone;
(**Right**) Phenyl swivel in the DBM ligand structure - phenyl-to-phenyl plane swivel.

121

Table 6.6 Selected dihedral angles for phenyl swiveling on individual DBM ligands as observed in the title compound.

Phenyl to ligand swivel (Figure 6.13a)		
Atoms in plane		**Dihedral angles (°)**
O_1—CCC—O_2	Ph_1	154.39(4)
O_1—CCC—O_2	Ph_2	141.88(4)
O_3—CCC—O_4	Ph_3	136.24(4)
O_3—CCC—O_4	Ph_4	157.73(6)
O_5—CCC—O_6	Ph_5	149.57(5)
O_5—CCC—O_6	Ph_6	152.95(4)
O_7—CCC—O_8	Ph_7	159.64(5)
O_7—CCC—O_8	Ph_8	159.27(4)
Phenyl to phenyl swivel (Figure 6.13b)		
Atoms in plane		**Dihedral angles (°)**
Ph_1	Ph_2	158.41(4)
Ph_3	Ph_4	119.80(5)
Ph_5	Ph_6	122.80(5)
Ph_7	Ph_8	154.46(5)

The compound itself packs in two observable ways in the lattice. Firstly, every organometallic molecule packs on top of another in a head-to-tail fashion along the *c*-axis, and head-to-head along the *a*-axis, as illustrated in Figure 6.14. Secondly, the most significant packing effect observed is a C—H···π interaction network, rigidly threading the entire crystal lattice together as a whole. This elaborate C—H···π interaction system found in the title compound could be the cause for the unique swivelling of each individual phenyl ring on each DBM ligand.

Table 6.7 Selected C—H···Cg (pi-ring) interactions (H···Cg < 3.0 Å, Gamma < 30.0 °) as observed in the title compound. H-Perp represents the perpendicular distance of H to Ph-ring plane; X-H, Pi represents the angle of the X-H bond to Pi-plane (perpendicular = 90 °, parallel = 0 °) (Å, °).

X—H···Cg	*H···Cg*	*H-Perp*	*Gamma*	*X—H···Cg*	*X···Cg*	*X—H, Pi*
C_{205}—H_{205}···$Ph_5{}^i$	2.73	2.708	5.27	149	3.556(2)	60
C_{204}—H_{204}···$Ph_4{}^i$	2.83	2.821	3.93	141	3.602(2)	55
C_{304}—H_{304}···$Ph_1{}^{ii}$	2.65	2.639	5.52	154	3.513(2)	62
C_{505}—H_{505}···$Ph_1{}^{iii}$	2.77	2.699	12.78	145	3.568(2)	58
Symmetry codes: (i) x,-1+y,z; (ii) x,1/2-y,-1/2+z; (iii) 1-x,1/2+y,1/2-z.						
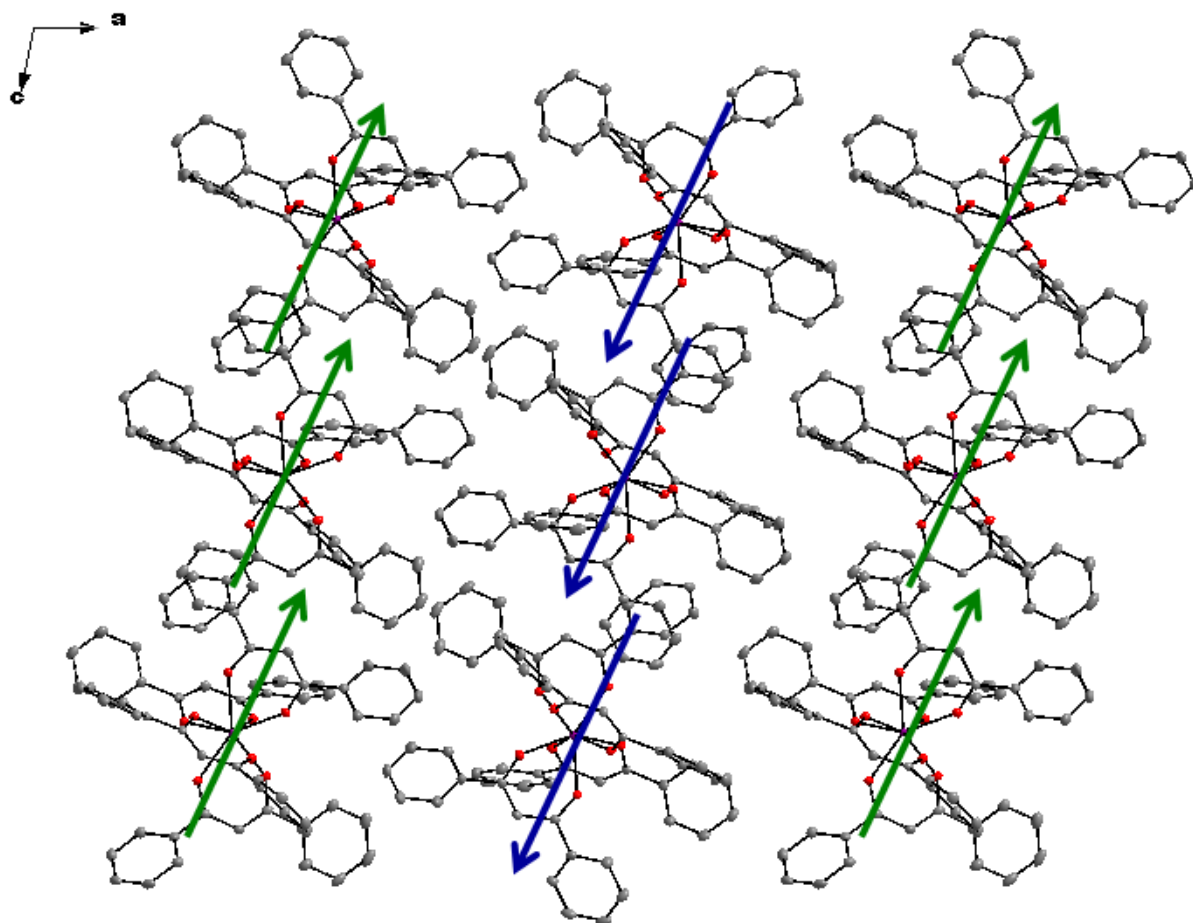
Figure 6.14 Graphical representation of molecular packing within the unit cell for the title compound, showing head-to-tail packing along the *c*-axis (***arrow direction***) and head-to-head packing along the *a*-axis (***alternating green and blue arrows***). Hydrogen atoms omitted for clarity, 50% probability displacement ellipsoids.

The effect of this best described, as illustrated in Figure 6.15a, as a "cross-stitching" and "threading" effect in the channelling of the head-to-tail packing along the *c*-axis in the crystal lattice. On one side of the stacked molecules, with a rigid "cross-stitching" of the C—H···π interactions of Ph_1, Ph_3 and Ph_5 (listed table 6.7), an intricate lattice assemblage of the symmetrically identical groups interacting and packing on their respective neighbours is observed. On the other side of the head-to-tail packed molecules, Ph_2 and Ph_4 show a looser, but still significant "threading" in their symmetrically placed neighbours (Figure 6.15b). This intricate network of C—H···π interactions gives rise to the possibility that no solvent molecules are caught inside the crystal lattice. Although there are no classical hydrogen-bonding or π-π stacking interactions, there is a weak intermolecular C—H···O interaction between C_{205}—H_{205} of the Ph_2 and an oxygen atom, O_4, on a neighbouring molecule (listed in Table 6.8).

Table 6.8 Hydrogen-bond geometry in the title compound (Å, °).

D—H⋯A	D—H	H⋯A	D⋯A	D—H⋯A
C_{205}—H_{205}⋯O4^i	0.93	2.6	3.512 (2)	169
Symmetry code: (i) x, y−1, z.				
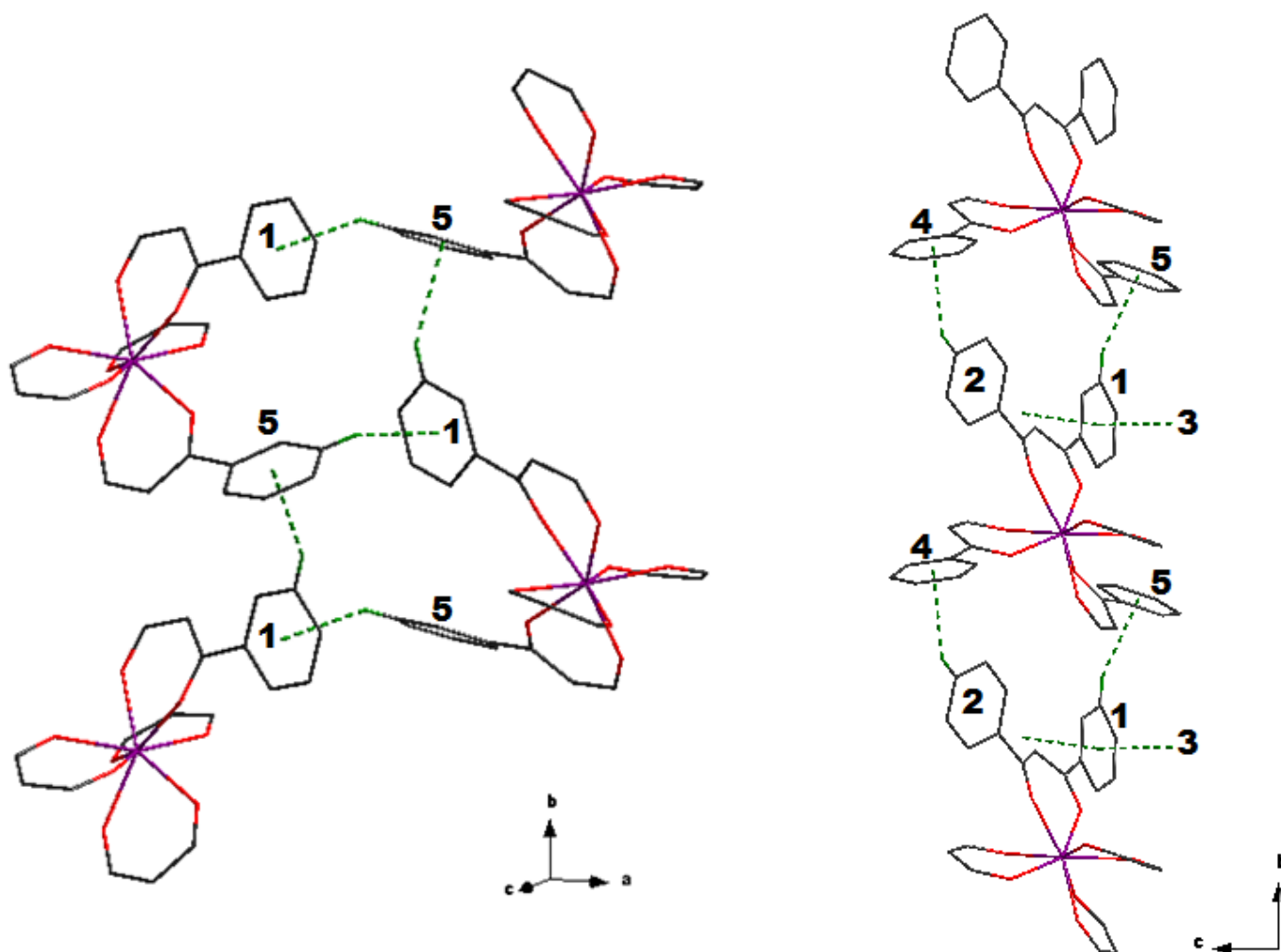
Figure 6.15 Illustration of C—H⋯π interactions found in the title compound.
(**Left**) As viewed along the *b*-axis, depicting the "cross-stitching" of Ph$_1$ & Ph$_5$;
(**Right**) showing the "threading" of Ph$_2$ & Ph$_4$, with Ph$_1$/Ph$_3$/Ph$_5$ in the background,
showing the entire network of C—H⋯π interactions found in lattice.

Furthermore, this very stable arrangement of the organometallic molecules as a whole, leads to two notable observations with regards to the nature of solid state behaviour of zirconium and its *β*-diketone chelated compounds. Firstly, it is a well-known fact that zirconium *β*-diketone complexes in general always show a square-antiprismatic coordination polyhedron.[14,15] This suggests that zirconium has a certain preference for the chelation sites

---

[14] J.V. Silverton & J.L. Hoard; *Inorg. Chem. 2* (**1963**), 243-249.
[15] W. Clegg; *Acta Cryst.C43* (**1987**), 789 -791.

of the coordinating atoms, regardless of the steric properties of the ligands as a whole.[16] This, in theory, could be mainly due to the fact that zirconium(IV) tends towards a maximum state of coordination, as preference, or as lowest crystallization state. This is in accordance of what is expected in these symbiotic systems.[17] However, the packing of each individual zirconium bidentate-ligand complex seems to be largely governed by the stabilization of the ligands themselves, and not from any discernible effect from the metal centre.

In other words, since the metal centre is entirely surrounded by the specific bidentate ligands coordinated, it has no influence on the packing of the organometallic molecule in the greater crystal lattice, but only influences the placement of the coordinating atoms around itself, thereby potentially not allowing for dimeric structures or other metal-to-linking-atom interactions.

As far as the physical structural characteristics of this *tetrakis(β-diketone)zirconium(IV)* complex are concerned, all aspects are in good comparison to other published structures containing such ligands (Table 6.8). All coordination bond lengths are in the average range of 2.1-2.2 Å and bite angles average the standard angle of 74-75 °. Furthermore, it is interesting to note that all these fully coordinated zirconium(IV) *β*-diketonates appear to prefer a monoclinic space group across the board.

Finally, in comparison to the previously published structure,[12] although the asymmetric unit appears identical and all structural characteristics are comparable (Table 6.9), these two crystals are not completely identical. When considering the smaller crystallographic cell volume for the title compound to that reported by Chun *et.al*, there does appear to be a tighter packing of the crystal lattice here.

Regardless of the final crystallographic findings, however, it is significant to note that Chun *et.al.*[12] reported a synthetic procedure of phosphite-catalyzed reflux in diethyl ether and crystallization method of benzene/hexane extraction after vigorous purification of the reaction solution, for producing of these specific crystals. This methodology in itself was most likely employed merely as a laboratory standard, but we can now report, with a certain amount of confidence, that zirconium as a metal reagent is more reactive than may have been expected in the last 30 years.

---

[16](a) M. Steyn, A. Roodt & G. Steyl; *Acta Cryst. E64* (**2008**), m827.
(b) M. Steyn, H. G. Visser, A. Roodt & T.J. Muller; *Acta Cryst. E67* (**2011**), m1240–m1241.
(c) M. Steyn, H. G. Visser & A. Roodt; *Acta Cryst. E68* (**2012**), m1344–m1345.
(d) M. Steyn, H. G. Visser & A. Roodt; *J. S. Afr. Inst. Min. Metall. 113* (**2013**), 105-108.
[17] J.E. Huheey, E.A. Keiter & R.L. Keiter; *Inorganic Chemistry - Principles of Structure and Reactivity, 4th Ed.* (**1993**) HarperCollins College Publishers, New York.

Table 6.9 Selected crystallographic characteristics, bond lengths and angles of zirconium(IV) β-diketonates.

	[Zr[DBM)$_4$][a]	[Zr[DBM)$_4$][b]	[Hf[DBM)$_4$][c]	[Zr(tFAcac)$_4$][d]	[Zr(hFAcac)$_4$][d]	[Zr(acac)$_4$][e]
Empirical formula	$C_{60}H_{44}O_8Zr$	$C_{60}H_{44}O_8Zr$	$C_{60}H_{44}O_8Hf$	$C_{20}H_{16}F_{12}O_8Zr$	$C_{20}H_4F_{24}O_8Zr$	$C_{20}H_{28}O_8Zr$
Formula weight (g.mol^{-1})	984.17	984.22	1071.44	703.55	919.45	487.7
Crystal system, Space Group	Monoclinic, $P2_1/c$	Monoclinic, $P2_1/c$	Monoclinic, $P2_1/c$	Monoclinic, $C2/c$	Monoclinic, $P2_1/c$	Monoclinic, $C2/c$
Unit cell dimensions:						
a, b, c (Å)	24.769(4), 10.216(5), 19.314(4)	25.241(5), 10.324(1), 19.395(4)	24.846(2), 10.224(8), 19.316(1)	21.506(2), 7.951(5), 16.051(1)	15.353(1), 20.261(2), 19.698(2)	21.662(2), 8.360(1), 14.107(1)
β (°)	101.541(5)	101.72(1)	101.618(4)	113.736(4)	95.828(2)	116.708(6)
Volume (Å^3), Z	4788(3), 4	4948, 4	4806(6), 4	628.13(3), 4	762.0(2), 4	2282.1, 4
R-Factor %	2.8	7.2	3.7	4.7	7.8	2
Average Zr—O (Å)	2.178(1)	2.171(5)	2.169(2)	2.189(2)	2.177(4)	2.188(1)
Shortest Zr—O (Å)	2.141(1)	2.1395(2)	2.133(2)	2.165(2)	2.141(4)	2.176(1)
Longest Zr—O (Å)	2.213(1)	2.2052(5)	2.200(2)	2.210(2)	2.225(4)	2.201(1)
Average O$_x$—Zr—O$_y$ (°)	74.53(4)	74.63(2)	74.74(9)	74.37(8)	74.58(2)	74.85(1)

a) This work, b) Ref. 12, c) Ref. 13, d) Ref. 18, e) Ref. 15.

These rigorous synthetic methods and laborious crystallization techniques are not always necessary. Organometallic chelation reactions of zirconium are often self-catalysed and crystallization can occur in ambient environments. Furthermore, application of DMF as a reaction and crystallization solvent in all processes further allows for less strict approaches to the impacts of hydration on the final product, since crystalline water could also be observed in some cases in the asymmetric unit, without any influence on the main metal-molecule as a whole.[16b]

[18]K.V. Zherikova, N.B. Morozova, N.V. Kurat'eva, I.A. Baidina, P.A. Stabnikov & I.K. Igumenov; *J. Struct. Chem. 46* (**2005**), 513–522.

6.4. Evaluation of Structural Characterisation – Zirconium(IV) Bidentate Ligand Complexes

In the presented crystallographic characterisation and description discussions presented in this and the previous chapters, a substantial amount of emphasis has been placed on elaborate, but concise structural trend identification for zirconium(IV) bidentate ligand complexes. It has been clearly highlighted in Chapter 2 that a complete understanding of the solid state behaviour of these compounds are necessary for a correlative study with hafnium(IV) counterparts with the intent of exploiting differences for separative experiments.

To this end, in Chapter 4 & 5, a comparison of oxine structural properties has been included and some conclusions were drawn as to the nature of zirconium(IV) chelation behaviour and preference. At this juncture, additional correlation of geometric characteristics of all compounds described can be presented. In all cases, a certain emphasis has been placed in three particular characteristics of the complexes described. Firstly, the coordination geometry observed in each instance was highlighted, which proved to be the *square antiprismatic polyhedra* (in almost all cases) as expected.[13,14] Secondly, it has been noted that for all zirconium(IV) complexes exhibiting *this* chelation geometry about the metal centre, there were a *deviation from the ideal* to a certain extent, measured by the distortion angle of the antiprism associated with an outward bend at the top and bottom (See Figure 6.16).
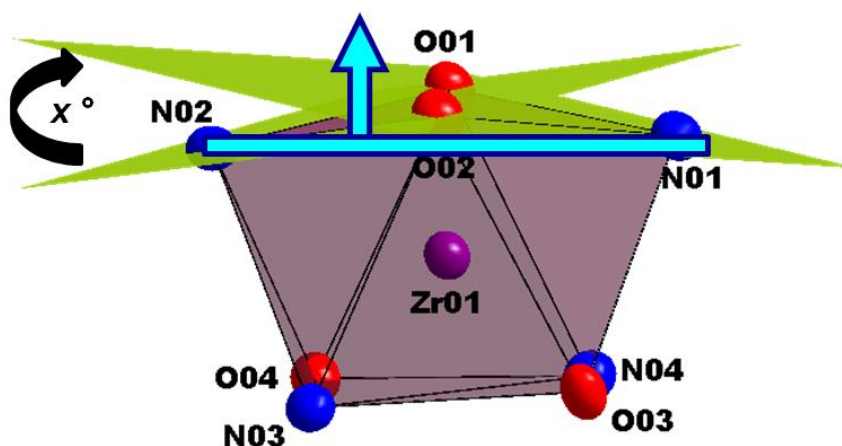
Figure 6.16 Illustration of the measure of the distortion of the square-antiprismatic coordination polyhedron found in zirconium(IV) complexes, showing the outward bend of the top-most atoms.

Finally, the measure of the angles at which ligand planes lie adjacent or opposite each other has been included for all structures. This has all been part of the complete structural description of zirconium(IV) complexes in the hopes that certain trends or aspects would be observed.

Table 6.10 Comparison of geometric characteristics of Zirconium(IV) Bidentate Ligand Complexes described in Chapters 4, 5 & 6.

Metal Complex	[Zr(diClOx)$_4$]	[Zr(5-ClOx)$_4$]	[Zr(5-ClOx)$_4$]	[Zr(diMeOx)$_4$]	[Zr(5-NO$_2$Ox)$_4$]	[Zr(5-NO$_2$Ox)$_4$]	[Zr(Pic)$_4$]	[Zr(Trop)$_4$]	[Zr(DBM)$_4$]
Ref	(§4.2)	(§4.3)	(§4.3)	(§5.2)	(§5.3)	(§5.3)	(§5.4)	(§6.2)	(§6.3)
Square Antiprismatic Polyhedron Isomer									
	D_2^z	D_2^x	D_2^x	D_2^x	C_2	--	C_2	--	D_2
Deviation from Ideal Square Antiprismatic Polyhedron (°)									
	19.5(1)	4.9(1)	5.3(1)	5.0(1)	17.5(6)	28.3(6)	21.0(1)	30.8(2)	3.71(4)
Ligand Plane Angles (°)									
L$_1$/L$_2$	80.45(4)	80.6(2)	80.6(2)	88.92(7)	78.3(5)	75.0(2)	74.28(5)	89.9(1)	39.52(4)
L$_2$/L$_3$	84.75(5)	75.9(2)	56.1(2)	61.26(7)	55.1(4)	60.7(2)	68.62(5)	89.7(1)	35.07(5)
L$_3$/L$_4$	84.69(4)	80.2(2)	76.8(2)	78.49(7)	78.3(5)	75.0(2)	74.29(5)	89.6(1)	33.69(4)
L$_4$/L$_1$	86.84(4)	59.1(2)	74.7(2)	83.73(7)	53.7(3)	61.2(2)	68.62(5)	89.2(1)	44.38(4)
L$_1$/L$_3$	151.21(4)	146.19(1)	132.3(2)	140.73(6)	102.4(5)	104.8(2)	111.38(5)	176.0(1)	163.88(4)
L$_2$/L$_4$	152.34(4)	134.2(2)	146.5(1)	142.21(6)	102.4(5)	104.8(2)	111.38(5)	176.8(1)	164.23(4)

In Table 6.10, these aspects are reported and correlated for consideration. These properties for individual cases could seem irrelevant, but with an overarching comparison considering the relation between square-antiprism isomer and the effect it has on the other geometric properties of a structure, some interesting tendencies come to light. In general, it would appear as though the compounds exhibiting the D_2/D_2^x isomer tend to have the least deviation from the ideal square antiprismatic geometry while D_2^z and C_2 isomer moieties tend more towards greater distortion and ultimately even a dodecahedral environment about the metal centre (e.g. [Zr(5-NO$_2$Ox)$_4$]). Furthermore, with regard to specific ligand plane geometries, a similar trend for these isomer types is observed. For D_2/D_2^x compounds, in general, the angles between adjacent planes are smaller than D_2^z and C_2 isomer counterparts (with the exception of [Zr(5-NO$_2$Ox)$_4$] – B).

With regard to the explicit tendency of a ligand to finally coordinate in any specific isomer, a broad generalisation or argument can be made with the data available at this stage. The **steric bulk** does seem to influence this trend, when considering the data presented in Table 6.10, where **D_2^z** {[Zr(diClOx)$_4$].2DMF] > **D_2^x/D$_2$** {[Zr(5-ClOx)$_4$].2DMF, [Zr(diMeOx)$_4$].2DMF, [Zr(DBM)$_4$]} > **C_2** {[Zr(5-NO$_2$Ox)$_4$], [Zr(Pic)$_4$].H$_2$O} > **Dodecahedral** {[Zr(Trop)$_4$].DMF}. The significance here, although not definitively proven, is that these observations can assist a great deal when designing/choosing ligands for separation studies.

6.5. Conclusion – Correlation of Zirconium(IV) Bidentate Ligand Complexes Characterised

By considering all of the structural detail discussed in this and previous chapters, some final conclusions are attempted with regard to all these endeavours of identifying the solid state tendencies of zirconium(IV) complexes containing N,O and O,O'-bidentate-ligands.

As far as general structural aspects (bond lengths and bite angles) and crystal lattice packing stabilization (π-stacking and hydrogen bonding) are considered, general trends are clearly observable. Certain aspects of the preferences of zirconium complex crystallization features become highly predictable. As in the case of the previously discussed (Chapter 4 & 5) oxine-type complexes, averages for physical properties were determined and all structures discussed held close to true in all cases. With regard to the expected lattice/crystalline network stabilization, it has become obvious in these systems to expect a certain extent of π-stacking to be present.

Furthermore, the intimate geometric properties in the immediate coordination polyhedron of the Zr(IV) metal are essentially reproduced in each case, but with correspondingly significant statistical implication. It has been shown, elaborately, that both oxine N,O-donating bidentate ligands, as well as O,O'-donating/β-diketone ligands chelate around zirconium and hafnium metal centres in square antiprismatic polyhedra, with negligible distortions towards a dodecahedral geometries in most cases, with the exception of [Zr(Trop)$_4$].DMF. This indicates that the susceptibility of chelation geometry to intermolecular forces is greater than that of ligand internal geometry.

In other words, when considering ligands for a study on purification/separation of these metals by means or organometallic chelation, the ligand coordination sites will have to be selected to specifically inhibit this kind of coordination geometry around the metal centres, since bidentate ligands *in general* will almost always yield a singular result.

Moreover, from these three crystallographic chapters, although a square antiprismatic coordination geometry and a series of very similar physical properties (bond lengths and bite angles) are observed for each example discussed, there is one aspect of these structures that does show different tendencies. The range of coordination isomers (D_2^x, D_2^z & C_2) described for each structure indicates that there are some aspects of Zr(IV) ligand chelation that allows for tinkering to yield chemically different behaviours of metal complexes. In Chapter 8 the theoretical optimization by means of computational modelling of some zirconium and hafnium complexes are described and discussed.

Chapter 7

Solution Formation Kinetics Study of

Tetrakis(oxine-type)zirconium(IV) Complexes

A fundamental question that has featured significantly throughout this project, and the related M.Sc.[1] study which preceded it, revolves around the issue of the step-wise formation process of *tetrakis*-coordinated bidentate ligands to form zirconium(IV) complexes. From theoretical considerations, synthetic processes results and the crystallographic characterisation chapters presented, the primary observation has been that only *tetrakis*-coordinated complexes are isolated in the final solid state. To answer this question of why this is occurring, in the broader sense, one needs to consider the intrinsic method by which zirconium(IV) behaves in chelation with ligands, in this case specifically oxine-type ligands. This method or reaction progress is most commonly evaluated by means of formation process kinetic studies.

In the previous project, a preliminary solution investigation, utilizing UV/Vis spectroscopic kinetics, was performed on the formation reaction of the *tetrakis*(8-quinolinolato-κ^2N,O)zirconium(IV) complex and a rudimentary mechanism was postulated from these results. In this chapter those experiments are repeated with three other oxine ligands (Figure 7.1), in an attempt to further elucidate the mechanism of formation of these complexes.

---

[1] M. Steyn; *Speciation And Interconversion Mechanism Of Mixed Halo And O,O- And O,N Bidentate Ligand Complexes Of Zirconium*, M.Sc. Dissertation (**2009**), University of the Free State, South Africa.

Thus, the three new sets of kinetic and equilibrium data are compared and correlated with the previous findings and general trends of formation processes and influences are discussed.
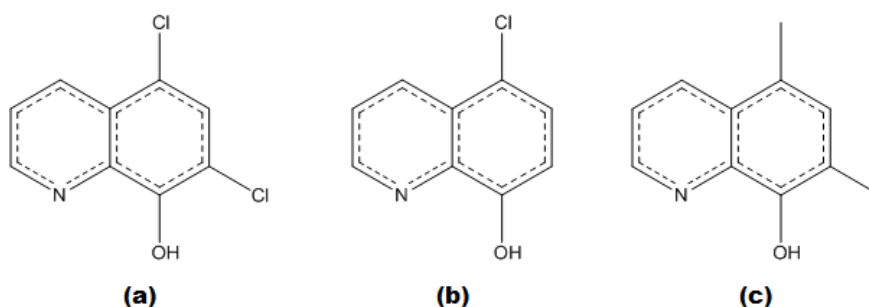
Figure 7.1 Oxine ligands employed in formation kinetic evaluations of zirconium; as discussed in this chapter. (**a**) 5,7-Dichloro-8-hydroxyquinoline (diClOxH); (**b**) 5-Chloro-8-hydroxyquinoline (5-ClOxH); (**c**) 5,7-Dimethyl-8-hydroxyquinoline (diMeOxH).

These ligands were selected to include a range of entering groups which increases in electron donating ability as indicated by their respective Bronsted pKa values. In increasing order, these range from diClOxH[2] (pKa$_1$ = 1.89; pKa$_2$ = 7.62) < 5-ClOxH[3] (pKa$_1$ = 3.56; pKa$_2$ = 9.34) < oxH[4] (pKa$_1$ = 5.02; pKa$_2$ = 9.81) < diMeOxH (pKa values unknown) [***Note***: pKa$_1$ represent the dissociation of the protonated pyridine moiety, while pKa$_2$ indicates the deprotonation of the hydroxyl]. It can be assumed that diMeOxH will have the highest values, however, when considering other organic compound families with different substituents. As listed in Table 7.1, the effect of increasing electron donating groups on a pyridine ring increases the pKa value. It can therefore be assumed that the Bronsted pKa values of diMeOxH will at least be as follows: pKa$_1$ = ± 6; pKa$_2$ = ± 10.5.

Table 7.1 Comparison of Pyridine-Type substrates and their pKa values.[5]

Pyridine - Specie	pKa
3-Chloropyridine	2.84
Pyridine	5.25
3-Methylpyridine	5.68
4-Methylpyridine	6.02
3,5-Dimethylpyridine	6.15
3,4-Dimethylpyridine	6.46
2,6-Dimethylpyridine	6.65
2,4,6-Trimethylpyridine	7.43

---

[2] J. Buckingham (ed.); *Dictionary of Organic Compounds 3* (**1996**), London: Chapman & Hall, 2063.
[3] J. Buckingham (ed.); *Dictionary of Organic Compounds 2* (**1996**), London: Chapman & Hall, 1383.
[4] D.R. Lide (ed.).; *CRC Handbook of Chemistry and Physics* (**2005**), *"Section 8: Dissociation Constants of Organic Acids and Bases"*, 85th Ed. Int.Vers. (http://www.hbcpnetbase.com), CRC Press, Boca Raton, FL, 8-48.
[5] ZirChrom Separations, Inc.; "*Dissociation Constants Of Organic Acids And Bases*" (**2014**), ZirChrom - http://www.zirchrom.com/organic.htm, retrieved 26 January 2014.

7.1. Theoretical Considerations – Formation Process[6] of

tetrakis(8-quinolinolato-κ^2N,O)zirconium(IV), [Zr(ox)$_4$]

During the course of the previous solution study concerning the formation mechanism of the zirconium complex containing 8-hydroxyquinoline (oxH) as chelating ligand, several key issues of interest were identified and investigated. The first of these points involves the consideration of the chemical reaction process by which a metal reagent, in this case ZrCl$_4$, goes about substituting all the initial monodentate halide ligands with four chelating bidentate oxine ligands. By means of simple deduction in this case, it becomes apparent that the metal centre itself undergoes a sterically influenced process with the addition of each doubly-bonded ligand that replaces the original reagent halides.

Furthermore, it is possible that a solvent influenced specie of this metal reagent exists when considering that the structure of the clioquinoline-zirconium(IV) structure described in § 4.4 contained a *coordinated* DMF solvent in the asymmetric unit. If it is, in fact, the case that a zirconium(IV)-chloro-DMF reagent is the initial starting point for *tetrakis*-coordinated complex formation, the entire scope of variables to consider become quite challenging.

(a)   **(b)**

Figure 7.2 Graphical representation of data obtained from UV/Vis spectroscopic kinetics for the formation of [Zr(ox)$_n$]: **(a)** Wavelength scans over time [~3 h]; **(b)** Absorbance vs. time trace at 380 nm for the initial 40 minutes (insert illustrates initial 5 minutes). [ZrCl$_4$] = 5.578 x10^{-5} M, [oxH] range = 5.61 x 10^{-4} to 5.61 x 10^{-3} M, Solvent: DMF, Temp: 25 °C.

---

[6] M. Steyn; *Speciation And Interconversion Mechanism Of Mixed Halo And O,O- And O,N Bidentate Ligand Complexes Of Zirconium*, M.Sc. Dissertation, *Chapter 6* (**2009**), University of the Free State, South Africa.

Furthermore, the significant point of interest that arises from such a *rudimentary* analogy of the entire process, is however the question of *how exactly* this occurs. In theory, bidentate ligands would in general coordinate in a multi-phase approach of firstly bonding at one site, followed by a ring-closing second step in the overall process. When one considers at this juncture, that there are a total of *four* bidentate ligands that are coordinating in a series of reaction steps, as well as the overarching liberation of the initial halide ligands from the metal centre, the total formation mechanism in its entirety becomes a daunting and complicated process.

From the initial reaction kinetic data obtained during the course of the previous study, it was observed that the initial *ca.* 60 seconds of the reaction process monitored by means of the slower minute-to-hour UV/Vis spectrophotometric equipment (Figure 7.2) was losing vital data of the first, fast reaction steps occurring almost instantly when the reaction solutions are mixed. This deficiency is due to the manual mixing process that is part of the experimental setup, and is unavoidable. However, this initial portion of the kinetic experimental data could be recorded by means of the fast millisecond-to-second Stopped-Flow equipment available.

Furthermore, it became apparent that individual reaction steps are not clearly identifiable from UV/Vis absorbance spectroscopic experimental results. In fact, the data obtained suggested that product formation occurs *via* a multi-step progression where overlapping influence of each intermediate product affects the overall observed process. This in itself challenged the efficient and scientifically accurate mathematical modelling of experimental data for prediction of reaction rates of individual/intermediate product formation steps.

From both sets of experimental data, it was determined that the mathematical model most adequately describing the absorbance spectroscopic experimental data was undoubtedly the multi-step *pseudo* first-order equations shown below. For the **faster** initial data, a **two**-consecutive step model (Eq.7.2) gave the most scientifically accurate rate data. For the **slower** minute-to-hour data, a **three**-consecutive step model (Eq.7.3) was determined to be most suitable, as illustrated in Figure 7.3. Correlation of the overlapping mechanistic steps from the faster (2nd observed step) *vs.* the slower (1st observed step) gave rise to the postulation that **a total of four** reaction steps are indeed observable by means of UV/Vis absorbance spectroscopic kinetic evaluations.

$$A_{obs} = A_\infty - (A_\infty - A_0)e^{-k_{obs}.t} \qquad\qquad \textbf{Eq.7.1}$$

$$A_{obs} = (A_0 - B_0)e^{(-k_{AB}.t)} + (B_0 - B_\infty)e^{(-k_{BC}.t)} + B_\infty \qquad\qquad \textbf{Eq.7.2}$$

$$A_{obs} = (A_0 - B_0)e^{(-k_{AB}.t)} + (B_0 - C_0)e^{(-k_{BC}.t)} + (C_0 - C_\infty)e^{(-k_{CD}.t)} + C_\infty \qquad\qquad \textbf{Eq.7.3}$$

In Eqs. 7.1, 7.2 & 7.3, A_{obs} is the observed absorbance at any time, t, A_0 is the initial absorbance at the start of the experiment, B_0 is the theoretical/calculated initial absorbance of the 2nd product, B_∞ is the infinite 2nd/final product absorbance, C_0 is the theoretical/calculated initial absorbance of the 3rd product while C_∞ is the infinite 3rd/final product absorbance. Furthermore, k_{xy} represents the observed rate constant for the specific step; k_{AB} represents k_{obs} for the 1st slow reaction; k_{BC} for the second and k_{CD} for the third.

The observed rate constants (k_{obs}) obtained from least-squares fits of the Absorbance vs. Time data, are subsequently fitted to a rate equation best describing each reaction step. In the case of the 1st fast initial reaction observed in Stopped-Flow experiments, a linear rate equation (Eq.7.4, derived in Appendix B.1) was most representative of the experimental data. The slope of this relation is representative of the forward reaction rate (k_{F1}) and the y-intercept by the reverse reaction rate (k_{F-1}).

$$k_{obs} = k_{F1}[\text{ox}] + k_{F-1} \qquad \textbf{Eq.7.4}$$

On the other hand, for the other three formation reaction steps, a limiting trend was observed for each one, which best corresponds to a rate equation as illustrated by Eq.7.5.

$$k_{Yobs} = (k_{Yn}K_{Yn}[\text{ox}]) / (1 + K_{Yn}[\text{ox}]) \quad + \quad k_r \qquad \textbf{Eq.7.5}$$

In Eq.7.5, k_{Yobs} is the observed rate constant obtained for step Yn [Y = Fast (F)/ Slow (S); n = 1, 2, 3]; K_{Yn} is the pre-equilibrium constant and k_{Yn} is the observed second order limiting rate constant for step Yn, while k_r is the reverse/ parallel reaction indicated by the intercept. The derivation of this rate equation is included in Appendix B.2. This limiting kinetic behaviour is generally associated with a two-phase reaction which becomes independent of ligand concentration at high [oxH] values.

The overall mechanism proposed from this, as illustrated in Scheme 7.1, describes an intricate and very complex process of bidentate ligand coordination with a fast initial reaction, followed by three multi-phase reaction steps wherein it is assumed that the chloride ligand is liberated as HCl (H$^+$ from oxH) in the ring-closing step in each of the four processes. The kinetic data from mathematical modelling of each individual step suggests that the coordination of the 2nd, 3rd and 4th ligands occur via a rapid pre-equilibrium initiation, followed by a slower second reaction.
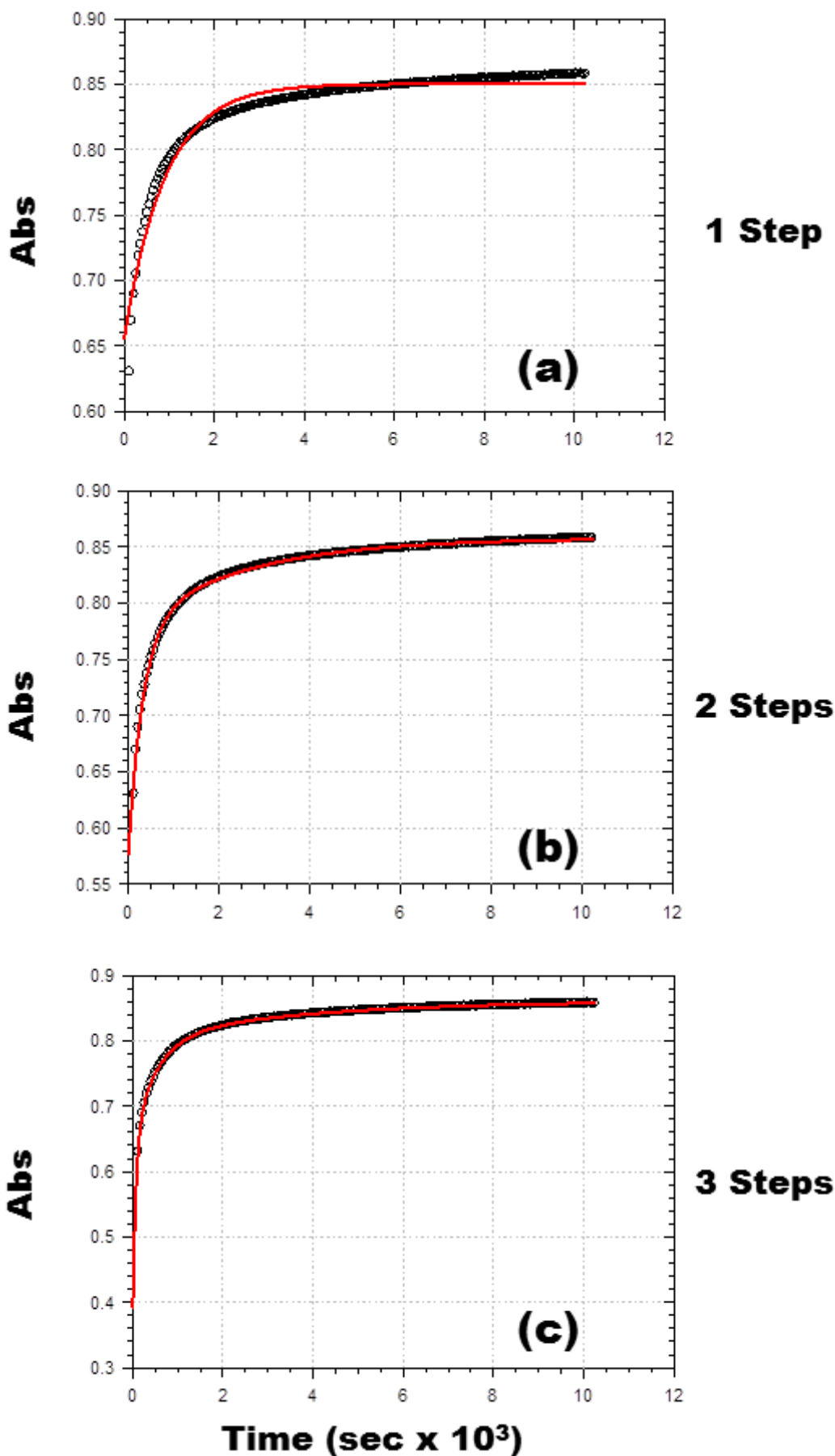
Figure 7.3 UV/Vis data fitted to a *pseudo* first-order (**a**) single-step; (**b**) two-steps; (**c**) three-steps reaction. (**black** circles - observed UV/Vis data; solid **red** line - calculated; using Eqs.7.1, 7.2 & 7.3, respectively) $[ZrCl_4]$ = 5.578 x10^{-5} M, $[oxH]$ = 5.61 x 10^{-3} M, Solvent: DMF, Temp: 25 °C.
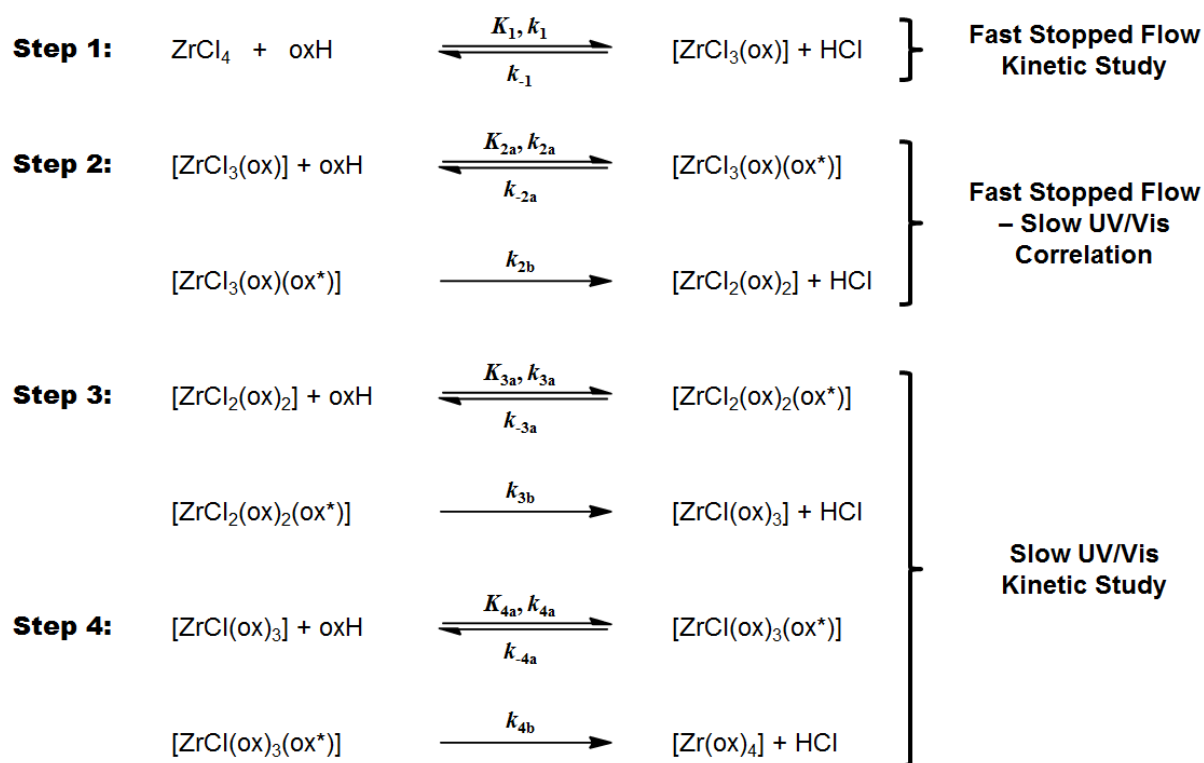
Scheme 7.1 Proposed overall scheme for the observed coordination of four oxine ligands to tetrachloridozirconium(IV) [intermediate products denoted by presence of (ox*)]. Please note that the 2nd observable step on the Fast Stopped Flow is equivalent to the 1st observable step on the Slow UV/Vis Study (See also § 7.7 and Table 7.1).

In another set of experiments, the influence on the reaction equilibrium was tested by means of artificially manipulation of the concentration of the leaving halide ligands in solution before mixing. By the addition of a large excess of Cl^- ions, a suppression of reaction step rates is in theory possible. The organic salt tetraphenylphosphonium chloride was introduced into the metal reaction solution as halide source in a 10^2-fold excess to suppress the forward reaction of ligand complex formation.

When the reaction rates of the observed formation mechanistic steps of the two different sets of experiments are compared, i.e. (i) **absence** and (ii) **presence** of additional leaving halide ligand (see Table 7.2); the effect on the equilibrium becomes strikingly apparent. For the first two observable reaction steps (fast 1st and 2nd – also correlated to slow 1st observable reaction) there appears to be no noteworthy effect on the reaction rates. However, for the 3rd and 4th overall reaction steps (2nd and 3rd observed reactions in slow experiments), the rate of these formation processes are significantly restrained by the presence of the additional Cl^- ions in solution.

Table 7.2 Comparative rate and equilibrium results obtained from formation kinetic studies of *tetrakis*(8-quinolinolato-κ^2N,O)zirconium(IV). Solvent: DMF, Temp: 25 °C

		Constant	No Cl⁻ Added	Cl⁻ Added
Fast Stopped-Flow	**1ˢᵗ Reaction**	k_{F1} ($M^{-1}s^{-1}$)	31±1	24±1
		k_{F-1} (s^{-1})	0.010±0.003	0.013±0.003
	2ⁿᵈ Reaction	k_{F2} (s^{-1})	0.021±0.005	0.015±0.003
		K_{F2} (M^{-1})	169±99	212±85
		k_{F2r} (s^{-1})	0.0029±0.0009	0.0029, Fixed
Slow UV/Vis	**2ⁿᵈ Reaction**	k_{S1} (s^{-1})	0.017±0.006	0.025±0.015
		K_{S1} (M^{-1})	149±107	115±98
		k_{S1r} (s^{-1})	0.0029±0.0008	0.0014, Fixed
	3ʳᵈ Reaction	k_{S2} (s^{-1})	0.0021±0.0002	0.0012±0.0007
		K_{S2} (M^{-1})	1897±754	90±69
		k_{S2r} (s^{-1})	0, Fixed	0, Fixed
	4ᵗʰ Reaction	k_{S3} (s^{-1})	0.00032±0.00005	0.00010±0.00001
		K_{S3} (M^{-1})	790±412	252±62
		k_{S3r} (s^{-1})	0, Fixed	0, Fixed

These observations suggest that as the number of bidentate ligands around the Zr(IV) metal centre are increased, so does the steric demand, and furthermore that both the thermodynamic equilibria of the higher coordinated oxine complexes are significantly more influenced. Furthermore, the forward rates for the formation of the *tris* and *tetrakis* moieties are significantly more affected than the first two steps.

The predominant aim of the kinetic study presented in this chapter is a direct result of the previously completed work. The main purpose here is to initially compare formation mechanisms of zirconium with three other oxine ligands which differ significantly in terms of electronic properties, yet remains constant with steric demand, to determine if the same consecutive multi-step progression of intermediate product formation holds true in all cases. The follow-up on the above is to determine firstly the comparative overall rates depending on the specific nature of the coordinating ligand. Secondly, the study is also intended to compare the influence on the reaction equilibrium (suppression of forward equilibria by a presence of excess leaving ligand in solution) in an overarching correlation of the effect of reaction retardation for each individual step for each ligand and for the series as a whole.

7.2. General Experimental Considerations

7.2.1.   Reagents

All reagents used for reaction solutions were of analytical grade and were purchased from Sigma-Aldrich, South Africa. Reagents were used as received, without further purification. The organic salt, tetraphenylphosphonium chloride, used in equilibrium/suppression experiments was dried at ca. 90 °C for 2 hours before solution preparation.

7.2.2.   Equipment

Kinetic measurements for slower reaction times were performed on a Varian Cary 50 Conc UV/Vis-spectrophotometer. Temperature control of the reaction solutions was maintained to within ±0.1 °C by means of a circulating water bath system. Faster reactions were monitored on a Hi-Tech SF-61DX2 Stopped-flow instrument, also equipped with a circulating water bath system, for which the dead time of the mixing unit was estimated to be less than 2.0 ms. The Stopped-Flow instrument is a multiple wavelength apparatus in the Diode-Array mode in which the initial reactions were collected in order to validate the appropriate wavelength of considerable absorbance change, already identified via the above mentioned spectrophotometer. After this specific wavelength was confirmed, the Stopped-Flow system was changed to the more sensitive Photo-Multiplier setup so that the complete kinetic study could be performed. The Hi-Tech Stopped-flow instrument is Microsoft Windows operated with KinetAsyst Stopped-Flow Kinetic Studio software[7] for the acquisition and analysis of kinetic data.

The *pseudo* first-order rate constants were determined from least-squares fits of the absorbance versus time data to single, double or triple exponentials (Eqs.7.1, 7.2 & 7.3) and then fitted to the relevant rate equations (Eqs.7.4 & 7.5 – derived in Appendix B). The software program Scientist[8] from Micromath was used for this purpose.

^{1}H FT-NMR solution-state spectra for formation kinetic experiment in § 7.3 were recorded at 300.13 MHz on a Bruker AXS 300 MHz at 25 °C.

---

[7] TgK Scientific Kinetic Studion, Version 1.0.8.32278, Copyright ©TgK Scientific, 2008.
[8] MicroMath Scientist for Windows, Version 2.01, Copyright © 1986 – 1995, MicroMath, Inc.

7.2.3.   Reaction Solutions

All the kinetic runs were performed under *pseudo* first-order reaction conditions with the ligand reagent in excess. Ligand stability in the reaction solvent, N,N'-Dimethylformamide (DMF), was confirmed for a *ca.* 48 hour period, for each of the three oxine ligands studied. Fresh reaction solutions were prepared for separate days of kinetic experiments, even though stability of solutions was confirmed, it was considered unwise to use solutions older than that time. All reaction experiments were performed at 25.0(1) °C.

The metal solution was prepared throughout to maintain a final concentration of 5.00×10^{-5} M ($ZrCl_4$: 116.5 mg, 0.5 mmol, dissolved in 50 ml DMF stock solution, from which reaction solutions were prepared by dilution – 0.05 ml diluted to 50 ml total volume). Ligand solutions were prepared as stock solution of 5.00×10^{-3} M final concentration and dilution was carried out across a series of 5 solutions with minimum final concentration solution of 5.00×10^{-4} M (5-ClOxH: 179.7 mg, 1.001 mmol; diClOxH: 214.2 mg, 1.001 mmol; diMeOxH: 173.4 mg, 1.001 mmol; each in 100 ml DMF total volume).   For   equilibrium   influencing/rate   suppression   experiments, tetraphenylphosphonium chloride (188.2 mg, 0.5 mmol, dissolved in $ZrCl_4$ reaction solution) was added to the metal reaction solution to maintain a 10^2 excess of free Cl^-.

7.3. The Search for Intermediate Species

In an attempt to elucidate the intermediate species of the previously described zirconium-oxine complex formation mechanism, a set of experiments utilizing NMR-spectroscopic techniques were performed. With this technique, the aim was to determine whether or not it is possible to observe the formation of different species in solution.

The premise here involves scanning, initially only the specific ligand in solution to obtain the basic spectrum of said ligand, and then subsequently adding the metal reagent (in solution) to this ligand solution and then further scanning this reaction solution over time. A series of such spectrums can be obtained at different times to identify all species of the reaction product observable in solution by this means.

In the specific set of experiments performed, ^{1}H-NMR spectroscopy was utilized as scanning technique. The ligand identified as most promising for this test, was 5,7-Dichloro-8-hydroxyquinoline (diClOxH), due to a its clearly identifiable and limited amount of proton peaks (Figure 7.4). The formation reaction process would be studied in Heptadeutero-N,N-dimethylformamide [N,N-Dimethylformamide-d_7 - DCON(CD$_3$)$_2$] to mimic the solution kinetic studies performed via UV/Vis Spectroscopic methods. The initial experimental setup involved different ratios of ligand vs. metal to determine if differing spectra would be obtained.
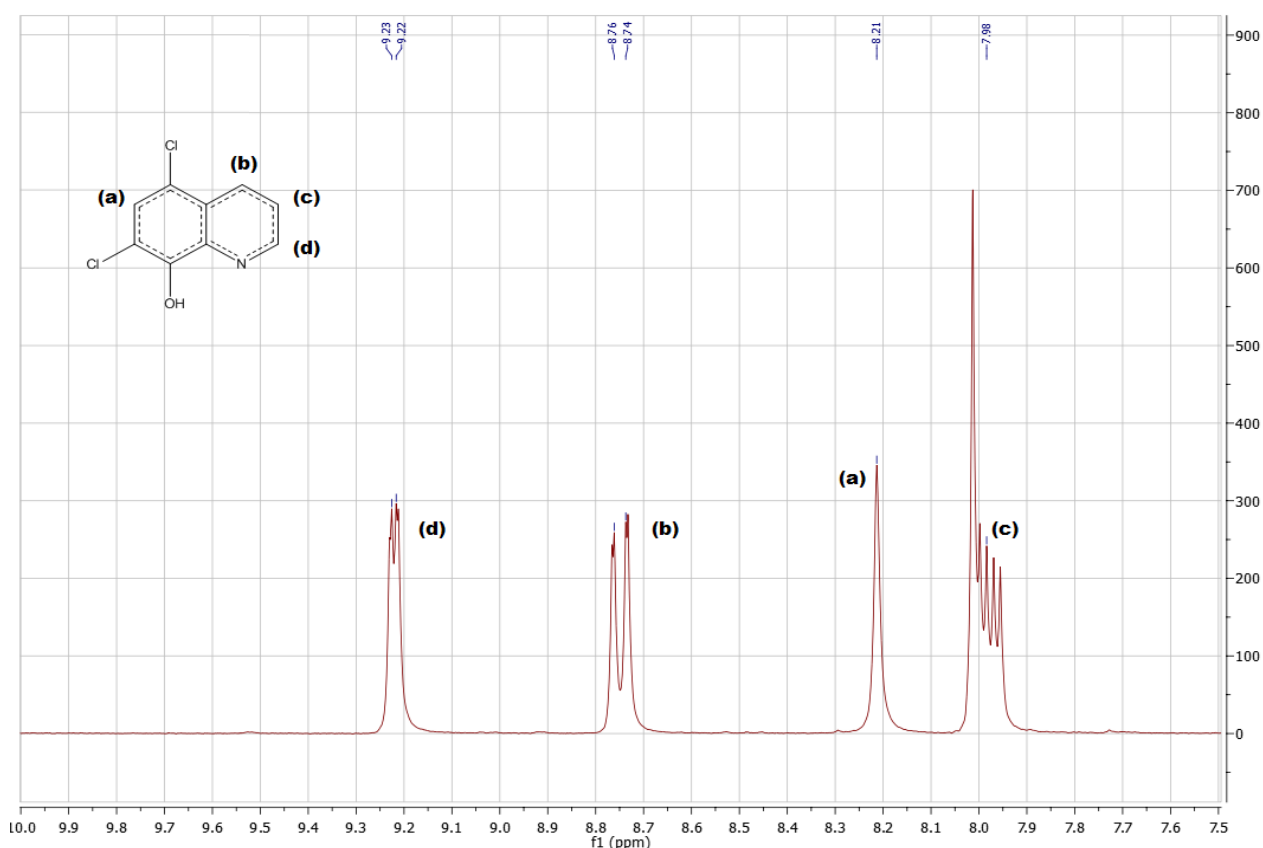
Figure 7.4 Illustration of ^{1}H-NMR spectrum of 5,7-Dichloro-8-hydroxyquinoline (diClOxH) in Heptadeutero-N,N-dimethylformamide (DMF-d_7). Peak assignment to specific protons on the oxine backbone (**a-d**) as per structure scheme insert.

In the 1st experiment performed, a 1:4 metal to ligand ratio was used as a point of reference. A DMF-d_7 solution of diClOxH (11.3 mg, 0.0528 mmol, 600 µl) was utilized to obtain the basic non-coordinated ligand spectrum. Subsequently, a ZrCl$_4$ solution (3.2 mg, 0.0137 mmol, 300 µl) was combined with the ligand solution and the resulting reaction in solution was scanned over time for 18 hours (initial 2 min intervals for 3 hours, 5 min intervals for next 3 hours, finally 15 min intervals for 10 hours).
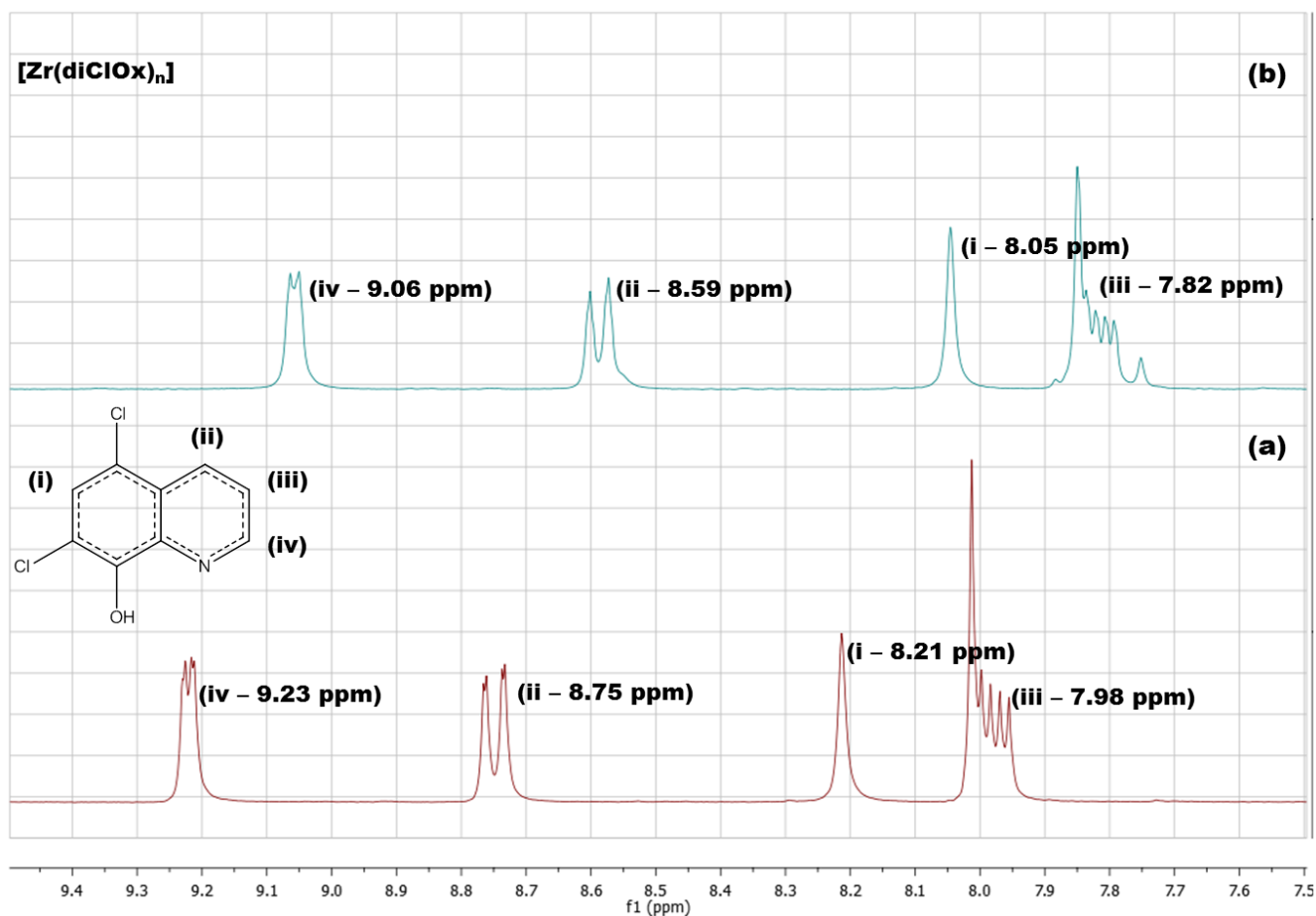
Figure 7.5 Illustration of ^{1}H-NMR spectrum of diClOxH (**a**) *before* and (**b**) *after* coordination with ZrCl$_4$ in DMF-d_7. Peak assignment to specific protons on the oxine backbone (**a-d**) as per structure scheme insert.

The results showed that one could indeed observe a clear shift in the proton peaks upon initiation of the reaction (Figure 7.5). However, although a particular peak at 7.75 ppm can be observed to increase in height over time (Figure 7.6), as the reaction proceeds, no other indications of intermediate-specific peak/s is found. Upon integration of the 7.75 ppm peak, in reference to the 1st observed peak directly after the reaction is initiated, a trend of peak height as a function of time can be presented as in Figure 7.7. This trend is very reminiscent of the UV/Vis Absorbance spectroscopic profiles found for oxine chelation kinetics (see Figure 7.2b), although very distorted in accuracy.
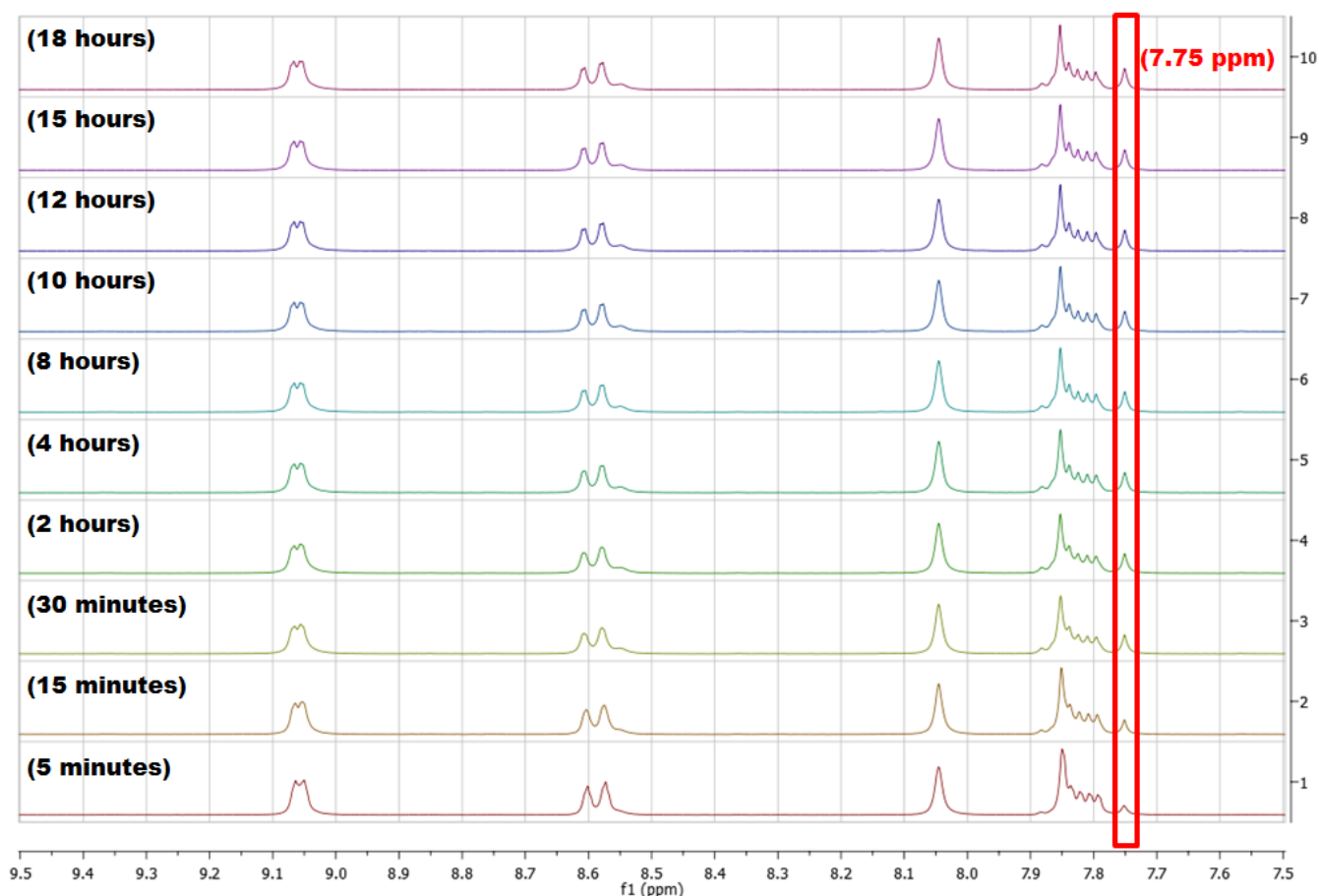
Figure 7.6 Illustration consecutive ^{1}H-NMR spectra from the formation reaction of [Zr(diClOx)$_n$] in DMF-d_7. Spectra shown chronologically from (**1**) earliest to (**10**) final product spectrum. Reference to peaks as illustrated in Figure 7.5; unique metal complex product peak at 7.75 ppm.

A follow-up experiment of a 1:1 metal to ligand ratio reaction solution was also subjected to time lapse scanning. A DMF-d_7 solution of diClOxH (2.9 mg, 0.0135 mmol, 400 µl) was combined with a ZrCl$_4$ solution (3.3 mg, 0.0142 mmol, 300 µl) and the resulting reaction in solution was scanned over time for 18 hours (initial 2 min intervals for 3 hours, 5 min intervals for next 3 hours, finally 15 min intervals for 10 hours). The results of this process, however, yielded no usable results. Again, as with the 1:4 ratio experiment, no specific intermediate product peaks could be observed during the course of the scanned reaction. In fact, no product peak growth could be observed at all in this instance.

The reaction solution used for the time-lapse scans in Figure 7.6 (i.e. 1:4 metal to ligand kinetic experiment) was subsequently scanned again over a period of two weeks, at certain daily intervals. These individual spectra, in comparison with the previously obtained kinetic study data is illustrated in Figure 7.8 along with the [1]H-spectrum of the crystalline product obtained during complex synthesis (reported in Chapter 3.2.1.1, structurally described in Chapter 4.2).
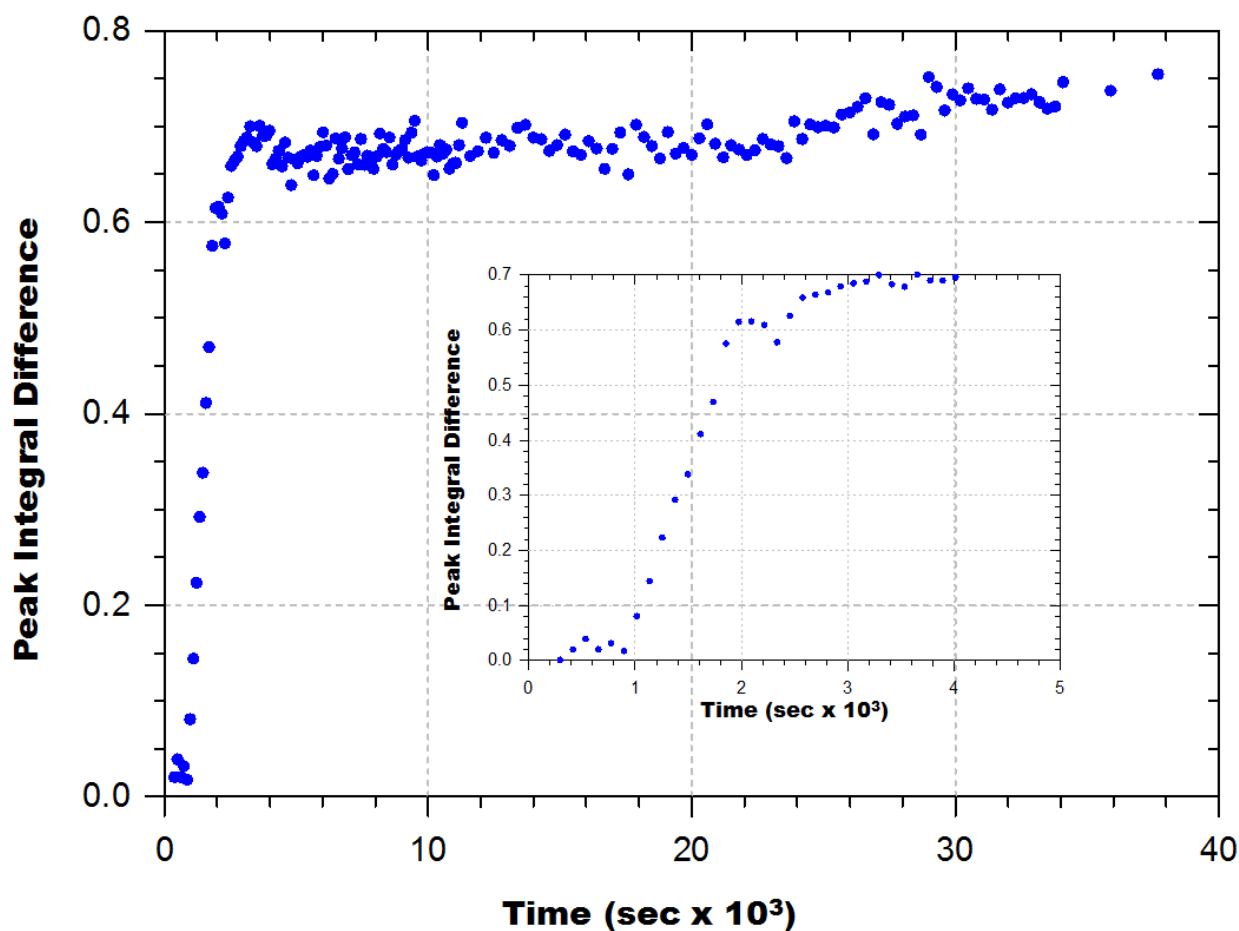
Figure 7.7 Illustration of measured peak integral, of observed unique product peak @ 7.75 ppm (See Figure 7.5) as a function of time for the formation reaction of $[Zr(diClOx)_n]$ in DMF-d_7. Insert illustrates the first 4000 seconds (~1 hour) of the experiment

From this rudimentary comparison it is clear that the metal complex formation process is not complete after 18 hours (comparing Figure 7.8 - Spectrum 1 & 6), when considering the extra set of ligand-specific peaks observable for the final crystal product, absent in the spectrum obtained after 18 hours. Over the course of several days, these peaks become observable, with subsequent degrading of the initial (previously clearly discernable) ligand proton peaks.

The overall result obtained here suggests that there are some form of intermediate formation and disappearance over time, but the entire process cannot be quantified with the current NMR setup. The initial peak at 7.75 ppm does appear to increase steadily over time (Figure 7.6 and 7.8), however the peaks observed at 7.98 ppm, 8.12 ppm and 8.86 ppm (see Figure 7.8) are erratic in there intensities over time and cannot be references to any usable standard for the same integral trend data. This formation rate is at best comparable to the slowest reaction observed, i.e. step 4 in Scheme 7.1 (See also Figure 7.2b).

Due to a large range of variables, uncertainties and experimental errors that can influence these spectra, the specific peak intensities cannot be integrated in a fashion that would yield viable kinetic data. Furthermore, the difficulty of temperature control and equipment calibration over such an extended time frame becomes near impossible.
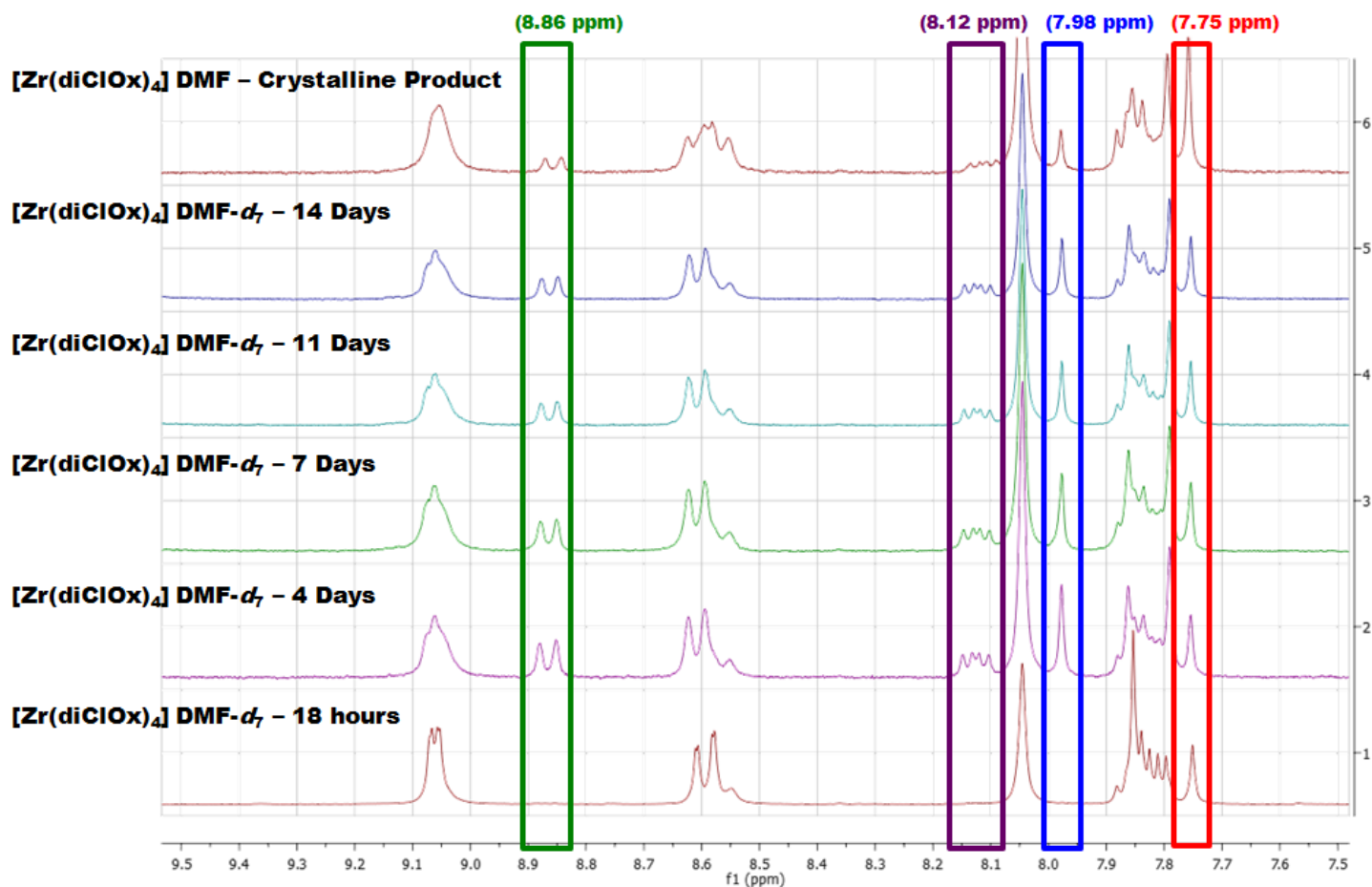
Figure 7.8 Comparison of ^{1}H-NMR spectra of different [Zr(diClOx)$_4$] product spectra. Spectra 1-5 illustrate time lapse scans over a two week period. Spectrum 6 refers to the specific crystalline product as reported in § 3.2.1.1 and discussed in § 4.2. All spectrums drawn in DMF-d_7, 25 °C.

Unfortunately, it is now obvious that any attempt to identify and account for intermediate, lesser coordinated zirconium compounds of oxine ligands would require more intricate planning and possibly other techniques. The time and planning scope required to complete this sub-study was unfortunately not feasible for the current project. Regardless, a series of solution kinetic experiments for the three additional oxine ligands (see Figure 7.1) were successfully completed by means of UV/Vis Absorbance spectroscopy and are reported in the following paragraphs, and compared to the oxine data obtained previously.[6]

7.4. Formation Kinetic Study of [Zr(diClOx)$_4$] –

tetrakis(5,7-dichloroquinolin-8-olato-κ^2N,O)zirconium(IV)

The solution behavioural analysis of 5,7-Dichloro-8-hydroxyquinoline (diClOxH) coordinating to Zr(IV) was performed as an example of a double (electron withdrawing) substituted oxine ligand chelation process. The synthesis and preliminary characterisation of this zirconium(IV) complex has been reported in § 3.2.1.1 and a detailed crystallographic structural characterisation of the solid state product obtained, was described in § 4.2. As with other oxine ligands, diClOxH yields a clear and definite colour change to a reaction solution when coordinated to Zr(IV), making it an ideal candidate for a UV/Vis absorbance spectroscopic solution kinetic evaluation.

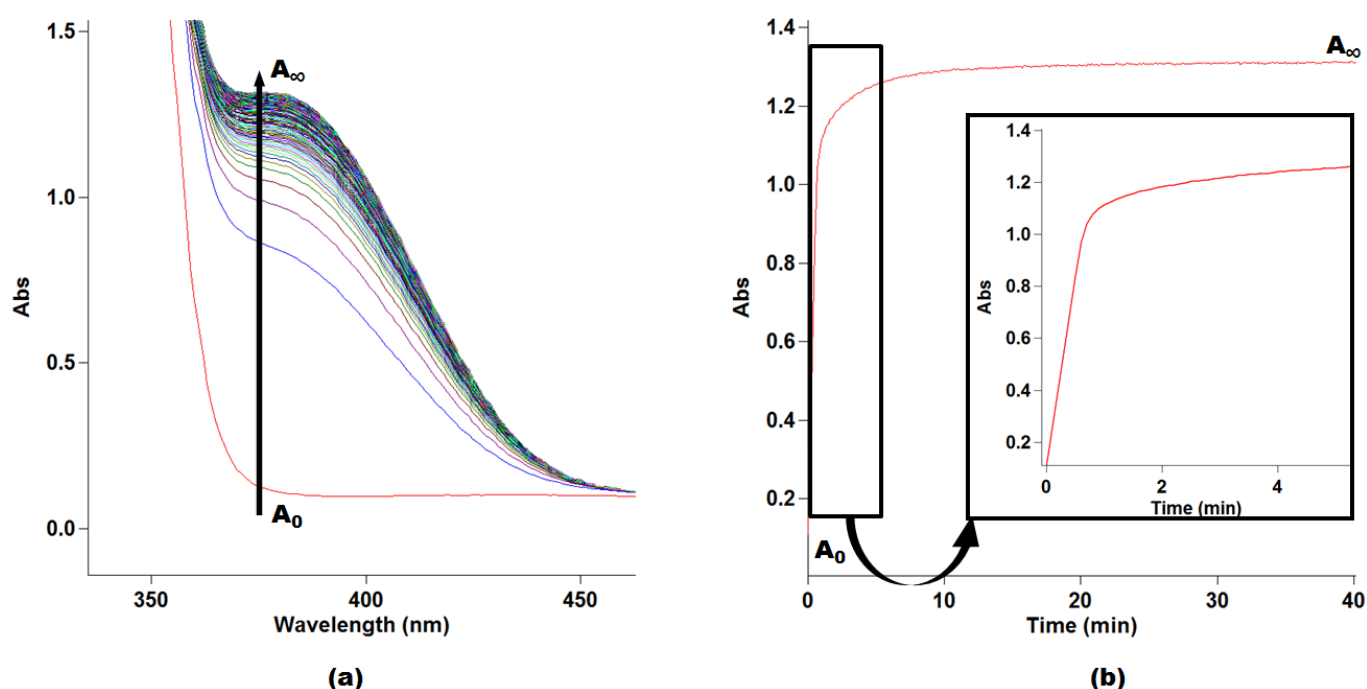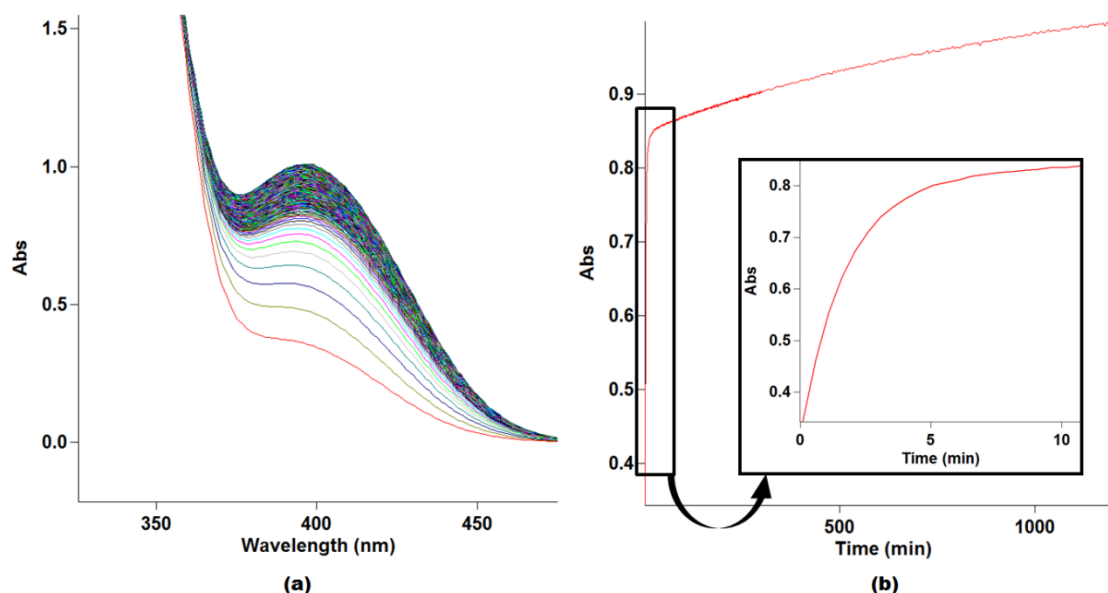**Figure 7.9** Graphical representation of data obtained from UV/Vis spectroscopic kinetics for the formation of [Zr(diClOx)$_4$]: (**a**) Wavelength scans over time [~24h]; (**b**) Absorbance vs. time trace at 400 nm (insert illustrates initial 10 minutes). [ZrCl$_4$] = 5.00 x10^{-5} M, [diClOxH] range = 5.00 x 10^{-4} to 5.00 x 10^{-3} M, Solvent: DMF, Temp: 25 °C

The reaction process of diClOxH with ZrCl$_4$ was followed over the 350-450 nm range to determine the ideal wavelength to follow product formation. As illustrated in Figure 7.9, the chosen wavelength in this case was 400 nm. Absorbance *vs.* Time traces were obtained for six different ligand concentrations. Two sets of experiments, on fast (millisecond-to-second range) Stopped-Flow equipment as well as slower (minute-to-hour range) UV/Vis absorbance spectroscopic analysis, were performed. As with the standard oxH formation kinetics described in § 7.1, the experimental absorbance data showed a fast initial reaction stage in the first *ca.* 60 seconds and a continuous reaction trend for up to 36 hours (See Figure 7.9b).

Figure 7.10 UV/Vis data fitted to a *pseudo* first-order (**a**) single step; (**b**) two step; (**c**) three-step reaction. **black** circles - observed UV/Vis data; solid **blue** line - calculated; using Eqs.7.1, 7.2 & 7.3, respectively) [ZrCl$_4$] = 5.00 x10^{-5} M, [diClOxH] = 5.00 x 10^{-3} M, Solvent: DMF, Temp: 25 °C.

The absorbance data obtained from these experiments were also subjected to mathematical modelling for all previously identified equations (7.1, 7.2 & 7.3) to determine the number of observable steps that can be predicted. For diClOxH reaction data, in the fast Stopped-Flow series, *two consecutive* steps are discernable, and *three consecutive* steps in the slower minute-to-hour data (Figure 7.10). This is in correlation with the predetermined oxH findings. The observed rate constants calculated for the fast and slow experimental data is reported in Table 7.3 and Table 7.4, respectively.

Table 7.3 Observed rate constants from the fast Stopped-Flow Study for the 1st and 2nd consecutive steps; $[ZrCl_4]$ = 5.00 x10^{-5} M, [salt] = 5.00 x 10^{-3} M, Solvent: DMF, Temp: 25 °C.

Observed rate constants (k_{Yn}) for two consecutive steps (s^{-1})				
	1st step: $k_{F1\ obs}$		2nd step: $k_{F2\ obs}$	
[diClOxH] (M)	No Cl⁻ Added	Cl⁻ Added	No Cl⁻ Added	Cl⁻ Added
5.00 x 10^{-4}	0.0351(12)	---	0.0017(6)	0.00081(9)
1.00 x 10^{-3}	0.0413(8)	0.00925(7)	0.0062(7)	0.00164(4)
2.00 x 10^{-3}	0.0541(15)	0.01558(7)	0.0092(5)	0.00399(9)
3.00 x 10^{-3}	0.0654(7)	0.02155(7)	0.0120(7)	0.00615(8)
4.00 x 10^{-3}	0.0744(7)	0.02837(14)	0.0132(7)	0.00676(15)
5.00 x 10^{-3}	0.0824(5)	0.03321(15)	0.0142(1)	0.00716(10)

Table 7.4 Comparison of observed rate constants for three consecutive steps of slow UV/VIS kinetics. $[ZrCl_4]$ = 5.00 x10^{-5} M, [salt] = 5.00 x 10^{-3} M, Solvent: DMF, Temp: 25°C. k_{Yn} – observed rate constant for specific steps; k_{S1} represents k_{obs} for the 1st slow reaction; k_{S2} for the second, k_{S3} for the third.

Observed rate constants (k_{Yn}) for three consecutive steps (s^{-1})						
[diClOxH] (M)	1st step: $k_{S1\ obs}$		2nd step: $k_{S2\ obs}$		3rd step: $k_{S3\ obs}$	
	No Cl⁻ Added	Cl⁻ Added	No Cl⁻ Added	Cl⁻ Added	No Cl⁻ Added	Cl⁻ Added
5.00 x 10^{-4}	0.00365(4)	0.00168(4)	0.00069(2)	0.00012(1)	0.000044(1)	0.0000135(1)
1.00 x 10^{-3}	0.00755(9)	0.00335(3)	0.00131(3)	0.00036(1)	0.000085(2)	0.0000287(9)
2.00 x 10^{-3}	0.0110(2)	0.00609(6)	0.00214(4)	0.00054(1)	0.000114(1)	0.0000433(8)
3.00 x 10^{-3}	0.0143(4)	0.00829(10)	0.00250(7)	0.00072(2)	0.000128(2)	0.0000514(7)
4.00 x 10^{-3}	0.0162(6)	0.00948(14)	0.00263(10)	0.00074(2)	0.000131(2)	0.0000540(4)
5.00 x 10^{-3}	0.0168(6)	0.00984(15)	0.00267(12)	0.00076(2)	0.000140(1)	0.0000544(7)

Additionally, the suppression reaction experiments were also performed in both time ranges. The Absorbance *vs.* Time data obtained from these analyses was mathematically modelled to correspond to the expected mechanistic fittings from the previous (absence of suppressant) data. In other words, the suppression reaction results from the Stopped-Flow time frame was fitted to conform with the expected *two consecutive* step model, whereas the slower experimental findings were fitted to *three consecutive* steps. The observed rate constants calculated for each concentration, in each time frame and each consecutive step is also reported in Table 7.3 (fast) and Table 7.4 (slow).
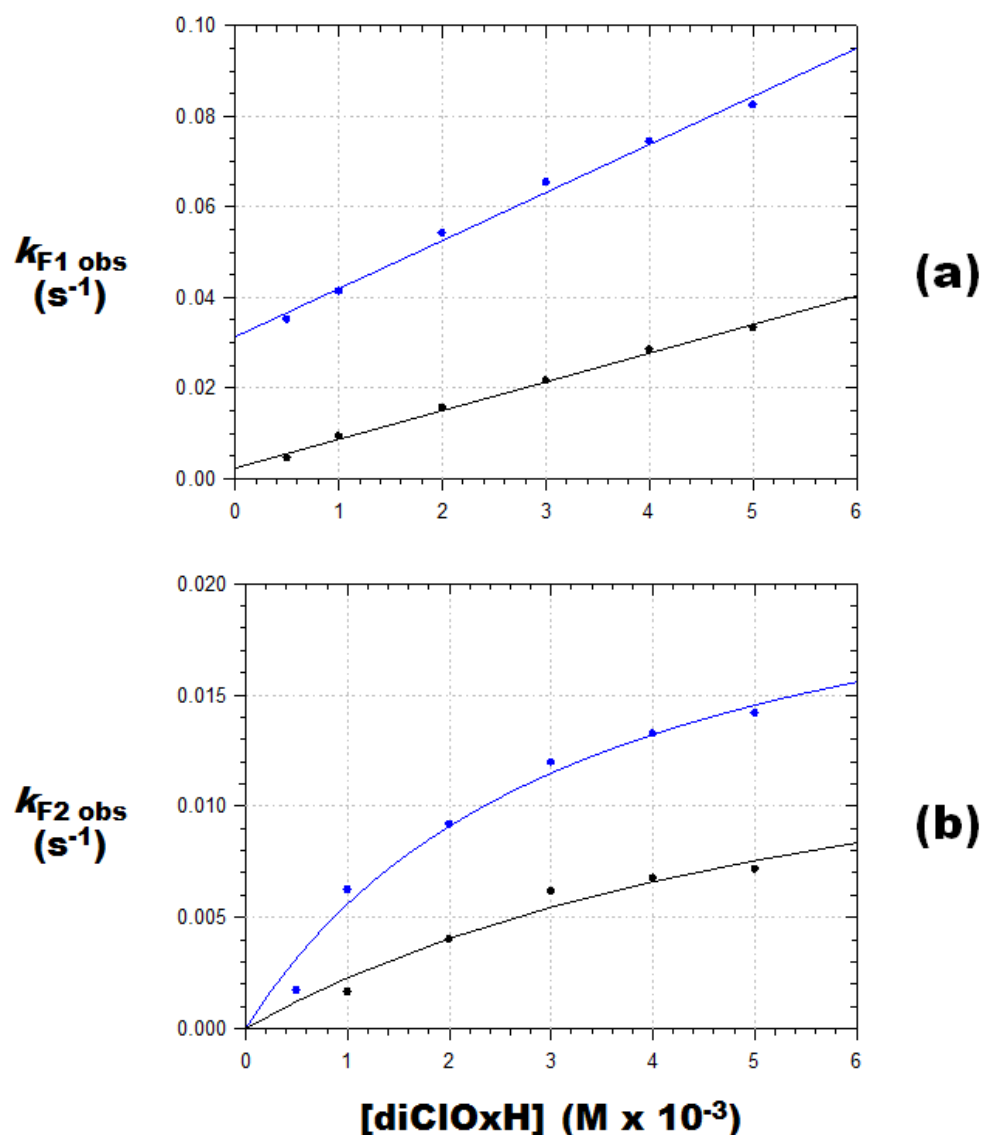
Figure 7.11 Plot of the observed rate constants for the (**a**) 1st and (**b**) 2nd observable reactions by Stopped-Flow Experiments, Table 7.3, modeled to Eq.7.4 and Eq7.5, respectively; $[ZrCl_4] = 5.00 \times 10^{-5}$ M, $[diClOxH] = 5.00 \times 10^{-4}$ - 5.00×10^{-3} M, Solvent: DMF, Temp: 25 °C. (Solid lines – fitted data; individual points – experimental data; **Blue** – *No Cl⁻ Added*; **Black** – *Cl⁻ Added*).

Figure 7.12 Plot of experimental data points (Table 7.4) modeled according to Eq.7.5.
(**a**) 1st observable slow reaction; (**b**) 2nd observable slow reaction; (**c**) 3rd observable slow reaction.
[ZrCl$_4$] = 5.00 x10^{-5} M, [diClOxH] = 5.00 x 10^{-4} - 5.00 x 10^{-3} M, Solvent: DMF, Temp: 25 °C. (Solid lines
– fitted data; individual points – experimental data; **Blue** – *No Cl$^-$ Added*; **Black** – *Cl$^-$ Added*).

The observed rate data, as listed in Table 7.3, for the faster Stopped-Flow kinetic analyses was subsequently fit to rate equations that most closely describe the trends observed. For the 1st observable step, F1, a linear trend was observed (Figure 7.11a), indicating a fast initial reaction. This is in accordance with the previous oxH solution behaviour example described in § 7.1, relating to a rate expression illustrated by Eq.7.5. The slope of this relation is representative of the forward reaction rate (k_{F1}) and the y-intercept by the backward reaction rate (k_{F-1}) as summarized in Table 7.5. The 2nd observable reaction, F2, yielded a limiting rate tendency was obtained (Figure 7.11b), again as with the oxH mechanism. This relation is mathematically described by Eq.7.5 and summarised in Table 7.5.

The slower minute-to-hour range of UV/Vis Absorbance spectroscopic results were also subjected to rate expression modelling to obtain a series of rate and equilibrium constants relevant to each observable step. For all three observable steps in this data, a limiting trend (Figure 7.12) was also observed, in good correlation to what is expected from previous mechanistic observations (§ 7.1). These trends are also best described by Eq.7.5 and the rate and equilibrium data obtained is reported in Table 7.5.

Table 7.5 Comparative rate and equilibrium results obtained from formation kinetic studies of *tetrakis*(5,7-dichloroquinolin-8-olato-κ^2N,O)zirconium(IV).

		Constant	No Cl⁻ Added	Cl⁻ Added
Fast Stopped-Flow	**1ˢᵗ Reaction**	k_{F1} (M⁻¹s⁻¹)	10.6±0.5	6.3±0.2
		k_{F-1} (s⁻¹)	0.031±0.001	0.0024±0.0007
	2ⁿᵈ Reaction	k_{F2} (s⁻¹)	0.024±0.004	0.018±0.007
		K_{F2} (M⁻¹)	301±94	148±94
		k_{F2r} (s⁻¹)	0, Fixed	0, Fixed
Slow UV/Vis	**2ⁿᵈ Reaction**	k_{S1} (s⁻¹)	0.026±0.002	0.019±0.002
		K_{S1} (M⁻¹)	374±51	233±53
		k_{S1r} (s⁻¹)	0, Fixed	0, Fixed
	3ʳᵈ Reaction	k_{S2} (s⁻¹)	0.0038±0.0003	0.0012±0.0002
		K_{S2} (M⁻¹)	557±116	401±133
		k_{S2r} (s⁻¹)	0, Fixed	0, Fixed
	4ᵗʰ Reaction	k_{S3} (s⁻¹)	0.000174±0.000009	0.000076±0.000006
		K_{S3} (M⁻¹)	858±141	587±129
		k_{S3r} (s⁻¹)	0, Fixed	0, Fixed

In all cases (fast and slow experiments), reverse reaction constant values (k_r) are kept constant at 0, due to an overall observation that these values tend to appear falsely negative, and negligibly small due to expected modelling errors in such scenarios were the least-squares fitting of data tend to involve a large amount of unknown variables.

Furthermore, in comparing the rate data for the 2nd observable step in the faster experiments with the 1st observable step of the slower sets, the same occurrence is observed as for the oxH mechanism before. These steps are in good correlation with each other, indicating that these steps are the same 2nd overall step of the entire formation mechanism. The discrepancy that is observed can be assigned to the fact that the faster Stopped-Flow data may not be complete for that specific step and is not as accurately defined by mathematical modelling as for the slower UV/Vis experiment.

In the case of the suppression experiments performed the observed rate results were also subjected to mechanistic evaluation in comparison with the unsuppressed data sets. In Figure 7.11 and Figure 7.12 the effect of this suppression on reaction rates become visually apparent. The findings in the case of diClOxH solution kinetic experiments, it is interesting to note that the equilibrium influencing suppression affects the entire mechanism of formation of the final zirconium product. This is in contrast to the previously discussed oxH findings, which only showed to have an observable influence on the reaction rates of the 3rd and 4th reaction steps.

Comparison of the rate data given in Table 7.5 shows that all four mechanistic reaction steps are significantly affected by the presence of the excess leaving ligand. The kinetic rate constants show that:

- The 1st observable step has its reaction rate slowed by approximately half, as is influenced by the addition of free chloride (k_{F1} of 10.6±0.5 s^{-1} vs. 6.3±0.2 s^{-1}).

- The 2nd observable step is also suppressed by approximately half [k_{S1} (= k_{F2}) of 0.026±0.002s^{-1} vs. 0.019±0.002s^{-1}].

- The 3rd observable step is suppressed more significantly by an approximate three-fold decrease (k_{S2} of 0.0038±0.0003 s^{-1} vs. 0.0012±0.0002 s^{-1}).

- The 4th observable step is also suppressed by an approximate three-fold decrease (k_{S3} of 0.000174±0.000009 s^{-1} vs. 0.000076±0.000006 s^{-1}).

The equilibrium constants follow a similar pattern of notable suppression:

- K_{S1} of 374±51 M^{-1} vs. 233±53 M^{-1}.

- K_{S2} of 557±116 M^{-1} vs. 401±133 M^{-1}.

- K_{S3} of 858±141 M^{-1} vs. 587±129 M^{-1}.

A result from this, as discussed in § 7.1, suggests that as the number of bidentate ligands around the Zr centre are increased, so does the steric demand. In this case all the thermodynamic equilibria of the diClOx-complexes are then significantly influenced. This type of information is vital for experiments that test the extraction capabilities of ligands for possible purification/separation of metals from solution, especially considering the extent of comparison that is available at this stage. It is however worth mentioning here that, however, even though the reaction rate information obtained here is directly applicable in separation studies, further information on hafnium counterparts is of paramount importance for success in solution extraction experiments.

7.5. Formation Kinetic Study of [Zr(5-ClOx)$_4$] –

tetrakis(5-chloroquinolin-8-olato-κ^2N,O)zirconium(IV)

The formation kinetics of 5-Chloro-8-hydroxyquinoline (5-ClOxH) and zirconium(IV) was studied as an example of a single (electron withdrawing) substituent oxine ligand coordination process. The synthesis and preliminary characterisation of this compound has been reported in § 3.2.1.6 and a detailed crystallographic structural characterisation of the solid state product obtained, was described in § 4.3. The ligand itself, when applied in metal complex synthesis, gives a clearly observable colour change in solution as it is combined with a reagent such as ZrCl$_4$. The ligand solution itself has a slight green hue, whereas the reaction with Zr(IV) yields a clear, bright yellow solution. This aspect in itself makes it yet another ideal candidate for an UV/Vis absorbance spectroscopic solution kinetic evaluation.
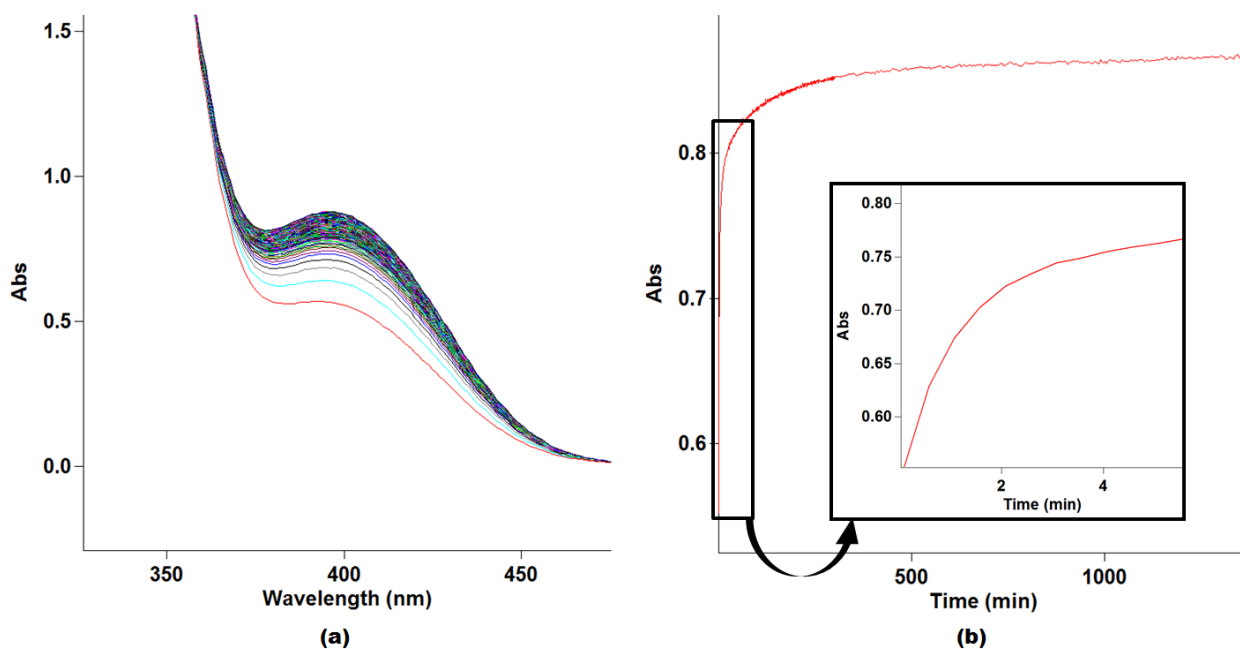
Figure 7.13 Graphical representation of data obtained from UV/Vis spectroscopic kinetics for the formation of [Zr(5-ClOx)$_4$]: **(a)** Wavelength scans over time [~24h]; **(b)** Absorbance vs. time trace at 400 nm (insert illustrates initial 5 minutes). [ZrCl$_4$] = 5.00 x10^{-5} M, [5-ClOxH] range = 5.00 x 10^{-4} to 5.00 x 10^{-3} M, Solvent: DMF, Temp: 25 °C

The reaction process of 5-ClOxH with ZrCl$_4$ was followed over the 350-450 nm range to determine the best wavelength to monitor product formation. As illustrated in Figure 7.13, the chosen wavelength in this case was 400 nm. Absorbance *vs.* Time traces were obtained for six different ligand concentrations. Two sets of experiments, on fast (millisecond-to-second range) Stopped-Flow equipment as well as slower (minute-to-hour range) UV/Vis absorbance spectroscopic analysis, were performed. As with the standard oxH formation kinetics described in § 7.1, the experimental absorbance data showed a fast initial reaction stage in the first *ca.* 60 seconds and a continuous reaction trend for up to 36 hours (See Figure 7.13b).

The absorbance data obtained from these experiments were also subjected to mathematical modelling for all previously identified equations (7.1, 7.2 & 7.3) to determine the number of observable steps that can be predicted. For 5-ClOxH reaction data, in the fast Stopped-Flow series, *two consecutive* steps are discernable, and *three consecutive* steps in the slower minute-to-hour data (Figure 7.14). This is in correlation with the predetermined oxH and diClOxH findings. The observed rate constants calculated for the fast and slow experimental data is reported in Table 7.6 and Table 7.7, respectively.

Table 7.6 Observed rate constants from the fast Stopped-Flow Study for the 1st and 2nd consecutive steps; [ZrCl$_4$] = 5.00 x10^{-5} M, [salt] = 5.00 x 10^{-3} M, Solvent: DMF, Temp: 25 °C.

	Observed rate constants (k_{Yn}) for two consecutive steps (s^{-1})			
	1st step: $k_{F1\ obs}$		**2nd step: $k_{F2\ obs}$**	
[5-ClOxH] (M)	**No Cl$^-$ Added**	**Cl$^-$ Added**	**No Cl$^-$ Added**	**Cl$^-$ Added**
5.00 x 10^{-4}	0.0110(3)	0.0040(4)	0.00303(8)	0.00050(7)
1.00 x 10^{-3}	0.0239(7)	0.0081(3)	0.00630(2)	0.00245(3)
2.00 x 10^{-3}	0.0405(1)	0.0135(2)	0.01031(3)	0.00395(5)
3.00 x 10^{-3}	0.0571(1)	0.0229(4)	0.01199(2)	0.00470(5)
4.00 x 10^{-3}	0.0707(1)	0.0291(8)	0.01287(1)	0.00563(10)
5.00 x 10^{-3}	0.0877(3)	0.0359(7)	0.01317(2)	0.00572(11)

Table 7.7 Comparison of observed rate constants for three consecutive steps of slow UV/VIS Study. [ZrCl$_4$] = 5.00 x10^{-5} M, [salt] = 5.00 x 10^{-3} M, Solvent: DMF, Temp: 25 °C. k_{Yn} – observed rate constant for specific steps; k_{S1} represents k_{obs} for the 1st slow reaction; k_{S2} for the second, k_{S3} for the third.

	Observed rate constants (k_{Yn}) for three consecutive steps (s^{-1})					
	1st step: k_{S1}		**2nd step: k_{S2}**		**3rd step: k_{S3}**	
[5-ClOxH] (M)	**No Cl$^-$ Added**	**Cl$^-$ Added**	**No Cl$^-$ Added**	**Cl$^-$ Added**	**No Cl$^-$ Added**	**Cl$^-$ Added**
5.00 x 10^{-4}	0.0056(2)	0.0014(1)	0.000502(5)	0.00014(4)	0.000048(4)	0.0000014(3)
1.00 x 10^{-3}	0.0094(6)	0.0030(6)	0.000646(6)	0.00034(7)	0.000077(7)	0.000018(2)
2.00 x 10^{-3}	0.0138(3)	0.0053(1)	0.000749(7)	0.00043(2)	0.000092(9)	0.000028(1)
3.00 x 10^{-3}	0.0157(2)	0.0061(2)	0.000866(8)	0.00049(1)	0.000102(1)	0.000033(1)
4.00 x 10^{-3}	0.0171(1)	0.0068(2)	0.000899(9)	0.00053(2)	0.000107(8)	0.000036(1)
5.00 x 10^{-3}	0.0176(3)	0.0071(2)	0.000918(5)	0.00057(3)	0.000111(1)	0.000037(9)

Additionally, the suppression reaction experiments were also performed in both time ranges. The Absorbance vs. Time data obtained from these analyses was mathematically modelled to correspond to the expected mechanistic fittings from the previous (absence of suppressant) data. In other words, the suppression reaction results from the Stopped-Flow time frame was fitted to conform with the expected *two consecutive* step model, whereas the slower experimental findings were fitted to *three consecutive* steps. The observed rate constants calculated for each concentration, in each time frame and each consecutive step are also reported in Table 7.6 (fast) and Table 7.7 (slow).
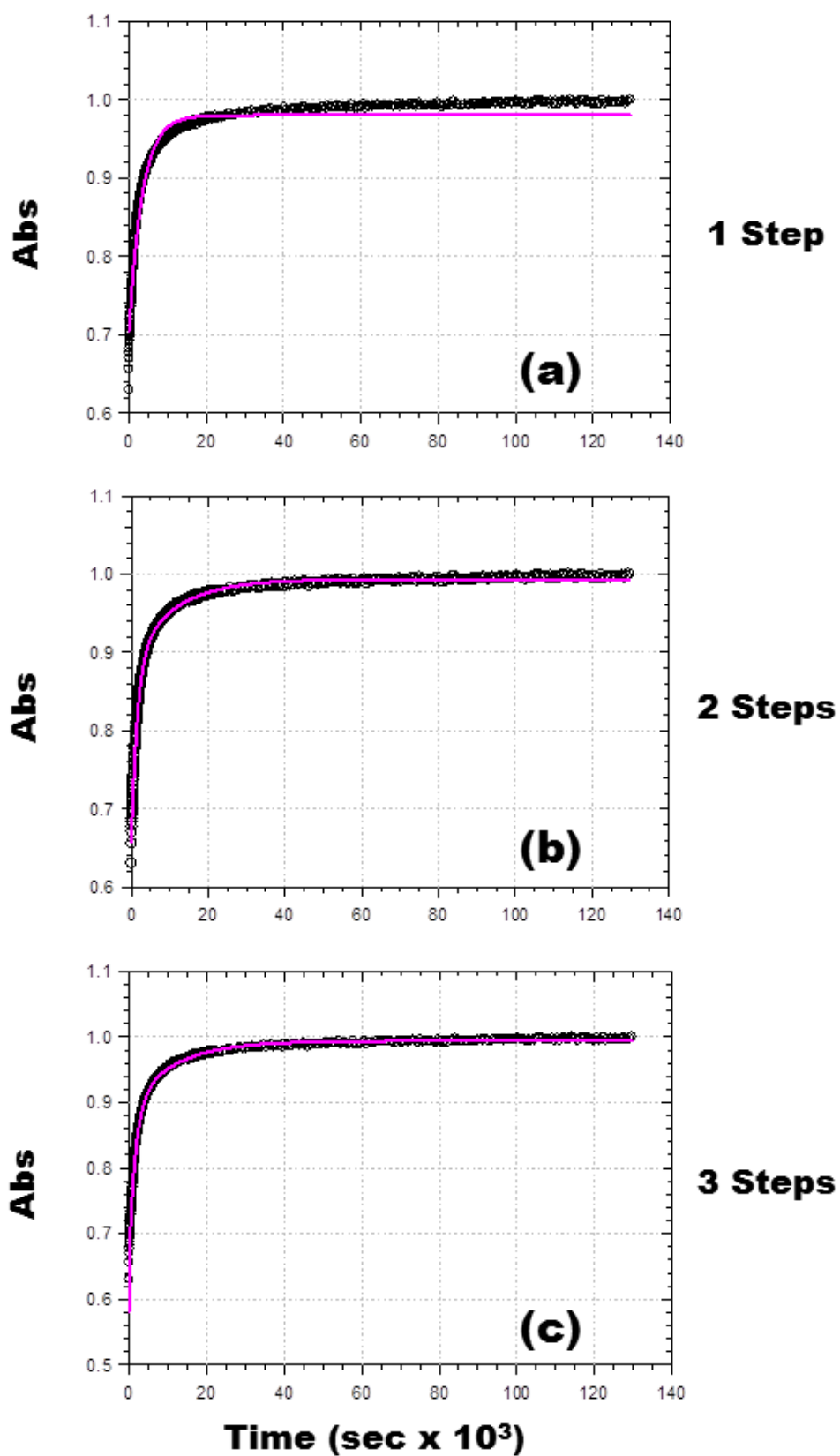
Figure 7.14 UV/Vis data fitted to a *pseudo* first-order (**a**) single step; (**b**) two step; (**c**) three-step reaction. **black** circles - observed UV/Vis data; solid **purple** line - calculated; using Eqs.7.1, 7.2 & 7.3, respectively) [ZrCl$_4$] = 5.00 x10^{-5} M, [5-ClOxH] = 5.00 x 10^{-3} M, Solvent: DMF, Temp: 25 °C.
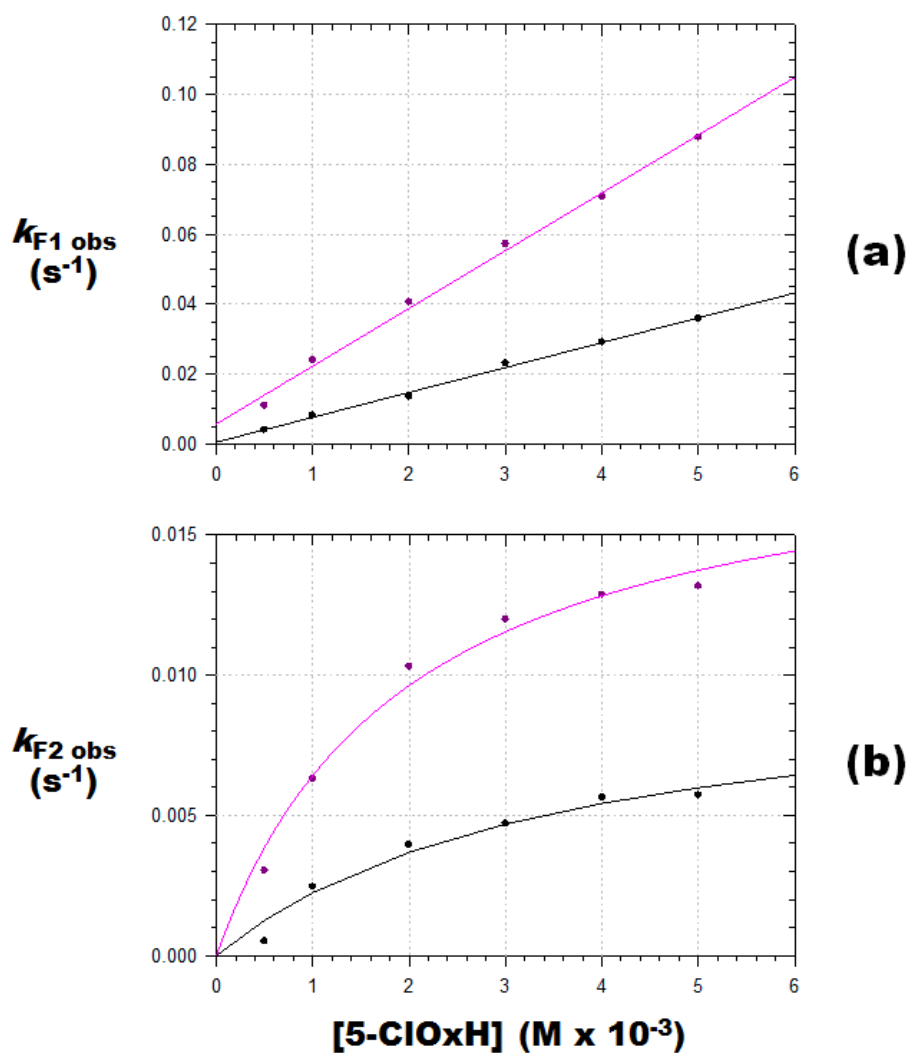
Figure 7.15 Plot of the observed rate constants for the (**a**) 1st and (**b**) 2nd observable reactions by Stopped-Flow Experiments, Table 7.6, modeled to Eq.7.4 and Eq7.5, respectively; [ZrCl$_4$] = 5.00 x10^{-5} M, [5-ClOxH] = 5.00 x 10^{-4} - 5.00 x 10^{-3} M, Solvent: DMF, Temp: 25°C. (Solid lines – fitted data; individual points – experimental data; **Purple** – *No Cl$^-$ Added*; **Black** – *Cl$^-$ Added*).

The observed rate data, as listed in Table 7.6, for the faster Stopped-Flow kinetic analyses was subsequently fit to rate equations that most closely describe the trends observed. For the 1st observable step, F1, a linear trend was observed (Figure 7.15a), indicating a fast initial reaction. This is in accordance with the previous oxH solution behaviour example described in § 7.1, relating to a rate expression illustrated by Eq.7.4. The slope of this relation is representative of the forward reaction rate (k_{F1}) and the y-intercept by the backward reaction rate (k_{F-1}) as summarized in Table 7.8. The 2nd observable reaction, F2, yielded a limiting rate tendency was obtained (Figure 7.15b), again as with the oxH mechanism. This relation is mathematically described by Eq.7.5 and summarised in Table 7.8.
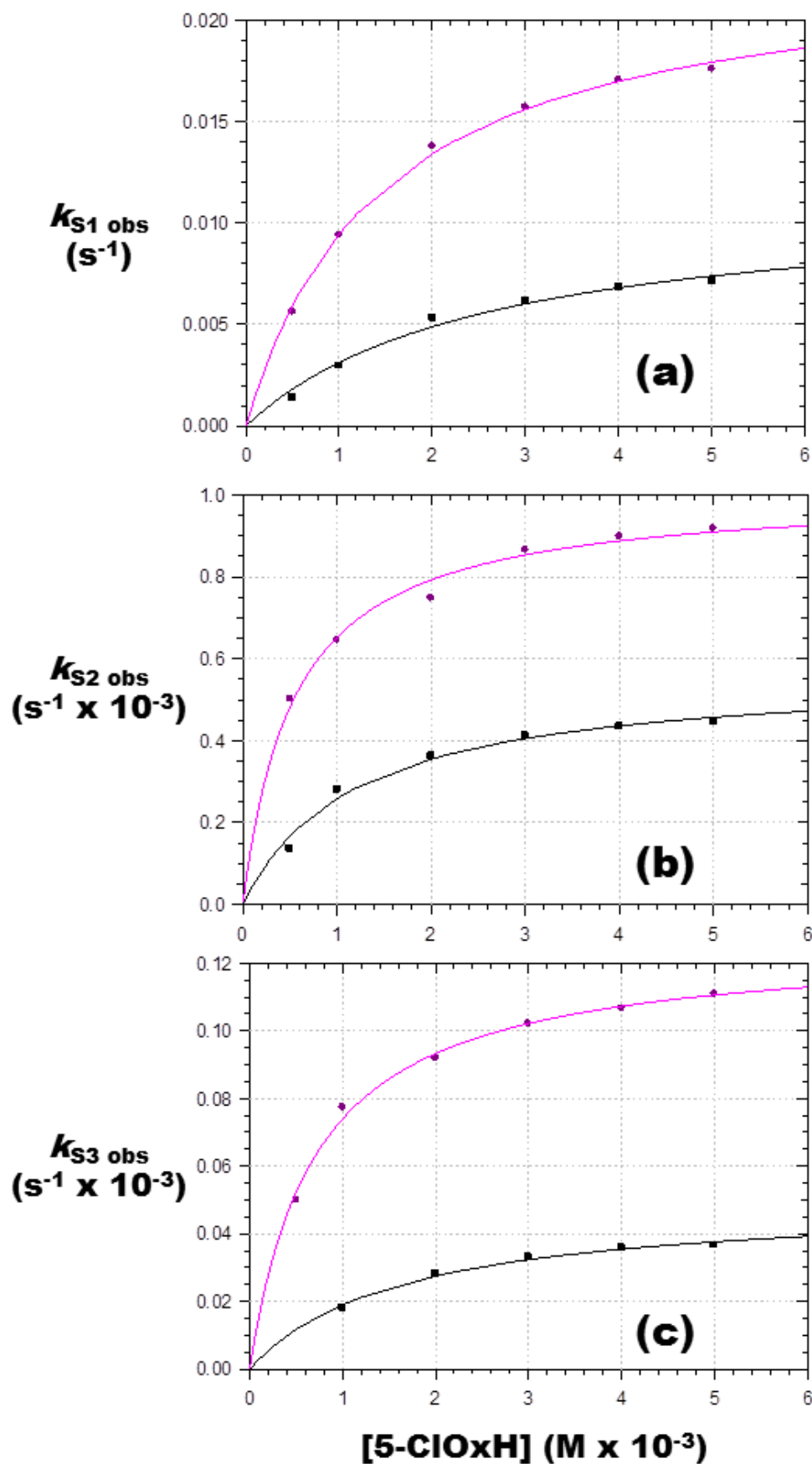
Figure 7.16 Plot of experimental data points (Table 7.7) modeled according to Eq.7.5.
(**a**) 1st observable slow reaction; (**b**) 2nd observable slow reaction; (**c**) 3rd observable slow reaction.
[$ZrCl_4$] = 5.00 x10^{-5} M, [5-ClOxH] = 5.00 x 10^{-4} - 5.00 x 10^{-3} M, Solvent: DMF, Temp: 25 °C. (Solid lines
– fitted data; individual points – experimental data; **Purple** – *No Cl⁻ Added*; **Black** – *Cl⁻ Added*).

Table 7.8 Comparative rate and equilibrium results obtained from formation kinetic studies of *tetrakis*(5-chloroquinolin-8-olato -κ^2N,O)zirconium(IV). Solvent: DMF, Temp: 25 °C

		Constant	No Cl⁻ Added	Cl⁻ Added
Fast Stopped-Flow	**1ˢᵗ Reaction**	k_{F1} $(M^{-1}s^{-1})$	16.5±0.6	7.1±0.2
		k_{F-1} (s^{-1})	0.0057±0.0017	0.0005±0.0007
	2ⁿᵈ Reaction	k_{F2} (s^{-1})	0.019±0.002	0.010±0.002
		K_{F2} (M^{-1})	503±107	281±115
		k_{F2r} (s^{-1})	0, Fixed	0, Fixed
Slow UV/Vis	**2ⁿᵈ Reaction**	k_{S1} (s^{-1})	0.023±0.002	0.011±0.001
		K_{S1} (M^{-1})	684±84	387±89
		k_{S1r} (s^{-1})	0, Fixed	0, Fixed
	3ʳᵈ Reaction	k_{S2} (s^{-1})	0.00101±0.0003	0.00056±0.0003
		K_{S2} (M^{-1})	1822±215	843±152
		k_{S2r} (s^{-1})	0, Fixed	0, Fixed
	4ᵗʰ Reaction	k_{S3} (s^{-1})	0.000126±0.000003	0.000050±0.000002
		K_{S3} (M^{-1})	1414±114	616±82
		k_{S3r} (s^{-1})	0, Fixed	0, Fixed

The slower minute-to-hour range of UV/Vis Absorbance spectroscopic results were also subjected to rate expression modelling to obtain a series of rate and equilibrium constants relevant to each observable step. For all three observable steps in this data, a limiting trend (Figure 7.16) was also observed, in good correlation to what is expected from previous mechanistic observations (§ 7.1 & 7.4). These trends are also best described by Eq.7.5 and the rate and equilibrium data obtained is reported in Table 7.8. In all cases (fast and slow experiments), reverse reaction constant values (k_r) are kept constant at 0, due to an overall observation that these values tend to appear falsely negative, and negligibly small due to expected modelling errors in such scenarios were the least-square fitting of data tend to involve a large amount of unknown variables.

Furthermore, in comparing the rate data for the 2ⁿᵈ observable step in the faster experiments with the 1ˢᵗ observable step of the slower sets, the same occurrence is observed as for the oxH mechanism before. These steps are in good correlation with each other, indicating that these steps are the same 2ⁿᵈ overall step of the entire formation mechanism. The discrepancy that is observed can be assigned to the fact that the faster Stopped-Flow data may not be complete for that specific step and is not as accurately defined by mathematical modelling as for the slower UV/Vis experiment.

In the case of the suppression experiments performed the observed rate results were also subjected to mechanistic evaluation in comparison with the unsuppressed data sets. In Figure 7.15 and Figure 7.16 the effect of this suppression on reaction rates become visually apparent. The findings in the case of 5-ClOxH solution kinetic experiments, it is interesting to note that the equilibrium influencing suppression affects the entire mechanism of formation of the final zirconium product. This is in contrast to the previously discussed oxH findings, which only showed to have an observable influence on the reaction rates of the 3rd and 4th reaction steps.

Comparison of the rate data given in Table 7.8 shows that all four mechanistic reaction steps are significantly affected by the presence of the excess leaving ligand. The kinetic rate constants show that:

- The 1st observable step has its reaction rate slowed by half, as is influenced by the addition of free chloride (k_{F1} of 16.5±0.6 s^{-1} vs. 7.1±0.2 s^{-1}).

- The 2nd and 3rd observable steps are also suppressed by half [k_{S1} (= k_{F2}) of 0.023±0.002s^{-1} vs. 0.011±0.001s^{-1}); k_{S2} of 0.00101±0.0003 s^{-1} vs. 0.00056±0.0003s^{-1}].

- The 4th observable step is further suppressed by an approximate three-fold decrease (k_{S3} of 0.000126±0.000003 s^{-1} vs. 0.000050±0.000002 s^{-1}).

The equilibrium constants follow a similar pattern:

- K_{S1} of 684±84 M^{-1} vs. 387±89 M^{-1}.

- K_{S2} of 1822±215 M^{-1} vs. 843±152M^{-1}.

- K_{S3} of 1414±114 M^{-1} vs. 616±82 M^{-1}.

A result from this, as proposed for the oxH kinetic findings before, suggests that as the number of bidentate ligands around the Zr centre are increased, so does the steric demand. In this case all the thermodynamic equilibria of the 5-ClOx-complexes are then significantly influenced. This type of information is vital for experiments that test the extraction capabilities of ligands for possible purification/separation of metals from solution.

7.6. Formation Kinetic Study of [Zr(diMeOx)₄] –

tetrakis(5,7-dimethylquinolin-8-olato-κ^2N,O)zirconium(IV)

The formation kinetics process of 5,7-Dimethyl-8-hydroxyquinoline (diMeOxH) chelation to zirconium(IV) was studied as an example of a double (electron donating) substituent oxine ligand coordination process. The synthesis and preliminary characterisation of this compound has been reported in § 3.2.1.5 and a detailed crystallographic structural characterisation of the solid state product obtained, was described in § 5.2. As with other oxine ligands, diMeOxH yields a clear and definite colour change to a reaction solution when coordinated to Zr(IV), making it yet another ideal candidate for a UV/Vis absorbance spectroscopic solution kinetic evaluation.

(a)   **(b)**
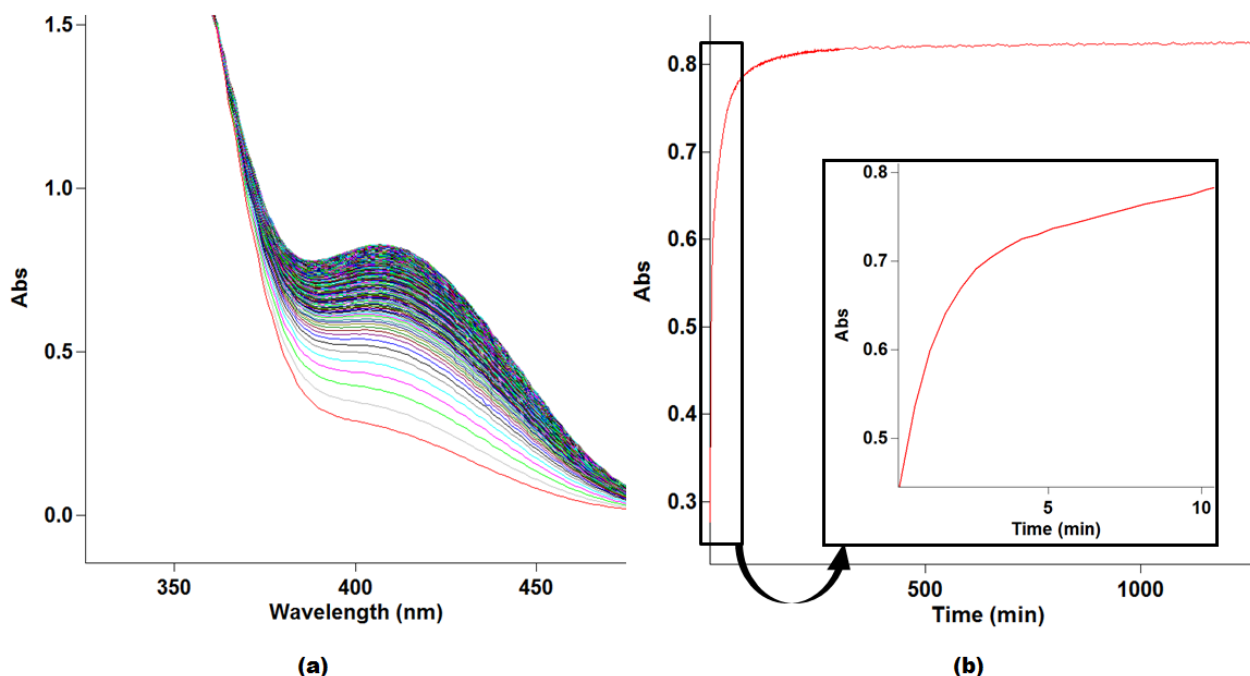
Figure 7.17 Graphical representation of data obtained from UV/Vis spectroscopic kinetics for the formation of [Zr(diMeOx)₄]: **(a)** Wavelength scans over time [~24h]; **(b)** Absorbance vs. time trace at 405 nm (insert illustrates initial 10 minutes). [ZrCl₄] = 5.00 x10⁻⁵ M, [diMeOxH] range = 5.00 x 10⁻⁴ to 5.00 x 10⁻³ M, Solvent: DMF, Temp: 25 °C

The reaction process of diMeOxH with ZrCl₄ was followed over the 350-450 nm range to determine the ideal wavelength to follow product formation. As illustrated in Figure 7.17, the chosen wavelength in this case was 405 nm. Absorbance vs. Time traces were obtained for six different ligand concentrations, as reported in Table 7.9 and 7.10. Two sets of experiments, on fast (millisecond-to-second range) Stopped-Flow equipment as well as slower (minute-to-hour range) UV/Vis absorbance spectroscopic analysis, were performed. As with the standard oxH formation kinetics described in § 7.1, the experimental absorbance

data showed a fast initial reaction stage in the first *ca.* 60 seconds and a continuous reaction trend for up to 36 hours (See Figure 7.17b).
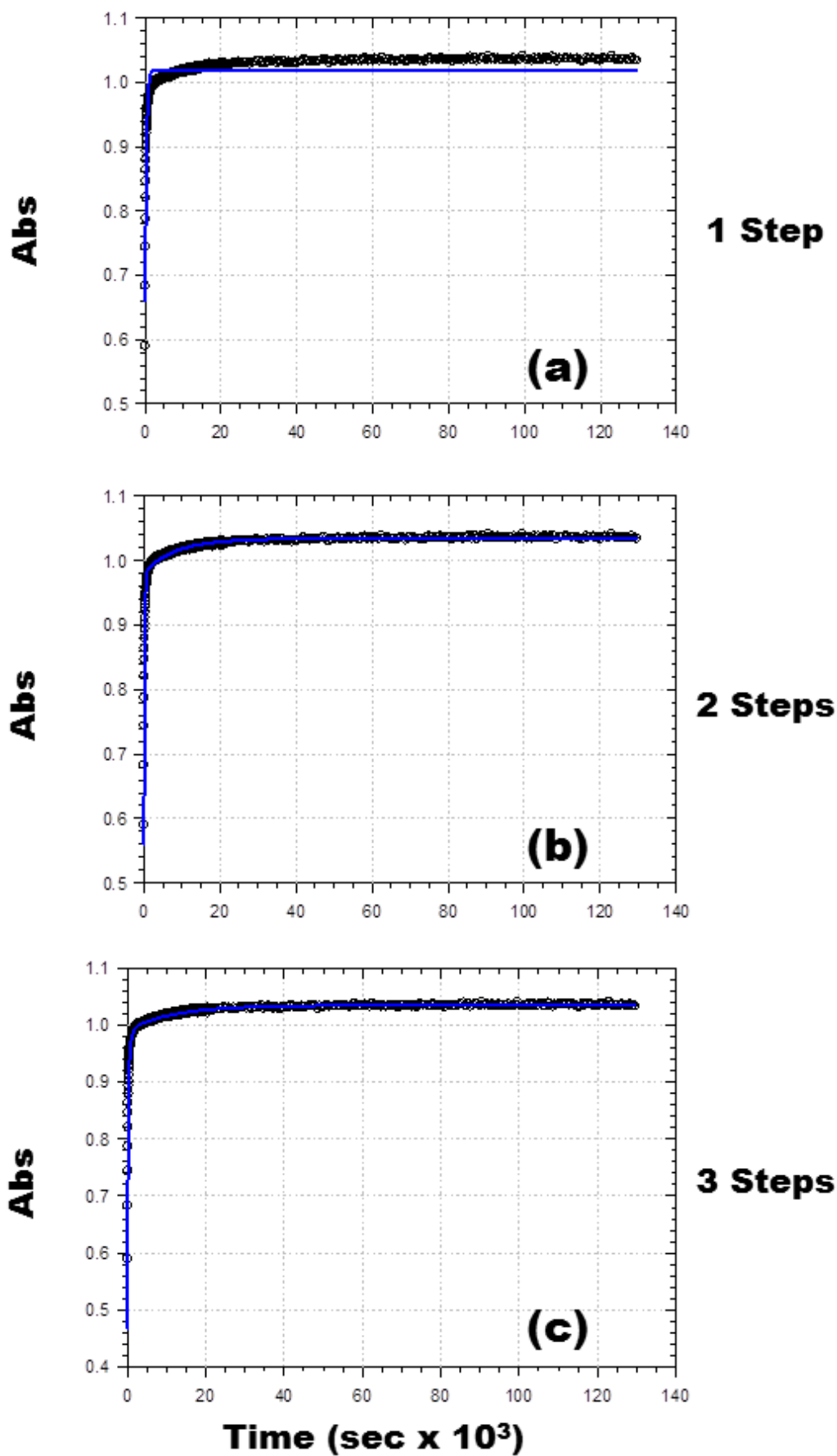
The absorbance data obtained from these experiments were also subjected to mathematical modelling for all previously identified equations (7.1, 7.2 & 7.3) to determine the number of observable steps that can be predicted. For diMeOxH reaction data, in the fast Stopped-Flow series, *two consecutive* steps are discernable, and *three consecutive* steps in the slower minute-to-hour data (Figure 7.18). This is in correlation with the other, predetermined oxine findings. The observed rate constants calculated for the fast and slow experimental data is reported in Table 7.9 and Table 7.10, respectively.

Table 7.9 Observed rate constants from the fast Stopped-Flow Study for the 1st and 2nd consecutive steps; [ZrCl$_4$] = 5.00 x10^{-5} M, [salt] = 5.00 x 10^{-3} M, Solvent: DMF, Temp: 25 °C.

Observed rate constants (k_{Yn}) for two consecutive steps (s^{-1})				
[diMeOxH] (M)	**1st step: $k_{F1\ obs}$**		**2nd step: $k_{F2\ obs}$**	
	No Cl$^-$ Added	**Cl$^-$ Added**	**No Cl$^-$ Added**	**Cl$^-$ Added**
5.00 x 10^{-4}	0.1843(5)	0.1517(8)	0.00117(3)	0.00113(12)
1.00 x 10^{-3}	0.4048(10)	0.2220(10)	0.00596(4)	0.00205(4)
2.00 x 10^{-3}	0.9716(8)	0.3058(14)	0.01059(4)	0.00312(4)
3.00 x 10^{-3}	1.2489(10)	0.3648(2)	0.01245(4)	0.00421(13)
4.00 x 10^{-3}	1.6496(14)	0.4303(11)	0.01327(7)	0.00493(4)
5.00 x 10^{-3}	1.8941(10)	0.5422(2)	0.01373(11)	0.00512(2)

Table 7.10 Comparison of observed rate constants for three consecutive steps[*] of slow UV/VIS kinetics.[ZrCl$_4$] = 5.00 x10^{-5} M, [salt] = 5.00 x 10^{-3} M, Solvent: DMF, Temp: 25 °C. k_{Yn} – observed rate constant for specific steps; k_{S1} represents k_{obs} for the 1st slow reaction; k_{S2} for the second, k_{S3} for the third.

Observed rate constants (k_{Yn}) for three consecutive steps (s^{-1})						
[diMeOxH] (M)	**1st step: k_{S1}**		**2nd step: k_{S2}**		**3rd step: k_{S3}**	
	No Cl$^-$ Added	**Cl$^-$ Added**	**No Cl$^-$ Added**	**Cl$^-$ Added**	**No Cl$^-$ Added**	**Cl$^-$ Added**
5.00 x 10^{-4}	0.0036(2)	0.00109(5)	0.000550(12)	0.000167(4)	0.0000309(13)	0.0000042(1)
1.00 x 10^{-3}	0.0067(2)	0.00153(8)	0.000809(9)	0.000219(5)	0.0000581(9)	0.0000091(1)
2.00 x 10^{-3}	0.0127(6)	0.00238(15)	0.001078(14)	0.000325(8)	0.0000681(8)	0.0000128(2)
3.00 x 10^{-3}	0.0149(6)	0.00365(19)	0.001106(12)	0.000412(8)	0.0000690(9)	0.0000145(3)
4.00 x 10^{-3}	0.0162(8)	0.00426(24)	0.001182(8)	0.000434(9)	0.0000721(7)	0.0000153(3)
5.00 x 10^{-3}	0.0171(9)	0.00448(27)	0.001178(8)	0.000446(8)	0.0000727(5)	0.0000154(3)
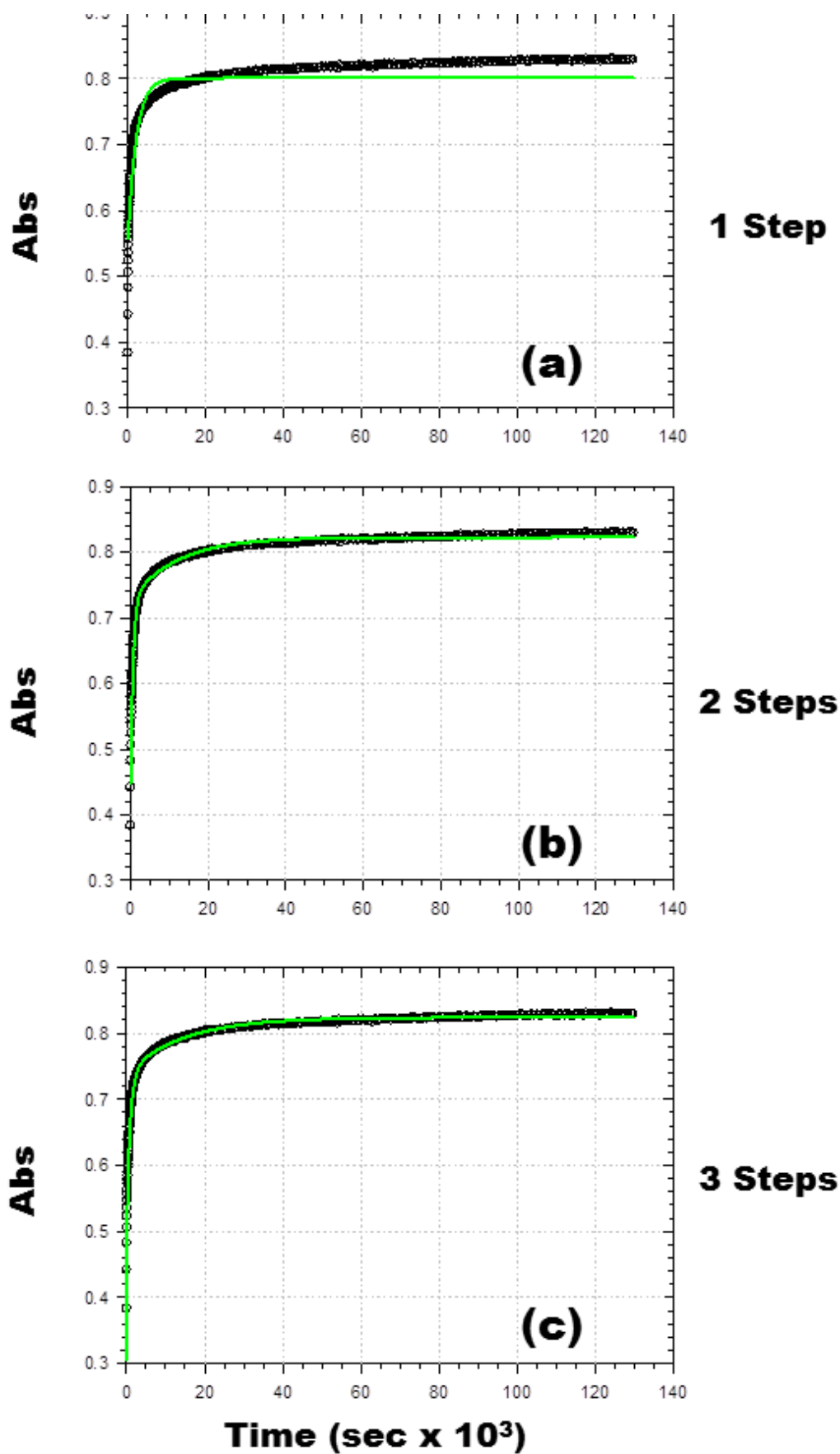
Figure 7.18 UV/Vis data fitted to a *pseudo* first-order (**a**) single step; (**b**) two step; (**c**) three-step reaction. **black** circles - observed UV/Vis data; solid **green** line - calculated; using Eqs.7.1, 7.2 & 7.3, respectively) [ZrCl$_4$] = 5.00 x10^{-5} M, [diMeOxH] = 5.00 x 10^{-3} M, Solvent: DMF, Temp: 25 °C.

Additionally, the suppression reaction experiments were also performed in both time ranges. The Absorbance vs. Time data obtained from these analyses was mathematically modelled to correspond to the expected mechanistic fittings from the previous (absence of suppressant) data. In other words, the suppression reaction results from the Stopped-Flow time frame was fitted to conform with the expected *two consecutive* step model, whereas the slower experimental findings were fitted to *three consecutive* steps. The observed rate constants calculated for each concentration, in each time frame and each consecutive step is also reported in Table 7.9 (fast) and Table 7.10 (slow).
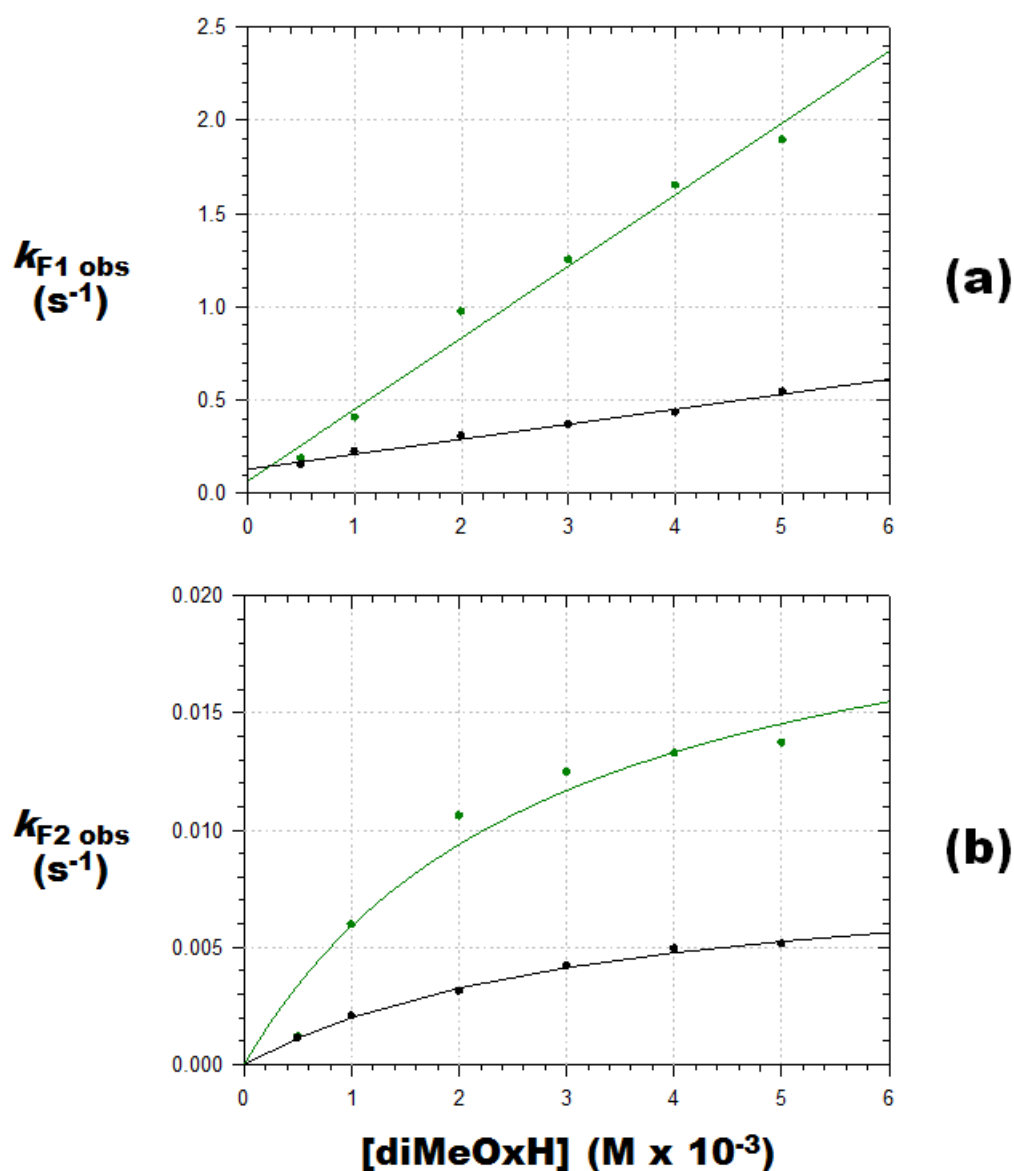
Figure 7.19 Plot of the observed rate constants for the (**a**) 1st and (**b**) 2nd observable reactions by Stopped-Flow Experiments, Table 7.9, modeled to Eq.7.4 and Eq7.5, respectively; [ZrCl$_4$] = 5.00 x10^{-5} M, [diMeOxH] = 5.00 x 10^{-4} - 5.00 x 10^{-3} M, Solvent: DMF, Temp: 25 °C. (Solid lines – fitted data; individual points – experimental data; **Green** – *No Cl⁻ Added*; **Black** – *Cl⁻ Added*).
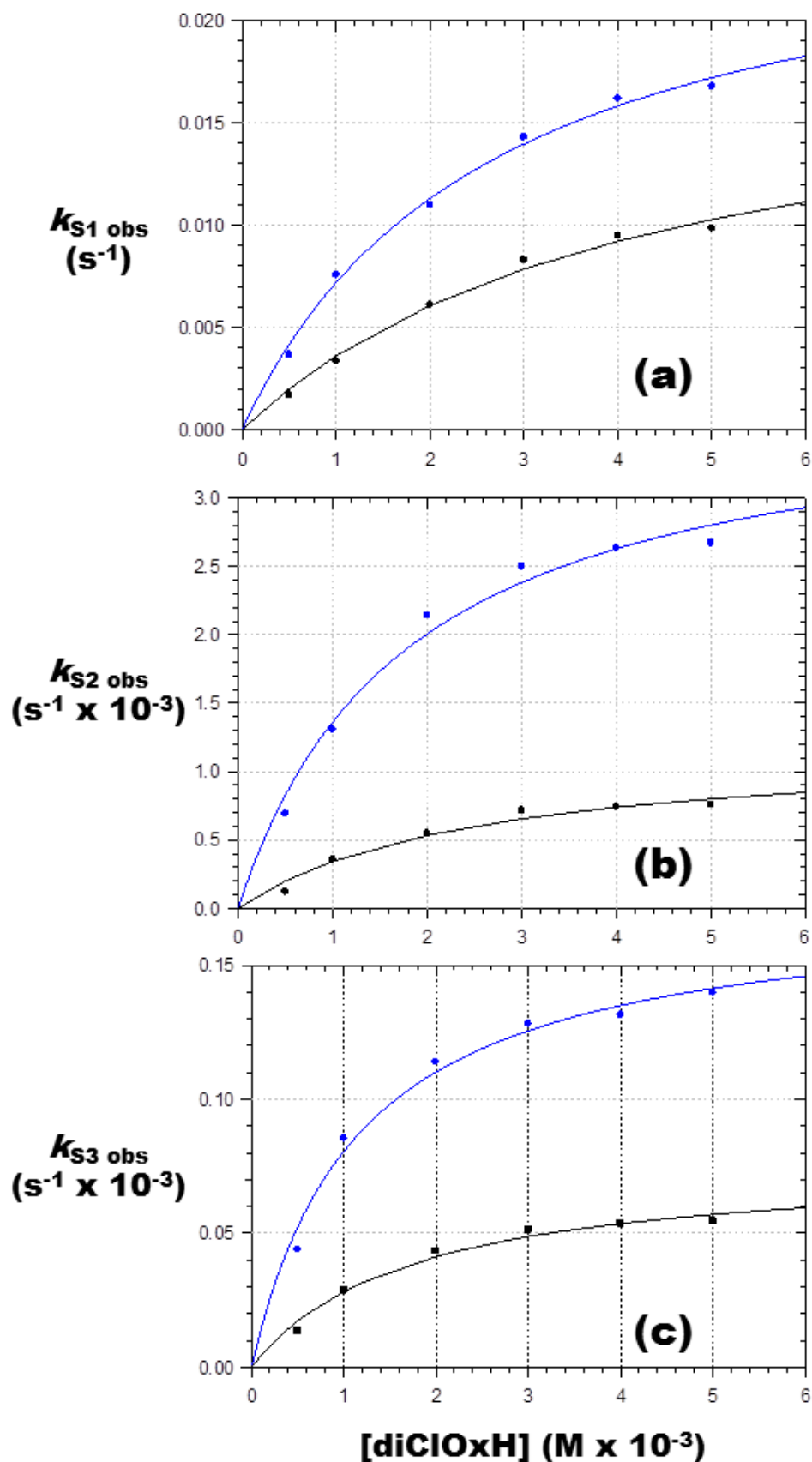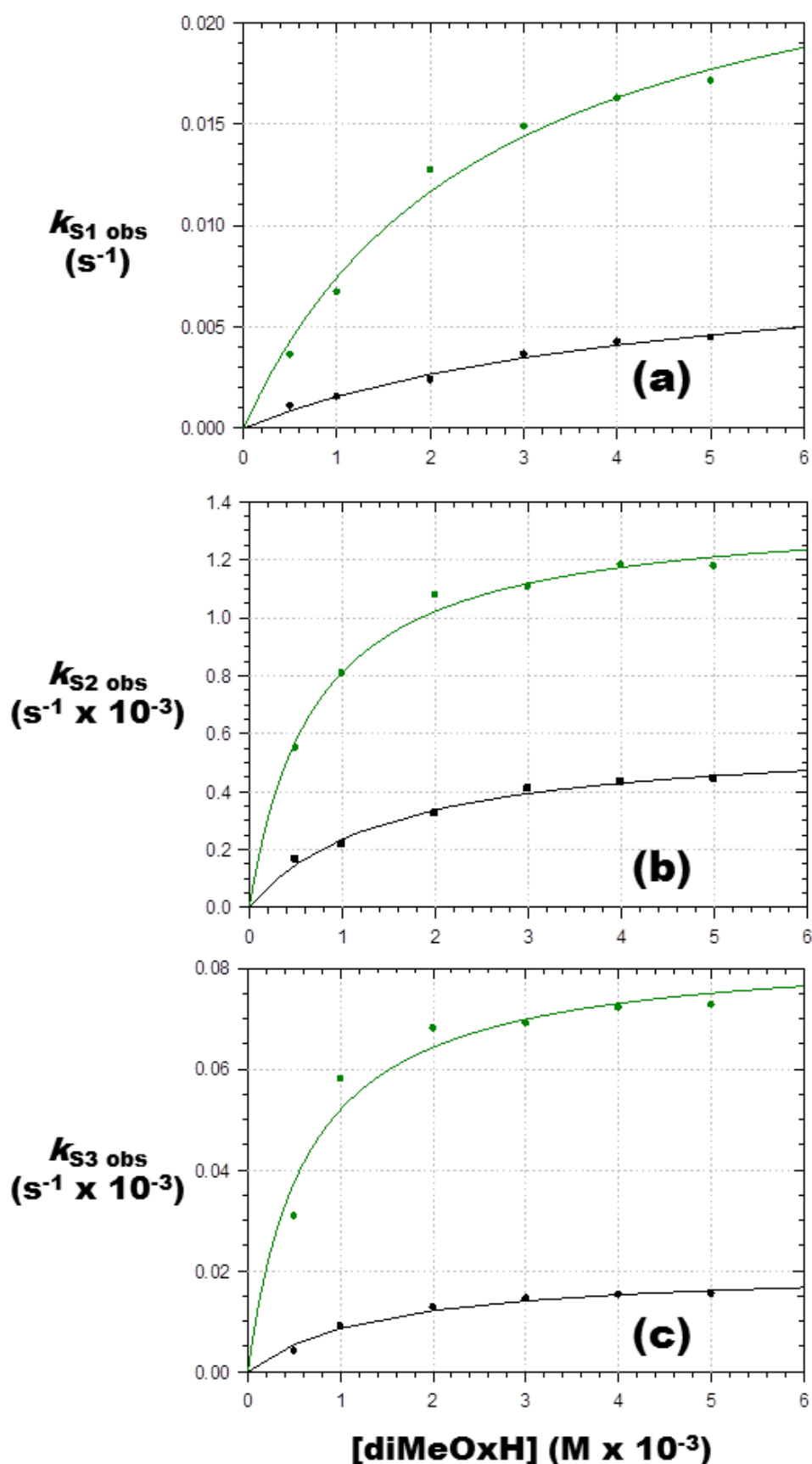
Figure 7.20 Plot of experimental data points (Table 7.10) modeled according to Eq.7.5. (**a**) 1st observable slow reaction; (**b**) 2nd observable slow reaction; (**c**) 3rd observable slow reaction. [ZrCl$_4$] = 5.00 x10^{-5} M, [diMeOxH] = 5.00 x 10^{-4} - 5.00 x 10^{-3} M, Solvent: DMF, Temp: 25 °C. (Solid lines – fitted data; individual points – experimental data; **Green** – *No Cl$^-$ Added*; **Black** – *Cl$^-$ Added*).

The observed rate data, as listed in Table 7.9, for the faster Stopped-Flow kinetic analyses was subsequently fit to rate equations that most closely describe the trends observed. For the 1st observable step, F1, a linear trend was observed (Figure 7.19), indicating a fast initial reaction. This is in accordance with the previous oxH solution behaviour example described in § 7.1, relating to a rate expression illustrated by Eq.7.4. The slope of this relation is representative of the forward reaction rate (k_{F1}) and the y-intercept by the backward reaction rate (k_{F-1}) as summarized in Table 7.11.

The 2nd observable reaction, F2, yielded a limiting rate tendency was obtained (Figure 7.19), again as with the oxH mechanism. This relation is mathematically described by Eq.7.5 and summarised in Table 7.11.

Table 7.11 Comparative rate and equilibrium results obtained from formation kinetic studies of *tetrakis*(5,7-dimethylquinolin-8-olato-κ^2N,O)zirconium(IV).

		Constant	No Cl⁻ Added	Cl⁻ Added
Fast Stopped-Flow	**1st Reaction**	k_{F1} $(M^{-1}s^{-1})$	384±25	81±5
		k_{F-1} (s^{-1})	0.066±0.076	0.13±0.01
	2nd Reaction	k_{F2} (s^{-1})	0.023±0.005	0.0088±0.0006
		K_{F2} (M^{-1})	347±166	294±40
		k_{F2r} (s^{-1})	0, Fixed	0, Fixed
Slow UV/Vis	**2nd Reaction**	k_{S1} (s^{-1})	0.027±0.003	0.0087±0.002
		K_{S1} (M^{-1})	380±87	215±64
		k_{S1r} (s^{-1})	0, Fixed	0, Fixed
	3rd Reaction	k_{S2} (s^{-1})	0.00138±0.00004	0.00059±0.00004
		K_{S2} (M^{-1})	1431±167	665±110
		k_{S2r} (s^{-1})	0, Fixed	0, Fixed
	4th Reaction	k_{S3} (s^{-1})	0.000084±0.000006	0.000021±0.000002
		K_{S3} (M^{-1})	1603±436	718±159
		k_{S3r} (s^{-1})	0, Fixed	0, Fixed

The slower minute-to-hour range of UV/Vis Absorbance spectroscopic results were also subjected to rate expression modelling to obtain a series of rate and equilibrium constants relevant to each observable step. For all three observable steps in this data, a limiting trend (Figure 7.20) was also observed, in good correlation to what is expected from previous mechanistic observations (§ 7.1, 7.4 & 7.5). These trends are also best described by Eq.7.5 and the rate and equilibrium data obtained is reported in Table 7.11. In all cases (fast and

slow experiments), reverse reaction constant values (k_r) are kept constant at 0, due to an overall observation that these values tend to appear falsely negative, and negligibly small due to expected modelling errors in such scenarios were the least-square fitting of data tend to involve a large amount of unknown variables.

Furthermore, in comparing the rate data for the 2nd observable step in the faster experiments with the 1st observable step of the slower sets, the same occurrence is observed as for the oxH mechanism before. These steps are in good correlation with each other, indicating that these steps are the same 2nd overall step of the entire formation mechanism. The discrepancy that is observed can be assigned to the fact that the faster Stopped-Flow data may not be complete for that specific step and is not as accurately defined by mathematical modelling as for the slower UV/Vis experiment.

In the case of the suppression experiments performed the observed rate results were also subjected to mechanistic evaluation in comparison with the unsuppressed data sets. In Figure 7.19 and Figure 7.20 the effect of this suppression on reaction rates become visually apparent. The findings in the case of diMeOxH solution kinetic experiments, it is interesting to note that the equilibrium influencing suppression affects the entire mechanism of formation of the final zirconium product to a greater extent than has been observed at this stage.

Comparison of the rate data given in Table 7.11 shows that all four mechanistic reaction steps are significantly affected by the presence of the excess leaving ligand. The kinetic rate constants show that:

- The 1st observable step has its reaction rate slowed by an astounding five-fold decrease in rate as influenced by the addition of free chloride (k_{F1} of 384±25 s^{-1} vs. 81±5 s^{-1}).

- The 2nd observable step is repressed by a three-fold decrease [k_{S1} (= k_{F2}) of 0.027±0.003s^{-1} vs. 0.0087±0.002s^{-1}].

- The 3rd observable step is suppressed by half (k_{S2} of 0.00138±0.00004 s^{-1} vs. 0.00059±0.00004 s^{-1}).

- The 4th observable step is further suppressed by a four-fold decrease (k_{S3} of 0.000084±0.000006 s^{-1} vs. 0.000021±0.000002 s^{-1}).

The equilibrium constants follow a similar pattern of notable suppression:

- K_{S1} of 380±87 M^{-1} vs. 215±64 M^{-1}.

- K_{S2} of 1431±167 M^{-1} vs. 665±110 M^{-1}.

- K_{S3} of 1603±436 M^{-1} vs. 718±159 M^{-1}.

A result from this, although as with all examples discussed before, suggests that as the number of bidentate ligands around the Zr centre are increased, so does the steric demand. In this case all the thermodynamic equilibria of the diMeOx-complexes are then significantly influenced. The significant difference observed here however is that the very fast initial reaction found for the diMeOx-complex formation process is very different from any of the other three systems described before. Furthermore, the fact that the initial reaction is suppressed by such a noteworthy extent does give a greater opportunity to apply this ligand in solution extraction experiments, in the presence of a suppressant, with a main aim at isolating different products for a zirconium moiety than its hafnium counterpart.

7.7. Comparative Evaluation of Formation Kinetic Findings

During the course of this project, a large range of oxine ligands were subjected to zirconium complex synthesis (described in Chapter 3). Most of these yielded crystalline products, although many could not be collected for crystallographic characterisation. In all cases, however, this type of ligand readily reacted in DMF with zirconium, in a visually obvious manner, without the need of laborious reaction conditions or additives (acid/base manipulation; counter ions; softer pre-chelators). In the hopes to better understand why exactly these ligands, that react so eagerly with zirconium, often gave poor quality crystalline products, this series of solution behavioural studies was initiated.

At this stage the bulk of formation mechanism information gathered, for each of the new ligands tested, has been presented individually, only in so far as describing for each their own reactions observed and how those reactions were able to be manipulated. The greater question that still remains unanswered here is *how* these ligands compare with each other in a coordination reaction process with zirconium. In each case, for each of the four separate experimental sets, the same four-consecutive step mechanism was categorised. Furthermore, in each case, the same steps can be identified with regard to specific rate

expression method of intermediate product formation. In other words, the overall mechanism for at least these four oxine ligands has been shown to have a fast, linear relation, initial step followed by three additional, consecutive, limiting kinetic tendency steps (indicative of multi-phase formation). Therefore, comparing each of these steps for each individual ligand is a plausible means to determine which ligand zirconium has a greater affinity for.

The first, most primary way, to compare the reaction rates and tendencies, can be illustrated as in Figure 7.21 and 7.22. An overlay of each mechanistic formation step for all four oxine ligands, in terms of reaction trend observed, gives a clear indication of correlation in each instance.
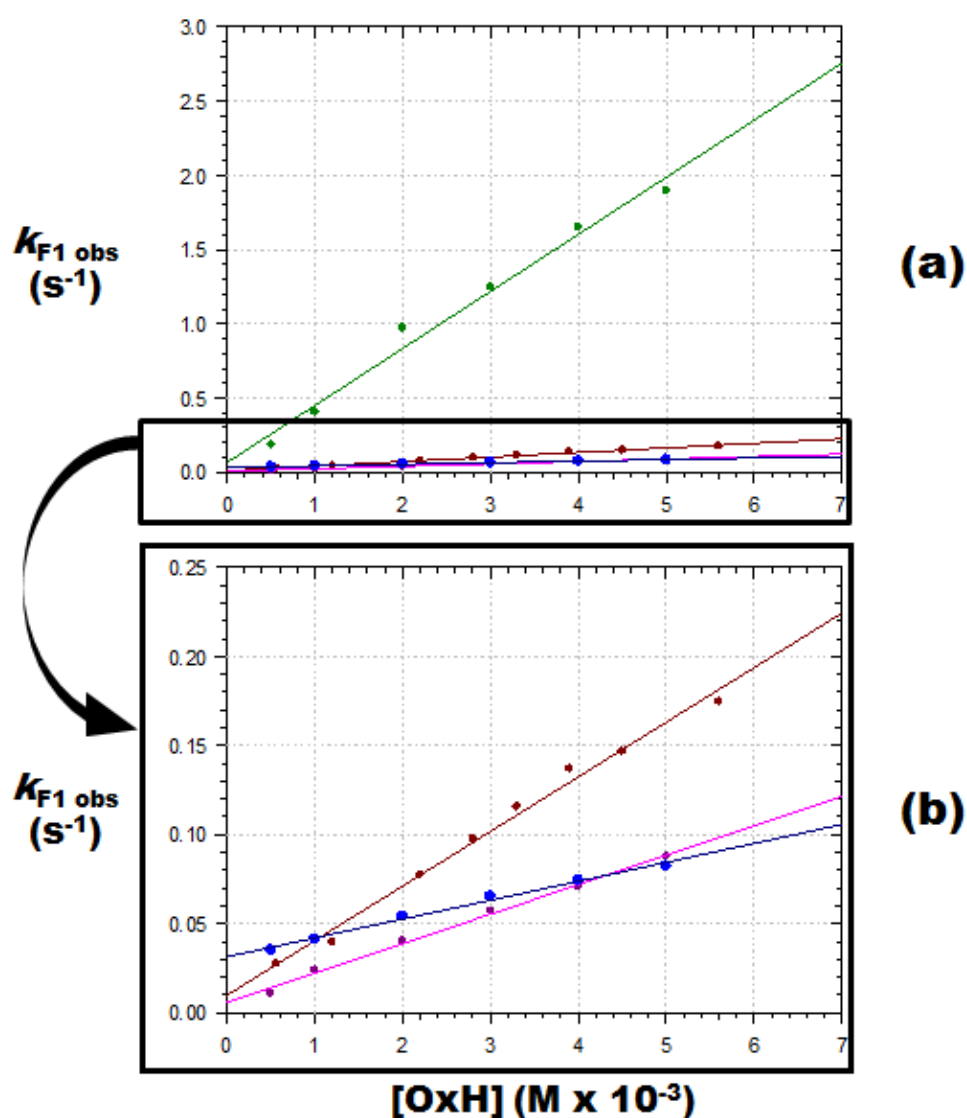
Figure 7.21 Plot of comparative formation mechanism rates of the 1st observable step for oxine ligands discussed in this chapter. Solid lines - calculated trends, circles - experimental data points; **Blue** = diClOxH, **Purple** = 5-ClOxH, **Red** = oxH, **Green** = diMeOxH; (**a**) Complete comparison showing all four ligands' trends, note diMeOxH with a forward reaction rate approximately a ten-fold larger than the other oxines. (**b**) Comparison of diClOxH, 5-ClOxH & oxH.
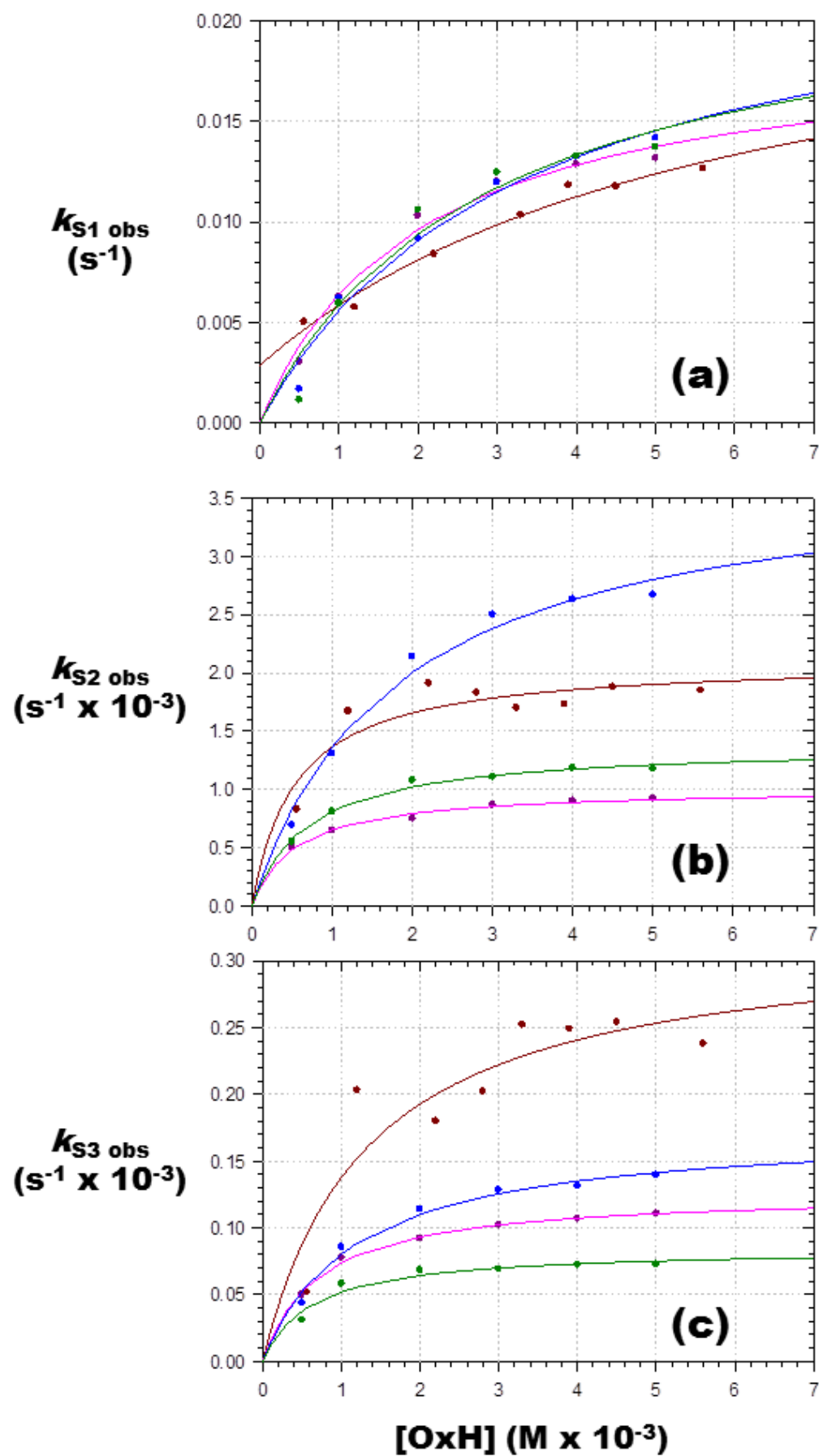
Figure 7.22 Plot of comparative formation mechanism rates of the (**a**) 2nd, (**b**) 3rd and (**c**) 4th observable steps for oxine ligands discussed in this chapter. Solid lines - calculated trends, circles - experimental data points; **Red** = oxH, **Purple** = 5-ClOxH, **Blue** = diClOxH, **Green** = diMeOxH;

169

Table 7.12 Comparative rate (*k*) and equilibrium (*K*) results obtained from formation kinetic studies of *tetrakis*(oxine)zirconium(IV) complexes discussed in this chapter.

	diClOxH		5-ClOxH		oxH		diMeOxH	
	No Cl⁻ Added	Cl⁻ Added	No Cl⁻ Added	Cl⁻ Added	No Cl⁻ Added	Cl⁻ Added	No Cl⁻ Added	Cl⁻ Added
k_{F1} $(M^{-1}s^{-1})$	10.6±0.5	6.3±0.2	16.5±0.6	7.1±0.2	31±1	24±1	384±25	81±5
k_{F-1} (s^{-1})	0.031 ±0.001	0.0024 ±0.0007	0.0057 ±0.0017	0.0005 ±0.0007	0.010 ±0.003	0.013 ±0.003	0.066 ±0.076	0.13 ±0.01
K_{F1} (M^{-1})	338 ±329	2663 ±329	2880 ±329	1420 ±329	3012 ±294	1061 ±294	5783 ±329	630 ±329
k_{F2} (s^{-1})	0.024 ±0.004	0.018 ±0.007	0.019 ±0.002	0.010 ±0.002	0.021 ±0.005	0.015 ±0.003	0.023 ±0.005	0.0088 ±0.0006
K_{F2} (M^{-1})	301±94	148±94	503±107	281±115	169±99	212±85	347±166	294±40
k_{F2r} (s^{-1})	0, Fixed	0, Fixed	0, Fixed	0, Fixed	0.0029 ±0.0009	0.0029, Fixed	0, Fixed	0, Fixed
k_{S1} (s^{-1})	0.026 ±0.002	0.019 ±0.002	0.023 ±0.002	0.011 ±0.001	0.017 ±0.006	0.025 ±0.015	0.027 ±0.003	0.0087 ±0.002
K_{S1} (M^{-1})	374±51	233±53	684±49	387±89	149±107	115±98	380±87	215±64
k_{S1r} (s^{-1})	0, Fixed	0, Fixed	0, Fixed	0, Fixed	0.0029 ±0.0008	0.0014, Fixed	0, Fixed	0, Fixed
k_{S2} (s^{-1})	0.0038 ±0.0003	0.0012 ±0.0002	0.00101 ±0.0003	0.00056 ±0.0003	0.0021 ±0.0002	0.0012 ±0.0007	0.00138 ±0.00004	0.00059 ±0.00004
K_{S2} (M^{-1})	557±116	401±133	1822±215	843±152	1897±754	90±69	1431±167	665±110
k_{S2r} (s^{-1})	0, Fixed	0, Fixed	0, Fixed	0, Fixed	0, Fixed	0, Fixed	0, Fixed	0, Fixed
k_{S3} (s^{-1})	0.000174 ±0.000009	0.000076 ±0.000006	0.000126 ±0.000003	0.000050 ±0.000002	0.00032 ±0.00005	0.00010 ±0.00001	0.000084 ±0.000006	0.000021 ±0.000002
K_{S3} (M^{-1})	858±141	587±129	1414±114	616±82	790±412	252±62	1603±436	718±159
k_{S3r} (s^{-1})	0, Fixed	0, Fixed	0, Fixed	0, Fixed	0, Fixed	0, Fixed	0, Fixed	0, Fixed

In Figure 7.21, the significantly increase in rate of the 1st reaction step for diMeOxH coordination with zirconium becomes vissually apparent. Although the trends for the other three ligands are in a sense comparable, diMeOxH has an initial reaction that occurs ten times faster than the rest (See Table 7.12 for exact values). From Figure 7.22, the other three mechanistic steps are overlayed in the same manner. The coordination step of the 2nd ligand appears comparable for all four oxines. The 3rd coordination step indicateds that diClOxH has a faster tendency than the rest and in the final (4th) step it appears that oxH chelates notably faster than the others.

Subsequently, a comparison of the exact forward reaction rate constants for each observed steps can also be made, in a visual manner. In Figure 7.23, a correlation of the k_{F1}, for the 1st observable mechanistic step is presented. Again as with Figure 7.21, the contrast in rate of the diMeOxH kinetic set against the other three ligands can be seen. Here the effect of suppresant is also more obvious, were the diMeOxH 1st step can clearly be seen to experience the greatest restraining of formation rate. Furthermore, a notable tendency emerges, from this visual comparison of rate data of each ligand. In Figure 7.23 it is clear that k_{F1} increases with and increase in the pKa value relation discussed earlier (***diClOxH < 5-ClOxH < oxH < diMeOxH***). This trend is exhbited for both experimental cases, without Cl$^-$ added and with Cl$^-$ added.
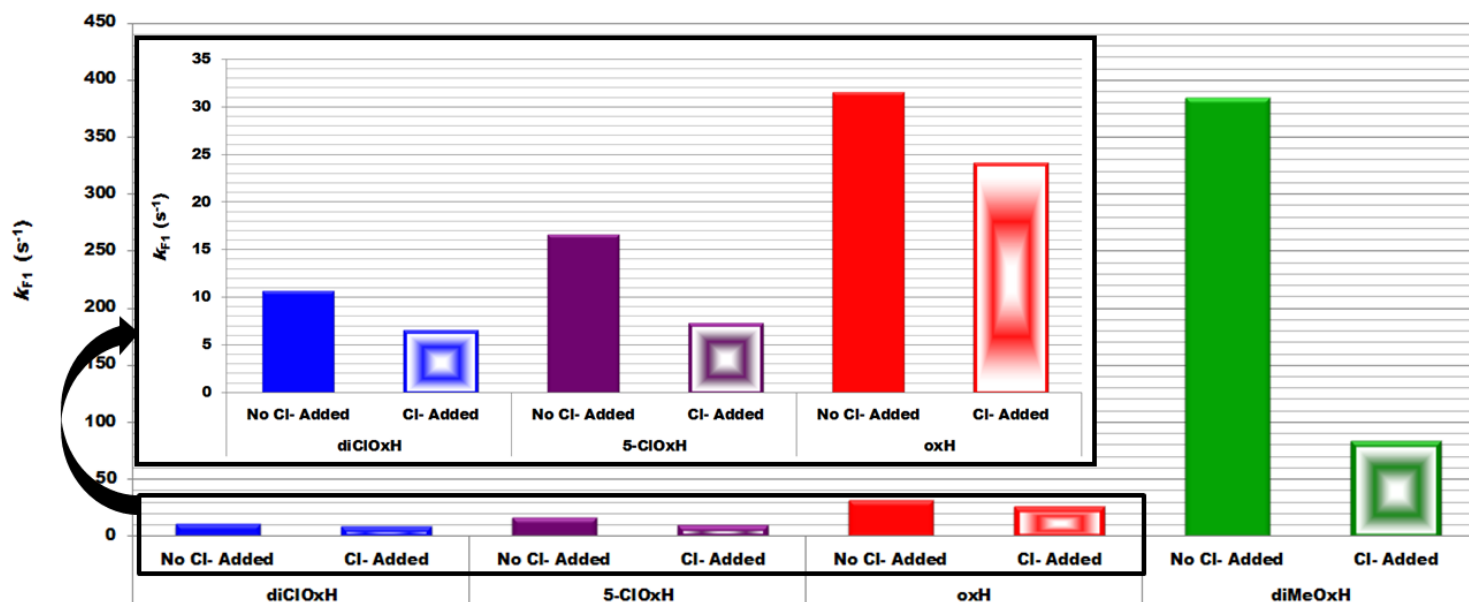
Figure 7.23 Comparison of reaction rate for the 1st observable coordination step, k_{F1}. Values listed in Table 7.12. (Solid columns – ***No Cl$^-$ Added***; Textured columns – ***Cl$^-$ Added***). **Blue** = diClOxH, **Purple** = 5-ClOxH, **Red** = oxH, **Green** = diMeOxH; Insert shows a scaled up representation for diClOxH, 5-ClOxH & oxH.

In Figure 7.24, the correlation of the forward reaction rate constants of 2nd observable step – k_{S1} $(=k_{F2})$ – is illustrated. As with Figure 7.22a, it is clear that this reaction step appears generally comparable for the four ligands tested. However, in comparison with the results of the suppressed reactions, it is notable here that diMeOxH and 5-ClOxH appear to feel the greatest effects of the presence of additional Cl⁻ in solution than the other two ligands. In this case, however, no specific rate data trend is observed, when considering pKa values. At the very least, it does appear as though this reaction step is slightly influenced by the steric bulk of the ligand in a way, if **_diClOxH > 5-ClOxH > oxH_** is considered.
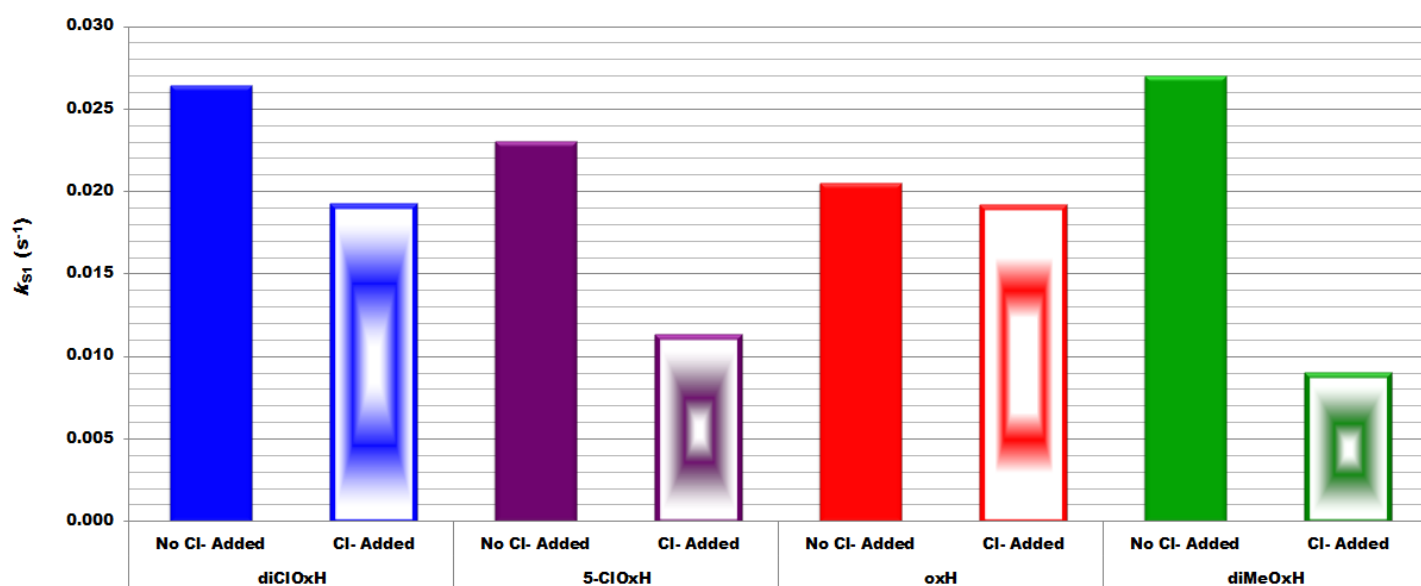
Figure 7.24 Comparison of reaction rates of the 2nd observable step – $k_{S1}(= k_{F2})$ – for oxine ligands discussed in this chapter. Values listed in Table 7.12. (Solid columns – **_No Cl⁻ Added_**; Textured columns – **_Cl⁻ Added_**). **Blue** = diClOxH, **Purple** = 5-ClOxH, **Red** = oxH, **Green** = diMeOxH.

For the 3rd observable step (k_{S2}) – illustrated in Figure 7.25 – diClOxH and its suppressed comparison show to be most prominent, with a reaction rate decrease for oxH now also being observed. In this case there appears to be no identifiable trend of influence, regarding pKa or steric characteristics of ligands. By the 4th step (k_{S3}) – illustrated in Figure 7.26 – the effect of excess Cl⁻ in solution for all four ligands has become significant. When the overall mechanism rates are considered in this manner, the effect of suppressant of on all oxine ligands tested becomes more substantial and at this juncture the merit of these solution behaviour studies come to light. From these results, the way forward for solution extraction experiments utilising these ligands can be performed with just cause, rather than merely grabbing at straws comparing coordination processes on synthesis success alone.
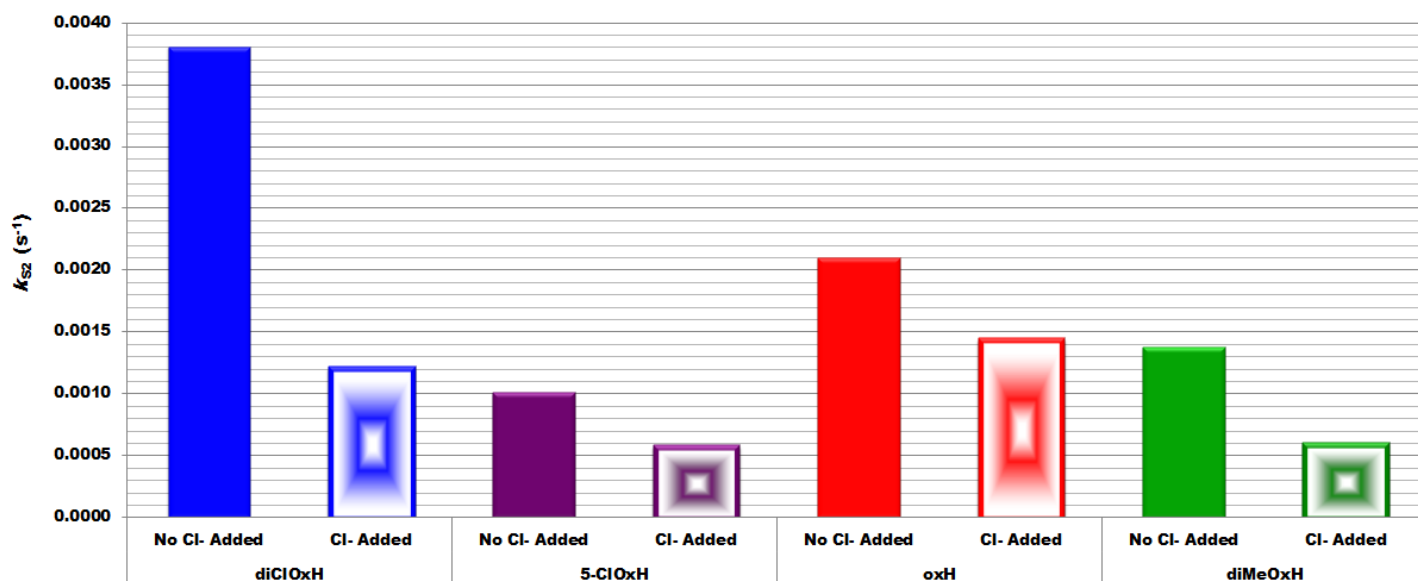
Figure 7.25 Comparison of reaction rates of the 3rd observable step – k_{S2} – for oxine ligands discussed in this chapter. Values listed in Table 7.12. (Solid columns – ***No Cl⁻ Added***; Textured columns – ***Cl⁻ Added***). **Blue** = diClOxH, **Purple** = 5-ClOxH, **Red** = oxH, **Green** = diMeOxH.
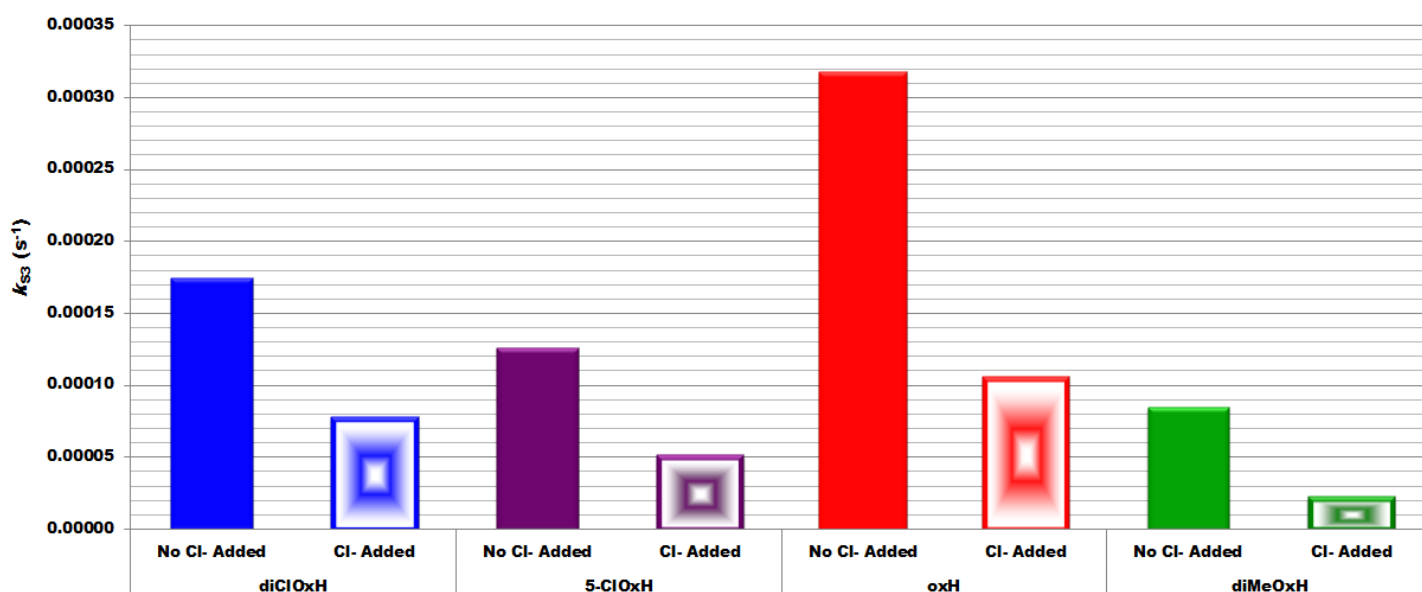
Figure 7.26 Comparison of reaction rates of the 4th observable step – k_{S3} – for oxine ligands discussed in this chapter. Values listed in Table 7.12. (Solid columns – ***No Cl⁻ Added***; Textured columns – ***Cl⁻ Added***). **Blue** = diClOxH, **Purple** = 5-ClOxH, **Red** = oxH, **Green** = diMeOxH.

Finally, a correlation of equilibrium rates determined, for all ligands, for all limiting trend mechanistic steps can visually presented as well. In Figure 7.27, these values shown to be compared on the same scale. At a glance, it is further apparent that the effect of additional Cl⁻ in solution, as suppressant affects all of the slower reaction steps across the board.
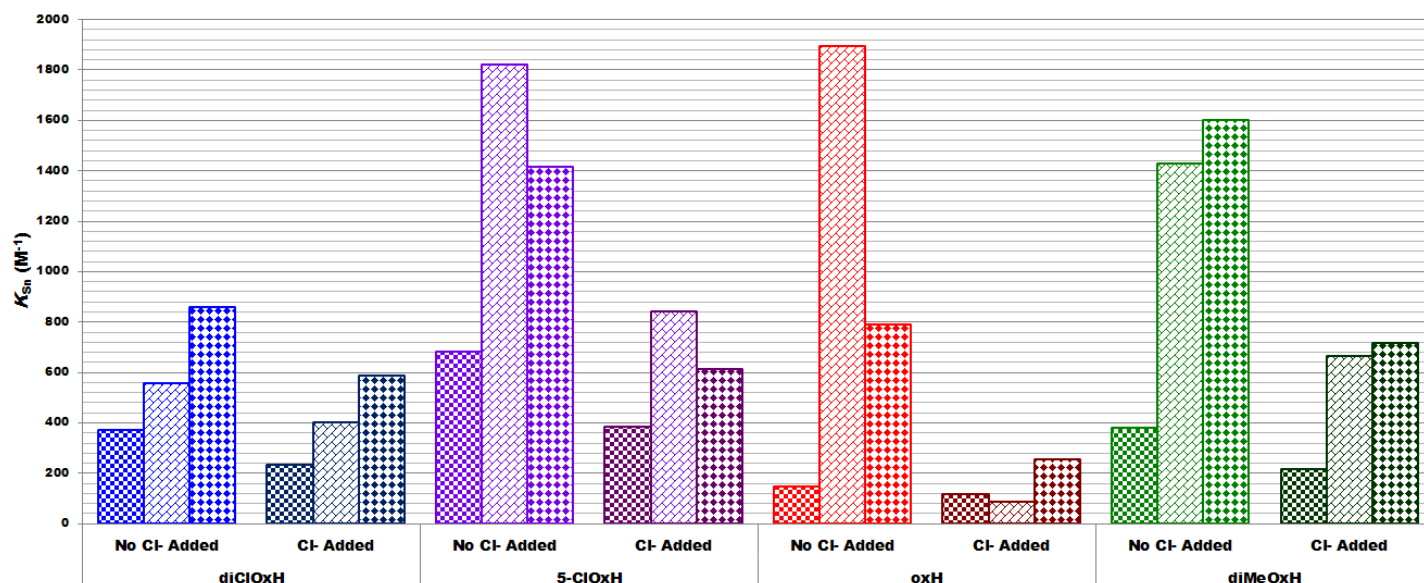
Figure 7.27 Comparison of equilibrium rate constants of the 2nd, 3rd and 4th observable steps for oxine ligands discussed in this chapter. Values listed in Table 7.12. (Lighter coloured columns – ***No Cl⁻ Added***; Darker coloured columns – ***Cl⁻ Added***). **Blue** = diClOxH, **Purple** = 5-ClOxH, **Red** = oxH, **Green** = diMeOxH. (**1st column**) $k_{S1}(= k_{F2})$ – 2nd coordination step; (**2nd column**) k_{S2}– 3rd coordination step; (**3rd column**) k_{S3}– 4th coordination step.

In an overarching manner presented as such, it does appear as though the overall equilibriums of oxH and 5-ClOxH are most affected by these suppression experiments. This seems to indicate that the ligands that have the *least amount of substitution* on the oxine backbone are *most influenced* by manipulation of formation reaction mechanism equilibria. On the other hand, from reaction rate data, it would appear as though the ligands with the *most amount of substitution* on the oxine backbone (diClOxH & diMeOxH) *chelate faster* to zirconium(IV), in an overall comparison, than the other two ligands. Unfortunately, from these equilibrium rate constants of all oxines tested no clear trend can be identified in terms of pKa or steric characteristics of ligands.

In Figure 7.28, a linear trend is observed in the comparison of pKa values for oxine ligands and their respective 1st observable reaction rate constants (k_{F1}). As is expected from a trend such as this, it highlights the effect of the ligand on the reaction mechanism, for this step. However, none of the limiting reaction steps (2nd, 3rd & 4th) exhibit the same tendency. This then goes even further in illustrating the complexity of the formation mechanism of oxine coordination to zirconium(IV).
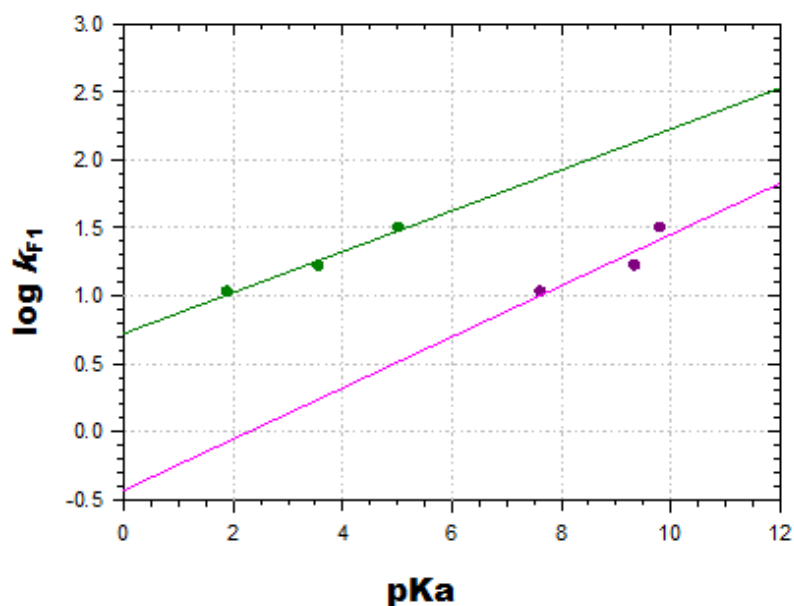
Figure 7.28 Plot of log k_{F1} vs. pKa for diClOxH, 5-ClOxH and oxH; **Purple** = pKa$_1$, **Green** = pKa$_2$.

7.8. Conclusion

The zirconium metal complex formation processes studies and reported to this point have led to some significant observations. In each set of the three additional oxine ligands subjected to solution behavioural analysis as a measure of chelation with zirconium, it could be shown that these ligands all follow the same mechanistic trend in complex formation. The previously postulated mechanism, consisting of a fast initial, linear trend, step followed by three additional limiting tendency reaction steps, still holds true.

The most noteworthy aspect in each case has been highlighted by the influenced by the addition of free chloride, as an equilibrium suppressant, on each individual ligand set. In each case it has been shown that the notably fast reactions that occur almost instantaneously in solution upon mixing of ligand and metal reagents, observed during synthesis and studied now *via* solution kinetics, can be considerably restrained by means of simple equilibrium manipulations. In this case, no other additives or competing extractants need to be utilized other than the simple and rudimentary knowledge of reaction rate adjustment via influence of a reverse reaction.

With regard to 'preference of coordination', the verdict is still out. From the current information available it can be postulated that:

i.   More substituted oxines (diClOxH & diMeOxH) appear to have faster formation reactions compared to lesser substituted species (oxH & 5-ClOxH), with the exception of the 1st observable reaction step which does not conform to this observation.

ii.   For the first reaction, the tendency is that the more electron donating the ligand is, the faster the reaction becomes [in agreement with an *Associative* mode of coordination]

iii.   However, the lesser substituted variety on the other hand appear to be more influenced by equilibrium suppressants.

In total, the reactions span about a five order-of-magnitude range, indicating a huge change in affecting all four the chlorido ligands to be substituted to form the corresponding tetrakis-oxine complexes. Where the first step showed an increase by more than 30 times as the donor ability of the entering ligand increased, the subsequent following three reactions indicated approximately one order-of-magnitude decrease in ligation rate.

Furthermore, the effect of this equilibrium suppression leads to further postulation as to the nature of the coordination mechanism of oxines to zirconium(IV). In the discussion and illustrations of Figures 7.24 - 7.26 in § 7.7 earlier, it has been explicitly pointed out that the effect of equilibrium suppression *increases* with each coordination step in the mechanism. The implication is that, as more incoming ligands coordinate to the metal centre, the leaving ligand is liberated into the solvent. If there is an oversaturation of this leaving ligand in solution already, the rate at which the liberation occurs, *decreases*, yielding slower conversion of intermediate forms to the final *tetrakis*-coordinated complex. This is by no means a definite and absolute finding, due to the little data available at this stage. However, since all four oxine ligands conform to this specific trend of equilibrium suppression, it is a valid assumption at this juncture.

Although many novel and noteworthy findings have been presented here, regarding zirconium-oxine chelation in solution, these findings are only half of the answer when it comes to separation/purification studies for zirconium and hafnium. It is vital that these results be related to hafnium counterparts if they are to be applied in any way in solution extraction experiments. Unfortunately at this time, hafnium solution behavioural characteristics are not available as yet. These correlations will form part of future, more in depth solution kinetic and separation studies.

Chapter **8**

Theoretical Study of Zirconium(IV)

O,O- and N,O-Bidentate Ligand Complexes

Computational chemistry is an analytical technique that employs theoretical simulation of structures or processes to yield insight into unknown or unobtainable chemical events. With the continual advancements being made into information technology and specifically hardware improvements (allowing more complex processing achievable), this specific branch of study grows increasingly viable and valid in its application. This method is progressively more often used to gather and assess information regarding metal complexes in organometallic chemistry.[1,2,3]

A broad variety of possible calculation methods exist. In general these range from the simpler Molecular Mechanics, to Semi-empirical methods and Density Functional Theory, to the more advanced *Ab Initio* method calculations.[4,5]

---

[1] T. Woo, E. Folga & T. Ziegler; *Organometallics 12* (**1993**), 1289-1297.

[2] V. Branchadell, M. Moreno-Manas, F. Pajuelo & R. Pleixtas; *Organometallics 18* (**1999**), 4934-4941.

[3] U. Burckhardt, G.L. Casty, T.D. Tilley, T. Woo & U. Rothlisberger; *Organometallics 19* (**2000**), 3830-3841.

[4] E. Lewars; "*Computation Chemistry: Introduction to the theory and applications of molecular and quantum mechanics"* (**2004**), Kluwer Academic, New York, USA.

[5] F.Jensen; "*Introduction to Computational Chemistry"*, *2nd Ed.* (**2007**), John Wiley & Sons Ltd., England, UK.

Density Functional Theory (DFT) is a quantum mechanical modelling technique employed in the study of the electronic structure of "many-body" systems, or more specifically, atoms and molecules. The characteristics of many-entity systems can be theoretically investigated by using *functionals* representative of electron density. This method has proved itself as reasonably accurate as well as less hardware intensive than other methods.[6]

In this current investigation, a series of zirconium(IV) complexes have been theoretically optimized and correlated to known solid state structures obtained by means of crystallographic characterisation, available in literature and acquired in this project. This was performed with an overarching aim to elucidate whether or not these calculated structures are comparable to those obtained by experimental methods. If the theoretical and actual structures are reasonably similar, it would be scientifically valid to predict the structures of currently unknown or unobtainable compounds. With this, the goal is to determine a characteristic profile of coordination trends and preferences for zirconium(IV), with the specific intention of correlating these nuances of chelation with that of hafnium(IV). If any chemical or physical differences are observed, they could, in theory, be exploited in separation experimentation.

8.1. Experimental Considerations

The DFT molecular orbital calculations were carried out using the Gaussian 09[7] software suite. Becke's three parameter hybrid (B3LYP)[8,9] exchange correlation functional was used. The basis set employed in this study was 6-311++G(d,p)[10,11,12] for the main group elements

---

[6] R.M. Dreizler & E.K.U. Gross; *"Density Functional Theory An Approach to the Quantum Many-Body Problem"* (**1990**), Springer-Verlag, Berlin Heidelberg, Germany.

[7] M.J. Frisch, G.W. Trucks, H.B. Schlegel, G.E. Scuseria, M.A. Robb, J.R. Cheeseman, J.A. Montgomery, T. Vreven, K.N. Kudin, J.C. Burant, J.M. Millam, S.S. Iyengar, J. Tomasi, V. Barone, B. Mennucci, M. Cossi, G. Scalmani, N. Rega, G.A. Petersson, H. Nakatsuji, M. Hada, M. Ehara, K. Toyota, R. Fukuda, J. Hasegawa, M. Ishida, T. Nakajima, Y. Honda, O. Kitao, H. Nakai, M. Klene, X. Li, J.E. Knox, H.P. Hratchian, J.B. Cross, C. Adamo, J. Jaramillo, R. Gomperts, R.E. Stratmann, O. Yazyev, A.J. Austin, R. Cammi, C. Pomelli, J.W. Ochterski, P.Y. Ayala, K. Morokuma, G.A. Voth, P. Salvador, J.J. Dannenberg, V.G. Zakrzewski, S. Dapprich, A.D. Daniels, M.C. Strain, O. Farkas, D.K. Malick, A.D. Rabuck, K. Raghavachari, J.B. Foresman, J.V. Ortiz, Q. Cui, A.G. Baboul, S. Clifford, J. Cioslowski, B.B. Stefanov, G. Liu, A. Liashenko, P. Piskorz, I. Komaromi, R.L. Martin, D.J. Fox, T. Keith, M.A. Al-Laham, C. Y. Peng, N. Nanayakkara, M. Challacombe, P.M.W. Gill, B. Johnson, W. Chen, M.W. Wong, C. Gonzalez, J. A. Pople; *Gaussian 09, Revision D.01* (**2009**), Gaussian, Inc, Pittsburgh PA.

[8] C. Lee, W. Yang & R.G. Parr; *Phys. Rev. B37* (**1988**); 785-789.

[9] A.D. Becke; *J. Chem. Phys. 98* (**1993**), 5648-5652.

[10] R. Ditchfield, W.J. Hehre & J.A. Pople; *J. Chem. Phys. 54* (**1971**), 724-728.

[11] M.S. Gordon; *Chem. Phys. Lett. 76* (**1980**), 163-168.

[12] V.A. Rassolov, M.A. Ratner, J.A. Pople, P.C. Redfern & L.A. Curiss; *J. Comp. Chem. 22* (**2001**), 976-984.

and LanL2DZ[13] for the middle to late transition metals. Vibrational frequencies were calculated at the 6-311++G(d,p) level for the main group elements and at the LanL2DZ level for the middle to late transition metals with minimum energies confirmed to have zero imaginary frequencies. The frequencies were unscaled and used to compute the zero-point vibrational energies. These optimized structures were then compared to the solid state crystallographic data of the corresponding complexes. Molecular graphics were obtained using DIAMOND,[14] while overlay graphics were obtained using HyperChem 7.5.[15] Selected geometric parameters of the calculated structures and corresponding crystal structures are presented and discussed. Cartesian coordinates and Gibbs free energies for all the computed structures are given in the supplementary data (Appendix C).

8.2. *Tetrakis*(acetylacetonato-κ^2O,O')zirconium(IV) – [Zr(Acac)$_4$] – Type Structures

The first series of structures theoretically optimised was chosen as a fair default example of zirconium(IV) solid state behaviour. In § 2.3.1 and § 6.3, the theoretical considerations of [Zr(Acac)$_4$] type structures were discussed and elaborated on. In summary, it is well known[16,17] that these types of compounds are classic examples of the square antiprismatic (*sap*) coordination geometry found in metal complexes. Although published structures of a wide range of these *β*-diketone ligand chelated compounds are available in literature,[18] this investigation focused specifically on three moieties containing symmetrical Acac-type ligands.

The structures of *Tetrakis*(acetylacetonato)zirconium(IV)[19] - [Zr(acac)$_4$], *Tetrakis*(hexafluoro-acetylacetonato)zirconium(IV)[20] - [Zr(hFAcac)$_4$] and *Tetrakis*(1,3-diphenyl-1,3-propanedionato) zirconium(IV)[21] - [Zr(DBM)$_4$] were used as a basis for this theoretical optimization and the results are compared and correlated here (See Figure 8.1).

[13] P.J. Hay & W.R. Wadt; *J. Chem. Phys.* 82 (1985), 299-310.
[14] K. Brandenburg & H. Putz; *DIAMOND, Release 3.0c* (**2006**), Crystal Impact GbR, Bonn, Germany.
[15] *HyperChemTM Release 7.52* (**2002**), Windows Molecular Modeling System, HyperCube Inc.
[16] J.V. Silverton & J.L. Hoard; *Inorg. Chem. 2* (**1963**), 243-249.
[17] W. Clegg; *Acta Cryst.C43* (**1987**), 789 -791.
[18] The Cambridge Structural Database, Licence Update Feb 2013; F. H. Allen; *Acta Cryst. B58* (**2002**), 380-388.
[19] S.C. Chaudhry, C. Verma, S.S. Bhatt & N. Sharma; *Indian J.Chem. 47A* (**2008**), 43-48.
[20] F. Calderazzo, U. Englert, C. Maichle-Mossmer, F. Marchetti, G. Pampaloni, D. Petroni, C. Pinzino, J. Strahle & G. Tripepi; *Inorg.Chim.Acta 270* (**1998**), 177-188.
[21] § 6.3; M. Steyn, H.G.Visser & A. Roodt; *J. S. Afr. Inst. Min. Metall.* (**2014**), In Press.
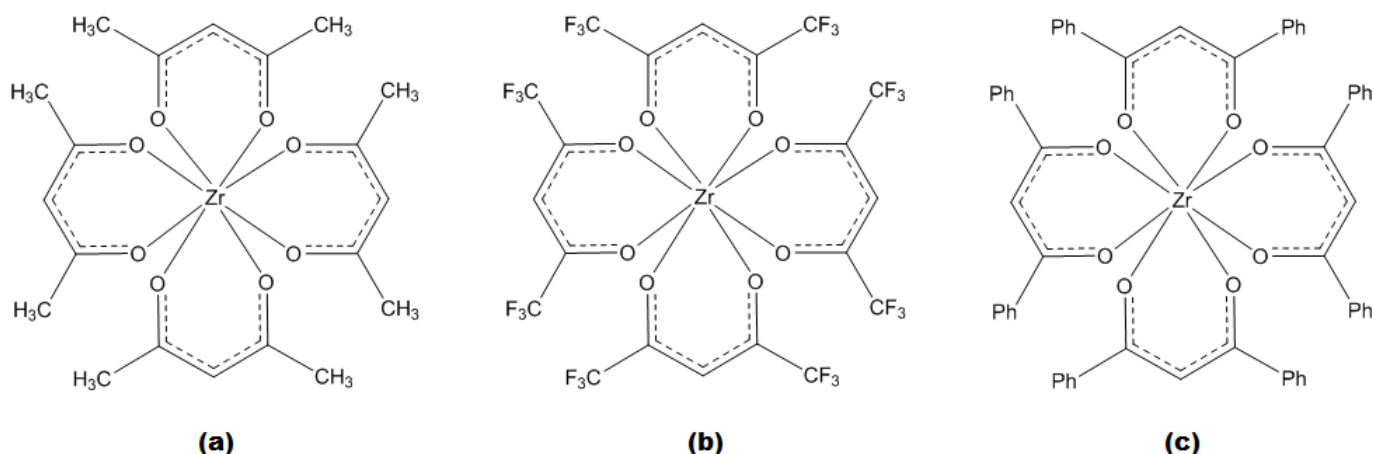
Figure 8.1 Schematic illustration of the *Tetrakis*(acetylacetonato-κ^2O,O')zirconium(IV)-type complexes optimized and discussed in this chapter; (**a**) [Zr(acac)$_4$], (**b**) [Zr(hFAcac)$_4$], (**c**) [Zr(DBM)$_4$].

8.2.1. *Tetrakis*(acetylacetonato)zirconium(IV) - [Zr(acac)$_4$]

The coordination compound [Zr(acac)$_4$] (**za**) is compared here to the theoretically optimized counterpart (**za***). Figure 8.2 illustrates the visual comparison of these two structures.

za   **za***

Figure 8.2 Graphical representation of [Zr(acac)$_4$]; (**za**) solid state structure at 50 % probability and (**za***) DFT optimized structure. Hydrogen atoms omitted for clarity.

The illustration in Figure 8.2 and geometric data presented in Table 8.1 give only a partial indication of the result of this structural optimization. From the table presented a general tendency of structural shift becomes clear.

The Zr—O bond lengths of the solid state structure (**za**) differ notably from that of the optimised counterpart (**za***). Although an overall average of Zr—O bond length of *ca.* 2.2 Å is observed, some discrepancies emerge. The average bond distance observed for **za** appears to be shorter than that of **za***, 2.191(8) Å *vs.* 2.212 Å.

Table 8.1 Comparison of selected geometric parameters for [Zr(acac)$_4$]; (**za**) solid state crystal structure and (**za***) DFT optimized structure.

Geometric Parameter	za	za*
Selected Bond Lengths (Å)		
Zr—O$_1$	2.177(7)	2.267
Zr—O$_2$	2.185(8)	2.156
Zr—O$_3$	2.208(9)	2.156
Zr—O$_4$	2.192(8)	2.267
Zr—O$_5$	2.177(7)	2.156
Zr—O$_6$	2.185(8)	2.267
Zr—O$_7$	2.208(9)	2.267
Zr—O$_8$	2.192(8)	2.156
Selected Bite Angles (°)		
O$_1$—Zr—O$_2$	74.90(3)	75.43
O$_3$—Zr—O$_4$	74.27(3)	75.42
O$_5$—Zr—O$_6$	74.90(3)	75.42
O$_7$—Zr—O$_8$	74.27(3)	75.43
Selected Torsion Angles (°)		
O$_1$—C$_{01}$—C$_{03}$—O$_2$	1.75(39)	3.27
O$_3$—C$_{04}$—C$_{06}$—O$_4$	0.03(31)	-3.28
O$_5$—C$_{07}$—C$_{09}$—O$_6$	1.75(39)	-3.26
O$_7$—C$_{10}$—C$_{12}$—O$_8$	0.03(31)	3.26

As per the discussion in Chapter 6 regarding the often observed phenomenon concerning acac-type coordination to zirconium(IV), whereby one Zr—O bond in a specific ligand is noticeably longer than the other, even for symmetric examples, in this case it becomes worth elaborating on. For the solid state structure (**za**), each ligand has one of these bond lengths notably longer than the other and the theoretically optimised counterpart (**za***) also shows this tendency. The average here for **za** is 2.185(8) Å for the shorter bonds *vs.* 2.197(9) Å for the longer. For **za*** this difference becomes more significant; 2.156 Å for shorter bonds *vs.* 2.267 Å for the longer.

Furthermore, the average ligand O—Zr—O bite angles also differ slightly; **za** = 74.59(3) ° *vs.* **za*** = 75.43 °. The observed O—C—C—O torsion angles of the ligand frame facing the O—Zr—O bite angles for **za** range from near flat, 0.03(31) °, to 1.75(39) °. On the other hand, **za*** exhibits torsion angles ranging from -3.28 ° to 3.27 °. In Figure 8.3, the greater extent of the structural difference between **za** and **za*** is illustrated visually with a Root-Mean-Square (RMS) fit and overlay.

(a)　　　　　　　　　　　　　　　　　　　**(b)**

Figure 8.3 Graphical representation of an overlay of the crystal structure **za** (**black**)
and the DFT optimized structure **za*** (**purple**) of [Zr(acac)$_4$]. RMS value = 1.183 Å. Overlay fit
excluded all hydrogen atoms. (**a**) Side view of *sap* arrangement, where the top and bottom of *sap* lie
parallel with the *x*-axis; (**b**) 45 ° rotation of **a** on the *x*-axis.

It does appear from Figure 8.3, as though these structures are notably different from each other, to the extent that they become incomparable. However, as with all aspects of structural characterization and description regarding zirconium(IV) complexes discussed so far, there is often more than one way to quantify structures. From summarizing discussions of the metal complexes described in Chapters 4-6, much effort and emphasis has been placed on the fact that mere geometric/structural data value comparisons are not entirely descriptive of what actually transpires from *tetrakis*(bidentate-ligand)zirconium(IV) complex formation.

Firstly, these theoretical optimizations assume a gas phase environment for these molecules. In other words, the effects of inter- and intramolecular forces and interactions that dictate crystal lattice packing in a solid state structure are not taken into consideration. In most cases, in the computational prediction of certain molecular structures, this issue does not interfere that significantly with the outcome of structural optimization. Unfortunately, as per the extensive discussions included in Chapters 4-6, it is clear that zirconium(IV) complexes do, in fact, experience a notable influence from these interactions and influences in the formation of final solid state crystal products.

Secondly, as discussed in detail in the crystallographic chapters (Chapters 4-6), these structural characteristics can all be near identical in some cases (See § 5.5, regarding oxine complexes of zirconium(IV)).

However, when the intimate coordination geometry around the metal centre is investigated and considered, these seemingly identical structures become clearly different, when the specific geometric isomers are identified.

Figure 8.4 Visual comparison of the square antiprismatic coordination polyhedron of $[Zr(acac)_4]$; (**za**) solid state structure at 50 % probability and (**za***) DFT optimized structure. Hydrogen atoms omitted for clarity.

From the visual comparison drawn in Figure 8.4, of the coordination polyhedra of **za** and **za***, a clearer description of the differences between these structures are possible. The structure of **za** is evidently the approximate standard square antiprismatic geometry expected for this type of compound.[16,17] However, **za*** exhibits a more distorted, almost dodecahedral polyhedron. Furthermore, **za** can be identified as a D_2 corner-bonded isomer while **za*** appears to have two ligands swiveled vertically to yield the C_2 counterpart.

From these observations it would appear that during the optimization of this structure, it became theoretically more stable for the compound to transform into a completely different isomer. As seen in Table 8.1, the ligands of **za*** appear to be identical in their sets of Zr—O bond lengths (Zr—O_{short} = 2.156 Å & Zr—O_{long} = 2.267 Å), as well as exhibiting *near identical* O—Zr—O bite angles (~75.4 °).

Although, in this case, theoretical optimization of the structure of *Tetrakis*(acetylacetonato)zirconium(IV) did not yield the ideal structure comparable results, it has still given valuable insights into the differences in behaviour of this compound between solid and gas phase conditions.

8.2.2. *Tetrakis*(hexafluoro-acetylacetonato)zirconium(IV) - [Zr(hFAcac)$_4$]

The coordination compound [Zr(hFAcac)$_4$] (**zf**) is compared here to the theoretically optimized counterpart (**zf***). Figure 8.5 illustrates the visual comparison of these two structures.

zf   **zf***
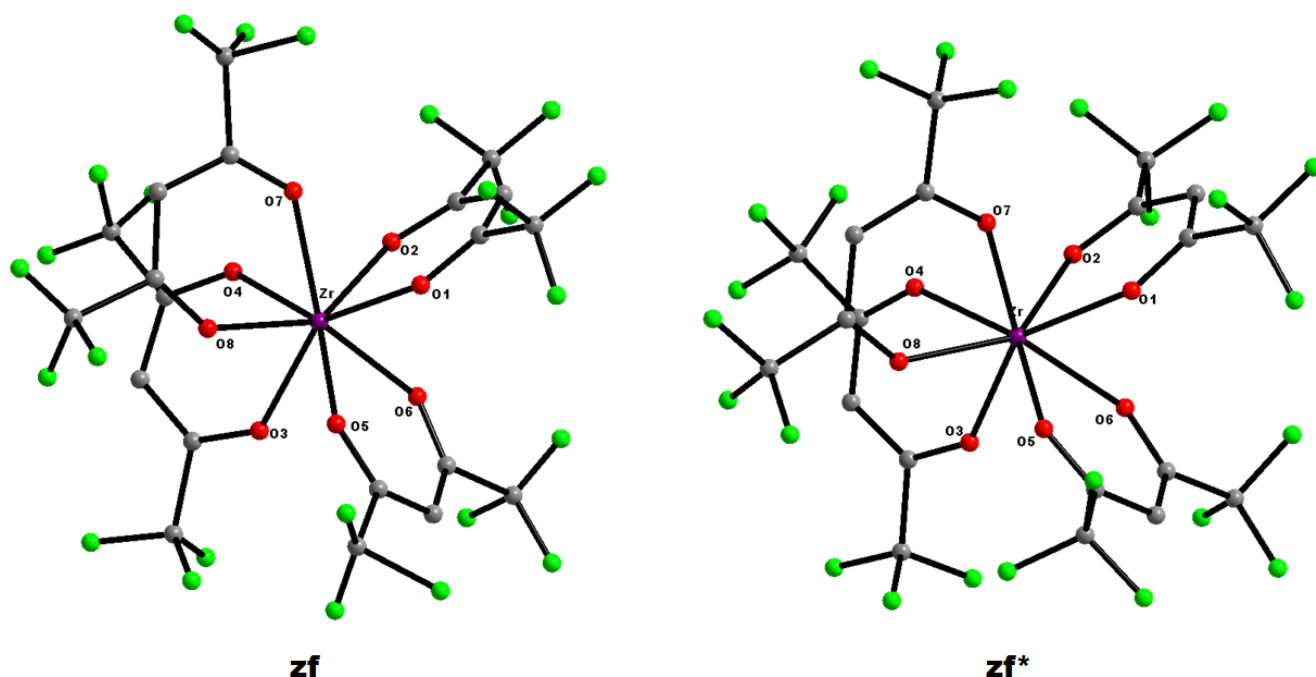
Figure 8.5 Graphical representation of [Zr(hFacac)$_4$]; (**zf**) solid state structure at 50 % probability and (**zf***) DFT optimized structure. Hydrogen atoms omitted for clarity.

As for the previously discussed example, the illustration presented above and the geometric data obtained, presented in Table 8.2, gives only a partial description of the structural optimization of this compound. The solid state structure (**zf**) used here as a basis for this computational prediction of an idealised coordination compound, is an example of a zirconium complex with each ligand coordinate, independently characterised. In other words, the ligands are not symmetrically placed or generated in the asymmetric unit. From the Zr—O bond lengths of **zf** it is clear that each ligand is structurally independent. The optimized structure (**zf***) however, appears to have favoured a more symmetrical placement of chelators, with only two independently identifiable ligands (the other two being symmetrically placed counterparts). Yet again, a tendency of Zr—O$_{short}$ & Zr—O$_{long}$ bond lengths can be observed in both these structures.

Table 8.2 Comparison of selected geometric parameters for [Zr(hFAcac)$_4$];
(**zf**) solid state crystal structure and (**zf***) DFT optimized structure.

Geometric Parameter	zf	zf*
Selected Bond Lengths (Å)		
Zr—O$_1$	2.152(9)	2.243
Zr—O$_2$	2.168(7)	2.149
Zr—O$_3$	2.194(8)	2.176
Zr—O$_4$	2.150(9)	2.234
Zr—O$_5$	2.199(7)	2.149
Zr—O$_6$	2.175(9)	2.243
Zr—O$_7$	2.225(8)	2.175
Zr—O$_8$	2.140(9)	2.234
Selected Bite Angles (°)		
O$_1$—Zr—O$_2$	78.03(3)	75.76
O$_3$—Zr—O$_4$	74.57(3)	75.76
O$_5$—Zr—O$_6$	76.59(3)	73.88
O$_7$—Zr—O$_8$	74.40(3)	73.88
Selected Torsion Angles (°)		
O$_1$—C$_{01}$—C$_{03}$—O$_2$	4.48(20)	1.82
O$_3$—C$_{04}$—C$_{06}$—O$_4$	2.79(18)	-1.28
O$_5$—C$_{07}$—C$_{09}$—O$_6$	2.62(21)	1.83
O$_7$—C$_{10}$—C$_{12}$—O$_8$	-4.57(19)	-1.29

The average Zr—O distances for **zf** – 2.175(8) Å – and **zf*** – 2.200 Å – also differ slightly as before (§ 8.2.1). The average lengths for **zf** range from 2.154(9) Å for the shorter bonds to 2.197(8) Å for the longer. For **zf*** this difference is again more considerable; 2.162 Å for shorter bonds *vs.* 2.239 Å for the longer. Furthermore, the average ligand O—Zr—O bite angles also differ substantially; **zf** = 75.90(3) ° *vs.* **zf*** = 74.82 °. The observed O—C—C—O torsion angles of the ligand frame facing the O—Zr—O bite angles for all four ligands in **zf** differ, ranging from -4.57(19) ° to 4.48(20) °, while **zf*** is shown to range only between -1.29 ° to 1.83 °.

In Figure 8.6, the larger extent of the structural difference between **zf** and **zf*** is illustrated visually with an RMS fit and overlay. Although these two structures are more similar than § 8.2.1, some discrepancies are still evident. Specific swivelling of the ligands around the metal centre in **zf***, in the square antiprismatic polyhedron observed, indicate that the absence of halogen intermolecular forces (as present for **zf**) allows for a different arrangement of all ligands in three dimensional space around the zirconium(IV) centre.
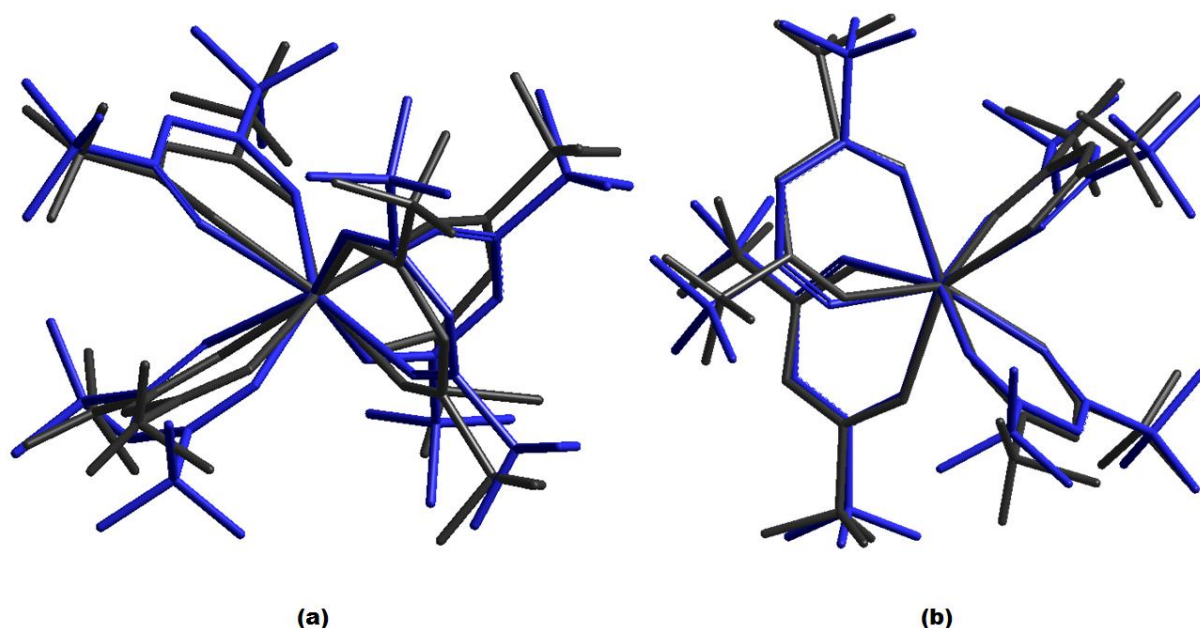
Figure 8.6 Graphical representation of an overlay of the crystal structure **zf** (**black**)
and the DFT optimized structure **zf*** (**blue**) of [Zr(hFAcac)$_4$]. RMS value = 0.346 Å. Overlay fit
excluded all hydrogen atoms. (**a**) Side view of *sap* arrangement, where the top and bottom of *sap*
lie parallel with the *x*-axis; (**b**) 45 ° rotation of **a** on the *x*-axis.

As further illustrated in Figure 8.7 below, although the structures of **zf** and **zf*** appear
more similar when considering the coordination geometries around the metal centre,
slight differences are still observable. Although both exhibit a C$_2$ isomer arrangement,
the exact placement of ligands on the antiprism is quite different. This difference in the
position of the ligands gives rise to the slightly larger (but still reasonable) RMS overlay
of 0.346 Å, as depicted by Figure 8.6.
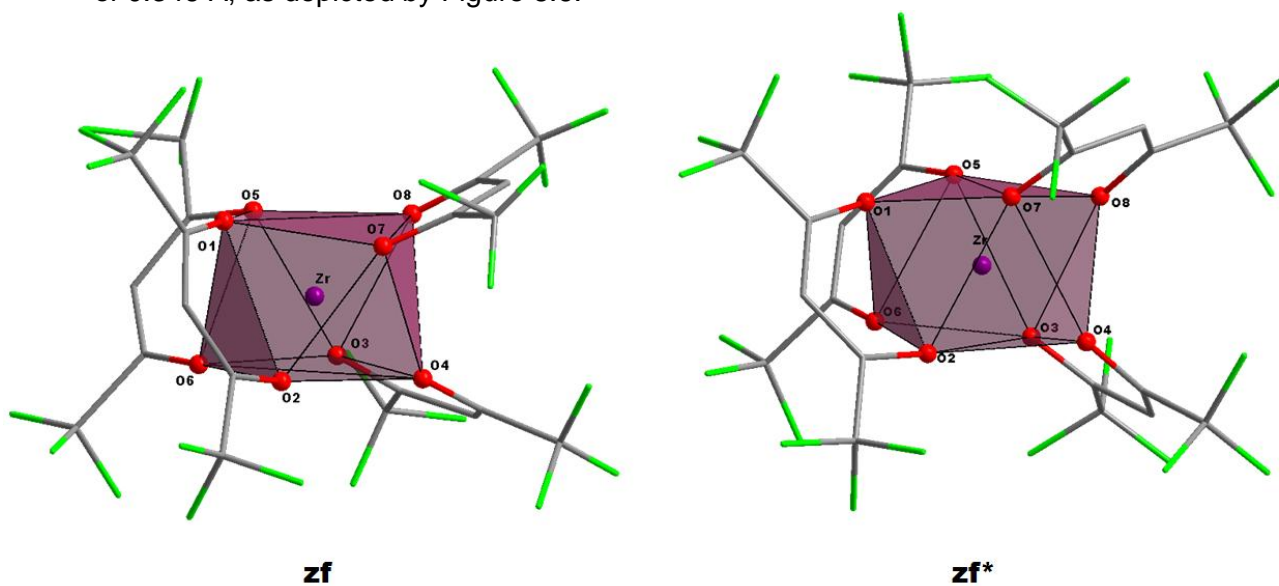
Figure 8.7 Visual comparison of the square antiprismatic coordination polyhedron of
[Zr(hFAcac)$_4$]; (**zf**) solid state structure at 50 % probability and (**zf***) DFT optimized structure.
Hydrogen atoms omitted for clarity.

8.2.3. *Tetrakis*(1,3-diphenyl-1,3-propanedionato)zirconium(IV) - [Zr(DBM)₄]

The coordination compound [Zr(DBM)$_4$] (**zd**) is compared here to the theoretically optimized counterpart (**zd***). Figure 8.8 illustrates the visual comparison of these two structures.

zd   **zd***
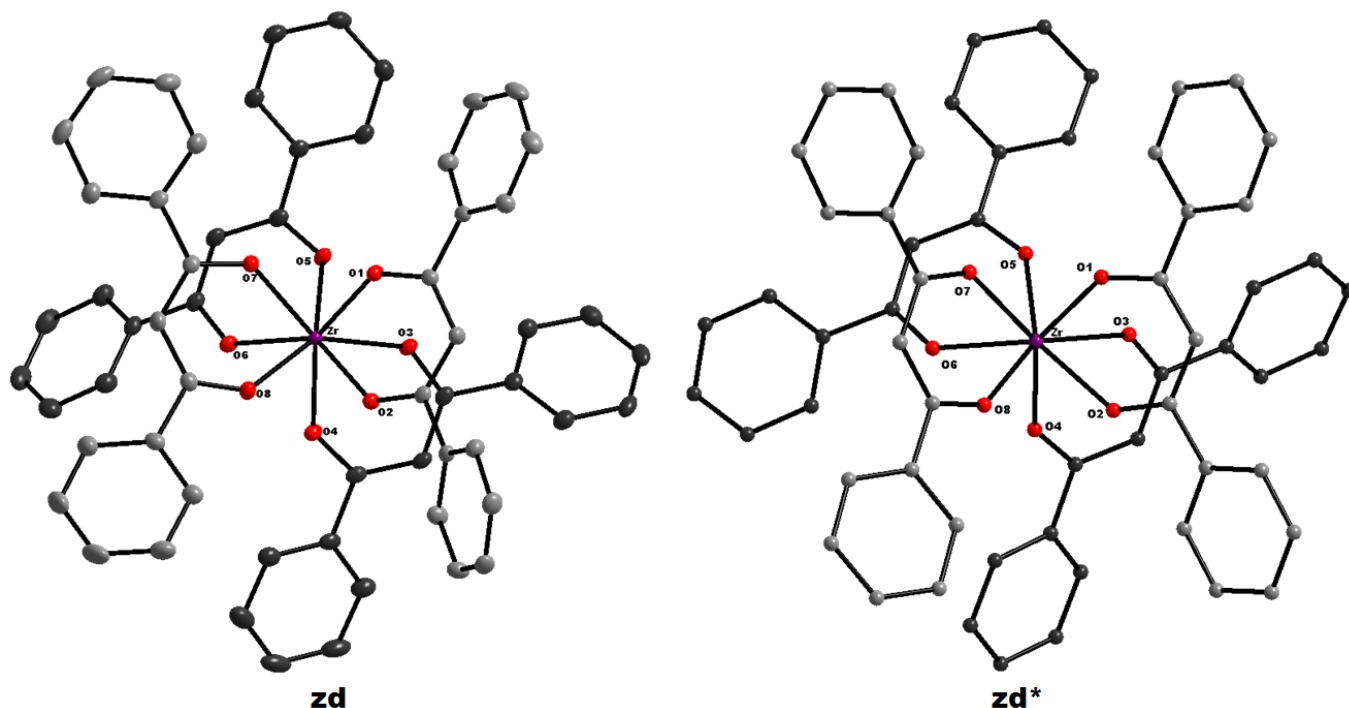
Figure 8.8 Graphical representation of [Zr(DBM)$_4$]; (**zd**) solid state structure at 50 % probability and (**zd***) DFT optimized structure. Hydrogen atoms omitted for clarity.

From the visual comparison in Figure 8.8 and the geometric data presented in Table 8.3 it would appear in this instance that the structures of **zd** and **zd*** are more comparable than the previously described examples. However, the average Zr—O distances for **zd** – 2.178(4) Å – and **zd*** – 2.204 Å – still differ marginally as before. The average lengths for **zd** range from 2.153(1) Å for the shorter bonds to 2.203(1) Å for the longer. For **zd*** this difference is again more considerable; 2.157 Å for shorter bonds *vs.* 2.251 Å for the longer. Furthermore, the average ligand O—Zr—O bite angles also differ notably; **zd** = 74.53(4) ° *vs.* **zd*** = 73.90 °. The observed O—C—C—O torsion angles of the ligand frame facing the O—Zr—O bite angles for all four ligands in **zd** differ, ranging from -1.54(11) ° to as great as 10.98(11) °, while **zd*** is shown to range only between 2.01 ° to 3.51 °.

Table 8.3 Comparison of selected geometric parameters for [Zr(DBM)$_4$];
(**zd**) solid state crystal structure and (**zd***) DFT optimized structure.

Geometric Parameter	zd	zd*
Selected Bond Lengths (Å)		
Zr—O$_1$	2.141(1)	2.154
Zr—O$_2$	2.207(1)	2.259
Zr—O$_3$	2.190(1)	2.253
Zr—O$_4$	2.162(1)	2.157
Zr—O$_5$	2.158(1)	2.159
Zr—O$_6$	2.201(1)	2.243
Zr—O$_7$	2.213(1)	2.249
Zr—O$_8$	2.152(1)	2.156
Selected Bite Angles (°)		
O$_1$—Zr—O$_2$	74.91(4)	73.79
O$_3$—Zr—O$_4$	74.53(4)	73.90
O$_5$—Zr—O$_6$	74.59(4)	73.99
O$_7$—Zr—O$_8$	74.10(4)	73.90
Selected Torsion Angles (°)		
O$_1$—C$_{01}$—C$_{03}$—O$_2$	6.02(11)	3.43
O$_3$—C$_{04}$—C$_{06}$—O$_4$	-1.39(11)	3.51
O$_5$—C$_{07}$—C$_{09}$—O$_6$	10.98(11)	2.01
O$_7$—C$_{10}$—C$_{12}$—O$_8$	-1.54(11)	2.20

(a)   (b)

Figure 8.9 Graphical representation of an overlay of the crystal structure **zd** (**black**)
and the DFT optimized structure **zd*** (**red**) of [Zr(DBM)$_4$]. RMS value = 0.322 Å.
Overlay fit excluded all hydrogen atoms. (**a**) Side view of *sap* arrangement, where the top and
bottom of *sap* lie parallel with the *x*-axis; (**b**) 45 ° rotation of **a** on the *y*-axis.

The RMS fit and overlay of these two structures is illustrated in Figure 8.9 clearly indicating the greater differences structurally for **zd** and **zd***. While the solid state structures exhibits a "flattening" of the ligands at the top and bottom of the coordination geometry around the metal centre, the gas-phase predicted structure visibly does not. The crystal packing intermolecular forces that dictate the exact arrangement of each of the DBM-ligands around the zirconium(IV) metal atom (See § 6.3), as well as the precise and independent swiveling of each phenyl on these ligands, is clearly not present for the optimized structure. This fact becomes more obvious in Figure 8.10, where the square antiprismatic coordination geometries for both **zd** and **zd*** are illustrated.

zd   **zd***

Figure 8.10 Visual comparison of the square antiprismatic coordination polyhedron of [Zr(DBM)$_4$]; (**zd**) solid state structure at 50 % probability and (**zd***) DFT optimized structure. Hydrogen atoms omitted for clarity.

From the illustration above it is visually clear that the structure of **zd** experiences more intermolecular interference than that of **zd***. The contortion of DBM ligands in **zd** show the independent swiveling of phenyls on the ligand backbone as well as strained "flattening" of the ligands, pinched inwards on the antiprism. However, **zd*** has its ligands arranged much more freely, and almost symmetrically, with no visible structural distortion.

8.2.4. Comparison of Theoretical Optimization Results - [Zr(Acac)₄] – Type Structures

From these observations, it appears plausible to suggest that structural optimization of zirconium(IV)-Acac compounds gives a fairly good correlation with solid state observations, given the right ligands are present. From a broad comparison of the three examples described, the steric bulk of the ligand in question does seem to have an effect on the predictability of the structure as a whole. Less bulky ligands (such as the standard acac) has a greater degree of freedom to be placed and optimized in, whereas the more bulky DBM has a slightly more rigid frame and space filling requirement. From the selected geometric data reported in Table 8.4, some broad generalizations could be made.

Table 8.4 Comparison of average geometric parameters of the structures of [Zr(acac)₄] – **za**, [Zr(hFAcac)₄] – **zf** and [Zr(DBM)₄] – **zd**, as well as their optimized counterparts (**za***, **zf*** & **zd***, respectively), as described Par.8.2.1-8.2.3.

	za	za*	zf	zf*	zd	zd*
Avg. Zr—O (Å)	2.191	**2.212**	2.175	**2.2**	2.178	**2.204**
Avg. Zr—O$_{Short}$ (Å)	**2.185**	2.156	2.154	**2.162**	2.153	**2.157**
Avg. Zr—O$_{Long}$ (Å)	2.197	**2.267**	2.197	**2.239**	2.203	**2.251**
Avg. O—Zr—O (°)	74.59	**75.43**	**75.9**	74.82	**74.53**	73.9

- It appears that for all three structures presented, there is a tendency for the optimized structures to prefer *longer* average Zr—O bond lengths and *smaller* ligand O—Zr—O bite angles than what has been structurally characterized.

- The extent of the difference between average Zr—O bond lengths for crystal structures (**z**) and optimized structures (**z***), appears to escalate with an increase in the steric bulk of the ligands coordinated: **za—za*** (0.021 Å) < **zf—zf*** (0.025 Å) < **zd—zd*** (0.026 Å). This could imply that for more sterically bulky ligand structures, optimized results would deviate increasingly from actual data than for smaller compounds.

- Although the solid state structures appear to have greater ligand O—Zr—O bite angles, in general, than their optimized counterparts, different tendencies for the range of these values are observed. For real structures, bite angles shrink with electron donating ability of the ligand; **zd** [74.53(4) °] < **za** [74.59(3) °] < **zf** [75.90(3) °]. However, the data from the optimized structures seem to suggest that bite angles shrink with an increase in steric bulk; **zd** [73.90 °] < **zf** [74.82 °] < **za** [75.43 °]. The discrepancies observed here leads to the conclusion that optimization of these types of compounds is not favorable and yields too many ambiguities if series trends are sought.
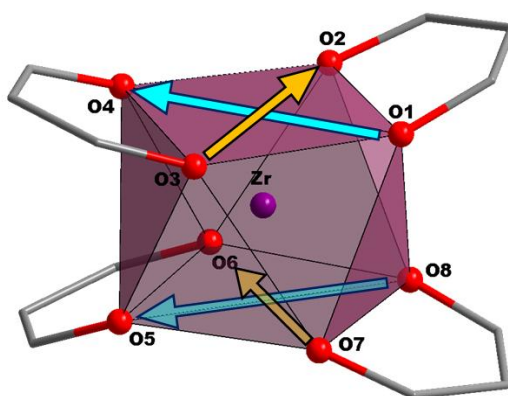
Figure 8.11 Illustration of the measurement of square antiprismatic corner-to-corner distances.

- Another point of interest that has arisen from these structural comparisons revolve around the differences in the coordination geometries around the zirconium(IV) metal center for each compound discussed. By a measure and comparison of the specific corner-to-corner distances of the top and bottom surface areas of the polyhedra in each case, a portrayal of the differences between solid state and optimized structures can be mathematically described. From the data reported in Table 8.5, it would appear that for each compound, there is a tendency where optimized structures have more extreme distortions in the coordination geometry than their solid state counterparts.

- For an ideal square antiprism (*isa*), the top and bottom square of the structure logically has corner-to-corner distances that are equal for each surface as well as equal in comparison of both areas. In other words, all four distances should be equal in the absolute ideal case and any deviation is a measure of distortion from this ideal. In this specific case, an artificial parameter is calculated measuring the "deviation from *isa*" by finding the difference between the two corner-to-corner distances for each surface as well as the average for the top and bottom (See Table 8.5).

Table 8.5 Comparison of square antiprismatic corner-to-corner distances of the structures of [Zr(acac)$_4$] – **za**, [Zr(hFAcac)$_4$] – **zf** and [Zr(DBM)$_4$] – **zd**, as well as their optimized counterparts (**za***, **zf*** & **zd***, respectively), as described Par.8.2.1-8.2.3.

	za	za*	zf	zf*	zd	zd*
Longest O—O (Å) - Top	O$_2$—O$_3$ 3.763(1)	**O$_1$—O$_4$** **4.123**	O$_5$—O$_7$ 3.868(1)	**O$_1$—O$_8$** **3.932**	O$_2$—O$_7$ 3.794(1)	**O$_2$—O$_7$** **3.959**
Longest O—O (Å) - Bottom	O$_6$—O$_7$ 3.763(1)	**O$_6$—O$_7$** **4.123**	O$_2$—O$_3$ 3.714(1)	**O$_4$—O$_6$** **3.932**	O$_3$—O$_6$ 3.712(1)	**O$_3$—O$_6$** **3.921**
Shortest O—O (Å) - Top	**O$_1$—O$_4$** **3.664(1)**	O$_2$—O$_5$ 3.19	**O$_1$—O$_8$** **3.495(1)**	O$_5$—O$_7$ 3.476	**O$_1$—O$_8$** **3.566(1)**	O$_1$—O$_8$ 3.445
Shortest O—O (Å) - Bottom	**O$_5$—O$_8$** **3.664(1)**	O$_3$—O$_8$ 3.19	**O$_4$—O$_6$** **3.612(1)**	O$_2$—O$_3$ 3.477	**O$_4$—O$_5$** **3.641(1)**	O$_4$—O$_5$ 3.485
Difference (Å) - Top	0.099	**0.933**	0.373	**0.456**	0.228	**0.514**
Difference (Å) - Bottom	0.099	**0.933**	0.102	**0.455**	0.071	**0.436**
Average Difference (Å)	0.099	**0.933**	0.238	**0.456**	0.15	**0.475**

By a measure of the scale of difference, in theory, the degree of distortion of a specific structure's coordination geometry can be quantified. It is important to note that this artificial parameter bears no significance on its own, but only in comparison with a series of similar structures (solid state and optimized). The result of these calculations shows that in all three cases, the optimized structures are more distorted from the *isa* than their solid state counterparts. The significance here is that optimization of these structures are therefore not viable, at least not for these types of ligands. Optimization of structures should theoretically tend towards less distorted and more symmetrical options, which is not the case here.

However, it seems a fair conclusion that in the gas phase, more freedom for the total structure is possible, thereby showing a larger tendency to occupy the dodecahedral geometry instead of the more compacted square antiprism.

8.3. Tetrakis(oxine-κ^2N,O)zirconium(IV) – [Zr(Ox)$_4$] – Type Structures

During the course of this project, significant advances has been made in the synthesis and classification of novel zirconium(IV) – oxine structures. In Chapter 4 and 5, the solid state characterisation of five novel oxine compounds was discussed and Chapter 7 contained a detailed account of a formation kinetic investigation of three of these complexes. In the following discussion, the structural optimization of three [Zr(Ox)$_4$] type compounds are reported (See Figure 8.12).
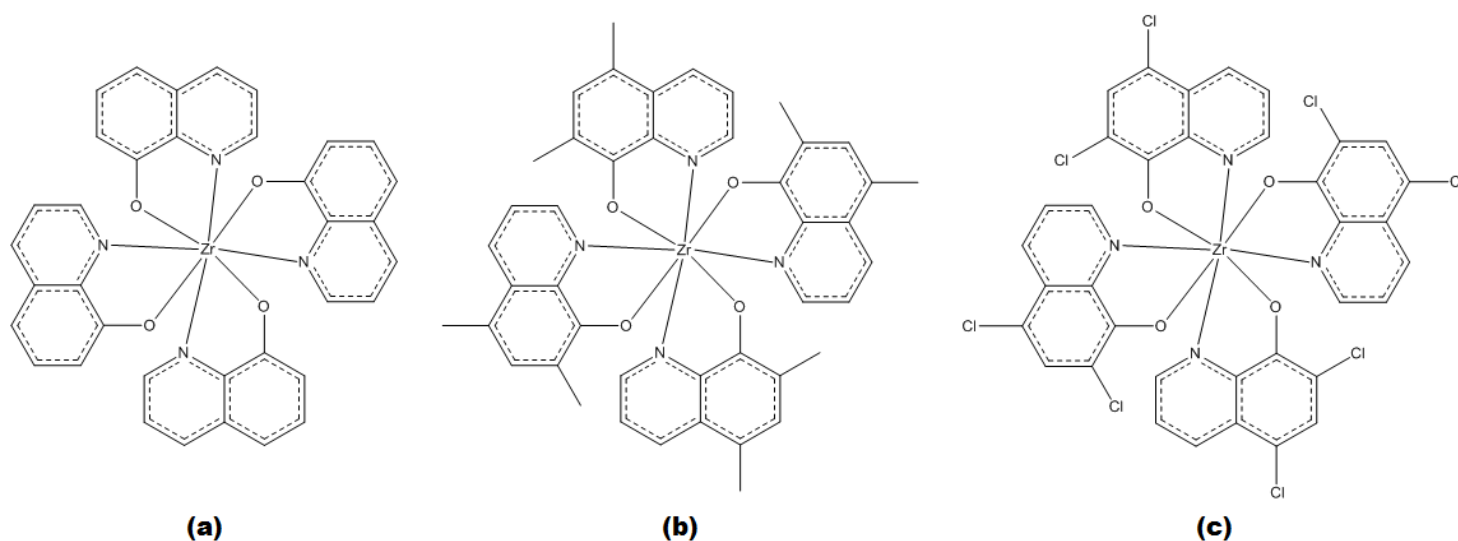
Figure 8.12 Schematic illustration of the *Tetrakis*(oxine-κ^2N,O)zirconium(IV)-type complexes optimized and discussed in this chapter; (**a**) [Zr(ox)$_4$], (**b**) [Zr(diMeOx)$_4$], (**c**) [Zr(diClOx)$_4$].

The structures of *Tetrakis*(8-quinolinolato-κ^2N,O)zirconium(IV)[22] - [Zr(ox)$_4$], *Tetrakis*(5,7-dimethylquinolin-8-olato-κ^2N,O)zirconium(IV)[23] - [Zr(diMeOx)$_4$] and *Tetrakis*(5,7-dichloroquinolin-8-olato-κ^2N,O) zirconium(IV)[24] - [Zr(diClOx)$_4$] were used as a basis for this theoretical optimization and the results are compared and correlated here.

Furthermore, these structures were not only optimized from the crystallographic solid state structure bases, but also for correlation with regard to coordination geometrical isomer possibilities. From the literary considerations in Chapter 2, § 2.4, known isomer possibilities[25,26] for discrete eight-coordinate species of zirconium(iv) compounds, containing four O,O'-donating ligands are the D$_2$, D$_4$ and C$_2$ species (See Figure 8.13).

[22] M. Steyn, H.G.Visser & A. Roodt; *J. S. Afr. Inst. Min. Metall. 113* (**2013**), 105-108.
[23] M. Steyn, H.G. Visser & A. Roodt; *Acta Cryst. E68* (**2012**), m1344–m1345.
[24] M. Steyn, H.G. Visser & A. Roodt; *Z. Kristallogr. - New Cryst. Struct. 228* (**2013**), 3, 413-415.
[25] J.L. Hoard & J.V. Silverton; *Inorg. Chem. 2* (**1963**), 235-242.
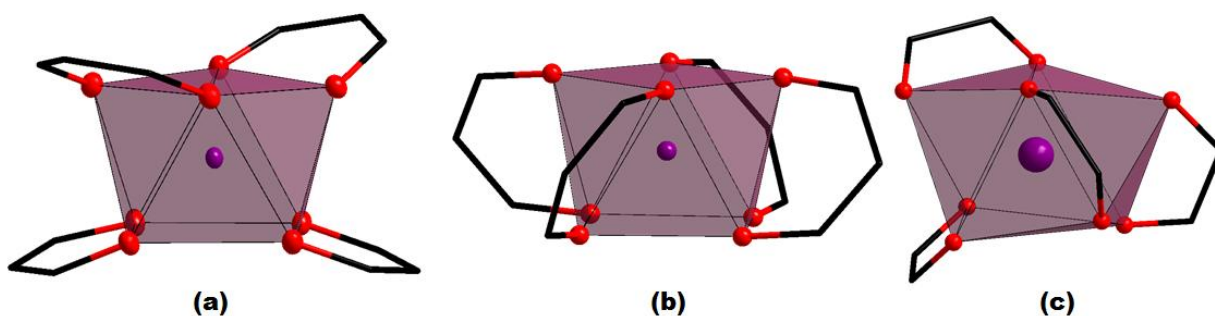
Figure 8. 13 Coordination isomers as defined for tetrakis(*β*-diketone)metal complexes exhibiting a square antiprismatic coordination polyhedron. (**a**) D_2 - Corner-clipped ligands; (**b**) D_4 - Side-clipped ligands; (**c**) C_2 - Combination corner- and side-clipped ligands.

Subsequent correlation with the novel $[Zr(Ox)_4]$ type structures described in Chapter 4 and 5, two sub-categories for the D_2 isomer were also identified (See Figure 8.14) – namely the D_2^x and D_2^z isomers.
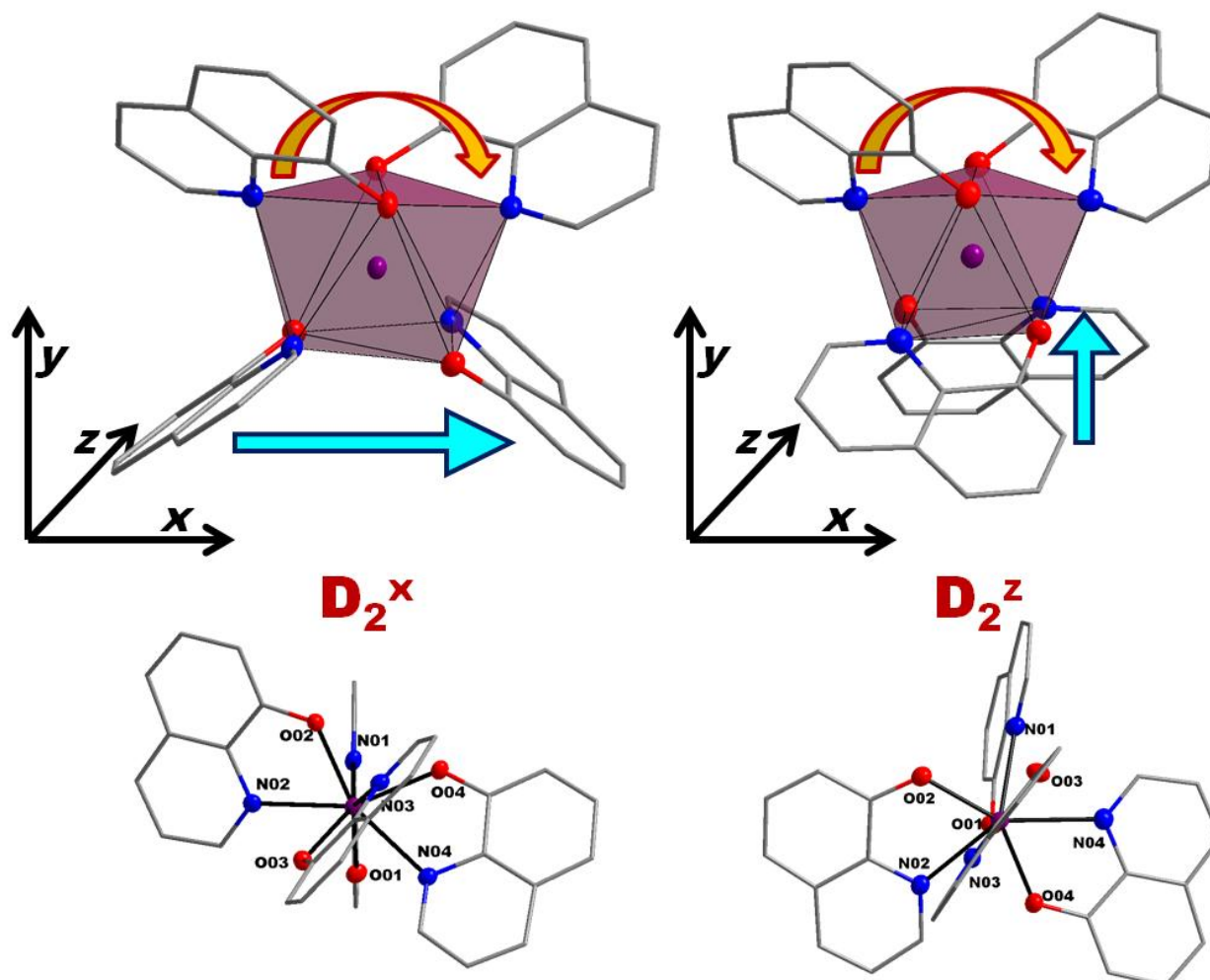
Figure 8. 14 Coordination isomer sub-category illustration of the corner-clipped D_2 species observed, when considering the arrangement of the ligands at the bottom square of the antiprism (**left**) D_2^x - ligands arranged across the *x*-axis; (**right**) D_2^z - ligands arranged across the *z*-axis.

[26] M.A. Porai-Koshits & L.A. Aslanov; *J. Struct. Chem. (Engl. Transl.) 13* (**1972**), 244-253.

From this standpoint, it became possible also to optimize structures for an isomer not identified for it. Since the solid state structures of both [Zr(diMeOx)$_4$] (D$_2^x$) and [Zr(diClOx)$_4$] (D$_2^z$) were fully characterised and described, they could be used as a bases for cross isomer optimization. By artificially adjusting the substituents on the original oxine ligands of the structure to match the desired moiety, all isomers could theoretically be optimized or predicted.

As a result, in the following section, a description of the correlation of optimized isomers with the original, published crystal structure is included. In all cases, D$_2^x$ isomers are denoted by **zx*** and D$_2^z$ isomers by **zx**** while solid state structures bear the reference **zx** [where **x = o** (ox), **m** (diMeOx) or **c** (diClOx)].

8.3.1. *Tetrakis(8-quinolinolato)zirconium(IV)* - **[Zr(ox)$_4$]**

The coordination compound [Zr(ox)$_4$] (**zo**) is compared here to the theoretically optimized counterparts; **zo*** = DFT structure of D$_2^x$ isomer and **zo**** = DFT structure of D$_2^z$ isomer. Figure 8.15 illustrates the visual comparison of these structures.
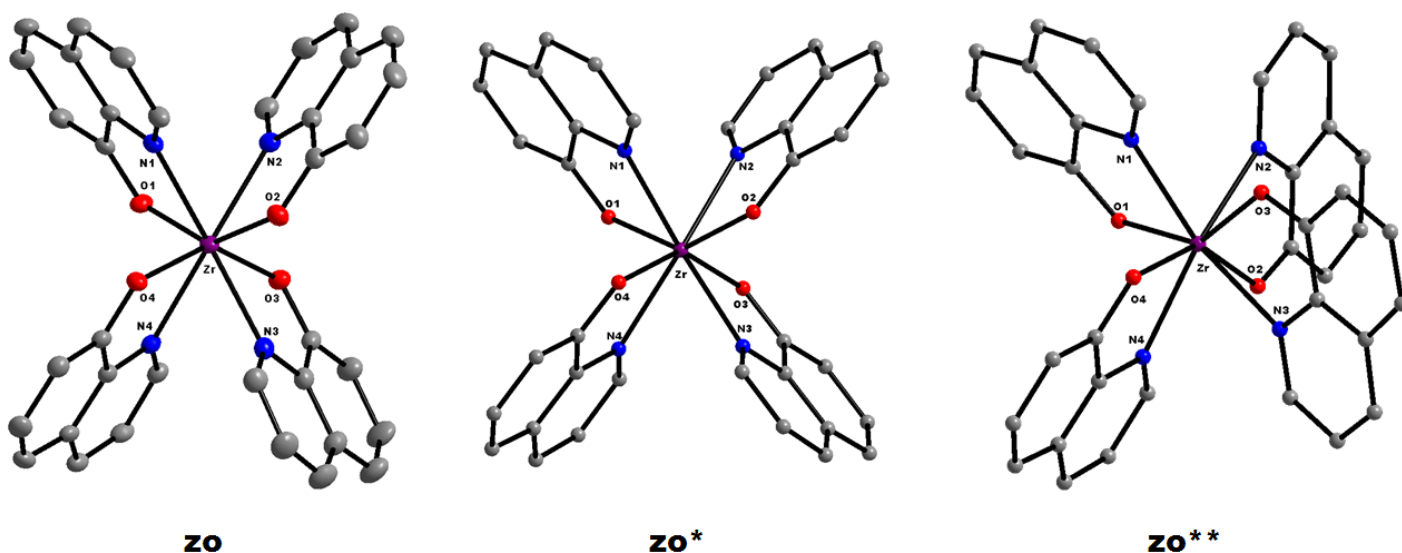
zo   **zo***   **zo****

Figure 8.15 Graphical representation of [Zr(ox)$_4$]; (**zo**) solid state structure at 50 % probability; (**zo***) DFT optimized structure for the D$_2^x$ isomer and (**zo****) DFT optimized structure for the D$_2^z$ isomer. Hydrogen atoms omitted for clarity.

The illustration in Figure 8.15 and geometric data presented in Table 8.6 give an indication of better comparability of solid state and optimized structures than reported for the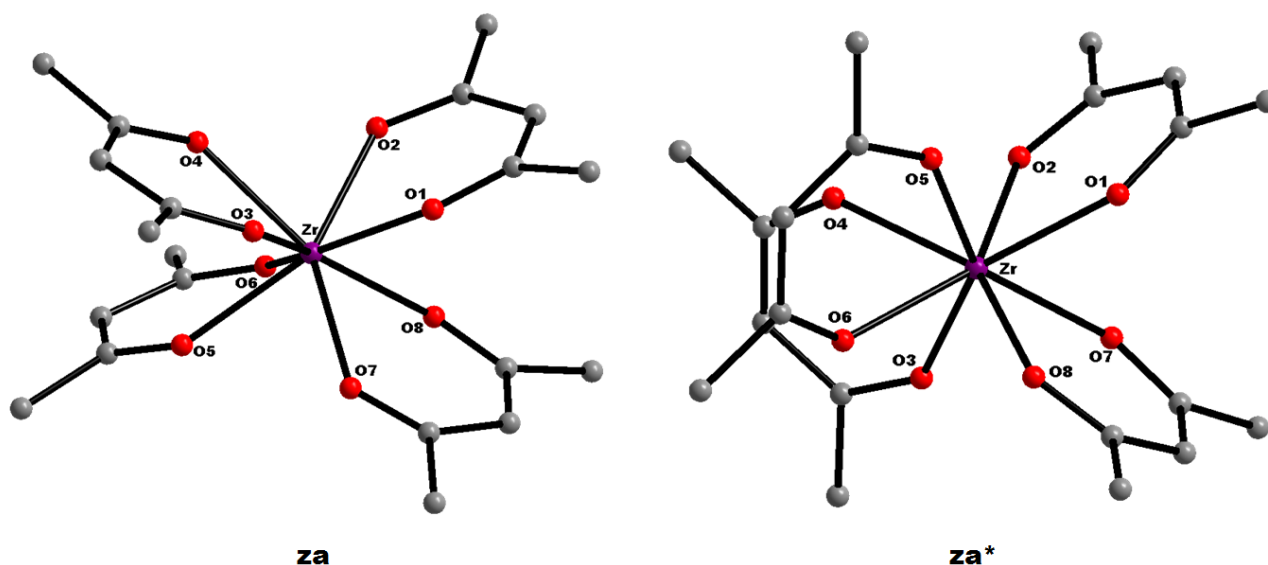 [Zr(Acac)$_4$] complexes discussed before. However, from the table presented a general tendency of structural shift is clear. The Zr—N and Zr—O bond lengths of the solid state structure (**zo**) differ notably from both optimised counterpart (**zo*** and **zo****). The average in each case – **zo**: 2.420(2) Å & 2.106(2) Å – is shorter than that of **zo*** – 2.441 Å & 2.133 Å – and **zo**** – 2.456 Å & 2.136 Å. However **zo** has a larger average N—Zr—O bite angle [70.43(7) °] than **zo*** [69.99 °] and **zo**** [69.45 °], respectively.

The observed N—C—C—O torsion angles of the ligand frame facing the N—Zr—O bite angles of **zo** are very similar, ranging from -1.25(32) ° to -1.03(33) ° and this tendency is also observed for **zo*** – 1.23 ° to 1.25 °. On the other hand, **za**** exhibits torsion angles ranging from -0.91 ° to 2.21 °, as could be expected for this more unsymmetrical isomer. In Figure 8.16, an RMS fit and overlay of **zo** and **zo*** (D$_2^x$ isomer examples) is illustrated.

Table 8.6 Comparison of selected geometric parameters for [Zr(ox)$_4$];
(**zo**) solid state structure, (**zo***) DFT optimized structure for D$_2^x$ isomer and
(**zo****) DFT optimized structure for D$_2^z$ isomer.

	zo	zo* (D$_2^x$)	zo** (D$_2^z$)
Selected Bond Lengths (Å)			
Zr—N$_1$	2.424(2)	2.442	2.434
Zr—N$_2$	2.415(2)	2.441	2.478
Zr—N$_3$	2.411(2)	2.441	2.478
Zr—N$_4$	2.431(2)	2.441	2.434
Zr—O$_1$	2.103(2)	2.133	2.134
Zr—O$_2$	2.086(2)	2.133	2.137
Zr—O$_3$	2.126(2)	2.133	2.137
Zr—O$_4$	2.108(2)	2.133	2.134
Selected Bite Angles (°)			
N$_1$—Zr—O$_1$	70.38(7)	69.98	69.54
N$_2$—Zr—O$_2$	70.89(7)	69.98	69.35
N$_3$—Zr—O$_3$	70.18(7)	69.99	69.35
N$_4$—Zr—O$_4$	70.27(7)	69.99	69.54
Selected Torsion Angles (°)			
N$_1$—C$_{09}$—C$_{08}$—O$_1$	-1.13(33)	1.24	2.21
N$_2$—C$_{18}$—C$_{17}$—O$_2$	-1.23(33)	1.23	-0.91
N$_3$—C$_{27}$—C$_{26}$—O$_3$	-1.03(33)	1.24	-0.90
N$_4$—C$_{36}$—C$_{35}$—O$_4$	-1.25(32)	1.23	2.21
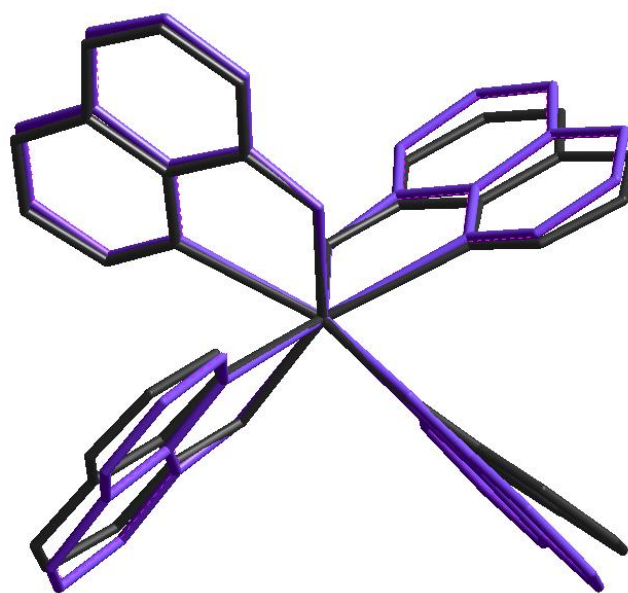
Figure 8.16 Graphical representation of an overlay of the crystal structure **zo** (**black**) and the DFT optimized structure **zo*** (**purple**) of [Zr(ox)$_4$]. RMS value = 0.123 Å. Overlay fit excluded all hydrogen atoms.

From Figure 8.16, it is clear that these two structures are geometrically very similar. The small structural discrepancy between the two illustrates again the difference between a solid state structure that experiences intermolecular packing stabilization and an optimized gas phase counterpart that does not.

(a)   (b)
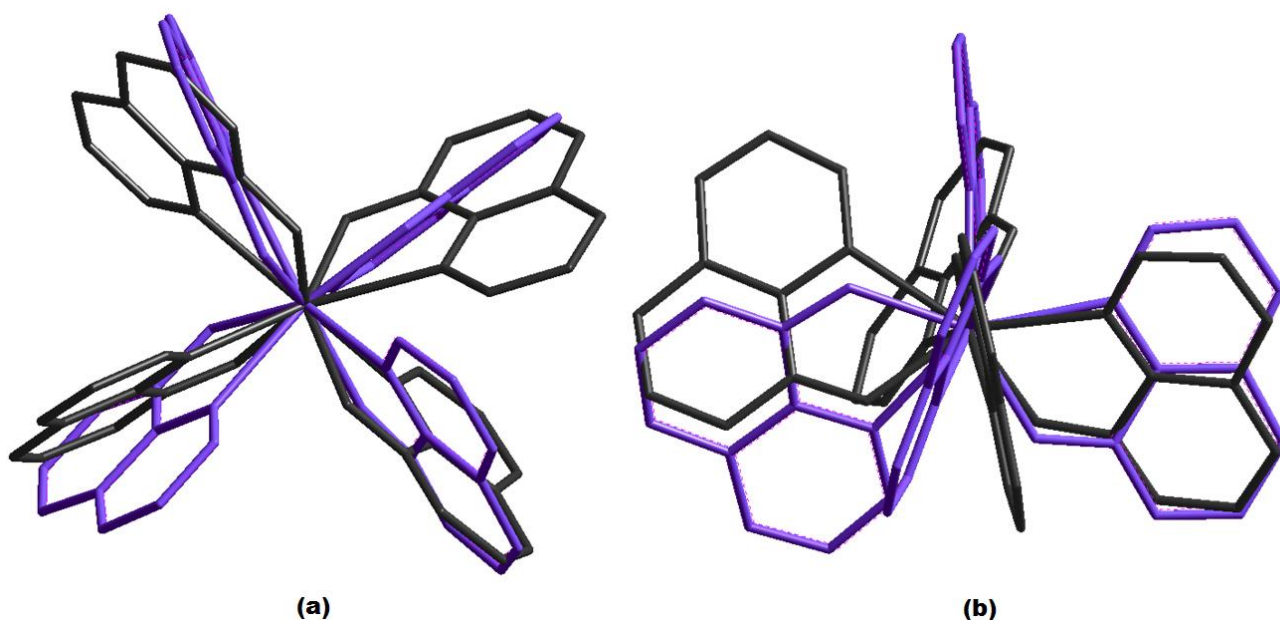
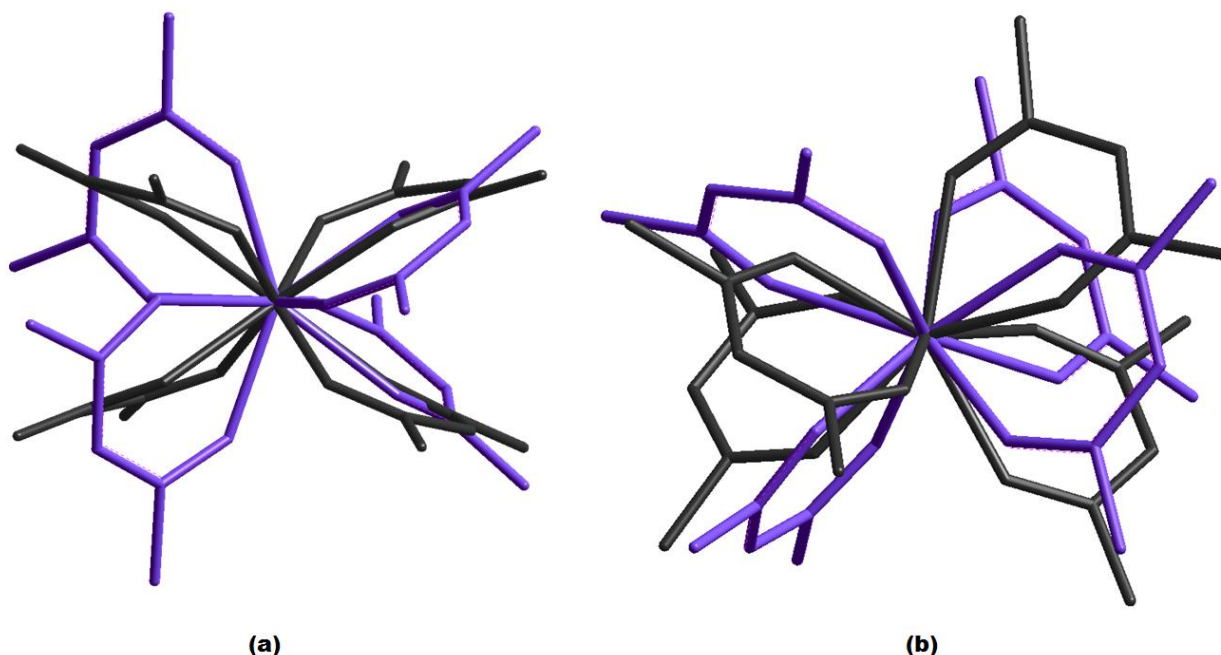**Figure 8. 17** Graphical representation of an overlay of the crystal structure **zo D$_2$^{x}** (**black**) and the DFT optimized structure **zo** D$_2$^{z}** (**purple**) of [Zr(ox)$_4$]. RMS value = 1.507 Å. Overlay fit excluded all hydrogen atoms. (**a**) Side view of Zr(IV) molecule aligned to the *ac*-plane; (**b**) Side view of Zr(IV) molecule aligned to the *ab*-plane.

An RMS fit and overlay of the solid state D_2^x **zo** and the theoretically optimized D_2^z **zo**** shows the extent of the difference between these two isomers (See Figure 8.17). As per the discussion in § 8.2.1 and § 5.5, although structural parameters of zirconium(IV) – oxine compounds can be similar or near identical, the intimate coordination geometry around the metal centre can show clear differences in the specific isomers discovered.

From the comparison drawn in Figure 8.18, the differences in the three-dimensional arrangement of ox-ligands around the metal centre are clearly visible. Although **zo** and **zo*** (D_2^x isomer structures) are very similar, it is also clear that crystal lattice packing affects (**zo**) the ligand orientation around the metal centre to a greater extent than is experienced by the gas phase counterpart (**zo***). Furthermore, although **zo** and **zo**** (D_2^z isomer structure) are in a sense comparable when considering the geometric data in Table 8.6, the visual evidence in Figure 8.18 clearly indicates the structural differences in the placement of these ligands.
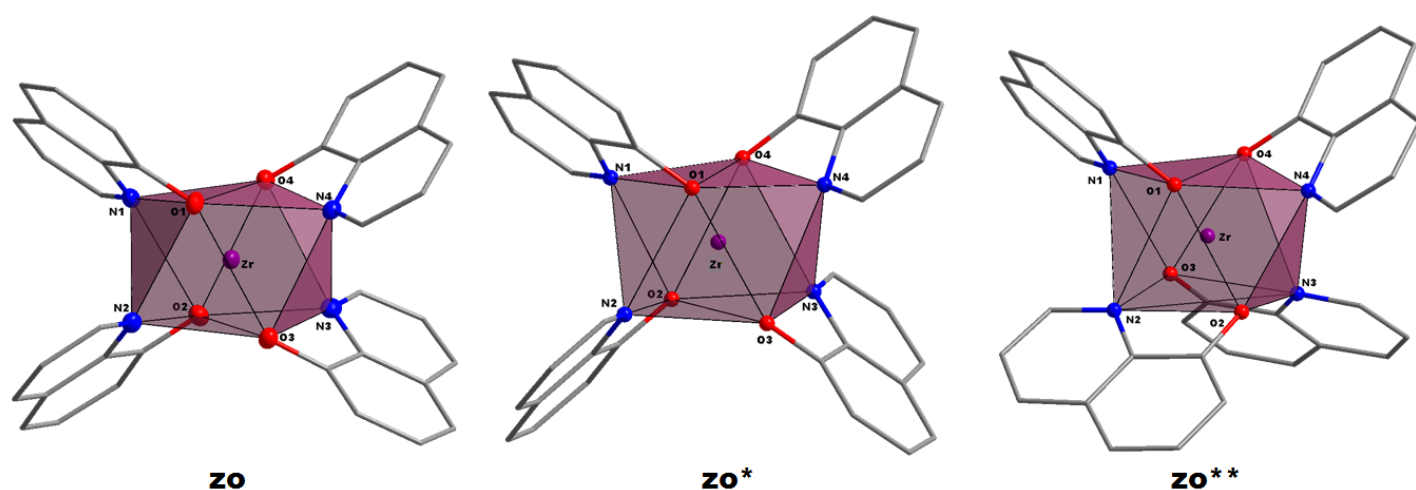
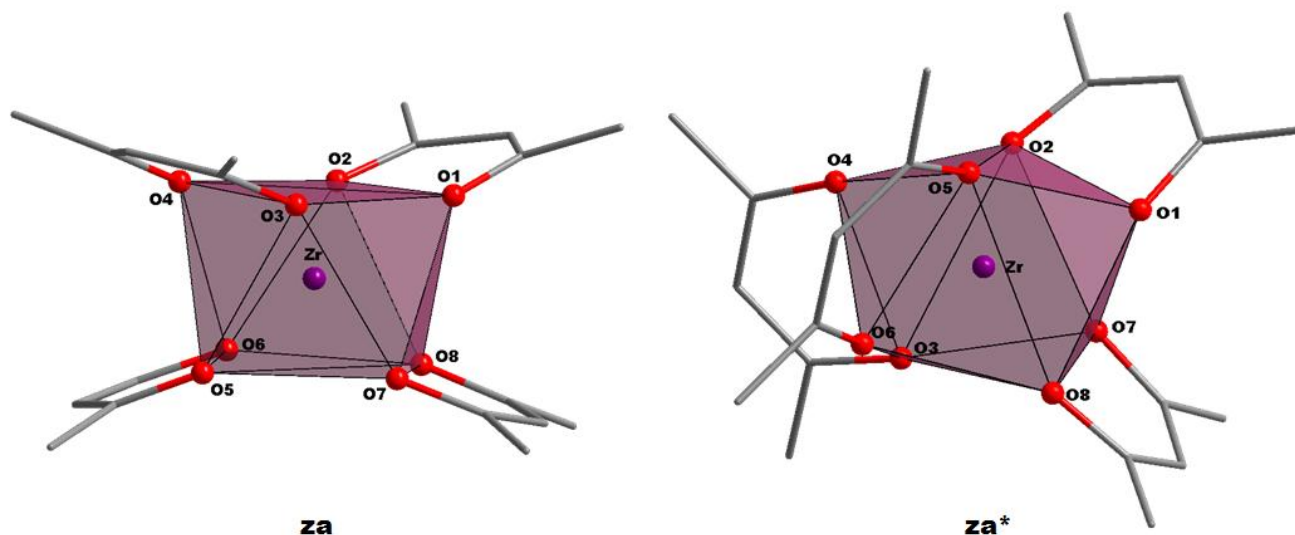**Figure 8.18** Visual comparison of the square antiprismatic coordination polyhedron of [Zr(ox)$_4$]; (**zo**) solid state structure at 50 % probability; (**zo***) DFT optimized structure for D_2^x isomer and (**zo****) DFT optimized structure for D_2^z isomer. Hydrogen atoms omitted for clarity.

8.3.2. *Tetrakis*(5,7-dimethylquinolin-8-olato)zirconium(IV) - [Zr(diMeOx)$_4$]

The coordination compound [Zr(diMeOx)$_4$] (**zm**) is compared here to the theoretically optimized counterparts; **zm*** = DFT structure of D$_2^x$ isomer and **zm**** = DFT structure of D$_2^z$ isomer. Figure 8.19 illustrates the visual comparison of these structures.
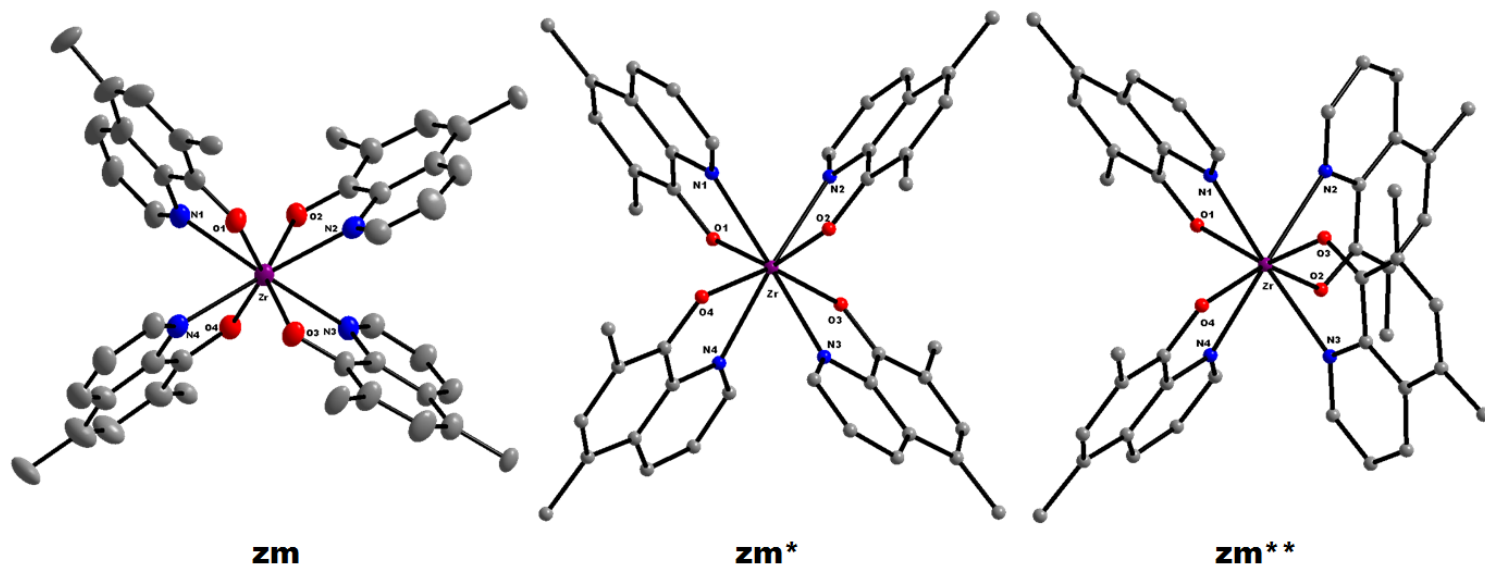
Figure 8.19 Graphical representation of [Zr(diMeOx)$_4$]; (**zm**) solid state structure at 50 % probability; (**zm***) DFT optimized structure for the D$_2^x$ isomer and (**zm****) DFT optimized structure for the D$_2^z$ isomer. Hydrogen atoms omitted for clarity.

As for the previously discussed example, the illustration in Figure 8.19 and geometric data presented in Table 8.7 give an indication of even better comparability of solid state and optimized structures than reported previously. However, from the table presented some notable differences are present. The Zr—N and Zr—O bond lengths of the solid state structure (**zm**) differ notably from both optimised counterpart (**zm*** and **zm****). The average in each case [**zm**: 2.418(2) Å & 2.106(2) Å] is shorter than that of **zm*** [2.444 Å & 2.133 Å] and **zm**** [2.466 Å & 2.136 Å], respectively. However **zm** has a larger average N—Zr—O bite angle [70.16(8) °] than **zm*** [69.89 °] and **zm**** [69.27 °], respectively.

The observed N—C—C—O torsion angles of the ligand frame facing the N—Zr—O bite angles of **zm** range from 0.49(41) ° to 2.85(41) °, while **zm*** exhibits a 1.19 ° for all ligands, indicating a more symmetrical optimized structure (as also evident from the Zr—N and Zr—O bond lengths). On the other hand, **zm**** exhibits torsion angles ranging from -0.47 ° to 2.36 °, as expected for a more unsymmetrical isomer. In Figure 8.20, an RMS fit and overlay of **zm** and **zm*** (D$_2^x$ isomer examples) is illustrated.

Table 8.7 Comparison of selected geometric parameters for [Zr(diMeOx)$_4$]; (**zm**) solid state structure, (**zm***) DFT optimized structure for D_2^x isomer and (**zm****) DFT optimized structure for D_2^z isomer.

	zm	zm* (D_2^x)	zm** (D_2^z)
Selected Bond Lengths (Å)			
Zr—N$_1$	2.433(3)	2.444	2.438
Zr—N$_2$	2.438(3)	2.444	2.493
Zr—N$_3$	2.402(3)	2.444	2.493
Zr—N$_4$	2.398(2)	2.444	2.438
Zr—O$_1$	2.105(2)	2.131	2.132
Zr—O$_2$	2.100(2)	2.131	2.129
Zr—O$_3$	2.094(2)	2.131	2.129
Zr—O$_4$	2.117(2)	2.131	2.132
Selected Bite Angles (°)			
N$_1$—Zr—O$_1$	70.10(9)	69.89	69.45
N$_2$—Zr—O$_2$	69.76(8)	69.88	69.08
N$_3$—Zr—O$_3$	70.55(8)	69.88	69.08
N$_4$—Zr—O$_4$	70.22(8)	69.89	69.45
Selected Torsion Angles (°)			
N$_1$—C$_{09}$—C$_{08}$—O$_1$	1.17(42)	1.19	2.36
N$_2$—C$_{18}$—C$_{17}$—O$_2$	0.49(41)	1.19	-0.47
N$_3$—C$_{27}$—C$_{26}$—O$_3$	2.72(40)	1.19	-0.47
N$_4$—C$_{36}$—C$_{35}$—O$_4$	2.85(41)	1.19	2.36
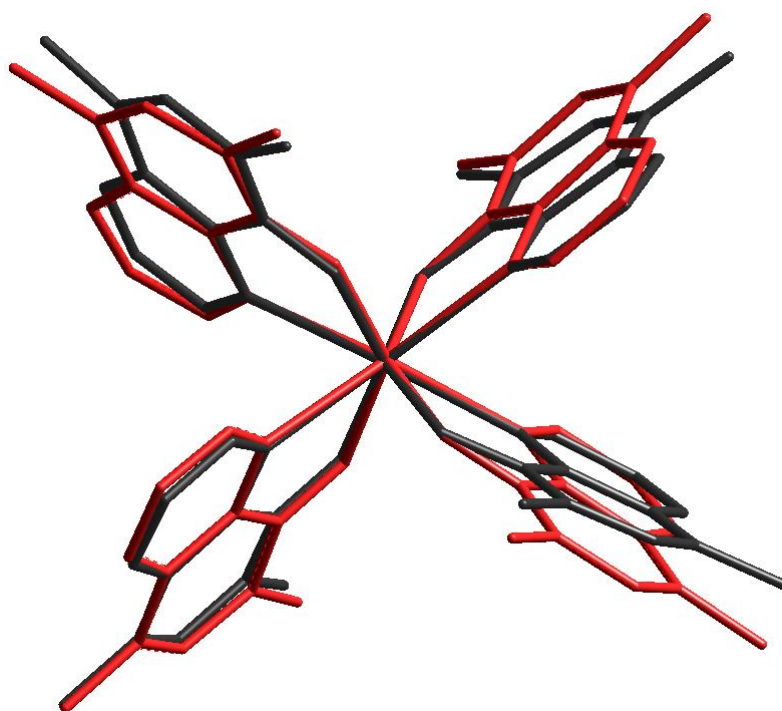
Figure 8.20 Graphical representation of an overlay of the crystal structure **zm** (**black**) and the DFT optimized structure **zm*** (**red**) of [Zr(diMeOx)$_4$]. RMS value = 0.138 Å. Overlay fit excluded all hydrogen atoms.

From Figure 8.20, it is clear that these two structures are highly comparable. The small structural discrepancy between the two illustrates again the difference between a solid state structure that experiences intermolecular packing stabilization and an optimized gas phase counterpart that does not.

(a)   (b)
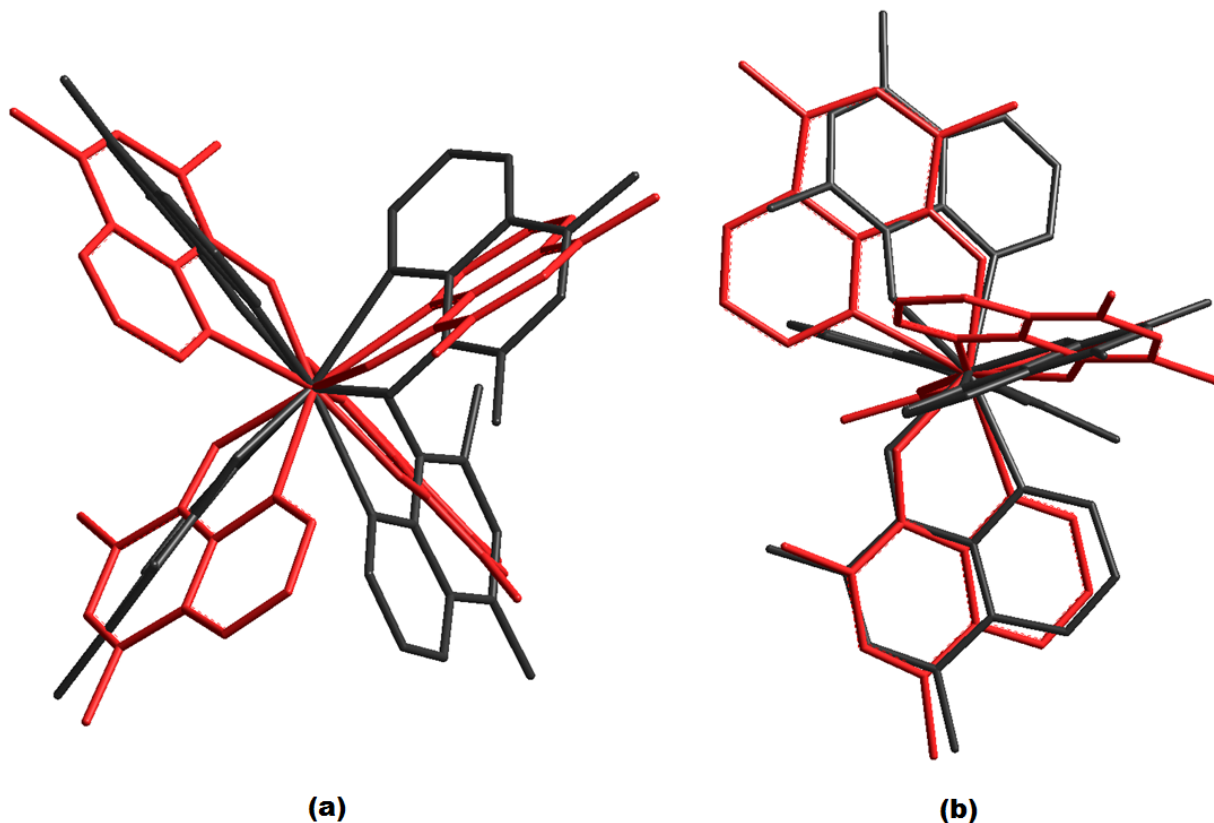
Figure 8.21 Graphical representation of an overlay of the crystal structure **zm D$_2$^{x}** (**black**) and the DFT optimized structure **zm** D$_2$^{z}** (**red**) of [Zr(diMeOx)$_4$]. RMS value = 1.491 Å. Overlay fit excluded all hydrogen atoms. (**a**) Side view of Zr(IV) molecule aligned to the *ac*-plane; (**b**) Side view of Zr(IV) molecule aligned to the *ab*-plane

An RMS fit and overlay of the solid state D$_2$^{x} **zm** and the theoretically optimized D$_2$^{z} **zm**** shows the extent of the difference between these two isomers (See Figure 8.21), as also described for the [Zr(ox)$_4$] structure before. From the comparison drawn in Figure 8.22, the differences in the three-dimensional arrangement of ox-ligands around the metal centre are clearly visible. Although **zm** and **zm*** (D$_2$^{x} isomer structures) are very similar, it is also clear that crystal lattice packing affects (**zm**) the ligand orientation around the metal centre to a greater extent than is experienced by the gas phase counterpart (**zm***). Furthermore, although **zm** and **zm**** (D$_2$^{z} isomer structure) are in a sense comparable when considering the geometric data in Table 8.7, the visual evidence in Figure 8.22 clearly indicates the structural differences in the placement of these ligands.
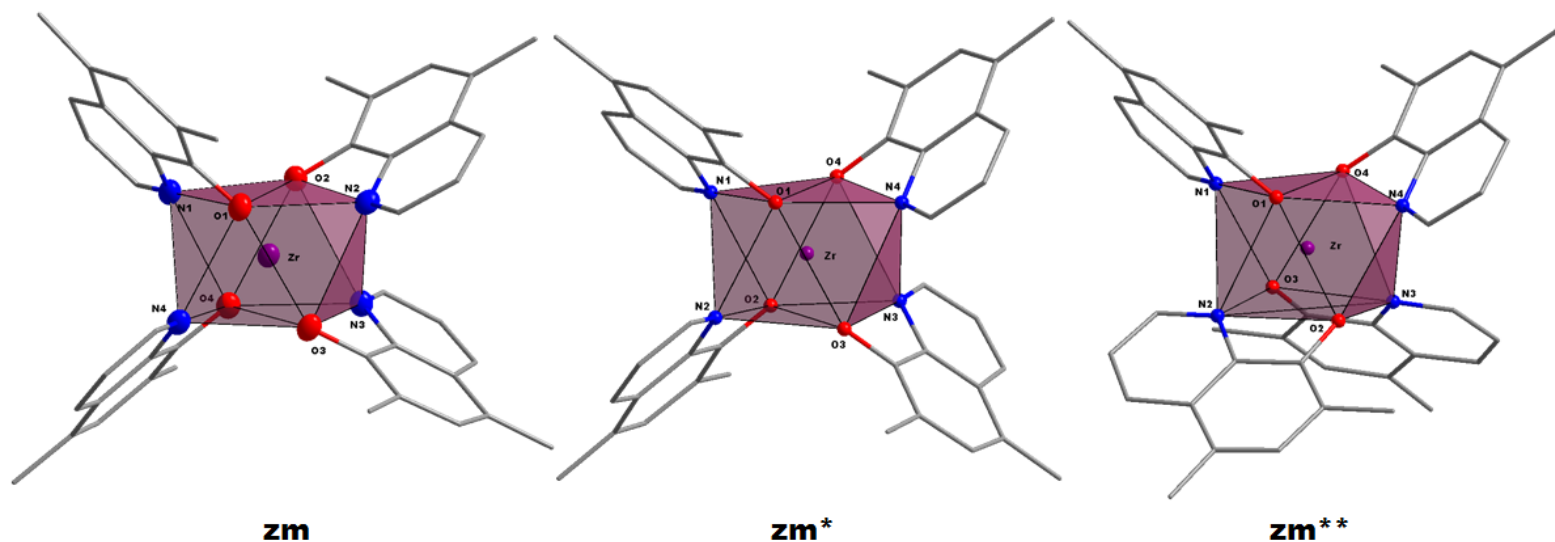
Figure 8.22 Visual comparison of the square antiprismatic coordination polyhedron of [Zr(diMeOx)$_4$]; (**zm**) solid state structure at 50 % probability; (**zm***) DFT optimized structure for D_2^x isomer and (**zm****) DFT optimized structure for D_2^z isomer. Hydrogen atoms omitted for clarity.

8.3.3. *Tetrakis*(5,7-dichloroquinolin-8-olato)zirconium(IV) - [Zr(diClOx)$_4$]

The coordination compound [Zr(diClOx)$_4$] (**zc**) is compared here to the theoretically optimized counterparts; **zc*** = DFT structure of the D_2^x isomer and **zc**** = DFT structure of the D_2^z isomer. Figure 8.23 illustrates the visual comparison of these structures.
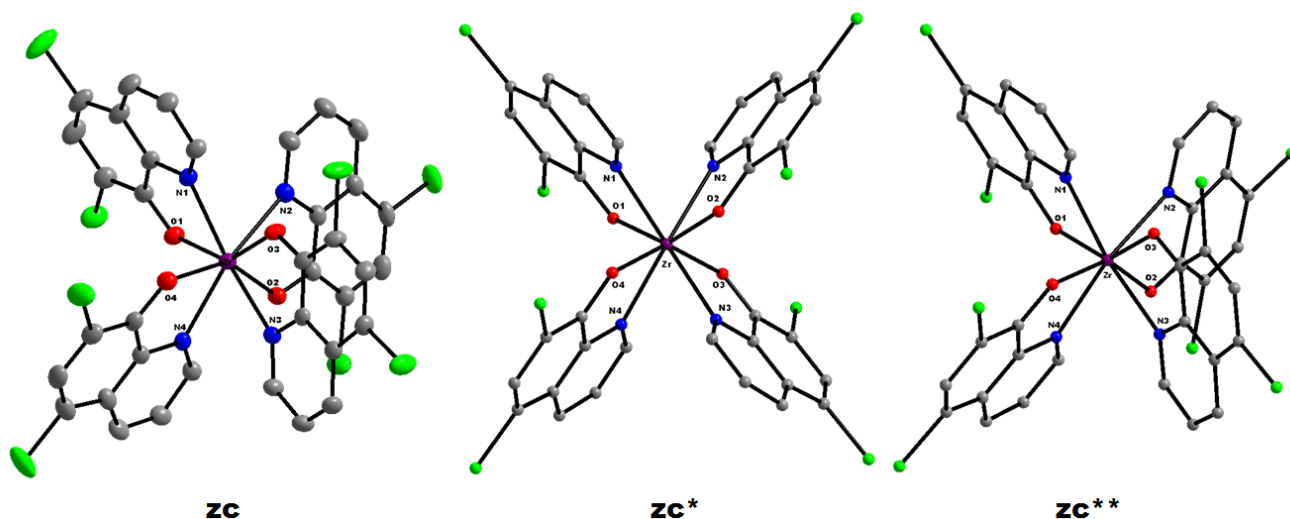
Figure 8.23 Graphical representation of [Zr(diClOx)$_4$]; (**zc**) solid state structure at 50 % probability; (**zc***) DFT optimized structure for D_2^x isomer and (**zc****) DFT optimized structure for D_2^z isomer. Hydrogen atoms omitted for clarity.

As for the previously discussed examples, the illustration in Figure 8.23 and geometric data presented in Table 8.8 give an indication of even better comparability of solid state and optimized structures than reported previously. However, from the table presented some notable differences are present. The Zr—N and Zr—O bond lengths of the solid state structure (**zc**) differ notably from both optimised counterpart (**zc*** and **zc****). In this case, other than for the previous D_2^x isomers discussed, the average Zr—N for **zc** – 2.452(2) Å – is *longer* than for the optimised **zc*** – 2.435 Å – or **zc**** – 2.448 Å. On the other hand, the average Zr—O for **zc** – 2.095(2) Å – is *shorter* than either **zc*** – 2.130 Å – or **zc**** – 2.136 Å. Furthermore **zc*** has a larger average N—Zr—O bite angle – 69.9 ° – than either of the D_2^z isomers **zc** – 69.77(7) ° – or **zc**** – 69.29 °. This is comparable to the previous D_2^x isomers discussed, in that these examples tend to have larger bite angles than their D_2^z counterparts.

Table 8.8 Comparison of selected geometric parameters for [Zr(diClOx)$_4$]; (**zc**) solid state structure, (**zc***) DFT optimized structure for D_2^x isomer and (**zc****) DFT optimized structure for D_2^z isomer.

	zc	zc* (D_2^x)	zc** (D_2^z)
Selected Bond Lengths (Å)			
Zr—N$_1$	2.417(2)	2.435	2.435
Zr—N$_2$	2.415(2)	2.435	2.460
Zr—N$_3$	2.485(2)	2.435	2.460
Zr—N$_4$	2.491(2)	2.435	2.436
Zr—O$_1$	2.113(2)	2.130	2.128
Zr—O$_2$	2.110(2)	2.130	2.143
Zr—O$_3$	2.075(2)	2.130	2.143
Zr—O$_4$	2.081(2)	2.130	2.128
Selected Bite Angles (°)			
N$_1$—Zr—O$_1$	70.21(7)	69.90	69.30
N$_2$—Zr—O$_2$	70.43(7)	69.90	69.28
N$_3$—Zr—O$_3$	69.28(7)	69.90	69.28
N$_4$—Zr—O$_4$	69.17(7)	69.90	69.29
Selected Torsion Angles (°)			
N$_1$—C$_{09}$—C$_{08}$—O$_1$	0.14(40)	1.93	2.08
N$_2$—C$_{18}$—C$_{17}$—O$_2$	1.17(39)	1.93	-1.49
N$_3$—C$_{27}$—C$_{26}$—O$_3$	1.19(37)	1.93	-1.48
N$_4$—C$_{36}$—C$_{35}$—O$_4$	0.79(39)	1.93	2.08

The observed N—C—C—O torsion angles of the ligand frame facing the N—Zr—O bite angles of **zc** range from 0.14(40) ° to 1.19(37) °, while **zc*** exhibits a 1.93 ° for all ligands, indicating a more symmetrical optimized structure (as also evident from the Zr—N and Zr—O bond lengths). On the other hand, **zc**** exhibits torsion angles ranging

from -1.49 ° to 2.08 °, as expected for a more unsymmetrical isomer. In Figure 8.24, an RMS fit and overlay of **zc** and **zc**** ($D_2{}^z$ isomer examples) is illustrated.

The observed N—C—C—O torsion angles of the ligand frame facing the N—Zr—O bite angles of **zc** range from 0.14(40) ° to 1.19(37) °, while **zc*** exhibits a 1.93 ° for all ligands, indicating a more symmetrical optimized structure (as also evident from the Zr—N and Zr—O bond lengths). On the other hand, **zc**** exhibits torsion angles ranging from -1.49 ° to 2.08 °, as expected for a more unsymmetrical isomer. In Figure 8.24, an RMS fit and overlay of **zc** and **zc**** ($D_2{}^z$ isomer examples) is illustrated.
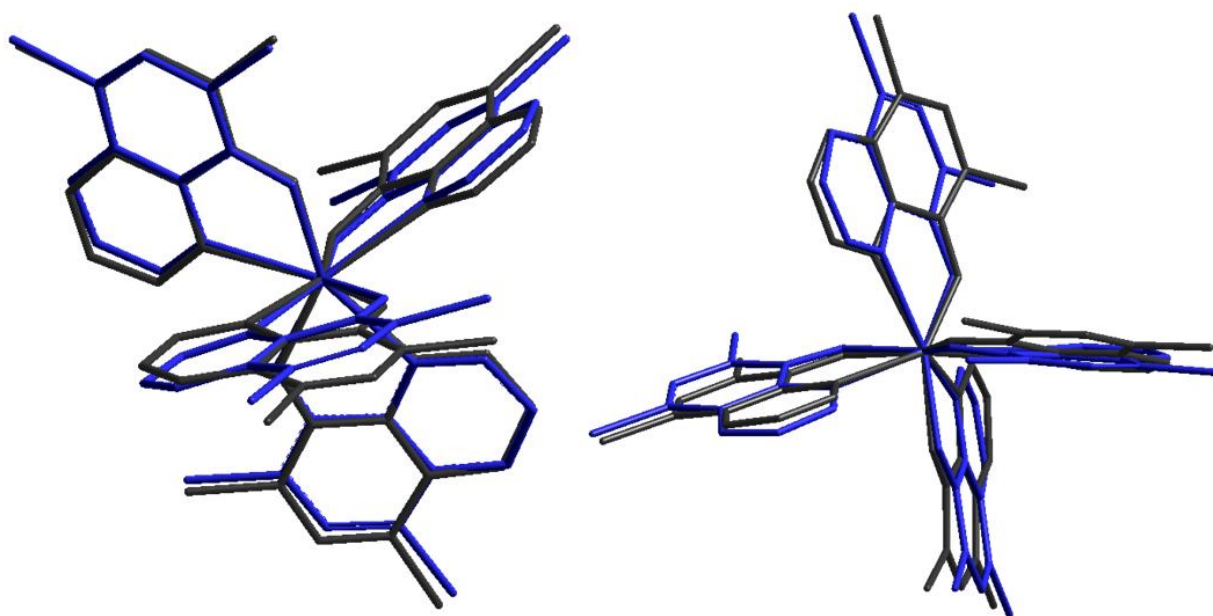
Figure 8.24 Graphical representation of an overlay of the crystal structure **zc** (**black**) and the DFT optimized structure **zc*** (**blue**) of [Zr(diClOx)$_4$]. RMS value = 0.173 Å. Overlay fit excluded all hydrogen atoms. (**a**) Side view of Zr(IV) molecule aligned to the ***bc***-plane; (**b**) Side view of Zr(IV) molecule aligned to the ***ac***-plane

From Figure 8.24, it is clear that these two structures are highly comparable. The small structural discrepancy between the two illustrates again the difference between a solid state structure that experiences intermolecular packing stabilization and an optimized gas phase counterpart that does not.

An RMS fit and overlay of the solid state $D_2{}^z$ **zc** and the theoretically optimized $D_2{}^x$ **zc*** shows the extent of the difference between these two isomers (See Figure 8.25), as also described for the other structures before. From the comparison drawn in Figure 8.26, the differences in the three-dimensional arrangement of ox-ligands around the metal centre are clearly visible.
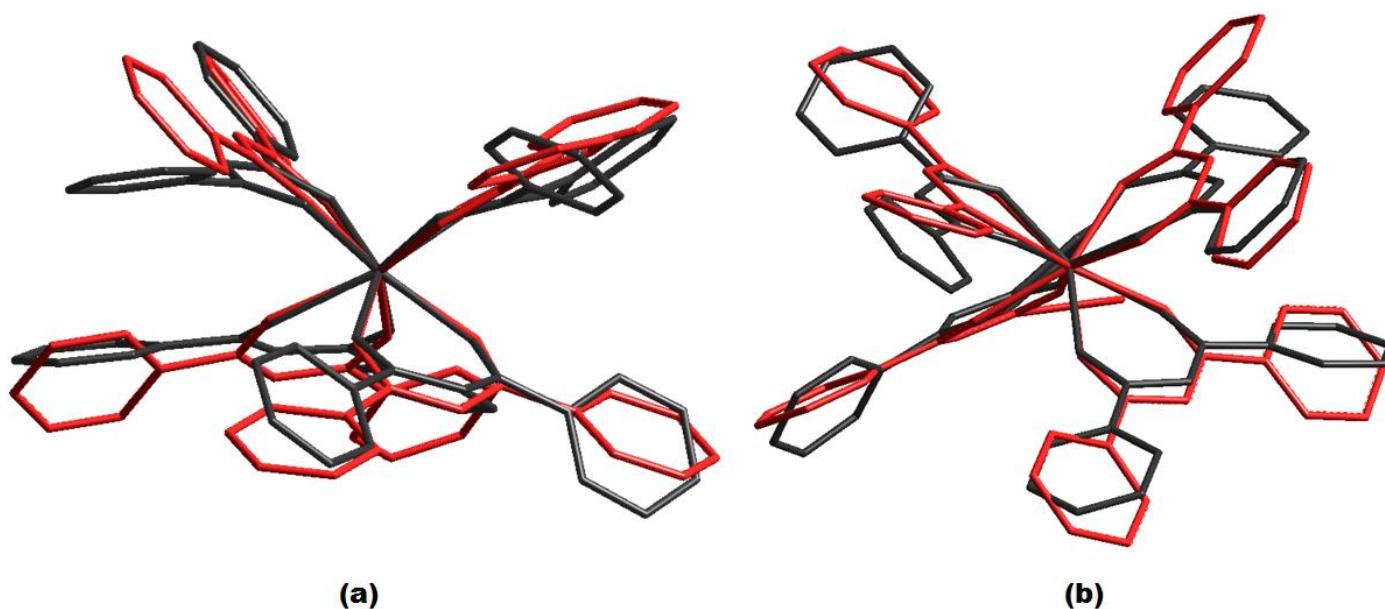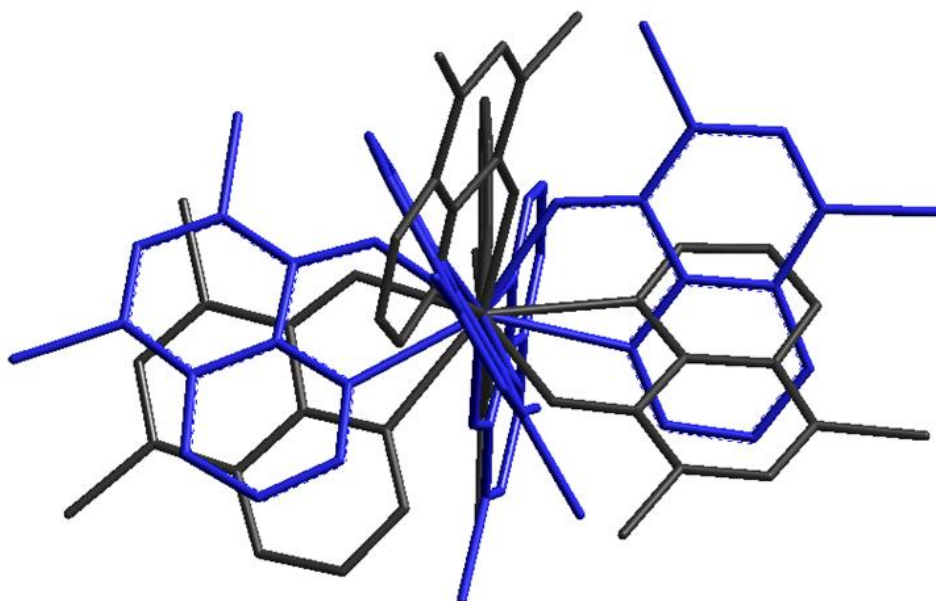
Figure 8.25 Graphical representation of an overlay of the crystal structure **zc D_2^z** (**black**) and the DFT optimized structure **zc* D_2^x** (**blue**) of [Zr(diClOx)$_4$]. RMS value = 1.901 Å. Overlay fit excluded all hydrogen atoms.

Although **zc** and **zc**** (D_2^z isomer structures) are very similar, it is also clear that crystal lattice packing affects (**zc**) the ligand orientation around the metal centre to a greater extent than is experienced by the gas phase counterpart (**zc***). Furthermore, although **zc** and **zc*** (D_2^x isomer structure) are in a sense comparable when considering the geometric data in Table 8.8, the visual evidence in Figure 8.26 clearly indicates the structural differences in the placement of these ligands.

zc   **zc***   **zc****

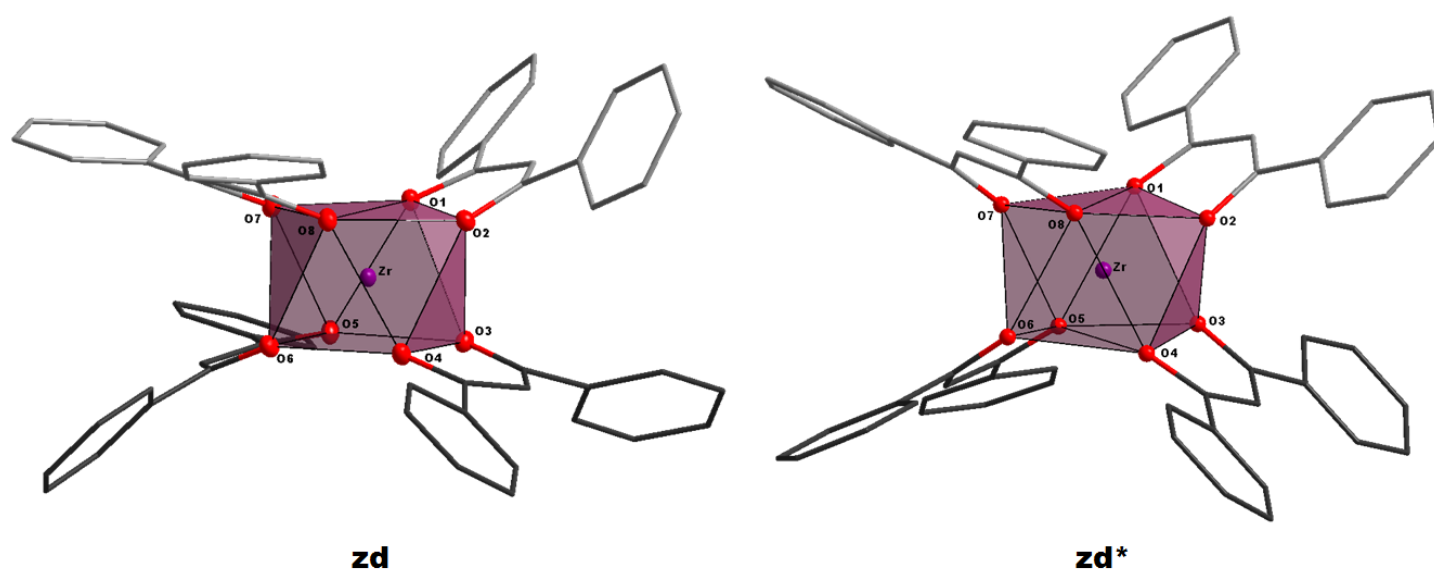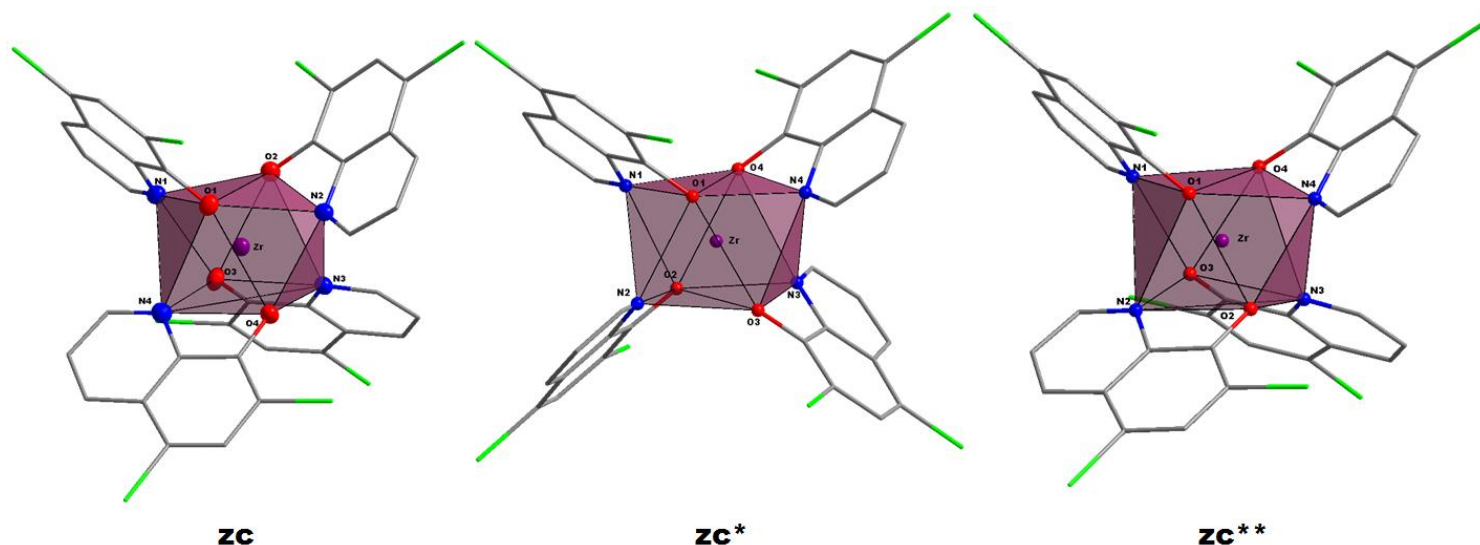**Figure 8.26** Visual comparison of the square antiprismatic coordination polyhedron of [Zr(diClOx)$_4$]; (**zc**) solid state structure at 50 % probability; (**zc***) DFT optimized structure for D_2^x isomer and (**zc****) DFT optimized structure for D_2^z isomer. Hydrogen atoms omitted for clarity.

8.3.4. Comparison of Theoretical Optimization Results –

[Zr(Ox)₄] – Type Structures

From these observations, it appears plausible to suggest that structural optimization of zirconium-oxine compounds is possible and more reliable than the zirconium-Acac examples discussed in § 8.3. From a broad comparison of the three examples described, all species investigated here seem equally adequate for structural optimization of zirconium(IV) complexes. This is of course limited to comparisons within specific coordination isomers as found for each individual moiety in the solid state structures previously characterized.

Table 8.9 Comparison of average geometric parameters of the structures of [Zr(ox)₄] – **zo**, [Zr(diMeOx)₄] – **zm** and [Zr(diClOx)₄] – **zc**, as well as their D_2^x (**zo***, **zm*** & **zc***, respectively) and D_2^z (**zo****, **zm**** & **zc****, respectively) optimized counterparts.

	zo	zo*	zo**	zm	zm*	zm**	zc	zc*	zc**
Avg. Zr—N (Å)	2.420(2)	2.441	**2.456**	2.418(2)	2.444	**2.466**	**2.452(2)**	2.435	2.448
Avg. Zr—O (Å)	2.106(2)	2.133	**2.136**	2.106(2)	2.133	**2.136**	2.095(2)	2.130	**2.136**
Avg. N—Zr—O (°)	**70.43(7)**	69.99	69.45	**70.16(8)**	69.89	69.27	69.77(7)	**69.90**	69.29

From the selected geometric data reported in Table 8.9, some broad generalizations could be made. It appears that for all three structures presented, there is a tendency for the optimized structures to prefer *longer* average Zr—N and Zr—O bond lengths and *smaller* ligand N—Zr—O bite angles than what has been structurally characterized. Furthermore, a tendency observed for specific isomers show that for D_2^x, the specific bond lengths are, although not comparable between solid state and optimized structures, almost identical for **zo** and **zm** (**z**: Zr—N = 2.420 Å; Zr—O = 2.106 Å; **z***: Zr—N = 2.444 Å; Zr—O = 2.133 Å). However the D_2^z example is notably different for only the solid state structure, but show very similar values for the optimized counterpart (**zc**: Zr—N = 2.452 Å; Zr—O = 2.095 Å; **zc***: Zr—N = 2.448 Å; Zr—O = 2.136 Å).

This does seem to imply that even during structural optimization, all zirconium(IV) oxine complexes become almost identical in their geometric parameters, as was seen for solid state products. Unfortunately, the comparison of all these structures is still not completely valid. Specific values differ too significantly. In general, although the solid

state structures appear to have greater ligand N—Zr—O bite angles than their optimized counterparts, no significant trend is observable with regard to the data available.

In a general sense, it does however appear that zirconium(IV) oxine compounds are good candidates for structural optimization *via* theoretical methods. The rigid ligand structure found here allows for less deviation from what is expected from real structures in comparison with optimized counterparts.

8.4. Conclusion

The aim of this particular investigation was to ascertain whether or not structural optimization of zirconium(IV) compounds *via* theoretical methods would be possible and viable and will produce good estimates of that observed in the solid state. A small set of examples published in literature were subjected to computational DFT calculation.

For $[Zr(Acac)_4]$ type compounds it has been shown that optimization of structures are possible, yielding stable complex data. However, the correlation of solid state parameters with that of the predicted counterparts was not ideal. In general, bond lengths, bite angles and coordination geometry comparisons all differed to some degree. The overall evaluation of the presented data in this is by no means a loss. The findings here are still novel research and opens new avenues of investigation for zirconium(IV) complex evaluation.

The fact that in the case of the $[Zr(acac)_4]$ structure, the optimized counterpart preferred a completely different isomer (C_2) than that which is known from literature (D_2),[16,17,19] is worth greater consideration. From this observation, it can be postulated with better certainty that zirconium(IV) complex structures experience a much greater influence from inter- and intramolecular interactions than previously considered. Clearly, the tighter arrangement within a crystal lattice is greatly governed by these influences, even if they are classified as "weak" bonding interactions.

On the other hand, for $[Zr(Ox)_4]$ type examples greater success, given the small sample group used, has been achieved. Structural overlays of geometric data and coordination environments were reasonably comparable, but only for the specific isomers that these compounds have been previously characterized in. The cross-isomer optimization of structures showed that it seems plausible the complexes described do, in fact, prefer a certain geometric placement of ligands around the metal center.

Furthermore, from initial postulation in § 6.4 regarding the influence of the steric bulk of a chelating ligand on the coordination environment (i.e. square antiprismatic geometry about the metal centre) in the final zirconium(IV) compound, this tendency of the $[Zr(acac)_4]$ structure to theoretically prefer a much looser arrangement of ligands in the complex, appear to support the postulated hypothesis. In the case of the fairly simple and sterically unhindered acac-ligand, the calculated structure finds an optimal placement of ligands in an almost dodecahedral coordination geometry, whereas the more encumbered DBM ligand counterpart conforms more accurately to the near ideal square antiprism. This observation is further verified by the greater accuracy of the (more bulky) oxine ligand structures also presented, which all conform to the expected square antiprismatic coordination geometry.

The fact that reasonable comparative data was obtained for the solid state and optimized structures, enables research to now pursue also different 'intermediate' structures in the complex formation process as described by solution behaviour kinetic studies (Chapter 7). However, clearly this is a complete study on its own and beyond the scope of this PhD project.

This analysis in itself has shown a proof of concept for the investigative method, at least. Theoretical prediction of zirconium(IV) structures is plausible, as shown to some extent in this chapter. The way forward from this point could allow for the determination of structural characteristics of more examples that could, until now, not be obtained from real-world laboratory experiments.

The greater significance here is that all the data for zirconium(IV) coordination compounds that could in theory be gathered and subsequently be compared to their hafnium(IV) counterparts, should be able to yield the illusive speciality differences for these metals, that would lead to easier and more effective separation methods.

Chapter **9**

Study Evaluation – Insight into Research Successes and Future Work

Zirconium(IV) complex synthesis, characterisation and quantification of solid state and solution behaviour of these compounds, highlights the comprehensive aims of this research study. In this endeavour, many novel findings have been noted and discussed in detail in each respective chapter pertaining to each separate field of the investigation. In this chapter is deliberated and elaborated on the successes attained and the significance these results have on the current knowledge base regarding zirconium(IV) chelation behaviour, as postulated theory and applied practise. Furthermore, future research possibilities and aims for subsequent investigations leading directly from these results are also included for consideration.

9.1. Zirconium(IV) Complex Synthesis

A wide range of zirconium(IV) complexes have been synthesised during the course of this project. Three sets of ligand 'families' were identified as excellent candidates for this chelation study, of which the theoretical considerations were discussed in detail in Chapter 2. These ligand categories or families were selected to exemplify a range of coordination abilities, bi- and multidentate as well as variation between O,O'-, N,O- and N,N-donating sites.

The first of these families that showed most synthetic success was the 8-Hydroxyquinoline (oxine, Ox) type ligands. A series of ten ligands was identified and applied in synthesis and all were successful in yielding coordination compound products, as confirmed by rudimentary characterisation *via* NMR-spectroscopy. The significance of the application of these ligands as chelators, lies in the fact that very few examples of zirconium(IV) complexes containing oxines were previously known in literature.[1]

The second group of ligands were chosen to expand on the *O,O'*-chelation possibilities for zirconium(IV), while the final series of ligands was a wide range of primarily pyridine type ligands, ranging from pyridine-carboxylic acids, tetradentate phenolic amines to also general bipyridyl en terpyridine examples. In all cases, as with the Ox-type ligands before, synthesis of metal complexes success was achieved, as confirmed by NMR-spectroscopy.

The noteworthy aspect worth mentioning here, regarding the success of zirconium(IV) complex synthesis, lies in the merit of the technique applied. The standard method utilized in all cases reported in Chapter 3 involved simple bench-top synthesis without any special precautions regarding anaerobic conditions (pre-dried solvents and reagents, inert atmosphere reaction setup). The chosen reaction solvent, N,N-Dimethylformamide (DMF), proved more than sufficient for controlling all aspects of the coordination formation reactions, even to the extent were crystalline water was observed in the asymmetric unit for the $[Zr(Pic)_4].2H_2O$[2] compound, without having any effect on the metal itself.

Consequently, it has been clearly illustrated that synthesis of zirconium(IV) complexes do not require rigorous synthesis methods and laborious crystallization techniques, in general. Formation reactions are often self-catalysed and crystallization can occur in ambient environments.

Finally, in all cases reported in Chapter 3 crystalline products were obtained. For those of sufficient quality and stability, the structural characterisation of the zirconium(IV) complexes was performed by means of single crystal X-Ray Diffraction studies (XRD). Unfortunately, many of these products were unstable for extended time or just of too poor quality to yield measurable diffraction data.

---

[1] The Cambridge Structural Database, Licence Update Feb 2013; F.H. Allen; *Acta Cryst. B58* (**2002**), 380-388.
[2] §5.4; M. Steyn, H.G. Visser, A. Roodt & T. J. Muller; *Acta Cryst. E67* (**2011**), m1240-m1241.

9.2. Crystallographic Structural Characterisation

Three-dimensional structural characterisation of six novel zirconium(IV) oxine complexes and two re-determined zirconium(VI) O,O'-donating ligand compounds has been performed and discussed in detail in Chapter 4, 5 and 6.

The description of the six oxine complexes yielded more insight into the intimate geometric coordination characteristics around the zirconium(IV) metal centre, as well as the crystal lattice packing stabilization as a whole. Correlation of these structures was shown to highlight that general structural properties (i.e. bond lengths, ligand bite angles, etc.) were similar for all compounds, in that they were near identical in most cases.

However, it was extensively pointed out that there were more factors at play in the case of *tetrakis*(ligand)zirconium(IV) structural characterisation. It has been established herein that these oxine complexes of zirconium(IV) also conform to the assumed square antiprismatic coordination geometry, previously only defined for O,O'-donating acetylacetonato-type complexes.[3,4] Furthermore, a series of different isomers of this chelation polyhedra was also identified and compared. It was noted that zirconium(IV) complexes, although all synthesised and crystallized by the same technique, do in fact yield slight variations in their nuances of coordination about the metal centre.

Moreover, the redetermination of the structures of *tetrakis*(tropolonato)zirconium(IV) - § 6.2 - and *tetrakis*(1,3-diphenyl-1,3-propanedionato)zirconium(IV) - § 6.3 - was included and compared with similar literary examples. In the case of the tropolone structure, the previously published[5] example included a chloroform solvate molecule in the asymmetric unit, to which the author made specific note of, as to the crystalline lattice packing stabilization *via* solvent interactions. Davis *et al.*[5] postulated that this solvate intermolecular packing stabilization defined the specific arrangement of the four tropolone ligands around the zirconium(IV) metal centre. It has been shown in this study for the DMF solvate counterpart, that the same influences can be observed for the DMF intermolecular interactions. However, the intimate geometry about the metal centre stayed essentially the same. This goes further into indicating that the susceptibility of chelation geometry to intermolecular forces is greater than that of ligand internal geometry or solvento molecule interference, but greatly governed by the metal centre itself.

---

[3] J.V. Silverton & J.L. Hoard; *Inorg. Chem. 2* (**1963**), 243-249.
[4] W. Clegg; *Acta Cryst.C43* (**1987**), 789 -791.
[5] A.R. Davis & F.W.B. Einstein; *Acta Cryst. B34* (**1978**), 2110-2115.

Finally, the redetermination of the structure of [Zr(DBM)$_4$] was discussed in detail. In this particular case, where no solvent molecule is present in the asymmetric unit, the structural characteristics as well as the chelation geometry gave a greater insight as to the nuances of coordination expected in zirconium(IV) Acac-type complexes. It was extensively shown that, although the four DBM ligands around the metal centre all participate to some extent in crystal lattice stabilization (by means of individual and, in each case unique, placement of ligand internal geometric fragments, i.e. phenyl ring swivelling observed), the final coordination environment around the zirconium(IV) centre was primarily dictated by the metal's preference for final solid state form. This aspect, the characteristic square antiprismatic polyhedron of chelated atoms, is definitively expected for this type of zirconium(IV) complex. However in this case it can be shown that is a phenomenon dictated by the metal itself, not the ligand species.

9.3. Solution Mechanistic Study

The investigation of the formation mechanism of three oxine-type ligand complexes for zirconium(IV) – [Zr(diClOx)$_4$], [Zr(5-ClOx)$_4$] & [Zr(diMeOx)$_4$] – was performed and described in detail in Chapter 7. The complexes examined, as crystallographically characterised in Chapter 4 and 5, were selected to include a range of entering groups which increases in electron donating ability as indicated by their respective Bronsted pKa values. Furthermore, since these ligands are structurally similar to the default oxine investigated in the previous M.Sc. project,[6] correlation over a series of four species could be included.

Initially, the formation mechanism for each of the new oxine ligands was evaluated, as comparison with the previously presented example. In all cases the same intricate process of bidentate ligand coordination was observed. This process involves a fast initial reaction, followed by three multi-phase reaction steps wherein it is assumed that the chloride ligand is liberated as HCl (H$^+$ from oxH) in the ring-closing step in each of the four processes.

Additionally, a subsequent set of experiments was performed to evaluate the effects of equilibrium suppression by presence of an excess of leaving ligand to the reaction solution. This was achieved by the addition of the organic salt tetraphenylphosphonium chloride, in an attempt to influence the reverse equilibrium reaction (chloride substitution), as preference. Again, as in the case of the [Zr(ox)$_4$] solution kinetic findings previously reported, reaction

---

[6] M. Steyn; *Speciation And Interconversion Mechanism Of Mixed Halo And O,O- And O,N Bidentate Ligand Complexes Of Zirconium*, M.Sc. Dissertation (**2009**), University of the Free State, South Africa.

steps could only be restrained to some extent, not completely stopped. However, in the case of the three new oxine ligands evaluated, this restraining influence was observed for all four mechanistic steps.

The final generalised conclusion from these findings, from correlation and comparison of reaction an equilibrium rate data obtained, could be summarised as follows:

i.   More substituted oxines (diClOxH & diMeOxH) appear to have faster formation reactions compared to lesser substituted species (oxH & 5-ClOxH), for the limiting reaction steps of the coordination of the 2nd, 3rd and 4th ligands.

ii.   For the first reaction, the tendency is that the more electron-donating the ligand is, the faster the reaction becomes [in agreement with an *Associative* mode of coordination]

ii.   However, the lesser substituted variety on the other hand appear to be more influenced by equilibrium suppressants.

9.4. Theoretical Calculations

Theoretical optimization, by means of computational chemistry techniques, of two different families of zirconium(IV) complexes was performed and the subsequent results evaluated by comparison with published structural data. The two families in question, the *tetrakis*(acetylacetonato-κ^2O,O')zirconium(IV)- and *tetrakis*(oxine-κ^2N,O)zirconium(IV) type examples, were each selected to represent the O,O- and N,O- coordination environments about the metal centre.

In the case of the [Zr(Acac)$_4$] type compounds, correlation of three optimized structures – [Zr(acac)$_4$], [Zr(hFacac)$_4$] & [Zr(DBM)$_4$] – with known characterised counterparts were not ideal but adequate. General comparison of geometric parameters (bond lengths, ligand bite angles, etc.) was shown to compare fairly well, from expected averages. However in the case of the structure of [Zr(acac)$_4$], the least substituted and complicated structure, the optimized counterpart proved to prefer a different isomer of chelation geometry. The expected square anti-prism was distorted significantly in the calculated structure, due mainly to the fact that this example optimized into a C_2 coordination isomer, as opposed to the D_2 example known to be the preference for this specific zirconium(IV) complex.

This observation can be attributed to the fact that theoretical optimization of molecular structures assumes a gas phase environment, without inter- or intramolecular forces governing lattice stabilization/packing. From this observation, it can be postulated with greater certainty that zirconium(IV) complex structures experience a much greater influence from these interactions than previously considered. Clearly, the tighter arrangement within a crystal lattice is greatly governed by these influences, even if they are classified as "weak" bonding interactions. This was furthermore elaborated on with the comparison of the [Zr(DBM)$_4$] crystal structure and optimized counterpart. In this case, as per the structural description included in §6.3, it was observed that the solid state structure of this particular zirconium(IV) complex exhibited and experience great influence from intermolecular packing effects, involving the phenyl rings on the DBM ligand structure. The arrangement of these ligands in the optimized stricter was shown to experience no such influences in the gas phase calculated environment.

Additionally, the optimization of three zirconium(IV) oxine complexes– [Zr(ox)$_4$], [Zr(diMeOx)$_4$] & [Zr(diClOx)$_4$] – was also accomplished to elucidate whether or not these ligands, with a more rigid frame and packing placement, would show better theoretical calculation possibility. This was performed for the specific isomer of each moiety known from crystallographic characterisation, D_2^x/D_2^z, but also in an environment of the opposite isomer possible.

The findings from this correlative endeavour showed that these oxine structures do, in fact, compare better when optimized, with the predetermined solid state structures. This is primarily accounted to the ligand rigidity, as postulated. This agreeable comparison of structures is however limited to the specific isomer defined from crystallographic characterisation. Nonetheless, the alternative isomers are theoretically possible but the probability appears to be lessened. This is further supported from the overarching comparison drawn in § 6.4, concerning the observed square antiprismatic isomers of each characterises structure with regard to the type of ligand yields a specific isomeric moiety.

In summary, with regard to the explicit tendency of a ligand to finally coordinate in any specific isomer, only a broad generalisation or argument can be made with the data available at this stage. The steric bulk of said ligand does seem to influence the trend that yields a specific isomer in the final solid state structure. As per the data presented in Table 6.10 where $\mathbf{D_2^z}$ {[Zr(diClOx)$_4$].2DMF] > $\mathbf{D_2^x/D_2}$ {[Zr(5-ClOx)$_4$].2DMF, [Zr(diMeOx)$_4$].2DMF, [Zr(DBM)$_4$]} > $\mathbf{C_2}$ {[Zr(5-NO$_2$Ox)$_4$], [Zr(Pic)$_4$].H$_2$O} > **Dodecahedral** {[Zr(Trop)$_4$].DMF}. The significance here, although not definitively proven, is that these observations can assist a great deal when designing/choosing ligands for separation studies.

9.5. Future Research

The research outputs presented throughout has yielded a significant amount of novel insights and fundamental knowledge into zirconium(IV) coordination behaviour for solid, solution and gas phase behaviours. Even so, the results discussed and quantified are only a proof of concept regarding the significance of a study to elucidate the intimate geometric nature and characteristics of zirconium(IV) coordination with organic ligands.

The possibilities leading directly out of the results obtained, that beg to ask even more questions in each field of characterisation, appear endless. However, a few key issues for immediate further investigation can be summarised, as below:

I. *Synthesis and Solid State Structure Characterisation*

Synthesis of complexes presented in Chapter 3 proved to yield crystalline products throughout, by means of the bench-top DMF solution method. However, most of the compounds were of too low quality to analyse via XRD. Effort into the production of better quality crystals would greatly increase the possibility of structural characterisation possibility, in turn expanding on the knowledge base of zirconium(IV) coordination behaviour properties.

II. *Solution Behaviour Manipulation Experiments (i.e. Solution Extraction Quantification)*

The application of the rudimentary findings of the solution kinetic studies presented herein can directly be applied at this stage on separation studies, involving Liquid-Liquid/ Solution Extraction experimentation. From the observations concerning the manipulation of formation mechanistic influences, suppression of certain intermediate products could be induced. If there is a difference in this solution behaviour for hafnium(IV) counterparts of these complexes, simple compound separation can be achieved *in principle*.

III. Theoretical Optimization – Solid State Structures

There is still much scope for structural computation regarding zirconium(IV) complexes. By increasing the evaluation data pool, even more information could be gathered regarding the relation between solid state and gas phase behaviours for the compounds. Of immediate interest is additional oxine complexes as well as investigating unsymmetrical acetylacetone type species of zirconium(IV). The correlative possibilities here would be of invaluable significance for future experimental design. Once the additional solid state structures have been optimised, transition state identification for the kinetic processes should be evaluated, to explain why different isomers are obtained when different ligands (and substituents thereupon) are utilised.

IV. Extraction Utilising the Above Fundamental Knowledge

Considering all of the discussed and postulated aims, the way forward for solution extraction separation studies has been set. The kinetic evaluations alone allow for a detailed solvent extraction study, also utilising modern dual flow techniques. This part of this parallel study is currently the aim of another PhD study in progress by J.A. Viljoen at the UFS.

SUMMARY

Zirconium and hafnium, the chemical twins in the titanium triad of the periodic table, are chemically very similar, but exhibit a significant difference in their nuclear properties, and also most noteworthy, their application in industry. Zirconium, with its very low affinity for thermal neutrons (radioactive energy), high thermal stability and exceptional anti-corrosive properties, is widely used as cladding material for nuclear reactor fuel rods. Hafnium, on the other hand, with its very high affinity for thermal neutrons is most often employed as control rods, used for regulating the rate of fission in nuclear reactors. For this application alone, it is apparent why the separation of these metals to their chemically pure state, is so important. Even the smallest impurity of one metal in the other would seriously degrade the ability of the metal to function in its particular role in a nuclear reactor.

In this study, the solid state and solution behaviour of zirconium(IV) coordination compounds, containing N- and O-donating multidentate ligands, is investigated. A detailed description of the synthesis of 25 zirconium(IV) complexes with three ligand families – *O,O'*-donating, oxines and pyridines – are reported and characterised by means of IR, UV/Vis and NMR (^{1}H & ^{13}C) spectroscopies.

Furthermore, the solid state structural characterisation, by means of single crystal X-Ray Diffraction spectroscopy, of eight of these synthesised complexes is described in detail. Six novel oxine-type complexes – [Zr(diClOx)$_4$]·2DMF, [Zr(5-ClOx)$_4$]·2DMF, [ZrCl(CliOx)$_2$(DMF)$_2$O]$_2$·DMF, [Zr(diMeOx)$_4$] ·2DMF, [Zr(5-NO$_2$Ox)$_4$] and [Zr(Pic)$_4$]·2H$_2$O – are discussed and compared with regard to the intimate geometric environment around the zirconium(IV) metal centre [where *5,7-Dichloro-8-hydroxyquinoline* (diClOxH), *5-Chloro-8-hydroxyquinoline* (5-ClOxH), *5-Chloro-7-iodo-8-hydroxyquinoline* (CliOxH), *5,7-Dimethyl-8-hydroxyquinoline* (diMeOxH), *5-Nitro-8-hydroxyquinoline* (5-NO$_2$OxH), *2-Picolinic acid* (PicH)]. It is shown here that these structures also exhibit the classic square antiprismatic coordination polyhedra as expected for the O,O'-donating acetylacetone-type complexes of zirconium(IV).

The redetermination for the structures [Zr(Trop)$_4$]·DMF and [Zr(DBM)$_4$] is also included and further discussed in detail [*Tropolone* (TropH), *Dibenzoylmethane* (DBM)]. In these examples, it is shown and concluded that zirconium(IV) complexes exhibit a natural tendency to form tetrakis- or eight-coordinate crystalline products, as preference, with a square antiprismatic chelation environment around the metal centre in most of the cases. From these findings it was postulated that, for this metal centre, the susceptibility of

chelation geometry to intermolecular forces seems greater than that of ligand internal geometry and is primarily governed by the zirconium(IV) centre itself.

In addition, a solution kinetic study (utilizing UV/Vis Absorbance spectroscopy) on the formation mechanism of three oxine complexes synthesised and crystallographically characterised, is also included. The rudimentary findings for [Zr(diClOx)$_4$], [Zr(5-ClOx)$_4$] and [Zr(diMeOx)$_4$] (from ZrCl$_4$ as reactant) is shown to correspond well with that of the [Zr(ox)$_4$] complex evaluated in the preliminary M.Sc. study. The entering ligands were selected to span a range of increasing donor ability utilising both chloro and methyl substituents on the oxine backbone. In all cases the same general intricate process of bidentate ligand coordination was observed. This process involves a fast initial reaction, followed by three slower multi-phase reaction steps wherein it is assumed that the chloride ligand is liberated as HCl (H$^+$ from oxH) in the ring-closing step in each of the four processes. In total, the reactions span about a five order-of-magnitude range, indicating a huge change in affecting all four the chlorido ligands to be substituted to form the corresponding tetrakis-oxine complexes. Where the first step showed an *increase* by more than 30 times as the donor ability of the entering ligand increased, the subsequent following three reactions indicated approximately one order-of-magnitude *decrease* in ligation rate.

Equilibrium suppression studies were also performed by means of stepwise increasing the concentration of the leaving ligand, in this case Cl$^-$, by the addition of a spectator organic salt, PPh$_4^+$Cl$^-$. The findings in this case show that all four reaction steps for all three zirconium(IV) complexes are significantly affected and restrained by this equilibrium manipulation process.

Next, theoretical optimization, by means of computational chemistry techniques, of two different families of zirconium(IV) complexes was performed and the subsequent results evaluated by comparison with the structural data obtained from single crystal studies. The two families in question, the tetrakis(acetylacetonato-κ^2O,O')zirconium(IV)- and tetrakis(oxine-κ^2N,O)zirconium(IV) type examples, were each selected to represent the O,O- and N,O- coordination environments of the metal polyhedron.

Fair correlation is observed for the [Zr(Acac)$_4$] type complexes, that is [Zr(acac)$_4$], [Zr(hFacac)$_4$] & [Zr(DBM)$_4$], with their optimized counterparts. However, for [Zr(acac)$_4$] a different coordination isomer was obtained from the optimization. This observation can be attributed to the fact that theoretical optimization of molecular structures assumes a gas phase environment, without inter- or intramolecular forces governing lattice stabilization/packing. It can therefore be postulated with more certainty that zirconium(IV)

complex structures experience a more significant influence from these interactions than previously considered.

Finally, the optimization of three zirconium(IV) oxine complexes– $[Zr(ox)_4]$, $[Zr(diMeOx)_4]$ & $[Zr(diClOx)_4]$ – was also accomplished to elucidate whether or not these ligands, with a more rigid frame and packing placement, would show similar optimisation. This was consequently illustrated to an acceptable accuracy with good correlation between crystallographically characterised structures and their theoretically optimised counterparts.

Key words: Zirconium; N- and O-donating ligands; synthesis; crystallographic characterisation; kinetic mechanistic study, theoretical optimization.

OPSOMMING

Sirkonium en hafnium, die chemiese tweeling in die titaangroep van die periodieke tabel, is chemies baie soortgelyk, maar toon 'n betekenisvolle verskil in hul kerneienskappe, ~~en~~ veral tov hul toepassing in die industrie. Sirkonium, met sy baie lae affiniteit vir termiese neutrone (radio-aktiewe energie), hoë termiese stabiliteit en uitsonderlike antikorrosie-eienskappe, word algemeen gebruik as dekmateriaal vir kernreaktorbrandstof. Hafnium daarteenoor, met sy hoë affiniteit vir termiese neutrone, word dikwels gebruik as beheerstawe in die kernbrandstof, wat gebruik word vir die temporegulering van die kernreaksie binne-in die reaktore. Deur bloot hierdie toepassing in aanmerking te neem blyk dit duidelik waarom die effektiewe skeiding van hierdie metale in hul chemiese suiwer toestand krities belangrik is. Selfs klein onsuiwerheid van een metaal in die ander kan die vermoë van die ander een betekenisvol negatief in 'n kernreaktor beïnvloed.

In hierdie studie is die vastetoestand- en oplossinggedrag van sirkonium(IV) koördinasieverbindings, met N- en O-elektrondonor multidentaatligande ondersoek. 'n Volledige beskrywing van die sintese van 25 sirkonium(IV)komplekse met drie reekse ligandgroepe – O,O'-donoratome (asetielasetonaattipe), sowel as beide oksien en piridien (d.w.s. O- en N-donoratoomligande) – word gerapporteer en is gekarakteriseer deur middel van IR, UV / Vis en KMR (^{1}H en ^{13}C) spektroskopie.

Die vastetoestandstrukture van agt van hierdie gesintetiseerde komplekse, soos bepaal deur middel van enkelkristal X-straaldiffraksie, word in detail beskryf. Ses nuwe oksien-tipe komplekse, nl. [Zr(diClOx)$_4$]·2DMF, [Zr(5-ClOx)$_4$]·2DMF, [ZrCl(CliOx)$_2$(DMF)$_2$O]$_2$·DMF, [Zr(diMeOx)$_4$]·2DMF, [Zr(5-NO$_2$Ox)$_4$] en [Zr(pic)$_4$]·2H$_2$O, word bespreek en die koördinasiepolihedra rondom die Zr(IV) vergelyk [met *5,7-Dichloro-8-hidroksiekinolien* (diClOxH), *5-Chloro-8-hidroksiekinolien* (5-ClOxH), *5-Chloro-7-iodo-8-hidroksiekinolien* (CliOxH), *5,7-Dimetiel-8-hidroksiekinolien* (diMeOxH), *5-Nitro-8-hidroksiekinolien* (5-NO$_2$OxH), *2-pikoliensuur* (PicH)]. Dit word ook illustreer dat al hierdie strukture die klassieke vierkantige antiprismatiese geometrie, met duidelike koördinasiemultivlakke soos verwag vir die O,O'-skenkende asetielasetoontipe komplekse van sirkonium(IV), vertoon.

Die herbepaling van die strukture [Zr(Trop)$_4$]·DMF en [Zr(DBM)$_4$] [*Tropoloon* (TropH), *Dibensoielmetaan* (DBM)] m.b.v. enkelkristal X-straaldiffraksie is ook ingesluit en verder in detail bespreek. In hierdie voorbeelde word dit geillustreer dat sirkonium(IV) komplekse 'n natuurlike neiging toon om by voorkeur die *tetrakis*- of agt-gekoördineerde produkte, met 'n vierkantige antiprismatiese chelering omgewing rondom die metaal-sentrum in die meeste

gevalle, te vorm. Dit is gevolglik voorlopig hieruit geformuleer dat die sirkonium(IV) metaalsenter se finale geometrie tot 'n groter mate deur intermolekulêre kragte as dié van ligande se interne eienskappe is en dus hoofsaaklik deur die metaalsentrum beheer word.

Die ondersoek het ook 'n oplossing kinetiese studie (m.b.v. UV/Vis absorbansie spektroskopie) van die vormingsmeganisme van drie oksienkomplekse soos gesintetiseer en kristallografies gekarakteriseer, ingesluit. Die basiese bevindings vir [Zr(diClOx)$_4$], [Zr(5-ClOx)$_4$] en [Zr(diMeOx)$_4$] (van ZrCl$_4$ as reaktant) toon goeie ooreenstemming met dié van die [Zr(ox)$_4$] komplekse soos geëvalueer in die voorlopige M.Sc. studie. Die inkomende ligande is gekies om 'n sistematiese reeks van toenemende elektronskenkervermoë te verteenwoordig deur van beide chloor- en metielsubstituente op die oksienruggraat gebruik te maak. In alle gevalle is dieselfde algemene ingewikkelde proses van bidentate ligand koördinasie waargeneem. Hierdie proses behels 'n vinnige aanvanklike reaksie, gevolg deur drie multi-fase reaksiestappe waarin dit aanvaar word dat die chloridoligand stapsgewys gesubstitueer word as HCl (H$^+$ uit oxH) in die ring-sluiting stap in elk van die vier prosesse. In geheel strek die reaksies ongeveer oor 'n vyf ordegrootte reeks, wat dui op 'n betekenisvolle verandering in al vier die chloridoligande wat wat verplaas word om die ooreenstemmende tetrakis-oksienkomplekse te vorm. In die geval van die eerste stap is daar 'n toename van meer as 30 keer gevind, in ooreenstemming met die toename in elektrondoneervermoë van die inkomende ligand. Daarteenoor toon die daaropvolgende drie reaksies 'n afname van een ordegrootte in substitusietempo vir die ooreenstemmende reaksies.

Ewewig onderdrukkingstudies is ook uitgevoer deur middel van stapsgewyse verhoging van die konsentrasie van die verlatende ligand, in hierdie geval Cl$^-$, deur die byvoeging van 'n toeskouer organiese sout, PPh$_4^+$Cl$^-$. Die resultate in hierdie geval toon dat al vier reaksiestappe vir al drie sirkonium(IV) komplekse beduidend beïnvloed en onderdruk word deur die ewewig manipulasieproses.

Die doktorale studie het ook teoretiese optimisering van twee verskillende families van sirkonium(IV)komplekse, deur middel van berekeningschemie, uitgevoer en die gevolglike resultate geëvalueer deur met die strukturele data vanaf die enkelkristal diffraksiestudies, te vergelyk. Twee reekse komplekse is ondersoek en geoptimiseer, nl. die *tetrakis*(asetielasetonato-κ^2O,O')sirkonium(IV)- en die tetrakis(oksien-κ^2N,O)sirkonium(IV) tipe, is elk gekies om die O,O- en N,O-koördinasie omgewings van die metaal poliheders te verteenwoordig.

'n Redelike goeie korrelasie is verkry tussen die kristalstruktuurstudies van die [Zr(Acac)$_4$] tipe komplekse, d.w.s. [Zr(acac)$_4$], [Zr(hFacac)$_4$] en [Zr(DBM)$_4$], met hul geoptimiseerde eweknië. Vir [Zr(acac)$_4$] egter, is 'n ander koördinasie-isomeer teoreties verkry. Hierdie waarneming kan toegeskryf word aan die feit dat teoretiese optimisering van molekulêre strukture in 'n gasfase omgewing verkry word, sonder inter-of intramolekulêre kragte wat roosterstabilisering/pakking beheer of beïnvloed. Hierdie waarneming dui aan dat sirkonium(IV)komplekse in die vaste toestand 'n meer beduidende invloed ervaar van hierdie eksterne interaksies.

Ten slotte, die optimisering van die drie sirkonium(IV) oksien komplekse, [Zr(ox)$_4$], [Zr(diMeOx)$_4$] en [Zr(diClOx)$_4$], is gedoen om te bepaal of dit vir hierdie ligande, met 'n meer stewige raam- en kristalpakkingplasing, ooreenstemmende teoretiese optimisering gedoen kan word. Dit is gevolglik geïllustreer tot 'n aanvaarbare akkuraatheid met 'n goeie korrelasie tussen kristallografiese gekarakteriseerde strukture en hul teoreties berekende eweknieë.

Sleutel woorde: *Sirkonium; N- en O-donorligande; sintese; kristallografiese karakterisering; kinetiese meganistiese studie, teoretiese optimisering.*

Appendix A

Supplementary Crystallographic Data

A.1. [Zr(diClOx)₄]·2DMF – § 4.2

Table A.1.1 Fractional atomic coordinates and isotropic or equivalent isotropic displacement parameters (Å^2) for [Zr(diClOx)$_4$]·2DMF.

	x	*y*	*z*	$U_{iso}*/U_{eq}$	*Occ. (<1)*
Zr01	0.882118 (9)	0.30434 (2)	0.486591 (10)	0.01945 (7)	
Cl02	0.99114 (3)	0.54916 (7)	0.65010 (3)	0.03764 (18)	
Cl08	1.02465 (3)	0.24999 (7)	0.44255 (4)	0.03864 (19)	
Cl05	0.72831 (3)	0.01637 (7)	0.22667 (3)	0.0412 (2)	
Cl06	0.77624 (3)	−0.01050 (7)	0.45093 (3)	0.0435 (2)	
Cl07	1.09534 (3)	−0.04033 (6)	0.60716 (4)	0.03833 (19)	
Cl04	0.72625 (3)	0.52899 (7)	0.42030 (4)	0.0442 (2)	
Cl01	0.87543 (3)	0.45185 (9)	0.74658 (4)	0.0526 (3)	
Cl03	0.82366 (3)	0.81099 (6)	0.36295 (5)	0.0506 (2)	
O01	0.92653 (7)	0.39597 (15)	0.55924 (8)	0.0244 (4)	
O04	0.94415 (7)	0.27077 (15)	0.47576 (8)	0.0232 (4)	
O03	0.83566 (7)	0.17677 (15)	0.46234 (8)	0.0248 (4)	
N02	0.89929 (8)	0.45787 (17)	0.44785 (9)	0.0206 (4)	
N03	0.84624 (8)	0.27202 (17)	0.38166 (9)	0.0211 (4)	
N04	0.93379 (9)	0.16689 (18)	0.55426 (10)	0.0246 (5)	
O02	0.81953 (7)	0.40289 (15)	0.45531 (8)	0.0250 (4)	
C13	0.86444 (10)	0.6254 (2)	0.40782 (12)	0.0265 (6)	
C22	0.78981 (10)	0.1528 (2)	0.30729 (11)	0.0228 (5)	
C01	0.81301 (10)	0.2383 (2)	0.55215 (12)	0.0256 (6)	
H01	0.7962	0.1949	0.5208	0.031*	
C31	1.01008 (11)	0.0673 (2)	0.58004 (12)	0.0267 (6)	

C29	0.96082 (13)	0.0356 (2)	0.62711 (15)	0.0382 (7)
H29	0.955	0.0005	0.6541	0.046*
C25	0.78089 (11)	0.0533 (2)	0.39612 (12)	0.0264 (6)
C35	0.97867 (10)	0.2015 (2)	0.50422 (11)	0.0229 (5)
C07	0.94232 (11)	0.4768 (2)	0.64791 (13)	0.0302 (6)
C33	1.05461 (11)	0.1059 (2)	0.52663 (13)	0.0305 (6)
H33	1.0814	0.0939	0.5195	0.037*
C11	0.94629 (11)	0.5774 (2)	0.42341 (12)	0.0273 (6)
H11	0.9756	0.5917	0.4218	0.033*
C10	0.94025 (10)	0.4826 (2)	0.44472 (12)	0.0244 (6)
H10	0.9662	0.4351	0.4572	0.029*
C08	0.91675 (10)	0.4104 (2)	0.60216 (11)	0.0236 (5)
N01	0.85143 (8)	0.29190 (18)	0.55578 (9)	0.0221 (5)
C18	0.86134 (10)	0.5276 (2)	0.42959 (11)	0.0219 (5)
O05	0.82431 (12)	0.6911 (3)	0.66107 (12)	0.0622 (9)
C27	0.81434 (9)	0.1899 (2)	0.36457 (11)	0.0195 (5)
C19	0.85475 (11)	0.3165 (2)	0.34182 (12)	0.0258 (6)
H19	0.8768	0.3716	0.3528	0.031*
C32	1.05037 (11)	0.0514 (2)	0.56792 (13)	0.0297 (6)
N05	0.85660 (14)	0.7125 (4)	0.60020 (18)	0.0750 (13)
C26	0.81010 (10)	0.1398 (2)	0.40983 (11)	0.0219 (5)
C34	1.01855 (11)	0.1805 (2)	0.49460 (12)	0.0266 (6)
C28	0.92730 (12)	0.1126 (2)	0.59270 (13)	0.0319 (6)
H28	0.8993	0.126	0.5972	0.038*
C05	0.89063 (11)	0.4348 (3)	0.69134 (13)	0.0344 (7)
C04	0.86212 (10)	0.3656 (2)	0.64594 (12)	0.0275 (6)
C14	0.82258 (12)	0.6904 (2)	0.39053 (13)	0.0327 (7)
C23	0.75946 (11)	0.0648 (2)	0.29647 (12)	0.0263 (6)
C20	0.83229 (12)	0.2848 (2)	0.28429 (12)	0.0305 (6)
H20	0.8396	0.3184	0.2581	0.037*
C02	0.79647 (10)	0.2443 (2)	0.59363 (12)	0.0278 (6)
H02	0.769	0.2061	0.5893	0.033*
C36	0.97464 (10)	0.1439 (2)	0.54742 (11)	0.0231 (5)
C12	0.90873 (11)	0.6481 (2)	0.40509 (13)	0.0298 (6)
H12	0.9123	0.711	0.3908	0.036*
C24	0.75476 (11)	0.0155 (2)	0.33929 (12)	0.0270 (6)
H24	0.7346	−0.0424	0.3311	0.032*
C06	0.92947 (11)	0.4890 (3)	0.69209 (13)	0.0358 (7)
H06	0.9475	0.5344	0.7221	0.043*
C03	0.82106 (11)	0.3068 (3)	0.64028 (13)	0.0331 (6)
H03	0.8108	0.3105	0.6683	0.04*
C16	0.77919 (11)	0.5632 (2)	0.41552 (12)	0.0294 (6)
C15	0.78131 (12)	0.6606 (2)	0.39459 (13)	0.0329 (7)
H15	0.7544	0.7053	0.3834	0.04*
C21	0.79956 (11)	0.2045 (2)	0.26676 (12)	0.0282 (6)
H21	0.7838	0.1839	0.2284	0.034*
C17	0.81860 (10)	0.4944 (2)	0.43388 (11)	0.0244 (6)
C30	1.00175 (12)	0.0127 (2)	0.62073 (14)	0.0335 (7)
H30	1.0239	−0.0383	0.643	0.04*

C09	0.87599 (10)	0.3552 (2)	0.60199 (11)	0.0227 (5)	
C39	0.8558 (3)	0.6574 (7)	0.5495 (3)	0.1196 (18)	
H39A	0.8751	0.6955	0.5358	0.179*	
H39B	0.8219	0.6515	0.5193	0.179*	
H39C	0.87	0.5902	0.5613	0.179*	
C42	0.9391 (3)	0.1164 (6)	0.7274 (3)	0.0331 (6)	0.475(6)
H42	0.9697	0.1154	0.7274	0.04*	0.475(6)
N06	0.9289 (4)	0.1857 (10)	0.7638 (4)	0.078 (4)	0.475(6)
C41	0.8875 (3)	0.1745 (7)	0.7742 (4)	0.053 (2)	0.475(6)
H41A	0.8641	0.1267	0.7471	0.08*	0.475(6)
H41B	0.8715	0.2397	0.77	0.08*	0.475(6)
H41C	0.8989	0.1493	0.8126	0.08*	0.475(6)
C40	0.9672 (3)	0.2595 (7)	0.8010 (4)	0.058 (2)	0.475(6)
H40A	0.9931	0.2633	0.79	0.087*	0.475(6)
H40B	0.9813	0.2375	0.8403	0.087*	0.475(6)
H40C	0.9522	0.3259	0.7969	0.087*	0.475(6)
O06	0.9051 (4)	0.0602 (13)	0.6972 (5)	0.214 (10)	0.475(6)
N07	0.8821 (4)	0.0778 (8)	0.7442 (3)	0.096 (3)	0.525(6)
C45	0.8865 (5)	−0.0244 (8)	0.7307 (4)	0.096 (3)	0.525(6)
H45A	0.8595	−0.064	0.7298	0.145*	0.525(6)
H45B	0.9179	−0.0519	0.7593	0.145*	0.525(6)
H45C	0.8852	−0.0273	0.6936	0.145*	0.525(6)
C43	0.9145 (7)	0.150 (2)	0.7467 (8)	0.147 (6)	0.525(6)
H43	0.9113	0.2132	0.7612	0.176*	0.525(6)
C44	0.8399 (5)	0.1012 (14)	0.7493 (6)	0.147 (6)	0.525(6)
H44A	0.8209	0.0399	0.7449	0.22*	0.525(6)
H44B	0.8197	0.1497	0.7201	0.22*	0.525(6)
H44C	0.8498	0.1304	0.7866	0.22*	0.525(6)
O07	0.9458 (8)	0.1454 (16)	0.7334 (8)	0.247 (10)	0.525(6)
C37	0.83135 (19)	0.6665 (5)	0.6224 (2)	0.0430 (17)	0.687(12)
H37	0.8166	0.6048	0.6049	0.052*	0.687(12)
C37B	0.8450 (4)	0.7340 (10)	0.6522 (5)	0.050 (4)	0.313(12)
H37B	0.8592	0.7915	0.675	0.06*	0.313(12)
C38	0.8863 (3)	0.8042 (6)	0.6151 (3)	0.1196 (18)	
H38A	0.8852	0.837	0.6471	0.179*	
H38B	0.8732	0.8499	0.5827	0.179*	
H38C	0.9203	0.7869	0.6254	0.179*	

Table A.1.2 Atomic displacement parameters (Å^2) for [Zr(diClOx)$_4$]·2DMF.

	U^{11}	U^{22}	U^{33}	U^{12}	U^{13}	U^{23}
Zr01	0.01698 (12)	0.02267 (13)	0.01735 (12)	0.00132 (10)	0.00705 (9)	0.00143 (9)
Cl02	0.0319 (4)	0.0485 (5)	0.0280 (4)	−0.0140 (3)	0.0106 (3)	−0.0077 (3)
Cl08	0.0357 (4)	0.0452 (5)	0.0452 (4)	0.0108 (3)	0.0275 (4)	0.0109 (4)
Cl05	0.0535 (5)	0.0435 (4)	0.0235 (4)	−0.0197 (4)	0.0158 (3)	−0.0098 (3)
Cl06	0.0538 (5)	0.0518 (5)	0.0280 (4)	−0.0263 (4)	0.0219 (4)	−0.0029 (3)
Cl07	0.0281 (4)	0.0283 (4)	0.0436 (4)	0.0108 (3)	0.0048 (3)	0.0009 (3)
Cl04	0.0318 (4)	0.0565 (5)	0.0519 (5)	0.0188 (4)	0.0262 (4)	0.0193 (4)

Cl01	0.0367 (4)	0.0931 (8)	0.0346 (4)	−0.0161 (5)	0.0222 (4)	−0.0299 (5)
Cl03	0.0391 (4)	0.0263 (4)	0.0697 (6)	0.0068 (3)	0.0122 (4)	0.0150 (4)
O01	0.0215 (9)	0.0304 (10)	0.0203 (9)	−0.0021 (8)	0.0092 (8)	−0.0014 (8)
O04	0.0216 (9)	0.0250 (10)	0.0223 (9)	0.0049 (8)	0.0097 (8)	0.0043 (7)
O03	0.0250 (10)	0.0317 (11)	0.0178 (9)	−0.0055 (8)	0.0102 (8)	−0.0019 (8)
N02	0.0192 (10)	0.0211 (11)	0.0177 (10)	0.0011 (9)	0.0058 (8)	−0.0018 (8)
N03	0.0199 (11)	0.0212 (11)	0.0199 (11)	0.0029 (9)	0.0076 (9)	0.0023 (9)
N04	0.0229 (11)	0.0242 (12)	0.0243 (12)	0.0002 (9)	0.0090 (9)	0.0002 (9)
O02	0.0210 (9)	0.0291 (10)	0.0242 (10)	0.0035 (8)	0.0102 (8)	0.0029 (8)
C13	0.0258 (14)	0.0216 (13)	0.0235 (13)	0.0003 (11)	0.0047 (11)	−0.0019 (11)
C22	0.0212 (13)	0.0241 (13)	0.0208 (13)	0.0040 (11)	0.0080 (10)	0.0011 (10)
C01	0.0210 (13)	0.0335 (15)	0.0216 (13)	0.0014 (11)	0.0095 (11)	−0.0011 (11)
C31	0.0265 (14)	0.0213 (13)	0.0241 (13)	0.0014 (11)	0.0055 (11)	−0.0021 (11)
C29	0.049 (2)	0.0268 (15)	0.0415 (18)	0.0040 (14)	0.0236 (16)	0.0100 (13)
C25	0.0251 (14)	0.0327 (15)	0.0224 (13)	−0.0036 (12)	0.0122 (11)	0.0014 (11)
C35	0.0197 (12)	0.0216 (13)	0.0226 (13)	0.0007 (10)	0.0062 (10)	−0.0012 (10)
C07	0.0226 (14)	0.0375 (16)	0.0255 (14)	−0.0027 (12)	0.0073 (12)	−0.0019 (12)
C33	0.0196 (13)	0.0311 (16)	0.0368 (16)	0.0041 (11)	0.0101 (12)	−0.0057 (13)
C11	0.0250 (14)	0.0275 (14)	0.0253 (14)	−0.0059 (11)	0.0085 (11)	−0.0016 (11)
C10	0.0208 (13)	0.0255 (14)	0.0225 (13)	0.0005 (11)	0.0066 (11)	−0.0008 (10)
C08	0.0194 (12)	0.0280 (14)	0.0196 (13)	0.0029 (11)	0.0063 (10)	0.0016 (10)
N01	0.0194 (10)	0.0259 (12)	0.0196 (11)	0.0019 (9)	0.0081 (9)	−0.0001 (9)
C18	0.0218 (13)	0.0220 (13)	0.0165 (12)	0.0008 (10)	0.0046 (10)	−0.0021 (10)
O05	0.0601 (19)	0.099 (3)	0.0382 (15)	0.0208 (18)	0.0317 (14)	0.0098 (15)
C27	0.0160 (11)	0.0217 (12)	0.0187 (12)	0.0045 (10)	0.0065 (10)	0.0005 (10)
C19	0.0289 (14)	0.0247 (14)	0.0220 (13)	−0.0030 (11)	0.0106 (11)	0.0014 (11)
C32	0.0232 (14)	0.0214 (14)	0.0334 (15)	0.0055 (11)	0.0044 (12)	−0.0040 (11)
N05	0.044 (2)	0.123 (4)	0.068 (2)	0.000 (2)	0.0355 (19)	0.038 (2)
C26	0.0174 (12)	0.0281 (14)	0.0198 (12)	0.0020 (10)	0.0085 (10)	−0.0003 (10)
C34	0.0244 (13)	0.0270 (14)	0.0279 (14)	0.0018 (11)	0.0120 (12)	−0.0001 (11)
C28	0.0353 (16)	0.0279 (15)	0.0352 (16)	0.0024 (13)	0.0188 (14)	0.0056 (12)
C05	0.0242 (14)	0.055 (2)	0.0219 (14)	0.0013 (14)	0.0095 (12)	−0.0085 (13)
C04	0.0201 (13)	0.0393 (16)	0.0210 (13)	0.0041 (12)	0.0081 (11)	−0.0022 (12)
C14	0.0315 (15)	0.0257 (15)	0.0301 (15)	0.0053 (12)	0.0059 (13)	0.0021 (12)
C23	0.0268 (14)	0.0275 (14)	0.0207 (13)	−0.0005 (11)	0.0082 (11)	−0.0038 (11)
C20	0.0390 (17)	0.0296 (15)	0.0220 (14)	−0.0017 (13)	0.0138 (12)	0.0045 (11)
C02	0.0209 (13)	0.0362 (16)	0.0287 (14)	−0.0003 (12)	0.0138 (12)	−0.0001 (12)
C36	0.0200 (12)	0.0204 (13)	0.0231 (13)	0.0001 (10)	0.0055 (10)	−0.0022 (10)
C12	0.0313 (15)	0.0221 (14)	0.0286 (15)	−0.0057 (12)	0.0081 (12)	−0.0009 (11)
C24	0.0244 (14)	0.0290 (15)	0.0267 (14)	−0.0065 (11)	0.0115 (12)	−0.0030 (11)
C06	0.0276 (15)	0.049 (2)	0.0242 (15)	−0.0050 (14)	0.0070 (12)	−0.0129 (13)
C03	0.0295 (14)	0.0460 (17)	0.0293 (14)	0.0025 (12)	0.0183 (12)	−0.0024 (12)
C16	0.0227 (14)	0.0391 (17)	0.0245 (14)	0.0075 (12)	0.0096 (11)	0.0017 (12)
C15	0.0298 (15)	0.0348 (16)	0.0278 (15)	0.0145 (13)	0.0085 (12)	0.0017 (12)
C21	0.0343 (15)	0.0293 (15)	0.0168 (12)	0.0000 (12)	0.0087 (11)	0.0004 (11)
C17	0.0236 (13)	0.0280 (14)	0.0188 (13)	0.0054 (11)	0.0078 (11)	−0.0006 (10)
C30	0.0361 (16)	0.0229 (14)	0.0337 (16)	0.0059 (12)	0.0103 (13)	0.0053 (12)
C09	0.0193 (12)	0.0277 (14)	0.0173 (12)	0.0047 (11)	0.0055 (10)	0.0007 (10)
C39	0.099 (4)	0.153 (5)	0.108 (4)	−0.013 (3)	0.050 (3)	−0.038 (3)

Atoms					
C42	0.0295 (14)	0.0460 (17)	0.0293 (14)	0.0025 (12)	0.0183 (12)	−0.0024 (12)
N06	0.055 (6)	0.136 (10)	0.042 (5)	0.040 (6)	0.022 (4)	0.009 (5)
C41	0.068 (6)	0.051 (5)	0.039 (4)	0.015 (4)	0.024 (4)	0.009 (4)
C40	0.053 (5)	0.061 (6)	0.047 (5)	0.015 (4)	0.014 (4)	0.008 (4)
O06	0.125 (9)	0.42 (2)	0.170 (11)	−0.159 (12)	0.128 (9)	−0.208 (14)
N07	0.090 (5)	0.148 (8)	0.053 (4)	0.004 (6)	0.035 (4)	−0.001 (4)
C45	0.090 (5)	0.148 (8)	0.053 (4)	0.004 (6)	0.035 (4)	−0.001 (4)
C43	0.094 (8)	0.224 (15)	0.138 (10)	0.056 (9)	0.069 (8)	0.129 (11)
C44	0.094 (8)	0.224 (15)	0.138 (10)	0.056 (9)	0.069 (8)	0.129 (11)
O07	0.261 (19)	0.27 (2)	0.230 (19)	−0.102 (17)	0.136 (16)	−0.167 (17)
C37	0.035 (3)	0.062 (4)	0.037 (3)	−0.006 (2)	0.021 (2)	−0.006 (3)
C37B	0.022 (6)	0.047 (8)	0.063 (9)	−0.009 (5)	0.006 (5)	0.013 (7)
C38	0.099 (4)	0.153 (5)	0.108 (4)	−0.013 (3)	0.050 (3)	−0.038 (3)

Table A.1.3 Bond lengths (Å) for [Zr(diClOx)₄]·2DMF.

Atoms	Bond length (Å)	Atoms	Bond length (Å)
Zr01—O03	2.075 (2)	O05—C37	1.183 (6)
Zr01—O04	2.0808 (19)	C27—C26	1.420 (4)
Zr01—O02	2.1102 (19)	C19—C20	1.399 (4)
Zr01—O01	2.1132 (19)	C19—H19	0.93
Zr01—N02	2.414 (2)	N05—C37	1.310 (6)
Zr01—N01	2.417 (2)	N05—C38	1.434 (8)
Zr01—N03	2.483 (2)	N05—C39	1.508 (8)
Zr01—N04	2.490 (2)	N05—C37B	1.595 (12)
Cl02—C07	1.735 (3)	C28—H28	0.93
Cl08—C34	1.727 (3)	C05—C06	1.366 (5)
Cl05—C23	1.741 (3)	C05—C04	1.419 (4)
Cl06—C25	1.731 (3)	C04—C03	1.410 (4)
Cl07—C32	1.738 (3)	C04—C09	1.416 (4)
Cl04—C16	1.729 (3)	C14—C15	1.364 (5)
Cl01—C05	1.739 (3)	C23—C24	1.365 (4)
Cl03—C14	1.739 (3)	C20—C21	1.365 (4)
O01—C08	1.313 (3)	C20—H20	0.93
O04—C35	1.315 (3)	C02—C03	1.365 (4)
O03—C26	1.317 (3)	C02—H02	0.93
N02—C10	1.325 (4)	C12—H12	0.93
N02—C18	1.363 (3)	C24—H24	0.93
N03—C19	1.329 (3)	C06—H06	0.93
N03—C27	1.368 (3)	C03—H03	0.93
N04—C28	1.326 (4)	C16—C17	1.386 (4)
N04—C36	1.369 (4)	C16—C15	1.399 (5)
O02—C17	1.314 (3)	C15—H15	0.93
C13—C14	1.411 (4)	C21—H21	0.93
C13—C12	1.411 (4)	C30—H30	0.93
C13—C18	1.420 (4)	C39—H39A	0.96
C22—C21	1.409 (4)	C39—H39B	0.96
C22—C23	1.414 (4)	C39—H39C	0.96

Atoms	Bond length	Atoms	Bond length
C22—C27	1.416 (4)	C42—O06	1.207 (5)
C01—N01	1.323 (4)	C42—N06	1.453 (13)
C01—C02	1.406 (4)	C42—H42	0.93
C01—H01	0.93	N06—C41	1.418 (13)
C31—C30	1.407 (4)	N06—C40	1.467 (12)
C31—C32	1.419 (4)	C41—H41A	0.96
C31—C36	1.420 (4)	C41—H41B	0.96
C29—C30	1.364 (5)	C41—H41C	0.96
C29—C28	1.411 (4)	C40—H40A	0.96
C29—H29	0.93	C40—H40B	0.96
C25—C26	1.373 (4)	C40—H40C	0.96
C25—C24	1.411 (4)	N07—C43	1.34 (2)
C35—C34	1.377 (4)	N07—C44	1.386 (12)
C35—C36	1.418 (4)	N07—C45	1.402 (2)
C07—C08	1.385 (4)	C45—H45A	0.96
C07—C06	1.403 (4)	C45—H45B	0.96
C33—C32	1.357 (5)	C45—H45C	0.96
C33—C34	1.407 (4)	C43—O07	1.16 (3)
C33—H33	0.93	C43—H43	0.93
C11—C12	1.364 (4)	C44—H44A	0.96
C11—C10	1.405 (4)	C44—H44B	0.96
C11—H11	0.93	C44—H44C	0.96
C10—H10	0.93	C37—H37	0.93
C08—C09	1.430 (4)	C37B—H37B	0.93
N01—C09	1.364 (3)	C38—H38A	0.96
C18—C17	1.422 (4)	C38—H38B	0.96
O05—C37B	0.949 (10)	C38—H38C	0.96

Table A.1.4 Bond angles (°) for [Zr(diClOx)$_4$]·2DMF.

Atoms	Bond angle (°)	Atoms	Bond angle (°)
O03—Zr01—O04	108.41 (8)	C29—C28—H28	118.4
O03—Zr01—O02	90.77 (8)	C06—C05—C04	121.1 (3)
O04—Zr01—O02	141.24 (7)	C06—C05—Cl01	119.5 (2)
O03—Zr01—O01	141.28 (7)	C04—C05—Cl01	119.4 (2)
O04—Zr01—O01	90.82 (7)	C03—C04—C09	116.9 (3)
O02—Zr01—O01	94.52 (8)	C03—C04—C05	126.1 (3)
O03—Zr01—N02	141.77 (7)	C09—C04—C05	116.9 (3)
O04—Zr01—N02	74.03 (8)	C15—C14—C13	121.6 (3)
O02—Zr01—N02	70.42 (8)	C15—C14—Cl03	119.4 (2)
O01—Zr01—N02	75.07 (8)	C13—C14—Cl03	119.0 (2)
O03—Zr01—N01	74.33 (8)	C24—C23—C22	122.0 (3)
O04—Zr01—N01	142.00 (7)	C24—C23—Cl05	119.1 (2)
O02—Zr01—N01	74.81 (7)	C22—C23—Cl05	118.9 (2)
O01—Zr01—N01	70.21 (7)	C21—C20—C19	119.7 (3)
N02—Zr01—N01	127.84 (8)	C21—C20—H20	120.1
O03—Zr01—N03	69.28 (7)	C19—C20—H20	120.1
O04—Zr01—N03	75.98 (7)	C03—C02—C01	119.4 (3)

O02—Zr01—N03	80.23 (7)	C03—C02—H02	120.3
O01—Zr01—N03	149.38 (7)	C01—C02—H02	120.3
N02—Zr01—N03	74.76 (7)	N04—C36—C35	114.8 (2)
N01—Zr01—N03	135.11 (7)	N04—C36—C31	123.2 (3)
O03—Zr01—N04	75.46 (8)	C35—C36—C31	122.0 (3)
O04—Zr01—N04	69.15 (8)	C11—C12—C13	119.8 (3)
O02—Zr01—N04	149.58 (8)	C11—C12—H12	120.1
O01—Zr01—N04	80.96 (8)	C13—C12—H12	120.1
N02—Zr01—N04	135.32 (8)	C23—C24—C25	119.2 (3)
N01—Zr01—N04	75.38 (8)	C23—C24—H24	120.4
N03—Zr01—N04	118.09 (8)	C25—C24—H24	120.4
C08—O01—Zr01	123.71 (17)	C05—C06—C07	120.5 (3)
C35—O04—Zr01	126.41 (17)	C05—C06—H06	119.7
C26—O03—Zr01	126.34 (17)	C07—C06—H06	119.7
C10—N02—C18	118.5 (2)	C02—C03—C04	119.8 (3)
C10—N02—Zr01	128.76 (18)	C02—C03—H03	120.1
C18—N02—Zr01	112.72 (17)	C04—C03—H03	120.1
C19—N03—C27	117.0 (2)	C17—C16—C15	122.1 (3)
C19—N03—Zr01	131.38 (18)	C17—C16—Cl04	119.1 (2)
C27—N03—Zr01	111.56 (16)	C15—C16—Cl04	118.8 (2)
C28—N04—C36	117.2 (2)	C14—C15—C16	120.4 (3)
C28—N04—Zr01	131.4 (2)	C14—C15—H15	119.8
C36—N04—Zr01	111.40 (17)	C16—C15—H15	119.8
C17—O02—Zr01	123.52 (17)	C20—C21—C22	119.4 (3)
C14—C13—C12	126.2 (3)	C20—C21—H21	120.3
C14—C13—C18	116.6 (3)	C22—C21—H21	120.3
C12—C13—C18	117.2 (3)	O02—C17—C16	125.2 (3)
C21—C22—C23	125.9 (3)	O02—C17—C18	118.5 (2)
C21—C22—C27	117.0 (3)	C16—C17—C18	116.4 (3)
C23—C22—C27	117.1 (2)	C29—C30—C31	119.2 (3)
N01—C01—C02	122.9 (3)	C29—C30—H30	120.4
N01—C01—H01	118.6	C31—C30—H30	120.4
C02—C01—H01	118.6	N01—C09—C04	122.8 (3)
C30—C31—C32	125.8 (3)	N01—C09—C08	114.3 (2)
C30—C31—C36	117.3 (3)	C04—C09—C08	122.9 (3)
C32—C31—C36	116.9 (3)	N05—C39—H39A	109.5
C30—C29—C28	119.8 (3)	N05—C39—H39B	109.5
C30—C29—H29	120.1	H39A—C39—H39B	109.5
C28—C29—H29	120.1	N05—C39—H39C	109.5
C26—C25—C24	122.3 (3)	H39A—C39—H39C	109.5
C26—C25—Cl06	118.2 (2)	H39B—C39—H39C	109.5
C24—C25—Cl06	119.5 (2)	O06—C42—N06	115.6 (8)
O04—C35—C34	124.3 (3)	O06—C42—H42	122.2
O04—C35—C36	118.2 (2)	N06—C42—H42	122.2
C34—C35—C36	117.5 (2)	C41—N06—C42	123.3 (9)
C08—C07—C06	122.2 (3)	C41—N06—C40	115.5 (9)
C08—C07—Cl02	119.0 (2)	C42—N06—C40	120.1 (9)
C06—C07—Cl02	118.7 (2)	N06—C41—H41A	109.5
C32—C33—C34	120.1 (3)	N06—C41—H41B	109.5

C32—C33—H33	120	H41A—C41—H41B	109.5
C34—C33—H33	120	N06—C41—H41C	109.5
C12—C11—C10	119.4 (3)	H41A—C41—H41C	109.5
C12—C11—H11	120.3	H41B—C41—H41C	109.5
C10—C11—H11	120.3	N06—C40—H40A	109.5
N02—C10—C11	122.9 (3)	N06—C40—H40B	109.5
N02—C10—H10	118.5	H40A—C40—H40B	109.5
C11—C10—H10	118.5	N06—C40—H40C	109.5
O01—C08—C07	125.3 (3)	H40A—C40—H40C	109.5
O01—C08—C09	118.4 (2)	H40B—C40—H40C	109.5
C07—C08—C09	116.3 (3)	C43—N07—C44	122.0 (16)
C01—N01—C09	118.2 (2)	C43—N07—C45	121.7 (15)
C01—N01—Zr01	128.56 (18)	C44—N07—C45	116.0 (13)
C09—N01—Zr01	113.05 (17)	N07—C45—H45A	109.5
N02—C18—C13	122.3 (3)	N07—C45—H45B	109.5
N02—C18—C17	114.7 (2)	H45A—C45—H45B	109.5
C13—C18—C17	123.0 (2)	N07—C45—H45C	109.5
C37B—O05—C37	62.2 (9)	H45A—C45—H45C	109.5
N03—C27—C22	123.4 (2)	H45B—C45—H45C	109.5
N03—C27—C26	114.6 (2)	O07—C43—N07	129 (3)
C22—C27—C26	121.9 (2)	O07—C43—H43	115.4
N03—C19—C20	123.5 (3)	N07—C43—H43	115.3
N03—C19—H19	118.2	N07—C44—H44A	109.5
C20—C19—H19	118.2	N07—C44—H44B	109.5
C33—C32—C31	121.7 (3)	H44A—C44—H44B	109.5
C33—C32—Cl07	119.4 (2)	N07—C44—H44C	109.5
C31—C32—Cl07	118.9 (2)	H44A—C44—H44C	109.5
C37—N05—C38	133.2 (5)	H44B—C44—H44C	109.5
C37—N05—C39	114.3 (5)	O05—C37—N05	130.2 (6)
C38—N05—C39	112.5 (5)	O05—C37—H37	114.9
C37—N05—C37B	44.0 (5)	N05—C37—H37	114.9
C38—N05—C37B	89.2 (6)	O05—C37B—N05	123.5 (12)
C39—N05—C37B	158.3 (6)	O05—C37B—H37B	118.3
O03—C26—C25	124.2 (2)	N05—C37B—H37B	118.3
O03—C26—C27	118.2 (2)	N05—C38—H38A	109.5
C25—C26—C27	117.5 (2)	N05—C38—H38B	109.5
C35—C34—C33	121.9 (3)	H38A—C38—H38B	109.5
C35—C34—Cl08	118.6 (2)	N05—C38—H38C	109.5
C33—C34—Cl08	119.6 (2)	H38A—C38—H38C	109.5
N04—C28—C29	123.3 (3)	H38B—C38—H38C	109.5
N04—C28—H28	118.4		

A.2. [Zr(5-ClOx)₄]·2DMF – § 4.3

Table A.2.5 Fractional atomic coordinates and isotropic or equivalent isotropic displacement parameters (Å^2) for [Zr(5-ClClOx)₄]·2DMF.

	x	*y*	*z*	$U_{iso}*/U_{eq}$	*Occ. (<1)*
C01	0.7436 (3)	0.6406 (3)	0.1078 (3)	0.0439 (13)	
H01	0.7635	0.6102	0.0803	0.053*	
C02	0.7497 (3)	0.7045 (3)	0.0899 (3)	0.0479 (14)	
H02	0.7743	0.7159	0.052	0.058*	
C03	0.7190 (3)	0.7498 (3)	0.1289 (3)	0.0498 (15)	
H03	0.7216	0.7921	0.1169	0.06*	
C04	0.6840 (3)	0.7321 (3)	0.1866 (3)	0.0478 (15)	
C05	0.6487 (3)	0.7727 (3)	0.2330 (4)	0.0553 (17)	
C06	0.6183 (4)	0.7501 (3)	0.2882 (4)	0.0625 (19)	
H06	0.5963	0.7781	0.3171	0.075*	
C07	0.6188 (3)	0.6861 (3)	0.3031 (3)	0.0583 (17)	
H07	0.5977	0.6718	0.3419	0.07*	
C08	0.6506 (3)	0.6433 (3)	0.2606 (3)	0.0484 (14)	
C09	0.6820 (3)	0.6667 (3)	0.2028 (3)	0.0437 (13)	
C10	0.7050 (4)	0.4500 (4)	0.3553 (3)	0.0602 (18)	
H10	0.6557	0.4444	0.3529	0.072*	
C11	0.7431 (4)	0.4298 (4)	0.4123 (3)	0.074 (2)	
H11	0.7184	0.4101	0.4463	0.089*	
C12	0.8156 (4)	0.4385 (4)	0.4189 (3)	0.070 (2)	
H12	0.84	0.4262	0.4574	0.084*	
C13	0.8523 (4)	0.4664 (3)	0.3660 (3)	0.0504 (15)	
C14	0.9271 (4)	0.4772 (3)	0.3635 (3)	0.0513 (15)	
C15	0.9578 (3)	0.5031 (3)	0.3091 (3)	0.0455 (14)	
H15	1.007	0.5097	0.3091	0.055*	
C16	0.9166 (3)	0.5201 (2)	0.2527 (3)	0.0387 (12)	
H16	0.9387	0.5381	0.2163	0.046*	
C17	0.8436 (3)	0.5102 (2)	0.2516 (3)	0.0366 (12)	
C18	0.8114 (3)	0.4845 (3)	0.3090 (3)	0.0403 (13)	
C19	0.7746 (3)	0.3809 (3)	0.1577 (3)	0.0469 (14)	
H19	0.8105	0.4079	0.1434	0.056*	
C20	0.7832 (4)	0.3155 (3)	0.1483 (4)	0.0606 (19)	
H20	0.8238	0.2999	0.1279	0.073*	
C21	0.7308 (4)	0.2748 (3)	0.1695 (3)	0.0574 (18)	
H21	0.7358	0.2314	0.1637	0.069*	
C22	0.6695 (3)	0.2994 (3)	0.2003 (3)	0.0453 (14)	
C23	0.6108 (4)	0.2643 (3)	0.2249 (3)	0.0520 (15)	
C24	0.5544 (3)	0.2938 (3)	0.2544 (3)	0.0525 (16)	
H24	0.5174	0.2696	0.2713	0.063*	
C25	0.5511 (3)	0.3593 (3)	0.2597 (3)	0.0513 (16)	
H25	0.5122	0.3781	0.2801	0.062*	
C26	0.6053 (3)	0.3966 (3)	0.2348 (3)	0.0423 (13)	
C27	0.6654 (3)	0.3659 (3)	0.2073 (2)	0.0371 (12)	

C28	0.5272 (3)	0.5888 (2)	0.1696 (3)	0.0425 (13)
H28	0.524	0.5918	0.2155	0.051*
C29	0.4732 (3)	0.6165 (3)	0.1293 (3)	0.0497 (15)
H29	0.4356	0.6379	0.1489	0.06*
C30	0.4754 (4)	0.6121 (3)	0.0623 (3)	0.0517 (15)
H30	0.4392	0.6296	0.036	0.062*
C31	0.5335 (3)	0.5804 (3)	0.0330 (3)	0.0447 (13)
C32	0.5442 (3)	0.5729 (3)	−0.0360 (3)	0.0463 (14)
C33	0.6036 (3)	0.5410 (3)	−0.0589 (3)	0.0453 (13)
H33	0.61	0.5369	−0.1044	0.054*
C34	0.6545 (3)	0.5146 (2)	−0.0149 (3)	0.0398 (12)
H34	0.6936	0.4927	−0.0314	0.048*
C35	0.6469 (3)	0.5210 (2)	0.0531 (3)	0.0361 (12)
C36	0.5856 (3)	0.5543 (2)	0.0765 (3)	0.0373 (12)
C37	0.7974 (3)	0.0761 (2)	0.1508 (2)	0.0372 (12)
H37	0.8469	0.0806	0.1535	0.045*
C38	0.7605 (3)	0.1013 (3)	0.0956 (3)	0.0468 (14)
H38	0.7851	0.124	0.0637	0.056*
C39	0.6879 (3)	0.0923 (3)	0.0891 (3)	0.0517 (16)
H39	0.6631	0.1088	0.0526	0.062*
C40	0.6512 (3)	0.0580 (3)	0.1378 (3)	0.0420 (13)
C41	0.5768 (3)	0.0445 (3)	0.1378 (3)	0.0517 (15)
C42	0.5452 (3)	0.0154 (3)	0.1900 (3)	0.0450 (13)
H42	0.4962	0.0075	0.1885	0.054*
C43	0.5861 (3)	−0.0029 (2)	0.2461 (3)	0.0369 (12)
H43	0.5635	−0.0222	0.2816	0.044*
C44	0.6594 (3)	0.0076 (2)	0.2495 (2)	0.0324 (11)
C45	0.6916 (3)	0.0376 (2)	0.1939 (2)	0.0339 (11)
C46	0.7597 (3)	−0.1304 (2)	0.3834 (3)	0.0393 (12)
H46	0.7389	−0.1022	0.4129	0.047*
C47	0.7567 (3)	−0.1955 (3)	0.3973 (3)	0.0469 (14)
H47	0.7335	−0.2098	0.4349	0.056*
C48	0.7878 (3)	−0.2372 (2)	0.3555 (3)	0.0479 (15)
H48	0.787	−0.2801	0.365	0.058*
C49	0.8209 (3)	−0.2155 (2)	0.2985 (3)	0.0390 (13)
C50	0.8554 (3)	−0.2533 (3)	0.2498 (3)	0.0464 (15)
C51	0.8860 (3)	−0.2271 (3)	0.1957 (3)	0.0492 (15)
H51	0.9081	−0.253	0.165	0.059*
C52	0.8848 (3)	−0.1609 (3)	0.1852 (3)	0.0428 (13)
H52	0.9064	−0.1437	0.148	0.051*
C53	0.8516 (3)	−0.1219 (2)	0.2302 (3)	0.0356 (12)
C54	0.8206 (3)	−0.1496 (2)	0.2867 (3)	0.0333 (11)
C55	0.9740 (3)	−0.0774 (2)	0.3252 (3)	0.0356 (11)
H55	0.9774	−0.077	0.2792	0.043*
C56	1.0267 (3)	−0.1094 (3)	0.3629 (3)	0.0434 (13)
H56	1.0637	−0.1303	0.3416	0.052*
C57	1.0240 (3)	−0.1101 (3)	0.4299 (3)	0.0449 (13)
H57	1.0593	−0.1307	0.4546	0.054*
C58	0.9674 (3)	−0.0795 (2)	0.4621 (3)	0.0395 (12)

C59	0.9562 (3)	−0.0772 (3)	0.5314 (3)	0.0449 (14)
C60	0.8980 (3)	−0.0460 (3)	0.5572 (3)	0.0456 (14)
H60	0.8916	−0.0452	0.6029	0.055*
C61	0.8480 (3)	−0.0151 (3)	0.5150 (3)	0.0393 (12)
H61	0.8095	0.0063	0.5333	0.047*
C62	0.8557 (3)	−0.0162 (2)	0.4471 (2)	0.0316 (11)
C63	0.9160 (3)	−0.0484 (2)	0.4209 (2)	0.0310 (10)
C64	0.7267 (3)	0.1316 (3)	0.3520 (4)	0.0561 (18)
H64	0.6917	0.1037	0.3661	0.067*
C65	0.7174 (4)	0.1965 (3)	0.3630 (4)	0.080 (3)
H65	0.6768	0.2108	0.3845	0.096*
C66	0.7673 (4)	0.2388 (3)	0.3426 (4)	0.065 (2)
H66	0.7606	0.2818	0.3492	0.078*
C67	0.8290 (3)	0.2164 (2)	0.3116 (3)	0.0427 (13)
C68	0.8865 (3)	0.2534 (2)	0.2875 (3)	0.0430 (13)
C69	0.9431 (3)	0.2264 (3)	0.2569 (3)	0.0450 (14)
H69	0.9791	0.2521	0.2406	0.054*
C70	0.9485 (3)	0.1611 (3)	0.2494 (3)	0.0416 (13)
H70	0.988	0.1437	0.2286	0.05*
C71	0.8956 (3)	0.1223 (2)	0.2729 (2)	0.0317 (11)
C72	0.8347 (3)	0.1500 (2)	0.3024 (2)	0.0317 (11)
N1	0.7109 (3)	0.6218 (2)	0.1620 (2)	0.0423 (11)
N2	0.7386 (3)	0.4770 (2)	0.3046 (2)	0.0445 (11)
N3	0.7176 (2)	0.4056 (2)	0.1861 (2)	0.0341 (9)
N4	0.5819 (2)	0.55909 (19)	0.1441 (2)	0.0366 (10)
N5	0.7640 (2)	0.04601 (19)	0.19945 (19)	0.0301 (9)
N6	0.7909 (2)	−0.10803 (18)	0.3302 (2)	0.0337 (9)
N7	0.9199 (2)	−0.04811 (18)	0.35307 (19)	0.0312 (9)
N8	0.7833 (2)	0.10900 (19)	0.3222 (2)	0.0338 (9)
O1	0.6532 (2)	0.5812 (2)	0.27121 (19)	0.0518 (11)
O2	0.8001 (2)	0.52381 (16)	0.20070 (17)	0.0375 (8)
O3	0.6046 (2)	0.45904 (19)	0.23524 (19)	0.0463 (10)
O4	0.6927 (2)	0.49868 (17)	0.09787 (17)	0.0391 (9)
O5	0.70164 (19)	−0.00805 (15)	0.29979 (17)	0.0324 (8)
O6	0.84785 (19)	−0.05972 (16)	0.22426 (17)	0.0372 (8)
O7	0.81045 (19)	0.01031 (15)	0.40398 (16)	0.0333 (8)
O8	0.89758 (18)	0.05949 (16)	0.27043 (16)	0.0334 (8)
Cl1	0.64751 (9)	0.85362 (8)	0.21638 (12)	0.0776 (6)
Cl2	0.98130 (11)	0.45327 (12)	0.43097 (8)	0.0802 (6)
Cl3	0.61074 (13)	0.18273 (8)	0.21530 (10)	0.0821 (6)
Cl4	0.48329 (10)	0.60358 (8)	−0.09325 (8)	0.0638 (5)
Cl5	0.52442 (9)	0.06726 (13)	0.06880 (9)	0.0827 (7)
Cl6	0.85753 (8)	−0.33485 (7)	0.26089 (11)	0.0660 (5)
Cl7	1.01634 (10)	−0.11397 (8)	0.58565 (8)	0.0621 (5)
Cl8	0.88468 (11)	0.33488 (7)	0.29928 (9)	0.0681 (5)
Zr01	0.68789 (3)	0.51544 (2)	0.20042 (2)	0.03697 (16)
Zr02	0.81423 (3)	0.00025 (2)	0.30052 (2)	0.02843 (15)
N9	0.7188 (4)	0.9073 (3)	0.0119 (3)	0.0756 (18)
C74	0.7645 (5)	0.9263 (4)	0.0653 (4)	0.092 (3)

H74A	0.8094	0.9044	0.0626	0.139*	
H74B	0.7423	0.9165	0.1067	0.139*	
H74C	0.7727	0.971	0.0628	0.139*	
O9	0.7888 (5)	0.8302 (4)	−0.0195 (4)	0.150 (3)	
C75	0.6503 (5)	0.9391 (5)	0.0059 (6)	0.130 (4)	
H75A	0.6242	0.9227	−0.0318	0.195*	
H75B	0.6579	0.9835	0.0002	0.195*	
H75C	0.6233	0.932	0.0454	0.195*	
C73	0.7361 (6)	0.8619 (7)	−0.0260 (7)	0.152 (6)	
H73	0.7055	0.8527	−0.0615	0.183*	
N10	0.4970 (6)	0.7253 (5)	0.5125 (4)	0.031 (3)	0.379(5)
C76	0.4283 (8)	0.7265 (7)	0.4913 (9)	0.074 (5)	0.379(5)
H76	0.4155	0.7443	0.4506	0.089*	0.379(5)
C77	0.5035 (14)	0.7023 (11)	0.5792 (7)	0.126 (10)	0.379(5)
H77A	0.5144	0.7368	0.6086	0.188*	0.379(5)
H77B	0.5412	0.6715	0.5818	0.188*	0.379(5)
H77C	0.4592	0.6831	0.592	0.188*	0.379(5)
C78	0.5616 (9)	0.7479 (7)	0.4849 (10)	0.077 (6)	0.379(5)
H78A	0.5506	0.777	0.4496	0.115*	0.379(5)
H78B	0.5885	0.7131	0.4677	0.115*	0.379(5)
H78C	0.5894	0.7691	0.5187	0.115*	0.379(5)
O10	0.3788 (6)	0.7010 (8)	0.5313 (7)	0.106 (6)	0.379(5)
N11	0.2481 (6)	0.8064 (6)	0.4983 (5)	0.020 (3)	0.242(7)
C79	0.2480 (9)	0.7432 (7)	0.4996 (9)	0.041 (3)	0.242(7)
H79	0.2039	0.723	0.4965	0.049*	0.242(7)
C80	0.3128 (7)	0.8452 (8)	0.4857 (7)	0.020 (3)	0.242(7)
H80A	0.3257	0.8682	0.5252	0.03*	0.242(7)
H80B	0.3029	0.8743	0.4503	0.03*	0.242(7)
H80C	0.3517	0.8181	0.4736	0.03*	0.242(7)
C81	0.1838 (7)	0.8454 (8)	0.5111 (7)	0.020 (3)	0.242(7)
H81A	0.1425	0.8185	0.514	0.03*	0.242(7)
H81B	0.1768	0.875	0.4755	0.03*	0.242(7)
H81C	0.1903	0.8679	0.5521	0.03*	0.242(7)
O11	0.3031 (8)	0.7089 (6)	0.5047 (7)	0.041 (3)	0.242(7)
N12	0.0057 (5)	0.7143 (5)	0.4807 (4)	0.0283 (19)	0.381(5)
C82	0.0743 (6)	0.7192 (6)	0.5013 (5)	0.0283 (19)	0.381(5)
H82	0.0853	0.7332	0.544	0.034*	0.381(5)
C83	−0.0148 (8)	0.6754 (10)	0.4274 (9)	0.076 (4)	0.381(5)
H83A	0.0266	0.6544	0.4104	0.114*	0.381(5)
H83B	−0.0365	0.7006	0.393	0.114*	0.381(5)
H83C	−0.0486	0.6445	0.4422	0.114*	0.381(5)
C84	−0.0543 (8)	0.7378 (10)	0.5162 (10)	0.076 (4)	0.381(5)
H84A	−0.0859	0.7035	0.5263	0.114*	0.381(5)
H84B	−0.0794	0.7683	0.4894	0.114*	0.381(5)
H84C	−0.0379	0.7573	0.5566	0.114*	0.381(5)
O12	0.1231 (6)	0.7048 (7)	0.4624 (8)	0.095 (6)	0.381(5)

Table A.2.6 Atomic displacement parameters (Å^2) for [Zr(5-ClOx)$_4$]·2DMF.

	U^{11}	U^{22}	U^{33}	U^{12}	U^{13}	U^{23}
C01	0.053 (4)	0.035 (3)	0.043 (3)	0.004 (2)	−0.002 (3)	−0.001 (2)
C02	0.052 (4)	0.037 (3)	0.054 (4)	−0.005 (3)	−0.009 (3)	0.003 (3)
C03	0.046 (4)	0.035 (3)	0.068 (4)	−0.001 (2)	−0.012 (3)	−0.002 (3)
C04	0.038 (3)	0.037 (3)	0.068 (4)	0.006 (2)	−0.015 (3)	−0.013 (3)
C05	0.037 (3)	0.045 (3)	0.084 (5)	0.010 (3)	−0.010 (3)	−0.029 (3)
C06	0.048 (4)	0.061 (4)	0.078 (5)	0.015 (3)	−0.009 (4)	−0.039 (4)
C07	0.055 (4)	0.067 (4)	0.052 (4)	0.021 (3)	−0.007 (3)	−0.022 (3)
C08	0.051 (4)	0.052 (4)	0.042 (3)	0.014 (3)	−0.003 (3)	−0.011 (3)
C09	0.044 (3)	0.040 (3)	0.047 (3)	0.012 (2)	−0.008 (3)	−0.012 (2)
C10	0.055 (4)	0.090 (5)	0.036 (3)	0.006 (3)	0.017 (3)	0.008 (3)
C11	0.065 (5)	0.120 (7)	0.037 (4)	0.003 (4)	0.017 (3)	0.029 (4)
C12	0.063 (5)	0.112 (6)	0.036 (3)	−0.003 (4)	0.011 (3)	0.018 (4)
C13	0.063 (4)	0.058 (4)	0.031 (3)	0.002 (3)	0.007 (3)	0.003 (3)
C14	0.058 (4)	0.059 (4)	0.037 (3)	−0.001 (3)	0.003 (3)	−0.005 (3)
C15	0.054 (4)	0.047 (3)	0.036 (3)	−0.005 (3)	0.002 (3)	−0.005 (2)
C16	0.052 (3)	0.030 (3)	0.034 (3)	−0.001 (2)	0.006 (2)	−0.006 (2)
C17	0.053 (3)	0.026 (2)	0.031 (3)	0.001 (2)	0.011 (2)	−0.0034 (19)
C18	0.048 (3)	0.040 (3)	0.034 (3)	0.004 (2)	0.010 (2)	−0.002 (2)
C19	0.042 (3)	0.039 (3)	0.060 (4)	−0.003 (2)	0.024 (3)	−0.007 (3)
C20	0.062 (4)	0.042 (3)	0.079 (5)	−0.005 (3)	0.040 (4)	−0.014 (3)
C21	0.076 (5)	0.032 (3)	0.065 (4)	−0.009 (3)	0.032 (4)	−0.011 (3)
C22	0.056 (4)	0.041 (3)	0.039 (3)	−0.009 (3)	0.014 (3)	0.002 (2)
C23	0.062 (4)	0.047 (3)	0.047 (4)	−0.014 (3)	0.010 (3)	0.009 (3)
C24	0.039 (3)	0.069 (4)	0.050 (4)	−0.005 (3)	0.008 (3)	0.026 (3)
C25	0.031 (3)	0.067 (4)	0.056 (4)	0.009 (3)	0.012 (3)	0.026 (3)
C26	0.036 (3)	0.055 (3)	0.036 (3)	0.010 (2)	0.013 (2)	0.017 (2)
C27	0.041 (3)	0.044 (3)	0.027 (3)	0.000 (2)	0.009 (2)	0.008 (2)
C28	0.045 (3)	0.038 (3)	0.045 (3)	0.004 (2)	0.015 (3)	0.003 (2)
C29	0.052 (4)	0.035 (3)	0.062 (4)	0.010 (3)	0.016 (3)	0.006 (3)
C30	0.060 (4)	0.041 (3)	0.054 (4)	0.012 (3)	0.010 (3)	0.014 (3)
C31	0.055 (4)	0.034 (3)	0.045 (3)	0.004 (2)	0.005 (3)	0.008 (2)
C32	0.056 (4)	0.042 (3)	0.041 (3)	0.000 (3)	0.000 (3)	0.011 (2)
C33	0.058 (4)	0.046 (3)	0.032 (3)	−0.005 (3)	0.008 (3)	0.003 (2)
C34	0.049 (3)	0.037 (3)	0.034 (3)	0.003 (2)	0.014 (2)	0.001 (2)
C35	0.044 (3)	0.033 (3)	0.032 (3)	0.002 (2)	0.009 (2)	0.002 (2)
C36	0.047 (3)	0.030 (3)	0.035 (3)	0.002 (2)	0.008 (2)	0.004 (2)
C37	0.034 (3)	0.046 (3)	0.032 (3)	0.003 (2)	0.005 (2)	0.000 (2)
C38	0.045 (3)	0.067 (4)	0.028 (3)	0.006 (3)	0.012 (2)	0.006 (3)
C39	0.046 (4)	0.078 (4)	0.031 (3)	0.019 (3)	0.002 (3)	0.005 (3)
C40	0.036 (3)	0.058 (3)	0.033 (3)	0.011 (2)	0.003 (2)	−0.004 (2)
C41	0.039 (3)	0.078 (4)	0.039 (3)	0.009 (3)	−0.005 (3)	−0.011 (3)
C42	0.036 (3)	0.057 (3)	0.042 (3)	0.001 (3)	0.001 (3)	−0.014 (3)
C43	0.036 (3)	0.037 (3)	0.037 (3)	−0.003 (2)	0.005 (2)	−0.008 (2)
C44	0.036 (3)	0.028 (2)	0.033 (3)	0.003 (2)	0.003 (2)	−0.0061 (19)
C45	0.032 (3)	0.037 (3)	0.032 (3)	0.006 (2)	0.005 (2)	−0.005 (2)
C46	0.044 (3)	0.033 (3)	0.041 (3)	−0.003 (2)	−0.004 (2)	−0.001 (2)

C47	0.047 (3)	0.035 (3)	0.059 (4)	−0.007 (2)	−0.008 (3)	0.009 (3)
C48	0.044 (3)	0.024 (3)	0.076 (4)	−0.003 (2)	−0.008 (3)	0.002 (3)
C49	0.032 (3)	0.028 (3)	0.056 (3)	0.002 (2)	−0.013 (2)	−0.004 (2)
C50	0.033 (3)	0.031 (3)	0.076 (4)	0.008 (2)	−0.010 (3)	−0.017 (3)
C51	0.039 (3)	0.044 (3)	0.065 (4)	0.011 (3)	−0.010 (3)	−0.023 (3)
C52	0.036 (3)	0.050 (3)	0.042 (3)	0.013 (2)	−0.004 (2)	−0.014 (2)
C53	0.036 (3)	0.034 (3)	0.036 (3)	0.010 (2)	−0.008 (2)	−0.012 (2)
C54	0.033 (3)	0.029 (2)	0.037 (3)	0.005 (2)	−0.007 (2)	−0.007 (2)
C55	0.042 (3)	0.035 (3)	0.030 (3)	0.001 (2)	0.007 (2)	−0.003 (2)
C56	0.042 (3)	0.040 (3)	0.048 (3)	0.008 (2)	0.005 (3)	0.002 (2)
C57	0.051 (4)	0.041 (3)	0.043 (3)	0.009 (3)	−0.004 (3)	0.005 (2)
C58	0.049 (3)	0.034 (3)	0.035 (3)	0.000 (2)	−0.004 (2)	0.002 (2)
C59	0.058 (4)	0.044 (3)	0.033 (3)	−0.001 (3)	−0.006 (3)	0.006 (2)
C60	0.066 (4)	0.046 (3)	0.024 (3)	−0.006 (3)	0.004 (3)	−0.002 (2)
C61	0.049 (3)	0.041 (3)	0.028 (3)	−0.002 (2)	0.003 (2)	−0.002 (2)
C62	0.038 (3)	0.028 (2)	0.029 (3)	−0.003 (2)	0.001 (2)	−0.0001 (19)
C63	0.040 (3)	0.028 (2)	0.025 (2)	0.001 (2)	0.001 (2)	−0.0004 (18)
C64	0.046 (4)	0.028 (3)	0.096 (5)	−0.006 (2)	0.043 (3)	−0.005 (3)
C65	0.077 (5)	0.037 (3)	0.129 (7)	−0.003 (3)	0.068 (5)	−0.018 (4)
C66	0.079 (5)	0.029 (3)	0.087 (5)	−0.005 (3)	0.043 (4)	−0.011 (3)
C67	0.057 (4)	0.029 (3)	0.042 (3)	−0.007 (2)	0.010 (3)	−0.003 (2)
C68	0.059 (4)	0.033 (3)	0.038 (3)	−0.014 (3)	0.003 (3)	0.003 (2)
C69	0.044 (3)	0.048 (3)	0.044 (3)	−0.014 (3)	−0.006 (3)	0.018 (3)
C70	0.032 (3)	0.054 (3)	0.039 (3)	−0.003 (2)	0.001 (2)	0.018 (2)
C71	0.034 (3)	0.039 (3)	0.023 (2)	0.002 (2)	−0.001 (2)	0.0049 (19)
C72	0.035 (3)	0.031 (2)	0.029 (2)	−0.004 (2)	0.006 (2)	0.0016 (19)
N1	0.052 (3)	0.036 (2)	0.038 (3)	0.009 (2)	0.005 (2)	−0.0071 (19)
N2	0.053 (3)	0.052 (3)	0.029 (2)	0.007 (2)	0.016 (2)	0.004 (2)
N3	0.034 (2)	0.037 (2)	0.031 (2)	−0.0009 (18)	0.0090 (18)	0.0015 (17)
N4	0.045 (3)	0.033 (2)	0.032 (2)	0.0032 (19)	0.0099 (19)	0.0029 (17)
N5	0.032 (2)	0.034 (2)	0.025 (2)	0.0047 (17)	0.0041 (17)	−0.0017 (16)
N6	0.041 (3)	0.027 (2)	0.033 (2)	0.0010 (17)	−0.0004 (19)	−0.0033 (17)
N7	0.038 (2)	0.027 (2)	0.029 (2)	0.0008 (17)	0.0020 (18)	−0.0006 (16)
N8	0.035 (2)	0.029 (2)	0.038 (2)	−0.0002 (17)	0.0095 (19)	−0.0010 (17)
O1	0.065 (3)	0.056 (3)	0.035 (2)	0.020 (2)	0.0146 (19)	−0.0031 (18)
O2	0.048 (2)	0.0339 (19)	0.0311 (19)	0.0033 (16)	0.0078 (16)	0.0000 (15)
O3	0.044 (2)	0.052 (2)	0.044 (2)	0.0137 (18)	0.0192 (18)	0.0154 (18)
O4	0.048 (2)	0.042 (2)	0.0279 (19)	0.0062 (16)	0.0111 (16)	0.0027 (15)
O5	0.038 (2)	0.0273 (17)	0.0324 (19)	0.0001 (14)	0.0045 (15)	−0.0007 (13)
O6	0.046 (2)	0.0354 (19)	0.0298 (18)	0.0115 (16)	0.0040 (16)	−0.0042 (14)
O7	0.038 (2)	0.0335 (18)	0.0282 (18)	0.0038 (14)	0.0030 (15)	−0.0047 (14)
O8	0.0331 (19)	0.0375 (19)	0.0297 (18)	0.0042 (14)	0.0066 (14)	0.0044 (14)
Cl1	0.0495 (10)	0.0417 (9)	0.1412 (19)	0.0065 (7)	−0.0114 (10)	−0.0345 (10)
Cl2	0.0743 (13)	0.1270 (18)	0.0390 (9)	−0.0108 (12)	−0.0111 (8)	0.0077 (10)
Cl3	0.1170 (17)	0.0488 (9)	0.0819 (13)	−0.0327 (10)	0.0433 (12)	−0.0023 (9)
Cl4	0.0779 (12)	0.0625 (10)	0.0508 (9)	0.0071 (8)	−0.0064 (8)	0.0173 (7)
Cl5	0.0412 (10)	0.161 (2)	0.0455 (10)	0.0104 (11)	−0.0070 (7)	0.0093 (11)
Cl6	0.0465 (9)	0.0294 (7)	0.1222 (16)	0.0060 (6)	−0.0022 (9)	−0.0195 (8)
Cl7	0.0841 (12)	0.0609 (10)	0.0406 (8)	0.0091 (8)	−0.0174 (8)	0.0094 (7)

Cl8	0.1059 (14)	0.0357 (8)	0.0634 (10)	−0.0278 (8)	0.0183 (10)	−0.0020 (7)
Zr01	0.0446 (3)	0.0382 (3)	0.0285 (3)	0.0102 (2)	0.0131 (2)	0.0026 (2)
Zr02	0.0343 (3)	0.0265 (2)	0.0247 (3)	0.00385 (18)	0.00527 (19)	−0.00106 (17)
N9	0.081 (5)	0.061 (4)	0.084 (5)	−0.001 (3)	−0.023 (4)	−0.016 (3)
C74	0.113 (7)	0.051 (4)	0.112 (7)	0.018 (4)	−0.054 (6)	−0.005 (4)
O9	0.188 (9)	0.120 (6)	0.141 (7)	0.045 (6)	−0.029 (6)	−0.062 (5)
C75	0.076 (7)	0.108 (8)	0.204 (13)	0.003 (6)	−0.028 (7)	−0.051 (8)
C73	0.108 (9)	0.172 (12)	0.176 (12)	0.059 (8)	−0.049 (8)	−0.130 (11)
N10	0.054 (7)	0.027 (5)	0.012 (5)	0.022 (5)	0.003 (4)	−0.011 (4)
C76	0.093 (12)	0.042 (8)	0.086 (11)	0.016 (8)	−0.018 (10)	−0.048 (8)
C77	0.22 (2)	0.097 (15)	0.066 (12)	0.087 (16)	0.099 (14)	0.025 (11)
C78	0.097 (14)	0.031 (8)	0.102 (14)	0.024 (9)	0.011 (12)	−0.037 (9)
O10	0.031 (6)	0.182 (14)	0.104 (10)	0.017 (7)	−0.003 (6)	−0.127 (10)
N11	0.011 (5)	0.043 (6)	0.004 (4)	0.005 (4)	−0.002 (3)	−0.007 (3)
C79	0.048 (7)	0.020 (5)	0.055 (7)	−0.014 (4)	0.008 (6)	−0.020 (5)
C80	0.011 (5)	0.043 (6)	0.004 (4)	0.005 (4)	−0.002 (3)	−0.007 (3)
C81	0.011 (5)	0.043 (6)	0.004 (4)	0.005 (4)	−0.002 (3)	−0.007 (3)
O11	0.048 (7)	0.020 (5)	0.055 (7)	−0.014 (4)	0.008 (6)	−0.020 (5)
N12	0.030 (4)	0.038 (4)	0.017 (4)	0.017 (3)	0.010 (3)	0.003 (3)
C82	0.030 (4)	0.038 (4)	0.017 (4)	0.017 (3)	0.010 (3)	0.003 (3)
C83	0.024 (6)	0.098 (10)	0.106 (11)	0.002 (6)	0.028 (6)	−0.034 (8)
C84	0.024 (6)	0.098 (10)	0.106 (11)	0.002 (6)	0.028 (6)	−0.034 (8)
O12	0.033 (7)	0.111 (11)	0.143 (13)	0.005 (7)	0.034 (8)	−0.075 (10)

Table A.2.7 Bond lengths (Å) for [Zr(5-ClOx)$_4$]·2DMF.

Atoms	Bond length (Å)	Atoms	Bond length (Å)
C01—N1	1.322 (7)	**C51—H51**	0.93
C01—C02	1.405 (8)	**C52—C53**	1.381 (7)
C01—H01	0.93	**C52—H52**	0.93
C02—C03	1.371 (8)	**C53—O6**	1.323 (6)
C02—H02	0.93	**C53—C54**	1.412 (8)
C03—C04	1.394 (9)	**C54—N6**	1.365 (6)
C03—H03	0.93	**C55—N7**	1.319 (6)
C04—C09	1.424 (8)	**C55—C56**	1.408 (7)
C04—C05	1.437 (8)	**C55—H55**	0.93
C05—C06	1.345 (10)	**C56—C57**	1.351 (8)
C05—Cl1	1.746 (7)	**C56—H56**	0.93
C06—C07	1.389 (10)	**C57—C58**	1.406 (8)
C06—H06	0.93	**C57—H57**	0.93
C07—C08	1.387 (8)	**C58—C59**	1.417 (8)
C07—H07	0.93	**C58—C63**	1.421 (7)
C08—O1	1.334 (7)	**C59—C60**	1.381 (8)
C08—C09	1.403 (9)	**C59—Cl7**	1.739 (6)
C09—N1	1.372 (7)	**C60—C61**	1.413 (8)
C10—N2	1.337 (7)	**C60—H60**	0.93
C10—C11	1.407 (9)	**C61—C62**	1.378 (7)
C10—H10	0.93	**C61—H61**	0.93

C11—C12	1.372 (10)	C62—O7	1.328 (6)
C11—H11	0.93	C62—C63	1.425 (7)
C12—C13	1.407 (8)	C63—N7	1.369 (6)
C12—H12	0.93	C64—N8	1.313 (6)
C13—C14	1.417 (9)	C64—C65	1.404 (8)
C13—C18	1.421 (8)	C64—H64	0.93
C14—C15	1.361 (8)	C65—C66	1.359 (9)
C14—Cl2	1.757 (6)	C65—H65	0.93
C15—C16	1.408 (8)	C66—C67	1.403 (8)
C15—H15	0.93	C66—H66	0.93
C16—C17	1.380 (8)	C67—C68	1.422 (7)
C16—H16	0.93	C67—C72	1.422 (7)
C17—O2	1.330 (6)	C68—C69	1.357 (8)
C17—C18	1.421 (7)	C68—Cl8	1.741 (5)
C18—N2	1.369 (7)	C69—C70	1.397 (8)
C19—N3	1.324 (7)	C69—H69	0.93
C19—C20	1.407 (8)	C70—C71	1.374 (7)
C19—H19	0.93	C70—H70	0.93
C20—C21	1.377 (8)	C71—O8	1.332 (6)
C20—H20	0.93	C71—C72	1.417 (7)
C21—C22	1.410 (8)	C72—N8	1.360 (6)
C21—H21	0.93	N1—Zr01	2.423 (5)
C22—C27	1.416 (8)	N2—Zr01	2.429 (5)
C22—C23	1.421 (8)	N3—Zr01	2.410 (4)
C23—C24	1.368 (9)	N4—Zr01	2.448 (4)
C23—Cl3	1.739 (6)	N5—Zr02	2.431 (4)
C24—C25	1.391 (9)	N6—Zr02	2.411 (4)
C24—H24	0.93	N7—Zr02	2.449 (4)
C25—C26	1.384 (8)	N8—Zr02	2.416 (4)
C25—H25	0.93	O1—Zr01	2.103 (4)
C26—O3	1.323 (7)	O2—Zr01	2.103 (4)
C26—C27	1.417 (7)	O3—Zr01	2.091 (4)
C27—N3	1.362 (6)	O4—Zr01	2.100 (4)
C28—N4	1.312 (7)	O5—Zr02	2.110 (3)
C28—C29	1.414 (8)	O6—Zr02	2.097 (3)
C28—H28	0.93	O7—Zr02	2.098 (3)
C29—C30	1.353 (9)	O8—Zr02	2.096 (3)
C29—H29	0.93	N9—C73	1.271 (11)
C30—C31	1.413 (8)	N9—C74	1.422 (9)
C30—H30	0.93	N9—C75	1.450 (11)
C31—C36	1.414 (8)	C74—H74A	0.96
C31—C32	1.416 (8)	C74—H74B	0.96
C32—C33	1.386 (8)	C74—H74C	0.96
C32—Cl4	1.734 (6)	O9—C73	1.197 (12)
C33—C34	1.407 (8)	C75—H75A	0.96
C33—H33	0.93	C75—H75B	0.96
C34—C35	1.386 (7)	C75—H75C	0.96
C34—H34	0.93	C73—H73	0.93
C35—O4	1.320 (6)	N10—C76	1.345 (14)

Atoms	Bond length	Atoms	Bond length
C35—C36	1.431 (7)	N10—C78	1.420 (14)
C36—N4	1.367 (6)	N10—C77	1.434 (14)
C37—N5	1.333 (6)	C76—O10	1.348 (17)
C37—C38	1.403 (8)	C76—H76	0.93
C37—H37	0.93	C77—H77A	0.96
C38—C39	1.374 (8)	C77—H77B	0.96
C38—H38	0.93	C77—H77C	0.96
C39—C40	1.408 (8)	C78—H78A	0.96
C39—H39	0.93	C78—H78B	0.96
C40—C45	1.417 (7)	C78—H78C	0.96
C40—C41	1.418 (8)	N11—C79	1.339 (14)
C41—C42	1.361 (9)	N11—C81	1.484 (13)
C41—Cl5	1.755 (6)	N11—C80	1.486 (14)
C42—C43	1.409 (8)	C79—O11	1.263 (16)
C42—H42	0.93	C79—H79	0.93
C43—C44	1.387 (7)	C80—H80A	0.96
C43—H43	0.93	C80—H80B	0.96
C44—O5	1.317 (6)	C80—H80C	0.96
C44—C45	1.429 (7)	C81—H81A	0.96
C45—N5	1.367 (6)	C81—H81B	0.96
C46—N6	1.318 (7)	C81—H81C	0.96
C46—C47	1.407 (7)	N12—C82	1.344 (12)
C46—H46	0.93	N12—C83	1.403 (14)
C47—C48	1.357 (8)	N12—C84	1.427 (12)
C47—H47	0.93	C82—O12	1.250 (13)
C48—C49	1.391 (8)	C82—H82	0.93
C48—H48	0.93	C83—H83A	0.96
C49—C54	1.417 (7)	C83—H83B	0.96
C49—C50	1.427 (8)	C83—H83C	0.96
C50—C51	1.357 (9)	C84—H84A	0.96
C50—Cl6	1.741 (6)	C84—H84B	0.96
C51—C52	1.419 (8)	C84—H84C	0.96

Table A.2.8 Bond angles (°) for [Zr(5-ClClOx)$_4$]·2DMF.

Atoms	Bond angle (°)	Atoms	Bond angle (°)
N1—C01—C02	122.8 (5)	C58—C59—Cl7	120.0 (5)
N1—C01—H01	118.6	C59—C60—C61	120.8 (5)
C02—C01—H01	118.6	C59—C60—H60	119.6
C03—C02—C01	119.3 (6)	C61—C60—H60	119.6
C03—C02—H02	120.3	C62—C61—C60	120.7 (5)
C01—C02—H02	120.3	C62—C61—H61	119.6
C02—C03—C04	119.8 (5)	C60—C61—H61	119.6
C02—C03—H03	120.1	O7—C62—C61	124.6 (5)
C04—C03—H03	120.1	O7—C62—C63	117.2 (4)
C03—C04—C09	117.7 (5)	C61—C62—C63	118.2 (5)
C03—C04—C05	127.5 (6)	N7—C63—C58	122.6 (5)
C09—C04—C05	114.8 (6)	N7—C63—C62	115.0 (4)

C06—C05—C04	122.0 (6)	C58—C63—C62	122.3 (4)
C06—C05—Cl1	120.2 (5)	N8—C64—C65	122.1 (5)
C04—C05—Cl1	117.8 (6)	N8—C64—H64	118.9
C05—C06—C07	121.6 (6)	C65—C64—H64	118.9
C05—C06—H06	119.2	C66—C65—C64	120.6 (6)
C07—C06—H06	119.2	C66—C65—H65	119.7
C08—C07—C06	120.4 (7)	C64—C65—H65	119.7
C08—C07—H07	119.8	C65—C66—C67	119.0 (5)
C06—C07—H07	119.8	C65—C66—H66	120.5
O1—C08—C07	124.1 (6)	C67—C66—H66	120.5
O1—C08—C09	117.8 (5)	C66—C67—C68	126.6 (5)
C07—C08—C09	118.1 (6)	C66—C67—C72	117.2 (5)
N1—C09—C08	115.2 (5)	C68—C67—C72	116.2 (5)
N1—C09—C04	121.7 (6)	C69—C68—C67	121.3 (5)
C08—C09—C04	123.1 (5)	C69—C68—Cl8	119.7 (4)
N2—C10—C11	121.2 (6)	C67—C68—Cl8	118.9 (5)
N2—C10—H10	119.4	C68—C69—C70	121.7 (5)
C11—C10—H10	119.4	C68—C69—H69	119.2
C12—C11—C10	121.5 (6)	C70—C69—H69	119.2
C12—C11—H11	119.2	C71—C70—C69	120.0 (5)
C10—C11—H11	119.2	C71—C70—H70	120
C11—C12—C13	118.4 (6)	C69—C70—H70	120
C11—C12—H12	120.8	O8—C71—C70	124.3 (5)
C13—C12—H12	120.8	O8—C71—C72	116.9 (4)
C12—C13—C14	125.9 (6)	C70—C71—C72	118.9 (5)
C12—C13—C18	117.6 (6)	N8—C72—C71	115.7 (4)
C14—C13—C18	116.5 (5)	N8—C72—C67	122.5 (5)
C15—C14—C13	121.5 (6)	C71—C72—C67	121.7 (5)
C15—C14—Cl2	119.6 (5)	C01—N1—C09	118.5 (5)
C13—C14—Cl2	118.9 (5)	C01—N1—Zr01	129.1 (4)
C14—C15—C16	121.4 (6)	C09—N1—Zr01	112.3 (4)
C14—C15—H15	119.3	C10—N2—C18	118.5 (5)
C16—C15—H15	119.3	C10—N2—Zr01	128.5 (4)
C17—C16—C15	120.1 (5)	C18—N2—Zr01	113.0 (3)
C17—C16—H16	119.9	C19—N3—C27	118.5 (5)
C15—C16—H16	119.9	C19—N3—Zr01	128.4 (3)
O2—C17—C16	124.9 (5)	C27—N3—Zr01	113.0 (3)
O2—C17—C18	116.7 (5)	C28—N4—C36	118.6 (5)
C16—C17—C18	118.4 (5)	C28—N4—Zr01	128.9 (4)
N2—C18—C17	115.0 (5)	C36—N4—Zr01	112.4 (3)
N2—C18—C13	122.9 (5)	C37—N5—C45	118.4 (4)
C17—C18—C13	122.1 (5)	C37—N5—Zr02	128.9 (3)
N3—C19—C20	122.7 (5)	C45—N5—Zr02	112.7 (3)
N3—C19—H19	118.6	C46—N6—C54	118.7 (4)
C20—C19—H19	118.6	C46—N6—Zr02	128.9 (3)
C21—C20—C19	119.5 (5)	C54—N6—Zr02	112.1 (3)
C21—C20—H20	120.3	C55—N7—C63	118.4 (4)
C19—C20—H20	120.3	C55—N7—Zr02	129.1 (3)
C20—C21—C22	119.3 (5)	C63—N7—Zr02	112.2 (3)

C20—C21—H21	120.3	C64—N8—C72	118.6 (4)
C22—C21—H21	120.3	C64—N8—Zr02	128.8 (3)
C21—C22—C27	117.2 (5)	C72—N8—Zr02	112.5 (3)
C21—C22—C23	126.6 (6)	C08—O1—Zr01	123.7 (4)
C27—C22—C23	116.2 (5)	C17—O2—Zr01	125.5 (3)
C24—C23—C22	121.0 (6)	C26—O3—Zr01	124.1 (3)
C24—C23—Cl3	120.3 (5)	C35—O4—Zr01	125.1 (3)
C22—C23—Cl3	118.7 (5)	C44—O5—Zr02	124.8 (3)
C23—C24—C25	121.6 (5)	C53—O6—Zr02	123.5 (3)
C23—C24—H24	119.2	C62—O7—Zr02	125.2 (3)
C25—C24—H24	119.2	C71—O8—Zr02	124.4 (3)
C26—C25—C24	120.4 (6)	O3—Zr01—O4	106.08 (16)
C26—C25—H25	119.8	O3—Zr01—O2	142.54 (14)
C24—C25—H25	119.8	O4—Zr01—O2	87.65 (14)
O3—C26—C25	124.1 (5)	O3—Zr01—O1	84.95 (16)
O3—C26—C27	118.0 (5)	O4—Zr01—O1	142.91 (15)
C25—C26—C27	117.9 (5)	O2—Zr01—O1	105.06 (16)
N3—C27—C22	122.8 (5)	O3—Zr01—N3	70.31 (14)
N3—C27—C26	114.5 (5)	O4—Zr01—N3	72.87 (14)
C22—C27—C26	122.6 (5)	O2—Zr01—N3	81.38 (14)
N4—C28—C29	121.7 (5)	O1—Zr01—N3	142.60 (15)
N4—C28—H28	119.1	O3—Zr01—N1	140.78 (15)
C29—C28—H28	119.1	O4—Zr01—N1	80.34 (14)
C30—C29—C28	120.8 (5)	O2—Zr01—N1	74.99 (15)
C30—C29—H29	119.6	O1—Zr01—N1	70.05 (15)
C28—C29—H29	119.6	N3—Zr01—N1	144.79 (15)
C29—C30—C31	119.0 (6)	O3—Zr01—N2	78.53 (16)
C29—C30—H30	120.5	O4—Zr01—N2	140.47 (15)
C31—C30—H30	120.5	O2—Zr01—N2	69.55 (15)
C30—C31—C36	116.9 (5)	O1—Zr01—N2	75.89 (15)
C30—C31—C32	125.8 (6)	N3—Zr01—N2	72.10 (15)
C36—C31—C32	117.3 (5)	N1—Zr01—N2	121.25 (16)
C33—C32—C31	120.6 (5)	O3—Zr01—N4	76.76 (14)
C33—C32—Cl4	118.8 (5)	O4—Zr01—N4	69.76 (14)
C31—C32—Cl4	120.7 (5)	O2—Zr01—N4	140.17 (14)
C32—C33—C34	121.4 (5)	O1—Zr01—N4	78.99 (15)
C32—C33—H33	119.3	N3—Zr01—N4	119.69 (14)
C34—C33—H33	119.3	N1—Zr01—N4	69.30 (15)
C35—C34—C33	120.4 (5)	N2—Zr01—N4	145.99 (14)
C35—C34—H34	119.8	O8—Zr02—O6	85.32 (14)
C33—C34—H34	119.8	O8—Zr02—O7	105.26 (13)
O4—C35—C34	124.3 (5)	O6—Zr02—O7	143.58 (13)
O4—C35—C36	117.6 (4)	O8—Zr02—O5	142.41 (13)
C34—C35—C36	118.0 (5)	O6—Zr02—O5	104.73 (14)
N4—C36—C31	122.9 (5)	O7—Zr02—O5	88.07 (13)
N4—C36—C35	114.7 (5)	O8—Zr02—N6	141.16 (14)
C31—C36—C35	122.3 (5)	O6—Zr02—N6	70.30 (14)
N5—C37—C38	122.3 (5)	O7—Zr02—N6	80.88 (13)
N5—C37—H37	118.8	O5—Zr02—N6	74.84 (13)

C38—C37—H37	118.8	O8—Zr02—N8	70.29 (13)
C39—C38—C37	119.6 (5)	O6—Zr02—N8	141.74 (14)
C39—C38—H38	120.2	O7—Zr02—N8	73.22 (13)
C37—C38—H38	120.2	O5—Zr02—N8	80.76 (13)
C38—C39—C40	119.7 (5)	N6—Zr02—N8	144.79 (14)
C38—C39—H39	120.1	O8—Zr02—N5	78.35 (13)
C40—C39—H39	120.1	O6—Zr02—N5	75.16 (13)
C39—C40—C45	117.0 (5)	O7—Zr02—N5	140.67 (13)
C39—C40—C41	126.3 (5)	O5—Zr02—N5	69.84 (13)
C45—C40—C41	116.6 (5)	N6—Zr02—N5	121.18 (14)
C42—C41—C40	121.9 (5)	N8—Zr02—N5	71.42 (14)
C42—C41—Cl5	119.5 (5)	O8—Zr02—N7	77.18 (13)
C40—C41—Cl5	118.6 (5)	O6—Zr02—N7	79.35 (13)
C41—C42—C43	120.5 (5)	O7—Zr02—N7	69.65 (13)
C41—C42—H42	119.7	O5—Zr02—N7	139.86 (13)
C43—C42—H42	119.7	N6—Zr02—N7	69.09 (14)
C44—C43—C42	121.2 (5)	N8—Zr02—N7	120.90 (14)
C44—C43—H43	119.4	N5—Zr02—N7	145.79 (13)
C42—C43—H43	119.4	C73—N9—C74	120.9 (8)
O5—C44—C43	125.3 (5)	C73—N9—C75	122.2 (8)
O5—C44—C45	117.4 (4)	C74—N9—C75	116.7 (7)
C43—C44—C45	117.3 (5)	N9—C74—H74A	109.5
N5—C45—C40	122.6 (5)	N9—C74—H74B	109.5
N5—C45—C44	115.0 (4)	H74A—C74—H74B	109.5
C40—C45—C44	122.4 (5)	N9—C74—H74C	109.5
N6—C46—C47	122.2 (5)	H74A—C74—H74C	109.5
N6—C46—H46	118.9	H74B—C74—H74C	109.5
C47—C46—H46	118.9	N9—C75—H75A	109.5
C48—C47—C46	119.7 (6)	N9—C75—H75B	109.5
C48—C47—H47	120.1	H75A—C75—H75B	109.5
C46—C47—H47	120.1	N9—C75—H75C	109.5
C47—C48—C49	119.8 (5)	H75A—C75—H75C	109.5
C47—C48—H48	120.1	H75B—C75—H75C	109.5
C49—C48—H48	120.1	O9—C73—N9	125.1 (11)
C48—C49—C54	117.6 (5)	O9—C73—H73	117.4
C48—C49—C50	126.4 (5)	N9—C73—H73	117.4
C54—C49—C50	116.0 (5)	C76—N10—C78	132.9 (13)
C51—C50—C49	121.5 (5)	C76—N10—C77	111.8 (13)
C51—C50—Cl6	120.0 (4)	C78—N10—C77	114.9 (15)
C49—C50—Cl6	118.5 (5)	N10—C76—O10	117.5 (14)
C50—C51—C52	121.3 (5)	N10—C76—H76	121.2
C50—C51—H51	119.4	O10—C76—H76	121.2
C52—C51—H51	119.4	C79—N11—C81	123.4 (12)
C53—C52—C51	119.9 (6)	C79—N11—C80	123.8 (12)
C53—C52—H52	120	C81—N11—C80	112.7 (12)
C51—C52—H52	120	O11—C79—N11	125.1 (15)
O6—C53—C52	124.0 (5)	O11—C79—H79	117.4
O6—C53—C54	117.7 (4)	N11—C79—H79	117.4
C52—C53—C54	118.4 (5)	N11—C80—H80A	109.5

N6—C54—C53	115.2 (4)	N11—C80—H80B	109.5
N6—C54—C49	121.9 (5)	H80A—C80—H80B	109.5
C53—C54—C49	122.9 (5)	N11—C80—H80C	109.5
N7—C55—C56	122.1 (5)	H80A—C80—H80C	109.5
N7—C55—H55	118.9	H80B—C80—H80C	109.5
C56—C55—H55	118.9	N11—C81—H81A	109.5
C57—C56—C55	120.4 (5)	N11—C81—H81B	109.5
C57—C56—H56	119.8	H81A—C81—H81B	109.5
C55—C56—H56	119.8	N11—C81—H81C	109.5
C56—C57—C58	119.8 (5)	H81A—C81—H81C	109.5
C56—C57—H57	120.1	H81B—C81—H81C	109.5
C58—C57—H57	120.1	C82—N12—C83	121.9 (10)
C57—C58—C59	126.5 (5)	C82—N12—C84	124.8 (11)
C57—C58—C63	116.7 (5)	C83—N12—C84	112.4 (11)
C59—C58—C63	116.8 (5)	O12—C82—N12	119.3 (11)
C60—C59—C58	121.1 (5)	O12—C82—H82	120.3
C60—C59—Cl7	118.9 (4)	N12—C82—H82	120.3

A.3. [ZrCl(CliOx)$_2$(DMF)$_2$O]$_2$·DMF − § 4.4

Table A.3.9 Fractional atomic coordinates and isotropic or equivalent isotropic displacement parameters (Å^2) for [ZrCl(CliOx)$_2$(DMF)$_2$O]$_2$·DMF.

	x	*y*	*z*	U_{iso}*/U_{eq}	*Occ. (<1)*
I02	0.558783 (18)	0.967373 (19)	0.85166 (2)	0.02738 (8)	
I01	1.226859 (19)	0.801616 (19)	0.84929 (2)	0.02659 (7)	
Zr1	0.92216 (2)	1.00615 (2)	0.85786 (2)	0.01317 (8)	
Cl04	0.83503 (7)	1.03980 (6)	0.67074 (7)	0.02185 (17)	
Cl02	0.66283 (8)	0.56358 (7)	0.87857 (9)	0.0328 (2)	
Cl01	1.40241 (8)	1.17698 (9)	0.89727 (9)	0.0375 (3)	
O01	1.04339 (18)	0.94572 (18)	0.83379 (19)	0.0184 (5)	
O02	0.78008 (18)	0.96852 (18)	0.8531 (2)	0.0194 (5)	
C03	1.1991 (3)	1.2591 (3)	0.8850 (3)	0.0248 (8)	
H03	1.252	1.3009	0.8936	0.03*	
C17	0.7491 (3)	0.8798 (3)	0.8568 (3)	0.0174 (7)	
O03	0.85605 (18)	1.14565 (18)	0.8800 (2)	0.0198 (5)	
C07	1.2148 (3)	0.9528 (3)	0.8567 (3)	0.0234 (8)	
C15	0.6314 (3)	0.7573 (3)	0.8651 (3)	0.0225 (8)	
H15	0.5699	0.7427	0.8662	0.027*	
N02	0.9035 (2)	0.8313 (2)	0.8593 (2)	0.0171 (6)	
N01	1.0377 (2)	1.1342 (2)	0.8607 (2)	0.0176 (6)	
O05	1	1	1	0.0166 (7)	
N03	0.7355 (2)	1.2485 (2)	0.8805 (3)	0.0260 (7)	
C12	0.8634 (3)	0.6328 (3)	0.8727 (3)	0.0216 (7)	
H12	0.8508	0.567	0.8773	0.026*	

C11	0.9509 (3)	0.6611 (3)	0.8712 (3)	0.0236 (8)	
H11	0.9989	0.6151	0.8745	0.028*	
C02	1.1085 (3)	1.2952 (3)	0.8796 (3)	0.0257 (8)	
H02	1.0994	1.3619	0.883	0.031*	
C10	0.9690 (3)	0.7626 (3)	0.8642 (3)	0.0203 (7)	
H10	1.0296	0.7814	0.8632	0.024*	
C09	1.1254 (3)	1.0976 (3)	0.8637 (3)	0.0192 (7)	
C18	0.8144 (3)	0.8018 (3)	0.8611 (3)	0.0176 (7)	
C20	0.8026 (3)	1.3292 (3)	0.9260 (3)	0.0305 (9)	
H20A	0.8704	1.3062	0.9533	0.046*	
H20B	0.7872	1.3567	0.9781	0.046*	
H20C	0.7945	1.3781	0.8766	0.046*	
C05	1.2959 (3)	1.1089 (3)	0.8796 (3)	0.0274 (8)	
C08	1.1260 (3)	0.9946 (3)	0.8504 (3)	0.0189 (7)	
C01	1.0304 (3)	1.2298 (3)	0.8687 (3)	0.0216 (7)	
H01	0.9708	1.255	0.8672	0.026*	
C14	0.6958 (3)	0.6841 (3)	0.8695 (3)	0.0210 (7)	
C19	0.7662 (3)	1.1649 (3)	0.8598 (3)	0.0257 (8)	
H19	0.7185	1.1172	0.8284	0.031*	
C13	0.7906 (3)	0.7031 (3)	0.8673 (3)	0.0190 (7)	
C06	1.2989 (3)	1.0113 (3)	0.8707 (3)	0.0273 (8)	
H06	1.3574	0.9819	0.8738	0.033*	
C16	0.6577 (3)	0.8555 (3)	0.8586 (3)	0.0190 (7)	
C21	0.6289 (3)	1.2670 (4)	0.8517 (5)	0.0502 (14)	
H21A	0.591	1.2111	0.8175	0.075*	
H21B	0.6088	1.3228	0.8085	0.075*	
H21C	0.617	1.2794	0.9102	0.075*	
C04	1.2090 (3)	1.1571 (3)	0.8771 (3)	0.0222 (7)	
C22	0.5733 (8)	0.4337 (10)	0.0978 (11)	0.065 (3)	0.5
H22	0.6195	0.4703	0.1492	0.078*	0.5
O04	0.5759 (7)	0.3476 (8)	0.1099 (10)	0.090 (4)	0.5
C24	0.4394 (9)	0.4351 (12)	−0.0680 (11)	0.065 (3)	0.5
H24A	0.3728	0.4566	−0.0809	0.097*	0.5
H24B	0.4449	0.3664	−0.054	0.097*	0.5
H24C	0.4533	0.4475	−0.1253	0.097*	0.5
C23	0.5110 (13)	0.5859 (9)	0.0225 (15)	0.079 (4)	0.5
H23A	0.5623	0.6046	0.0855	0.118*	0.5
H23B	0.4474	0.609	0.0181	0.118*	0.5
H23C	0.5249	0.6138	−0.0304	0.118*	0.5
N04	0.5085 (17)	0.4858 (10)	0.0144 (14)	0.079 (4)	0.5

Table A.3.10 Atomic displacement parameters ($\mathring{A}^2$) for [ZrCl(CliOx)$_2$(DMF)$_2$O]$_2$·DMF.

	U^{11}	U^{22}	U^{33}	U^{12}	U^{13}	U^{23}
I02	0.01650 (11)	0.02674 (13)	0.04142 (16)	0.00410 (9)	0.01439 (11)	0.00543 (11)
I01	0.02509 (13)	0.02988 (14)	0.02848 (14)	0.00673 (10)	0.01469 (11)	−0.00208 (10)
Zr1	0.01301 (14)	0.01184 (15)	0.01599 (16)	0.00071 (11)	0.00727 (12)	0.00093 (12)
Cl04	0.0241 (4)	0.0220 (4)	0.0178 (4)	0.0006 (3)	0.0069 (3)	0.0027 (3)

Cl02	0.0285 (5)	0.0190 (4)	0.0523 (7)	−0.0078 (4)	0.0179 (5)	0.0004 (4)
Cl01	0.0234 (5)	0.0485 (6)	0.0451 (6)	−0.0143 (4)	0.0186 (5)	−0.0032 (5)
O01	0.0176 (12)	0.0179 (12)	0.0242 (13)	−0.0010 (9)	0.0131 (10)	−0.0013 (10)
O02	0.0163 (11)	0.0166 (12)	0.0279 (14)	0.0021 (9)	0.0118 (10)	0.0036 (10)
C03	0.0238 (18)	0.036 (2)	0.0139 (17)	−0.0145 (16)	0.0068 (14)	−0.0020 (15)
C17	0.0170 (16)	0.0189 (16)	0.0172 (17)	−0.0006 (13)	0.0079 (13)	0.0024 (13)
O03	0.0175 (12)	0.0155 (12)	0.0272 (14)	0.0021 (9)	0.0100 (10)	0.0014 (10)
C07	0.0223 (18)	0.029 (2)	0.0222 (19)	0.0001 (15)	0.0122 (15)	0.0015 (15)
C15	0.0159 (16)	0.0268 (19)	0.0251 (19)	−0.0056 (14)	0.0086 (14)	0.0017 (15)
N02	0.0157 (13)	0.0173 (14)	0.0184 (15)	0.0005 (11)	0.0069 (12)	−0.0017 (12)
N01	0.0188 (14)	0.0176 (14)	0.0175 (15)	−0.0026 (11)	0.0084 (12)	0.0019 (11)
O05	0.0188 (16)	0.0134 (15)	0.0177 (17)	0.0026 (13)	0.0075 (14)	0.0009 (13)
N03	0.0242 (16)	0.0203 (16)	0.0355 (19)	0.0075 (12)	0.0142 (14)	0.0041 (14)
C12	0.0306 (19)	0.0120 (15)	0.0213 (18)	−0.0034 (14)	0.0098 (15)	−0.0043 (13)
C11	0.0231 (18)	0.0262 (19)	0.0203 (18)	0.0055 (15)	0.0076 (15)	−0.0039 (15)
C02	0.032 (2)	0.0232 (19)	0.0199 (19)	−0.0093 (15)	0.0082 (16)	0.0028 (15)
C10	0.0192 (16)	0.0210 (17)	0.0211 (18)	−0.0004 (13)	0.0087 (14)	−0.0024 (14)
C09	0.0180 (16)	0.0240 (18)	0.0164 (17)	−0.0044 (13)	0.0078 (13)	0.0017 (14)
C18	0.0172 (16)	0.0195 (17)	0.0161 (17)	−0.0020 (13)	0.0070 (13)	−0.0018 (13)
C20	0.035 (2)	0.023 (2)	0.031 (2)	0.0070 (16)	0.0111 (18)	−0.0035 (17)
C05	0.0184 (17)	0.041 (2)	0.026 (2)	−0.0076 (16)	0.0122 (15)	−0.0002 (17)
C08	0.0190 (16)	0.0241 (18)	0.0165 (17)	−0.0021 (13)	0.0100 (14)	−0.0005 (14)
C01	0.0244 (18)	0.0202 (17)	0.0199 (18)	−0.0019 (14)	0.0088 (15)	0.0015 (14)
C14	0.0202 (17)	0.0163 (16)	0.0246 (19)	−0.0076 (13)	0.0071 (15)	−0.0005 (14)
C19	0.0231 (18)	0.0180 (17)	0.035 (2)	0.0013 (14)	0.0108 (16)	0.0029 (16)
C13	0.0178 (16)	0.0195 (17)	0.0175 (17)	−0.0026 (13)	0.0051 (14)	−0.0027 (14)
C06	0.0173 (17)	0.040 (2)	0.029 (2)	−0.0019 (16)	0.0140 (16)	−0.0039 (18)
C16	0.0144 (15)	0.0202 (17)	0.0228 (18)	0.0012 (13)	0.0079 (14)	0.0005 (14)
C21	0.027 (2)	0.032 (2)	0.091 (4)	0.0130 (19)	0.024 (3)	0.006 (3)
C04	0.0208 (17)	0.0284 (19)	0.0195 (18)	−0.0078 (15)	0.0102 (14)	0.0018 (15)
C22	0.034 (4)	0.076 (7)	0.085 (7)	−0.008 (4)	0.024 (4)	−0.022 (6)
O04	0.048 (5)	0.066 (6)	0.142 (10)	0.010 (5)	0.024 (6)	0.022 (7)
C24	0.034 (4)	0.076 (7)	0.085 (7)	−0.008 (4)	0.024 (4)	−0.022 (6)
C23	0.097 (7)	0.051 (6)	0.137 (10)	−0.030 (6)	0.098 (7)	−0.040 (6)
N04	0.097 (7)	0.051 (6)	0.137 (10)	−0.030 (6)	0.098 (7)	−0.040 (6)

Table A.3.11 Bond lengths (Å) for [ZrCl(CliOx)$_2$(DMF)$_2$O]$_2$·DMF.

Atoms	Bond length (Å)	Atoms	Bond length (Å)
I02—C16	2.082 (4)	C12—C13	1.415 (5)
I01—C07	2.088 (4)	C12—H12	0.93
Zr1—O05	1.9322 (7)	C11—C10	1.428 (5)
Zr1—O01	2.115 (2)	C11—H11	0.93
Zr1—O02	2.116 (3)	C02—C01	1.410 (5)
Zr1—O03	2.227 (3)	C02—H02	0.93
Zr1—N02	2.414 (3)	C10—H10	0.93
Zr1—N01	2.426 (3)	C09—C04	1.415 (5)
Zr1—Cl04	2.5597 (13)	C09—C08	1.427 (5)

Cl02—C14	1.741 (4)	C18—C13	1.409 (5)
Cl01—C05	1.744 (4)	C20—H20A	0.96
O01—C08	1.316 (4)	C20—H20B	0.96
O02—C17	1.307 (4)	C20—H20C	0.96
C03—C02	1.385 (6)	C05—C06	1.347 (6)
C03—C04	1.417 (6)	C05—C04	1.420 (6)
C03—H03	0.93	C01—H01	0.93
C17—C16	1.389 (5)	C14—C13	1.426 (5)
C17—C18	1.419 (5)	C19—H19	0.93
O03—C19	1.253 (5)	C06—H06	0.93
C07—C08	1.388 (5)	C21—H21A	0.96
C07—C06	1.412 (5)	C21—H21B	0.96
C15—C14	1.359 (5)	C21—H21C	0.96
C15—C16	1.415 (5)	C22—O04	1.193 (13)
C15—H15	0.93	C22—N04	1.402 (16)
N02—C10	1.323 (5)	C22—H22	0.93
N02—C18	1.376 (4)	C24—N04	1.405 (17)
N01—C01	1.324 (5)	C24—H24A	0.96
N01—C09	1.362 (5)	C24—H24B	0.96
O05—Zr1i	1.9322 (7)	C24—H24C	0.96
N03—C19	1.313 (5)	C23—N04	1.376 (15)
N03—C20	1.449 (5)	C23—H23A	0.96
N03—C21	1.461 (5)	C23—H23B	0.96
C12—C11	1.347 (5)	C23—H23C	0.96

Table A.3.12 Bond angles (°) for [ZrCl(CliOx)$_2$(DMF)$_2$O]$_2$·DMF.

Atoms	Bond angle (°)	Atoms	Bond angle (°)
O05—Zr1—O01	89.97 (7)	N02—C10—C11	123.1 (3)
O05—Zr1—O02	99.36 (8)	N02—C10—H10	118.5
O01—Zr1—O02	141.19 (10)	C11—C10—H10	118.5
O05—Zr1—O03	88.79 (7)	N01—C09—C04	122.8 (3)
O01—Zr1—O03	143.64 (9)	N01—C09—C08	114.8 (3)
O02—Zr1—O03	74.61 (9)	C04—C09—C08	122.4 (3)
O05—Zr1—N02	88.05 (7)	N02—C18—C13	123.0 (3)
O01—Zr1—N02	73.60 (10)	N02—C18—C17	113.8 (3)
O02—Zr1—N02	69.22 (10)	C13—C18—C17	123.1 (3)
O03—Zr1—N02	142.62 (10)	N03—C20—H20A	109.5
O05—Zr1—N01	85.07 (7)	N03—C20—H20B	109.5
O01—Zr1—N01	70.13 (10)	H20A—C20—H20B	109.5
O02—Zr1—N01	147.75 (10)	N03—C20—H20C	109.5
O03—Zr1—N01	73.56 (10)	H20A—C20—H20C	109.5
N02—Zr1—N01	143.03 (10)	H20B—C20—H20C	109.5
O05—Zr1—Cl04	170.65 (3)	C06—C05—C04	121.6 (4)
O01—Zr1—Cl04	88.54 (8)	C06—C05—Cl01	118.9 (3)
O02—Zr1—Cl04	87.53 (8)	C04—C05—Cl01	119.4 (3)
O03—Zr1—Cl04	86.95 (7)	O01—C08—C07	124.5 (3)
N02—Zr1—Cl04	100.37 (8)	O01—C08—C09	118.2 (3)

N01—Zr1—Cl04	85.75 (7)	C07—C08—C09	117.3 (3)
C08—O01—Zr1	122.7 (2)	N01—C01—C02	123.2 (4)
C17—O02—Zr1	125.3 (2)	N01—C01—H01	118.4
C02—C03—C04	118.4 (3)	C02—C01—H01	118.4
C02—C03—H03	120.8	C15—C14—C13	121.7 (3)
C04—C03—H03	120.8	C15—C14—Cl02	119.8 (3)
O02—C17—C16	125.2 (3)	C13—C14—Cl02	118.6 (3)
O02—C17—C18	117.7 (3)	O03—C19—N03	123.7 (4)
C16—C17—C18	117.1 (3)	O03—C19—H19	118.2
C19—O03—Zr1	128.5 (2)	N03—C19—H19	118.2
C08—C07—C06	120.8 (4)	C18—C13—C12	117.2 (3)
C08—C07—I01	120.2 (3)	C18—C13—C14	116.5 (3)
C06—C07—I01	119.0 (3)	C12—C13—C14	126.3 (3)
C14—C15—C16	120.3 (3)	C05—C06—C07	121.1 (4)
C14—C15—H15	119.8	C05—C06—H06	119.4
C16—C15—H15	119.8	C07—C06—H06	119.4
C10—N02—C18	117.4 (3)	C17—C16—C15	121.3 (3)
C10—N02—Zr1	128.7 (2)	C17—C16—I02	118.6 (3)
C18—N02—Zr1	113.8 (2)	C15—C16—I02	120.1 (3)
C01—N01—C09	118.1 (3)	N03—C21—H21A	109.5
C01—N01—Zr1	129.5 (2)	N03—C21—H21B	109.5
C09—N01—Zr1	112.0 (2)	H21A—C21—H21B	109.5
Zr1i—O05—Zr1	180	N03—C21—H21C	109.5
C19—N03—C20	122.8 (3)	H21A—C21—H21C	109.5
C19—N03—C21	120.7 (4)	H21B—C21—H21C	109.5
C20—N03—C21	116.3 (3)	C09—C04—C03	117.9 (3)
C11—C12—C13	120.1 (3)	C09—C04—C05	116.7 (4)
C11—C12—H12	119.9	C03—C04—C05	125.4 (3)
C13—C12—H12	119.9	O04—C22—N04	127.2 (13)
C12—C11—C10	119.1 (3)	O04—C22—H22	116.4
C12—C11—H11	120.4	N04—C22—H22	116.4
C10—C11—H11	120.4	C23—N04—C22	116.6 (16)
C03—C02—C01	119.5 (4)	C23—N04—C24	123.6 (16)
C03—C02—H02	120.3	C22—N04—C24	119.6 (13)
C01—C02—H02	120.3		

A.4. [Zr(diMeOx)$_4$]·2DMF − § 5.2

Table A.4.13 Fractional atomic coordinates and isotropic or equivalent isotropic displacement parameters (Å^2) for [Zr(diMeOx)$_4$]·2DMF.

	x	*y*	*z*	U_{iso}*/U_{eq}	*Occ. (<1)*
Zr01	0.966492 (14)	0.144909 (13)	0.35472 (2)	0.02309 (7)	
N02	0.96038 (15)	0.03649 (14)	0.43983 (17)	0.0263 (6)	
O01	0.89104 (13)	0.17186 (11)	0.46022 (13)	0.0298 (5)	
O04	1.02831 (11)	0.19246 (11)	0.24984 (13)	0.0272 (5)	
N04	0.87762 (15)	0.23774 (13)	0.29760 (17)	0.0264 (6)	
O03	0.85770 (12)	0.09319 (11)	0.30678 (14)	0.0280 (5)	
N01	1.01715 (16)	0.25660 (13)	0.41570 (17)	0.0293 (6)	
N03	1.01036 (15)	0.04556 (13)	0.26891 (17)	0.0254 (6)	
O02	1.08753 (12)	0.12303 (11)	0.40712 (14)	0.0273 (5)	
C16	1.1888 (2)	0.04676 (17)	0.4779 (2)	0.0325 (7)	
C28	0.79972 (18)	0.25710 (16)	0.3226 (2)	0.0296 (7)	
H28	0.7761	0.2349	0.3697	0.036*	
C10	0.8931 (2)	−0.00204 (18)	0.4598 (2)	0.0340 (8)	
H10	0.8392	0.0135	0.4426	0.041*	
C22	0.95416 (19)	−0.05991 (17)	0.1977 (2)	0.0259 (7)	
C07	0.8620 (2)	0.23819 (18)	0.5857 (2)	0.0352 (8)	
C25	0.79018 (19)	−0.01000 (18)	0.2459 (2)	0.0365 (8)	
C21	1.03964 (19)	−0.07792 (19)	0.1757 (2)	0.0321 (8)	
H21	1.0504	−0.1192	0.1447	0.039*	
C18	1.03967 (18)	0.01547 (17)	0.46770 (19)	0.0249 (6)	
C11	0.8992 (2)	−0.0660 (2)	0.5062 (2)	0.0420 (9)	
H11	0.8502	−0.0923	0.5188	0.050*	
C09	0.97620 (19)	0.27291 (17)	0.4898 (2)	0.0291 (7)	
C20	1.1060 (2)	−0.03518 (18)	0.1996 (2)	0.0352 (8)	
H20	1.162	−0.0464	0.1842	0.042*	
C14	1.1373 (2)	−0.06655 (18)	0.5408 (2)	0.0331 (8)	
C17	1.1079 (2)	0.06290 (17)	0.4491 (2)	0.0279 (7)	
C29	0.75126 (19)	0.30986 (17)	0.2807 (2)	0.0350 (8)	
H29	0.6965	0.3216	0.2997	0.042*	
C19	1.0886 (2)	0.02636 (18)	0.2480 (2)	0.0308 (7)	
H19	1.1344	0.0545	0.2658	0.037*	
C34	1.03498 (19)	0.27827 (19)	0.1370 (2)	0.0355 (8)	
C27	0.94305 (19)	0.00393 (16)	0.2438 (2)	0.0251 (7)	
C35	0.9944 (2)	0.24634 (17)	0.2046 (2)	0.0271 (7)	
C31	0.8680 (2)	0.32476 (19)	0.1830 (2)	0.0343 (8)	
C12	0.9788 (2)	−0.0889 (2)	0.5328 (2)	0.0391 (9)	
H12	0.9837	−0.1312	0.5632	0.047*	
C15	1.2007 (2)	−0.01837 (18)	0.5217 (2)	0.0383 (8)	
H15	1.2562	−0.0294	0.5391	0.046*	
C01	1.0838 (2)	0.29612 (16)	0.3916 (2)	0.0341 (8)	
H01	1.1107	0.2858	0.3407	0.041*	
C13	1.0527 (2)	−0.04865 (18)	0.5143 (2)	0.0299 (7)	

C02	1.1149 (2)	0.35303 (18)	0.4411 (3)	0.0428 (9)
H02	1.1621	0.3795	0.4232	0.051*
C04	1.0027 (2)	0.32917 (19)	0.5430 (3)	0.0403 (9)
C36	0.91150 (19)	0.27065 (17)	0.2282 (2)	0.0294 (7)
C4B	1.1235 (2)	0.2566 (2)	0.1105 (2)	0.0411 (9)
H4B1	1.1651	0.2818	0.144	0.062*
H4B2	1.1318	0.2681	0.0521	0.062*
H4B3	1.1305	0.2061	0.1186	0.062*
C33	0.9899 (3)	0.3324 (2)	0.0926 (3)	0.0465 (10)
H33	1.017	0.3533	0.0465	0.056*
C26	0.86087 (18)	0.03012 (16)	0.2668 (2)	0.0271 (7)
C2A	1.1541 (2)	−0.13465 (18)	0.5889 (2)	0.0426 (9)
H2A1	1.2148	−0.1407	0.5965	0.064*
H2A2	1.1316	−0.1745	0.5579	0.064*
H2A3	1.1266	−0.1321	0.643	0.064*
C24	0.8030 (2)	−0.07531 (18)	0.2025 (2)	0.0429 (9)
H24	0.7546	−0.1024	0.1898	0.051*
C08	0.9077 (2)	0.22612 (17)	0.5113 (2)	0.0305 (7)
C03	1.0751 (2)	0.36920 (19)	0.5160 (3)	0.0462 (10)
H03	1.0957	0.4065	0.5491	0.055*
C3A	0.8898 (2)	−0.17101 (18)	0.1313 (3)	0.0423 (9)
H3A1	0.8341	−0.1915	0.122	0.063*
H3A2	0.9241	−0.2034	0.164	0.063*
H3A3	0.9173	−0.1625	0.078	0.063*
C06	0.8904 (2)	0.2956 (2)	0.6375 (2)	0.0472 (10)
H06	0.8612	0.3029	0.688	0.057*
C1B	0.7879 (2)	0.1918 (2)	0.6074 (2)	0.0417 (9)
H1B1	0.7387	0.206	0.5749	0.062*
H1B2	0.7752	0.1963	0.6664	0.062*
H1B3	0.8018	0.1429	0.5948	0.062*
C05	0.9567 (3)	0.3408 (2)	0.6198 (3)	0.0512 (12)
C3B	0.7014 (2)	0.0168 (2)	0.2668 (3)	0.0577 (12)
H3B1	0.6853	0.0004	0.3219	0.086*
H3B2	0.6612	−0.0010	0.2259	0.086*
H3B3	0.7011	0.0681	0.2657	0.086*
C2B	1.2621 (2)	0.09889 (19)	0.4672 (3)	0.0432 (9)
H2B1	1.2871	0.0929	0.4123	0.065*
H2B2	1.3048	0.09	0.5096	0.065*
H2B3	1.2409	0.1468	0.4729	0.065*
C4A	0.8653 (3)	0.4166 (3)	0.0640 (3)	0.0686 (14)
H4A1	0.9049	0.4358	0.0234	0.103*
H4A2	0.8481	0.4537	0.1023	0.103*
H4A3	0.8157	0.3983	0.0353	0.103*
C30	0.7852 (2)	0.34338 (18)	0.2126 (2)	0.0379 (8)
H30	0.7538	0.3788	0.1852	0.046*
C23	0.8804 (2)	−0.10147 (17)	0.1780 (2)	0.0329 (8)
C32	0.9087 (3)	0.3562 (2)	0.1132 (3)	0.0497 (10)
C1A	0.9854 (3)	0.3987 (3)	0.6802 (3)	0.0792 (17)
H1A1	0.9753	0.4447	0.6553	0.119*

H1A2	1.0455	0.3932	0.6919	0.119*	
H1A3	0.9534	0.3948	0.7318	0.119*	
N05	0.5984 (2)	0.0129 (2)	0.8445 (3)	0.0738 (11)	
C38	0.5443 (3)	−0.0454 (3)	0.8136 (3)	0.0689 (13)	
H38A	0.556	−0.0535	0.7549	0.103*	
H38B	0.4849	−0.0327	0.8205	0.103*	
H38C	0.5563	−0.0881	0.845	0.103*	
C39	0.5748 (5)	0.0406 (5)	0.9249 (5)	0.145 (3)	
H39A	0.608	0.0827	0.9367	0.217*	
H39B	0.5857	0.0053	0.9676	0.217*	
H39C	0.5149	0.0526	0.9248	0.217*	
C37	0.6631 (3)	0.0338 (3)	0.7988 (5)	0.0922 (18)	
H37	0.6961	0.0693	0.8241	0.111*	
O05	0.6878 (2)	0.0166 (2)	0.7324 (3)	0.0954 (13)	
N06	0.367 (2)	0.2636 (14)	0.8657 (9)	0.136 (5)	0.358(10)
C41	0.458 (2)	0.265 (2)	0.8603 (11)	0.123 (7)	0.358(10)
C42	0.317 (3)	0.3238 (14)	0.8704 (14)	0.139 (8)	0.358(10)
C40	0.3340 (18)	0.1919 (13)	0.8686 (12)	0.148 (6)	0.358(10)
H40	0.277	0.1785	0.8757	0.177*	0.358(10)
O06	0.4027 (14)	0.1472 (8)	0.8588 (10)	0.175 (7)	0.358(10)
N07	0.5373 (19)	0.2729 (12)	0.8523 (17)	0.165 (8)	0.280(7)
C45	0.462 (2)	0.3160 (16)	0.8425 (17)	0.153 (9)	0.280(7)
C44	0.529 (2)	0.2033 (12)	0.8762 (12)	0.173 (10)	0.280(7)
C43	0.619 (2)	0.3016 (17)	0.843 (2)	0.204 (11)	0.280(7)
H43	0.6232	0.3504	0.8321	0.245*	0.280(7)
O07	0.6920 (19)	0.2630 (16)	0.8476 (15)	0.255 (13)	0.280(7)
N08	0.3765 (18)	0.2737 (12)	0.8781 (14)	0.133 (5)	0.362(8)
C48	0.4665 (19)	0.2784 (19)	0.8670 (17)	0.114 (7)	0.362(8)
C47	0.3564 (17)	0.2039 (8)	0.9056 (9)	0.117 (6)	0.362(8)
C46	0.318 (2)	0.3254 (15)	0.854 (2)	0.133 (6)	0.362(8)
H46	0.3358	0.3639	0.8218	0.160*	0.362(8)
O08	0.2331 (12)	0.3208 (7)	0.8783 (8)	0.130 (6)	0.362(8)

Table A.4.14 Atomic displacement parameters (Å^2) for [Zr(diMeOx)$_4$]·2DMF.

	U^{11}	U^{22}	U^{33}	U^{12}	U^{13}	U^{23}
Zr01	0.01672 (11)	0.02220 (12)	0.03037 (13)	0.00032 (10)	−0.00127 (16)	−0.00252 (17)
N02	0.0215 (13)	0.0291 (15)	0.0283 (15)	0.0004 (11)	0.0023 (11)	−0.0050 (12)
O01	0.0277 (11)	0.0254 (11)	0.0362 (13)	0.0038 (9)	0.0013 (9)	−0.0052 (10)
O04	0.0178 (10)	0.0271 (11)	0.0366 (12)	0.0001 (8)	−0.0011 (9)	−0.0013 (10)
N04	0.0178 (11)	0.0265 (13)	0.0348 (15)	0.0009 (10)	−0.0018 (10)	−0.0048 (12)
O03	0.0166 (10)	0.0281 (11)	0.0394 (12)	0.0007 (8)	−0.0009 (9)	−0.0066 (10)
N01	0.0253 (13)	0.0242 (14)	0.0385 (16)	0.0035 (10)	−0.0081 (11)	−0.0033 (12)
N03	0.0171 (12)	0.0254 (14)	0.0337 (15)	0.0004 (10)	0.0017 (11)	−0.0004 (12)
O02	0.0196 (10)	0.0245 (11)	0.0376 (12)	0.0013 (9)	−0.0036 (9)	−0.0007 (10)
C16	0.0260 (16)	0.0304 (18)	0.0410 (19)	0.0008 (13)	−0.0038 (14)	0.0015 (15)
C28	0.0205 (14)	0.0277 (17)	0.0405 (17)	0.0008 (12)	0.0013 (12)	−0.0039 (13)
C10	0.0224 (16)	0.042 (2)	0.0373 (19)	0.0005 (14)	0.0033 (14)	0.0018 (17)

C22	0.0218 (15)	0.0225 (16)	0.0334 (17)	0.0000 (12)	−0.0005 (13)	−0.0028 (14)
C07	0.0312 (17)	0.041 (2)	0.0332 (18)	0.0200 (15)	−0.0068 (14)	−0.0059 (16)
C25	0.0209 (15)	0.0358 (19)	0.053 (2)	−0.0037 (13)	0.0038 (14)	−0.0126 (17)
C21	0.0261 (17)	0.033 (2)	0.038 (2)	0.0020 (14)	0.0041 (14)	−0.0104 (16)
C18	0.0216 (15)	0.0272 (16)	0.0260 (17)	0.0034 (12)	0.0047 (13)	−0.0006 (13)
C11	0.0295 (18)	0.044 (2)	0.053 (2)	−0.0062 (16)	0.0080 (17)	0.0112 (19)
C09	0.0297 (17)	0.0242 (17)	0.0335 (18)	0.0100 (13)	−0.0109 (14)	−0.0070 (14)
C20	0.0211 (15)	0.040 (2)	0.045 (2)	0.0003 (14)	0.0041 (14)	−0.0125 (17)
C14	0.0278 (16)	0.0341 (19)	0.0374 (19)	0.0057 (14)	−0.0001 (14)	0.0050 (16)
C17	0.0279 (16)	0.0258 (17)	0.0299 (16)	0.0041 (13)	0.0012 (13)	−0.0007 (14)
C29	0.0195 (15)	0.0331 (18)	0.052 (2)	0.0028 (13)	−0.0028 (15)	−0.0009 (17)
C19	0.0220 (15)	0.0337 (19)	0.0369 (19)	−0.0021 (13)	0.0015 (14)	−0.0029 (15)
C34	0.0252 (16)	0.044 (2)	0.0372 (18)	0.0000 (14)	−0.0011 (14)	0.0033 (16)
C27	0.0203 (14)	0.0279 (17)	0.0271 (17)	−0.0024 (13)	0.0004 (12)	−0.0037 (14)
C35	0.0217 (14)	0.0270 (18)	0.0327 (17)	0.0000 (13)	−0.0053 (13)	−0.0015 (14)
C31	0.0291 (16)	0.0387 (19)	0.0351 (19)	0.0027 (14)	−0.0048 (14)	0.0045 (16)
C12	0.0354 (19)	0.034 (2)	0.048 (2)	0.0045 (15)	0.0085 (16)	0.0068 (18)
C15	0.0287 (17)	0.038 (2)	0.048 (2)	0.0093 (15)	−0.0044 (15)	0.0041 (17)
C01	0.0266 (16)	0.0250 (16)	0.051 (2)	0.0009 (13)	−0.0092 (14)	−0.0023 (15)
C13	0.0318 (17)	0.0272 (18)	0.0308 (18)	0.0025 (14)	0.0052 (14)	−0.0001 (15)
C02	0.0318 (17)	0.0268 (18)	0.070 (3)	0.0010 (14)	−0.0182 (18)	−0.0059 (18)
C04	0.0322 (17)	0.0320 (19)	0.057 (2)	0.0134 (16)	−0.0177 (17)	−0.0134 (18)
C36	0.0234 (15)	0.0298 (17)	0.0350 (18)	−0.0042 (13)	−0.0023 (13)	−0.0025 (15)
C4B	0.0285 (17)	0.052 (2)	0.043 (2)	−0.0002 (15)	0.0010 (15)	0.0110 (18)
C33	0.041 (2)	0.059 (2)	0.039 (2)	0.008 (2)	0.0064 (19)	0.018 (2)
C26	0.0219 (14)	0.0235 (16)	0.0359 (18)	−0.0007 (12)	0.0015 (13)	−0.0036 (14)
C2A	0.0373 (19)	0.039 (2)	0.052 (2)	0.0083 (16)	−0.0011 (17)	0.0088 (18)
C24	0.0271 (17)	0.038 (2)	0.063 (2)	−0.0140 (15)	−0.0017 (16)	−0.0140 (19)
C08	0.0291 (16)	0.0291 (17)	0.0332 (17)	0.0120 (14)	−0.0088 (14)	−0.0045 (15)
C03	0.0324 (19)	0.035 (2)	0.072 (3)	0.0065 (15)	−0.0233 (19)	−0.0210 (19)
C3A	0.0358 (19)	0.0308 (18)	0.060 (2)	−0.0056 (15)	0.0000 (17)	−0.0133 (18)
C06	0.041 (2)	0.062 (3)	0.038 (2)	0.029 (2)	−0.0100 (17)	−0.0192 (19)
C1B	0.0339 (18)	0.056 (2)	0.0349 (19)	0.0197 (17)	−0.0002 (15)	−0.0065 (18)
C05	0.045 (2)	0.054 (3)	0.054 (3)	0.020 (2)	−0.021 (2)	−0.032 (2)
C3B	0.0235 (17)	0.057 (2)	0.093 (3)	−0.0050 (16)	−0.003 (2)	−0.031 (2)
C2B	0.0260 (16)	0.043 (2)	0.061 (2)	−0.0029 (15)	−0.0113 (16)	0.0138 (19)
C4A	0.055 (3)	0.090 (4)	0.061 (3)	0.032 (2)	0.007 (2)	0.034 (3)
C30	0.0279 (16)	0.041 (2)	0.045 (2)	0.0100 (15)	−0.0068 (15)	0.0013 (17)
C23	0.0295 (16)	0.0274 (18)	0.042 (2)	−0.0038 (14)	0.0029 (14)	−0.0051 (15)
C32	0.041 (2)	0.062 (3)	0.046 (2)	0.0143 (19)	0.0002 (18)	0.017 (2)
C1A	0.057 (3)	0.092 (4)	0.088 (4)	0.020 (3)	−0.021 (3)	−0.064 (3)
N05	0.0427 (18)	0.080 (2)	0.098 (3)	0.0169 (18)	0.001 (2)	0.007 (3)
C38	0.042 (2)	0.081 (3)	0.084 (3)	0.003 (2)	−0.001 (2)	0.009 (3)
C39	0.095 (5)	0.184 (8)	0.154 (7)	0.069 (5)	−0.008 (5)	−0.075 (6)
C37	0.049 (3)	0.091 (4)	0.137 (5)	0.010 (3)	0.005 (3)	0.013 (4)
O05	0.0440 (19)	0.111 (3)	0.132 (4)	0.0007 (19)	0.018 (2)	0.027 (3)
N06	0.254 (12)	0.120 (9)	0.035 (8)	0.046 (9)	0.010 (9)	−0.008 (8)
C41	0.227 (15)	0.093 (14)	0.051 (12)	−0.032 (13)	0.000 (14)	0.007 (12)
C42	0.270 (18)	0.094 (12)	0.053 (14)	0.039 (15)	−0.036 (14)	−0.002 (10)

C40	0.274 (15)	0.115 (11)	0.054 (10)	0.039 (11)	0.019 (12)	0.024 (11)
O06	0.299 (19)	0.158 (12)	0.068 (7)	0.052 (12)	0.002 (15)	0.016 (10)
N07	0.29 (2)	0.162 (15)	0.041 (8)	0.021 (17)	0.056 (15)	0.010 (12)
C45	0.29 (2)	0.142 (18)	0.032 (13)	−0.023 (17)	−0.012 (14)	0.003 (13)
C44	0.37 (3)	0.112 (16)	0.038 (12)	0.052 (19)	0.065 (15)	0.001 (11)
C43	0.34 (2)	0.20 (2)	0.071 (14)	0.03 (2)	0.03 (2)	0.021 (16)
O07	0.39 (3)	0.31 (3)	0.064 (11)	0.15 (2)	−0.027 (19)	0.055 (17)
N08	0.254 (12)	0.101 (9)	0.043 (7)	0.021 (9)	−0.004 (9)	−0.012 (7)
C48	0.213 (15)	0.087 (15)	0.041 (12)	−0.020 (13)	0.027 (12)	−0.005 (10)
C47	0.292 (18)	0.027 (7)	0.031 (7)	0.010 (9)	−0.040 (10)	−0.002 (6)
C46	0.261 (14)	0.095 (11)	0.043 (9)	0.038 (11)	−0.021 (11)	−0.010 (10)
O08	0.216 (15)	0.078 (8)	0.095 (11)	0.023 (10)	−0.010 (11)	0.005 (7)

Table A.4.15 Bond lengths (Å) for [Zr(diMeOx)$_4$]·2DMF.

Atoms	Bond length (Å)	Atoms	Bond length (Å)
Zr01—O03	2.094 (2)	C20—C19	1.410 (5)
Zr01—O02	2.100 (2)	C14—C15	1.370 (4)
Zr01—O01	2.105 (2)	C14—C13	1.422 (4)
Zr01—O04	2.117 (2)	C14—C2A	1.508 (5)
Zr01—N04	2.398 (2)	C29—C30	1.356 (5)
Zr01—N03	2.402 (3)	C34—C35	1.381 (5)
Zr01—N01	2.433 (3)	C34—C33	1.419 (5)
Zr01—N02	2.438 (3)	C34—C4B	1.497 (4)
N02—C10	1.310 (4)	C27—C26	1.418 (4)
N02—C18	1.369 (4)	C35—C36	1.419 (4)
O01—C08	1.325 (4)	C31—C32	1.405 (5)
O04—C35	1.345 (4)	C31—C36	1.414 (4)
N04—C28	1.326 (4)	C31—C30	1.416 (4)
N04—C36	1.366 (4)	C12—C13	1.406 (5)
O03—C26	1.340 (4)	C01—C02	1.408 (5)
N01—C01	1.331 (4)	C02—C03	1.373 (6)
N01—C09	1.371 (4)	C04—C03	1.420 (6)
N03—C19	1.314 (4)	C04—C05	1.428 (6)
N03—C27	1.365 (4)	C33—C32	1.379 (5)
O02—C17	1.345 (4)	C24—C23	1.359 (4)
C16—C17	1.375 (4)	C3A—C23	1.504 (5)
C16—C15	1.415 (5)	C06—C05	1.364 (6)
C16—C2B	1.510 (4)	C05—C1A	1.513 (6)
C28—C29	1.408 (4)	C4A—C32	1.530 (5)
C10—C11	1.407 (5)	N05—C37	1.301 (7)
C22—C27	1.411 (4)	N05—C39	1.425 (8)
C22—C21	1.417 (4)	N05—C38	1.462 (6)
C22—C23	1.421 (4)	C37—O05	1.166 (7)
C07—C08	1.395 (5)	N06—C42	1.371 (17)
C07—C06	1.424 (5)	N06—C41	1.428 (16)
C07—C1B	1.485 (5)	N06—C40	1.435 (17)
C25—C26	1.373 (4)	C40—O06	1.37 (2)

Atoms	Length	Atoms	Length
C25—C24	1.416 (5)	N07—C44	1.361 (17)
C25—C3B	1.508 (4)	N07—C43	1.385 (18)
C21—C20	1.360 (4)	N07—C45	1.431 (18)
C18—C17	1.415 (4)	C43—O07	1.35 (2)
C18—C13	1.423 (5)	N08—C46	1.383 (17)
C11—C12	1.378 (5)	N08—C47	1.411 (17)
C09—C04	1.410 (5)	N08—C48	1.416 (16)
C09—C08	1.421 (5)	C46—O08	1.37 (3)

Table A.4.16 Bond angles (°) for [Zr(diMeOx)$_4$]·2DMF.

Atoms	Bond angle (°)	Atoms	Bond angle (°)
O03—Zr01—O02	141.24 (8)	C15—C14—C2A	122.8 (3)
O03—Zr01—O01	86.99 (8)	C13—C14—C2A	120.6 (3)
O02—Zr01—O01	103.49 (9)	O02—C17—C16	124.3 (3)
O03—Zr01—O04	106.08 (8)	O02—C17—C18	116.8 (3)
O02—Zr01—O04	89.11 (8)	C16—C17—C18	118.8 (3)
O01—Zr01—O04	140.99 (8)	C30—C29—C28	119.4 (3)
O03—Zr01—N04	74.37 (8)	N03—C19—C20	122.6 (3)
O02—Zr01—N04	143.94 (8)	C35—C34—C33	117.9 (3)
O01—Zr01—N04	78.72 (9)	C35—C34—C4B	121.5 (3)
O04—Zr01—N04	70.22 (8)	C33—C34—C4B	120.7 (3)
O03—Zr01—N03	70.55 (8)	N03—C27—C22	122.7 (3)
O02—Zr01—N03	79.51 (8)	N03—C27—C26	114.9 (3)
O01—Zr01—N03	142.55 (8)	C22—C27—C26	122.4 (3)
O04—Zr01—N03	75.58 (8)	O04—C35—C34	124.0 (3)
N04—Zr01—N03	120.70 (9)	O04—C35—C36	117.2 (3)
O03—Zr01—N01	143.44 (8)	C34—C35—C36	118.8 (3)
O02—Zr01—N01	73.69 (8)	C32—C31—C36	118.9 (3)
O01—Zr01—N01	70.10 (9)	C32—C31—C30	124.7 (3)
O04—Zr01—N01	78.69 (9)	C36—C31—C30	116.4 (3)
N04—Zr01—N01	73.46 (8)	C11—C12—C13	120.4 (4)
N03—Zr01—N01	142.84 (8)	C14—C15—C16	125.5 (3)
O03—Zr01—N02	77.58 (8)	N01—C01—C02	121.9 (3)
O02—Zr01—N02	69.76 (8)	C12—C13—C14	124.7 (3)
O01—Zr01—N02	74.79 (8)	C12—C13—C18	116.3 (3)
O04—Zr01—N02	143.32 (8)	C14—C13—C18	118.9 (3)
N04—Zr01—N02	142.08 (8)	C03—C02—C01	119.5 (3)
N03—Zr01—N02	71.39 (8)	C09—C04—C03	116.4 (4)
N01—Zr01—N02	120.46 (9)	C09—C04—C05	118.4 (4)
C10—N02—C18	119.0 (3)	C03—C04—C05	125.1 (3)
C10—N02—Zr01	128.5 (2)	N04—C36—C31	123.1 (3)
C18—N02—Zr01	112.47 (19)	N04—C36—C35	114.8 (3)
C08—O01—Zr01	124.1 (2)	C31—C36—C35	122.1 (3)
C35—O04—Zr01	123.72 (18)	C32—C33—C34	124.5 (4)
C28—N04—C36	118.1 (3)	O03—C26—C25	124.5 (3)
C28—N04—Zr01	127.8 (2)	O03—C26—C27	117.3 (2)
C36—N04—Zr01	114.04 (19)	C25—C26—C27	118.2 (3)

C26—O03—Zr01	123.27 (17)	C23—C24—C25	125.1 (3)
C01—N01—C09	119.0 (3)	O01—C08—C07	122.7 (3)
C01—N01—Zr01	128.0 (2)	O01—C08—C09	118.2 (3)
C09—N01—Zr01	112.4 (2)	C07—C08—C09	119.1 (3)
C19—N03—C27	118.9 (3)	C02—C03—C04	120.2 (3)
C19—N03—Zr01	128.2 (2)	C05—C06—C07	125.7 (4)
C27—N03—Zr01	112.84 (19)	C06—C05—C04	117.5 (4)
C17—O02—Zr01	124.74 (18)	C06—C05—C1A	122.4 (5)
C17—C16—C15	118.2 (3)	C04—C05—C1A	120.0 (4)
C17—C16—C2B	120.9 (3)	C29—C30—C31	120.3 (3)
C15—C16—C2B	120.8 (3)	C24—C23—C22	117.2 (3)
N04—C28—C29	122.7 (3)	C24—C23—C3A	122.6 (3)
N02—C10—C11	122.7 (3)	C22—C23—C3A	120.2 (3)
C27—C22—C21	116.4 (3)	C33—C32—C31	117.7 (3)
C27—C22—C23	118.6 (3)	C33—C32—C4A	121.5 (4)
C21—C22—C23	125.1 (3)	C31—C32—C4A	120.8 (3)
C08—C07—C06	116.8 (3)	C37—N05—C39	126.0 (6)
C08—C07—C1B	119.9 (3)	C37—N05—C38	119.0 (5)
C06—C07—C1B	123.3 (3)	C39—N05—C38	115.0 (5)
C26—C25—C24	118.5 (3)	O05—C37—N05	132.5 (7)
C26—C25—C3B	120.0 (3)	C42—N06—C41	123.7 (19)
C24—C25—C3B	121.5 (3)	C42—N06—C40	124.4 (18)
C20—C21—C22	120.4 (3)	C41—N06—C40	111.9 (16)
N02—C18—C17	115.4 (3)	O06—C40—N06	106.9 (19)
N02—C18—C13	122.5 (3)	C44—N07—C43	119.2 (19)
C17—C18—C13	122.0 (3)	C44—N07—C45	119 (2)
C12—C11—C10	119.0 (3)	C43—N07—C45	121.2 (19)
N01—C09—C04	122.8 (3)	O07—C43—N07	124 (3)
N01—C09—C08	114.7 (3)	C46—N08—C47	125.7 (17)
C04—C09—C08	122.4 (3)	C46—N08—C48	125.4 (18)
C21—C20—C19	119.1 (3)	C47—N08—C48	108.3 (16)
C15—C14—C13	116.6 (3)	O08—C46—N08	121 (2)

A.5. [Zr(5-NO$_2$Ox)$_4$] – § 5.3

Table A.5.17 Fractional atomic coordinates and isotropic or equivalent isotropic displacement parameters (Å^2) for [Zr(5-NO$_2$Ox)$_4$].

	x	*y*	*z*	*U$_{iso}$*/U$_{eq}$*	*Occ. (<1)*
C4A	0.5579 (14)	0.1525 (13)	0.5766 (8)	0.074 (7)	0.512(8)
C9A	0.5536 (12)	0.1118 (12)	0.6356 (8)	0.063 (4)	0.512(8)
N2A	0.6555 (11)	0.2054 (8)	0.4892 (5)	0.096 (3)	0.512(8)
C5A	0.6507 (16)	0.1693 (9)	0.5506 (6)	0.077 (4)	0.512(8)
C3A	0.4696 (15)	0.1771 (9)	0.5533 (7)	0.059 (4)	0.512(8)
H3A	0.4672	0.2078	0.5155	0.071*	0.512(8)
C6A	0.7254 (11)	0.1406 (11)	0.5815 (7)	0.081 (3)	0.512(8)
H6A	0.7813	0.1386	0.5604	0.097*	0.512(8)
C7A	0.724 (3)	0.112 (2)	0.6456 (14)	0.156 (16)	0.512(8)
H7A	0.7786	0.1094	0.6685	0.188*	0.512(8)
C1A	0.3952 (10)	0.1124 (13)	0.6333 (7)	0.051 (4)	0.512(8)
H1A	0.3415	0.0933	0.6532	0.062*	0.512(8)
C2A	0.3902 (14)	0.1592 (12)	0.5817 (8)	0.095 (7)	0.512(8)
H2A	0.334	0.1789	0.5657	0.115*	0.512(8)
C8A	0.6384 (14)	0.0898 (9)	0.6721 (7)	0.063 (4)	0.512(8)
O1A	0.6201 (9)	0.0464 (10)	0.7125 (5)	0.064 (3)	0.512(8)
O2A	0.5963 (9)	0.1986 (6)	0.4524 (4)	0.096 (3)	0.512(8)
O3A	0.7247 (15)	0.2375 (14)	0.4755 (9)	0.157 (5)	0.512(8)
N1A	0.4762 (10)	0.0926 (11)	0.6570 (8)	0.038 (2)	0.512(8)
C5B	0.6941 (10)	0.1664 (9)	0.5685 (7)	0.057 (3)	0.488(8)
C9B	0.5832 (12)	0.1080 (12)	0.6321 (9)	0.049 (3)	0.488(8)
C4B	0.6014 (12)	0.1577 (12)	0.5804 (7)	0.053 (4)	0.488(8)
N2B	0.7203 (12)	0.2114 (11)	0.5111 (6)	0.116 (5)	0.488(8)
C3B	0.5240 (14)	0.1876 (8)	0.5523 (6)	0.049 (3)	0.488(8)
H3B	0.5299	0.2212	0.5159	0.059*	0.488(8)
C7B	0.7381 (14)	0.0835 (12)	0.6464 (13)	0.093 (7)	0.488(8)
H7B	0.7844	0.0555	0.6695	0.111*	0.488(8)
C6B	0.7655 (9)	0.1291 (11)	0.6012 (7)	0.081 (3)	0.488(8)
H6B	0.8274	0.1368	0.5909	0.097*	0.488(8)
C1B	0.4312 (9)	0.1208 (9)	0.6346 (6)	0.038 (3)	0.488(8)
H1B	0.3741	0.1103	0.653	0.045*	0.488(8)
C2B	0.4333 (12)	0.1704 (8)	0.5754 (5)	0.051 (4)	0.488(8)
H2B	0.3802	0.189	0.5548	0.061*	0.488(8)
C8B	0.6552 (11)	0.0692 (7)	0.6662 (6)	0.049 (3)	0.488(8)
O1B	0.6359 (7)	0.0314 (7)	0.7253 (4)	0.0332 (15)	0.488(8)
O2B	0.7986 (13)	0.2192 (12)	0.4990 (12)	0.157 (5)	0.488(8)
O3B	0.6673 (12)	0.2477 (11)	0.4797 (4)	0.116 (5)	0.488(8)
N1B	0.5054 (10)	0.0904 (12)	0.6633 (9)	0.038 (2)	0.488(8)
Zr1	0.5	0	0.75	0.0390 (2)	

Table A.5.18 Atomic displacement parameters (Å^2) for [Zr(5-NO$_2$Ox)$_4$].

	U^{11}	U^{22}	U^{33}	U^{12}	U^{13}	U^{23}
C4A	0.133 (18)	0.028 (5)	0.062 (9)	−0.023 (10)	0.048 (12)	−0.010 (6)
C9A	0.081 (8)	0.048 (5)	0.060 (6)	−0.007 (6)	0.042 (6)	−0.011 (4)
N2A	0.156 (8)	0.063 (3)	0.070 (4)	0.017 (5)	0.033 (4)	0.026 (4)
C5A	0.128 (14)	0.052 (6)	0.052 (6)	−0.016 (9)	0.026 (9)	0.007 (5)
C3A	0.081 (10)	0.046 (7)	0.050 (9)	0.014 (8)	−0.007 (10)	−0.005 (7)
C6A	0.051 (7)	0.101 (7)	0.090 (8)	0.015 (7)	0.024 (6)	0.034 (6)
C7A	0.21 (3)	0.16 (3)	0.106 (16)	−0.10 (2)	0.023 (18)	−0.025 (17)
C1A	0.039 (7)	0.073 (9)	0.042 (5)	0.021 (7)	−0.021 (6)	0.000 (5)
C2A	0.112 (15)	0.087 (11)	0.088 (11)	0.031 (10)	0.073 (11)	0.020 (8)
C8A	0.081 (8)	0.048 (5)	0.060 (6)	−0.007 (6)	0.042 (6)	−0.011 (4)
O1A	0.052 (6)	0.101 (8)	0.038 (5)	0.008 (5)	−0.017 (3)	0.023 (4)
O2A	0.156 (8)	0.063 (3)	0.070 (4)	0.017 (5)	0.033 (4)	0.026 (4)
O3A	0.168 (11)	0.152 (8)	0.150 (10)	0.020 (9)	0.088 (11)	0.058 (8)
N1A	0.036 (9)	0.0347 (14)	0.043 (4)	0.015 (6)	−0.031 (6)	−0.0005 (19)
C5B	0.051 (7)	0.051 (6)	0.071 (8)	0.018 (5)	0.008 (5)	0.027 (5)
C9B	0.060 (6)	0.032 (3)	0.053 (6)	0.007 (4)	0.030 (4)	−0.007 (3)
C4B	0.083 (10)	0.034 (6)	0.043 (6)	0.003 (8)	0.022 (8)	0.011 (5)
N2B	0.158 (10)	0.121 (7)	0.068 (5)	0.076 (8)	0.058 (6)	0.049 (5)
C3B	0.082 (9)	0.026 (4)	0.038 (6)	0.000 (5)	0.009 (7)	0.004 (3)
C7B	0.081 (8)	0.056 (7)	0.141 (16)	−0.003 (6)	0.073 (10)	0.020 (8)
C6B	0.051 (7)	0.101 (7)	0.090 (8)	0.015 (7)	0.024 (6)	0.034 (6)
C1B	0.030 (6)	0.039 (5)	0.044 (5)	0.001 (6)	−0.024 (6)	−0.007 (4)
C2B	0.072 (11)	0.058 (6)	0.022 (5)	0.021 (7)	0.021 (5)	0.014 (4)
C8B	0.060 (6)	0.032 (3)	0.053 (6)	0.007 (4)	0.030 (4)	−0.007 (3)
O1B	0.029 (4)	0.044 (3)	0.027 (4)	0.004 (2)	−0.012 (3)	0.022 (2)
O2B	0.168 (11)	0.152 (8)	0.150 (10)	0.020 (9)	0.088 (11)	0.058 (8)
O3B	0.158 (10)	0.121 (7)	0.068 (5)	0.076 (8)	0.058 (6)	0.049 (5)
N1B	0.036 (9)	0.0347 (14)	0.043 (4)	0.015 (6)	−0.031 (6)	−0.0005 (19)
Zr1	0.0387 (3)	0.0387 (3)	0.0396 (3)	0	0	0

Table A.5.19 Bond lengths (Å) for [Zr(5-NO$_2$Ox)$_4$].

Atoms	Bond length (Å)	Atoms	Bond length (Å)
C4A—C9A	1.44 (3)	**C9B—C8B**	1.42 (2)
C4A—C3A	1.45 (3)	**C4B—C3B**	1.38 (2)
C4A—C5A	1.51 (2)	**N2B—O3B**	1.177 (19)
C9A—N1A	1.27 (2)	**N2B—O2B**	1.195 (17)
C9A—C8A	1.53 (2)	**C3B—C2B**	1.46 (2)
N2A—O3A	1.17 (2)	**C3B—H3B**	0.95
N2A—O2A	1.198 (15)	**C7B—C6B**	1.27 (3)
N2A—C5A	1.459 (13)	**C7B—C8B**	1.32 (2)
C5A—C6A	1.37 (2)	**C7B—H7B**	0.95
C3A—C2A	1.36 (2)	**C6B—H6B**	0.95
C3A—H3A	0.95	**C1B—N1B**	1.344 (13)
C6A—C7A	1.47 (3)	**C1B—C2B**	1.50 (2)

Atoms	Bond length (Å)	Atoms	Bond length (Å)
C6A—H6A	0.95	C1B—H1B	0.95
C7A—C8A	1.44 (4)	C2B—H2B	0.95
C7A—H7A	0.95	C8B—O1B	1.450 (16)
C1A—C2A	1.33 (2)	O1B—Zr1	2.134 (11)
C1A—N1A	1.341 (13)	N1B—Zr1	2.34 (2)
C1A—H1A	0.95	Zr1—O1Ai	2.078 (15)
C2A—H2A	0.95	Zr1—O1Aii	2.078 (15)
C8A—O1A	1.13 (2)	Zr1—O1Aiii	2.078 (15)
O1A—Zr1	2.078 (15)	Zr1—O1Bii	2.134 (11)
N1A—Zr1	2.493 (17)	Zr1—O1Biii	2.134 (11)
C5B—C6B	1.393 (16)	Zr1—O1Bi	2.134 (11)
C5B—C4B	1.40 (2)	Zr1—N1Bi	2.34 (2)
C5B—N2B	1.484 (18)	Zr1—N1Biii	2.34 (2)
C9B—N1B	1.37 (2)	Zr1—N1Bii	2.34 (2)
C9B—C4B	1.38 (2)		

Table A.5.20 Bond angles (°) for [Zr(5-NO$_2$Ox)$_4$].

Atoms	Bond angle (°)	Atoms	Bond angle (°)
C9A—C4A—C3A	112.7 (13)	C9B—N1B—Zr1	123.5 (12)
C9A—C4A—C5A	117.1 (18)	O1Ai—Zr1—O1Aii	99.1 (2)
C3A—C4A—C5A	130.0 (18)	O1Ai—Zr1—O1Aiii	133.0 (6)
N1A—C9A—C4A	118.2 (17)	O1Aii—Zr1—O1Aiii	99.1 (2)
N1A—C9A—C8A	119.7 (12)	O1Ai—Zr1—O1A	99.1 (2)
C4A—C9A—C8A	122.1 (13)	O1Aii—Zr1—O1A	133.0 (6)
O3A—N2A—O2A	120.1 (15)	O1Aiii—Zr1—O1A	99.1 (2)
O3A—N2A—C5A	115.5 (17)	O1Ai—Zr1—O1Bii	88.7 (5)
O2A—N2A—C5A	124.2 (13)	O1Aii—Zr1—O1Bii	11.6 (3)
C6A—C5A—N2A	122.6 (15)	O1Aiii—Zr1—O1Bii	103.1 (6)
C6A—C5A—C4A	119.6 (13)	O1A—Zr1—O1Bii	140.9 (3)
N2A—C5A—C4A	117.3 (17)	O1Ai—Zr1—O1Biii	140.9 (3)
C2A—C3A—C4A	124.4 (16)	O1Aii—Zr1—O1Biii	88.7 (5)
C2A—C3A—H3A	117.8	O1Aiii—Zr1—O1Biii	11.6 (3)
C4A—C3A—H3A	117.8	O1A—Zr1—O1Biii	103.1 (6)
C5A—C6A—C7A	124.0 (18)	O1Bii—Zr1—O1Biii	93.73 (12)
C5A—C6A—H6A	118	O1Ai—Zr1—O1Bi	11.6 (3)
C7A—C6A—H6A	118	O1Aii—Zr1—O1Bi	103.1 (6)
C8A—C7A—C6A	118 (3)	O1Aiii—Zr1—O1Bi	140.9 (3)
C8A—C7A—H7A	121.2	O1A—Zr1—O1Bi	88.7 (5)
C6A—C7A—H7A	121.2	O1Bii—Zr1—O1Bi	93.73 (12)
C2A—C1A—N1A	119.7 (15)	O1Biii—Zr1—O1Bi	150.4 (5)
C2A—C1A—H1A	120.2	O1Ai—Zr1—O1B	103.1 (6)
N1A—C1A—H1A	120.2	O1Aii—Zr1—O1B	140.9 (3)
C1A—C2A—C3A	116.7 (17)	O1Aiii—Zr1—O1B	88.7 (5)
C1A—C2A—H2A	121.7	O1A—Zr1—O1B	11.6 (3)
C3A—C2A—H2A	121.7	O1Bii—Zr1—O1B	150.4 (5)
O1A—C8A—C7A	132 (2)	O1Biii—Zr1—O1B	93.73 (12)
O1A—C8A—C9A	110.0 (15)	O1Bi—Zr1—O1B	93.73 (12)

C7A—C8A—C9A	117.5 (17)	O1Ai—Zr1—N1Bi	57.0 (4)
C8A—O1A—Zr1	134.9 (13)	O1Aii—Zr1—N1Bi	81.3 (5)
C9A—N1A—C1A	127.7 (16)	O1Aiii—Zr1—N1Bi	83.8 (5)
C9A—N1A—Zr1	107.6 (11)	O1A—Zr1—N1Bi	143.6 (6)
C1A—N1A—Zr1	124.6 (14)	O1Bii—Zr1—N1Bi	71.2 (5)
C6B—C5B—C4B	127.5 (13)	O1Biii—Zr1—N1Bi	87.0 (4)
C6B—C5B—N2B	114.9 (12)	O1Bi—Zr1—N1Bi	68.6 (4)
C4B—C5B—N2B	117.1 (13)	O1B—Zr1—N1Bi	137.8 (5)
N1B—C9B—C4B	133.0 (18)	O1Ai—Zr1—N1Biii	83.8 (5)
N1B—C9B—C8B	106.6 (13)	O1Aii—Zr1—N1Biii	143.6 (6)
C4B—C9B—C8B	120.3 (13)	O1Aiii—Zr1—N1Biii	57.0 (4)
C3B—C4B—C9B	112.3 (15)	O1A—Zr1—N1Biii	81.3 (5)
C3B—C4B—C5B	134.5 (13)	O1Bii—Zr1—N1Biii	137.8 (5)
C9B—C4B—C5B	113.1 (14)	O1Biii—Zr1—N1Biii	68.6 (4)
O3B—N2B—O2B	118.1 (18)	O1Bi—Zr1—N1Biii	87.0 (4)
O3B—N2B—C5B	122.3 (15)	O1B—Zr1—N1Biii	71.2 (5)
O2B—N2B—C5B	119.2 (15)	N1Bi—Zr1—N1Biii	70.0 (8)
C4B—C3B—C2B	123.6 (12)	O1Ai—Zr1—N1Bii	143.6 (6)
C4B—C3B—H3B	118.2	O1Aii—Zr1—N1Bii	57.0 (4)
C2B—C3B—H3B	118.2	O1Aiii—Zr1—N1Bii	81.3 (5)
C6B—C7B—C8B	130 (2)	O1A—Zr1—N1Bii	83.8 (5)
C6B—C7B—H7B	115	O1Bii—Zr1—N1Bii	68.5 (4)
C8B—C7B—H7B	115	O1Biii—Zr1—N1Bii	71.2 (5)
C7B—C6B—C5B	112.0 (15)	O1Bi—Zr1—N1Bii	137.8 (5)
C7B—C6B—H6B	124	O1B—Zr1—N1Bii	87.0 (4)
C5B—C6B—H6B	124	N1Bi—Zr1—N1Bii	132.2 (5)
N1B—C1B—C2B	123.9 (16)	N1Biii—Zr1—N1Bii	132.2 (5)
N1B—C1B—H1B	118.1	O1Ai—Zr1—N1B	81.3 (5)
C2B—C1B—H1B	118.1	O1Aii—Zr1—N1B	83.8 (5)
C3B—C2B—C1B	114.2 (11)	O1Aiii—Zr1—N1B	143.6 (6)
C3B—C2B—H2B	122.9	O1A—Zr1—N1B	57.0 (4)
C1B—C2B—H2B	122.9	O1Bii—Zr1—N1B	87.0 (4)
C7B—C8B—C9B	117.1 (16)	O1Biii—Zr1—N1B	137.8 (5)
C7B—C8B—O1B	122.9 (17)	O1Bi—Zr1—N1B	71.2 (5)
C9B—C8B—O1B	119.0 (11)	O1B—Zr1—N1B	68.6 (4)
C8B—O1B—Zr1	119.9 (8)	N1Bi—Zr1—N1B	132.2 (5)
C1B—N1B—C9B	112.7 (16)	N1Biii—Zr1—N1B	132.2 (5)
C1B—N1B—Zr1	123.3 (14)	N1Bii—Zr1—N1B	70.0 (8)

A.6. [Zr(Pic)₄]·2H₂O – § 5.4

Table A.6.21 Fractional atomic coordinates and isotropic or equivalent isotropic displacement parameters (Å^2) for [Zr(Pic)₄]·2H₂O.

	x	*y*	*z*	U_{iso}*/U_{eq}
Zr1	0.25	0.25	0.75	0.01305 (15)
O1	0.41797 (14)	0.31522 (14)	0.82454 (18)	0.01305 (15)
O2	0.56146 (18)	0.33223 (18)	0.9859 (2)	0.0263 (4)
C3	0.4700 (2)	0.1154 (2)	1.1212 (3)	0.0195 (5)
H3	0.5415	0.144	1.1601	0.023*
N1	0.31289 (18)	0.13671 (18)	0.9505 (2)	0.0157 (4)
C2	0.4174 (2)	0.1737 (2)	1.0089 (3)	0.0169 (5)
C5	0.3088 (2)	−0.0267 (2)	1.1131 (3)	0.0206 (5)
H5	0.2707	−0.0959	1.1461	0.025*
C6	0.2603 (2)	0.0372 (2)	1.0016 (3)	0.0178 (5)
H6	0.1891	0.01	0.961	0.021*
C4	0.4143 (2)	0.0137 (2)	1.1748 (3)	0.0222 (5)
H4	0.4473	−0.0269	1.251	0.027*
C1	0.4728 (2)	0.2822 (2)	0.9379 (3)	0.0183 (5)
O03	0.25	0.75	0.3385 (4)	0.0472 (9)
H03A	0.274 (4)	0.815 (3)	0.396 (4)	0.068 (15)*

Table A.6.22 Atomic displacement parameters (Å^2) for [Zr(Pic)₄]·2H₂O.

	U^{11}	U^{22}	U^{33}	U^{12}	U^{13}	U^{23}
Zr1	0.01054 (17)	0.01054 (17)	0.0181 (2)	0	0	0
O1	0.01054 (17)	0.01054 (17)	0.0181 (2)	0	0	0
O2	0.0201 (9)	0.0257 (10)	0.0332 (11)	−0.0070 (8)	−0.0066 (8)	0.0008 (8)
C3	0.0170 (11)	0.0211 (12)	0.0205 (12)	0.0015 (9)	−0.0014 (9)	−0.0035 (10)
N1	0.0141 (9)	0.0136 (9)	0.0194 (10)	−0.0005 (8)	0.0000 (8)	−0.0002 (8)
C2	0.0145 (11)	0.0160 (11)	0.0203 (12)	0.0000 (9)	0.0007 (9)	−0.0030 (9)
C5	0.0221 (12)	0.0178 (12)	0.0220 (13)	0.0026 (9)	0.0043 (10)	0.0027 (10)
C6	0.0158 (11)	0.0154 (11)	0.0223 (12)	−0.0003 (9)	0.0005 (9)	0.0003 (9)
C4	0.0236 (13)	0.0240 (13)	0.0191 (13)	0.0056 (10)	0.0003 (10)	0.0020 (10)
C1	0.0148 (11)	0.0171 (11)	0.0231 (12)	−0.0001 (9)	0.0006 (9)	−0.0032 (9)
O03	0.059 (2)	0.038 (2)	0.045 (2)	−0.0011 (18)	0	0

Table A.6.23 Bond lengths (Å) for [Zr(Pic)₄]·2H₂O.

Atoms	Bond length (Å)	Atoms	Bond length (Å)
Zr1—O1i	2.1200 (18)	**C3—C4**	1.384 (4)
Zr1—O1	2.1200 (18)	**C3—H3**	0.93
Zr1—O1ii	2.1200 (18)	**N1—C6**	1.340 (3)
Zr1—O1iii	2.1200 (18)	**N1—C2**	1.349 (3)
Zr1—N1i	2.393 (2)	**C2—C1**	1.511 (4)
Zr1—N1ii	2.393 (2)	**C5—C4**	1.384 (4)

Atoms		Atoms	
Zr1—N1iii	2.393 (2)	C5—C6	1.386 (4)
Zr1—N1	2.393 (2)	C5—H5	0.93
O1—C1	1.294 (3)	C6—H6	0.93
O2—C1	1.218 (3)	C4—H4	0.93
C3—C2	1.381 (4)	O03—H03A	0.941 (19)

Table A.6.24 Bond angles (°) for [Zr(Pic)$_4$]·2H$_2$O.

Atoms	Bond angle (°)	Atoms	Bond angle (°)
O1i—Zr1—O1	96.47 (3)	N1i—Zr1—N1	129.78 (7)
O1i—Zr1—O1ii	96.47 (3)	N1ii—Zr1—N1	73.76 (11)
O1—Zr1—O1ii	140.77 (10)	N1iii—Zr1—N1	129.78 (7)
O1i—Zr1—O1iii	140.77 (10)	C1—O1—Zr1	126.61 (15)
O1—Zr1—O1iii	96.47 (3)	C2—C3—C4	118.7 (2)
O1ii—Zr1—O1iii	96.47 (3)	C2—C3—H3	120.7
O1i—Zr1—N1i	69.79 (7)	C4—C3—H3	120.7
O1—Zr1—N1i	145.95 (7)	C6—N1—C2	118.2 (2)
O1ii—Zr1—N1i	73.05 (7)	C6—N1—Zr1	126.65 (17)
O1iii—Zr1—N1i	78.95 (7)	C2—N1—Zr1	114.94 (16)
O1i—Zr1—N1ii	145.95 (7)	N1—C2—C3	122.8 (2)
O1—Zr1—N1ii	78.95 (7)	N1—C2—C1	113.9 (2)
O1ii—Zr1—N1ii	69.79 (7)	C3—C2—C1	123.3 (2)
O1iii—Zr1—N1ii	73.05 (7)	C4—C5—C6	119.3 (2)
N1i—Zr1—N1ii	129.78 (7)	C4—C5—H5	120.4
O1i—Zr1—N1iii	78.95 (7)	C6—C5—H5	120.4
O1—Zr1—N1iii	73.05 (7)	N1—C6—C5	122.1 (2)
O1ii—Zr1—N1iii	145.95 (7)	N1—C6—H6	118.9
O1iii—Zr1—N1iii	69.79 (7)	C5—C6—H6	118.9
N1i—Zr1—N1iii	73.76 (11)	C3—C4—C5	118.9 (2)
N1ii—Zr1—N1iii	129.78 (7)	C3—C4—H4	120.6
O1i—Zr1—N1	73.05 (7)	C5—C4—H4	120.6
O1—Zr1—N1	69.79 (7)	O2—C1—O1	124.4 (2)
O1ii—Zr1—N1	78.95 (7)	O2—C1—C2	121.4 (2)
O1iii—Zr1—N1	145.95 (7)	O1—C1—C2	114.2 (2)

A.7. [Zr(Trop)₄]·DMF – § 6.2

Table A.7.25 Fractional atomic coordinates and isotropic or equivalent isotropic displacement parameters (Å^2) for [Zr(Trop)₄]·DMF.

	x	y	z	$U_{iso}*/U_{eq}$
C01	0.5459 (6)	0.3086 (4)	0.3610 (4)	0.0225 (11)
C02	0.4966 (7)	0.2505 (5)	0.4436 (4)	0.0319 (13)
H02	0.5402	0.1985	0.4645	0.038*
C03	0.3938 (6)	0.2573 (5)	0.4996 (4)	0.0317 (13)
H03	0.3818	0.2137	0.556	0.038*
C04	0.3063 (6)	0.3183 (5)	0.4851 (5)	0.0353 (15)
H04	0.2378	0.3066	0.5291	0.042*
C05	0.3072 (6)	0.3950 (5)	0.4134 (5)	0.0373 (15)
H05	0.2375	0.4274	0.4143	0.045*
C06	0.3927 (6)	0.4306 (5)	0.3420 (5)	0.0325 (14)
H06	0.3765	0.4871	0.303	0.039*
C07	0.5010 (6)	0.3962 (4)	0.3175 (4)	0.0233 (11)
C08	0.5142 (5)	0.2060 (4)	0.0012 (4)	0.0193 (10)
C09	0.4158 (6)	0.0883 (5)	−0.0684 (4)	0.0260 (12)
H09	0.4056	0.0151	−0.0418	0.031*
C10	0.3306 (6)	0.0606 (5)	−0.1701 (4)	0.0281 (12)
H10	0.2755	−0.0285	−0.2045	0.034*
C11	0.3136 (6)	0.1435 (5)	−0.2292 (4)	0.0293 (13)
H11	0.247	0.1039	−0.2975	0.035*
C12	0.3815 (6)	0.2767 (5)	−0.2012 (4)	0.0267 (12)
H12	0.353	0.317	−0.2518	0.032*
C13	0.4855 (6)	0.3594 (4)	−0.1091 (4)	0.0252 (12)
H13	0.5189	0.4484	−0.1066	0.03*
C14	0.5497 (5)	0.3330 (4)	−0.0191 (4)	0.0195 (11)
C15	0.9463 (5)	0.2667 (4)	0.1828 (4)	0.0215 (11)
C16	1.0110 (6)	0.1864 (5)	0.2032 (4)	0.0278 (12)
H16	0.9802	0.141	0.2565	0.033*
C17	1.1143 (6)	0.1640 (5)	0.1561 (5)	0.0364 (14)
H17	1.1409	0.1033	0.1809	0.044*
C18	1.1833 (6)	0.2152 (5)	0.0802 (5)	0.0343 (14)
H18	1.2492	0.1843	0.0583	0.041*
C19	1.1684 (6)	0.3085 (5)	0.0305 (5)	0.0307 (13)
H19	1.2261	0.3329	−0.0205	0.037*
C20	1.0813 (6)	0.3690 (4)	0.0461 (4)	0.0245 (11)
H20	1.091	0.432	0.0063	0.029*
C21	0.9804 (6)	0.3525 (4)	0.1113 (4)	0.0224 (11)
C22	0.9714 (6)	0.6257 (4)	0.3844 (4)	0.0222 (11)
C23	1.0709 (6)	0.6871 (5)	0.4843 (4)	0.0269 (12)
H23	1.075	0.6326	0.53	0.032*
C24	1.1639 (7)	0.8161 (5)	0.5253 (5)	0.0364 (15)
H24	1.2256	0.8371	0.5942	0.044*
C25	1.1810 (7)	0.9209 (5)	0.4807 (5)	0.0400 (16)

H25	1.2552	1.0023	0.5213	0.048*
C26	1.1034 (7)	0.9198 (5)	0.3853 (4)	0.0353 (15)
H26	1.1261	1.0022	0.3718	0.042*
C27	0.9972 (6)	0.8170 (4)	0.3058 (4)	0.0247 (12)
H27	0.9604	0.8392	0.2447	0.03*
C28	0.9351 (5)	0.6842 (4)	0.3016 (4)	0.0191 (10)
C29	1.4162 (9)	−0.0727 (9)	0.3024 (6)	0.064 (2)
H29	1.4561	0.0167	0.3054	0.076*
C30	1.2403 (9)	−0.2876 (7)	0.2058 (9)	0.097 (4)
H30A	1.2773	−0.3093	0.2699	0.145*
H30B	1.2582	−0.3315	0.1411	0.145*
H30C	1.1367	−0.3154	0.1975	0.145*
C31	1.2663 (8)	−0.0982 (7)	0.1332 (6)	0.0596 (19)
H31A	1.3322	−0.0064	0.1482	0.089*
H31B	1.1684	−0.1083	0.1323	0.089*
H31C	1.2692	−0.1435	0.0624	0.089*
O1	0.6429 (4)	0.2874 (3)	0.3188 (3)	0.0238 (8)
O2	0.5751 (4)	0.4455 (3)	0.2482 (3)	0.0250 (8)
O3	0.5861 (4)	0.2106 (3)	0.0930 (3)	0.0223 (8)
O4	0.6499 (4)	0.4270 (3)	0.0562 (3)	0.0219 (8)
O5	0.8450 (4)	0.2673 (3)	0.2314 (3)	0.0210 (8)
O6	0.9058 (4)	0.4175 (3)	0.1097 (3)	0.0253 (8)
O7	0.8955 (4)	0.5006 (3)	0.3595 (3)	0.0258 (8)
O8	0.8414 (4)	0.6032 (3)	0.2167 (3)	0.0229 (8)
O9	1.4645 (8)	−0.1065 (9)	0.3747 (6)	0.124 (3)
Zr01	0.74269 (5)	0.39447 (4)	0.20449 (4)	0.01594 (16)
N1	1.3103 (5)	−0.1532 (5)	0.2188 (4)	0.0388 (12)

Table A.7.26 Atomic displacement parameters (Å^2) for [Zr(Trop)$_4$]·DMF.

	U^{11}	U^{22}	U^{33}	U^{12}	U^{13}	U^{23}
C01	0.035 (3)	0.009 (2)	0.018 (3)	0.005 (2)	0.006 (2)	0.0030 (18)
C02	0.048 (4)	0.017 (2)	0.027 (3)	0.008 (2)	0.013 (3)	0.007 (2)
C03	0.040 (3)	0.024 (3)	0.027 (3)	0.006 (2)	0.017 (3)	0.009 (2)
C04	0.034 (3)	0.028 (3)	0.035 (3)	0.003 (3)	0.022 (3)	0.004 (2)
C05	0.030 (3)	0.030 (3)	0.045 (4)	0.009 (3)	0.008 (3)	−0.002 (3)
C06	0.041 (4)	0.025 (3)	0.034 (3)	0.017 (3)	0.009 (3)	0.007 (2)
C07	0.024 (3)	0.017 (2)	0.018 (3)	0.002 (2)	−0.001 (2)	0.0020 (19)
C08	0.023 (3)	0.018 (2)	0.020 (2)	0.012 (2)	0.004 (2)	0.0063 (19)
C09	0.030 (3)	0.017 (2)	0.029 (3)	0.009 (2)	0.002 (2)	0.008 (2)
C10	0.025 (3)	0.021 (2)	0.030 (3)	0.005 (2)	0.001 (2)	0.002 (2)
C11	0.025 (3)	0.028 (3)	0.029 (3)	0.010 (2)	−0.001 (2)	0.002 (2)
C12	0.033 (3)	0.026 (3)	0.023 (3)	0.013 (2)	0.005 (2)	0.010 (2)
C13	0.033 (3)	0.014 (2)	0.025 (3)	0.008 (2)	0.002 (2)	0.004 (2)
C14	0.021 (3)	0.017 (2)	0.019 (3)	0.006 (2)	0.004 (2)	0.0054 (19)
C15	0.027 (3)	0.010 (2)	0.017 (2)	0.0010 (19)	0.000 (2)	−0.0007 (18)
C16	0.033 (3)	0.022 (3)	0.032 (3)	0.009 (2)	0.011 (2)	0.019 (2)
C17	0.034 (3)	0.028 (3)	0.058 (4)	0.018 (3)	0.013 (3)	0.024 (3)

C18	0.034 (3)	0.031 (3)	0.050 (4)	0.020 (3)	0.019 (3)	0.018 (3)
C19	0.030 (3)	0.025 (3)	0.033 (3)	0.006 (2)	0.014 (2)	0.009 (2)
C20	0.032 (3)	0.015 (2)	0.026 (3)	0.008 (2)	0.009 (2)	0.011 (2)
C21	0.027 (3)	0.013 (2)	0.022 (3)	0.004 (2)	0.003 (2)	0.0048 (19)
C22	0.028 (3)	0.017 (2)	0.020 (3)	0.007 (2)	0.006 (2)	0.008 (2)
C23	0.036 (3)	0.018 (2)	0.022 (3)	0.009 (2)	0.000 (2)	0.005 (2)
C24	0.048 (4)	0.020 (3)	0.028 (3)	0.006 (3)	−0.008 (3)	0.009 (2)
C25	0.057 (4)	0.015 (2)	0.031 (3)	0.005 (3)	−0.002 (3)	0.002 (2)
C26	0.054 (4)	0.013 (2)	0.031 (3)	0.007 (2)	0.007 (3)	0.006 (2)
C27	0.032 (3)	0.016 (2)	0.025 (3)	0.009 (2)	0.006 (2)	0.008 (2)
C28	0.022 (3)	0.014 (2)	0.021 (3)	0.007 (2)	0.005 (2)	0.0064 (19)
C29	0.067 (6)	0.081 (6)	0.042 (4)	0.032 (5)	0.010 (4)	0.016 (4)
C30	0.057 (5)	0.047 (5)	0.170 (10)	0.010 (4)	0.070 (6)	−0.011 (5)
C31	0.058 (5)	0.066 (5)	0.058 (5)	0.031 (4)	0.015 (4)	0.013 (4)
O1	0.030 (2)	0.0180 (17)	0.0244 (19)	0.0113 (15)	0.0050 (16)	0.0066 (14)
O2	0.029 (2)	0.0173 (16)	0.0266 (19)	0.0080 (15)	0.0029 (16)	0.0096 (14)
O3	0.028 (2)	0.0144 (16)	0.0221 (18)	0.0080 (15)	0.0004 (15)	0.0071 (14)
O4	0.030 (2)	0.0146 (16)	0.0177 (18)	0.0075 (14)	−0.0001 (15)	0.0064 (13)
O5	0.026 (2)	0.0170 (16)	0.0173 (17)	0.0066 (15)	0.0047 (15)	0.0061 (13)
O6	0.030 (2)	0.0225 (18)	0.030 (2)	0.0140 (16)	0.0110 (16)	0.0146 (15)
O7	0.038 (2)	0.0142 (16)	0.0199 (18)	0.0083 (15)	−0.0006 (16)	0.0052 (14)
O8	0.0251 (19)	0.0148 (16)	0.0237 (19)	0.0062 (14)	−0.0011 (15)	0.0040 (14)
O9	0.108 (6)	0.218 (9)	0.074 (4)	0.081 (6)	0.031 (4)	0.074 (5)
Zr01	0.0216 (3)	0.0095 (2)	0.0144 (2)	0.00463 (19)	0.0011 (2)	0.00527 (16)
N1	0.038 (3)	0.040 (3)	0.035 (3)	0.015 (2)	0.009 (2)	0.003 (2)

Table A.7.27 Bond lengths (Å) for [Zr(Trop)$_4$]·DMF.

Atoms	Bond length (Å)	Atoms	Bond length (Å)
C01—O1	1.299 (6)	C19—H19	0.95
C01—C02	1.401 (7)	C20—C21	1.405 (7)
C01—C07	1.453 (7)	C20—H20	0.95
C02—C03	1.389 (8)	C21—O6	1.294 (6)
C02—H02	0.95	C22—O7	1.306 (6)
C03—C04	1.386 (8)	C22—C23	1.401 (7)
C03—H03	0.95	C22—C28	1.450 (7)
C04—C05	1.393 (9)	C23—C24	1.379 (7)
C04—H04	0.95	C23—H23	0.95
C05—C06	1.363 (8)	C24—C25	1.401 (7)
C05—H05	0.95	C24—H24	0.95
C06—C07	1.401 (8)	C25—C26	1.371 (8)
C06—H06	0.95	C25—H25	0.95
C07—O2	1.312 (6)	C26—C27	1.382 (7)
C08—O3	1.291 (5)	C26—H26	0.95
C08—C09	1.391 (6)	C27—C28	1.412 (6)
C08—C14	1.462 (6)	C27—H27	0.95
C09—C10	1.383 (7)	C28—O8	1.284 (5)
C09—H09	0.95	C29—O9	1.200 (10)

Atoms		Atoms	
C10—C11	1.383 (7)	C29—N1	1.323 (9)
C10—H10	0.95	C29—H29	0.95
C11—C12	1.383 (7)	C30—N1	1.410 (9)
C11—H11	0.95	C30—H30A	0.98
C12—C13	1.386 (7)	C30—H30B	0.98
C12—H12	0.95	C30—H30C	0.98
C13—C14	1.404 (7)	C31—N1	1.480 (9)
C13—H13	0.95	C31—H31A	0.98
C14—O4	1.292 (5)	C31—H31B	0.98
C15—O5	1.299 (6)	C31—H31C	0.98
C15—C16	1.404 (7)	O1—Zr01	2.190 (4)
C15—C21	1.448 (7)	O2—Zr01	2.177 (4)
C16—C17	1.395 (8)	O3—Zr01	2.193 (3)
C16—H16	0.95	O4—Zr01	2.184 (3)
C17—C18	1.367 (8)	O5—Zr01	2.207 (3)
C17—H17	0.95	O6—Zr01	2.179 (4)
C18—C19	1.409 (7)	O7—Zr01	2.176 (3)
C18—H18	0.95	O8—Zr01	2.203 (3)
C19—C20	1.378 (7)		

Table A.7.28 Bond angles (°) for [Zr(Trop)$_4$]·DMF.

Atoms	Bond angle (°)	Atoms	Bond angle (°)
O1—C01—C02	119.4 (5)	C23—C24—C25	129.8 (5)
O1—C01—C07	114.7 (4)	C23—C24—H24	115.1
C02—C01—C07	125.9 (5)	C25—C24—H24	115.1
C03—C02—C01	129.9 (6)	C26—C25—C24	127.7 (5)
C03—C02—H02	115.1	C26—C25—H25	116.2
C01—C02—H02	115.1	C24—C25—H25	116.1
C04—C03—C02	129.5 (6)	C25—C26—C27	129.8 (5)
C04—C03—H03	115.3	C25—C26—H26	115.1
C02—C03—H03	115.3	C27—C26—H26	115.1
C03—C04—C05	127.4 (6)	C26—C27—C28	129.8 (5)
C03—C04—H04	116.3	C26—C27—H27	115.1
C05—C04—H04	116.3	C28—C27—H27	115.1
C06—C05—C04	130.0 (6)	O8—C28—C27	119.7 (5)
C06—C05—H05	115	O8—C28—C22	114.3 (4)
C04—C05—H05	115	C27—C28—C22	125.9 (4)
C05—C06—C07	129.6 (6)	O9—C29—N1	123.6 (9)
C05—C06—H06	115.2	O9—C29—H29	118.2
C07—C06—H06	115.2	N1—C29—H29	118.2
O2—C07—C06	119.9 (5)	N1—C30—H30A	109.5
O2—C07—C01	112.6 (5)	N1—C30—H30B	109.5
C06—C07—C01	127.5 (5)	H30A—C30—H30B	109.5
O3—C08—C09	120.6 (4)	N1—C30—H30C	109.5
O3—C08—C14	113.3 (4)	H30A—C30—H30C	109.5
C09—C08—C14	126.1 (4)	H30B—C30—H30C	109.5
C10—C09—C08	130.4 (5)	N1—C31—H31A	109.5

C10—C09—H09	114.8	N1—C31—H31B	109.5
C08—C09—H09	114.8	H31A—C31—H31B	109.5
C09—C10—C11	129.6 (5)	N1—C31—H31C	109.5
C09—C10—H10	115.2	H31A—C31—H31C	109.5
C11—C10—H10	115.2	H31B—C31—H31C	109.5
C12—C11—C10	128.1 (5)	C01—O1—Zr01	120.7 (3)
C12—C11—H11	116	C07—O2—Zr01	121.9 (3)
C10—C11—H11	116	C08—O3—Zr01	121.6 (3)
C11—C12—C13	128.6 (5)	C14—O4—Zr01	121.5 (3)
C11—C12—H12	115.7	C15—O5—Zr01	120.4 (3)
C13—C12—H12	115.7	C21—O6—Zr01	122.1 (3)
C12—C13—C14	130.5 (5)	C22—O7—Zr01	122.3 (3)
C12—C13—H13	114.7	C28—O8—Zr01	121.4 (3)
C14—C13—H13	114.7	O7—Zr01—O2	95.19 (14)
O4—C14—C13	119.5 (4)	O7—Zr01—O6	95.03 (13)
O4—C14—C08	114.0 (4)	O2—Zr01—O6	148.34 (13)
C13—C14—C08	126.5 (4)	O7—Zr01—O4	140.65 (12)
O5—C15—C16	119.0 (5)	O2—Zr01—O4	75.84 (13)
O5—C15—C21	114.3 (5)	O6—Zr01—O4	77.29 (13)
C16—C15—C21	126.6 (5)	O7—Zr01—O1	76.54 (13)
C17—C16—C15	129.2 (5)	O2—Zr01—O1	69.88 (13)
C17—C16—H16	115.4	O6—Zr01—O1	141.75 (13)
C15—C16—H16	115.4	O4—Zr01—O1	131.65 (12)
C18—C17—C16	130.4 (5)	O7—Zr01—O3	149.78 (12)
C18—C17—H17	114.8	O2—Zr01—O3	92.56 (12)
C16—C17—H17	114.8	O6—Zr01—O3	93.50 (13)
C17—C18—C19	127.7 (5)	O4—Zr01—O3	69.56 (12)
C17—C18—H18	116.2	O1—Zr01—O3	78.85 (13)
C19—C18—H18	116.2	O7—Zr01—O8	69.11 (12)
C20—C19—C18	128.6 (5)	O2—Zr01—O8	78.63 (13)
C20—C19—H19	115.7	O6—Zr01—O8	77.23 (13)
C18—C19—H19	115.7	O4—Zr01—O8	71.56 (12)
C19—C20—C21	130.4 (5)	O1—Zr01—O8	130.41 (13)
C19—C20—H20	114.8	O3—Zr01—O8	141.11 (12)
C21—C20—H20	114.8	O7—Zr01—O5	77.34 (12)
O6—C21—C20	119.4 (5)	O2—Zr01—O5	142.04 (13)
O6—C21—C15	113.6 (5)	O6—Zr01—O5	69.56 (13)
C20—C21—C15	127.0 (5)	O4—Zr01—O5	131.95 (12)
O7—C22—C23	119.2 (4)	O1—Zr01—O5	72.19 (13)
O7—C22—C28	112.8 (4)	O3—Zr01—O5	78.63 (12)
C23—C22—C28	128.0 (4)	O8—Zr01—O5	129.80 (12)
C24—C23—C22	128.8 (5)	C29—N1—C30	123.8 (8)
C24—C23—H23	115.6	C29—N1—C31	117.6 (6)
C22—C23—H23	115.6	C30—N1—C31	118.6 (7)

A.8. [Zr(DBM)₄] – § 6.3

Table A.8.29 Fractional atomic coordinates and isotropic or equivalent isotropic displacement parameters (Å^2) for [Zr(DBM)₄].

	x	*y*	*z*	U_{iso}*/U_{eq}
C01	0.32906 (5)	0.25074 (13)	0.25634 (6)	0.0129 (2)
C02	0.29255 (5)	0.17791 (13)	0.20714 (7)	0.0152 (3)
H02	0.305	0.1034	0.1876	0.018*
C03	0.23707 (5)	0.21512 (13)	0.18646 (6)	0.0130 (2)
C04	0.27005 (5)	0.46966 (13)	0.09367 (7)	0.0152 (3)
C05	0.21426 (6)	0.48748 (14)	0.06293 (7)	0.0170 (3)
H05	0.2012	0.4607	0.0166	0.02*
C06	0.17804 (5)	0.54473 (13)	0.10071 (7)	0.0153 (3)
C07	0.34396 (5)	0.71092 (13)	0.32003 (7)	0.0154 (3)
C08	0.30840 (5)	0.80010 (14)	0.34239 (7)	0.0179 (3)
H08	0.3227	0.8635	0.3756	0.021*
C09	0.25144 (5)	0.79581 (13)	0.31563 (7)	0.0152 (2)
C10	0.25311 (5)	0.54297 (13)	0.41773 (7)	0.0140 (2)
C11	0.19547 (5)	0.54132 (14)	0.40868 (7)	0.0177 (3)
H11	0.1791	0.5692	0.4454	0.021*
C12	0.16226 (5)	0.49877 (13)	0.34566 (7)	0.0147 (2)
C101	0.38680 (5)	0.20586 (13)	0.28358 (6)	0.0140 (2)
C102	0.40195 (5)	0.07454 (14)	0.28648 (7)	0.0174 (3)
H102	0.376	0.011	0.2687	0.021*
C103	0.45578 (6)	0.03784 (15)	0.31582 (8)	0.0219 (3)
H103	0.4657	−0.0501	0.3183	0.026*
C104	0.49465 (6)	0.13320 (17)	0.34144 (8)	0.0239 (3)
H104	0.5307	0.109	0.361	0.029*
C105	0.47999 (6)	0.26403 (16)	0.33798 (8)	0.0238 (3)
H105	0.5063	0.3276	0.3546	0.029*
C106	0.42615 (5)	0.30070 (14)	0.30970 (7)	0.0188 (3)
H106	0.4163	0.3886	0.3082	0.023*
C201	0.19649 (5)	0.12231 (13)	0.14562 (7)	0.0138 (2)
C202	0.15174 (5)	0.16915 (14)	0.09583 (7)	0.0183 (3)
H202	0.1478	0.2585	0.0871	0.022*
C203	0.11322 (5)	0.08190 (15)	0.05952 (8)	0.0206 (3)
H203	0.0845	0.1126	0.0248	0.025*
C204	0.11744 (5)	−0.05090 (14)	0.07478 (7)	0.0194 (3)
H204	0.091	−0.1087	0.0513	0.023*
C205	0.16115 (6)	−0.09729 (14)	0.12516 (7)	0.0197 (3)
H205	0.1636	−0.186	0.1362	0.024*
C206	0.20121 (6)	−0.01110 (13)	0.15905 (7)	0.0166 (3)
H206	0.2315	−0.0431	0.191	0.02*
C301	0.30922 (5)	0.42685 (14)	0.04883 (7)	0.0159 (3)
C302	0.29581 (6)	0.32759 (15)	−0.00101 (7)	0.0204 (3)
H302	0.2622	0.2846	−0.0059	0.024*
C303	0.33279 (6)	0.29252 (15)	−0.04354 (7)	0.0232 (3)

H303	0.324	0.2256	−0.0765	0.028*
C304	0.38249 (6)	0.35716 (16)	−0.03662 (7)	0.0220 (3)
H304	0.4067	0.3353	−0.0659	0.026*
C305	0.39649 (6)	0.45437 (15)	0.01370 (8)	0.0221 (3)
H305	0.4303	0.4968	0.0185	0.026*
C306	0.36042 (6)	0.48867 (14)	0.05688 (7)	0.0190 (3)
H306	0.3702	0.5528	0.0912	0.023*
C401	0.12044 (5)	0.58238 (13)	0.06640 (7)	0.0173 (3)
C402	0.08224 (6)	0.60088 (14)	0.10956 (8)	0.0212 (3)
H402	0.0926	0.5877	0.158	0.025*
C403	0.02866 (6)	0.63899 (16)	0.08037 (9)	0.0283 (3)
H403	0.0032	0.651	0.1093	0.034*
C404	0.01319 (6)	0.65908 (16)	0.00802 (9)	0.0300 (4)
H404	−0.0227	0.6844	−0.0116	0.036*
C405	0.05097 (6)	0.64142 (16)	−0.03452 (9)	0.0288 (3)
H405	0.0405	0.6552	−0.0829	0.035*
C406	0.10461 (6)	0.60333 (15)	−0.00601 (8)	0.0235 (3)
H406	0.1299	0.5919	−0.0352	0.028*
C501	0.40419 (5)	0.71404 (13)	0.35042 (7)	0.0163 (3)
C502	0.42407 (6)	0.75737 (15)	0.41934 (7)	0.0204 (3)
H502	0.3997	0.7892	0.4462	0.024*
C503	0.48002 (6)	0.75301 (16)	0.44778 (8)	0.0249 (3)
H503	0.4931	0.781	0.4939	0.03*
C504	0.51649 (6)	0.70721 (15)	0.40786 (8)	0.0243 (3)
H504	0.554	0.705	0.4271	0.029*
C505	0.49724 (6)	0.66453 (15)	0.33917 (8)	0.0224 (3)
H505	0.5219	0.6348	0.3122	0.027*
C506	0.44117 (6)	0.66626 (14)	0.31071 (7)	0.0189 (3)
H506	0.4282	0.6355	0.2651	0.023*
C601	0.21456 (6)	0.90465 (14)	0.32851 (7)	0.0170 (3)
C602	0.15813 (6)	0.88157 (15)	0.31898 (7)	0.0220 (3)
H602	0.1443	0.7981	0.3072	0.026*
C603	0.12265 (6)	0.98201 (17)	0.32702 (8)	0.0266 (3)
H603	0.0851	0.9656	0.3214	0.032*
C604	0.14275 (7)	1.10729 (16)	0.34337 (8)	0.0285 (3)
H604	0.1187	1.1748	0.3486	0.034*
C605	0.19858 (7)	1.13180 (15)	0.35193 (8)	0.0262 (3)
H605	0.212	1.2161	0.3622	0.031*
C606	0.23454 (6)	1.03059 (15)	0.34519 (7)	0.0215 (3)
H606	0.2722	1.0469	0.3518	0.026*
C701	0.28841 (5)	0.58066 (13)	0.48706 (7)	0.0154 (3)
C702	0.26803 (6)	0.65460 (15)	0.53695 (7)	0.0212 (3)
H702	0.2314	0.681	0.5276	0.025*
C703	0.30220 (7)	0.68901 (15)	0.60050 (8)	0.0245 (3)
H703	0.2884	0.7392	0.6332	0.029*
C704	0.35658 (7)	0.64893 (15)	0.61519 (8)	0.0254 (3)
H704	0.3792	0.6707	0.6581	0.031*
C705	0.37734 (6)	0.57610 (16)	0.56574 (8)	0.0260 (3)
H705	0.4139	0.5491	0.5756	0.031*

C706	0.34364 (6)	0.54332 (15)	0.50156 (8)	0.0211 (3)
H706	0.358	0.4963	0.4682	0.025*
C801	0.10143 (5)	0.48467 (14)	0.33845 (7)	0.0173 (3)
C802	0.07291 (6)	0.40422 (15)	0.28496 (7)	0.0206 (3)
H802	0.0917	0.3628	0.254	0.025*
C803	0.01653 (6)	0.38595 (18)	0.27783 (8)	0.0285 (3)
H803	−0.0021	0.3304	0.243	0.034*
C804	−0.01201 (6)	0.4503 (2)	0.32257 (9)	0.0348 (4)
H804	−0.0497	0.4376	0.3179	0.042*
C805	0.01573 (6)	0.5335 (2)	0.37416 (9)	0.0348 (4)
H805	−0.0036	0.5783	0.4033	0.042*
C806	0.07229 (6)	0.55041 (18)	0.38261 (8)	0.0265 (3)
H806	0.0908	0.6057	0.4178	0.032*
O1	0.31617 (4)	0.35793 (9)	0.28337 (5)	0.01409 (18)
O2	0.21792 (4)	0.32398 (9)	0.20176 (5)	0.01359 (18)
O3	0.29096 (4)	0.49389 (9)	0.15825 (5)	0.01450 (18)
O4	0.19106 (4)	0.57241 (9)	0.16635 (5)	0.01536 (18)
O5	0.32838 (4)	0.62352 (9)	0.27261 (5)	0.01565 (19)
O6	0.22768 (4)	0.70181 (9)	0.27807 (5)	0.01485 (18)
O7	0.27859 (4)	0.51013 (9)	0.36924 (5)	0.01434 (18)
O8	0.18056 (4)	0.46568 (9)	0.29101 (5)	0.01504 (19)
Zr1	0.254666 (5)	0.505417 (12)	0.252589 (6)	0.01025 (4)

Table A.8.30 Atomic displacement parameters (Å^2) for [Zr(DBM)$_4$].

	U^{11}	U^{22}	U^{33}	U^{12}	U^{13}	U^{23}
C01	0.0134 (6)	0.0135 (6)	0.0123 (6)	0.0000 (5)	0.0035 (5)	0.0020 (5)
C02	0.0143 (6)	0.0135 (6)	0.0176 (6)	0.0006 (5)	0.0027 (5)	−0.0026 (5)
C03	0.0154 (6)	0.0132 (6)	0.0109 (5)	−0.0018 (5)	0.0035 (5)	−0.0001 (5)
C04	0.0188 (6)	0.0132 (6)	0.0136 (6)	−0.0032 (5)	0.0033 (5)	−0.0004 (5)
C05	0.0181 (6)	0.0198 (7)	0.0121 (6)	−0.0032 (5)	0.0004 (5)	−0.0020 (5)
C06	0.0174 (6)	0.0117 (6)	0.0151 (6)	−0.0029 (5)	−0.0010 (5)	0.0011 (5)
C07	0.0163 (6)	0.0159 (6)	0.0140 (6)	−0.0051 (5)	0.0031 (5)	−0.0004 (5)
C08	0.0189 (6)	0.0165 (7)	0.0175 (6)	−0.0046 (5)	0.0019 (5)	−0.0052 (5)
C09	0.0202 (6)	0.0130 (6)	0.0124 (6)	−0.0022 (5)	0.0031 (5)	−0.0001 (5)
C10	0.0171 (6)	0.0121 (6)	0.0128 (6)	0.0002 (5)	0.0028 (5)	0.0008 (5)
C11	0.0173 (6)	0.0209 (7)	0.0159 (6)	0.0011 (5)	0.0059 (5)	−0.0025 (5)
C12	0.0152 (6)	0.0133 (6)	0.0165 (6)	0.0004 (5)	0.0049 (5)	0.0009 (5)
C101	0.0124 (6)	0.0190 (7)	0.0108 (5)	0.0005 (5)	0.0027 (4)	0.0009 (5)
C102	0.0160 (6)	0.0189 (7)	0.0177 (6)	−0.0003 (5)	0.0043 (5)	0.0016 (5)
C103	0.0215 (7)	0.0226 (7)	0.0226 (7)	0.0066 (6)	0.0068 (6)	0.0074 (6)
C104	0.0133 (6)	0.0367 (9)	0.0211 (7)	0.0046 (6)	0.0018 (5)	0.0067 (6)
C105	0.0158 (6)	0.0309 (8)	0.0229 (7)	−0.0046 (6)	−0.0006 (5)	−0.0010 (6)
C106	0.0183 (6)	0.0187 (7)	0.0183 (6)	−0.0003 (5)	0.0016 (5)	−0.0004 (5)
C201	0.0131 (6)	0.0146 (6)	0.0142 (6)	−0.0021 (5)	0.0041 (5)	−0.0026 (5)
C202	0.0173 (6)	0.0132 (6)	0.0236 (7)	−0.0009 (5)	0.0022 (5)	−0.0012 (5)
C203	0.0144 (6)	0.0216 (7)	0.0239 (7)	−0.0006 (5)	−0.0007 (5)	−0.0016 (6)
C204	0.0162 (6)	0.0193 (7)	0.0227 (7)	−0.0068 (5)	0.0041 (5)	−0.0070 (6)

C205	0.0225 (7)	0.0138 (7)	0.0230 (7)	−0.0030 (5)	0.0052 (5)	−0.0031 (5)
C206	0.0176 (6)	0.0157 (7)	0.0158 (6)	−0.0006 (5)	0.0018 (5)	−0.0017 (5)
C301	0.0185 (6)	0.0169 (7)	0.0119 (6)	0.0011 (5)	0.0022 (5)	0.0015 (5)
C302	0.0214 (7)	0.0226 (7)	0.0163 (6)	−0.0022 (5)	0.0018 (5)	−0.0013 (5)
C303	0.0301 (7)	0.0240 (8)	0.0135 (6)	0.0074 (6)	−0.0002 (5)	−0.0047 (5)
C304	0.0226 (7)	0.0312 (8)	0.0128 (6)	0.0111 (6)	0.0047 (5)	0.0039 (6)
C305	0.0174 (6)	0.0247 (8)	0.0243 (7)	0.0020 (6)	0.0047 (5)	0.0038 (6)
C306	0.0191 (6)	0.0182 (7)	0.0190 (6)	0.0000 (5)	0.0023 (5)	−0.0020 (5)
C401	0.0166 (6)	0.0129 (6)	0.0201 (6)	−0.0021 (5)	−0.0019 (5)	−0.0021 (5)
C402	0.0190 (6)	0.0187 (7)	0.0244 (7)	−0.0017 (5)	0.0007 (5)	−0.0031 (6)
C403	0.0182 (7)	0.0233 (8)	0.0423 (9)	−0.0008 (6)	0.0036 (6)	−0.0059 (7)
C404	0.0196 (7)	0.0197 (8)	0.0445 (10)	0.0008 (6)	−0.0087 (7)	−0.0025 (7)
C405	0.0283 (8)	0.0241 (8)	0.0275 (8)	−0.0014 (6)	−0.0104 (6)	0.0002 (6)
C406	0.0236 (7)	0.0221 (8)	0.0220 (7)	−0.0012 (6)	−0.0020 (6)	0.0001 (6)
C501	0.0158 (6)	0.0141 (6)	0.0182 (6)	−0.0043 (5)	0.0017 (5)	−0.0024 (5)
C502	0.0194 (6)	0.0227 (7)	0.0189 (7)	−0.0035 (5)	0.0035 (5)	−0.0059 (6)
C503	0.0235 (7)	0.0282 (8)	0.0204 (7)	−0.0025 (6)	−0.0018 (6)	−0.0069 (6)
C504	0.0170 (6)	0.0249 (8)	0.0277 (7)	0.0001 (6)	−0.0035 (6)	−0.0046 (6)
C505	0.0190 (7)	0.0230 (8)	0.0256 (7)	0.0007 (6)	0.0054 (6)	−0.0052 (6)
C506	0.0218 (7)	0.0187 (7)	0.0158 (6)	−0.0032 (5)	0.0028 (5)	−0.0037 (5)
C601	0.0220 (6)	0.0161 (7)	0.0122 (6)	0.0020 (5)	0.0016 (5)	−0.0007 (5)
C602	0.0231 (7)	0.0206 (7)	0.0204 (7)	0.0007 (6)	0.0001 (5)	−0.0011 (6)
C603	0.0216 (7)	0.0327 (9)	0.0236 (7)	0.0051 (6)	0.0001 (6)	−0.0001 (6)
C604	0.0359 (8)	0.0260 (8)	0.0213 (7)	0.0153 (7)	0.0002 (6)	−0.0016 (6)
C605	0.0398 (9)	0.0150 (7)	0.0213 (7)	0.0027 (6)	0.0002 (6)	−0.0023 (6)
C606	0.0265 (7)	0.0196 (7)	0.0177 (6)	−0.0011 (6)	0.0026 (5)	−0.0018 (5)
C701	0.0186 (6)	0.0144 (6)	0.0127 (6)	−0.0021 (5)	0.0024 (5)	0.0010 (5)
C702	0.0225 (7)	0.0228 (7)	0.0186 (7)	−0.0003 (6)	0.0052 (5)	−0.0033 (6)
C703	0.0345 (8)	0.0227 (8)	0.0175 (7)	−0.0065 (6)	0.0084 (6)	−0.0063 (6)
C704	0.0343 (8)	0.0220 (8)	0.0162 (7)	−0.0098 (6)	−0.0038 (6)	−0.0006 (6)
C705	0.0221 (7)	0.0246 (8)	0.0269 (8)	−0.0001 (6)	−0.0056 (6)	−0.0021 (6)
C706	0.0214 (7)	0.0205 (7)	0.0205 (7)	0.0004 (5)	0.0022 (5)	−0.0049 (6)
C801	0.0138 (6)	0.0209 (7)	0.0172 (6)	0.0011 (5)	0.0030 (5)	0.0031 (5)
C802	0.0171 (6)	0.0251 (8)	0.0195 (6)	−0.0004 (5)	0.0035 (5)	−0.0001 (6)
C803	0.0182 (7)	0.0404 (10)	0.0251 (7)	−0.0051 (6)	−0.0001 (6)	−0.0026 (7)
C804	0.0139 (7)	0.0640 (13)	0.0266 (8)	−0.0025 (7)	0.0044 (6)	0.0003 (8)
C805	0.0183 (7)	0.0616 (12)	0.0262 (8)	0.0051 (7)	0.0083 (6)	−0.0085 (8)
C806	0.0193 (7)	0.0396 (9)	0.0207 (7)	0.0027 (6)	0.0040 (6)	−0.0062 (7)
O1	0.0147 (4)	0.0137 (5)	0.0127 (4)	0.0013 (3)	0.0001 (3)	−0.0021 (3)
O2	0.0127 (4)	0.0122 (4)	0.0154 (4)	−0.0004 (3)	0.0018 (3)	−0.0017 (3)
O3	0.0155 (4)	0.0167 (5)	0.0109 (4)	−0.0030 (4)	0.0017 (3)	−0.0019 (3)
O4	0.0171 (4)	0.0140 (5)	0.0136 (4)	0.0017 (4)	−0.0002 (3)	−0.0017 (4)
O5	0.0155 (4)	0.0172 (5)	0.0145 (4)	−0.0051 (4)	0.0036 (3)	−0.0050 (4)
O6	0.0152 (4)	0.0127 (4)	0.0157 (4)	−0.0016 (3)	0.0007 (3)	−0.0025 (4)
O7	0.0137 (4)	0.0164 (5)	0.0128 (4)	0.0008 (3)	0.0025 (3)	−0.0014 (4)
O8	0.0147 (4)	0.0154 (5)	0.0157 (4)	−0.0020 (3)	0.0046 (3)	−0.0032 (4)
Zr1	0.00969 (6)	0.01078 (6)	0.00978 (6)	−0.00062 (4)	0.00074 (4)	−0.00173 (4)

Table A.8.31 Bond lengths (Å) for [Zr(DBM)$_4$].

Atoms	Bond length (Å)	Atoms	Bond length (Å)
C01—O1	1.2807 (16)	C401—C402	1.393 (2)
C01—C02	1.3893 (18)	C402—C403	1.390 (2)
C01—C101	1.4937 (17)	C402—H402	0.93
C02—C03	1.4046 (17)	C403—C404	1.388 (2)
C02—H02	0.93	C403—H403	0.93
C03—O2	1.2670 (17)	C404—C405	1.375 (2)
C03—C201	1.4881 (17)	C404—H404	0.93
C04—O3	1.2754 (16)	C405—C406	1.388 (2)
C04—C05	1.4025 (18)	C405—H405	0.93
C04—C301	1.4896 (19)	C406—H406	0.93
C05—C06	1.393 (2)	C501—C506	1.3953 (19)
C05—H05	0.93	C501—C502	1.3957 (19)
C06—O4	1.2757 (16)	C502—C503	1.385 (2)
C06—C401	1.4981 (18)	C502—H502	0.93
C07—O5	1.2820 (16)	C503—C504	1.381 (2)
C07—C08	1.3944 (19)	C503—H503	0.93
C07—C501	1.4904 (18)	C504—C505	1.387 (2)
C08—C09	1.4026 (18)	C504—H504	0.93
C08—H08	0.93	C505—C506	1.3876 (19)
C09—O6	1.2744 (16)	C505—H505	0.93
C09—C601	1.4912 (19)	C506—H506	0.93
C10—O7	1.2746 (16)	C601—C602	1.393 (2)
C10—C11	1.4032 (18)	C601—C606	1.393 (2)
C10—C701	1.4957 (18)	C602—C603	1.380 (2)
C11—C12	1.3952 (19)	C602—H602	0.93
C11—H11	0.93	C603—C604	1.387 (2)
C12—O8	1.2749 (16)	C603—H603	0.93
C12—C801	1.4921 (18)	C604—C605	1.382 (2)
C101—C102	1.391 (2)	C604—H604	0.93
C101—C106	1.3954 (19)	C605—C606	1.388 (2)
C102—C103	1.3918 (19)	C605—H605	0.93
C102—H102	0.93	C606—H606	0.93
C103—C104	1.389 (2)	C701—C706	1.3937 (19)
C103—H103	0.93	C701—C702	1.3959 (19)
C104—C105	1.383 (2)	C702—C703	1.390 (2)
C104—H104	0.93	C702—H702	0.93
C105—C106	1.3875 (19)	C703—C704	1.382 (2)
C105—H105	0.93	C703—H703	0.93
C106—H106	0.93	C704—C705	1.388 (2)
C201—C206	1.388 (2)	C704—H704	0.93
C201—C202	1.3984 (18)	C705—C706	1.390 (2)
C202—C203	1.3889 (19)	C705—H705	0.93
C202—H202	0.93	C706—H706	0.93
C203—C204	1.388 (2)	C801—C806	1.395 (2)
C203—H203	0.93	C801—C802	1.396 (2)
C204—C205	1.386 (2)	C802—C803	1.388 (2)

Atoms	Bond length	Atoms	Bond length
C204—H204	0.93	C802—H802	0.93
C205—C206	1.3886 (19)	C803—C804	1.387 (2)
C205—H205	0.93	C803—H803	0.93
C206—H206	0.93	C804—C805	1.383 (3)
C301—C302	1.392 (2)	C804—H804	0.93
C301—C306	1.3972 (19)	C805—C806	1.388 (2)
C302—C303	1.394 (2)	C805—H805	0.93
C302—H302	0.93	C806—H806	0.93
C303—C304	1.380 (2)	O1—Zr1	2.1405 (11)
C303—H303	0.93	O2—Zr1	2.2069 (12)
C304—C305	1.384 (2)	O3—Zr1	2.1904 (10)
C304—H304	0.93	O4—Zr1	2.1621 (10)
C305—C306	1.384 (2)	O5—Zr1	2.1578 (10)
C305—H305	0.93	O6—Zr1	2.2014 (13)
C306—H306	0.93	O7—Zr1	2.2125 (11)
C401—C406	1.391 (2)	O8—Zr1	2.1517 (10)

Table A.8.32 Bond angles (°) for [Zr(DBM)$_4$].

Atoms	Bond angle (°)	Atoms	Bond angle (°)
O1—C01—C02	123.74 (12)	C506—C501—C502	119.35 (12)
O1—C01—C101	114.71 (11)	C506—C501—C07	119.44 (12)
C02—C01—C101	121.51 (12)	C502—C501—C07	121.12 (12)
C01—C02—C03	121.02 (12)	C503—C502—C501	120.13 (13)
C01—C02—H02	119.5	C503—C502—H502	119.9
C03—C02—H02	119.5	C501—C502—H502	119.9
O2—C03—C02	124.19 (12)	C504—C503—C502	120.24 (13)
O2—C03—C201	115.98 (11)	C504—C503—H503	119.9
C02—C03—C201	119.81 (12)	C502—C503—H503	119.9
O3—C04—C05	124.18 (12)	C503—C504—C505	120.15 (13)
O3—C04—C301	116.18 (12)	C503—C504—H504	119.9
C05—C04—C301	119.55 (12)	C505—C504—H504	119.9
C06—C05—C04	121.06 (12)	C504—C505—C506	120.00 (13)
C06—C05—H05	119.5	C504—C505—H505	120
C04—C05—H05	119.5	C506—C505—H505	120
O4—C06—C05	123.52 (12)	C505—C506—C501	120.12 (13)
O4—C06—C401	114.31 (12)	C505—C506—H506	119.9
C05—C06—C401	122.15 (12)	C501—C506—H506	119.9
O5—C07—C08	123.90 (12)	C602—C601—C606	119.19 (13)
O5—C07—C501	115.52 (12)	C602—C601—C09	118.93 (13)
C08—C07—C501	120.57 (12)	C606—C601—C09	121.75 (13)
C07—C08—C09	121.10 (12)	C603—C602—C601	120.27 (14)
C07—C08—H08	119.5	C603—C602—H602	119.9
C09—C08—H08	119.5	C601—C602—H602	119.9
O6—C09—C08	123.32 (12)	C602—C603—C604	120.28 (15)
O6—C09—C601	115.35 (12)	C602—C603—H603	119.9
C08—C09—C601	121.32 (12)	C604—C603—H603	119.9
O7—C10—C11	123.12 (12)	C605—C604—C603	119.97 (14)

O7—C10—C701	116.03 (11)	C605—C604—H604	120
C11—C10—C701	120.84 (12)	C603—C604—H604	120
C12—C11—C10	121.33 (12)	C604—C605—C606	119.96 (15)
C12—C11—H11	119.3	C604—C605—H605	120
C10—C11—H11	119.3	C606—C605—H605	120
O8—C12—C11	124.04 (12)	C605—C606—C601	120.32 (14)
O8—C12—C801	114.63 (11)	C605—C606—H606	119.8
C11—C12—C801	121.30 (12)	C601—C606—H606	119.8
C102—C101—C106	119.46 (12)	C706—C701—C702	119.04 (12)
C102—C101—C01	122.80 (12)	C706—C701—C10	118.95 (12)
C106—C101—C01	117.69 (12)	C702—C701—C10	121.99 (12)
C101—C102—C103	120.32 (13)	C703—C702—C701	120.40 (14)
C101—C102—H102	119.8	C703—C702—H702	119.8
C103—C102—H102	119.8	C701—C702—H702	119.8
C104—C103—C102	119.69 (14)	C704—C703—C702	120.20 (14)
C104—C103—H103	120.2	C704—C703—H703	119.9
C102—C103—H103	120.2	C702—C703—H703	119.9
C105—C104—C103	120.25 (13)	C703—C704—C705	119.83 (13)
C105—C104—H104	119.9	C703—C704—H704	120.1
C103—C104—H104	119.9	C705—C704—H704	120.1
C104—C105—C106	120.16 (14)	C704—C705—C706	120.26 (14)
C104—C105—H105	119.9	C704—C705—H705	119.9
C106—C105—H105	119.9	C706—C705—H705	119.9
C105—C106—C101	120.11 (14)	C705—C706—C701	120.23 (14)
C105—C106—H106	119.9	C705—C706—H706	119.9
C101—C106—H106	119.9	C701—C706—H706	119.9
C206—C201—C202	119.35 (12)	C806—C801—C802	119.25 (13)
C206—C201—C03	120.26 (12)	C806—C801—C12	122.20 (13)
C202—C201—C03	120.32 (12)	C802—C801—C12	118.54 (12)
C203—C202—C201	119.84 (13)	C803—C802—C801	120.17 (14)
C203—C202—H202	120.1	C803—C802—H802	119.9
C201—C202—H202	120.1	C801—C802—H802	119.9
C204—C203—C202	120.35 (13)	C804—C803—C802	120.17 (15)
C204—C203—H203	119.8	C804—C803—H803	119.9
C202—C203—H203	119.8	C802—C803—H803	119.9
C205—C204—C203	119.89 (13)	C805—C804—C803	119.90 (14)
C205—C204—H204	120.1	C805—C804—H804	120
C203—C204—H204	120.1	C803—C804—H804	120
C204—C205—C206	119.87 (14)	C804—C805—C806	120.36 (15)
C204—C205—H205	120.1	C804—C805—H805	119.8
C206—C205—H205	120.1	C806—C805—H805	119.8
C201—C206—C205	120.60 (13)	C805—C806—C801	120.10 (15)
C201—C206—H206	119.7	C805—C806—H806	120
C205—C206—H206	119.7	C801—C806—H806	120
C302—C301—C306	119.47 (13)	C01—O1—Zr1	135.26 (8)
C302—C301—C04	121.53 (12)	C03—O2—Zr1	134.47 (8)
C306—C301—C04	119.00 (12)	C04—O3—Zr1	132.06 (9)
C301—C302—C303	120.06 (13)	C06—O4—Zr1	134.09 (9)
C301—C302—H302	120	C07—O5—Zr1	129.82 (8)

C303—C302—H302	120	C09—O6—Zr1	133.45 (9)
C304—C303—C302	119.91 (14)	C10—O7—Zr1	133.07 (8)
C304—C303—H303	120	C12—O8—Zr1	134.80 (8)
C302—C303—H303	120	O1—Zr1—O8	112.35 (4)
C303—C304—C305	120.31 (13)	O1—Zr1—O5	79.29 (5)
C303—C304—H304	119.8	O8—Zr1—O5	142.50 (4)
C305—C304—H304	119.8	O1—Zr1—O4	143.62 (3)
C306—C305—C304	120.25 (14)	O8—Zr1—O4	77.58 (4)
C306—C305—H305	119.9	O5—Zr1—O4	114.90 (4)
C304—C305—H305	119.9	O1—Zr1—O3	78.78 (4)
C305—C306—C301	119.97 (13)	O8—Zr1—O3	142.86 (3)
C305—C306—H306	120	O5—Zr1—O3	72.88 (4)
C301—C306—H306	120	O4—Zr1—O3	74.53 (4)
C406—C401—C402	119.47 (13)	O1—Zr1—O6	144.15 (4)
C406—C401—C06	122.41 (13)	O8—Zr1—O6	77.10 (4)
C402—C401—C06	118.09 (12)	O5—Zr1—O6	74.59 (4)
C403—C402—C401	120.20 (14)	O4—Zr1—O6	71.14 (4)
C403—C402—H402	119.9	O3—Zr1—O6	115.37 (4)
C401—C402—H402	119.9	O1—Zr1—O2	74.91 (4)
C404—C403—C402	119.91 (15)	O8—Zr1—O2	71.98 (4)
C404—C403—H403	120	O5—Zr1—O2	143.92 (3)
C402—C403—H403	120	O4—Zr1—O2	75.58 (4)
C405—C404—C403	119.88 (14)	O3—Zr1—O2	77.65 (3)
C405—C404—H404	120.1	O6—Zr1—O2	138.44 (4)
C403—C404—H404	120.1	O1—Zr1—O7	72.65 (3)
C404—C405—C406	120.77 (15)	O8—Zr1—O7	74.10 (4)
C404—C405—H405	119.6	O5—Zr1—O7	76.16 (3)
C406—C405—H405	119.6	O4—Zr1—O7	141.54 (3)
C405—C406—C401	119.78 (15)	O3—Zr1—O7	141.02 (4)
C405—C406—H406	120.1	O6—Zr1—O7	77.52 (3)
C401—C406—H406	120.1	O2—Zr1—O7	118.29 (4)

273

Appendix B

Kinetic Rate Equations

B.1. Derivation of: $k_{obs} = k_1[L] + k_{-1}$ – § 7.1, Eq.7.4

Consider the reaction

$$M + L \underset{k_{-1}}{\overset{k_1}{\rightleftharpoons}} ML \qquad (1)$$

The rate of this reaction can be expressed as

$$-\frac{d[M]}{dt} = \frac{d[ML]}{dt} = k_1[M][L] - k_{-1}[ML] \qquad (2)$$

Where [M] = concentration of metal M;

[L] = concentration of ligand L;

[ML] = concentration of complex ML.

Under *pseudo* first-order conditions where [L] >> [M], equation 2 simplifies to

$$-\frac{d[M]}{dt} = \frac{d[ML]}{dt} = k_1^*[L] - k_{-1}[ML] \qquad (3)$$

Where $k_1^* = k_1[B]$

If the reaction reaches equilibrium, the following equation would be true

$$-\frac{d[M]_{eq}}{dt} = \frac{d[ML]_{eq}}{dt} = 0 \tag{4}$$

Where [M] = concentration of metal M at equilibrium

[ML] = concentration of product ML at equilibrium

From equations 2 & 4 we obtain

$$\frac{k_1^*}{k_{-1}} = \frac{[ML]_{eq}}{[M]_{eq}} \tag{5}$$

If the initial concentration of M is given the vale M_0 we can manipulate equation 5 to

$$\frac{k_1^*}{k_{-1}} = \frac{[M]_0 - [M]_{eq}}{[M]_{eq}}$$

$$[M]_{eq} = \left(\frac{k_{-1}}{k_1^* + k_{-1}}\right)[M]_0 \tag{6}$$

We also apply this manipulation to equation 3

$$\begin{aligned}
\frac{d[M]}{dt} &= -k_1^*[M] + k_{-1}\left([M]_0 - [M]\right) \\
&= -k_1^*[M] + k_{-1}[M]_0 - k_{-1}[M] \\
&= -\left(k_1^* + k_{-1}\right)[M] + k_{-1}[M]_0 \\
&= -\left(k_1^* + k_{-1}\right)\left([M] - \frac{k_{-1}}{k_1^* + k_{-1}}[M]_0\right)
\end{aligned} \tag{7}$$

From equations 6 & 7 it follows

$$\frac{d[M]}{dt} = -\left(k_1^* + k_{-1}\right)\left([M] - [M]_{eq}\right) \tag{8}$$

By ordering of variables in equation 8

$$\frac{d[M]}{[M]-[M]_{eq}} = -\left(k_1^* + k_{-1}\right)$$

$$\int_{[M]_0}^{[M]} \frac{d[M]}{[M]-[M]_{eq}} = -\left(k_1^* + k_{-1}\right) \int_{t=0}^{t=t} dt \qquad (9)$$

$$\ln\left(\frac{[M]_0-[M]_{eq}}{[M]-[M]_{eq}}\right) = \left(k_1^* + k_{-1}\right)t$$

The sum of the two constants (k_1^* + k_{-1}) is defined as the observed rate constant k_{obs}, therefore:

$$k_{obs} = k_1^* + k_{-1} \qquad (10)$$

And consequently, from $k_1^* = k_1[B]$:

$$k_{obs} = k_1[L] + k_{-1} \qquad (11)$$

B.2. Derivation of: $k_{obs} = \dfrac{k_1 K_1[L]}{1 + K_1[L]}$ – § 7.1, Eq.7.5

Consider the following reactions

$$[M] + [L] \underset{}{\overset{K_{1a}}{\rightleftharpoons}} [ML^*] \qquad (12)$$

$$[ML^*] \xrightarrow{k_{1b}} [ML] \qquad (13)$$

Where [M] = concentration of metal M;

[L] = concentration of ligand L;

[ML*] = concentration of the intermediate product ML*

[ML] = concentration of complex ML.

The rate of equation 13 is expressed as

$$k_{obs} = k_{1b}[ML]$$ (14)

The equilibrium constant K_1, of equation 12 can be expressed as

$$K_{1a} = \frac{[ML^*]}{[M][L]}$$ (15)

Equation 15 can be transformed as such

$$[M] = \frac{[ML^*]}{K_{1a}[L]}$$ (16)

The total concentration of the reactant M in equations 12 & 13 is given by

$$[M]_T = [ML] + [M]$$ (17)

By substitution of equation 16 into equation 17, we obtain

$$[ML]_T = [ML] + \frac{[ML]}{K_{1a}[L]}$$ (18)

And by rearrangement, subsequently obtain

$$[ML] = \frac{[ML]_T K_1[L]}{1 + K_{1a}[L]}$$ (19)

Under *pseudo* first-order conditions, where [L] >> [M], equation 19 simplifies to

$$[ML] = \frac{K_{1a}[L]}{1 + K_{1a}[L]}$$ (20)

By substitution of equation 20 into equation 14 the rate equation for this reaction becomes

$$k_{obs} = \frac{k_{1b}K_{1a}[L]}{1 + K_{1a}[L]}$$ (21)

Appendix C

Theoretical Optimization –

DFT Calculated Supplementary Data

Table C.1 Calculated Single Point and Optimized energies of Zr(IV) complexes in Chapter 7.

Zr(IV) Complex	Abbreviation	$-(10^{-6})$ $E_{Single\ Point}$ (kJ.mol^{-1})	$-(10^{-6})$ $E_{Optimized}$ (kJ.mol^{-1})
[Zr(acac)$_4$]	za*	3.747	3.748
[Zr(hFAcac)$_4$]	zf*	9.999	10.000
[Zr(DBM)$_4$]	zd*	7.693	7.775
[Zr(ox)$_4$] – D$_2$^{x}	zo*	5.126	5.127
[Zr(ox)$_4$] – D$_2$^{z}	zo**	5.056	5.127
[Zr(diMeOx)$_4$] – D$_2$^{x}	zm*	5.951	5.953
[Zr(diMeOx)$_4$] – D$_2$^{z}	zm**	5.953	5.953
[Zr(diClOx)$_4$] – D$_2$^{x}	zc*	5.427	5.428
[Zr(diClOx)$_4$] – D$_2$^{z}	zc**	5.428	5.428

C.1. [Zr(acac)₄] − § 8.2.1

Table C.2 Calculated atomic coordinates for [Zr(acac)₄].

	x	*y*	*z*
Zr	0.00272	0.001215	-0.0053
O	-1.833019	0.934417	0.942441
O	-0.655329	-1.452002	1.448435
O	0.669534	-1.450845	-1.452884
O	1.838727	-0.939128	0.933383
O	-0.670223	1.444687	-1.458028
O	-1.829932	-0.949706	-0.946264
O	0.660886	1.455348	1.444443
O	1.829613	0.955515	-0.945582
H	-3.458471	-0.926078	3.196706
H	3.48182	-3.183494	-0.923133
H	-3.50076	0.916683	-3.161914
H	3.470437	3.194388	0.919602
H	-0.76089	-3.122445	3.519028
H	-1.724134	-3.790168	2.1982
H	-2.546196	-3.095766	3.626154
H	3.324988	-2.556039	2.489449
H	4.512947	-2.880315	1.195497
H	4.31654	-1.23407	1.867458
H	1.739065	2.190442	3.783883
H	0.776991	3.51626	3.124271
H	2.562735	3.619468	3.093679
H	-4.298502	1.874852	1.241544
H	-4.514373	1.178269	2.875528
H	-3.322473	2.475807	2.585178
H	3.318925	2.596886	-2.485042
H	-1.767888	3.782311	-2.17655
H	-2.599542	3.090263	-3.600387
H	-0.813259	3.128478	-3.510394
H	-4.533075	-1.197508	-2.848117
H	1.740879	-2.193921	-3.790599
H	-3.338648	-2.494144	-2.557746
H	0.790123	-3.523258	-3.122449
H	2.576196	-3.614914	-3.096886
H	-4.307248	-1.885694	-1.212537
H	4.295035	1.25004	-1.891432
H	4.515849	2.881311	-1.190186
C	-2.676192	-0.695591	2.483364
C	-2.699249	0.566906	1.831737
C	-1.67051	-1.65024	2.25112
C	-3.784503	1.574005	2.162946
C	-1.690956	-2.992253	2.951379
C	1.688586	-2.249479	-1.65

	x	y	z
C	2.709185	-1.825541	0.569648
C	-1.699981	1.643041	-2.243369
C	-2.712412	-0.58033	-1.817816
C	1.679454	2.254413	1.644116
C	2.701719	1.837818	-0.576408
C	1.715244	-2.947451	-2.992816
C	2.69391	-2.475983	-0.693834
C	3.791421	-2.153789	1.580886
C	-1.736892	2.988939	-2.934625
C	-2.704959	0.68589	-2.463759
C	-3.79854	-1.589913	-2.138574
C	1.705519	2.947311	2.989381
C	2.684251	2.485483	0.688668
C	3.783581	2.171341	-1.586099

C.2. [Zr(hFAcac)₄] – § 8.2.2

Table C.3 Calculated atomic coordinates for [Zr(hFacac)₄].

	x	y	z
Zr	-0.020222	0.000081	-0.000347
O	-1.82766	-1.009262	0.862125
O	-0.690602	-1.311842	-1.565464
O	0.618038	1.84996	-0.950668
O	1.778331	-0.517718	-1.220047
O	-0.688576	1.312832	1.565022
O	-1.826742	1.011481	-0.862382
O	0.615088	-1.850476	0.950495
O	1.779259	0.515349	1.219245
H	-3.339088	-3.305931	-1.060371
H	3.445788	1.956093	-2.752941
H	-3.334739	3.31014	1.060418
H	3.441885	-1.960548	2.754022
F	-4.554586	-3.322864	0.989279
F	-4.51622	-1.21133	1.770413
F	-3.152547	-2.767487	2.658764
F	-2.686483	-3.715718	-3.316251
F	-1.720824	-1.857255	-4.1417
F	-0.443588	-3.535611	-3.355699
F	0.428353	4.15541	-2.611095
F	1.587444	4.512616	-0.715684
F	2.678278	4.227203	-2.664496
F	4.735242	-0.01847	-3.172536
F	4.442231	-1.426162	-1.438933
F	3.282296	-1.727239	-3.346491
F	-2.681065	3.719329	3.316054
F	-1.717474	1.859762	4.141424

F	-0.438388	3.536482	3.35496
F	-4.550964	3.328311	-0.988745
F	-4.515229	1.216774	-1.76998
F	-3.150002	2.771396	-2.658626
F	0.420733	-4.155032	2.611417
F	1.58054	-4.5148	0.716928
F	2.670507	-4.230413	2.666382
F	4.734535	0.012026	3.173153
F	3.284646	1.723571	3.345316
F	4.444799	1.41904	1.438439
F	4.444799	1.41904	1.438439
C	-2.603869	-2.55381	-0.812609
C	-2.627442	-1.927366	0.449855
C	-1.633634	-2.179923	-1.748619
C	-3.714611	-2.316465	1.468429
C	-1.624065	-2.824968	-3.143591
C	1.616829	2.285568	-1.650383
C	2.653817	0.120231	-1.912953
C	-1.630481	2.1821	1.748293
C	-2.62527	1.930595	-0.449901
C	1.612858	-2.28746	1.65082
C	2.653381	-0.12375	1.912793
C	1.582848	3.79922	-1.913297
C	2.65775	1.506035	-2.1665
C	3.781021	-0.762975	-2.477418
C	-1.619785	2.827275	3.143199
C	-2.600515	2.5571	0.812499
C	-3.712275	2.320966	-1.468158
C	1.576276	-3.800954	1.914285
C	2.65485	-1.509441	2.167041
C	3.781958	0.757786	2.477134

C.3. [Zr(DBM)₄] – § 8.2.3

Table C.4 Calculated atomic coordinates for [Zr(DBM)₄].

	x	y	z
Zr	-0.015743	-0.002816	-0.005447
O	0.218062	1.667448	1.333961
O	1.955492	-0.31387	1.052746
O	1.49077	1.281537	-1.081231
O	1.066204	-1.325496	-1.322321
O	-1.10608	1.398386	-1.234439
O	-1.532951	-1.214807	-1.127991
O	-1.965078	0.235518	1.089807
O	-0.217477	-1.748851	1.242525
H	3.11579	2.215067	2.898419

H	2.460564	3.873238	3.923586
H	-0.975302	3.688781	1.320195
H	1.785451	6.126118	4.67882
H	-1.665836	5.978501	2.078924
H	3.756245	-1.827722	0.745056
H	4.612491	1.124085	3.773795
H	-0.277953	7.198229	3.764982
H	5.913906	-2.985124	1.268832
H	6.741977	-0.011872	4.296432
H	3.828041	-0.283102	-2.881237
H	-3.832485	0.435218	-2.901257
H	-3.046081	-2.34979	2.907454
H	7.412896	-2.071618	3.051797
H	4.484643	1.427303	-3.820576
H	2.255866	3.512421	-0.770933
H	1.195187	-3.680352	-1.195088
H	4.086328	-2.040594	-3.946821
H	-4.669503	2.361009	-2.912054
H	-0.6561	3.616769	-1.947535
H	-1.784126	-3.511201	-1.660934
H	-5.14236	-1.150847	-2.986897
H	-4.947948	-1.661167	3.112105
H	-3.455331	2.028457	1.447778
H	1.335088	-3.382072	1.98594
H	-2.739184	-4.426484	2.947262
H	5.704605	3.505059	-4.36786
H	3.488417	5.623458	-1.31931
H	1.849118	-5.997692	-1.897403
H	4.732583	-4.320639	-4.648325
H	-5.221068	4.652661	-3.663359
H	-1.205748	5.942806	-2.709897
H	-2.990691	-5.60259	-2.343893
H	-6.339415	-3.205171	-3.659513
H	-7.057753	-0.542941	3.736543
H	-5.595831	3.172799	2.079101
H	2.095757	-5.636396	2.781968
H	-1.998267	-6.652319	3.732542
H	5.220651	5.61718	-3.12425
H	3.624249	-6.315339	-3.63109
H	-3.496586	6.458505	-3.571387
H	-5.276014	-5.444393	-3.347802
H	-7.401823	1.879198	3.229447
H	0.420534	-7.274099	3.658881
C	1.145491	2.264891	2.043152
C	2.390386	1.667738	2.315526
C	0.788594	3.627533	2.548919
C	2.733431	0.377195	1.833962
C	1.566586	4.324652	3.503944
C	-0.384206	4.238809	2.045451

C	4.036849	-0.267714	2.200555
C	1.182778	5.603843	3.939574
C	-0.764509	5.519307	2.477662
C	4.420687	-1.442217	1.511315
C	4.889785	0.238782	3.209762
C	0.017371	6.207701	3.426396
C	2.52121	1.093335	-1.854302
C	2.173146	-1.351882	-2.023292
C	-2.216662	1.461086	-1.928086
C	-2.585109	-0.984764	-1.85921
C	-2.737094	-0.500917	1.834911
C	-1.129107	-2.378425	1.944153
C	5.630175	-2.087381	1.812744
C	6.098817	-0.409156	3.514815
C	2.915594	-0.190825	-2.311395
C	3.290668	2.322415	-2.234866
C	2.600197	-2.704734	-2.500139
C	-2.972738	0.320118	-2.258016
C	-2.607892	2.828128	-2.393268
C	-3.361629	-2.192277	-2.288778
C	-2.374165	-1.804509	2.261725
C	-4.040547	0.118399	2.24203
C	-0.740085	-3.738769	2.42933
C	6.475752	-1.572647	2.815707
C	4.26921	2.330073	-3.257065
C	3.014162	3.527444	-1.546998
C	1.968465	-3.840331	-1.939785
C	3.60175	-2.894096	-3.48192
C	-3.902368	3.129189	-2.879183
C	-1.642922	3.860977	-2.328146
C	-2.774205	-3.465722	-2.103031
C	-4.655974	-2.112696	-2.854948
C	-5.069348	-0.605379	2.890252
C	-4.249951	1.486918	1.95056
C	0.62525	-4.106064	2.373881
C	-1.681502	-4.672417	2.923625
C	4.959465	3.511747	-3.575956
C	3.706944	4.706897	-1.861946
C	2.33857	-5.134008	-2.341023
C	3.967046	-4.188632	-3.887397
C	-4.220802	4.431853	-3.298342
C	-1.959797	5.160703	-2.754964
C	-3.457241	-4.630733	-2.485706
C	-5.34238	-3.279383	-3.231856
C	-6.274065	0.026317	3.242323
C	-5.451723	2.119158	2.30571
C	1.041969	-5.370961	2.819301
C	-1.264533	-5.940646	3.361431
C	4.684031	4.70385	-2.877585

	x	y	z
C	3.339681	-5.313888	-3.316256
C	-3.249747	5.451638	-3.242211
C	-4.744542	-4.542496	-3.052514
C	-6.469443	1.391421	2.95418
C	0.099091	-6.293385	3.315458

C.4. [Zr(ox)₄] – D₂ˣ – § 8.3.1

Table C.5 Calculated atomic coordinates for [Zr(ox)₄] – D₂ˣ.

	x	y	z
Zr	-0.000038	-0.000035	-0.00008
O	-0.711464	-1.353875	-1.486622
O	-0.711251	1.353867	1.486558
O	0.711349	1.353851	-1.486597
O	0.711212	-1.35398	1.486497
N	1.963199	-1.192732	-0.826806
N	-1.963234	1.192677	-0.826734
N	-1.963365	-1.192564	0.826705
N	1.963295	1.192476	0.826698
H	2.077627	-0.371451	-2.716549
H	-2.077708	0.371375	-2.716464
H	-2.077727	-0.371226	2.716431
H	2.077705	0.37107	2.71639
H	4.051612	-1.778342	-3.413333
H	-4.051443	1.778561	-3.413364
H	-4.051435	-1.778381	3.413465
H	4.051429	1.778204	3.413426
H	5.017614	-3.427507	-1.787579
H	-3.710656	-4.58734	-2.786034
H	-3.710165	4.58754	2.786094
H	-5.01729	3.427876	-1.787671
H	3.710515	4.587355	-2.785978
H	-5.017428	-3.42767	1.787833
H	5.017387	3.427544	1.787825
H	3.710422	-4.587338	2.78612
H	-1.734367	3.131266	3.257155
H	-4.884483	4.5005	0.594668
H	1.734435	-3.1313	3.257103
H	4.884831	-4.500147	0.594751
H	-1.734811	-3.131169	-3.257215
H	-4.884815	-4.500275	-0.594533
H	1.734655	3.131203	-3.257157
H	4.884725	4.500219	-0.594508
C	2.519826	-1.093071	-2.038758
C	2.46579	-2.10406	0.075063
C	-1.778952	-2.168097	-1.336899

C	-1.778669	2.168178	1.336853
C	-2.519818	1.093085	-2.03871
C	-2.46572	2.104109	0.075089
C	1.778837	2.168073	-1.336872
C	-2.465914	-2.104003	-0.07508
C	-2.519874	-1.092952	2.038717
C	2.519836	1.09282	2.038691
C	2.465827	2.103942	-0.07507
C	1.778695	-2.168209	1.336803
C	3.632136	-1.89579	-2.419081
C	3.584966	-2.944857	-0.215414
C	-2.246502	-3.066374	-2.301428
C	-2.246118	3.066501	2.301397
C	-3.631987	1.89597	-2.419099
C	-3.584775	2.945048	-0.215439
C	2.246368	3.066378	-2.301384
C	-3.584987	-2.944893	0.215514
C	-3.632035	-1.895814	2.419178
C	3.632006	1.895669	2.419153
C	3.58491	2.944819	0.215524
C	2.246207	-3.066483	2.30136
C	4.164497	-2.809944	-1.514774
C	4.034903	-3.851827	0.7928
C	-3.370848	-3.895602	-2.017991
C	-3.370442	3.895778	2.018033
C	-4.164263	2.810205	-1.514825
C	-4.034644	3.852075	0.792755
C	3.370721	3.895595	-2.017948
C	-4.164391	-2.810036	1.514938
C	-4.034957	-3.851888	-0.792665
C	4.164342	2.80992	1.51493
C	4.034859	3.851843	-0.792638
C	3.370645	-3.895621	2.018044

C.5. [Zr(ox)₄] – D₂ᶻ – § 8.3.1

Table C.6 Calculated atomic coordinates for [Zr(ox)₄] – D₂ᶻ.

	x	y	z
Zr	-0.00002	0.031367	-0.000098
O	-1.276815	-1.33727	-1.024183
O	-0.07433	1.202097	-1.786685
O	0.073714	1.20209	1.786518
O	1.277433	-1.336663	1.024018
N	1.444021	-1.129333	-1.579072
N	2.07351	1.386372	0.071845
N	-2.07392	1.38581	-0.071698

N	-1.443523	-1.129835	1.578872
H	0.748021	-0.276034	-3.317422
H	2.872262	0.990523	-1.795603
H	-2.872271	0.989748	1.795876
H	-0.747866	-0.276166	3.317177
H	2.192419	-1.713446	-4.819909
H	4.943274	2.347499	-1.436096
H	-4.943753	2.346082	1.436656
H	-2.191869	-1.713911	4.819728
H	-4.553139	-4.559965	-0.904217
H	-2.394924	3.909542	-4.680507
H	2.39306	3.910249	4.680672
H	3.758284	-3.378522	-3.783689
H	5.261277	3.559332	0.741006
H	-5.262451	3.557784	-0.740416
H	4.554913	-4.55818	0.904186
H	-3.757129	-3.379603	3.783588
H	-4.668906	-4.463503	1.57844
H	-2.973667	-3.109566	-2.187932
H	4.281956	4.150449	3.077042
H	0.38401	2.541263	4.113587
H	4.670538	-4.461902	-1.578487
H	2.974977	-3.10823	2.187834
H	-0.385375	2.541168	-4.113711
H	-4.283655	4.149177	-3.076599
C	-2.187935	-2.137792	-0.439524
C	-1.125587	1.944969	-2.185418
C	1.124689	1.945276	2.185408
C	1.422273	-1.022478	-2.914275
C	2.277138	-2.05631	-0.992639
C	2.219486	2.067545	1.263276
C	3.029734	1.508673	-0.858563
C	-3.030046	1.507828	0.858849
C	-2.220282	2.066917	-1.263121
C	2.188835	-2.136878	0.439377
C	-1.421869	-1.022855	2.914066
C	-2.276316	-2.057133	0.992484
C	-3.024279	-3.039914	-1.105539
C	-1.209154	2.616818	-3.409742
C	1.207871	2.617156	3.409741
C	2.249073	-1.832807	-3.74233
C	3.155975	-2.898887	-1.74302
C	3.362945	2.873355	1.565612
C	4.199579	2.289961	-0.647499
C	-4.20016	2.288755	0.647948
C	-3.364033	2.872375	-1.565296
C	3.025529	-3.038647	1.105434
C	-2.248442	-1.83338	3.742156
C	-3.154895	-2.899946	1.742902

C	-3.916948	-3.86408	-0.361166
C	-2.357493	3.400508	-3.719661
C	2.355927	3.401197	3.719825
C	3.114807	-2.757461	-3.16393
C	3.991734	-3.812612	-1.031271
C	3.418118	3.539283	2.828078
C	4.371323	2.960798	0.558675
C	-4.372289	2.95952	-0.558211
C	-3.419594	3.538277	-2.827759
C	3.918459	-3.862563	0.361099
C	-3.11384	-2.758376	3.163801
C	-3.990305	-3.814025	1.031196

C.6. [Zr(diMeOx)$_4$] – D$_2$^{x} – § 8.3.2

Table C.7 Calculated atomic coordinates for [Zr(diMeOx)$_4$] – D$_2$^{x}.

	x	y	z
Zr	0.000011	-0.000054	0.000035
O	-0.709228	-1.358514	-1.480799
O	-0.709609	1.358219	1.480879
O	0.709272	1.358501	-1.480701
O	0.709617	-1.358403	1.480818
N	1.970389	-1.187866	-0.824238
N	-1.970371	1.187697	-0.824111
N	-1.970119	-1.188101	0.824079
N	1.970211	1.188068	0.824176
H	2.085424	-0.344265	-2.702332
H	-2.085432	0.344021	-2.702167
H	-2.085319	-0.344456	2.702136
H	2.085551	0.344298	2.702173
H	4.065303	-1.742235	-3.411199
H	-4.065234	1.742072	-3.41111
H	-4.06506	-1.742662	3.410973
H	4.065088	1.74273	3.411103
H	5.025518	-3.401769	-1.808261
H	-3.689827	-4.599128	-2.759734
H	-1.528649	-2.221921	-4.162355
H	-1.963038	-3.9453	-4.268884
H	-0.451114	-3.429394	-3.479333
H	-1.533083	2.222408	4.164272
H	-1.96162	3.947378	4.267469
H	-0.451099	3.424896	3.479432
H	-3.690556	4.598596	2.759597
H	-5.025375	3.401722	-1.808248
H	3.689617	4.599392	-2.759502
H	1.527372	2.221715	-4.161557

H	1.963679	3.944568	-4.269182
H	0.45128	3.430823	-3.479175
H	-5.024989	-3.402385	1.808062
H	5.024815	3.402665	1.808287
H	3.690804	-4.598481	2.759651
H	1.527218	-2.221054	4.16121
H	1.965255	-3.943434	4.26966
H	0.452371	-3.431574	3.479383
H	5.425914	-5.414221	1.396275
H	6.150045	-4.216878	0.312824
H	5.057343	-5.449679	-0.33404
H	-5.425627	5.414373	1.396199
H	-6.149829	4.217094	0.312728
H	-5.056968	5.449772	-0.334101
H	-6.149273	-4.217795	-0.313016
H	-5.05639	-5.450419	0.333877
H	-5.424933	-5.415028	-1.396447
H	5.424574	5.415475	-1.396138
H	6.149053	4.21824	-0.312801
H	5.056062	5.450715	0.334194
C	2.529166	-1.073255	-2.033351
C	2.471264	-2.107006	0.072005
C	-1.779631	-2.175622	-1.325589
C	-1.780096	2.175208	1.325593
C	-2.529142	1.073065	-2.033223
C	-2.471208	2.106895	0.072087
C	1.77962	2.175678	-1.325443
C	-2.470838	-2.107342	-0.072139
C	-2.528952	-1.073523	2.033167
C	2.529065	1.073485	2.033254
C	2.470815	2.107427	-0.071987
C	1.780138	-2.175337	1.325505
C	3.641657	-1.869725	-2.419812
C	3.59354	-2.945565	-0.224706
C	-2.227567	-3.080115	-2.298553
C	-2.228203	3.079636	2.298544
C	-3.641587	1.869581	-2.419727
C	-3.59344	2.945495	-0.224659
C	2.227484	3.080239	-2.298376
C	-3.593008	-2.946044	0.224546
C	-3.641356	-1.870129	2.419608
C	3.641363	1.870213	2.419749
C	3.592892	2.946239	0.224743
C	2.228267	-3.079738	2.29847
C	4.171824	-2.793158	-1.522531
C	4.046481	-3.868162	0.777982
C	-3.356515	-3.900717	-1.992838
C	-1.510414	-3.18104	-3.626577
C	-1.511281	3.180481	3.626702

C	-3.357168	3.90018	1.992739
C	-4.171714	2.793079	-1.522488
C	-4.046326	3.868162	0.777991
C	3.356351	3.900938	-1.992624
C	1.510292	3.181179	-3.626378
C	-4.171364	-2.793671	1.522344
C	-4.045755	-3.868749	-0.778133
C	4.171257	2.793873	1.522538
C	4.04556	3.86902	-0.777901
C	3.357326	-3.900171	1.992734
C	1.511133	-3.180787	3.626494
C	5.230682	-4.782614	0.522884
C	-5.230417	4.782737	0.522823
C	-5.229817	-4.783387	-0.523055
C	5.229537	4.783757	-0.522785

C.7. [Zr(diMeOx)$_4$] – D$_2$^{z} – § 8.3.2

Table C.8 Calculated atomic coordinates for [Zr(diMeOx)$_4$] – D$_2$^{z}.

	x	*y*	*z*
Zr	-0.000009	0.068187	-0.000011
O	1.402592	-1.319689	0.807134
O	0.322122	1.277702	1.722601
O	-0.322175	1.27776	-1.722573
O	-1.40255	-1.319727	-0.807189
N	-1.184314	-1.090044	1.789016
N	-2.107756	1.382506	0.216669
N	2.107694	1.382636	-0.216651
N	1.184408	-1.08995	-1.789085
H	-0.253746	-0.196416	3.390376
H	-2.690443	0.882161	2.138409
H	2.690426	0.882383	-2.138401
H	0.253865	-0.196307	-3.390452
H	-1.43111	-1.635248	5.111806
H	-4.802175	2.219799	2.079562
H	4.802092	2.220117	-2.079488
H	1.431338	-1.635047	-5.111884
H	4.561381	-4.579059	0.171857
H	2.95052	4.104647	4.189515
H	-2.950749	4.104625	-4.189398
H	-3.095855	-3.335294	4.346253
H	-5.372901	3.52795	0.02444
H	5.372734	3.528231	-0.024319
H	-4.561243	-4.579198	-0.171921
H	3.096107	-3.335064	-4.346322
H	-5.94502	3.920005	-2.40258

H	-5.088706	5.306744	-1.712351
H	-5.001277	4.988632	-3.450725
H	-0.417105	2.76442	3.856055
H	0.672602	1.767558	4.82233
H	0.743357	3.532988	4.970895
H	-3.926435	-5.406526	3.15604
H	-5.212751	-4.193368	3.236254
H	-5.208955	-5.395331	1.937467
H	3.556292	-2.190781	2.562002
H	2.309944	-3.428892	2.595762
H	4.015933	-3.905439	2.40074
H	5.212995	-4.193098	-3.236282
H	5.209192	-5.395102	-1.937535
H	3.926711	-5.406295	-3.156149
H	-3.555751	-2.19071	-2.562091
H	-2.310022	-3.429446	-2.595808
H	-4.016241	-3.905143	-2.400788
H	0.416952	2.764561	-3.855997
H	-0.672712	1.767688	-4.822307
H	-0.743549	3.533121	-4.9708
H	5.944815	3.920243	2.402711
H	5.088429	5.306956	1.71252
H	5.001009	4.988787	3.450883
C	2.203621	-2.128102	0.080556
C	1.414573	2.039145	1.961148
C	-1.414676	2.039138	-1.961104
C	-0.965764	-0.961028	3.103867
C	-2.080102	-2.038159	1.34264
C	-2.394737	2.114597	-0.9193
C	-2.955448	1.443588	1.252075
C	2.955396	1.443792	-1.252046
C	2.394634	2.114694	0.919349
C	-2.203546	-2.128181	-0.080617
C	0.965901	-0.960902	-3.10394
C	2.080217	-2.038042	-1.342704
C	3.112851	-3.046031	0.626191
C	1.621176	2.763894	3.143734
C	-1.621326	2.763909	-3.143667
C	-1.643077	-1.771504	4.055704
C	-2.823175	-2.885563	2.22742
C	-3.575133	2.918056	-1.051611
C	-4.149226	2.212937	1.212282
C	4.149136	2.213194	-1.212215
C	3.574988	2.918209	1.051697
C	-3.112767	-3.046118	-0.626253
C	1.643273	-1.771326	-4.055778
C	2.823346	-2.885397	-2.227486
C	3.862462	-3.868659	-0.268501
C	2.80849	3.548061	3.263652

C	-2.808683	3.548017	-3.263553
C	-2.5684	-2.71894	3.62312
C	-3.746218	-3.827387	1.661
C	-3.783927	3.648084	-2.270305
C	-4.461087	2.938784	0.067306
C	4.460951	2.939019	-0.067212
C	3.783737	3.648209	2.270415
C	-3.862327	-3.868794	0.268438
C	2.568611	-2.718745	-3.62319
C	3.746401	-3.827208	-1.661065
C	-5.018548	4.50903	-2.466132
C	0.600768	2.710756	4.259831
C	-4.564106	-4.751177	2.544961
C	3.264659	-3.155775	2.126536
C	4.564343	-4.750948	-2.545028
C	-3.264606	-3.155834	-2.126597
C	-0.600919	2.710866	-4.259771
C	5.01831	4.509215	2.466276

C.8. [Zr(diClOx)₄] – D₂ˣ – § 8.3.3

Table C.9 Calculated atomic coordinates for [Zr(diClOx)₄] – D₂ˣ.

	x	y	z
Zr	-0.000018	-0.000017	0.00011
O	-0.728525	1.345503	1.482045
O	-0.728244	-1.345682	-1.481887
O	0.728552	-1.345525	1.482028
O	0.728146	1.345644	-1.481904
N	1.944527	1.200259	0.842449
N	-1.944475	-1.20026	0.842525
N	-1.944798	1.19983	-0.842339
N	1.944706	-1.199834	-0.842417
H	1.998556	0.40931	2.749674
H	-1.998378	-0.409275	2.749737
H	-1.998668	0.408746	-2.749515
H	1.99846	-0.408762	-2.7496
H	3.959027	1.814961	3.47833
H	-3.958803	-1.814913	3.478549
H	-3.959111	1.814309	-3.478417
H	3.958949	-1.814228	-3.478568
H	4.984804	3.428658	1.853394
H	-3.796912	4.519868	2.78776
H	-3.796279	-4.520365	-2.787663
H	-4.984677	-3.428651	1.853715
H	3.797093	-4.519794	2.787614
H	-4.985099	3.428037	-1.853644

H	4.985071	-3.427904	-1.853829
H	3.796127	4.520269	-2.787934
Cl	5.473935	-4.895456	0.460619
Cl	1.536342	-3.114424	3.915349
Cl	5.473217	4.896198	-0.461158
Cl	1.535419	3.114578	-3.915352
Cl	-5.473225	-4.896253	-0.460775
Cl	-1.535647	-3.114686	-3.915248
Cl	-5.473822	4.895603	0.460827
Cl	-1.536169	3.114412	3.915405
C	2.465844	1.115159	2.072095
C	2.472942	2.097756	-0.058136
C	-1.799733	2.139223	1.330135
C	-1.799337	-2.139551	-1.32997
C	-2.465713	-1.115136	2.072202
C	-2.472947	-2.097778	-0.058004
C	1.799773	-2.139218	1.330072
C	-2.473305	2.097377	0.058144
C	-2.466015	1.114641	-2.072023
C	2.465871	-1.114627	-2.072121
C	2.473293	-2.097347	0.058054
C	1.799255	2.139505	-1.330066
C	3.570556	1.916588	2.470553
C	3.592401	2.930486	0.256043
C	-2.315245	3.017302	2.286188
C	-2.314751	-3.017681	-2.286036
C	-3.570397	-1.91656	2.470749
C	-3.592381	-2.930508	0.256264
C	2.31535	-3.017283	2.286101
C	-3.592795	2.930017	-0.256157
C	-3.570716	1.916018	-2.470619
C	3.570598	-1.915949	-2.470754
C	3.592805	-2.929941	-0.25629
C	2.314618	3.017607	-2.286183
C	4.137102	2.812776	1.570135
C	4.049108	3.804571	-0.774903
C	-3.434978	3.84884	2.01632
C	-3.434423	-3.849312	-2.016208
C	-4.136999	-2.812769	1.570387
C	-4.049146	-3.80462	-0.774634
C	3.435106	-3.848777	2.016189
C	-4.137379	2.812223	-1.570291
C	-4.049651	3.804101	0.774724
C	4.137335	-2.812125	-1.570445
C	4.049735	-3.804009	0.774573
C	3.434312	3.849237	-2.016441

C.9. [Zr(diClOx)₄] – D₂ᶻ – § 8.3.3

Table C.10 Calculated atomic coordinates for [Zr(diClOx)₄] – D₂ᶻ.

	x	*y*	*z*
Zr	-0.0001	-0.115859	0.000022
O	-1.538881	1.22328	0.604262
O	-0.63306	-1.239487	1.711782
O	0.632303	-1.239287	-1.712067
O	1.539401	1.222635	-0.60391
N	0.927475	1.054453	1.924047
N	1.932536	-1.532593	0.554069
N	-1.933661	-1.531589	-0.554383
N	-0.926844	1.055071	-1.923581
H	-0.27276	0.235705	3.387025
H	2.00744	-1.263547	2.603529
H	-2.008605	-1.262015	-2.603772
H	0.27304	0.235775	-3.386542
H	0.671715	1.671773	5.232733
H	4.087418	-2.625711	2.916109
H	-4.089308	-2.62304	-2.916494
H	-0.670367	1.672663	-5.232159
H	-4.692443	4.410593	-0.443307
H	-3.843437	-3.782858	3.802705
H	3.841568	-3.783743	-3.803404
H	2.508291	3.301078	4.704858
H	5.165322	-3.703528	0.921531
H	-5.16757	-3.7008	-0.922079
H	4.694885	4.407964	0.443819
H	-2.50602	3.303002	-4.70427
Cl	-3.737874	3.023582	1.90434
Cl	-1.428004	-2.35437	4.500673
Cl	1.426911	-2.353862	-4.501225
Cl	3.739257	3.021836	-1.90391
Cl	4.411139	4.77208	3.300704
Cl	5.649969	-4.546158	-1.676685
Cl	-5.65241	-4.543824	1.675953
Cl	-4.408173	4.774939	-3.300109
C	-2.245152	2.017786	-0.2093
C	-1.761465	-1.953805	1.773567
C	1.760347	-1.954154	-1.773986
C	0.50226	0.966638	3.19276
C	1.914035	1.963801	1.607688
C	2.487599	-2.148787	-0.548302
C	2.496232	-1.724275	1.754964
C	-2.497559	-1.722698	-1.755276
C	-2.488927	-2.147767	0.547894
C	2.246176	2.016605	0.209743

C	-0.501551	0.967157	-3.192261
C	-1.91289	1.964976	-1.607214
C	-3.256494	2.904536	0.16729
C	-2.287246	-2.558689	2.917781
C	2.285917	-2.55901	-2.918311
C	1.054466	1.776144	4.223
C	2.536836	2.799715	2.58665
C	3.671734	-2.949346	-0.470548
C	3.669687	-2.507654	1.92188
C	-3.671426	-2.505438	-1.922275
C	-3.673472	-2.947714	0.470046
C	3.257992	2.902828	-0.166823
C	-1.053156	1.777139	-4.222452
C	-2.535092	2.801387	-2.586129
C	-3.914537	3.733805	-0.77991
C	-3.473317	-3.336427	2.886255
C	3.471593	-3.337355	-2.886876
C	2.06993	2.680575	3.929551
C	3.557304	3.679653	2.118471
C	4.140575	-3.5265	-1.687864
C	4.264211	-3.107613	0.817176
C	-4.266146	-3.10537	-0.817662
C	-4.142499	-3.524933	1.687257
C	3.916625	3.731581	0.780416
C	-2.068107	2.682146	-3.928994
C	-3.555098	3.681855	-2.117935